PACIFIC EARTHQUAKE ENGINEERING RESEARCH CENTER

Urban Earthquake Engineering

Proceedings of the U.S.-Iran Seismic Workshop
December 18-20, 2012

Tehran, Iran

PEER 2013/26
DECEMBER 2013

Disclaimer

The opinions, findings, and conclusions or recommendations expressed in this publication are those of the author(s) and do not necessarily reflect the views of the study sponsor(s) or the Pacific Earthquake Engineering Research Center.

Urban Earthquake Engineering

Proceedings of the U.S.-Iran Seismic Workshop
December 18-20, 2012

Tehran, Iran

PEER Report 2013/26
Pacific Earthquake Engineering Research Center
Headquarters at the University of Califronia

December 2013

ABSTRACT

The 4th U.S.-Iran Seismic Workshop was held on December 18-20, 2012 in Tehran, Iran. The workshop was supported by the U.S. National Academy of Sciences in collaboration with the Sharif University of Technology, Iran, and the Pacific Earthquake Engineering Research Center, University of California, Berkeley, USA. The theme of the workshop was ***Urban Earthquake Engineering***. This report contains the collection of papers presented at the 2012 seismic workshop.

INTRODUCTION

2008, 2009 , and 2010 U.S.–Iran Seismic Workshops

Following an extended period of planning, on June 8-9, 2008, a U.S. –Iran invitational workshop on *Seismic Performance of Adobe and Masonry Structures* was held at the Sharif University of Technology in Tehran. The workshop was organized by the Sharif University of Technology, in collaboration with the U.S. National Academy of Sciences and the Pacific Earthquake Engineering Research Center (PEER), University of California, Berkeley. It involved specialists from fourteen Iranian institutions, and seven earthquake experts from the United States.

The topic of adobe and masonry vulnerability was selected because of the extensive damage to this form of construction from earthquakes in Iran, including the Bam earthquake of December 26, 2003. Twenty-three technical papers were presented. The workshop concluded with a panel session that identified topics for future research collaboration. The workshop was followed with a one-day public seminar on June 10, 2008, on *Seismic Hazard Reduction*, also held at Sharif University.

The second U.S.-Iran seismic workshop was held on June 29-July 1, 2009, at the Arnold and Mabel Beckman Center of the National Academies of Sciences and Engineering, Irvine, California. The workshop was supported by the U.S. National Academy of Sciences, in collaboration with PEER, and Sharif University of Technology. The theme of this workshop was *Improving Earthquake Mitigation through Innovations and Applications in Seismic Science, Engineering, Communication, and Response*. Numerous American and Iranian earthquake engineers and scientists participated in the workshop and gave presentations. The proceedings of the 2009 seismic workshop were published by PEER as *PEER Report 2009/02*.

The third seismic workshop was held on December 14-16, 2010, in Istanbul, Turkey with participation of American, Iranian and Turkish earthquake experts. The theme of the workshop was *Seismic Risk Management in Urban Areas.* The 2010 seismic workshop was hosted by the Bogazici University–Kandilli Observatory and Earthquake Research Institute in Istanbul, Turkey, in collaboration with the U.S. National Academy of Sciences, Sharif University of Technology, and PEER. The participants of the workshop included nine experts from the United States, twelve from Iran, and fifteen from Turkey. The proceedings of the 2010 seismic workshop were published by PEER as *PEER Report 2011/07.*

2012 U.S.–Iran Seismic Workshop

The fourth seismic workshop, which is the subject of this report, was held on December 18-20, 2012, in Tehran, Iran. The theme was *Urban Earthquake Engineering.* This workrshop was hosted by the Sharif University of Technology, in collaboration with the U.S. National Academy of Sciences and PEER. The participants of the workshop included four earthquake experts from the United States, along with numerous Iranian earthquake engineers and scientists. The workshop was also attended by over 80 enthusiastic Iranian graduate students from various universities in Iran.

We thank all participants of the 2012 workshop from both Iran and the U.S. for their time and efforts. The seismic workshops in 2008, 2009, 2010, and 2012 would not have been possible without the continuous support and encouragement of **Glenn Schweitzer** of the U.S. National Academy of Sciences. Dr. **Fayaz Rahimzadeh Rofooei** (Sharif University of Technology) was the host and coordinator of the Iranian team of participants, and we appreciate his continuous cooperation.

Finally, we recently lost Dr. **William Anderson**. Bill actively participated in all U.S.-Iran seismic workshops, including the 2012 workshop in Tehran. He always provided guidance and encouragement. Bill's contributions to our seismic collaborations will be remembered forever. We lost a great colleague, educator, and friend.

Yousef Bozorgnia and Sanaz Rezaeian

Sharif University of Technology, Tehran, Iran, December 20, 2012

AGENDA

Urban Earthquake Engineering
The U.S.-Iran Seismic Workshop
December 18-20, 2012
Tehran, Iran

TUESDAY, DECEMBER 18, 2012

7:45–8:15 AM **Registration**

8:15–8:30 AM **Welcoming Remarks: Dr. Roosta Azad**, President, Sharif University of Technology

8:30–9:00 AM **Introductory Remarks: Fayaz Rahimzadeh,** Session Chair

9:00–10:30 AM **Seismic Risk and Hazard Analysis—Fayaz Rahimzadeh**, Session Chair

- **Ghafori Ashtinay, M.,** ***International Institute Earthquake Engineering and Seismology***
  An Index Model for Evaluating Urban Earthquake Risk
- **Tehranizadeh, M.,** ***Amirkabir University of Technology***
  Directivity Effects on Near-Fault Amplification
- **Ghaya-Maghamian, G. R.,** ***International Institute Earthquake Engineering and Seismology***
  Near-Field Low-Frequency Ground Motion Simulation in Tehran

10:30–11:00 AM **Break**

11:00–12:30 PM **Seismic Hazard and Lifelines—William Anderson**, Session Chair

- **Borzognia, Y.,** ***PEER, University of California, Berkeley***
  Latest Developments in Probabilistic Seismic Hazard Analysis and Performance-Based Earthquake Engineering
- **Ahmadi, M. T.,** ***Tarbiat Modares University, Tehran***
  Methods for Design of Large Dam Gates under Seismic Hydrodynamic Action
- **Ghaemian, M.,** ***Sharif University of Technology, Tehran***
  Seismic Damage Assessment of Concrete Arch Dams

12:30–1:30 PM **Lunch**

1:30–3:00 PM **<u>Lifelines</u>—Morteza Talebian**, Session Chair

- **Fujisaki, E., *PG&E, San Francisco, California***
  Seismic Performance and Qualification of Electric Substation Equipment
- **Rahimzadeh, F., *Sharif University of Technology***
  Assessment of the Seismic Behavior of Buried Gas Pipelines under Reverse Faulting
- **Jafarzadeh F., *Sharif University of Technology***
  Evaluation of Dynamic Response and Vulnerability of Tehran Buried Gas Network Pipelines in Slopes by In Situ Explorations, 1g Shaking Table Tests and Numerical Modeling

3:00–3:30 PM **Break**

3:30–6:00 PM **<u>Seismic Performance of Structural Systems (I)</u>—Abolhassan Vafael**, Session Chair

- **Shakib, H., *Tarbiat Modares University, and the City Council of Tehran***
  An Overview of the Seismic Code Provision for Vertical Irregularity Criteria: A Proposal
- **Abrahms, D., *University of Illinois, Urbana-Champaign***
  Latest Development in Seismic Performance of Masonry Buildings
- **Mehdizadeh, A. R., *State Organization of Schools Renovation***
  A Report on the State of the Practice in Retrofitting Procedures of School Buildings in Tehran
- **Mostofinejad, D., *Isfahan University of Technology***
  Performance of Grooving Method (GM) for FRP Strengthening of Concrete Structures
- **Estekanchi, H., *Sharif University of Technology***
  Recent Advances in Seismic Assessment of Structures by Endurance Time Method
- **Yahyaii, M., *Khaje Nasir Toosi University of Technology***
  Behavior of Steel Frames under Post-Earthquake Fire

WEDNESDAY, DECEMBER 19, 2012

7:45–8:00 AM — **Overview of the Second Day Program—Yousef Bozorgnia and Fayaz Rahimzadeh**

8:00–10:30 AM — **Seismic Risk and Resilient Community—Eric Fujisaki**, Session Chair

- **Anderson, W.,** ***National Academy of Sciences***
  Preparedness Planning and the August 28, 2011, Virginia Earthquake
- **Hosseini, M.,** ***Tehran Municipality***
  Design of the Tehran Earthquake Damage and Lost Estimation System
- **Bonowitz, D.,** ***Consulting Engineer, San Francisco, California***
  Engineering for Resilient Communities
- **Zolfaghari, M. R.,** ***Khaje Nasir Toosi University of Technology***
  Design and Development of Real Time Seismic Damage and Casualty Estimation Tools toward Urban Disaster Management
- **Ghodrati Amiri, G. R.,** ***Iran University of Science and Technology***
  Hybrid Wavelet Neuro-PSO Algorithm for Generation of Pulse-Like Near-Fault Earthquake Time Histories Compatible with NGA Predicted Spectrum

10:30–11:00 AM — **Break**

11:00–12:30 PM — **Seismic Performance of Structural Systems (II)—M. T. Kazemi** Session Chair

- **Honarbakhsh, T.,** ***Sarzamin Consulting Engineers Company***
  Guidelines for Relative Rehabilitation of Common Buildings (Up to Four Stories) in Tehran
- **Kheyroddin, A.,** ***Semnan University***
  Structural Application of HPFRCC in Earthquake Resistant Reinforced Concrete Structures
- **Khonsari, V.,** ***Sharif University of Technology***
  A New Replaceable Bracing System

12:30–1:30 PM — **Lunch**

1:30–3:00 PM — **Seismic Performance of Structural Systems (III)—D. Bonowitz** Session Chair

- **Aghakochak, A. A.,** ***Tarbiat Modares University Tehran***
  Current Research on the Seismic Behavior of Steel Structures Commonly Used in Iran
- **Khoushnodian, F.,** ***Amir Kabir University Technology***
  New Pushover Procedure for Estimating Seismic Demands of Tall Buildings

	• **Banan, M. R., *Shiraz University*** *Damage-Based Seismic Design of RC Buildings: Estimation of Relations among Hysteretic Indices and Design Parameters for RC Beam-Columns*
3:00–3:30 PM	**Break**
3:30–6:00 PM	**Seismic Performance of Structural Systems (IV)—A. Bakhshi,** Session Chair
	• **Halabian, M. M., *Isfahan University of Technology*** *A Hybrid SPH-FEM Model to Evaluation Seismic Response of TSD-Equipped Structures*
	• **Zareian, F., *University of California, Irvine*** *Seismic Performance of Skewed Bridges*
	• **Baziar, M. H., *Sharif University of Technology*** *Behavior of Pile Raft Foundation under Seismic Loading: Connected versus Non-Connected System*
	• **Moghaddam, H., *Sharif University of Technology*** *On the Ductility of Retrofitted RC Columns*
	• **Asgarian, B., *Khaje Nasir Toosi University of Technology*** *Hybrid Devices to Reduce Residual Displacement of Structural Systems Subjected to Strong Ground Motion*

THURSDAY, DECEMBER 20, 2012

7:45–8:00 AM	**Overview of the Third Day Program—Yousef Bozorgnia and Fayaz Rahimzadeh**
8:00–9:00 AM	**Research Center and Current State of Construction—M.A. Ghannad**, Session Chair
	• **Sinaeian, F.,** Building and Housing Research Center *On Recent Achievements and Activities of Building and Housing Research Center of Iran* *On the Construction of SADR Bridge in Tehran*
9:00–10:15 AM	**Hashash, Y., University of Illinois, Urbana-Champaign** *Short Course (Session 1): Advances in Equivalent and Linear and Nonlinear Site Response Analysis*
10:15–10:45 AM	**Break**
10:45–12:00 PM	**Hashash, Y., University of Illinois, Urbana-Champaign** *Short Course (Session 2): Advances in Equivalent and Linear and Nonlinear Site Response Analysis*
12:00–1:00 PM	**Lunch**

1:00–2:15 PM	**Hashash, Y., University of Illinois, Urbana-Champaign** *Short Course (Session 3): Advances in Equivalent and Linear and Nonlinear Site Response Analysis*
2:15–3:15 PM	**Future of Seismic Cooperation Discussion: ALL**
3:15–3:30 PM	**Closing Remarks: Fayaz Rahimzadeh and Yousef Bozorgnia**
3:30 PM	**Adjourn**

CONTENTS

SEISMIC PERFORMANCE OF STRUCTURAL SYSTEMS (I)

SEISMIC RISK AND RESILIENT COMMUNITY

SEISMIC PERFORMANCE OF STRUCTURAL SYSTEMS (II)

Seismic Performance of Structural Systems (III)

Seismic Performance of Structural Systems (IV)

Research Centers and Current State of Construction

Short Course

AN INDEX MODEL FOR EVALUATING URBAN EARTHQUAKE RISK

Hooman Motamed[1] and Mohsen Ghafory-Ashtiany[2]

ABSTRACT

In the recent years, various earthquake damage estimation methodologies such as RADIUS, HAZUS-MH, and MaeVIZ developed to perform earthquake damage and loss assessment. The output of such risk models is supposed to be used by disaster risk decision-makers for risk reduction planning purposes. The usual missing link in this regard, is a decision support medium that interprets the technical risk analysis outputs to the non-technical stakeholders. To overcome this problem, user-friendly tools can be employed to translate the disaster risk analysis results to an understandable language to the decision-maker in different areas of risk reduction planning. This paper, comprised of one qualitative and two quantitative models, attempts to address three different examples of such decision support mediums. The first model, UERI, is structured to incorporate several urban risk components (hazard, physical exposure, disaster management facilities and human exposure) based on the 69 earthquake risk indicators. The second proposed model quantifies the monetary value of earthquake losses, and finds an optimal budget allocation mitigation the seismic risk. The model consists of five main modules: (1) building damage module; (2) mitigated damage module; (3) cost estimation module; (4) optimization module; and (5) user interface module. The third model presented here uses the mixed integer quadratic programming (MIQP) to find an optimal spatial land-use allocation pattern for a defined urban environment.

All three models are capable of assisting decision-makers in using the output results of existing damage and loss estimation methodologies and also facilitate the process of risk reduction planning by providing proposal solutions to stakeholders. The performance of proposed models is demonstrated by applying them to a seismically vulnerable urban district in Tehran, Iran.

Keywords: *budget allocation, earthquake risk index, land-use allocation, optimization analyss, seismic risk reduction*

INTRODUCTION

The city of Tehran is the political, economical, and social capital of Iran. It is located on a seismically active zone at the foot of the Alborz Mountains and is surrounded by three main active faults that have caused serious damages to the city in cycles of approximately 180 years. The earthquake of 1830 was been the last event that devastated Tehran; however, local seismologists are expecting the possibility of another large quake in the near future [Abbasi and Shabanian 1999; Berberan and Yeats 2001; Hessami et al. 2003]. Hitherto, previous researchers have estimated potential seismic losses in Tehran and have shown that the occurrence of an

1 Iranian Earthquake Engineering Association and SPRMI.
[2] President of Iranian Earthquake Engineering Association and Prof. of IIEES.

expected large earthquake can bring about intensive human and economic consequences [Ghafory-Ashtiany et al. 1992; Ghafory-Ashtiany 2001; Ghafory-Ashtiany and Jafari 2003; JICA 2000].

Having an estimated static population of more than 8 million, Tehran has experienced the highest rate of urbanization compared to any other city in the country. In the absence of an appropriate urban planning and a sound construction practice, the city is considerably vulnerable to natural hazards, namely earthquakes [Amini-Hosseini and Jafari 2006]. High population density, galloped expansion of the city, inappropriate structural design and poor construction standards, and insufficient urban planning are the main contributors of Tehran's vulnerability to seismic hazard.

So far, several seismic hazard analyses and risk assessment studies have been carried out for the city of Tehran [JICA 2000 2004, 2010; Jafari et al. 2005]. In addition, a limited number of funded projects have proposed mitigation policies and improving measures aiming to reduce the seismic damage cost [JICA 2004; Amini-Hosseini and Jafari 2007]. Arguably, an important challenge that still exists is the lack of methodological processes and practices that incorporate results of risk analyses and disaster loss estimations into the decision-making process of institutions that are responsible for land use and urban development planning, construction and building licensing, environmental management, and social welfare [Amini-Hosseini and Jafari 2007; Amini-Hosseini et al. 2009]. This requires a high-level understanding of the technical elements of earthquake risk and analysis, and, at the same time, the requirements determined by high-level disaster risk managers. Therefore, tools that support non-technical decision-makers in using the outputs of disaster risk analyses for large scale planning purposes can create a better stream of information and ultimately help increase the chance of more successful adoption of mitigations strategies.

Based on the information collected in a survey the first part of this paper adopts a qualitative approach to address the key components of earthquake risk in Tehran. The second and third parts of the study present quantitative models originally developed to be deployed as decision support tools in disaster risk reduction process. The performance of proposed models has been demonstrated by their implementation in a vulnerable urban area in Tehran.

URBAN EARTHQUAKE RISK INDEX (UERI)

Background

Over the last several decades qualitative analysis of earthquake risk has been an interesting topic to the disaster risk researchers. This is mainly because the fact that some aspects of seismic risk, which are inherently subjective and hence an not be easily investigated through numerical measurements, have been to some extent neglected and the major of disaster risk-related studies have been devoted to the physical seismic risk assessment [Carreno et al. 2007]. However, in the 1990s saw the emergence of several researches that targeted disaster risk management and natural hazard around the globe in terms of seismic hazard. The 1997 pioneer study by Davidson and Shah presented a composite index (EDRI) for measuring earthquake disaster risk. They first defined the list of key factors contributing to urban earthquake risk as hazard, exposure, vulnerability, external context, and emergency response. Then, based on the constraints of quantitativeness, measurability, and data availability, they selected a set of indicators to represent those factors. The final composite risk index was calculated by mathematically combining all the indicators [Davidson and Shah 1997]. A weighted linear summation technique used in this study, assuming that indictors are independent and there is no interaction mechanism between them. A number of sample earthquake prone cities were selected to implement the model and their holistic seismic risk indices were compared.

In 2001 the European commission conducted a comprehensive research project called RISK-EU to assess the different aspects of earthquake risk in seven earthquake-prone towns based on defined scenarios. Apart from physical dimensions of earthquake risk, this study covered socio-economic and emergency response aspects of seismic risk in the pilot cities. An index based technique also employed to estimate the physical damage of the earthquake [Mouroux et al. 2004]. In 2007 Carreno et al. introduced an urban seismic risk model that incorporated physical damage, the number and type of casualties or economic losses, and also the conditions relating to social fragility and lack of resilience, which facilitated determining the indirect effects of earthquakes in urban settlements [Carreno et al. 2007]. They redefined the seismic risk as the summation of physical core and non-physical component, which amplifies the effects of the former. In this study, similar to Davidson and Shah's research (1997), a weighted summation technique was used to combine different indicators. They implemented the model on Barcelona and Bogota and compared the urban seismic risk index associated to these cities with a resolution of city's districts.

In recent years, researchers tried to capture other components of disaster rather than just physical risk, in part, Cardona and Carreno [2011] carried out a study introducing four composite risk indicator of Disaster Deficit Index (DDI), Local Disaster Index (LDI), Prevalent Vulnerability Index (PVI) and Risk Management Index (RMI). These indicators were designed to cover the organisational, development capacity, and institutional actions taken to reduce overall vulnerability and losses from disasters. They applied the proposed model to 19 countries in Latin America in the Caribbean region. Recent research has addressed the performance of the critical facilities and urban utilities, and derived index-based model to quantify the performance and functionality of such infrastructures in aftermath of disasters [Cavalieri et al. 2010; Motamed et al. 2012b].

Identifying the Seismic Risk Components

In this section of the study, a survey comprising academic and governmental organisations were asked about the key factors contributing to earthquake risk and possible indicators. Hazard, physical vulnerability, human vulnerability, and disaster risk centers (critical facilities) were selected as the risk components, and a set of indicators were adopted to quantify these factors. Based on the first-stage results of the survey, a questionnaire was designed and distributed to a larger number of sample interviewees, and their opinion about the relative importance of indicators were collected using pairwise AHP methodology. Figure 1 shows the contribution weights of earthquake risk components and risk indicators, respectively. The two models proposed in the following sections of this study are constructed based on the results obtained from this survey.

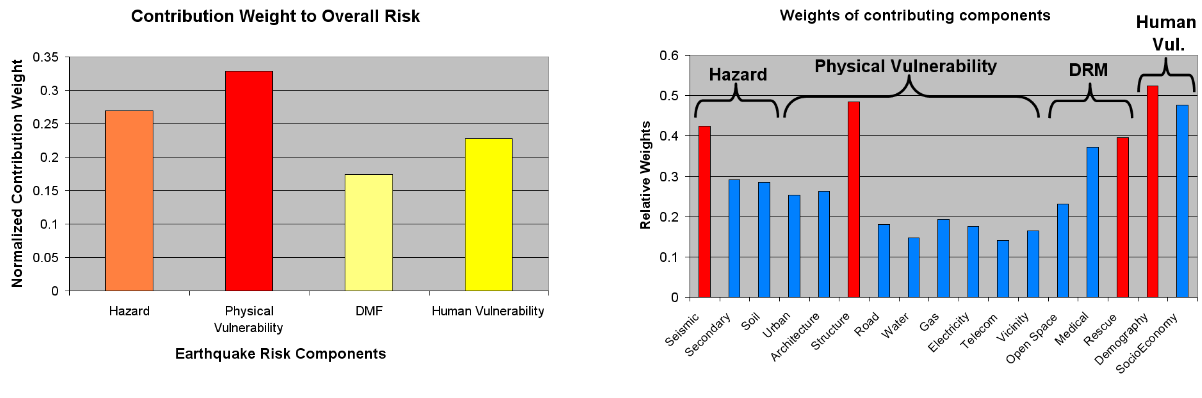

(a) (b)

Figure 1 (a) The contribution weight of various urban risk components; and (b) The contribution weight of urban risk indicators.

OPTIMIZED BUDGET ALLOCATION MODEL FOR EARTHQUAKE MITIGATION IN URBAN SETTLEMENTS

Literature Review

Recent works in mitigation budget allocation are classified into four main approaches: deterministic Net Percent Value (NPV) analysis, probabilistic NPV, multi-attribute utility models, and optimization models. Deterministic NPV (cost-benefit) analysis, which is the simplest method, consists of: (1) estimating the cost of implementing each mitigation options; (2) estimating the mitigation benefit gained; and (3) comparing options according to the decision criteria: benefit-cost ratio, benefit minus cost, or net present value [Dodo et al. 2005].

Stochastic NPV analysis is similar to the previous method except it employs a probabilistic approach instead of a deterministic one. The procedure includes: (1) estimating the cost of implementing each mitigation alternative; (2) estimating probability density function of benefits for each mitigation alternative (where the uncertainty is due to uncertainty in earthquake occurrence); and (3) comparing alternatives according to one or more decision criteria, such as expected value and variance of NVP.

In multi-attribute utility models, different factors are taken into account. For instance, Nuti and Vanzi [1998] compared structural upgrading strategies for hospitals based on various performance indices for the response of associated system of hospitals, e.g., including average distance traveled for a casualty, and a decrease in number of damaged beds. In the optimization method, contrary to three fore-mentioned methods, there is no need to have predefined mitigation strategies to run the analysis. The optimization method can be used to select a set of mitigation strategies from an existing menu of mitigation alternatives by maximizing the expected NVP given a constraint (such as budget limitations). For example, Shah et al. [1992] performed an optimization analysis with a budget constraint to maximize the NVP of an investment to improve 15 buildings at the Stanford University campus against earthquakes, where four different structural mitigation alternatives were considered. Benefits were estimated assuming a deterministic earthquake scenario. Shah et al. also performed a dynamic investment optimization that had three two-year stages. Dodo et al. [2005] proposed a linear program that selects buildings for mitigation based on mitigation costs and the resulting reductions in reconstruction costs. Vaziri et al. [2009] modified Dodo's model and added new features, which include: (1) allowing reconstruction to be delayed (at a penalty) if the funds are not immediately available; (2) allowing changes in the structural types during both mitigation and reconstruction period; and (3) including an objective to minimize the chance of an extremely large death toll. In 2012, Motamed et al. [2012a] proposed and optimization model that took into account the effect of critical facilities and secondary human loss to the analysis.

Model Design

A model was developed to optimize the allocation of a limited mitigation budget to a number of mitigation alternatives, and assists the user in prioritizing urban improvement options by interactively displaying the costs and benefits of each mitigation alternative. The model and all of its components, which are selected based on the first stage of the present study, have been developed in MATLAB. The model design integrates HAZUS-MH [FEMA 2003] earthquake loss estimation methodology for estimating building damage, human casualties, displaced households, debris volume, and direct economic losses. A user interface allows stakeholders to interact with the software and define input values for a number of mitigation strategies. These values are used in the optimization model to determine which of the selected mitigation measures are most effective for the given budget limit.

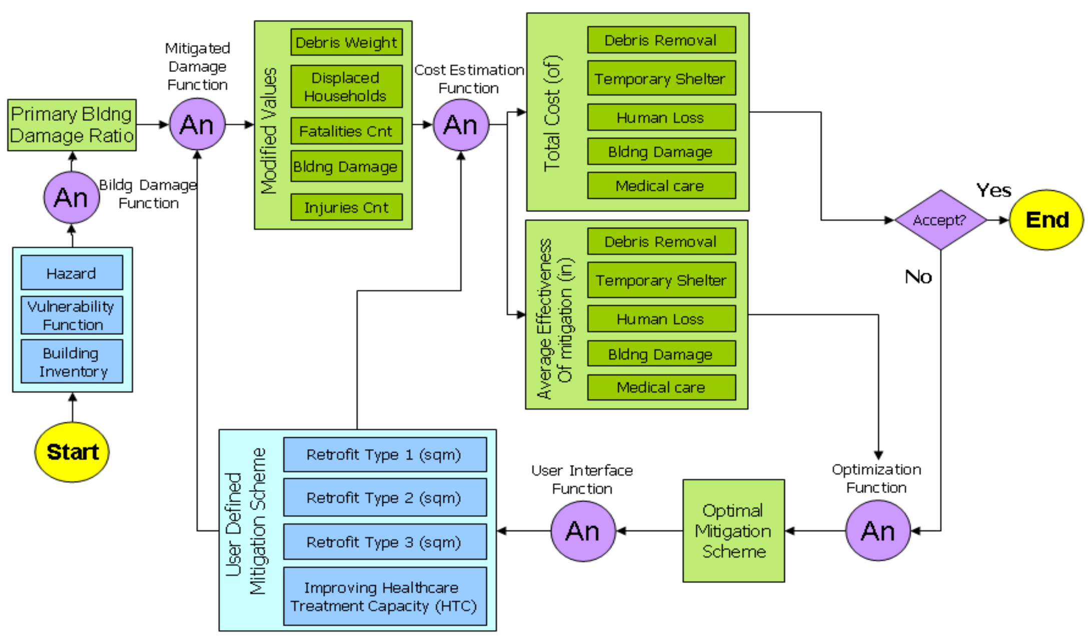

Figure 2 General flow chart of model.

The model consists of five main modules: (1) building damage function; (2) mitigated damage function; (3) cost estimation function; (4) optimization function; and (5) user interface function. Figure 2 illustrates the different modules of the model and the relations between them. In addition to the interactive procedure that takes stakeholder input into account (via the user interface function), the model is designed so that the computations are iterative and converge on an optimal solution. The discussion to follow will provide a description of the functions and mathematical formulations used in each of the five modules.

Implementation of Model

The city of Tehran is composed of 22 administrative districts. District 17 of Tehran has been used as a pilot area in previous earthquake vulnerability studies due to its adjacency to the active Ray fault, population of vulnerable buildings, narrow road networks, and inadequate emergency facilities (e.g., hospitals and fire departments). In addition, the hazard employed in this investigation included ground shaking for three different scenario events representing the South Tehran, North Tehran, and Mosha Fault. Besides these three events, a floating earthquake scenario, which varied in accordance with soil amplification factor of subsurface soil, was considered.

Table (1) tabulates the damage cost and fatality counts in the pilot area for four different earthquake scenarios before implementation of any mitigation strategy. Two earthquake scenarios of South Ray Fault and Floating caused the highest rate of damages and fatalities.

Figure 3 shows an example output of the proposed model that is the spatial distribution of mitigation plan with a budget of 50 million US$ for 4 different earthquake scenarios. In those earthquakes with high rate of fatality, e.g., the South Ray and Floating scenarios, a reduction in human casualty is the first priority. Threfore, for a rather low mitigation budget of 50 Million US$, the optimization model allocates the money to a structural retrofitting strategy that has the highest effect in decreasing casualties, which is masonry building type. On the other hand, in those earthquakes with low degree of fatality, e.g., Mosha and NTF scenarios, reducing building damage is the first priority. Therefore, the optimization model looks for the most economical way of retrofitting buildings, which is the steel building retrofit strategy.

Table 1 Damage costs and fatality count when subjected to scenario earthquakes.

Earthquake Scenario	South Ray Fault	Floating	North Tehran Fault	Mosha Fault
Max. PGA (Gal)	531	362	246	157
Damage Cost (US$)	1042644	586051	165143	69862
Fatality Count	1263	514	25	1

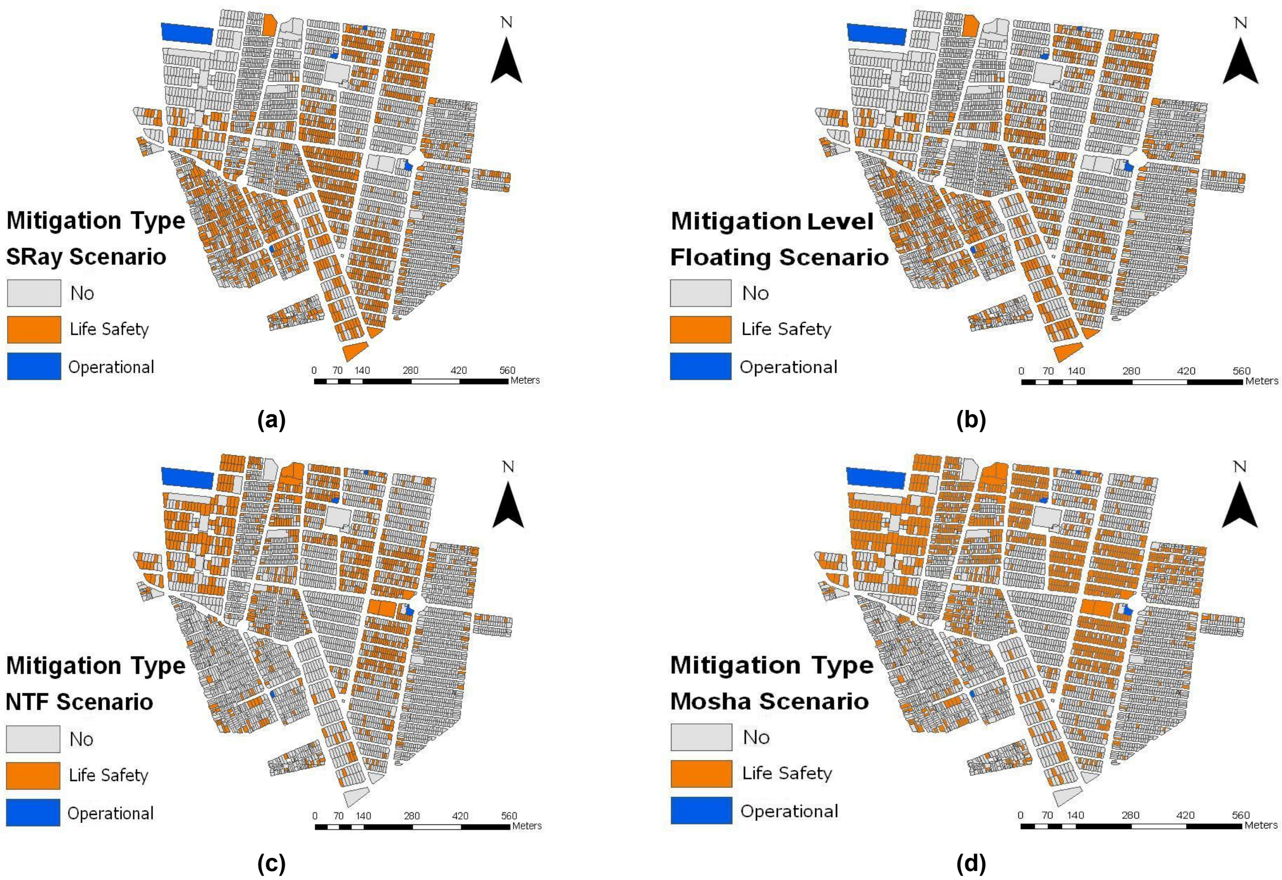

Figure 3 **Distribution of mitigation alternative in the pilot area for (a) South Ray Fault scenario, (b) Floating scenario, (c) North Tehran Fault scenario, and (d) Mosha Fault scenario.**

AN EARTHQUAKE RISK-SENSITIVE MODEL FOR SPATIAL ALLOWCATION LAND-USE ALLOCATIONS

Literature Review

Dokmeci et al. [1993] presented a generalized land-use model to determine the most efficient utilization of land based on two interactive objectives: (1) maximization of return; and (2) minimization of the sum of weighted distances among the different land-use units. Aerts et al. [2003] addressed the use of spatial optimization techniques for solving the optimal allocation of multiple sites of different land uses to an area. They solved an MLUA problem using four different integer programs (IP), of which three were linear integer programs. The IPS were formulated for a raster-based GIS environment and were designed to minimize development costs and to maximize compactness of the allocated land use. They used a weighting factor for preferring either minimizing costs or maximizing compactness. Banba et al. [2004] focused on land use management planning processes and divided these processes into three phases: (1) planning background analysis; (2) planning strategy development; and (3) implementation strategies development. They identified factors of each phase and applicable land use control and potential management methods for Marikina City, Philippines. Ligmann-Zielinska et al. [2008]

presented a new multiobjective spatial optimization model that minimized the conflicting objectives of open space development, infill and redevelopment, land-use neighborhood compatibility, and cost distance to already urbanized areas. Tudes and Ygiter [2010] determined six land use categories for Adana, one of the most earthquake prone provinces of Turkey, by the use of an analytical hierarchical process (AHP) and GSI. According to the authors, little work has been done to employ optimization techniques for disaster risk reduction purposes.

Model Design

The proposed model is capable of choosing the optimal spatial pattern of land-uses among several possible alternatives through solving a mixed integer quadratic programming (MIQP) problem that considers boundary conditions. Since the problem involves spatial allocation of land uses, a raster model of the study area was used. This raster model allowed the mathematical core to utilize the topological data at different pixels. Using a raster definition for modeling urban areas does, however, enter some uncertainties in the problem [Motamed et al. 2012b].

The aim of this model is to optimize a multi-objective problem by using a weighted summation method. The objectives of the optimization were to (1) minimize the susceptibility to earthquake hazard, (2) maximize the permeability of critical facilities, (3) minimize the average distance to critical facilities, (4) maximize the compatibility of adjacent land uses, and (5) minimize the redevelopment. Figure 4 illustrates the sequential steps involved in using the proposed land-use allocation model.

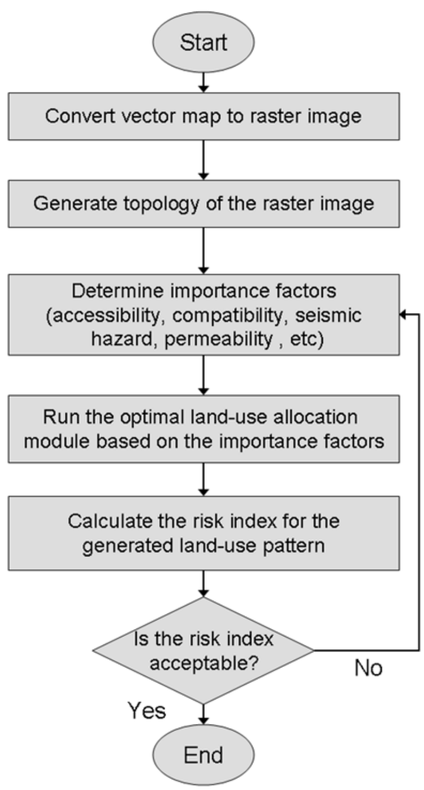

Figure 4 The sequential steps of using the land-use allocation model.

Implementation of Model in Pilot Area

The proposed land-use allocation model was applied to a neighborhood in 17th district of Tehran. The earthquake hazard in the northern region of the area is the lowest and gradually increases to its highest value (the most severe) in the southern region. A risk index was used to evaluate the performance of the model for different importance factors. Figure 5 shows the trade-off between importance factors of earthquake hazard and accessibility. As the accessibility importance factor exceeds the earthquake hazard factor, the land-use pattern takes a more uniform shape to provide the maximum accessibility. On the contrary, when hazard importance factor is dominant, all the critical facilities are piled in the upper region where the earthquake hazard is the minimum.

The results obtained from the proposed model were compared to a real land-use allocation done by an experienced urban planner. The automated results have very close risk index values to the real allocation pattern.

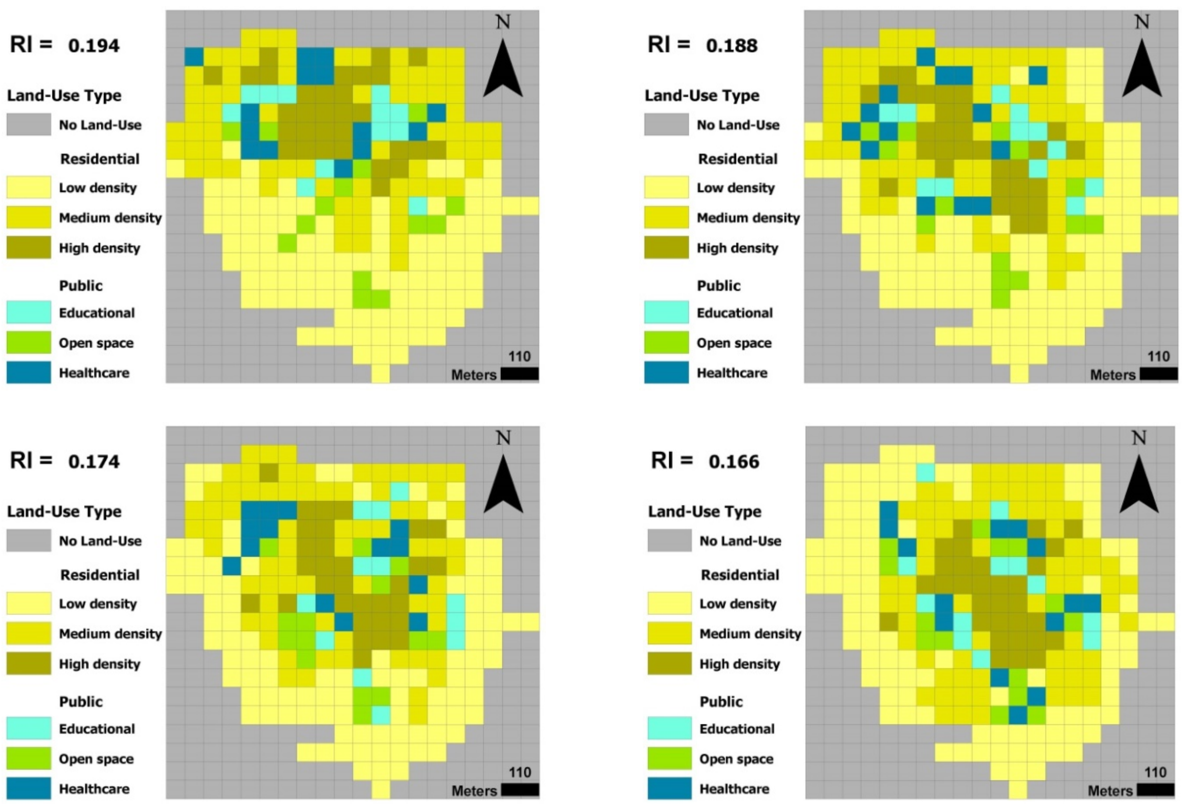

Figure 5 Comparisonbetween importance factors of earthquake hazard and accessibility.

CONCLUSIONS

This paper presented an index-based model to identify the most influential seismic risk factors and indicators for Tehran, Iran. Engineering judgement and expert opinion were collected to determine the importance of each risk component. The second part of the study presented a budget allocation model for earthquake risk reduction planning. This models benefitted from an optimization module that assists disaster risk decision-makers in finding the most cost-effective improvement schedule. It covered a variety of possible development alternatives, i.e., different structural retrofitting, and replacement and improvement of healthcare capacity. The third part of the research approached earthquake risk management from a more general point of view: seismic hazard-sensitive land-use allocation. An optimization model was developed to facilitate the process of land-use planning in earthquake-prone urban areas. Examples of the outputs of three proposed models were demonstrated by applying them to reduce the risk in the seismically vulnerable 17^{th} in Tehran.

REFERENCES

Abbasi M.R., Shabanian E. (1999), *Fault Map of North Tehran*, International Institute of Earthquake Engineering and Seismology, Tehran, Iran.

Aerts J.C.J.H, Eisinger E., Heuvelink G.B.M., Stewart T.J. (2003). Using linear integer programming for multi-site land-use allocation, *Geographical Analysis*, 35(2): 148−169.

Amini-Hosseini K., Jafari M.K. (2006). Seismic risk assessment for Tehran, *J. Seismol. Earthq. Eng*., 9(1): 11−21.

Amini-Hosseini K., Jafari M.K. (2007). Development guidelines for disaster management in Tehran, *Proceedings, 5th International Conf. on Seismology and Earthquake Engineering*, Tehran, Iran.

Amini-Hosseini K., Hosseini M,. Jafari M.K., Hosseinioun S. (2009). Recognition of vulnerable urban fabrics in earthquake zones: A case study of Tehran Metropolitan Area, *J. Seismol. Earthq. Eng*., 10(4): 175−187.

Banba M., Maki N., Topping K., Hayashi H., Kondo T., Tamura K., Tatsuki S., Tanaka S., Fukasawa Y., Karatani Y. (2004). Analysis of land use management for earthquake disaster reduction in the Asia Pacific, *Proceedings, 13^{th} World Conference on Earthquake Engineering*, Vancouver B.C., Canada.

Berberian M., Yeats R.S. (2001). Contribution of archaeological data to studies of earthquake history in the Iranian Plateau, J. Structural Geol., 23: 563−584.

Cardona O.D., Carreno M.L. (2011). Updating the indicators of disaster risk and risk management for the Americas, *J. Integrated Risk Management*, 1(1): 1–21.

Carreno M.L., Cardona O.D., Barbat A.H. (2007) A disaster risk management performance index, *Natural Hazards*, 41: 1–20.

Cavalieri F., Franchin P., Gehl P., Khazai B. (2012). Quantitative assessment of socio-economic performance measures accounting for seismic damage to buildings and functional interaction with infrastructural systems, *Proceedings, 15^{th} World Conference on Earthquake Engineering*, Lisbon, Portugal.

Davidson R.A., Shah H.C. (1997). An urban earthquake disaster risk index, *Report No. 121*, The John H Blume Earthquake Engineering Center, Stanford University, Stanford, CA.

Dodo A., Xu N., Davidson R., Nozick L. (2005). Optimizing regional earthquake mitigation investment strategies, *Earthq. Spectra*, 21(2): 305–327.

Dokmeci V.F., Cagdas G., Tokcan S. (1993). Multiobjective land-use planning model, *J. Urban Plann. Dev.,* vol. 119(1): 15−22.

Ghafory-Ashtiany M., Jafari M.K., Shadi Talab J., Eshghi S., Qurashi M. (1992). Tehran vulnerability analysis, *Proceedings, 10th World Conference on Earthquake Engineering*, Balkema, Rotterdam.

Ghafory-Ashtiany M. (2001). *Tehran Earthquake Risk Reduction Plan*, I.R. Housing Foundation, Tehran, Iran.

Ghafory-Ashtiany M., Jafari M.K. (2003). Tehran geotechnical microzonation, *Proceedings, SEE4*, Tehran, Iran.

FEMA (2003). *Multi-hazard Loss Estimation Methodology, Earthquake Model, HAZUS-MH MR1*, Federal Emergency Management Agency, Washington D.C.

Hessami K., Jamali F., Tabassi H. (2003). *Active Fault Maps of Iran*, Seismotectonic Dept., Seismology Research Center, IIEES, Iran.

Jafari M.K., Amini-Hosseini K., Hosseini M., Kamalian M., Askari F., Razmkhah A., Davoodi M., Mahdavifar M.R, Sohrabi Bidar A., Keshavarz Bakhshayesh M. (2005) *Seismic Hazard Study, Final Report for Tehran Comprehensive Plan*, International Institute of Earthquake Engineering and Seismology, Iran.

JICA (2000). The study on seismic microzoning of the Greater Tehran Area in the Islamic Republic of Iran, *Final Report to the Government of the Islamic Republic of Iran*, Japan International Cooperation Agency, Tokyo, Japan.

JICA, TDMMC (2004). *The Comprehensive Master Plan on Urban Seismic Disaster Management ffor The Greater Tehran Area in the Islamic Republic of Iran*, Japan International Cooperation Agency and Tehran Disaster Mitigation and Management Center, Tokyo, Japan.

JICA, TDMMO (2010). *Establishment of Emergency Response Plan for the 1st 72 Hours after an Earthquake in Tehran*, Japan International Cooperation Agency and Tehran Disaster Mitigation and Management Organization, Tehran, Iran.

Ligmann-Zielinska A., Church R, Jankowski P. (2008). Spatial optimization as a generative technique for sustainable multiobjective landuse allocation, *Int. J. Geographical Information Sci*., 22(6): 601‒622.

Motamed H., Khazai B., Ghafory-Ashtiany M., Amini-Hosseini K. (2012a). An automated model for optimizing budget allocation in earthquake mitigation scenarios, *Nat. Hazards*, 70(1): 51‒68.

Motamed H., Ghafory-Ashtiany M., Amini-Hosseini K. (2012b). An earthquake risk–sensitive model for spatial land-use allocation, *Proceedings, 15th World Conference on Earthquake Engineering*, Lisbon, Portugal.

Mouroux P., Bertrand E., Bour M., LeBrun B., Depinois P., Masure P. (2004). The European Risk Project: An advanced approach to earthquake risk scenarios with applications to different European towns, *Proceedings, 13th World Conference on Earthquake Engineering,* Paper No. 3329, Vancouver, B.C., Canada.

Nutti C., Vanzi I. (1998). Assessment of post-earthquake availability of hospital system and upgrading strategies, *Earthq. Eng. Struct. Dyn*., 27: 1403‒1423.

Shah H.C., Bendimerad M.F., Stojanovski P. (1992). Resource allocation in seismic risk mitigation, *Proceedings, 10th World Conference on Earthquake Engineering*, Balkema, Rotterdam, pp. 6007‒6011.

Simpson D.M., Katirai M. (2006). Indicator issues and proposed framework for a Disaster Preparedness Index (DPI), *Working Paper 06-03*, Center for Hazard Research and Policy Development, University of Louieville, Kentucky.

Tudes S., Yigter N.D. (2010). Preparation of land use planning model using GIS based on AHP: Case study Adana-Turkey, *Bull. Eng. Geol. Environ*., 69: 235‒245.

Vaziri P., Davidson R., Nozick L.K., Hosseini M. (2009). Resource allocation for regional earthquake risk mitigation: A case study of Tehran, Iran, *Nat. Hazards*, 53: 527‒546.

DIRECTIVITY EFFECTS ON NEAR-FAULT AMPLIFICATION FACTOR

Mohsen Tehranizadeah[1] and Homa Shanehsazzadeh[2]

ABSTRACT

Presence of pulse in fault-normal component of near-fault velocity time history is one of the important and practical specifications of near-fault records. Velocity pulses are often caused by directivity effects. Previous researches have shown that this kind of pulse has most likely been the main cause of damage to structures. These pulses, which appear at the beginning of the velocity time history records, apply a lot of energy in a short period of time to structures. Since these pulses usually cause amplification in acceleration response spectra, we used this idea in order to consider near-fault amplification factors resulting from directivity effects. In this paper, the mentioned pulse is identified and extracted by wavelet analysis. This method includes some criteria to identify velocity pulse. These criteria are for the purpose of selecting records that contains pulses caused by forward directivity effects and discriminate them from ordinary pulses that do not impose a lot of energy to the structures and are not related to forward directivity effects. Using records that have been identified as having pulses and records from which pulses have been extracted, corresponding response acceleration spectra were calculated and the spectra amplifications of pulse-like records were calculated related to which their pulses were extracted as a function of period. This amplification is provided as a near-fault design spectrum amplification. Records were selected from the PEER database and BHRC, the Iranian strong-motion database; the results were compared with modifications by Somerville et al. [1997]. The results show that they are close to each other, especially in way of increasing as a function of period. Somerville at al. [1997] has provided modifications for sites that are located at short distance to faults considering forward directivity and polarization effects. In this model, the basic criterion for classifying records was the site geometry related to rupture directivity effect.

Keywords: *directivity effects, near-fault effects, pulse amplification, pulse-like records, velocity pulse, wavelet analysis*

INTRODUCTION

According to research that has been done on wavelet procedure for identifying pulse-like ground motion and removing the velocity pulse from them [Baker 2007], pulse-like records were usually located at sites with forward directivity effect [Baker 2007]. The presence of a large pulse in the fault-normal component is one of the specifications of near fault motions, which is due to rupture directivity effect (forward directivity and polarization).

The quantitative procedure to extract the pulse from pulse-like motions has been developed. Furthermore, it has been mentioned that when the pulses were extracted from pulse-like records, the residual ground motions were well described by existing ground motion

[1] Department of Civil and Environment Engineering, Amirkabir University of Technology, Tehran, Iran; email: dtehz@yahoo.com.
[2] Department of Civil and Environment Engineering, Amirkabir University of Technology, Tehran, Iran; email: homa.shanehsaz@gmail.com.

prediction models, which do not include near fault effects. So according to the above, it is suggested that the pulse extraction method, which will be explained below, is able to identify a suitable amount of amplification to near-fault effect for near-fault sites in relation to far-field one. Basically, the pulse extraction method is based on the ratio of acceleration response spectrum of a pulse-like record to that of the pulse extracted one. In this way we were able to find amplification as a function of period.

In this paper we consider another important parameter to classify near-fault ground motions that are the closest distance to fault, in addition to Baker's quantitative procedure, which contains other important aspects like: PGV larger than 30 cm/sec and pulse indicator more than 0.85 [Baker 2008].

Finally, by taking into account some considerations, results were compared with Somerville et al. model [1997]. There were not observed any distinctions between results but there were differences for dip-slip fault, and it is reasonable to say that they are close to each other for strike-slip mechanism and distance equal to or less than 2 km.

NEAR-FAULT STRONG-MOTION RECORDS

In this research 91 fault-normal pulse-like records from NGA, and two fault-normal pulse-like records from Iran are used as a data set. The other two records, which are mentioned as well as 91 pulse-like records from NGA, belong to Tabas and Bam earthquakes. They are two important records from Iran owing to some bold specifications like having distance shorter than or equal to 2 km and being pulse-like in fault normal component regarding to Baker's quantitative wavelet procedure. They were recognized as pulse-like records by a written MATLAB program by Baker for this purpose [Baker N.D.].

At first, all records were classified according to distance; they were also classified into two kinds of mechanism of faulting: strike-slip and dip-slip. In these two types of mechanism we expect different result, as it was mentioned before by Somerville et al.'s model [1997] as well. So we found groups for two distances: less than or equal to 2 km and about 5 km. Other distances are ignored, because the number of records was less than 5 due to dividing them into strike-slip and dip-slip. Classified records with some of their characteristics are shown in Tables 1, 2, and 3.

Table 1 Strike-slip records for 2 km distance.

No.	Event	Year	Station	PGV (cm/sec)	M_w	T_p Wavelet	T_p S_v	Closest Distance (km)	Epicentral Distance (km)	Pulse Indicator	Mechanism
1	Morgan Hill	1984	Coyote Lake Dam (SW Abut)	62.3	6.2	1.0	0.7	0.5	24.6	0.99	Strike-slip
2	Kobe, Japan	1995	Takarazuka	72.6	6.9	1.4	1.2	0.3	38.6	0.87	Strike-slip
3	Kobe, Japan	1995	Takatori	169.6	6.9	1.6	1.3	1.5	13.1	0.96	Strike-slip
4	Superstition Hills-02	1987	Parachute Test Site	106.8	6.5	2.3	1.9	1.0	16.0	1.00	Strike-slip
5	Imperial Valley-06	1979	Agrarias	54.4	6.5	2.3	1.9	0.7	2.6	1.00	Strike-slip
6	Imperial Valley-06	1979	Aeropuerto Mexicali	44.3	6.5	2.4	1.6	0.3	2.5	0.99	Strike-slip
7	Imperial Valley-06	1979	EC Meloland Overpass FF	115.0	6.5	3.3	2.9	0.1	19.4	1.00	Strike-slip
8	Imperial Valley-06	1979	El Centro Array #6	111.9	6.5	3.8	3.5	1.4	27.5	1.00	Strike-slip
9	Imperial Valley-06	1979	El Centro Array #7	108.8	6.5	4.2	3.3	0.6	27.6	1.00	Strike-slip
10	Landers	1992	Lucerne	140.3	7.3	5.1	4.2	2.2	44.0	1.00	Strike-slip
11	Bam	2003	Bam	64	(Ms=6.7)	2	1.44	<2	2.0	1.00	Strike-slip

Table 2 Dip-slip records for 2 km distance.

No.	Event	Year	Station	PGV (cm/sec)	M_w	T_p Wavelet	T_p S_v	Closest distance (km)	Epicentral distance (km)	Pulse indicator	Mechanism
1	San Fernando	1971	Pacoima Dam (upper left abut)	116.5	6.6	1.6	1.1	1.8	11.9	0.97	Reverse
2	Chi-Chi, Taiwan	1999	TCU075	88.4	7.6	5.1	4.5	0.9	20.7	1.00	Reverse oblique
3	Chi-Chi, Taiwan	1999	TCU065	127.7	7.6	5.7	4.5	0.6	26.7	0.96	Reverse oblique
4	Chi-Chi, Taiwan	1999	TCU102	106.6	7.6	9.7	2.5	1.5	45.6	0.97	Reverse oblique
5	Chi-Chi, Taiwan	1999	TCU101	68.4	7.6	10.0	8.8	2.1	45.1	1.00	Reverse oblique
6	Chi-Chi, Taiwan	1999	TCU068	191.1	7.6	12.2	9.4	0.3	47.9	1.00	Reverse oblique
7	Tabas,Iran	1978	Tabas	118.8	7.4	6.2	5.0	2.0	-	1.00	Reverse

Table 3 Dip-slip records for 5 km distance.

No.	Event	Year	Station	PGV (cm/sec)	M_w	T_p Wavelet	T_p S_v	Closest distance (km)	Epicentral distance (km)	Pulse indicator	Mechanism
1	Northridge-01	1994	LA Dam	77.1	6.69	1.7	1.3	5.92	11.79	1.00	Reverse
2	Northridge-01	1994	Jensen Filter Plant Generator	67.4	6.69	3.5	2.7	5.43	13	1.00	Reverse
3	Northridge-01	1994	Newhall-W.Pico Canyon Rd.	87.8	6.69	2.4	2.0	5.48	21.55	1.00	Reverse
4	Northridge-01	1994	Sylmar - Converter Sta	130.3	6.69	3.5	2.7	5.35	13.11	0.92	Reverse
5	Northridge-01	1994	Sylmar - Converter Sta East	116.6	6.69	3.5	2.9	5.19	13.6	1.00	Reverse
6	Northridge-01	1994	Sylmar - Olive View Med FF	122.7	6.69	3.1	2.4	5.3	16.77	1.00	Reverse
7	Chi-Chi, Taiwan	1999	TCU082	56.1	7.62	9.2	6.9	5.18	36.2	0.95	Reverse Oblique
8	Chi-Chi, Taiwan	1999	TCU053	41.8	7.62	12.8		5.97		1.00	Reverse Oblique

PULSE EXTRACTION METHOD

After classifying records according to mechanism and distance, and finding the final sets of data, for each record in its group we obtained 5% damping acceleration response spectrum for ‘original’ and ‘residual’ records. The term of ‘original record’ indicates record that has velocity pulse (pulse-like records), and ‘residual record’ indicates the record which its velocity pulse has been extracted, so it does not have pulse any more in velocity time history. We also have a record of the pulse that had been removed, but it has not been used here. The pulse extraction process was performed, as described above. The amplification was calculated from the ratio of acceleration response spectrum of original to that of residual one. This amplification was obtained for each record and then for each group they were averaged. The average amplification is able to represent both forward directivity and polarization effects, in relation to far field records, because selected original records have velocity pulse (due to forward directivity effect), and the pulse was indicated in fault normal component (due to polarization effect). In most of text, both effects are together called forward directivity, but we prefer to deal with them separately.

For first category, strike-slip mechanism and distance less than or equal to 2 km, acceleration response spectra for original and residual selected records are shown in logarithmic scale in Figure 1; the period of pulse is also shown at the top of the figures. We can see that the maximum amplification will be at a period about period of pulse [Baker 2007].

The results in this step were compared with corresponding results that have been developed by Somerville et al. [1997]. They have provided modifications for sites that are located in short distance to faults considering forward directivity and polarization effects. In this model the set of records includes both pulse-like and non pulse-like records. In fact the basic criterion (for forward directivity effect) was the site geometry related to rupture directivity effect. Site geometric parameters are indicated in Figure 2.

The average amplification from each category was approximated by least-squares fitting method after transition period 0.5 sec. The reason of selecting 0.5 sec as a transition period in order to take into account amplification is clear in figures. The values of amplification increase significantly after about transition period to values more than 1, and before this period amplification values are about 1. This period is so close to which Somerville et al. have mentioned 0.6 sec. Results are indicated in Figures 3 and 4.

For a more sensible comparison, in Figures 5 and 6 an optional spectrum, which is New Zealand Standard Class A and B [Building Design Standards 2004] that does not include near fault effect, has been selected to amplify by developed near fault amplification factors by two mentioned research.

It is observed that the results of two research for strike slip faults and distances equal to or less than 2 km are so close to each other as it is indicated in Figure 5 the difference on the optional spectrum [Building Design Standards 2004] with hazard factor Z=0.4, is not distinguishable.

For dip-slip fault and distance about 5 km, values of pulse extraction method are more than Somerville et al. model. We can see in Figure 6 that the near fault spectrum which is amplified by obtained pulse extraction amplification is more conservative than that by Somerville et al. amplification, but the difference is not remarkable.

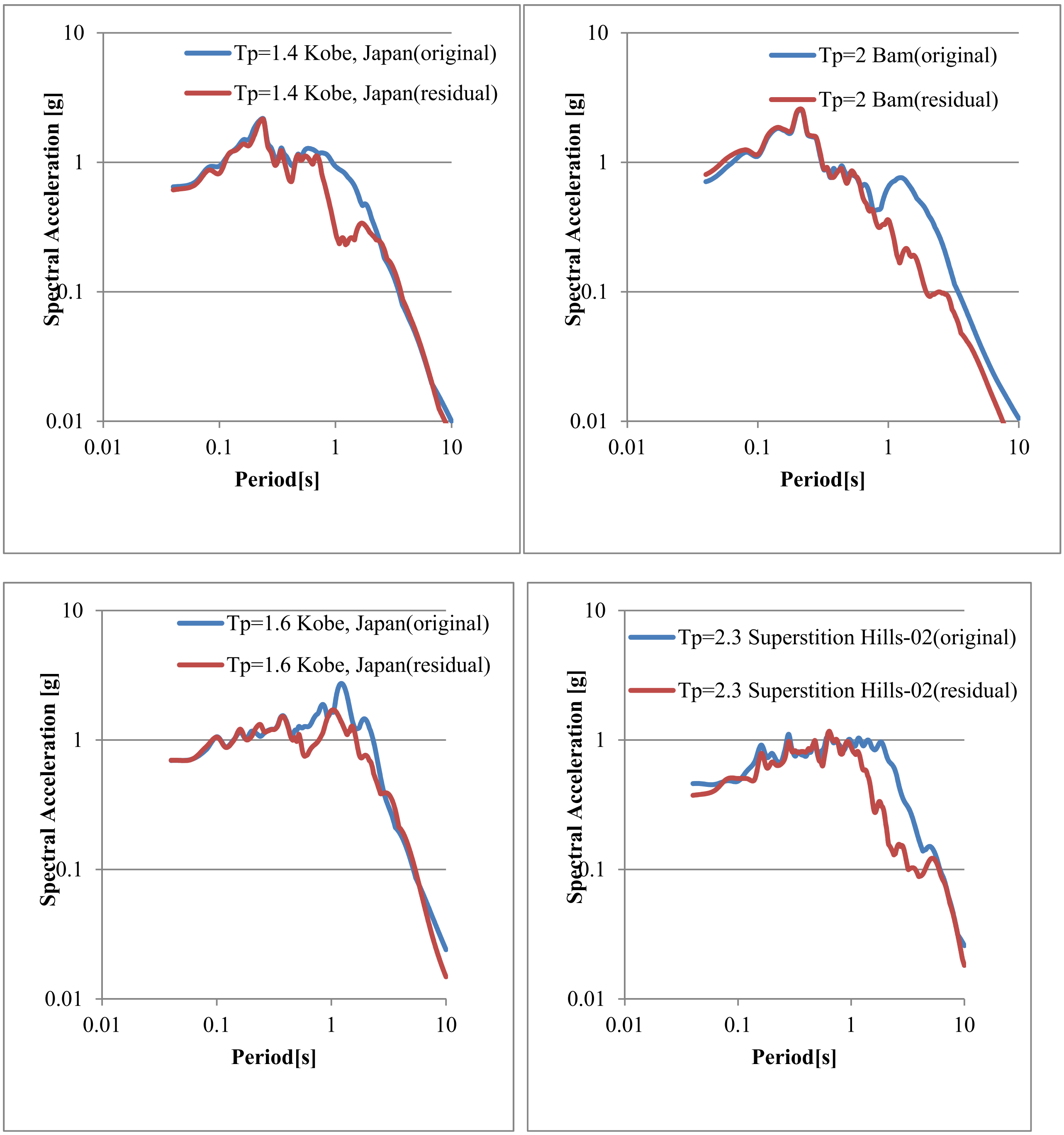

Figure 1 Original and residual spectra.

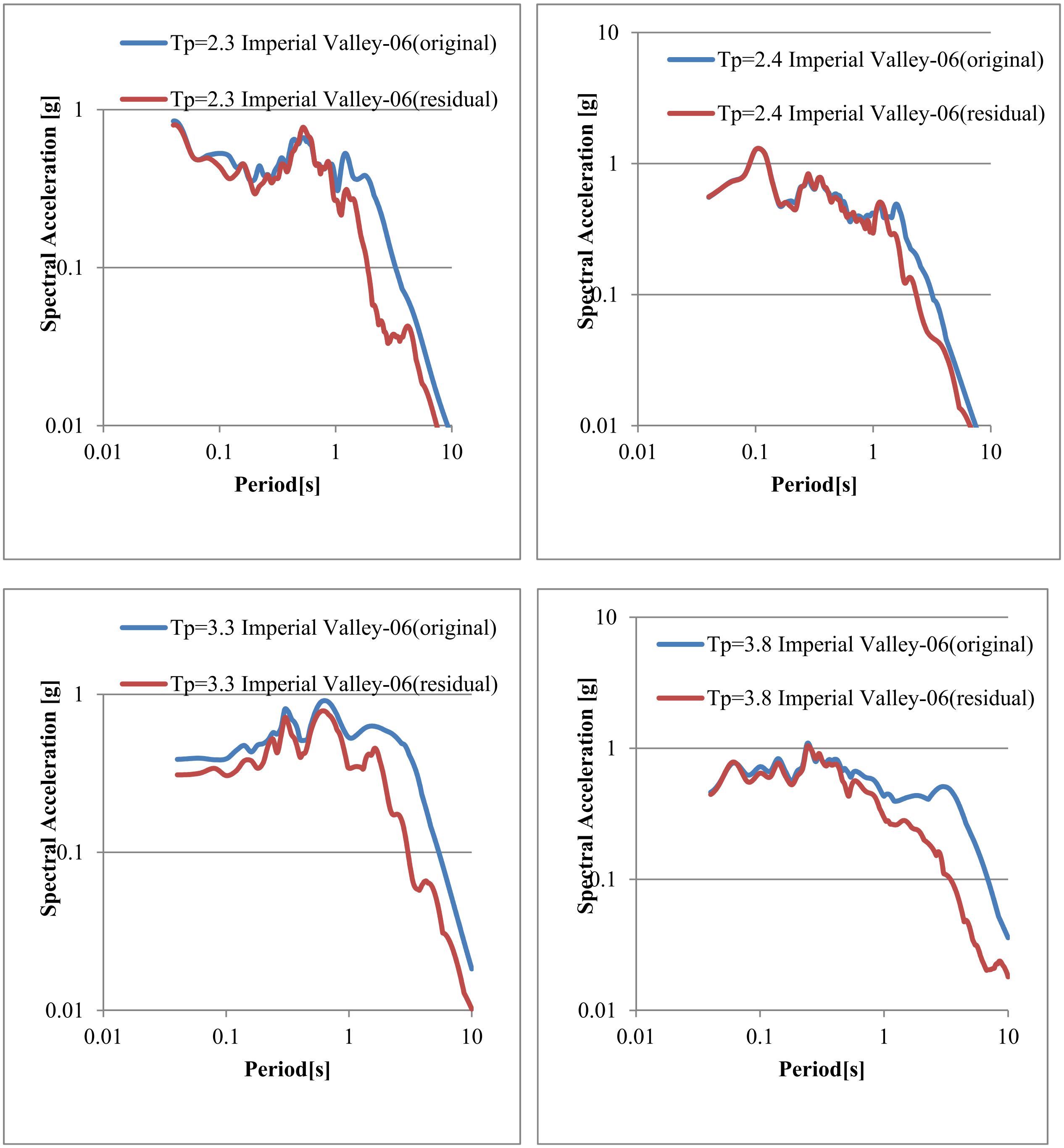

Figure 1 Continued.

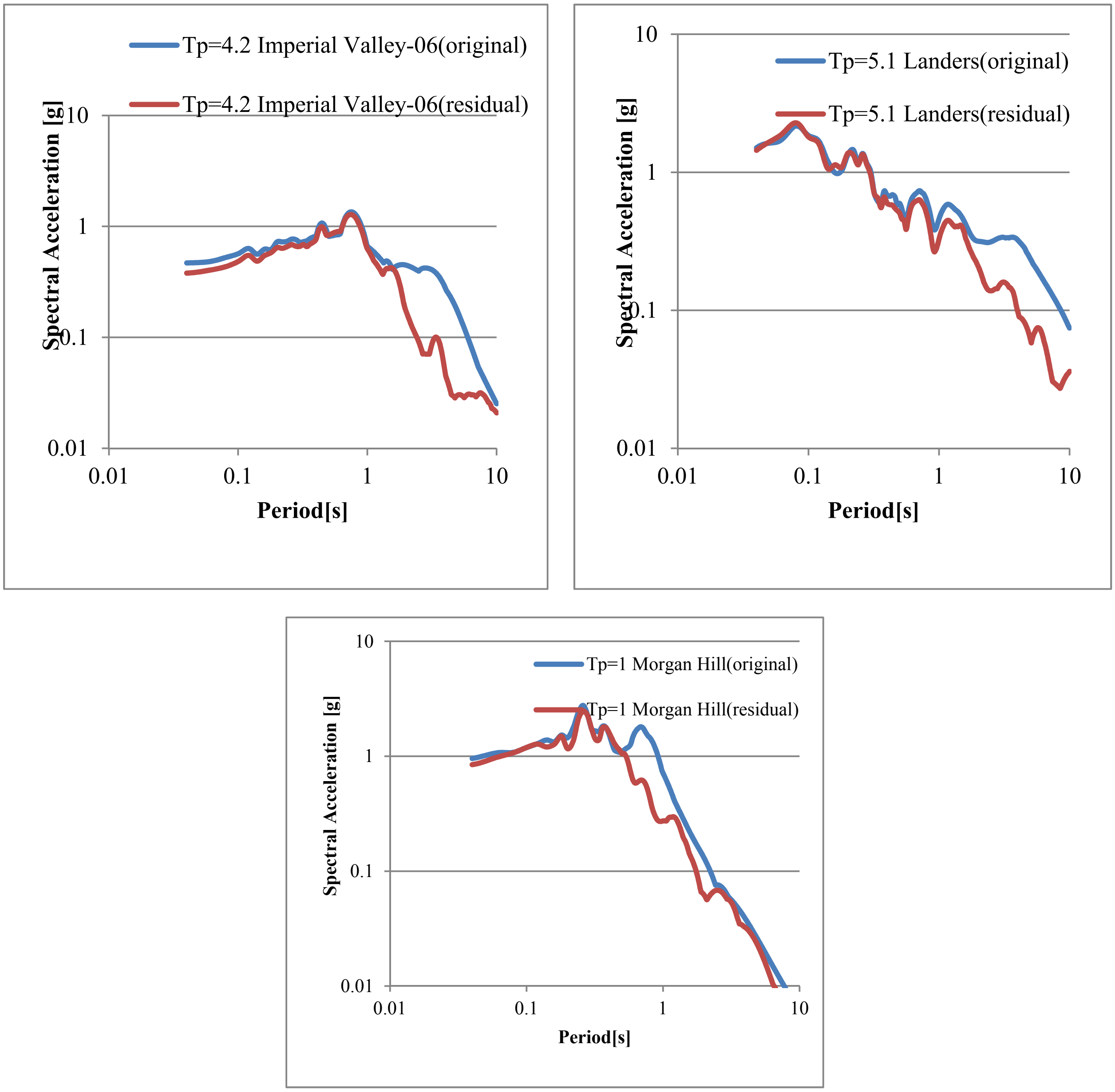

Figure 1 Continued.

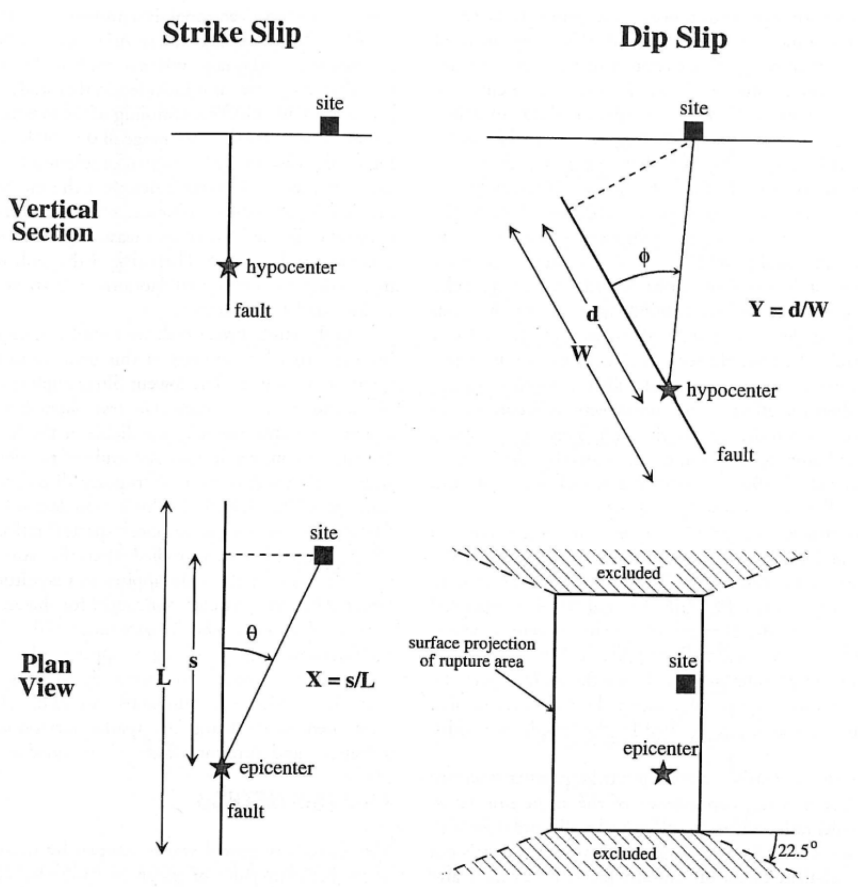

Figure 2 **Definition of rupture directivity parameters ϴ and X for strike-slip faults, and ϕ and Y for dip-slip faults in Somerville et al.'s model [1997].**

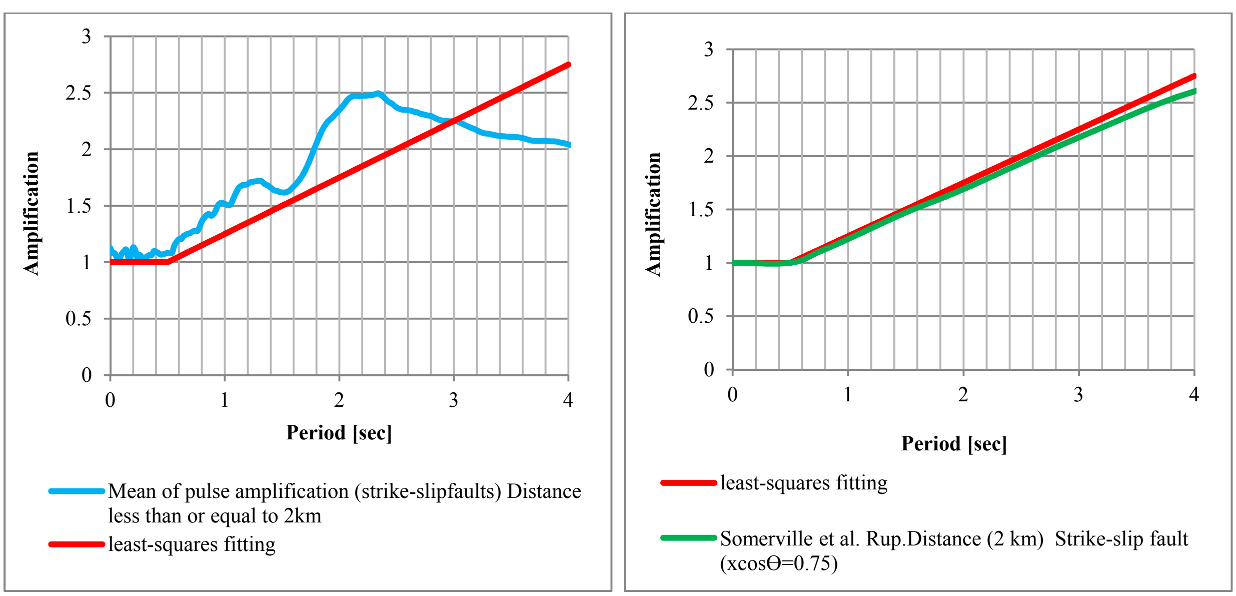

Figure 3 **Comparison of Somerville et al. model and pulse extraction.**

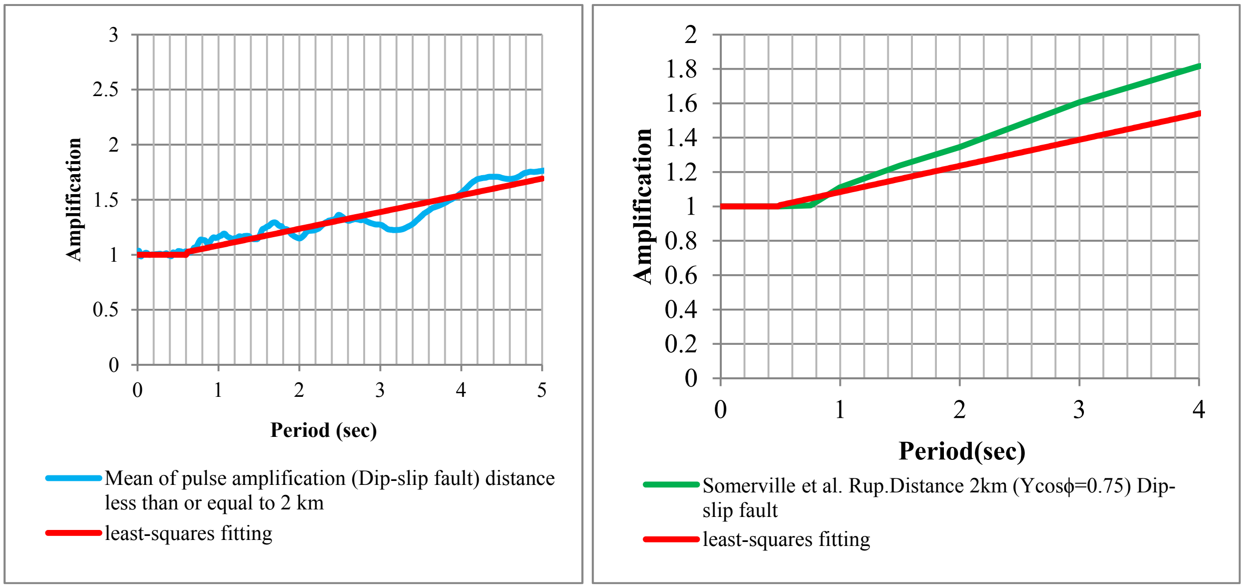

Figure 4 Comparison of Somerville et al. model and pulse extraction.

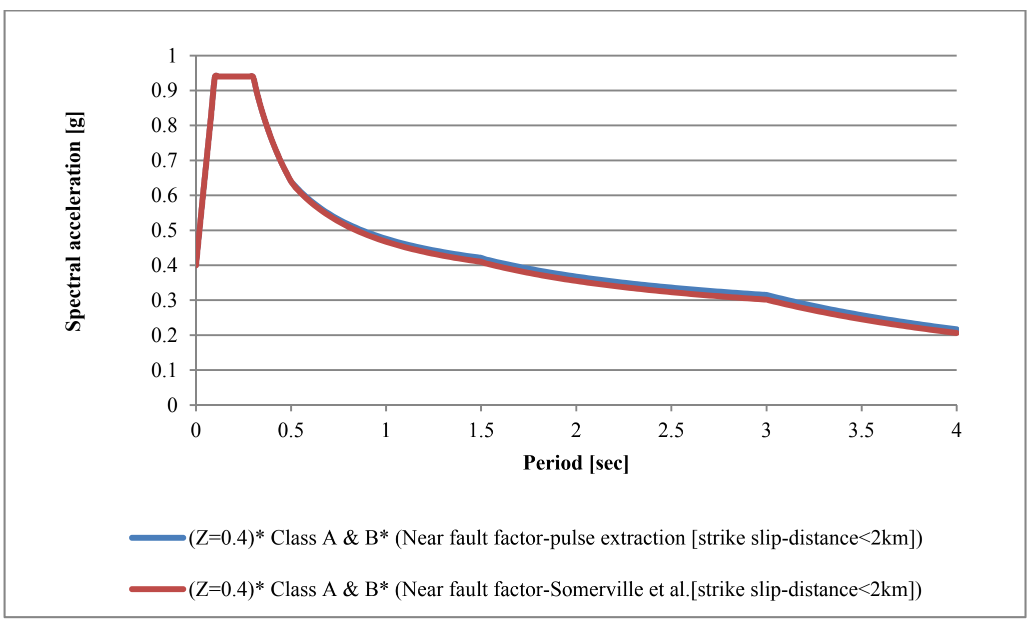

Figure 5 Comparison of Somerville et al.'s model [1997] and pulse extraction method to New Zealand Standard spectrum Building Design Standard [2004].

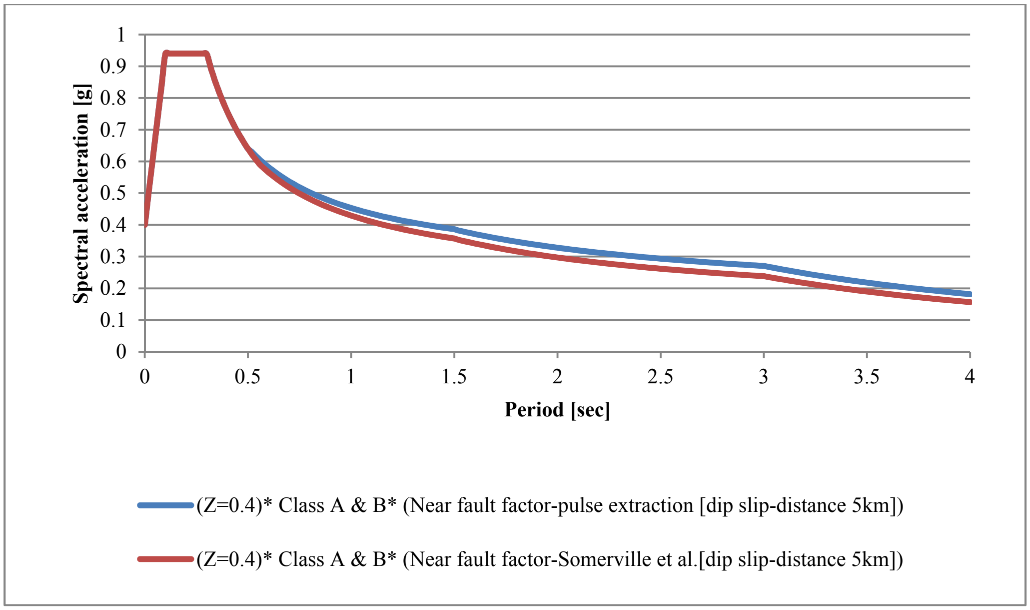

Figure 6 Comparison of Somerville et al.'s model [1997] and pulse extraction method to New Zealand Standard spectrum Building Design Standard [2004].

CONCLUSIONS

According to above, generally, for distances about 2 km and strike-slip fault values of two methods are close to each other. For 5 km category where some differences for dip-slip fault were observed, as you can see pulse amplification's values are more than Somerville et al. model. The difference does not look significantly regarding to Figure 6 that shows comparison of two types of amplifications on an optional far field spectrum. Surly we expected differences due to different records were used in two methods and also other reasons. Since we have ignored the geometric parameters like X and Θ in pulse extraction method, we tried to compared results with maximum values ($Y\cos\phi$=1) or average ones ($X\cos\Theta$=0.75).

We can mention the difference of magnitudes, which seems ignorable in comparison with the important parameters such as distance, which was used for classifying records. Moreover, we should pay attention that there are relationships between pulse period and magnitude. They are used extensively in probabilistic seismic hazard analysis and to identify a representative earthquake for a site. In pulse extraction method as the amplification has been obtained as a function of period, and we also find the largest amount of amplification at a period about period of pulse, it is reasonable to say that we have considered period of pulse effect as well, and this method strongly depends on period of pulse. This method can be used for special zone with its records more accurately. By classifying records with respect to closest distance to fault, the near-fault factor could be calculated as a function of distance and period. We did not take into account of the variation of near fault effect for different soil sites. We have supposed near fault amplification independent from soil effects. Near-fault effect might be different for different soil types. Soil amplification at near-fault sites might be more than far field or even less than on account of nonlinearity.

REFERENCES

Baker J.W. (2007). Quantitative classification of near-fault ground motions using wavelet analysis, *Bull Seismol. Soc. Am.,* 97(5): 1486–1501.

Baker J.W. (2008). Identification of near-fault velocity pulses and prediction of resulting response spectra, *Proceedings, Geotechnical Earthquake Engineering and Soil Dynamics IV*, Sacramento, CA, doi: http://dx.doi.org/10.1061/40975(318)4.

Baker, J.W. (N.D.). http://www.stanford.edu/~bakerjw/gm-selection.html.

Somerville P.G, Smith N.F, Graves R.W, Abrahamson N.A (1997). Modification of strong ground motion attenuation relations to include the amplitude and duration effects of rupture directivity, *Seismol. Res. Lett*., 68(1): 199–222.

Standards New Zealand (2004). *Building Design Standard, NZS 1170, Part 5*, Wellington, New Zealand.

LONG-PERIOD GROUND MOTION SIMULATION FOR NORTH TEHRAN FAULT SCENARIO IN TEHRAN CITY

M. R. Ghayamghamian[1] and K. Gheisari[2]

ABSTRACT

Tehran, the capital city of Iran, is a megacity situated at the southern part of the Central Alborz Mountains with more than 12 million inhabitants. North Tehran Fault (NTF) is one of the major active faults that directly threaten metropolitan area of Tehran. The NTF is the most prominent tectonic structure in the immediate vicinity of Tehran whose trace is EW to ENE-WSW and slightly concave to the south. The NTF would have been the source of several major historical earthquakes in the past, which the last one occurred in 1830 killing about 45000 people. Therefore, it is an important task to identify the characteristics of long-period strong ground motions for seismic hazard mitigation plan and design of long structures.

The kinematic model with non-uniform slip distribution on the fault plane is employed to simulate acceleration and velocity waveforms at the sites. To this end, several rupture scenarios for NTF are assumed. Then, the long-period velocity and acceleration motions for these rupture scenarios are simulated at 250 points in a grid of 2.5 km×2.5 km covering whole Tehran region. The simulated motions show near-fault directivity pulse with different peaks and periods depending on the site azimuth and distance to the fault. Based on simulated acceleration and velocity waveforms, the worst rupture scenario for Tehran is defined. The peak ground acceleration (PGA) and velocity (PGV) are found to be in the range of 20 to 120 cm/sec and 50 to 800 cm/sec^2, respectively. Finally, the estimated PGA and PGV at the simulated sites are used to develop acceleration and velocity microzonation maps for Tehran City.

Keywords: *asperity, ground motion simulation, kinematic model, microzonation maps, near-fault directivity pulse, PGA and PGV, Tehran*

INTRODUCTION

Metropolis of Tehran is the political and commercial capital of Iran. The city accommodates about 15% of total Iran population and hosts many important industries and infrastructures of Iran. Tehran is located in the southern part of central Alborz mountains in north of Iran (Figure 1). Alborz Mountains is part of the Alps-Himalayan organic zone and is known to have high potential of seismic activities with many active faults [Nazarian 2003]. Thus, the disaster mitigation and management are of great importance in Tehran. The North Tehran Fault (NTF) with EW strike dipping to the north is one of the most important active faults that directly menacing this metropolitan and would have been the source of several major historical earthquakes in the past [Berberian 1983; Ambraseys 1982]. According to the historical seismic data, Tehran region has been hit by several strong earthquakes with return period of about 150

[1] Associate Professor, International Institute of Earthquake Engineering and Seismology Tehran, Iran; email: mrgh@.iiees.ac.ir.
[2] M.S. of Geophysics, International Institute of Earthquake Engineering and Seismology, Tehran, Iran; email: koroush.gheisari@gmail.com.

years and has not experienced any disastrous earthquake since 1830, when an estimated 45,000 people were killed [Moinfar et al. 1994; Berberian and Yeats 1999]. Consequently, a strong earthquake is expected to occur in the Tehran region. The most important historical (e.g., Ambraseys and Melville [1982]) and instrumental (Iranian Seismological Center, IRSC) earthquakes that occurred in the Tehran region are highlighted in Figure 2 and are listed in Table 1. This has led many seismologists to believe that there is a high possibility that a strong earthquake strikes Tehran in the near future. Therefore, the hazard mitigation studies for decreasing the damage severity from a most probable earthquake in future are inevitable.

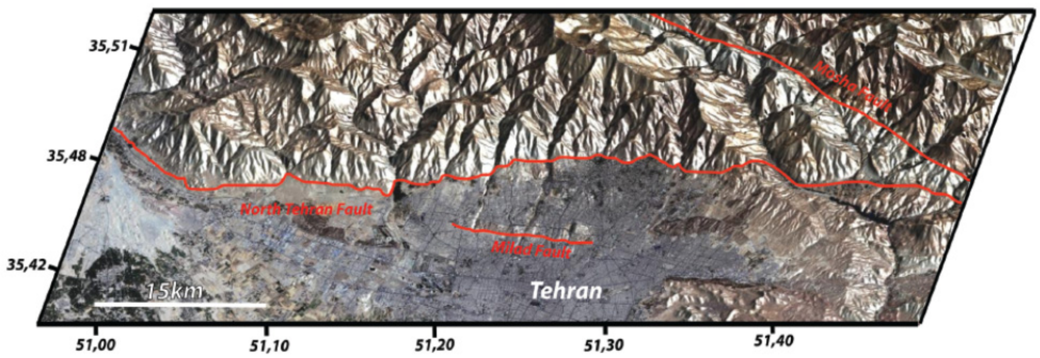

Figure 1 Three-dimensional view of Tehran region and the North Tehran fault (NTF).

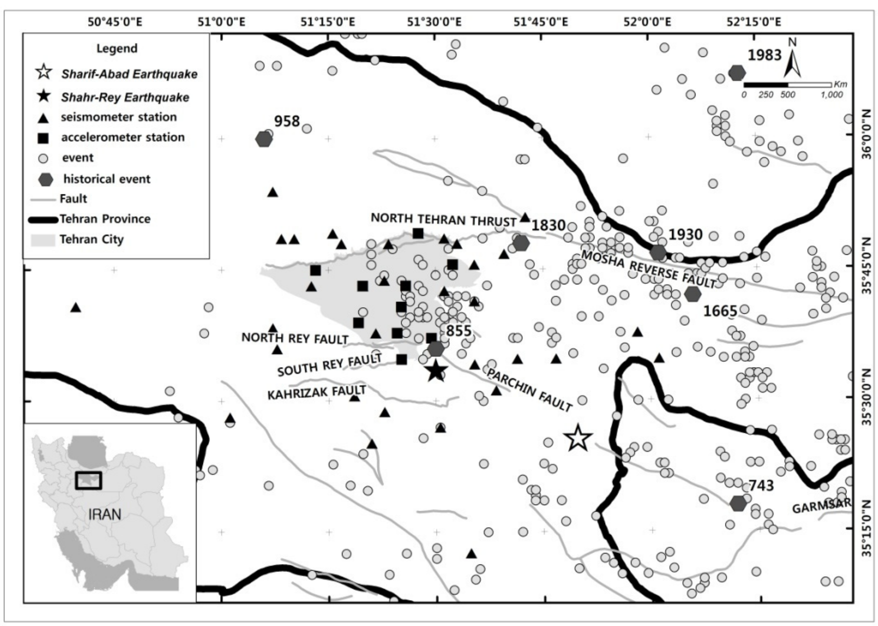

Figure 2 The location of some historic and instrumental earthquakes on the background of Tehran city and tectonic faults in Tehran region.

Table 1 **A list of some historical earthquakes around the study area from Ambraseys and Melville (1982).**

Year	Latitude	Longitude	M_s
743	35.50	52.20	7.2
855	35.60	51.50	7.1
958	36.00	51.00	7.7
1665	35.70	51.00	6.5
1830	35.80	52.70	7.1
1930	35.78	52.00	5.4
1983	35.12	52.21	5.4

Most of strong-motion estimations in earthquake hazard analysis are still inclined to the probabilistic seismic hazard analysis (PSHA) method. In this method, attenuation relations have been used extensively to predict simple parameters characterizing ground motion intensity, such as peak ground acceleration (PGA) or spectral acceleration (SA), as a function of earthquake size and distance. Conventional attenuation relations predict ground motion parameters using simplified model in which the effects of earthquake source are presented by earthquake magnitude; the effects of wave propagation from the earthquake source to site are specified by a distance; and the effects of the site are specified by a simple site category. These relations have a large degree of uncertainty in the estimation of strong ground parameter, especially in the near-fault area [Ghayamghamian 2007; Ghayamghamian and Hisada 2007]. The damage distribution of the large earthquakes such as the 1995 Hyogo-ken Nanbu (Japan) 1999 Kocaeli (Turkey), 1999 Chi-Chi (Taiwan), and 2003 Bam (Iran) earthquakes revealed that the ground motions in near-fault area have two special characteristics, namely rupture directivity and fling effects, which need to be carefully treated in the seismic hazard evaluation.

In principle, when an earthquake fault ruptures and propagates towards a site at a speed close to the shear wave velocity, the generated waves will arrive at the site at approximately the same time, generating a "distinct" velocity pulse in the ground motion time history in the strike-normal direction [Singh 1985; Somerville et al. 1999]. This intense velocity pulse usually occurs at the beginning of a record. This is referred to as the forward directivity effect, which has been known for more than a decade to have the potential to cause severe damage to the structures [Bertero et al. 1978; Singh 1985; Hall et al. 1995; Hall 1998; Wald and Heaton 1998; Iwan et al. 2000; Aagaard et al. 2000; 2001; Alavi and Krawinkler 2001; 2004, MacRae et al. 2001]. The analyses of elastic and inelastic multiple degree-of-freedom system indicate that the amplitude and period of the pulse in the velocity time history are key parameters which control the performance of structures [Kranwinkler and Alavi 2001].

Furthermore, many researchers have shown that a ground motion with a distinct velocity pulse tends to cause heightened elastic response only in a narrow period range of structures, namely those with a natural period close to the pulse period (e.g., Alavi and Krawinkler [2001], Mavroeidis and Papageorgiou [2003], Somerville [2003], Baker and Cornell [2005], Fu [2005], Tothong and Cornell [2006a], and Tothong and Cornell [2007]). Then, the question will be how to estimate the ground motion hazard for a site that may experience such a forward directivity effect.

In this paper, long-period ground motions are simulated using kinematic model for different rupture scenarios of the NTF. A finite fault model with non-uniform slip distribution on the fault plane (asperity) is assumed. Different rupture scenarios and source parameters for NTF are examined. Then, the acceleration and velocity ground motions are simulated at 250 points, which cover whole Tehran region by a 2.5 km×2.5 km grid size. The simulated ground motions in near-fault area consistency show a forward directivity pulse that its period and peak values show significant variations with respect to the site to source distance and azimuth to rupture nucleation points. Finally, the peak ground acceleration (PGA) and velocity (PGV) are estimated from simulated motions at the sites and PGA together with PGV microzonation maps are provided for Tehran City.

GEOLOGIC SETTINGS OF TEHRAN

North of Tehran is a part of Central Alborz Mountains with height of almost 3000 m, while southern part is located in plain like low lands (Figure 1). The thickness of the sediments increases from north to south. The study area mainly consists of sedimentary deposits of Quaternary era, which has been known as Tehran alluvial formation. This formation often is a result of erosion and re-deposition of former sediments, which has extended to the south as a young fan and generally consists of unsorted fluvial and river deposits. Both, the effects of climate processes and tectonic young activities caused a miscellaneous alluvium of type, thickness and grain size to be formed.

As shown in Figure 3, Tehran is spread on four typical alluvial formations [Rieben 1955] as:

- “A” formation (Hezardarreh formation) is considered to be of the Pliocene-Pleistocene and essentially include conglomerates with a few lenses of sandstone, siltstone and mudstone and covers northeast and east of Tehran city.
- “B” formation covers “A” formation and includes two facieses such as “Bn” (North Tehran inhomogeneous alluvial formation) which Consist of conglomeratic mixture of gravel, pebble, and clastic size cobble and “Bs” (South Tehran clayey silt or Kahrizak formation) composed of reddish brown and beige-colored silt with some clayey component.
- “C” formation (Tehran alluvial formation [Rieben 1955] includes homogenous conglomerates, composed of gray to brown colored gravel with mixture of silt and sand.
- “D” formation (Recent Alluvium) is the youngest stratigraphic unit within the Tehran region and is present as alluvial and fluvial deposits. This formation is subdivided

into two different stratigraphic units, called “D1” as a veneer, covers the “Bs” formation in the south and is composed of line silt with a grayish cream and gray color and “D2” units is composed of silty gravel, clastic size pebble, and covered “C” formation in north.

Geotechnical observations of drilled boreholes and also other previous studies reveal that sediments of northern and eastern parts of the studied area are mostly sand and gravel [JICA 2000; Ghayamghamian et al. 2011]. These cemented coarse grained deposits (except at upper 5m band) have a high density and strength. The maximum depth of these deposits has been estimated to be 200m. In the middle zone of region, both fine and coarse grained materials have deposited consequently. Furthermore, the deposits grain size decreases with distance from marginal elevations, so that southern part of area comprises mostly of low plastic silty and clayey materials. This transformation from coarse to fine grain size is gradually throughout the region. The low plastic silty and clayey materials usually have a plasticity index of less than 20 and a fine content of more than 75%. The maximum thickness of fine-grained deposits has been estimated to be 150m.

Here, we simulated ground motion on the engineering bedrock, where the shear wave velocity exceeds 600 m/sec or the NSPT exceeds 100. The depth of engineering bedrock in south of Tehran reached to the 150 m, which is the deepest part in study area [JICA 2000; Ghayamghamian et al. 2011]. From this area, the depth of engineering bedrock becomes shallower towards the north and east. The depth becomes about 35 m at the boundary of the fan and the plain. It reaches to near 20 m in C and D2 formations. Furthermore, A and B formations are firmly cemented, and are considered as engineering bedrock.

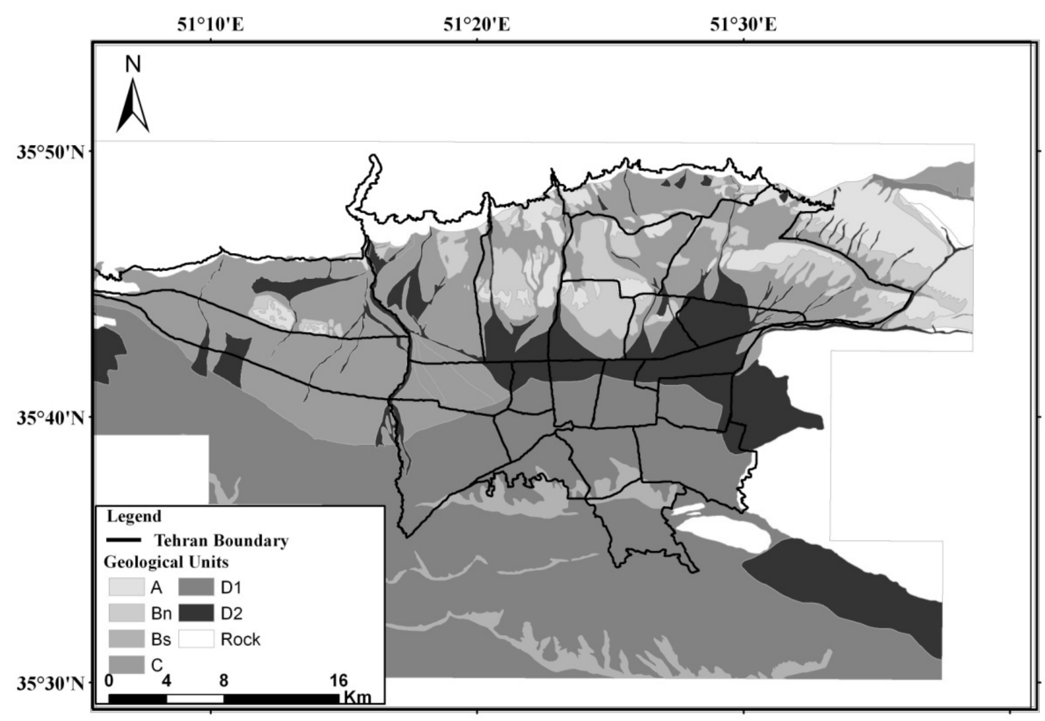

Figure 3 Geological map of Tehran region.

TECTONIC INFORMATION OF THE NORTH TEHRAN FAULT

North Tehran fault with almost EW strike dipping to the north separates Tehran Plain in south from central Alborz Mountains in the north. Based on GPS measurements, the central Alborz is affected by a NS shortening comprised between 5±2 mm/year [Vernant et al. 2004], which represents 20 % of the ~ 22 mm/yr NS convergence of the Arabian plate (Figure 4). Central Alborz is also affected by left-lateral shearing comprised between 2.5±1.5 mm/yr [Vernant et al. 200]). These data confirm the active strain partitioning observed across Alborz as interpreted by analyses of the seismological and morphotectonics data [Jackson et al. 2002; Allen et al. 2003; Ritz et al. 2006]. The NTF extends over approximately 110 km, with a general "V" shape trace at the surface, switching from the NW-SE direction to NE-SW between the cities of Karaj and Tehran (Figure 1). The fault trace is, however, difficult to follow—mainly because of urban development—and it appears to be divided into several segments [Nazari 2006; Nazari et al. 2008].

Paleoseismological investigations within two trenches dug across the fault scarp zone reveals evidence for 8 surface-rupturing events within the past ~30,000 years (optically stimulated luminescence ages). The two last events involved 2.35 m of total reverse displacement along the fault during the last ~ 8000 years (0.77 m for the latest event and 1.58 m for the penultimate). The eight events have magnitudes in the range of 6.5 to 7.1, and the mean return period is 3175–4075 yrs. [Nazari et al. 2008].

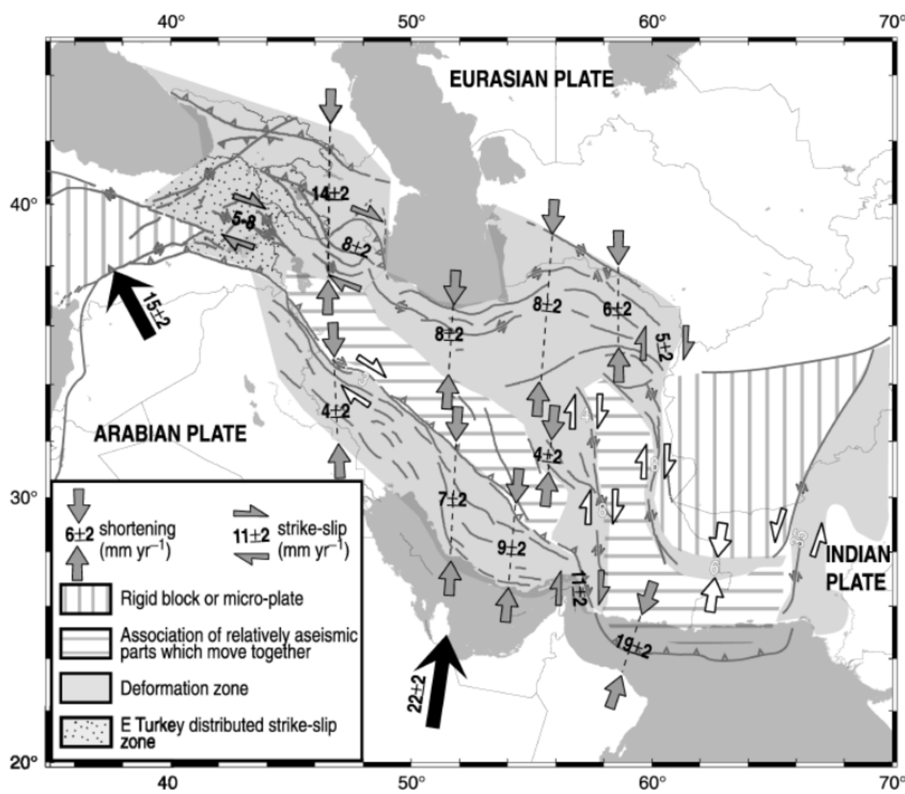

Figure 4 Shortening rate in different parts of Iran (after Vernant et al. [2004]).

KINEMATIC METHOD

Ground motion from an earthquake can be simulated if a slip distribution across a fault surface (i.e., source effects) and a Green's function, which represents the impulse response of propagation medium (i.e., propagation path effects), are known. There are two ways to characterize a fault motion at an earthquake source, namely kinematic and dynamic source models. The kinematic source models give arbitrarily the slip space-time functions on the fault plane without physical considerations regarding stress conditions. In spite of the inadequacy in the handling of the physical condition in the source, the kinematic model yields numerous important results in interpreting ground motions from earthquakes and in estimating slip distributions and rupture propagating over the fault planes [Rouhollahi et al. 2012]. Haskell [1964] made the pioneer work on kinematic model to express the source effect defining fault length, fault width, final slip, rise time, and rupture velocity. This method has been also successfully employed in ground motion simulation and determining source characteristics of some large earthquakes in Iran by first author [Ghayamghamian 2007; Ghayamghamain and Hisada 2007; Rouhollahi et al. 2012], which used to validate its application and accuracy for ground motion simulation in Tehran.

Starting from representation theorem [Aki and Richards 1980], it can be shown that in homogenous, isotropic, and infinite medium, the displacement $\vec{u}_i(\vec{x},t)$ of P and S waves at point $(\vec{x},t)$ due to a displacement discontinuity $\vec{u}(\vec{\xi},\tau)$ at point $(\vec{\xi},\tau)$ across an internal surface $\sum$ can be given by:

$$\overrightarrow{u_i}(\vec{x},t) = \frac{R_c(\phi,\delta)}{4\pi\rho c^3 r}\cdot\mu\iint_{\Sigma}\ \Delta\dot{U}_J\left(\vec{\xi},t-\frac{r}{c}\right)d\Sigma \qquad (1)$$

where μ is the rigidity, r is the distance between the fault plane Σ and point of observation, R_c (subscript c indicates the wave type: P, SV, or SH) is the radiation pattern coefficient along the strike ϕ and dip δ of the fault. The function Δu is a scalar, called the "source function" or the "slip function" in case of a shear fault. For a fault of length L and width W, the displacement waveform can be written in a simple form given by:

$$\overrightarrow{u_i}(\vec{x},t) = \int_0^L\int_0^W \Delta\dot{u}\,(\xi,\eta) * \vec{G}(\vec{x},\xi,\eta,t)d\xi d\eta \qquad (2)$$

where G is the Green's function, and $*$ represent convolution. To simulate ground motion due to an extended fault, the fault surface is divided into small sub-faults. Assuming that the fault plane is divided into l elements along the strike of the fault and m elements along its down-dip direction, the above integral can be rewritten in the following form:

$$\overrightarrow{u_i}(\vec{x},t) = \sum_{i=1}^{l}\sum_{j=1}^{m}\int_{L_i}^{L_i+\Delta L_i}\int_{W_i}^{W_i+\Delta W_i}\Delta\dot{U}\left(\xi_i,\eta_j,t-\tau_{ij}\right) * \vec{G}\left(\vec{x},\xi_i,\eta_j,t\right)d\xi d\eta \qquad (3)$$

where τ_{ij} is the time taken by the rupture front to propagate from hypocenter to the i,j sub-fault. The rise time of the dislocation function is small for the smaller event and is also scaled by the similarity condition of earthquakes as:

$$\frac{\tau}{\tau_e} = \left(\frac{M}{M_e}\right)^{1/3} \qquad (4)$$

where the parameters with a subscript e correspond to the small earthquake and without, to the large earthquake [Kanamori and Anderson 1975; Hardly and Helmberger 1980; Irikura 1983)]. M is the seismic moment of an event. The above ratio is a constant and is approximated by an integer n. Thus, $\vec{u}\,(\vec{x},t)$ can be expressed as:

$$\vec{u_i}(\vec{x},t) = \sum_{k=1}^{n}\sum_{j=1}^{m}\sum_{i=1}^{l}\int_{L_i}^{L_i+\Delta L_i}\int_{W_i}^{W_i+\Delta W_i} \Delta\dot{U}\left(\xi_i,\eta_j,t-\tau_{ij}-(k-1)\right) * \vec{G}\left(\vec{x},\xi_i,\eta_j,t\right) d\xi d\eta \tag{5}$$

where k is a random number, which prevents an artificial periodicity in simulated motion [Joyner and Boore 1988]. Equation (5) is the base of simulation studies that have been done to date. The parameter n is the number of sub-sources per sub-fault. The simulated motion of the large event is then the summation of contributions from l fault element along strike, m fault elements down-dip and n source functions lagged in time on each fault element.

SOURCE PARAMETERS AND LONG-PERIOD GROUND MOTION SIMULATION IN TEHRAN

Based on the earlier studies and explanation given earlier, a most probable segment of NTF with length of 60 km is assumed as shown in Figure 5 [Nazari et al. 2006; JICA 2000]; the source parameters for NTF scenario are defined as listed in Table 2. These source parameters as well as number, area and slip of the asperities- the areas on the fault plane with large slip relative to the average slip on the fault - are defined based on recent investigation on the NTF by Nazari et al. [2006] and the relationships given by Somerville et al. [1999; 2003]. Since the location of asperities and nucleation point as well as rupture direction have a large influence on the simulated ground motions, three rupture scenarios are assumed for NTF as schematically shown in Figure 6 (Models A, B and C). Then, the Tehran region was divided into 250 grids with a grid size of 2.5 km×2.5 km to simulate acceleration and velocity waveforms, and to compute PGV and PGA microzonation maps of Tehran (Figure 5).

The long-period ground motion for three components (NS, EW and UP) are simulated for the NTF rupture scenarios at 250 points covering Tehran region. The examples of simulated acceleration and velocity waveforms for three rupture models are shown in Figure 7. To explain the variations of simulated motions, the velocity waveforms at the 20 sites located along two parallel and perpendicular lines to the fault strike (see blue rectangular in Figure 5) for Model A are illustrated in Figures 8 and 9, respectively. From these figures, a clear rupture directivity pulse with the peak values of 30 to 90 cm can be seen in the NS component, which is almost located in fault normal direction (FN). The rupture directivity pulse characteristics vary with respect to the sites distance from the source and its azimuth. The PGV at the sites in perpendicular direction to the fault strike decreases as going from the north toward the south. Meanwhile, the PGV at the sites in fault parallel direction increases from east to the middle of the fault and then decreases from middle to the west. Furthermore, the peak values of simulated velocity and acceleration waveforms at the sites are estimated for the models. Then, the PGV and

PGA microzonation maps of Tehran are developed as shown in Figures 10 and 11, respectively. The comparison among estimated PGVs and PGAs for different rupture Models shows that the rupture scenario for Model A could produce the largest PGV and PGA in Tehran City, and can be considered as the worst rupture scenario for Tehran. For this Model, the PGV and PGA with maximum value of 120 cm/sec and 800 cm/sec^2 can be seen in the northeast of Tehran. They decrease to about 50 cm/sec^2 and 30 cm/sec toward the south.

Table 2 Source parameters for NTF scenario.

Source Parameters	Value
Mw	7.0
Fault length	60 km
Fault width	20 km
Dip	75°
Strike	83°
Rake	0°
Max slip of asperity 1	200 cm
Max. slip of asperity 2	90 cm
Raise time	1 sec
Rupture velocity	2.5 km/sec

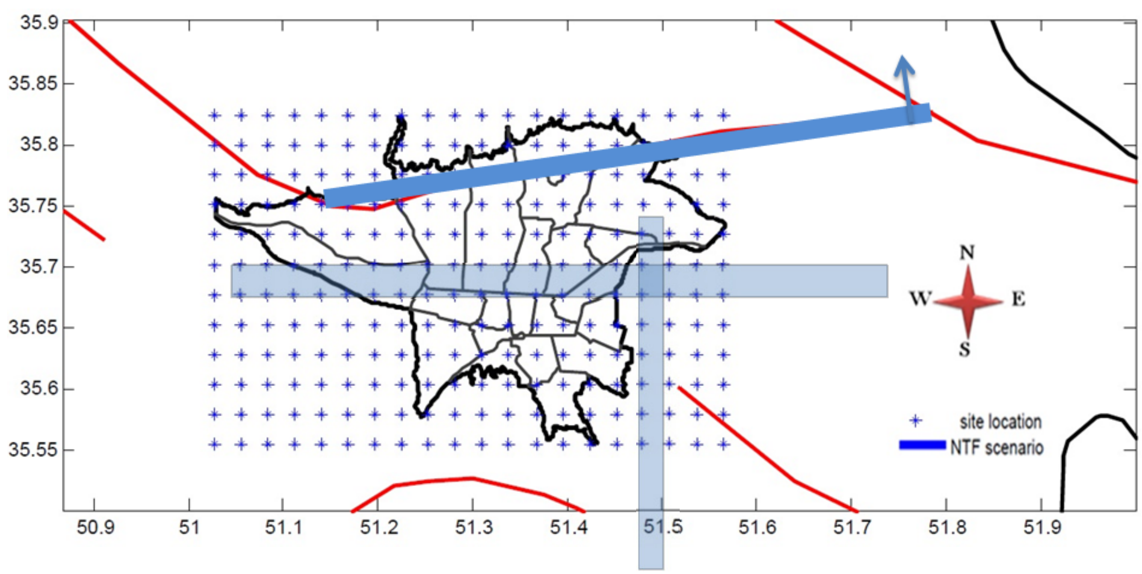

Figure 5 The assumed segment for NTF with boundary of Tehran City in the background. The plus signs show the location of the sites where the ground motions were simulated.

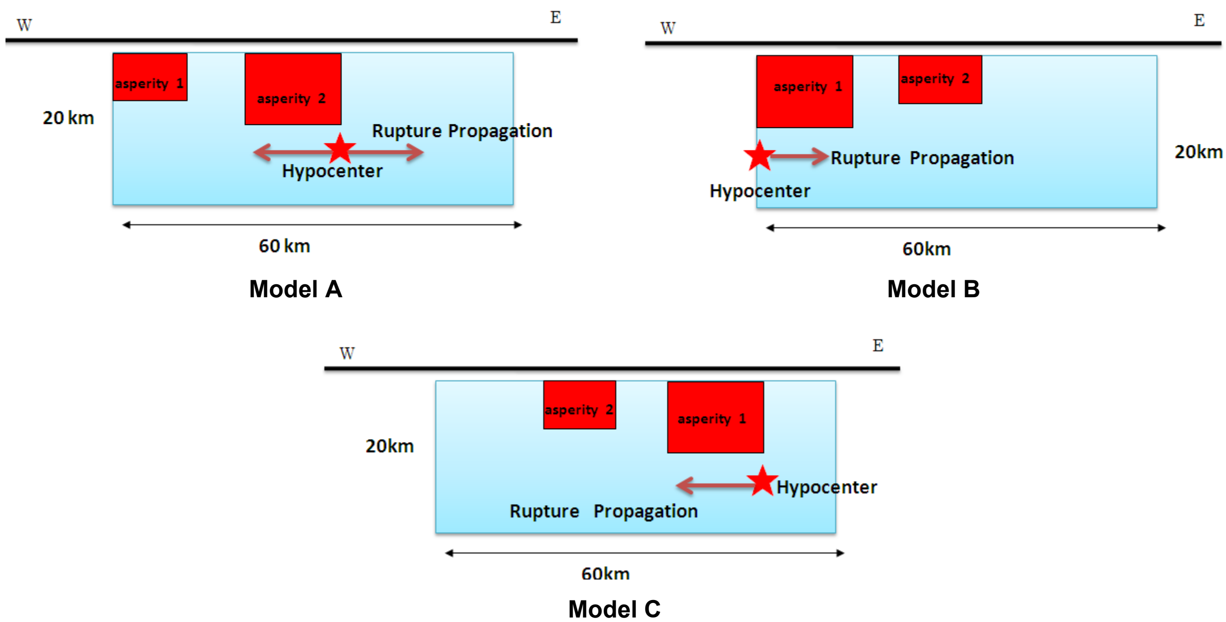

Figure 6 **A schematic for different rupture scenarios showing the location of the asperity, nucleation point and rupture direction on the fault plan.**

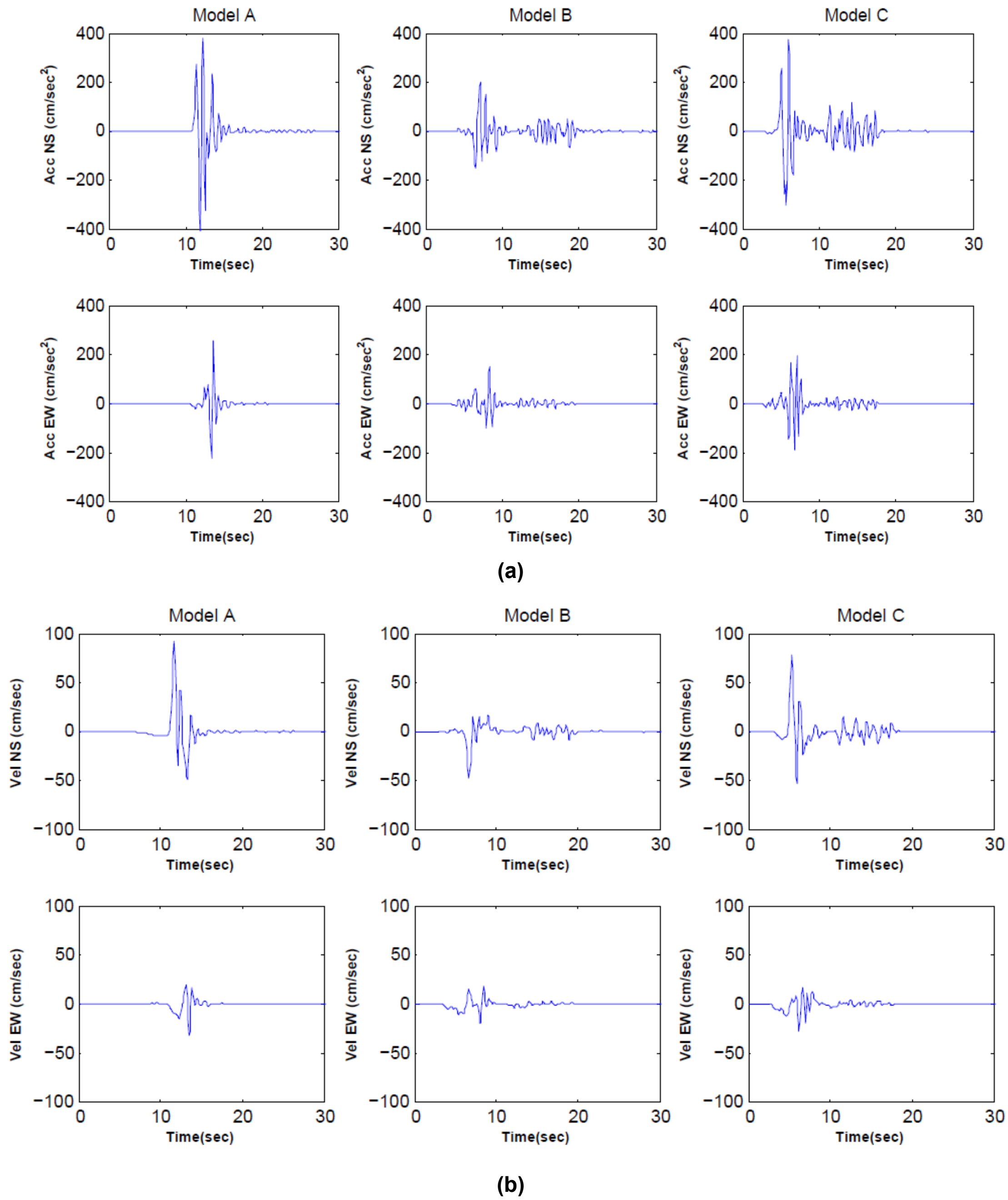

Figure 7 Examples of simulated waveforms for different rupture models (A, B and C): (a) acceleration waveforms; and (b) velocity waveforms.

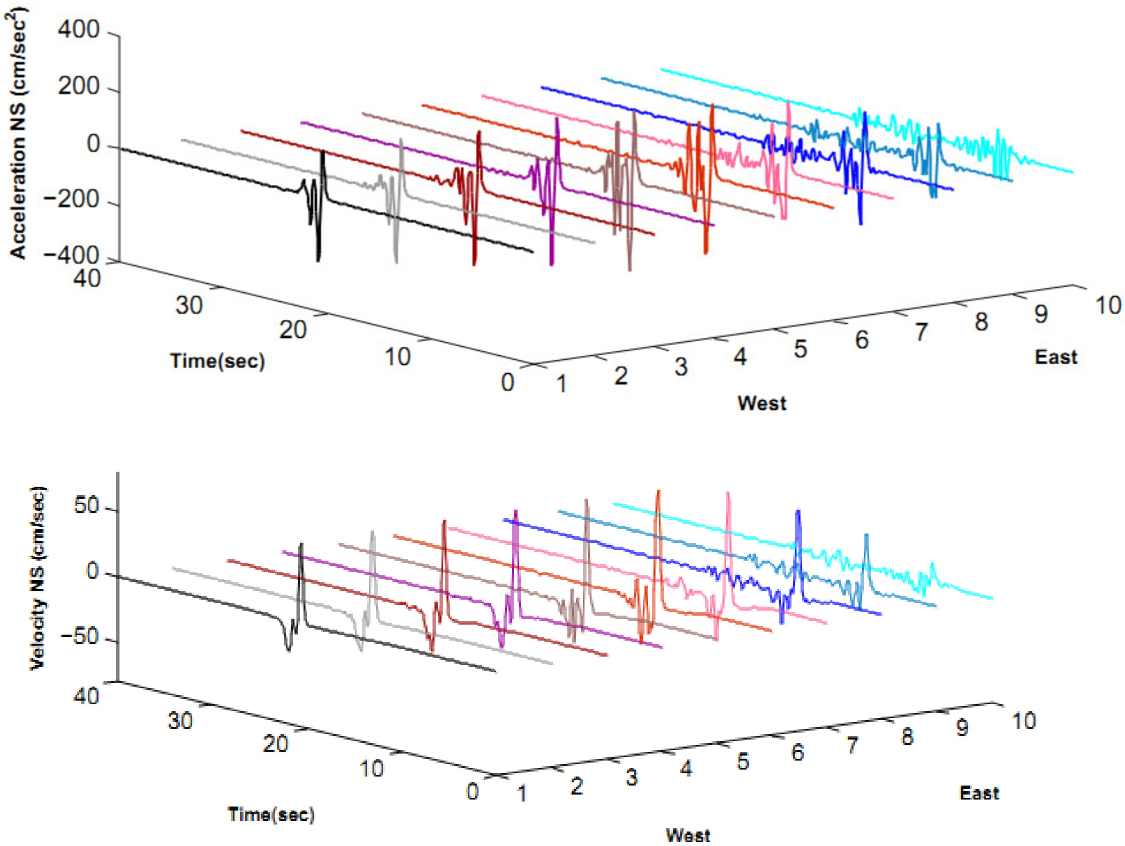

Figure 8 **Variation of simulated velocity and acceleration waveforms for NS component at 10 sites which are located along a line almost parallel to the fault strike.**

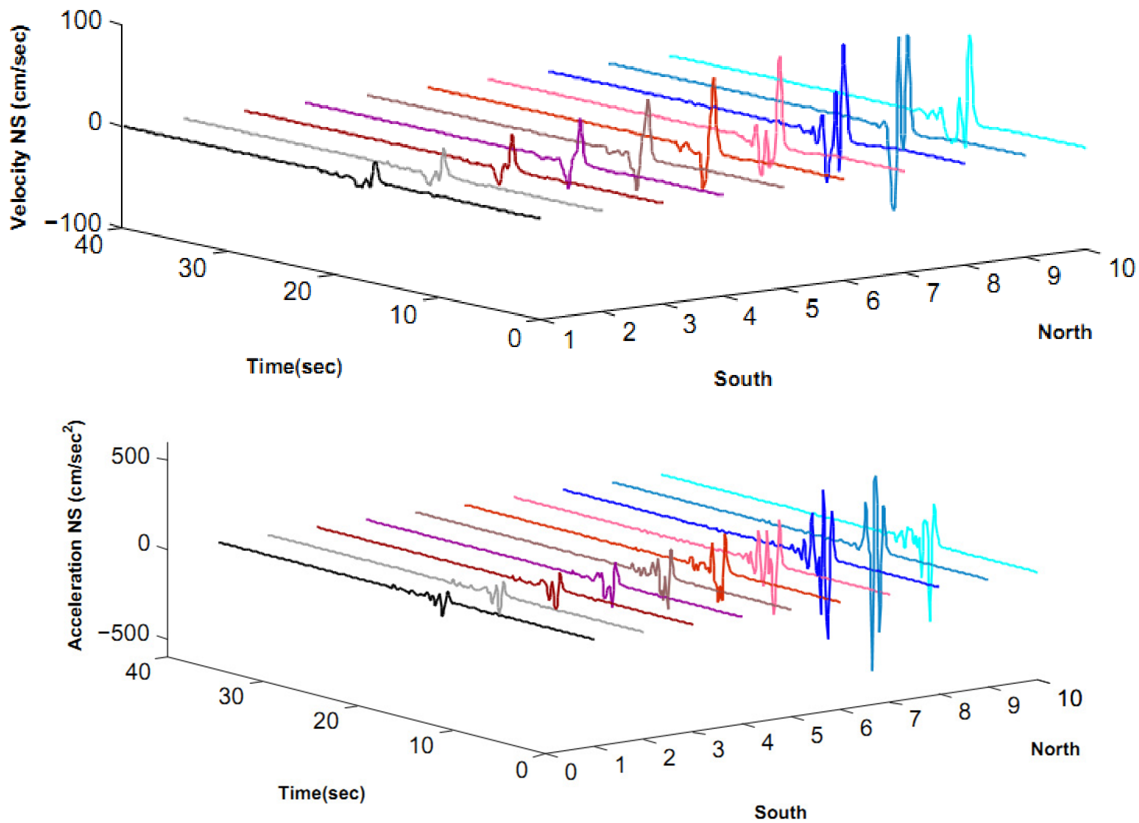

Figure 9 **Variation of simulated velocity and acceleration waveforms for NS component at 10 sites, which are located along a line almost perpendicular to the fault strike.**

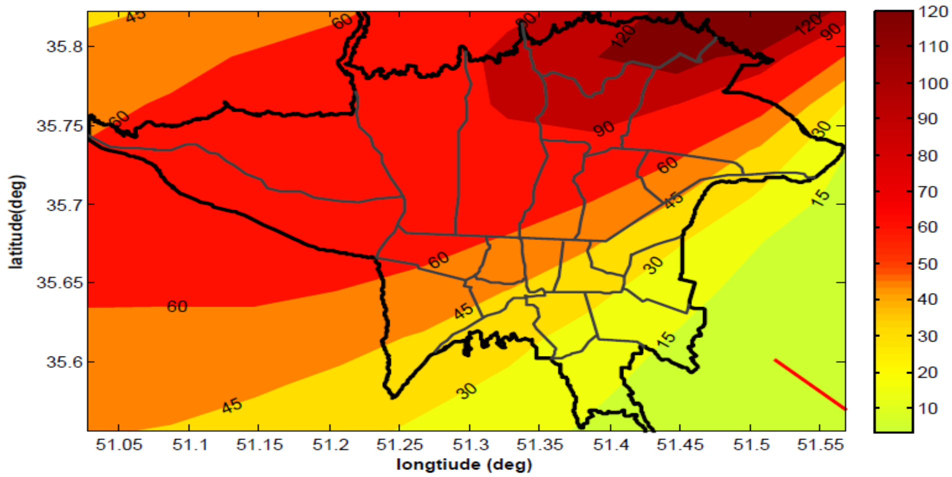

Model A

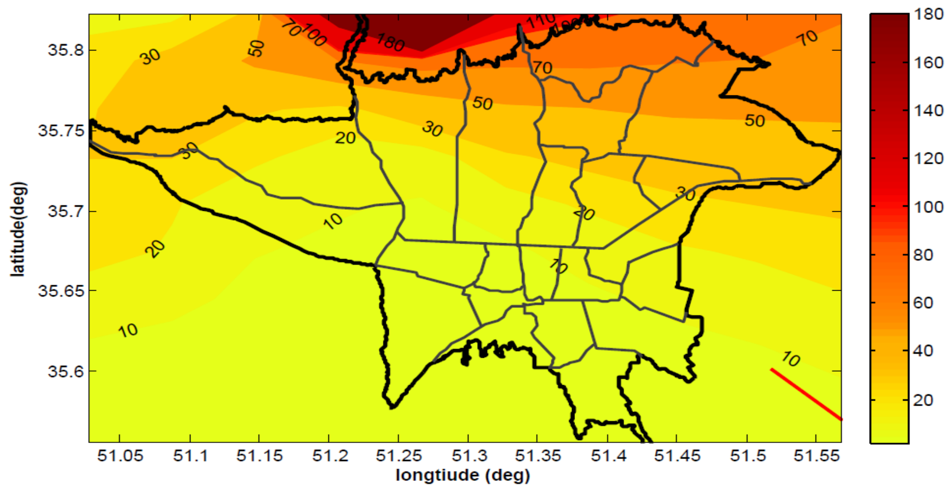

Model B

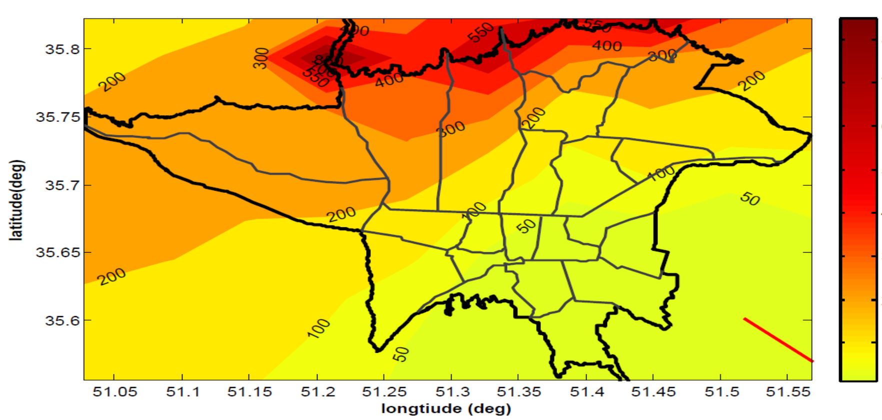

Model C

Figure 10 The distribution of PGVs (cm/sec) for simulated waveforms at 250 sites for different rupture scenarios (Models A, B, and C).

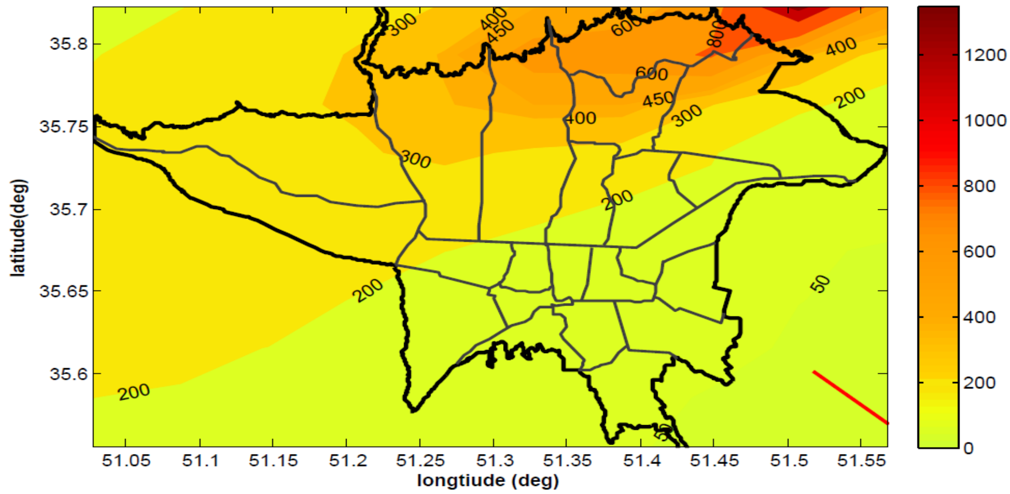

Model A

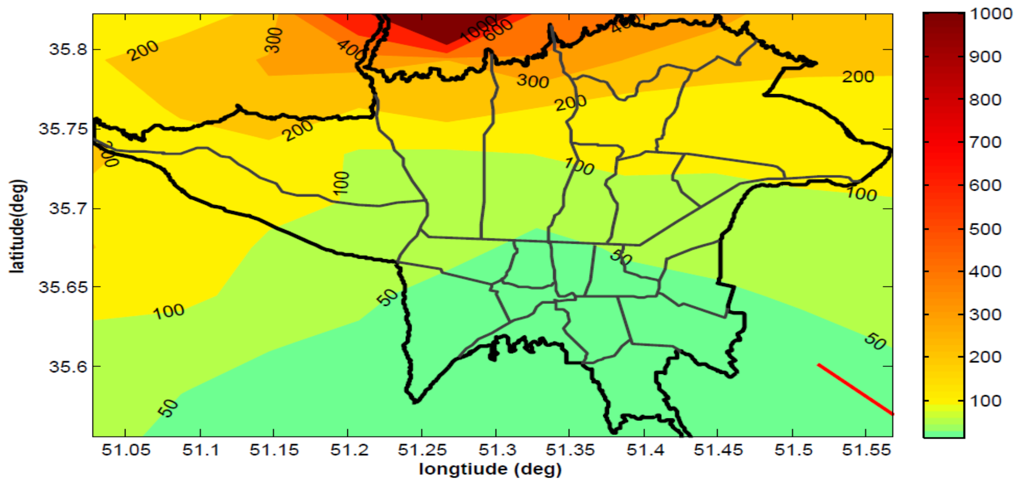

Model B

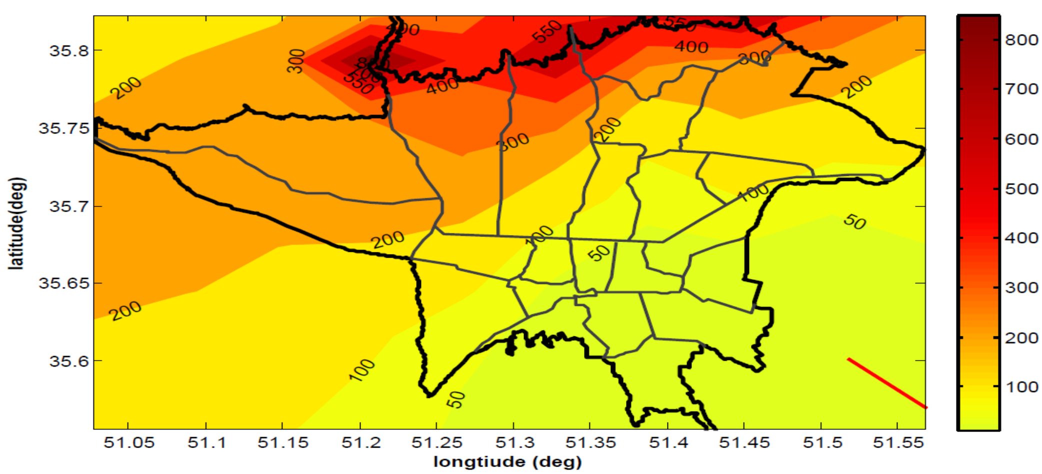

Model C

Figure 11 **The distribution of PGAs (cm/sec^2) for simulated waveforms at 250 sites for different rupture scenarios (Models A, B and C).**

CONCLUSIONS

In this paper, the long-period velocity and acceleration waveforms were simulated using kinematic method for different rupture scenarios of NTF. The worst rupture scenario was defined for different configurations of source parameters, asperity and nucleation point locations as well rupture directions on the fault. The velocity and acceleration waveforms were simulated at 250 sites covering whole Tehran region. The simulated motions for the worst rupture scenario consistently show a near-fault directivity pulse with maximum PGV and PGA values in the ranges of 30–120 cm/sec and 50–800 cm/sec^2, respectively. From the simulated velocity and acceleration waveforms, the PGV and PGA microzonation maps for Tehran is developed in a grid of 2.5 x 2.5 km.

REFERENCES

Aagaard B.T., Hall J.F., Heaton T.H. (2000). Sensitivity study of near-source ground motion, *Proceedings, 12th World Conference on Earthquake Engineering, New Zealand Society for Earthquake Engineering*, Upper Hutt, New Zealand.

Aagaard B.T., Hall J.F., Heaton T.H. (2001). Characterization of near-source ground motions with earthquake simulations, *Earthq. Spectra*, 17, 177–207.

Aki K., Richards P.G. (1980). *Quantitative Seismology: Theory and Methods*, W.H. Freeman and Co. New York.

Alavi B., Krawinkler H. (2004). Behavior of moment-resisting frame structures subjected to near-fault ground motions, *Earthq. Eng. Struct. Dyn*., 33: 687–706.

Alavi B., Krawinkler H. (2001). *Effects of Near-Fault Ground Motion on Building Structures*, CUREE-Kajima Joint Research Program Report, Richmond, CA.

Allen M.B., Ghassemi M.R., Sharabi M., Qoraishi M. (2003). Accommodation of late Cenozoic oblique shortening in the Alborz range, northern, *Iran. J. Struct. Geol*., 25: 659– 672.

Ambraseys N.N., Melville C.P. (1982). *A History of Persian Earthquakes,* Cambridge University Press, New York.

Baker J.W., Cornell C.A. (2005). A vector-valued ground motion intensity measure consisting of spectral acceleration and epsilon, *Earthq. Eng. Struct. Dyn*., 34: 1193–1217.

Berberian M. (1983). The southern Caspian: A comparison depression floored by a trapped, modified oceanic crust, *Can. J. Earth Sci.,* 20: 163–183.

Berberian M., Yeats R.S. (1999). Patterns of historical earthquake rupture in the Iranian Plateau, *Bull. Seismol. Soc. Am.*, 89(1): 120-139.

Bertero V.V., Mahin S.A., Herrera R.A. (1978). A seismic design implication of near-fault San Fernando earthquake records, *Earthq. Eng. Struct. Dyn*., 6: 31–34.

Fu Q. (2005). *Modeling and Prediction of Fault-Normal Near-Field Ground Motions and Structural Response*, PhD Dissertation, Department of Civil and Environmental Engineering, Stanford University, Stanford, CA.

Ghayamghamian, M.R., Haghshenas E., Amini Hosseini K., Mansouri B. (2011). *Estimation of Site Amplification Factor in Tehran City for Rapid Damage Estimation*, Tehran Disaster Mitigation and Management Organization Report, Tehran, Iran.

Ghayamghamian M.R., Rafiee Gazani M., Mahrabian S. (2010). Site effect estimation in Tehran using Firoozabad-Koojour (2003) earthquake and Tehran earthquake (2009) data, *Proceedings, 14th Iranian Geophysical Conference,* Tehran, Iran.

Ghayamghamian M.R. (2007). Directional damage due to near-fault and site effects in the M6.4 Changureh-Avaj earthquake of 22 June 2002, *J. Seismology*, DOI 10.1007/s10950-006-9026-y.

Ghayamghamian M.R., Hisada Y. (2007). Near-fault strong motion complexity of the 2003 Bam earthquake (Iran) and low-frequency ground motion simulation, *Geophys. J. Inter.,* 170(2): 679–686.

Ghayamghamian M.R. (2003). Near-field ground motion simulation for heterogeneous faulting, *Proceedings, 4th International Conference on Earthquake Engineering and Seismology*, Tehran, Iran.

Hall J.F., Aagaard B.T. (1998). Fundamentals of the near-source problem, *Proceedings, 5th Caltrans Seismic Research Workshop*, Sacramento, CA.

Hall J.F., Heaton T.H., Halling M.W., Wald D.J. (1995). Near-source ground motion and its effects on flexible buildings, *Earthq. Spectra*, 11(4): 569–605.

Irikura K. (1983). Semi-empirical estimation of strong ground motions during large earthquakes, *Bull. Disaster Prevention Res. Institute*, Kyoto University, Kyoto, Japan, 33: 63–104.

Iwan W.D., Huang C. Guyader A.C., (2000). Important features of the response of inelastic structures to near-field ground motion, *Proceedings, 12th World Conference on Earthquake Engineering*, Paper No. 1740, New Zealand Society for Earthquake Engineering, Lower Hutt, New Zealand.

Jackson J., Priestley K., Allen M., Berberian M. (2002). Active tectonics of the South Caspian Basin, *Geophys. J. Inter*., 148: 214–245.

JICA (2000). *The Study on Seismic Microzoning of the Greater Tehran Area in the Islamic Republic of Iran*, Japan International Cooperation Agency, Final Report.

MacRae G.A., Morrow D.V., Roeder C.W (2001). Near-fault ground motion effects on simple structures, *J. Struct. Eng*., ASCE, 127: 996–1004.

Mavroeidis G.P., Papageorgiou A.S. (2003). A mathematical expression of near-fault ground motions, *Bull. Seismol. Soc. Am.* 93(3): 1099–1131.

Mavroeidis G.P., Dong G., Papageorgiou A.S. (2004). Near-fault ground motions, and the response of elastic and inelastic single-degree-freedom SDOF systems, *Earthq. Eng. Struct. Dyn*., 33: 1023–1049.

Moinfar A.A., Mahdavian A., Maleky E. (1994), *Historical and Instrumental Data Collection of Iran*, Iranian Cultural Affairs Institute, Tehran, Iran.

Nazari H., Ritz J.-F. (2008). Neotectonic in Central Alborz, *Geosciences*, 17(1): 74–92.

Nazari H. (2006). *Analyse de la Tectonique Recente et Active dans l'Alborz Central et la Region de Teheran:Approche Morphotectonique et Paleoseismologique*, PhD thesis, Montpellier II, Montpellier, France.

Ritz J.-F., Nazari H., Ghassemi A. Salamati R., Shafei A., Solaymani S., Vernant P. (2006). Active transtention inside Central Alborz: A new insight into the Northern Iran-Southern Caspian geodynamics, *Geology*, 34 (6): 477–480.

Ritz J.-F., Nazari H., Salamati H.A.R., Shafeii A., Solaymani S. (2006). Active transtension inside Central Alborz: a new insight into the Northern Iran–Southern Caspian geodynamics, *Geology*, 34: 477–480

Ritz J.F., Nazari H., Balescu S., Mamothe, Salamati R., Ghassemi A., Shafei A., Ghorashi M., Saidi A. (2012). Paleoearthquakes of the past 30,000 years along the North Tehran Fault (Iran), *J. Geophys. Res: Solid Earth*, 117(B6).

Rouhollahi R., Ghayamghamian M.R., Yaminifard F., Suhadolc P. Tatar M. (2012). Source process and slip model of 2005 Dahuiyeh-Zarand earthquake (Iran) using inversion of near-field strong motion data, *Geophys. J. Inter.*, 189: 669–680.

Singh J.P. (1985). Earthquake ground motions: Implications for designing structures and reconciling structural damage, *Earthq. Spectra*, 1(2): 239–270.

Somerville P.G, Irikura K., Graves R., Sawada S., Wald D.J., Abrahamson N.A., Iwasaki Y., Smith N., Kowada A., (1999). Characterizing crustal earthquake slip models for the prediction of strong ground motion, *Seismol. Res. Lett.*, 70(1) 59–80.

Somerville P.G. (2003). Magnitude scaling of the near fault rupture directivity pulse, *Phys. Earth Planet. Int*., 137(1–4): 201–212.

Somerville P.G., Smith N.F., Graves R.W., Abrahamson N.A. (1997). Modification of empirical strong ground motion attenuation relations to include the amplitude and duration effects of rupture directivity, *Seismol. Res. Lett*., 68: 199–222.

Tothong P., Cornell C.A. (2007). Structural performance assessment under near-source pulse-like ground motions using advanced ground motion intensity measures, *Earthq. Eng. Struct. Dyn*., 36(13): 1837–1860.

Tothong P., Cornell C.A. (2006). Probabilistic seismic demand analysis using advanced ground motion intensity measures, attenuation relationships, and near-fault effects, *PEER Report 2006/11*, Pacific Earthquake Engineering Research Center, University of California, Berkeley, CA.

Vernant P., Nilforoushan F., Chery J., Bayer R., Djamour Y., Masson F., Nankali H., Ritz J.F., Sedighi M., Tavakoli F. (2004b). Deciphering oblique shortening of central Alborz in Iran using geodetic data, *Earth Planetary Sci. Lett.*, 223: 177–185.

Wald D.J., Heaton T.H. (1998). Forward and inverse modeling of near-source ground motions for use in engineering response analysis, Paper T162-1, *Proceedings, of the American Society of Civil Engineering*, San Francisco, CA.

METHODS FOR DESIGN OF LARGE DAM GATES UNDER SEISMIC HYDRODYNAMIC ACTION

M. T. Ahmadi[1] and M. Haghani[1]

ABSTRACT

Large dams are major infrastructures of the Iranian national plan of urban and industrial economic development. Concrete dams are subjected to large seismic excitations in this country, and although nowadays they are well designed against inertia and hydrodynamic actions, but their vital secondary structures are less being focused on during the seismic loading. The International Commission on Large Dams (ICOLD) recommendations require safe operation of major outlets of large reservoirs to enable lowering the water head in case of destructive earthquakes causing considerable risk of collapse for the dam body or its appurtenant structures. As major outlets such as spillway gates, orifices, and bottom outlets are usually positioned in the dam body, their safety becomes a strategic concern. Most times these are located at quite high elevations where dynamic amplification of accelerations and displacements exceed several folds those of ground motion. Indeed several performance observations during important seismic events in dam sites have proven that the risk of malfunctioning of such outlets is quite high. Unfortunately research in this field are rather scarce worldwide, and almost all design codes related to dam and appurtenant structures neglect such complications and suggest over-simplified methods of loading and analysis. In this research a consistent simplified approach is devised based on rigorous dam-reservoir interaction analysis. Due to large dependency of secondary structures dynamic loads on their detailed specifications, their direct modeling in such rigorous analysis is cumbersome and needs more than usual engineering skill. The method yields pseudo-static loading similar to that of Westergaard's for estimating the design hydrodynamic pressure under horizontal ground motion, but employs actual relevant floor spectral acceleration. Based on a variety of gravity dam geometries, dam heights, gate dimensions, gate boundary conditions, reservoir bottom reflection coefficients, and seismic load frequency contents; formulae have been fitted and proposed for hydrodynamic pressures acting on elevated rectangular slide gates. Two categories of gate elevations are considered. The algorithm requires obtaining the floor response spectrum at the gate level; a trivial task possible once the dam-reservoir dynamic analysis is carried out as a standard procedure of dam design. It also requires the fundamental coupled frequency of the gate. It is believed that the simplified proposed method of hydrodynamic design load approximation is very reliable for seismic design of gates positioned in the body of concrete gravity dams.

Keywords: *floor response spectrum, fluid-structure interaction, hydrodynamic pressure, secondary systems, sliding rectangular gate*

[1] Civil Engineering Department, Tarbiat Modares University, Tehran, Iran.

INTRODUCTION

To guarantee reliable operation of concrete dams and safe using of the impounded water, the reliability of secondary structures such as spillways, gates, control valves, intake towers and other related equipment must be ensured. In fact the security of dam body itself is greatly dependent on its appurtenant structures in case of severe earthquakes when emergency operation of these should be guaranteed. Therefore, main hydraulic structures related to reservoir must be resistant against the design earthquake for which the dam would be designed for [ICOLD 1999]. One of the important challenges in seismic design of hydraulic structures is the consistent estimation of the induced hydrodynamic pressure on the gate vibrating at certain elevations in the dam body as a secondary structure and adjacent to an excited reservoir.

Seismic hydrodynamic pressure evaluation for dams was initiated by Westergaard who assumed horizontal harmonic excitation of a rigid wall against a two-dimensional semi-infinite reservoir and tailored his solution into a depth-wise parabolic maximum hydrodynamic pressure distribution. He evolved his solution to an equivalent added mass form for the design of Hoover Dam [1933]. Chopra studied for a simplified evaluation of added mass for intake towers in reservoirs [1989]. There were also several works by others mostly in frequency domain and for flat plates at fluid contact. Kojic and Trifunac [1988] used finite element analysis for dam bottom outlets with rigid gates and showed that dynamic pressure in the adjacent conduits could be two to threefold the hydrostatic pressure. Sanabria et al. [1998] conducted an experimental study and suggested an added mass expression for the first mode approximation of vibrating sliding inclined gate of Olmset dam in contact to incompressible fluid body. Daniell and Taylor [2000] conducted a three-dimensional seismic performance evaluation of radial gates in a gravity dam using finite elements. They showed that gates not designed for seismic forces, are quite vulnerable. Wieland [2005] investigated the hydrodynamic pressure induced in hydropower penstock pipes during earthquake using one-dimensional analytic solution of wave equation and concluded that such pressures may be several folds higher than usually assumed values. Almost all the previous studies did not include most of several influencing factors such as reservoir compressibility, reservoir wave radiation at upstream, reservoir bottom partial wave absorption, gate flexibility, gate joint condition, and gate position with interactive seismic input (as a secondary structure inside the flexible dam body). The relationship offered in valid codes such as codes for hydraulic structures of Japan [Hydraulic Gate and Penstock Assoc. 1996] and the U.S. Army Corps of Engineers [1997] are based on that of Westergaard's although the latter uses the peak ground acceleration but the former uses the gate support peak acceleration. In this study all predominant factors mentioned above are included in an extensive parametric study to arrive at a simplified formula employed in a methodology applicable to engineering application in a straight forward manner. Several numerical tests due to different values of factors and loading functions are examined using standard finite element modeling of fluid-structure dynamic interaction software capable of including such parameters.

THEORIES AND BASIC RELATIONS

Acoustic Waves Propagation in Fluid

Considering a compressible fluid with homogenous, isotropic, invicid with irrotational small amplitude motion, hydrodynamic pressure is governed by the equation:

$$\nabla^2 P = \frac{1}{c^2}\frac{\partial^2 P}{\partial t^2} \tag{1}$$

where c denotes for the acoustic wave velocity in water.

The interaction boundary condition between the dam (or gate) and the reservoir is expressed as:

$$\frac{1}{\rho_f}\frac{\partial p}{\partial n} + \ddot{u}.n = 0 \tag{2}$$

Here ρ_f is water mass density, $\ddot{u}$ the structural acceleration (equal to ground acceleration if the dam is rigid) and "n" the unit outward normal vector to the interface surface. Assuming rigid vertical dam with horizontal harmonic motion the simple Westergaard type solution of maximum pressure for the above equations is expressed as

$$P = 0.875\gamma a_e \sqrt{Hy} \tag{3}$$

in which γ is the water weight density, a_e the seismic coefficient based on the maximum ground (or the dam body) acceleration, H is the reservoir maximum depth, and y the local depth of water. Here the pressure coefficient is constant and equal to 0.875 according to Westergaard's assumptions. Due to deficiencies mentioned earlier, we elaborate further for the time-domain numerical solution.

Reservoir upstream truncation boundary condition is a radiation boundary of Sommerfeld type transparent to travelling waves toward large positive x direction. It is expressed as:

$$\frac{\partial P}{\partial x} = -\frac{1}{c}\dot{P} \tag{4}$$

Reservoir bottom is partially absorbing the incident acoustic waves due to its elastic nature and also due to soft materials and sediments present there. It is well-known that such damping mechanism is significantly affecting the response of the system [Fenves and Chopra 1983]. As the reservoir bottom is assumed horizontal, the boundary condition of reservoir bottom is expressed as:

$$\frac{\partial P}{\partial y} = -\frac{1}{\eta c}\dot{P} \tag{5}$$

where y is the vertical direction, η is the relative acoustic impedance of the reservoir bottom in respect to water. The bottom reflection coefficient of acoustic waves is also defined as α, given by:

$$\alpha = \frac{\eta - 1}{\eta + 1} \tag{6}$$

The two recent boundary conditions cause significant external (versus internal) damping mechanisms. Gravity type surface waves do not contribute much to seismic induced hydrodynamic pressure and thus the free surface boundary condition is simply expressed as

$$P = 0 \tag{7}$$

As the reservoir and the dam are assumed considerably continuous in the transverse direction the reservoir sides boundaries are equivalent to rigid condition and therefore the following relation holds;

$$\frac{\partial P}{\partial n} = 0 \tag{8}$$

in which the unit vector n is parallel to the dam axis coinciding with the z direction.

FINITE ELEMENT MODEL OF THE DAM-GATE-RESERVOIR COUPLED SYSTEM

Foundation interaction has been ignored. The coupled system of dam-gate-reservoir has two separate parts. The part due to the dam and the gate is modeled by Lagrangian approach and the reservoir part by Eulerian approach. The Euler-Lagrangian finite element equation of the dam-gate-reservoir dynamic system is expressed as:

$$\begin{bmatrix} [M] & 0 \\ [h_I] & [E] \end{bmatrix} \begin{Bmatrix} \ddot{u}(t) \\ \ddot{p}(t) \end{Bmatrix} + \begin{bmatrix} [C] & 0 \\ 0 & [A] \end{bmatrix} \begin{Bmatrix} \dot{u}(t) \\ \dot{p}(t) \end{Bmatrix} + \begin{bmatrix} [K] & [f_I] \\ 0 & [H] \end{bmatrix} \begin{Bmatrix} u(t) \\ p(t) \end{Bmatrix} + \begin{Bmatrix} [f_0] \\ [h_0] \end{Bmatrix} = 0 \tag{9}$$

In the above relation, $[M]$ is the mass matrix of the solid part, $[h_I]$ the fluid-structure interaction matrix for fluid excitation, $[E]$ the fluid inertia matrix due to water compressibility, $[C]$ the non-proportional damping matrix pertaining both internal and external damping, $[K]$ the solid part stiffness matrix, $[f_I]$ the fluid-structure interaction matrix for structural hydrodynamic loading, $[H]$ fluid stiffness matrix, $[f_0]$ seismic load of the structure, and $[h_0]$ seismic load of the reservoir through reservoir banks if any. In all models, the internal damping ratio of dam-gate system is considered as ζ=0.05. Mechanical properties of all materials are assumed as linear and constant for all cases considered as in Table 1.

Table 1 Materials mechanical properties.

Gate Steel			Reservoir Water		Dam Concrete		
Elasticity Modulus (GPa)	Poisson's Ratio	Mass Density $\frac{kg}{m^3}$	Bulk Modulus (GPa)	Mass Density $\frac{kg}{m^3}$	Elasticity Modulus (GPa)	Poisson's Ratio	Mass Density $\frac{kg}{m^3}$
211	0.3	7800	2.07	1000	21	0.2	2400

DERIVING A SIMPLIFIED CONSISTENT HYDRODYNAMIC PRESSURE ESTIMATION RELATIONSHIP

Employing the above mathematical forms the following eight steps are taken for each numerical test in order to estimate appropriate value of the hydrodynamic pressure coefficient on the gate to be used in a simplified consistent formula of Westergaard's type.

- construct the rigorous coupled model of the dam, reservoir and the gate
- conduct numerical test as by seismic analysis of the rigorous model
- calculate reservoir hydrodynamic pressure time histories
- collect hydrodynamic pressure time histories at gate nodes facing the reservoir
- allocate time-wise gate local hydrodynamic pressure to its tributary area
- calculate maximum flexural moment M_{max} due to hydrodynamic pressure at the gate section during the seismic excitation
- back-calculate the equivalent Westergaard's pressure to conserve the same internal maximum flexural moment M_{max} at the gate section
- obtain the non-dimensional pressure coefficient: $\beta = \dfrac{P}{A_t \gamma \sqrt{H_y}}$

Here, A_t is the seismic coefficient due to the maximum absolute acceleration of the dam body at the gate center location. The above type of numerical test and process are performed within an extensive parametric study due to a group of test parameters which may vary from one site to another. The parameters are listed as:

- Dam height and profile type
- Gate elevation (position) on the dam body
- Gate plate thickness & slenderness ratio
- Gate supports boundary conditions
- Reservoir bottom acoustic wave reflection coefficient
- Seismic input frequency content

The ranges of variation of these parameters are within appropriate intervals assigned for each, and are based on known dam engineering experiences.

Dam Height, Profile Types, and Gate Elevations

Two monoliths of 50 m width from the two different types of gravity dams, one similar to the famous American Pine Flat dam as a classic profile, and the other similar to the Iranian Shafarood Dam as a modern profile were considered (Figure 1). In addition to the original dam height, two alternative heights equal to 80 and 200 m are also considered for each profile type.

The original dam height and reservoir depth for Shafarood dam are 142.9 and 140 m respectively, whereas for Pine Flat dam these are equal to 122 and 116.9 m. The reservoir models lengths are almost twice their corresponding depth as shown typically in Figure 2 along with different gate locations. Gates are placed on the upstream side of the dam body and adjacent to reservoir.

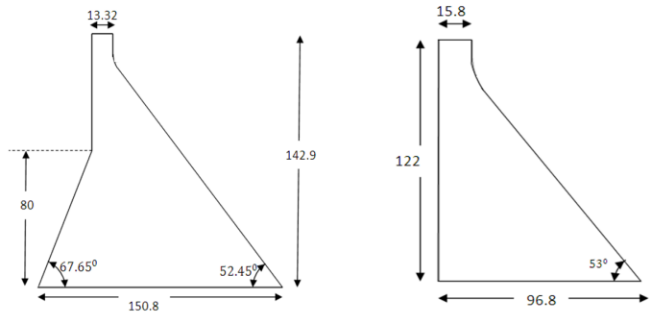

Shafarood Dam **Pine Flat Dam**

Figure 1 Original geometry of dam types

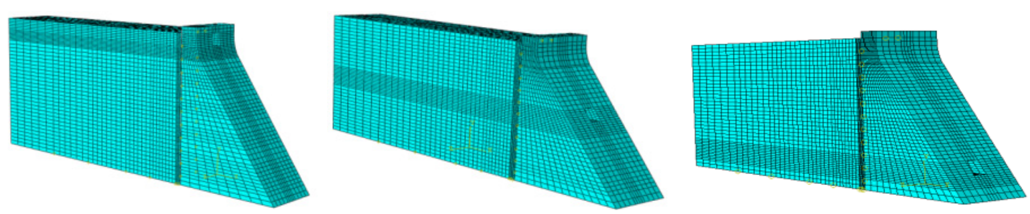

(a) (b) (c)

Figure 2 Three-dimensional view of Pine Flat dam-reservoir system and gate position in the dam body: (a) upper gate or spillways; (b) mid-height gate or orifice; and (c) bottom gate or bottom outlet.

Gate Plate Thickness and Gate Supports Boundary Conditions

Gates are rectangular with thicknesses of 4 to 25 cm and width to thickness (or slenderness) ratios varying between 40 and 333. The equivalent thickness has been calculated in order to conserve the actual moment of inertia when using stiffeners against flexural lateral deformation. Eight-node shell elements have been used to model these gates. These gates are sliding type ones and may have different boundary condition types in their connection with the supporting structure, i.e., the dam body. Therefore three types of usual boundary conditions are considered as “3-sides hinged and one side free”, “all-sides hinged”, and “all-sides clamped.”

Reservoir Bottom Reflection Coefficient and Seismic Input Types

In all analyses cases, the reflection coefficient of acoustic waves at the reservoir bottom is considered at one of the three conditions of full absorption (α=0), medium absorption (α=0.5), and considerable reflection of acoustic waves (α=0.8).

As for the seismic input types, main shocks of three natural and one artificial accelerograms are used with a time duration of about 10 sec. All the natural records correspond to rock foundations and include Northridge (1994), Koyna (1967), and San Fernando (1971) ground motions. All the selected records are scaled as to fit the original Koyna dam earthquake that is their peak ground accelerations are equal to 0.47*g*. Furthermore as a different type of ground motion, using the Iranian Seismic Code [Standard 2800] soil type-I spectrum an additional record of artificial type with the same PGA is also generated for analysis (Figures 3 and 4).

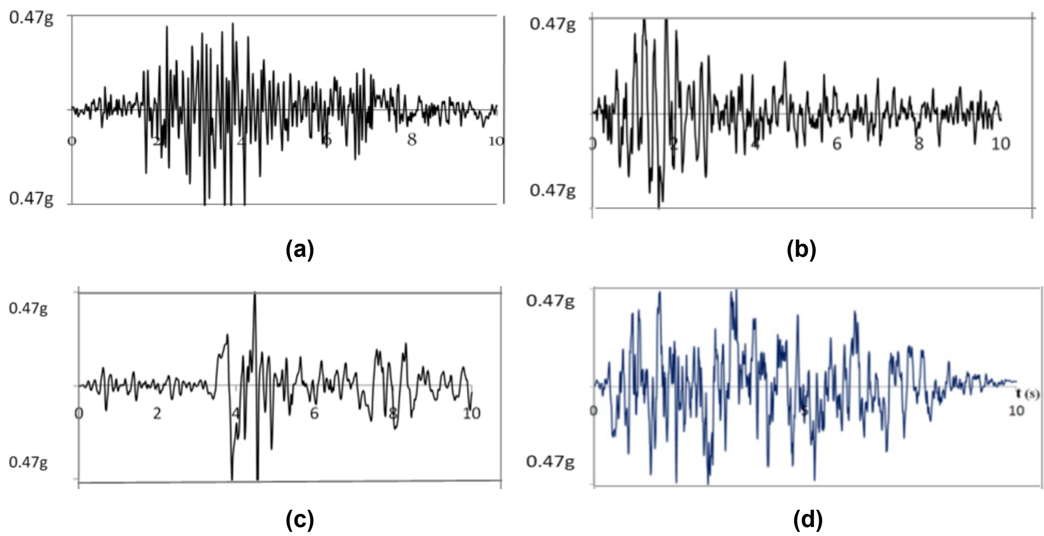

Figure 3 Different horizontal ground motion records employed: (a) Koyna Dam Station 11 December 1967; (b) San Fernando Fairmont Dam Station 9 February 1971; (c) Northridge Pacoima Dam 17 January 1994; and (d) Iran Standard 2800 spectrum compatible.

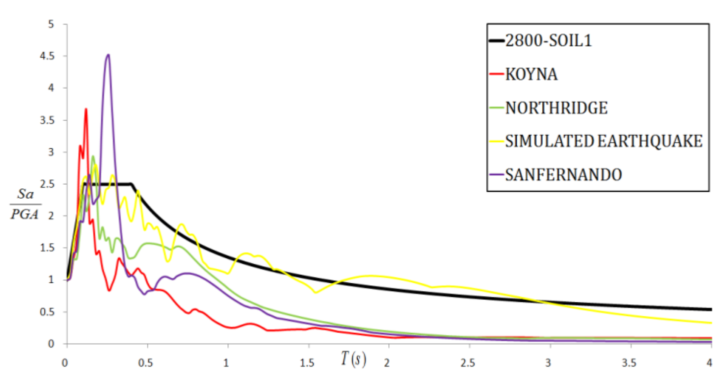

Figure 4 Response spectra of ground motion records employed in the analyses

ANALYSIS RESULTS AND DISCUSSIONS

Extensive number of analyses are made for the types of dams with different heights including the original ones. Typical variations of the pressure coefficient β versus gate slenderness ratios (b/t values) are shown in Figure 5 for totally hinged support top gate under the Iranian Code compatible ground motion. It is seen that once slenderness coefficient reaches a specific value (e.g., b/t=140), an amplification of response may occur. This phenomenon should be due to the resonance of the gate local mode of vibration (coupled with the neighboring reservoir and with circular frequency of $\omega_{G\text{-}R}$) with its supporting dam response dominated by a major system natural mode. Different bottom reflection coefficients, α are also examined and proved to be of medium importance for the hydrodynamic pressure coefficient. It is also well seen that the pressure coefficient is far from a constant value and its variation intervals are rather large; 0.25−2.25 for the Pine Flat Dam, and 0.25−1.9 for the Shafarood Dam (both with original height). Westergaard's coefficient (β=0.875) is only a near-average value for β. It could not be reliable due to excessive underestimation of hydrodynamic forces in a large interval of plate slenderness ratios; i.e., when b/t corresponds to a value of $\omega_{G\text{-}R,}$ falling in the vicinity of the dominant frequency of the dam-reservoir system response.

As shown the Figures 6 and 7, additional tests on Pine Flat dam with original height and under the same conditions stated above suggests more or less similar patterns and explanations regardless to different boundary conditions of gate support, different gate elevations, different seismic motions etc. although additional observation suggests higher pressure coefficient for lower gates. The tests process is fully followed for different dam heights as well to accomplish a statistically valid population of data for each gate elevation condition. The produced data corresponding to each gate elevation amounts to 210 numerical tests results.

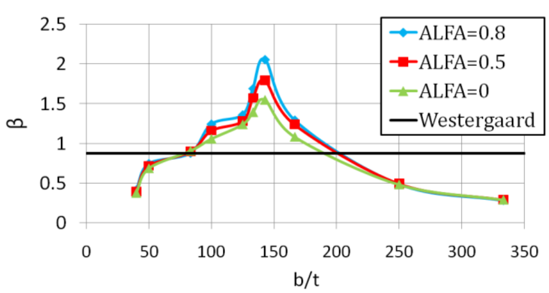

Pine Flat Dam

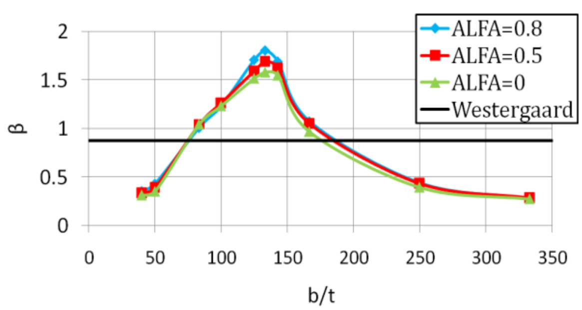

Shafarood Dam

Figure 5 Hydrodynamic pressure coefficient variation versus plate slenderness ratios for the top gates of original height dams (all-sides hinged gate) due to Iranian Seismic Code compatible ground motion

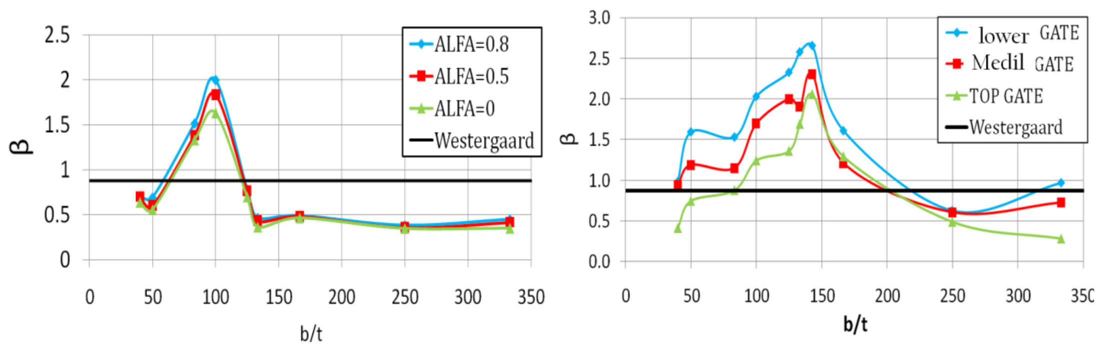

(a) Pine Flat Dam **(b) Shafarood Dam**

Figure 6 Hydrodynamic pressure coefficient variation versus plate slenderness ratios: (a) for the top gate of Pine Flat dam (3-sides hinged and one side free gate); and (b) for different gates positions on the original Pine Flat dam (all-sides hinged gate and *α* = 0.8) due to Iranian Seismic Code compatible ground motion.

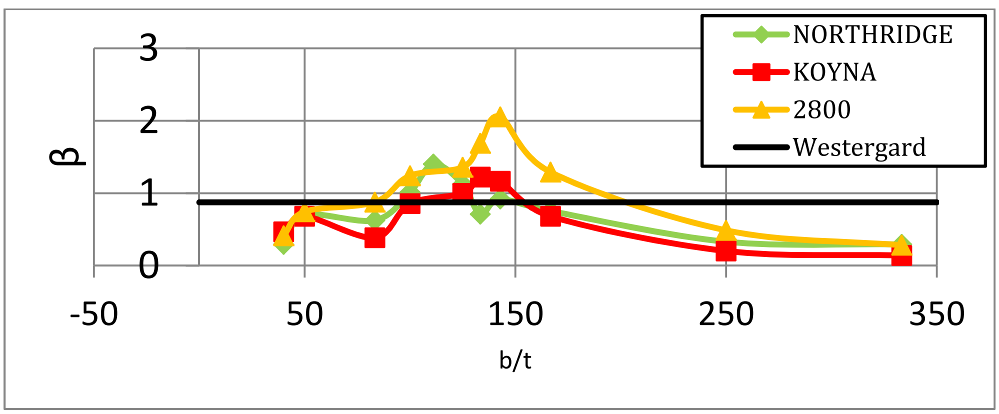

Figure 7 Hydrodynamic pressure coefficient variation versus plate slenderness ratios for top gate on the original Pine Flat dam (all-sides hinged gate and *α* = 0.8) due to different ground motions.

FLOOR-SPECTRAL FORMULATION OF HYDRODYNAMIC PRESSURE

The highly variable β value during these tests prevents simple and constant determination of its value. Indeed, correlation of the gate natural frequency and the predominant response of the dam-reservoir system affected by the input motion may well describe the high fluctuation of β. Thus response spectrum of the gate support motion (or floor response spectrum) is studied for each test set. For example, Figure 8 shows the floor response spectra of top gate position in Pine Flat dam due to three types of ground motion. The corresponding pressure coefficient variations are already plotted in Figure 7. Typical high similarities of these figures curves support the idea and thus it is decided to re-establish the basic relation of hydrodynamic pressure in terms of floor spectral peak acceleration (or corresponding seismic coefficient S_a) values [Equation (10)] rather than ground or absolute peak acceleration (or corresponding seismic coefficient A_t) values used in Equation (3). In fact the peak value of S_a in each floor spectrum corresponds to $\omega_{G\text{-}R}$. The floor spectra needs to be obtained at the damping level ζ, assigned for the system. In most cases 0.05 for the damping level may be assigned. It is so fortunate that the new version of pressure coefficient, λ, is statically more reliable as its variation interval is quite limited (0.5 to 0.99 for top gates) compared to the corresponding β values varying between 0.25 to 2.5, i.e., a tenfold change.

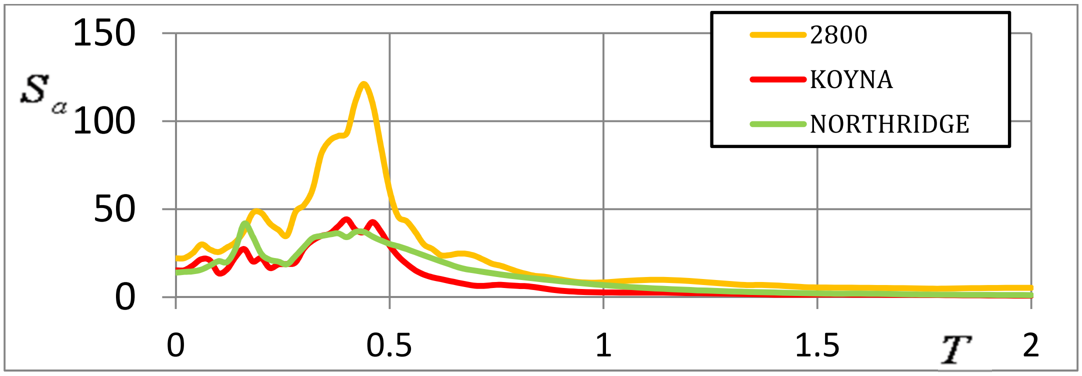

Figure 8 **Floor response spectra of top gate support on the Pine Flat Dam body due to different earthquakes.**

$$P = \lambda S_a\left(\omega_{G-R}, \xi\right).\gamma.\sqrt{H.y} \tag{10}$$

$$\lambda = \frac{P}{S_a\left(\omega_{G-R}, \xi\right).\gamma.\sqrt{H.y}} \tag{11}$$

STATISTICAL DETERMINATION OF THE MODIFIED PRESSURE COEFFICIENT Λ

Limiting ourselves to conservative tests with bottom reflection coefficient α = 0.8 and including different dam geometry, dam height, gate support B.Cs., and ground motion type, the probability distribution of λ for the top gate is fitted with standard lognormal distribution. The corresponding mean and standard deviation values are found equal to 0.65 and 0.14, respectively. Based on engineering judgment, the mean plus half the standard deviation is expedited as sufficiently safe value and thus the final prescribed value of the non-dimensional hydrodynamic pressure coefficient for top gate floor-spectral formulation could be assumed constant and equal to λ=0.72. The same process for the mid-height and bottom gates (which proved to be close together) yields λ= 0.98.

CONCLUSIONS

Large dam gates are of major importance for safe operation of dams. Seismically induced hydrodynamic pressure exerted to such gates have proved to be critical. Thus the present work has exploited the state-of-the-art modeling techniques of fluid-structure dynamic interaction in order to derive a reliable simplified relationship applicable to gravity dams with different gate dimensions, gate position, dam geometry, gate connection conditions, reservoir bottom reflection coefficient, and ground motion types. Application of the formula to actual new cases is quite compatible with the standard dam design and analysis procedure and is presented in the flow-chart shown below, Figure 9.

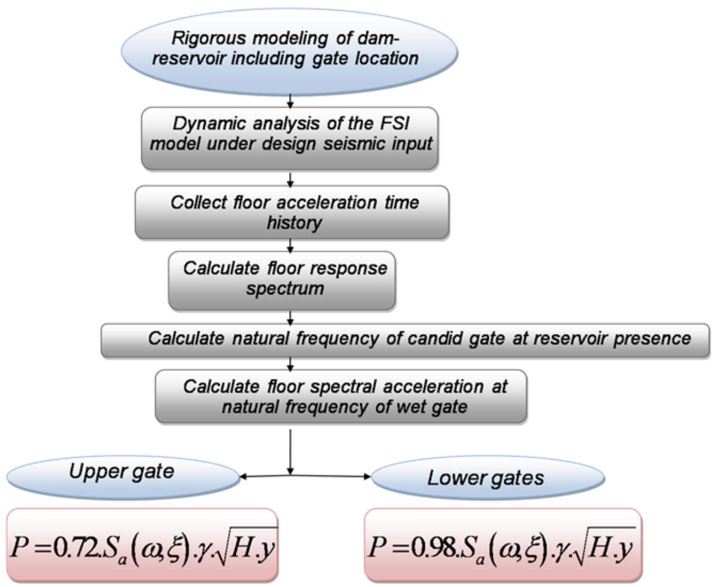

Figure 9 Algorithm of seismic hydrodynamic pressure estimation for gravity dam gates

REFERENCES

Chopra A.K. (1989). Simplified evaluation of added mass for intake towers, ASCE, *J. Struct. Eng.*, ASCE, 115: 1393−1412.

Daniell W.E. Taylor C.A. (2000). The seismic safety evaluation of a radial flood gate, *Proceedings, ICOLD 20th Congress on Large Dams, IV*, Q79-R9, pp. 123−132.

Fenves G.L., Chopra A.K. (1983). Effects of reservoir bottom absorption on earthquake response of concrete gravity dams, *Earthq. Eng. Struct. Dyn.*, 11(6): 809–829.

Hydraulic Gate and Penstock Association [1996]. *Technical Standards for Gates and Penstocks*, Japanese Standards.

ICOLD (1999). Design and evaluation of appurtenant structures to seismic shaking, International Committee on Large Dams, *Bulletin 123*, Paris, France.

Kojic S.B., Trifunac M.D. (1988). Transient pressures in hydrotechnical tunnels during earthquakes, *Earthq. Eng. Struct. Dyn.*, 16: 523–539.

Seda-Sanabria Y., Hall R.L., Suarez L.E. (1998). Hydrodynamic study of the Olmset wicket gate using a 1:25-scale model, *J. Mech. Systems*, 12(5): 661−677.

USACE [1997]. *Vertical Lift Gates, EM 1110–2–2701*, U.S. Army Corps of Engineers, Washington, D.C.
Westergaard H.M. (1933). Dynamic water pressure on dams during earthquake, ASCE, *Transactions*, 98: 418–433.
Wieland M. (2005). Hydrodynamic pressures, in: *International Water Power and Dam Construction*, 20 September.

SEISMIC DAMAGE ASSESSMENT OF CONCRETE ARCH DAMS

Mohammad Alembagheri[1] and Mohsen Ghaemian[2]

ABSTRACT

Damage assessment of concrete arch dams is carried out through nonlinear Incremental Dynamic Analysis (IDA) of a typical arch dam. In this study the Morrow Point arch dam is subjected to a set of twelve three-component earthquakes each scaled to twelve increasing intensity levels. Damage propagation through the dam body is investigated and various IDA curves are created. The performance and various limit-states of the dam structure are examined based on the obtained results. Simple damage indices are proposed through comparison of response demands in earthquake analysis with the determined structural capacities. It was found that the proposed damage indices can properly indicate state of damage in the dam body.

INTRODUCTION

Throughout the world there are hundreds of high concrete dams, the failure of which due to seismic activities could result in heavy loss of human life and substantial property damages [Valliappan et al. 1999]. Behavior of a concrete dam in an earthquake and its structural losses is an important issue in seismic assessment of concrete dams. Concrete arch dams are among large concrete dams that need to be investigated for this purpose. Potentially an arch dam may fail as a result of (a) excessive contraction joint opening combined with cantilever tensile cracking, (b) movements of abutment rock wedges formed by rock discontinuities, and (c) in certain cases sliding along the gently sloped dam-abutment interface [Ghanaat 2004]. There are generally two sources of nonlinearity in behavior of arch dams: material nonlinearity due to tensile cracking or compressive crushing of mass concrete; and geometric nonlinearity due to the opening of contraction or lift joints. Several methods such as fracture and damage mechanics have been utilized for nonlinear analysis of concrete dams for detection of crack initiation and its propagation through the dam body [Dowling and Hall 1989; Niwa and Clough 1982; Feng et al. 1996; Cervera et al. 1996; Lofti and Espoandar 2004]. Using the well-established methods and with the aid of powerful computers it is now possible to efficiently perform time-consuming analysis methods such as incremental dynamic analysis (IDA) for large structures such as arch dams. In the IDA a series of earthquake records has been applied with increasing intensity to the structure that leads the structure to its severer limit-states [Vamvatsikos and Cornell 2002]. Performance and various limit-states of the structure, thus, can be determined through the IDA.

Presented herein is the IDA of Morrow Point arch dam, which has been extensively investigated by other researchers. Morrow Point dam is an almost perfectly symmetric arch dam, 142 m height, 219 m crest length, 3.7 m crest thickness, and 16 m base thickness [Hall 1998].

[1] PhD Candidate, Department of Civil Engineering, Sharif University of Technology, Tehran, Iran; email: Alembagheri@mehr.sharif.edu
[2] Associate Professor, Department of Civil Engineering, Sharif University of Technology, Tehran, Iran; email: Ghaemian@sharif.edu, Tel: +98 21 66164242, Fax: +98 21 66014828.

The IDA study of the Morrow Point arch dam is presented using a set of twelve earthquake ground motions. The objective is deep investigation of a case study using one of the proposed nonlinear models of the mass concrete to rigorously determine its seismic performance and various limit-states under different earthquake ground motions. The dam is modeled using finite-elements along with its reservoir and foundation in three-dimensional space. The plastic-damage model proposed by Lee and Fenves [1998] is utilized for nonlinear analyses and determination of damage propagation in the dam body. Three components of the selected earthquakes are scaled simultaneously with respect to the spectral intensity of the stream component. The performance and various limit-states of the dam structure are recognized and it is attempted to categorize the damage imposed to the dam body in terms of the ground shaking intensity. Finally some damage indexes are proposed for assessment of imposed damage and determination of residual structural capacity after any seismic event.

NUMERICAL MODELING

The Morrow Point dam-reservoir-foundation system is modeled using finite-elements as shown in Figure 1. The undamaged modulus of elasticity (E_0), Poisson's ratio (υ_c), density (ρ_c), dynamic tensile strength (σ_{t0}) and compressive strength of the mass concrete of the dam is considered 27.579 GPa, 0.2, 2483 kg/m^3, 2.9 MPa and 30 MPa, respectively. For the foundation rock layer, Young's modulus (E_f) is considered same as the dam's one, with Poisson's ratio υ_f =0.2 and density ρ_f =2643 kg/m^3. In this study the effects of stiffness, inertia and damping of the foundation are considered to more precisely model the actual system. The density of water is assumed to be ρ_w=1000 kg/m^3. The transmitting boundary conditions are applied at the reservoir far-end; and infinite elements are used for modeling of wave radiation at the foundation edges. The non-absorptive reservoir boundary is considered for the reservoir bottom. The damping for the dam and foundation materials is considered using the Rayleigh method [Hall 2006]. The mass- and stiffness-proportional damping coefficients are set as 1.679 and 0.001026 so that produce approximately 5% critical damping for the first six vibration modes of the system. The dam is modeled without any joints, thus the potential failure mode of the dam structure is tensile cracking along the abutments and through the dam body [Ghanaat 2004].

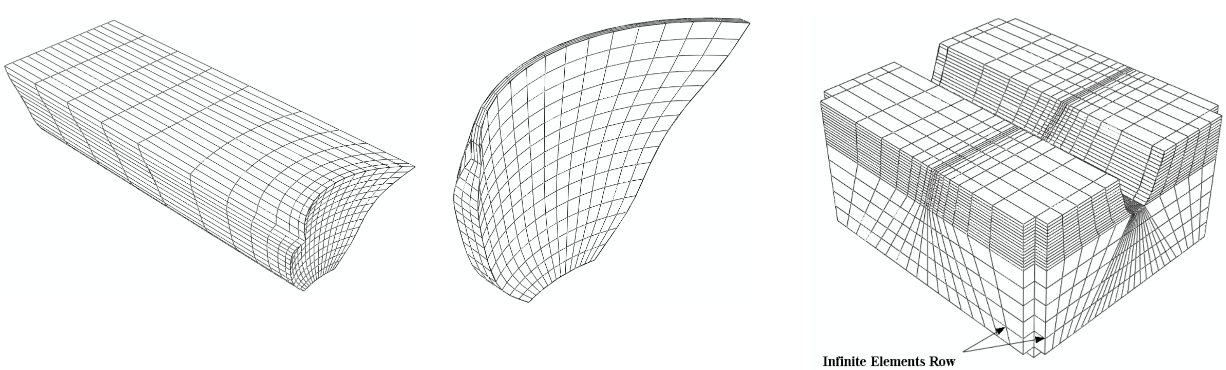

Figure 1 Finite-elements mesh of the dam, reservoir, and foundation.

The 8-node cubic elements are used for entire model; three finite element rows are placed through the dam thickness to distinguish the damage of the upstream and downstream faces. The plastic-damage model [Lee and Fenves 1998], which is a continuum homogenous damage mechanics approach, is used for modeling the nonlinear behavior of the mass concrete. In this approach the tensile damage is addressed by normal strain at any point. After the elastic limit, the material is softened based on a considered constitutive behavior. This behavior is characterized by tensile damage (d_t) parameter that shows stiffness degradation at any normal strain. The considered behavior of the mass concrete in this study is shown in Figure 2.

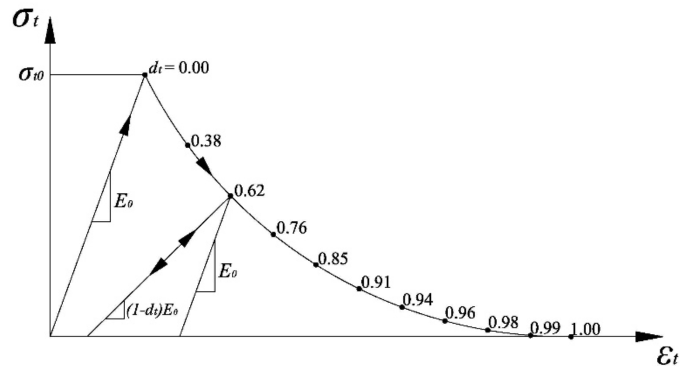

Figure 2 Considered constitutive behavior of mass concrete in tension.

THREE-DIMENSIONAL IDA

In an IDA study, a series of earthquake ground motions are applied to structure. By increasing the earthquakes intensity, the structure is shifted from its initial elastic state into a series of successive inelastic states and finally to the collapse. In this way its seismic performance and structural capacities can be identified [Vamvatsikos and Cornell 2002]. Determination of the structural capacities makes possible the determination of the structure's safety margin after seismic events. An IDA curve is a curve in which the horizontal axis is the damage measure (DM) or engineering demand parameter (EDP) that shows the structural responses; and vertical axis is the intensity measure (IM) that shows the shaking intensity [Vamvatsikos and Cornell 2004]. The IDA studies are normally performed using one-component earthquakes. Thus the PGA or spectral acceleration of that component is a good choice for IM. In arch dams it is required to do three-dimensional seismic analysis using three-component earthquakes. In this study different parameters are set as IM to investigate the effects of each parameter in scattering of the DM values. The selected DMs were chosen to be maximum radial and vertical crest displacement at crown cantilever, and damage energy dissipation.

In each seismic analysis first the static loads including the self-weight of the dam and the hydrostatic load on upstream face of the dam are applied and then the three components of the selected earthquakes are uniformly applied at the dam-foundation interface. The earthquakes are tabulated in Table 2. These earthquakes belong to a bin of relatively large magnitude records each recorded on stiff soil (rock), and extracted from PEER strong-motion database. Since the stream component is the most significant one in seismic response of arch dams [Fok and Chopra

1986], the earthquakes are scaled based on the 5% damping spectral acceleration of the stream components at the first-mode period of the coupled dam-reservoir-foundation system. The earthquakes are scaled so that they have 0.1*g* to 1.2*g* spectral acceleration with 0.1*g* steps in stream direction.

The IDA curves are plotted using spline interpolation between discrete points. The running mean and median methods are used to summarize an IDA curve set to one representative IDA curve. In these methods the mean and median of the DMs at each level of IM is calculated to form the Mean and Median representative curves, respectively. In addition, the mean plus one standard deviation (STDEV), i.e., 84% fractile, and the mean minus one standard deviation, i.e., 16% fractile, representative curves can be plotted [Vamvatsikos and Cornell 2004].

Table 2 The earthquakes used in the IDA analysis.

No	Earthquake	Name	Magnitude (M)	Distance (R)	USGS Soil Classification	Un-scaled PGA (g) Stream	Cross-Stream	Vertical
1	Imperial Valley, 1940	IVELC	7.0	8.3	C	0.313	0.215	0.205
2	Imperial Valley, 1977	IVPTS	6.5	14.2	B	0.204	0.111	0.159
3	Kern County, 1952	KCTAF	7.4	41.0	B	0.178	0.156	0.109
4	Landers, 1992	LADSP	7.3	23.2	B	0.171	0.154	0.167
5	Loma Prieta, 1989	LPAND	6.9	21.4	B	0.244	0.240	0.151
6	Loma Prieta, 1990	LPGIL	6.9	11.6	B	0.357	0.325	0.191
7	Loma Prieta, 1991	LPSTG	6.9	13.0	B	0.512	0.324	0.389
8	Morgan Hill, 1984	MHG06	6.2	11.8	B	0.292	0.222	0.405
9	Northridge, 1994	NRORR	6.7	22.6	B	0.514	0.568	0.217
10	Northridge, 1995	NRPUL	6.7	8.0	A	1.585	1.285	1.229
11	San Fernando, 1971	SFPAS	6.6	31.7	B	0.110	0.088	0.095
12	San Fernando, 1972	SFPPP	6.6	38.9	B	0.136	0.102	0.050

RESULTS AND DISCUSSION

The IDA curves sets of the maximum radial crest displacement are shown in Figure 3 in which the PGA and 5% damping first- and second-mode spectral accelerations of various components are selected as IM. As can be seen the minimum dispersion belongs to the curves set in which the first-mode spectral acceleration of stream component, i.e., $S_{a,\mathrm{stream}}(T_1,5\%)$, is selected as IM. In this curve [Figure 3(b)] there is strict consistency between various records; almost records have IDA curves between 16% and 84% fractiles in total range of IM. This consistency is observed for other DMs. Results show that the dam's response is essentially dependent on the first-mode spectral acceleration of stream component; and the response to different earthquakes scaled to the same $S_{a,\mathrm{stream}}(T_1,5\%)$ is predictable. The low dispersion improves the accuracy of determined limit-states especially the ultimate one from IDA curves. Thus the first-mode spectral acceleration of the stream components is considered as IM in the rest of the study. The IDA curves set for maximum vertical crest displacement is shown in Figure 4. As can be seen from

Figures 3 and 4 there is excellent agreement between the mean and median curves over all range of $S_{a,\mathrm{stream}}(T_1,5\%)$. This shows that the DM values are evenly distributed at each level of IM.

An investigation of the dam's damage contours shows that there is no damage up to the $S_{a,\mathrm{stream}}(T_1,5\%)=0.2g$, the value at which the first damage has appeared at the dam's heel on the upstream face (see Figure 10). This value can be an indicator of "yielding" or "base-cracking" limit-state. In this state the dam crest on the crown cantilever has mean maximum displacements of 1.18cm in radial and 0.09 cm in vertical directions with the 0.15 cm and 0.02 cm standard deviations (STDEV), respectively. Low amount of normalized dispersion (STDEV/mean; i.e., 0.12 and 0.22 for radial and vertical displacements) implies that the "yielding" limit-state can be defined based on both IM ($S_{a,\mathrm{stream}}(T_1,5\%)$) and DM (maximum crest displacement). By increasing the shaking intensity the damage is propagated along the dam base and abutment on the upstream face until $S_{a,\mathrm{stream}}(T_1,5\%)\approx 0.6g$. From Figures 3(b) and 4 it is seen that the IDA curves apparently follow the elastic section until this limit. This shows that the base and abutment cracking do not significantly alter the crest displacements. The damage rises to about half of the dam height and is observed only on the upstream face, and is appeared on the top of the dam in more intense shakings. Normally, vertical cracks are developed at the midpoint and quarter-points of the crest after $S_{a,\mathrm{stream}}(T_1,5\%)=0.7g$ that propagate from the dam crest to its base and observed on the both upstream and downstream faces. They can be related to the opening of the contraction joints that are not modeled in this study. The above explanations can be clearly seen in Figure 5 that shows the IDA curves set of the damage energy dissipation. The hardening problem which is a common issue in IDA curves of buildings is not significantly observed in the IDA curves of the arch dam. This can be attributed to the very brittle nature of the mass concrete and shows that as the intensity of the shaking increases more damages appear.

As can be seen in Figure 5, the amount of the damage, which can be assessed by the damage energy dissipation, has negligible value up to $S_{a,\mathrm{stream}}(T_1,5\%)=0.2g$; and approximately the same value until the $S_{a,\mathrm{stream}}(T_1,5\%)=0.6g$. It was observed that the dam suffered almost the same damage under various earthquakes with intensity up to the mentioned limit. Initiation of cracking at the top of the dam body after $S_{a,\mathrm{stream}}(T_1,5\%)=0.7g$ is simultaneous with the increase of the damage energy dissipation rate. This rate growth is also observed in the maximum displacement IDA curves (Figures 3 and 4), that shows the significant effects of the top cracking on the displacements. After $S_{a,\mathrm{stream}}(T_1,5\%)=0.7g$ the amount of residual crest displacements highly increase, always in upstream and up-direction for radial and vertical displacements, respectively. Thus the $S_{a,\mathrm{stream}}(T_1,5\%)=0.6g$ can be considered as "top-cracking" limit-state. In this state the dam has the mean maximum crest displacements of 3.47 cm and 0.26 cm in radial and vertical directions with the 0.51 cm and 0.07 cm standard deviations, respectively. There is mean damage energy dissipation of 3.12 MJ at this limit-state. Again the low normalized dispersion (0.15 and 0.27 for radial and vertical displacements) implies that this limit-state can be defined both on IM and DM. Until $S_{a,\mathrm{stream}}(T_1,5\%)=0.7g$ there is no damage-through along the dam thickness in none of the earthquake analyses. There is no damage-through at the base of the dam even at high shaking intensities such as $S_{a,\mathrm{stream}}(T_1,5\%)=1.2g$.

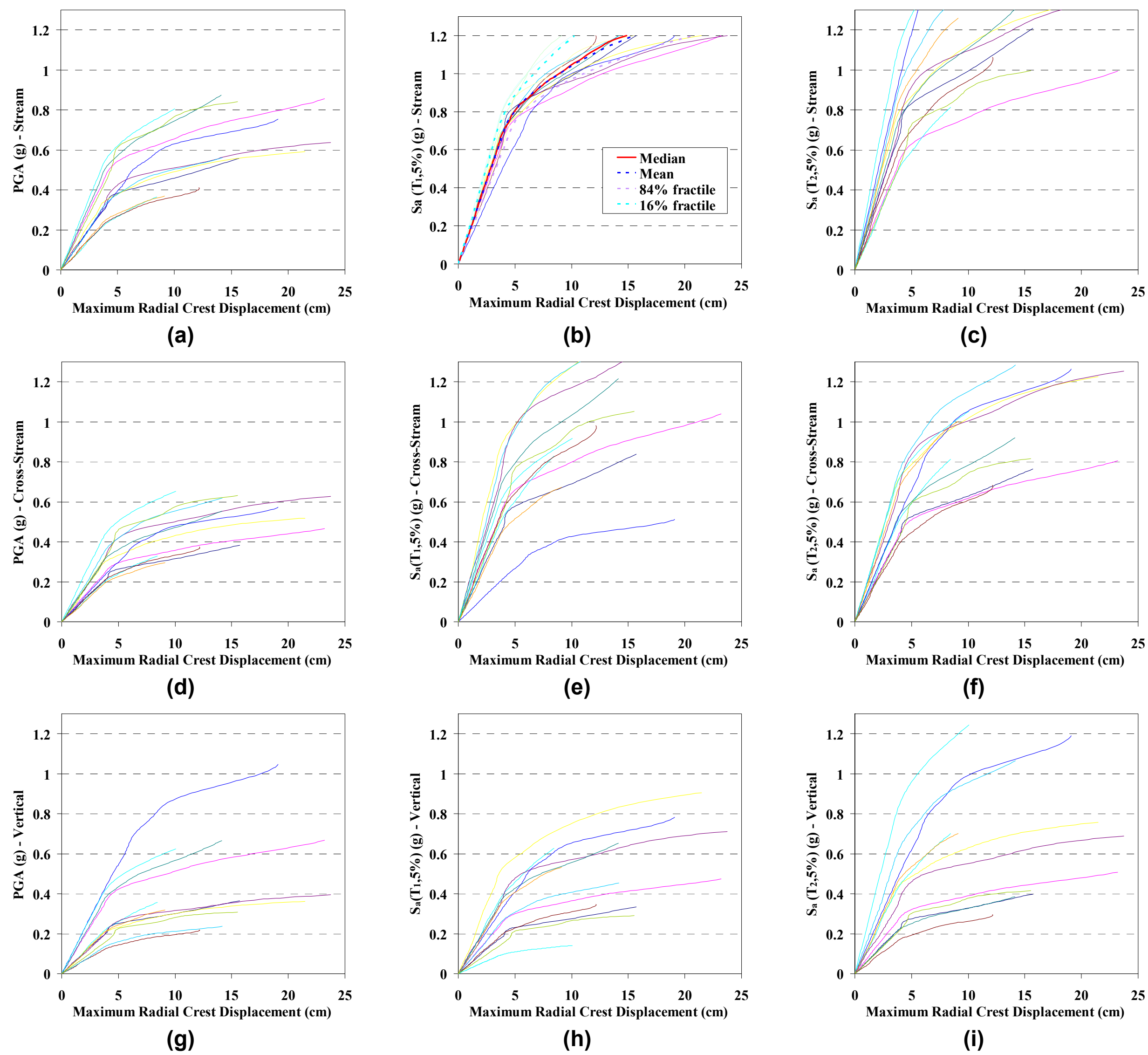

Figure 3 **The IDA curves sets of maximum radial crest displacement in terms of various IMs**

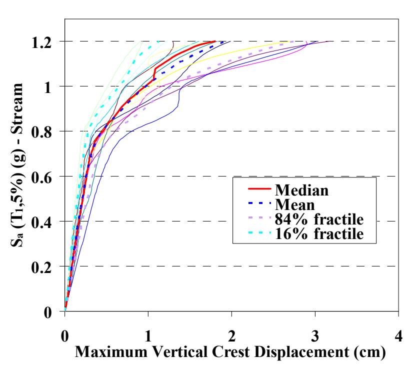

Figure 4 **The IDA curves set for maximum vertical crest displacement**

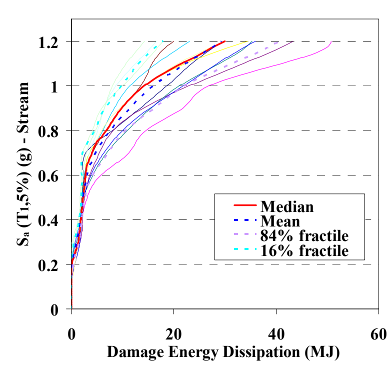

Figure 5 **The IDA curves set for damage energy dissipation.**

After formation of vertical cracks, stress values in the vertical (cantilever) direction increase, causing the horizontal cracks between the vertical ones. This is sometimes simultaneous with a diffused cracking pattern that shows the vastness of the damage. Observation of such damages on the both upstream and downstream faces shows the possibility of generation of the partially-free blocks that can individually vibrate (Figure 6) [Ghanaat 2004]. This state can be structurally attributed to the ultimate state where the dam structure requires substantial repairs. It is decided to determine this limit-state based on the IM [Vamvatsikos and Cornell 2002]. At high earthquake intensities the amount of damage is more on the downstream face than the upstream one. After $S_{a,\mathrm{stream}}(T_1,5\%)=1.0g$, the damage-through state is observed such that the generation of the above-mentioned partially-free blocks are possible. However this limit is not the same among all records, but it can be said that the earthquake with $S_{a,\mathrm{stream}}(T_1,5\%)\geq 1.2g$ causes excessive cracking that can be considered as "ultimate" limit-state or "collapse." At the "ultimate" limit-state the dam crest on the crown cantilever has maximum deflections in the range of 9.13–23.73 cm and 0.91–3.17 cm in radial and vertical directions, respectively. The above-mentioned limit-states are shown on the Mean IDA curves in Figure 7.

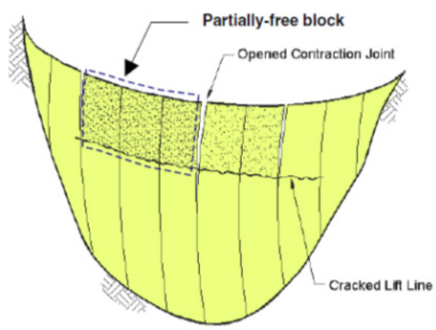

Figure 6 Generation of partially-free blocks [Ghanaat 2004].

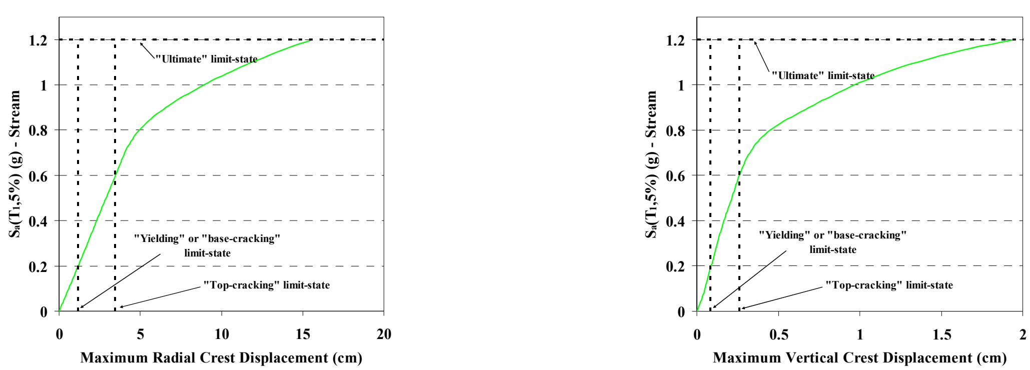

Figure 7 The dam's limit-states on the mean IDA curves.

DAMAGE INDEX PROPOSAL

Based on the obtained results of the IDA study, now it is possible to calculate the damage imposed to the dam body in earthquakes by comparison of the responses demanded in seismic events with the determined structural capacities from the IDA study. Two damage indices can be defined as follows:

Based on the maximum crest displacement:

$$DI_u = \frac{u_{\max} - u_y}{u_u - u_y} \tag{1}$$

in which u_{max} is the maximum crest displacement in an earthquake analysis, u_u and u_y are respectively the maximum crest displacement at "ultimate" and "yielding" limit-states that are defined from the IDA study. If $u_{max} < u_y$ then DI_u=0.0 and if $u_{max} > u_u$ then DI_u=1.0.

Based on the damage energy dissipation

$$DI_E = \frac{E_{\max}}{E_u} \tag{2}$$

in which E_{max} is the damage energy dissipation in an earthquake analysis and E_u is the damage energy dissipation at "ultimate" limit-state that is defined from the IDA study. If $E_{max} > E_u$, then DI_E=1.0.

For the studied dam model, the values of u_y and u_u are 1.18 cm and 15.56 cm for radial direction and 0.09 cm and 1.945 cm for vertical direction; and the value of E_u is 29.28MJ. The normalized dispersion (the coefficient of variation, c_v) of the response results (DMs) at every level of IM for the dam model is shown in Figure 8. The low amount of dispersion at "yielding" and "ultimate" limit-states can imply the accuracy of the defined structural capacities.

In addition to the defined damage indices a global damage index can be defined as

$$D_{global,1} = \frac{\sqrt{\sum_e \int_{v_e} (d_t)^2 \, dv_e}}{\sqrt{\sum_e \int_{v_e} dv_e}} \tag{3a}$$

$$D_{global,2} = \frac{\sum_e \int_{v_e} (d_t) \, dv_e}{\sum_e \int_{v_e} dv_e} \tag{3b}$$

where d_t is the tensile damage at individual elements. These indexes are linear and quadratic weighted average of the damage of individual elements over their volume (v_e). They are directly related to the damage energy dissipation. They have "unit" value when all elements of the dam model are totally damaged. This state is not realistic, thus they can be defined over regions of the dam which experience damage in the determined "ultimate" limit-state, e.g., at $S_{a,\mathrm{stream}}(T_1,5\%)=1.2g$ for the studied dam model. These regions are shown in Figure 9. Also these indices can be set such that they are calculated over entire dam model but have "unit" value at the "ultimate" state. The damage contours of the studied dam model under KCTAF record at some shaking intensity levels are shown in Figure 10.

The determined limit-states of the studied arch dam now can be defined based on these global cumulative indices. For the studied dam model, the calculated global indices over entire dam for the performed seismic analyses are shown in Figure 11. They have a trend same as the damage dissipated energy IDA curves. At $S_{a,\mathrm{stream}}(T_1,5\%)=0.2g$, the mean values of the global damage indices are $D_{global,1}=0.036$ and $D_{global,2}=0.003$ that is assumed as "yielding" limit-states. However, the $D_{global,2}$ more clearly shows the negligible damage. At $S_{a,\mathrm{stream}}(T_1,5\%)=0.6g$, i.e., "top-cracking" limit-state, the mean indices are $D_{global,1}=0.203$ and $D_{global,2}=0.043$. The dispersion of the global indices at various intensity levels are low, depicted in Figure 12. The lower dispersion shows the higher accuracy of the defined indices. At the "ultimate" limit-state the mean indices are $D_{global,1}=0.577$ and $D_{global,2}=0.352$. These values can be scaled to 1.0 to present total "collapse" at "ultimate" limit-state and then based on the determined scale factors other indices at various limit-states can be obtained. The scaled mean global indices at various limit-states for the dam model are tabulated in Table 3.

Table 3 Mean scaled values of global indices.

Limit-State	$D_{global,1}$	$D_{global,2}$
Yielding (Base-cracking)	0.062	0.008
Top-cracking	0.352	0.122
Ultimate (Collapse)	1.000	1.000

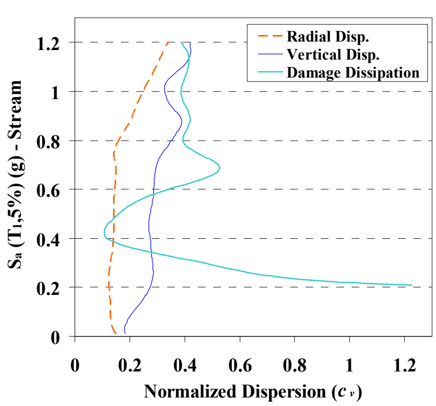

Figure 8 Normalized dispersion of the IDA results at various intensity levels.

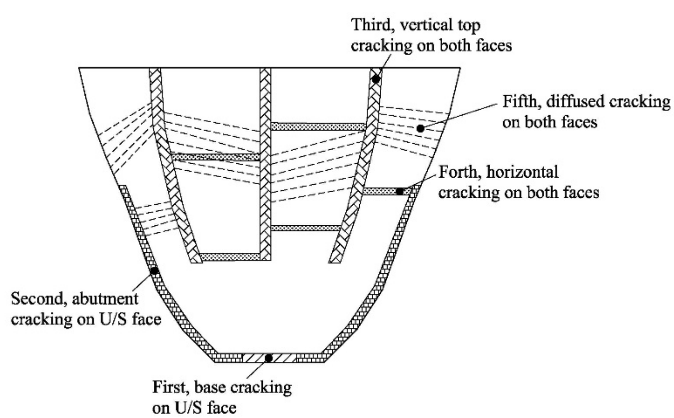

Figure 9 Sequence of the damage in the dam body.

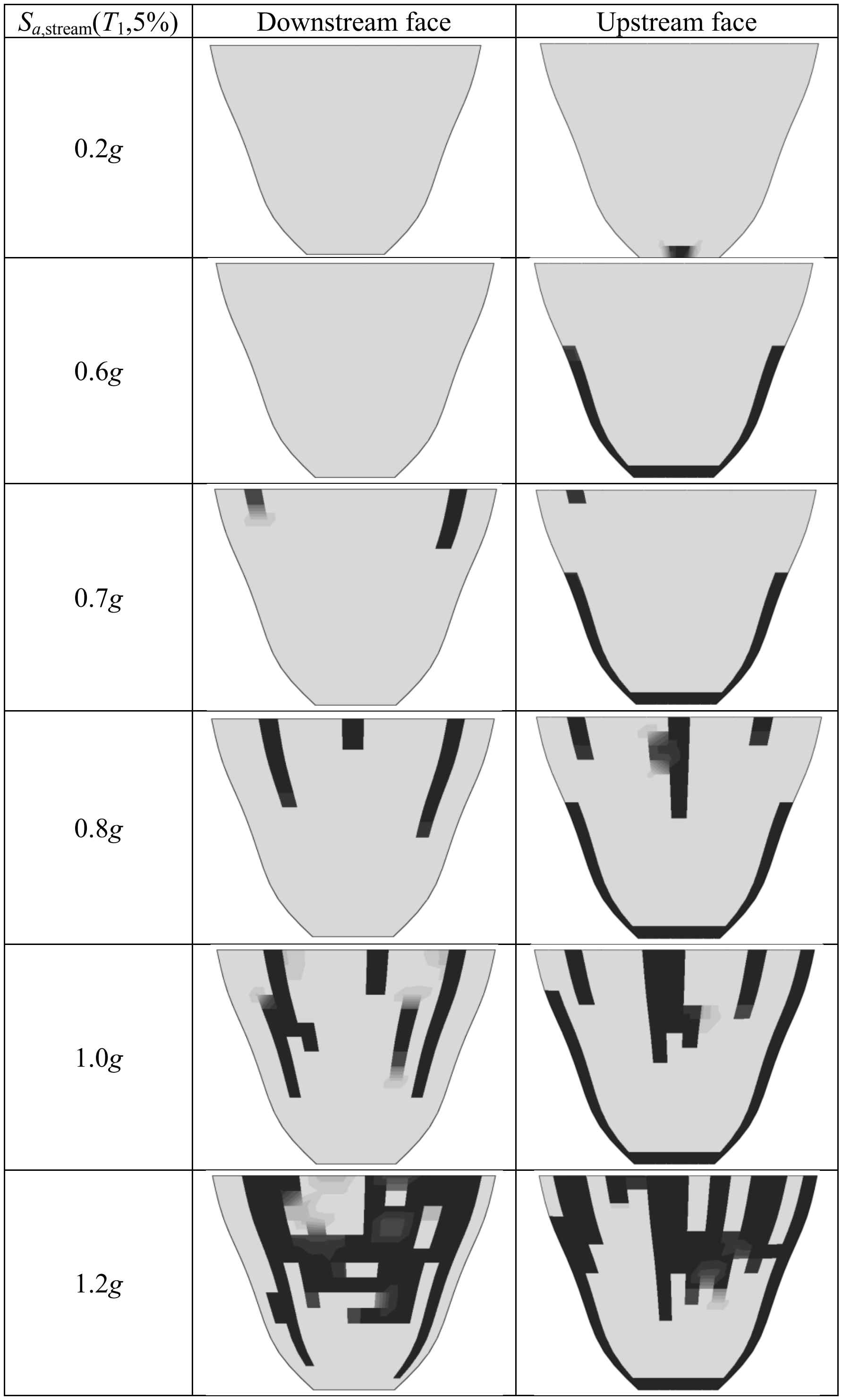

Figure 10 Damage contours of the Morrow Point Dam under KCTAF record at various intensity levels presented based on the spectral acceleration of the stream component.

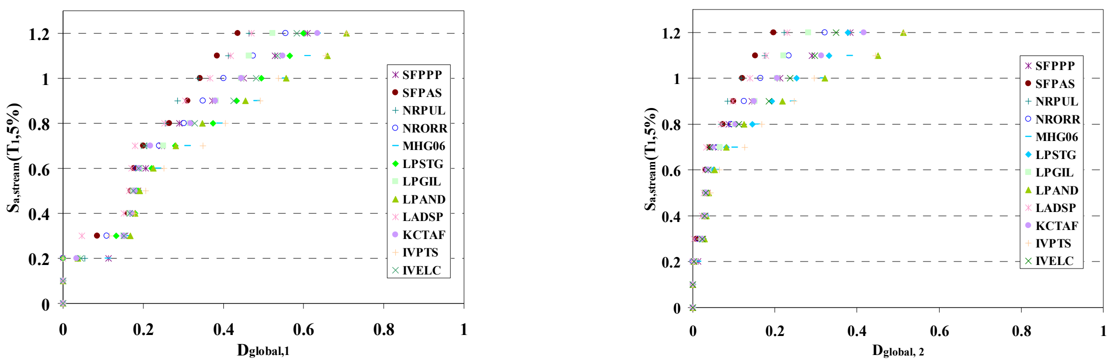

(a) (b)

Figure 11 The global damage indices, (a) $D_{global,1}$, (b) $D_{global,2}$.

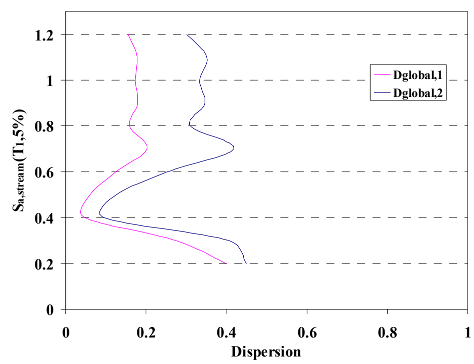

Figure 12 Normalized dispersion of the global indexes.

CONCLUSIONS

The seismic damage of concrete arch dams has been investigated by applying the incremental dynamic analysis method (IDA) to the Morrow Point arch dam. The dam is modeled using finite-elements and its interaction with reservoir and foundation is considered in the analysis. The inertia and damping of the foundation is considered along with its stiffness. Twelve three-component earthquake records recorded on stiff soil are selected for the purpose of the analysis. Each record is scaled to twelve increasing intensity levels categorized based on the 5% damping first-mode spectral acceleration of the stream component ($S_{a,\text{stream}}(T_1,5\%)$). Three components of the selected records are scaled simultaneously and applied at the dam-foundation interface. Based on the obtained results it is attempted to define the seismic performance of the selected arch dam and its various limit-states. It is concluded that the dam responds with low normalized dispersion to different earthquakes scaled to the same $S_{a,\text{stream}}(T_1,5\%)$. For the dam model, the $S_{a,\text{stream}}(T_1,5\%)=0.2g$ is defined as the "yielding" limit-state before that the dam suffers no damage. Up to $S_{a,\text{stream}}(T_1,5\%)=0.6g$ the damage is concentrated at the dam's base and abutment, after that the damage is appeared at the crest level as vertical cracks at mid- and quarter-points. By increasing the shaking intensity these vertical cracks propagate toward the base and horizontal cracks are developed between them. After $S_{a,\mathrm{stream}}(T_1,5\%)=1.1g$ the damage is imposed to the both faces of the dam such that the generation of partially-free blocks are possible. At $S_{a,\mathrm{stream}}(T_1,5\%)=1.2g$ the generation of these blocks and diffused pattern of cracking causes the selection of this intensity level as "ultimate" limit-state or "collapse". The generated bias in the response results is much more for damage energy dissipation with respect to maximum crest displacement. The values of the dam responses under different records at various limit-states have such dispersion that these limits can be defined based on the dam responses. The defined limit-states can be used in the seismic vulnerability analysis of an arch dam.

REFERENCES

Dowling M.J., Hall J.F. (1989). Nonlinear seismic analysis of arch dams, ASCE, *J. Eng. Mech.*, 115: 768−789.

Cervera M., Oliver J., Manzoli O. (1996). A rate-dependent isotropic damage model for the seismic analysis of concrete dams, *Earthq. Eng. Struct. Dyn.*, 25: 987−1010.

Feng L.M., Pekau O.A., Zhang C.H. (1996). Cracking analysis of arch dams by 3D boundary element method, ASCE, *J. Struct. Eng.*, 122: 691−699.

Fok K.L., Chopra A.K. (1986). Hydrodynamic and foundation flexibility effects in earthquake response of arch dams, ASCE, *J. Struct. Eng.*,112: 1810−1828.

Ghanaat Y. (2004). Failure modes approach to safety evaluation of dams, *Proceedings of 13th World Conference on Earthquake Engineering*, Vancouver, Canada.

Ghrib F., Tinawi R. (1995). Nonlinear behavior of concrete dams using damage mechanics, ASCE, *J. Eng. Mech.*, 121: 513−527.

Hall J.F. (1988). The dynamic and earthquake behaviour of concrete dams: review of experimental behaviour and observational evidence, *Soil Dyn. Earthq. Eng.*, 7: 58−121.

Hall J.F. (2006). Problems encountered from the use (or misuse) of Rayleigh damping, *Earthq. Eng. Struct. Dyn.*, 35: 525−545.

Lee J.-H., Fenves G.L. (1998). A plastic-damage concrete model for earthquake analysis of dams, *Earthq. Eng. Struct. Dyn.*, 27: 937−956.

Lotfi V., Espandar R. (2004). Seismic analysis of concrete arch dams by combined discrete crack and non-orthogonal smeared crack technique, *Eng. Struct.*, 26: 27−37.

Niwa A., Clough R.W. (1982). Seismic response of arch dams, *Earthq. Eng. Struct. Dyn.*, 10: 267−281.

Valliappan S., Yazdchi M., Khalili N. (1999). Seismic analysis of arch dams—A continuum damage mechanics approach, *Inter. J. Numerical Methods Eng.*., 45: 1695−1724.

Vamvatsikos D., Cornell C.A. (2002). Incremental dynamic analysis, *Earthq. Eng. Struct. Dyn.*, 31 491−514.

Vamvatsikos D., Cornell C.A. (2004). Applied incremental dynamic analysis, *Earthq. Spectra*, 20: 523−553.

SEISMIC PERFORMANCE AND QUALIFICATION OF ELECTRIC SUBSTATION EQUIPMENT

Eric Fujisaki[1]

ABSTRACT

High voltage electric substation equipment has been historically vulnerable as evidenced in numerous large earthquakes world-wide. Such equipment often includes acceleration-sensitive, lightly-damped, massive, porcelain components, metal castings, and fragile electro-mechanical parts and assemblies. Many of these items are brittle and have little ability to deform and dissipate energy through inelastic behavior. Damage to the electric system in large California earthquakes of the 1980–1990s spurred the development of modern seismic design standards specifically intended for substation equipment. Standards for equipment design including seismic design provide benefits to both utility users and equipment manufacturers. Manufacturers and utilities have important roles in the implementation of standards, and cooperation is necessary to achieve the best seismic performance. Research, testing, and other engineering activities toward an improved understanding of the behavior and performance of substation equipment and better methods of design and qualification continue through the efforts of the user community. As the importance of reliable electric power increases in the modern world, so does the necessity to provide the robust infrastructure needed to survive and operate with minimal disruption following large earthquakes. Standard-making plays an important role in moving the industry toward this goal.

INTRODUCTION

High voltage electric substation equipment has historically been one of the weak links in the electric power system as observed in numerous past earthquakes around the world. Equipment damage in substations has resulted in significant financial losses for utilities as well as sometimes prolonged power outages for industrial, commercial, and residential customers. Early seismic design codes and standards focused on protecting life safety, and for good reason. As building codes became more effective in protecting life safety, more attention was given to other aspects of building and infrastructure performance. Not until about the early to mid-1990s did more comprehensive efforts gain traction to develop standards for seismic design of electric substation equipment. Prior to that time, the conventional practice for most substation seismic design involved the use of rather low static lateral force coefficients derived from building codes.

In an analogous way, recent years have seen increased interest in the protection of expensive building contents, and the continued occupancy and operability of buildings following large earthquakes. The interest in the seismic design of these "non-building" or "non-structural" components reflects a recognition of the effect survival and continued availability of these

[1] P.E., Principal Civil Engineer, Substation Project Engineering Department, Pacific Gas and Electric Company, 1919 Webster Street, Oakland, California 94612, USA; email: eric.fujisaki@pge.com.

facilities have on the resiliency of individual businesses or other entities, institutions, communities, or entire regions.

SUBSTATION DAMAGE IN EARTHQUAKES

High voltage electric substation equipment are complex machines that often consist of acceleration-sensitive components such as massive, brittle porcelain insulators and other rather fragile items designed to close tolerances in order to perform their functions. In many cases, electrical substation equipment are lightly-damped and have little capability to dissipate energy from earthquake response without structural or functional failure. Because higher voltage air-insulated equipment generally requires greater clearances between energized parts and the ground, they tend to require the use of the tallest and most massive porcelain insulators, and are also the most vulnerable to earthquake motions. Figures 1 through 8 illustrate some of the equipment damaged in large earthquakes in the California. Similar damage has been observed in world-wide earthquakes.

Live tank circuit breakers (the interrupter tank is at line potential, hence “live”) generally consist of massive interrupters supported on porcelain columns. At the higher voltages, older models of these types of breakers have performed poorly (Figure 1a) and are not favored by utilities in seismically active areas. Instead, seismically rugged dead tank (the tank is at ground potential, hence “dead”) circuit breakers are more often used in such areas (Figure 1b).

Instrument transformers have suffered damage due to insulator failures as well as brittle metal parts of the tank located below the insulator. The rotational flexibility of the mounting cover of the tank may have contributed to some failures. In Figure 2, higher mode effects may have caused the tapered insulator to fracture in the upper portion.

Transformers and bushings (Figures 3 and 4) are among the most important equipment in a substation. Bushings, particularly at higher voltage classes, have been damaged in even relatively small earthquakes. Transformers, while generally rugged, have experienced damage to the piping of large radiators when inadequately braced.

Air disconnect switches (Figure 5) particularly in high voltage classes have often been damaged due to support flexibility and to the mass and cantilever strength of post insulators. In some cases, the failure of adjacent bus work caused the damage to the switch.

Surge arresters (Figure 6) mounted on flexible booms extending from transformer tanks have commonly failed.

Rigid bus work (Figure 7) is vulnerable to shaking especially at high voltage levels due to inadequacy of porcelain post insulators to resist inertial loading. Brittle metal castings that are commonly used for attaching bus work to the tops of post insulators possess far less ductility than the aluminum buses and have often fractured.

Utilities maintain an inventory of spare parts and materials to respond to random failures as well as the consequences of larger, more damaging events. Insufficient attention to the restraint of stored items has sometimes resulted in spares being damaged (Figure 8). Warehouse seismic performance should provide for post-earthquake entry, protection of stored materials (e.g., from falling hazards), and located such that they can be accessed by the transportation network. Numerous other types of equipment have also been damaged.

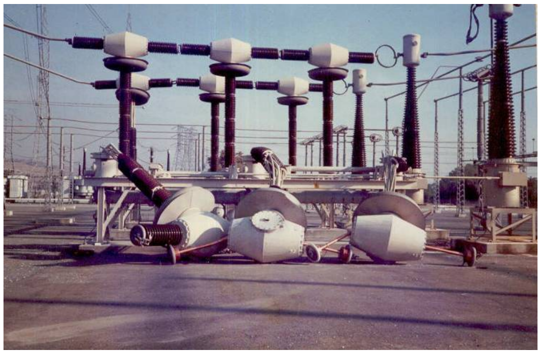

Figure 1a **Live tank circuit breaker failures (photo courtesy of Pacific Gas and Electric Company).**

Figure 1b **Dead tank circuit breaker (photo courtesy of Pacific Gas and Electric Company).**

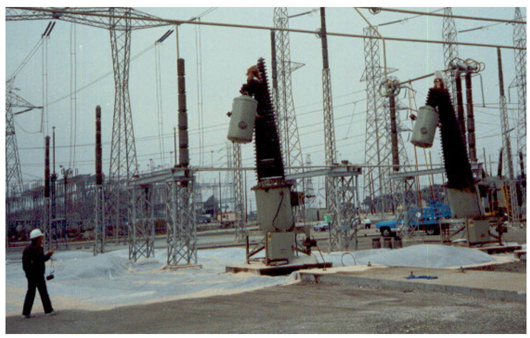

Figure 2 **Current transformer failures (photo courtesy of Pacific Gas and Electric Company).**

Figure 3 **Transformer radiator leaks (Photo courtesy of Pacific Gas and Electric Company).**

Figure 4 **Transformer bushing damage (Photo courtesy of Pacific Gas and Electric Company).**

Figure 5 Air disconnect switches (photo courtesy of Pacific Gas and Electric Company).

Figure 6 Surge arresters (photo courtesy of Pacific Gas and Electric Company).

Figure 7 Damaged rigid bus work (photo courtesy of Pacific Gas and Electric Company).

Figure 8 Spare parts damage (photo courtesy of Pacific Gas and Electric Company).

SEISMIC QUALIFICATION OF SUBSTATION EQUIPMENT

Modern North American standards for seismic design of electric substation equipment began their development following the large California earthquakes of the 1980s and 1990s. Among these, the 1989 Loma Prieta and 1994 Northridge earthquakes had the greatest impact, although several moderate and large earthquakes also occurred during that period but resulted in more limited damage. The large California electric utilities suffered significant damage to their systems in these earthquakes which provided some of the impetus for the formation of the Inter-

Utility Seismic Working Group, composed of the large California utilities as well as other utility members from the western U.S. with an interest in improving seismic design practices. This group eventually formed the core membership of the Institute of Electrical and Electronic Engineers (IEEE) Std. 693 Working Group on seismic design of substations.

Today, the leading seismic design standards for electric substation equipment are the IEEE Std 693, Recommended Practice for the Seismic Design of Substations [IEEE 2006a], and the standards of the International Electrotechnical Commission (IEC) [IEC 2006]. (. The former has been adopted by most utilities in the high seismic hazards North America, and other places worldwide, while the latter is used mostly in Europe and parts of Asia. Some countries have adopted their own national standards, some of which may depend upon or accept the IEEE or IEC standards as alternatives to their own.

Prior to the development of these modern seismic design standards for substation equipment, electric utilities each developed their own internal standards, which made their way into procurement specifications for equipment. There was significant variation in these design requirements, depending upon the experience and expertise of each utility's engineering department. These practices resulted in custom designs for each utility client, and a corresponding wide range of seismic capability. The absence of consensus standards also created no particular incentive and little guidance for manufacturers to improve the seismic performance of their designs.

The development and implementation of standards for the seismic design of substation equipment thus provides important benefits for the equipment manufacturer and the utilities that procure equipment from them. Most importantly, standards provide a common basis of understanding for both parties. Widespread adoption of such standards provides guidance for the manufacturer to use during design development, and a yard-stick with which to assess his customer's acceptance, and other customers who have adopted the same standard. For utilities, standards provide the means for specifying equipment that will satisfy the desired performance objectives, provide for uniformity in equipment design and deployed inventory, and reduce lead time and cost of procurement. Utilities also need not depend so heavily upon the expertise of their own engineering staffs, but instead rely upon the collective knowledge and judgment of standards developers.

The IEEE and IEC standards have similar performance objectives for qualified equipment:

- Minor or no damage after the design earthquake used for qualification
- Equipment remains functional after the design earthquake

Discrete levels of qualification are used in both standards, as opposed to site-specific designs such as those used for buildings. This approach is helpful in limiting the number of different design configurations for different customers who require seismic qualification, and hence simplifies the qualification process. This is particularly important for equipment that is designed in advance of a customer order and is intended to serve multiple customers. Such equipment includes air disconnect switches, instrument transformers, surge arrester, transformer bushings, and circuit breakers.

METHODS OF QUALIFICATION

Seismic qualification standards for equipment generally specify two categories of qualification methods which are analysis and testing. Analysis may include static or dynamic methods, usually by linear elastic methods. Testing includes shake table testing using time history records as well as single frequency tests such as sine-beat testing. Static pull testing may also be specified for the qualification of certain components. In addition, exploratory tests such as resonance search are generally required to identify the frequencies associated with the important modes of vibration. As an example, the qualification methods required by IEEE 693-2005 are summarized in Tables 1 and 2. As a semi-empirically-based standard, IEEE 693 requires that equipment that have historically exhibited vulnerability in earthquakes or possess characteristics that are believed to make them vulnerable, are subjected to more rigorous methods of qualification. In general, equipment of higher voltage classes fall into this category. Other standards may not take such an approach and instead permit any method of qualification.

Table 1 Methods of qualification required for equipment by IEEE 693-2005.

Equipment Type	Method of Qualification Required for Voltage Class (kV)			
	Inherently Acceptable	Static or Static Coefficient Analysis	Dynamic Analysis	Time History Test
Circuit breaker	< 35	35 to <121	121 to < 169	≥ 169[1]
Transformer	< 35	≥ 35	--	--
Air disconnect switch	< 35	35 to < 121	121 to < 169	≥ 169
Instrument transformer	< 35[2]	35 to < 69[2]	69 to < 230[2]	≥ 230[2]
Air core reactor	< 35	35 to < 115	≥ 115	--
Circuit switcher	< 35	35 to < 121	121 to < 169	≥ 169
Surge arrester	< 35[3]	35 to < 54[3]	54 to < 90[3]	≥ 90[3]
Metal clad switchgear	< 35	--	≥ 35	--
Gas insulated switchgear	< 35	35 to < 121	121 to < 169	≥ 169
Capacitor	< 38	38 to < 230	≥ 230	--

[1]Also requires sine beat test.
[2]Time history test required when height of equipment on support ≥ 20 ft.
[3]Duty cycle voltage rating.

Table 2 Methods of qualification required for components by IEEE 693-2005.

Component Type	Method of Qualification Required for Voltage Class (kV)		
	Inherently Acceptable	Static Pull Test	Time History Test
Transformer bushing	<35	35 to < 161	≥ 161
Cable termination	<35	35 to < 220	≥ 220

INPUT MOTIONS

Unlike buildings which are often designed for site-specific ground motions, standards for equipment seismic qualification utilize standard spectra assigned to discrete levels of qualification (typically termed low, moderate or high, or similar designations) in order to simplify the qualification process for mass-produced items. Similar to design spectra for buildings, standard spectra are usually broad-band type spectra as depicted in Figure 9. These spectra form the basis for static and dynamic analysis qualification as well as time history tests. Input motions used for time history tests are usually spectrum-compatible records created by modifying empirical records from real earthquakes, or synthetically generated records. In addition to spectral matching, other requirements such as duration or number of strong-motion cycles may also be specified.

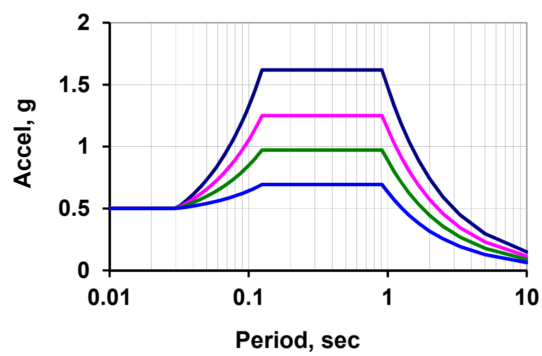

Figure 9a. IEEE 693 high required response spectra 2, 5, 10, and 20% damping.

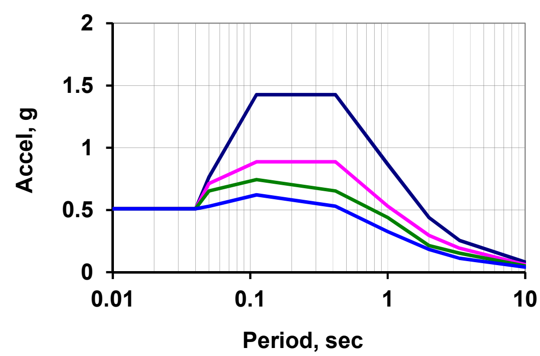

Figure 9b IEC 62271-300 high required response spectra 2, 5, 10, and 20% damping.

IMPLEMENTATION OF SEISMIC DESIGN AND QUALIFICATION STANDARDS

The implementation of seismic design standards for electric substation equipment requires a degree of cooperation and coordination between the end user utility and the manufacturer of the equipment.

The end user or utility generally specifies the level of qualification defined by the standard that is suitable for the site where the equipment is to be installed. In order to do this, the utility should have an understanding of the seismic hazard and soil conditions at the site that can modify the ground motions. The utility should also consider amplification or modification of input motions that result from mounting the equipment on the upper floors of a multi-story building. If the spectra defined by the standard are insufficient, the utility has the option of specifying site-specific input motions; however, this has the effect of requiring the equipment manufacturer to perform a customized qualification. While this is sometimes necessary in specific instances, specifying a customized qualification is more costly and should be avoided whenever possible.

The equipment manufacturer generally qualifies the equipment in accordance with the standard or utility specifications in case of customized qualifications and prepares the documentation for the qualification activities. The end user or utility sometimes will specify a support structure of its own design that must be considered in the seismic qualification. The variation of support conditions creates problems for manufacturers wishing to simplify and streamline the qualification process. In many cases, the manufacturer will perform a seismic qualification in advance of a specific customer order, usually for catalog-type items such as air switches, instrument transformers or surge arresters. In those cases, the manufacturer must anticipate the range of support structure types and properties that may be employed, and in some cases select the qualification parameters that are expected to envelop most if not all of the likely support configurations. The manufacturer also provides the means for anchoring the equipment, for example, by providing anchor brackets, anchor bolt holes, or baseplates for welding. These means for anchorage must be designed to transfer the anchorage forces resulting from the qualification.

Once the utility has accepted the qualification and documentation, it must install the equipment in a manner consistent with the qualification. This series of steps is as important as the qualification activity itself. A support structure with sufficient strength and stiffness must be used. The utility usually also designs and constructs the anchorages (e.g., embedments in concrete) and the bus work for connecting the equipment. The latter should be configured with enough displacement capacity (e.g., conductor slack) or flexibility so as to limit the effects of interaction with the adjacent equipment or components.

CONTEMPORARY ISSUES

Standard-making groups and their member communities continue to work toward improvements to address issues identified during application of the standards, as well as to incorporate new data from research and real earthquake experience. Some of these topics are discussed here.

SEISMIC PROTECTION TECHNOLOGIES

For several decades, building seismic design has incorporated the use of seismic protection technologies such as base isolation of supplemental damping systems. Utilities have in the past been skeptical about the efficacy of such protection systems because they often result in large conductor terminal displacement demand. However, interest in the application of these devices has increased somewhat because of the appeal of protecting the equipment and assuring its functionality following large earthquakes, the introduction of new protection devices, and the maturation of protection technologies. The deployment of these technologies may be facilitated by the development of shake table test protocols for equipment with low frequencies. The displacement limits of most shake tables in use today make them unable to deliver the required motion in the low frequency range (typically < 1Hz). Standardized methods for dynamic testing of low frequency equipment will need to be developed and make their way into standards.

INTERACTION OF CONNECTED EQUIPMENT

One recognized area for improvement is the development of guidance for the treatment of interaction effects. Engineers have recognized that conductors with insufficient slack used to connect electrical substation equipment can adversely affect the equipment when the slack is used up. IEEE 1527, Recommended Practice for the Design of Flexible Bus Work [IEEE 2006b] provides estimation methods for the loading effects (which can be significant) on the connected equipment. Since equipment is generally qualified in the unconnected condition (Figure 10), the provision for interaction effects during the qualification process needs further development.

Figure 10 Equipment is qualified in the unconnected condition, but connected in service (photos courtesy of Pacific Gas and Electric Company).

CABLE TERMINATIONS

Standard EEE 693 has included requirements for the qualification of cable terminations since the 1997 version. Recent earthquakes and recognition of the importance of these components in the scheme of substation operability have resulted in an increased interest in revisiting the requirements for this component. The qualification of terminations poses several challenging problems including the definition and practical implementation of post-shaking electrical function tests, and the qualification test conditions for systems operating at high gas or fluid pressure.

NETWORK PERFORMANCE FOLLOWING EARTHQUAKE

Large scale disasters including but not limited to large earthquakes in recent years have likely influenced risk management thinking at many utilities. Risk management and mitigation efforts at some electric utilities in North America have resulted in an increased interest in studying the performance of electric transmission/ substation networks. These network performance models may be used to develop estimates of the damage state of the system from scenario earthquakes, utility direct losses, indirect economic losses, outage duration, and resource demands. Development of moderately detailed models and supporting databases requires network geographic information, ground motion prediction equations, equipment seismic fragility estimates for applicable equipment failure modes, equipment repair/ replacement cost data, among others. Although significant uncertainty is associated with the results of such studies, they may yield valuable insights to system performance.

CONCLUSIONS

Substation equipment has historically been observed to be vulnerable in large earthquakes. Such experiences were a major motivating factor for the development of the most modern seismic design standards for electric substation equipment. These design standards are an important tool with which utilities can cost-effectively deploy robust equipment that are expected to perform significantly better than "legacy" equipment designed before introduction of those standards. At the same time, seismic design standards assist manufacturers in developing equipment with fewer customized qualifications that are expected to be acceptable to their utility customers who have adopted those standards. Similar to building design standards, those for substation equipment seismic design remain a work in progress. The member communities (utilities, equipment manufacturers, consulting engineers, academic/ research engineers) forming standard-development organizations are actively engaged in improvements on a wide variety of topics of interest to the user community. Standards that are widely adopted and applied provide a cost-effective means for improving the performance of the electric system. Because of the significant capital investment and long life cycle of high voltage substation equipment, legacy equipment may remain in service for some time to come, but steady progress will continue to occur as new seismically qualified equipment enters service for capacity expansion and as replacements.

REFERENCES

IEEE (2006a). *IEEE Std 693-2005, Recommended Practice for Seismic Design of* Substations, Institute of Electrical and Electronic Engineers, Piscataway, NJ.

IEEE (2006b). *IEEE Std 1527-2006, Recommended Practice for Design of Flexible Buswork in Seismically Active Areas,* Institute of Electrical and Electronic Engineers, Piscataway, NJ.

IEC (2006). *IEC 62271-300, High Voltage Switchgear and Control Gear-Part 300: Seismic Qualification of Alternating Current Circuit Breakers*, International Electrotechnical Commission, Geneva, Switzerland.

EVALUATION OF DYNAMIC RESPONSE AND VULNERABILITY OF TEHRAN BURIED GAS NETWORK PIPELINES IN SLOPES BY *IN SITU* EXPLORATIONS, 1G SHAKING TABLE TESTS AND NUMERICAL MODELING

Fardin Jafarzadeh[1], Hadi Farahi Jahromi[2], Masoud Samadian[3], Mehdi Sehizadeh[4], Mohammad Joshaghani[4], and Siyamak Yousfi[4]

INTRODUCTION

The cause of pipelines' structural and slopes' geotechnical failures in the traverse region are matters of controversy; therefore, comprehensive research to understand these failure mechanisms have been performed or are now in progress. Great emphasis on rehabilitation of important structures to endure earthquake loading has compelled Iranian governmental organizations to allot parts of their budget to conduct research with the goal of retrofitting underground systens and above ground structures. The Tehran Gas Company is one such organization and has initiated several research projects to retrofit gas pipelines and networks in Tehran against major earthquake-related hazards, including liquefaction, landslides, wave propagation, and faulting. The Sharif University of Technology is in charge of performing analysis on the faulting in the region and landslide potential . This paper discusses the results of an ongoing project by Sharif University of Technology to evaluate and analyse current systems and suggest retrofitting strategies for gas pipeline and network system against probable landslides in Tehran's megacity. This project is in progress and is supported by Tehran Gas Distribution Company. The activities completed thus far include:

- recognition of probable landslides in Tehran urban areas
- investigating pipelines routes and geometrical characteristics of the pipelines and points where pipelines cross slopes
- performing parametrical and actual numerical modeling
- conducting physical model tests with shaking table device

LITERATURE REVIEW

The vulnerability of piplines to earthquake loading has been evidenced in many events worldwide and the damage records are available in literature. For cases of buried pipeline in slopes, the potential damage ranges from minor to severe and is mainly dependent on slope

[1] Associate Professor, Sharif University of Technology, Tehran, Iran.
[2] PhD Candidate, Sharif University of Technology, Tehran, Iran.
[3] Head of Research & Technology Department, Tehran Gas Company, Iranian National Gas Co., Tehran, Iran.
[4] Former Graduate Students, Sharif University of Technology, Tehran, Iran.
[4] Former Graduate Students, Sharif University of Technology, Tehran, Iran.
[4] Former Graduate Students, Sharif University of Technology, Tehran, Iran.

geometry and materials used. The physical and functional damages to pipelines, generating economical and human loss, can be more severe for pipes conveying fuel. In the last three decades, many countries have developed scientifically-based regulations regarding buried pipes. These include: ASCE guidelines for the design of buried pipes against permanent ground deformation (PGD) [1984], Japanese released standards for pipeline designs against PGDs, the ALA [American Lifeline Alliance 2005], and Indian standards for pipelines [IITK-GSDM 2007].

Landslides are a critical component when considering crossing pipelines. There are many records reporting the pipeline damage related to earthquake-induced landslides. For example, landslide and land subsidence during 1971 San Fernando earthquake, particularly in Sylmar area, resulted in gas, water, and sewage pipeline buckling and failures. Youd [1973] found that even though strong, flexible steel pipes can withstand large earthquakes, they are vulnerable and do not perform well in events with large PGDs. Although PGDs occur in all earthquakes, the geology determines the type and degree of deformation. Although the three major modes of failure in straight pipelines are tension rupture, local buckling due to compression, and general buckling, more than 80% of pipeline failures occur because of joint ruptures. Consequently, there are several damage scenarios possible in considering pipeline failure: pipe up-heaving, joint rupture, buckling, bend dislocation, cross-section torsion, concrete block separation and fracture, manhole dislocation, and longitudinal fracture.

In 1975 Newmark and Hall [1975] considered tensile strain of 4% as a limit of pipe failure; ASCE regulations suggest 2–5% strain as an upper and lower bound. Pipe wall deformation and cracks, which are representative of local buckling, occurs in 1.3 to 1.4 of 0.6 t/R (t is pipe thickness and R is pipe radius). Although pipe wall deformation is considered a buckling failure mode, beam buckling similar to column buckling is another cause of pipeline failures. In conditions where the burial depth of pipe is less than 1 m and loose material lets the pipe to deform, the continuous pipe tends to protrude the overburden material and general buckling will occur. Failure controlling parameters are δ (displacement), L (pipe length), δ_{cr} (critical displacement), pipe material, R/t, and burial depth specifications.

In general, the angle between the pipe axis and the loading direction (similar to faulting), is an influential parameter affecting the pipeline behavior; however, a slope's stability complicates the problem. Although instability may occur due to two static and dynamic mechanisms, the major consideration is stability itself [Kramer 1996]. Thus there are two ways to ensure pipeline safety: (1) control the parameters influencing the interaction between the pipe and the slope' and (2) stabilize the slope to ensure that no excess loading will be imposed on pipeline in future. Even though there are only a few methods to control the interaction, there many ways to stabilize a slope. Geological, hydrological, topographical, geometrical, and material characteristics can all influence slope stability. Static and dynamic stability analysis should rely on scientifically acceptable parameters. These parameters can be determined from available documents, field reconnaissance reports, field monitoring, subsurface investigation, and material testing [Kramer 1996].

Each slide can be categorized as disrupted, coherent, and lateral spreads and flows in liquefiable soils [Kramer 1996]. To analyze slope stability or any fact relevant to slope and landslide, the slope mechanism should be known first. Any slope can be categorized as debris flowing, rock falling, toppling, planer, wedge, and/or rotational sliding.

Although stability analysis is divided to two static and dynamic procedures, each category includes several sub-methods. For instance, a static slope stability analysis can be performed by limit equilibrium and stress-deformation method. Similarly, dynamic analysis includes two major sub-methods, including inertial and weakening stability. The inertial method is also varied: pseudo-static, Newmark sliding block, Makdisi-Seed, and stress-deformation analysis. The weakening analysis has been implemented by two techniques, the so-called flow failure and deformation failure analysis [Kramer 1996].

Because the interaction between the pipeline and the slope is of major consideration, the crossing angle, relative geometry of pipeline and the slope, pipeline features (buried or above ground) and the pipeline characteristics should be considered. Some other factors, such as internal pressure, duration of service, type of welding, and the pipe material, can also affect the durability and serviceability of pipeline during a dynamic event.

A recent and more advanced procedure has been developed which is basically a stability analysis of the whole model (slope and crossing pipeline) and can be performed by two deterministic and probabilistic methods. In both approaches the whole system with its geometrical, mechanical, and geotechnical parameters is modeled. In deterministic approach, the result is only concerned with a safety factor, which determines whether or not the pipeline does not fail. In contrast, the probabilistic approach provides us the failure probability of pipeline for a specific level of damage and loading during its lifetime. In both approaches, some structural analysis must be perfomred to indicate the severity and type of damage to pipeline. Having this information, practical stabilization techniques can be selected regarding to numerical modeling and work experiences by an expert engineer. Many techniques for slope stabilization have been proposed in literature, including: slope geometry change, water drainage, stabilizing structure construction, route change, and directional drilling [Boivin et al. 1993]. The first research step focused on the efficacy of altering the route as an effective method of minimizing the dynamic forces impose to a pipeline in the even of an earthquake.

Numerical calculations and physical modeling tests are two major techniques widely used by researchers for the subject. ABAQUS and FLAC3D computer programs, which are based on finite element or finite difference methods, respectively, are used for numerical calculations. Centrifuge and shaking table facilities can be used in dynamic physical modeling.

Modes of pipeline deformations are greatly dependent on loading direction. As a case in point, the ground deformation can be parallel or normal to pipe axis, in addition to considering the oblique mode. In this case, there are variety combinations of deformation modes. For example, a pipeline can cross the slope in 30, 45, 60 and 75°.Two extreme cases are 0 and 90° crossing angles, which impose pure axial or bending strains on pipes; respectively. However other cases that are also probable and common place is a combination of both bending and axial deformations.

Cocchetti et al. [2009] performed many numerical analyses to determine the influence of several parameters including traverse angle, pipeline material behavior, pipe-to-slope relative geometry, etc., on pipeline deformations. They concluded that the safest place for pipeline passage is behind the rotational curve line. Figure 1 shows the concept of their analysis.

Qiao et al. [2008] conducted several 1g shaking table tests and numerical modeling to simulate lateral spreading, subsidence, and sand boiling during liquefaction. They imposed harmonic sinusoidal loading with the amplitude of 0.1–0.5*g* to a slope having 2H:1V gradient. They used a 180×60×80 cm (*L.W.H.)* soil container with fixed boundaries. The soil and silicon sand, was uniformly poured in the water to form a 40-cm layer below the slope and had 70% relative density. The slope was 20 cm in height, and the pipe had the overburden of 10 cm. Figure 2 shows the box and slope configuration. The PVC pipe had 25 mm outer diameter and was loaded by a harmonic 5 Hz frequency loading. The graphical charts and reported results show that the slope experienced a three-dimensional slide and the center zone of the slope had maximum displacement. In addition to physical models, several numerical analyses were performed using the two-dimensional FLAD program to show the accuracy of physical tests. They suggested that centrifuge modeling can much appropriately model the landslide.

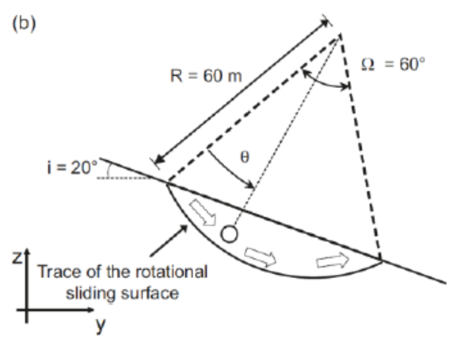

Figure 1 Concept of pipe to slope relative geometry and angle of pipe placing in the slope [Cocchetti et al.2009].

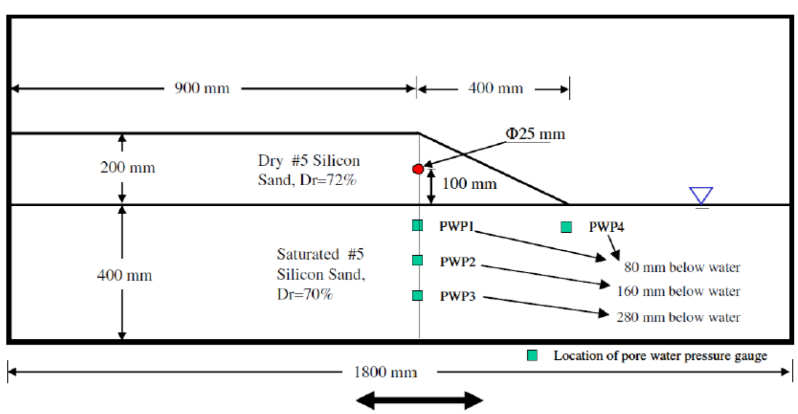

Figure 2 Constructed slope and pipe model and sensors configuration in the rigid box.

Besides the aforementioned tests, a substantial cooperative research program was conducted between the U.S. and Japan by Professor D. Brand of Cornell University and Professor M. Hamada (from Waseda University) representing the Tokyo Gas Company, [2000]. The performance of pipelines in response to the 1994 Northridge, California, and 1995 Kobe, Japan, earthquakes prompted the scientists to focus on pipeline vulnerability. In the tests performed at Cornell, four L-shaped and 30-m-long steel pipes were buried in a soil container made out of reinforced wood structure with dimensions 30×14 cm (*L.W.)*. The box had two fixed and moveable parts to model the strike-slip faulting, with a maximum offset of 4 ft, which simulated a 7.0 magnitude earthquake.

The overburden depth was 3 ft, which covered the 4-in.-diameter simulated gas pipes. One hundred and twenty strain gauges and many load cells and LVDTs recorded the required deformation and force parameters during four tests. Designed test were able to model direct shear and lateral spreading (by changing relative density and moisture) that simulated fault movement, liquefaction, and slip. The deformed shape of the 60-ton sand in the container is shown in Figure 3.

Brusshi [1995] modeled the slow soil movement for intersection angle of 10, 40, and 70° and concluded that the induced axial force of pipe increases with decreasing pipe-slope angle; however, the bending moment has a direct relationship with the PGD perpendicular to pipe axis and can be considered spatially distributed or localized. While the first type is attributed to lateral spreading or some type of slides, the second is allotted to faulting or slope instability. These phenomena were analytically, numerically, and physically analyzed. For example, O'Rourke and Liu [1999] proposed two spatially distributed deformation pattern, as shown in Figure 4.

Figure 3 The surface of 60 tons of shearing sand buckled and fissured due to simulated earthquake, resembling the typical surface distortions following a real earthquake [Brand 2000].

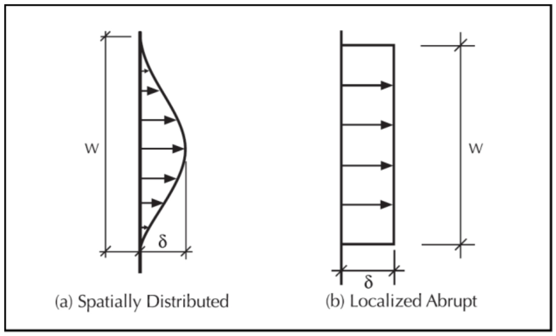

Figure 4 Two ground deformation type perpendicular to pipe axis (after O'Rourke and Liu [1999]).

Besides soil movement, boundary conditions are also of major consideration in numerical modeling. The Winkler spring, a routine way of surrounding soil modeling, has been widely used in previous studies. To take into account the pipe-soil interaction, M.J. O'Rourke et al. [1995] used this method (elasto-plastic spring) along with Ramber-Osgood model for steel pipe. Incorporating some simplifying assumptions, T. O'Rourke [1988], Suzuki et al. [1988], Liu and M. O'Rourke [1997] and Maugeri [2004] presented several analytic formulas to predict PGD with elastic-plastic Winkler soil model; here the influence of shear stress between two adjacent springs was not considered. As a result, these assumptions could not actually calculate the induced dynamic forces caused by seismic slope failure or soil settlement. To compensate the shortcomings of this approach, finite element modeling that considers the slope as a continuum media has been increasingly applied for soil-structure interaction modeling. This paper uses finite element analysis to evaluate the pipe seismic performance buried in a potential slope.

RESEARCH PROJECT ACTIVITIES

Tehran has a widespread and dense gas network and related installations and elements. More than 10,000 km basic grid, 700,000 local distribution points, and 300 pressure control stations characterize this network. The Tehran area is highly seismic but the region has been relatively quiet during last 100 years. Given the potential for a major earthquake, government authorities have supported a number of research and engineering projects to evauate the seismic vulnerability and retrofitting methods of Tehran and suburb gas network.

As mentioned earlier, the project reported here is being done in the framework of a contract between Sharif University of Technology and the Tehran Gas Company, and has two major components, including the numerical modeling and physical testing. A summary of the conducted activities in the framework of the project are presented next.

Tehran Tectonics and Geological Characteristics

Tehran, a city with high risk of earthquakes, has several faults. The fault geometry and characteristics are reviewed through geological maps (the map scales were 1:250,000 and 1:100,000), aerial photographs (1:55,000), the available documents from Tehran municipality, relevant ministries, and engineering consultants. Based on the obtained geological investigations, ground in Tehran is divided to 4 major categories including alluvium type “A,” which is composed of conglomerates and cobbles, heterogeneous alluvium Type “B,” which is largely composed of gravel and cobbles, however sand and clays are also present. This formation is up to 60 m thick, which includes the most slopes in the city. In addition, Tehran has two other formations, named “C” and “D,” which include recent sedimentations being formed by finer materials.

Based on previous studies, Tehran has several active faults, including Mosha, Northern Tehran, Parchin, Northern and Southern Ray, Kahrizak, Niavaran, Mahmoodieh, TalvPayin, Shianand Kosar, GhasreFiroozeh, Latian, TalvBala, SorkheHesar, and Southern Mehrabad Faults. These faults, which are listed based on importance, have caused several severe earthquakes in the past and are capable of producing earthquakes of magnitude 7+ events.

Strong Ground Motion

Strong ground movement characterization was performed based on statistical and artificially produced parameters approaches; the more deleterious scenarios were selected by the following calculations.

1. The potential faults in Tehran area (mentioned above) were identified through many seismic reports and work experiences and then, the ability of each fault to produce an event was assessed based on geological, geophysical and historical records through earthquake catalogs. These catalogs were chosen in a way to cover all earthquakes in a 120 km radius around Tehran.
2. Each fault was weighted based on its ability to generate an event with moment magnitude "M", and the coefficients β and λ were calculated. Table 1 and Figure 5 show the seismic coefficient calculation results and moment magnitude-return period graph for this area.
3. The ground motion parameters were calculated using attenuation formulas (Campbell and Bozorgnia [2003]; Ambraseys et al. (2005); Boore and Atkinson [2008]; Campbell and Bozorgnia [2008]; Akkar and Bommer [2010]; Motazedian [2006]), for three return periods of 475, 975, and 2475 years. Depending on the response expectation from gas pipes and networks; each return period was a representative for loading level of serviceability, moderate earthquake, and severe one; respectively.
4. The computer program SEISRISK–III [1987] was used to calculate the maximum earthquake parameters.

Based on the above, the following results were obtained: The north of Tehran is considered to have the highest seismic risk, with the maximum parameters compared to the other regions, followed by southeastern and the northwestern regions. Table 2 summarizes the calculated measures of design spectra for a typical selected site northwestern Tehran (Islamic Azad University site - Olum-Tahghighat) for various frequency and damping measures. Also, the response spectra of this site for three return periods of 475, 975, and 2475 years (5% damping and mean+1σ standard deviation (84%) level) is presented in Figure 6.

Table 1 Seismicity parameters calculated for Tehran area in a 120 km radius.

β	M_{max}		Pre His.	His	Complete part		
	Obs.	Cal.	1800<	1800-1899	1900-1963	1964-1979	>1979
1.37±0.12	7.5	7.58+0.51	9	6	13	10	31

Magnitude Mw	Annual Activity Rate (λ)	Return Period (Year)	Occurrence Probability			
			1yr	50yr	100yr	1000yr
4.0	0.55251	1.8	42%	100%	100%	100%
4.1	0.48102	2.1	38%	100%	100%	100%
4.2	0.41915	2.4	34%	100%	100%	100%
4.3	0.36553	2.7	30%	100%	100%	100%
4.4	0.31901	3.1	27%	100%	100%	100%
4.5	0.27860	3.6	24%	100%	100%	100%
4.6	0.24346	4.1	21%	100%	100%	100%
4.7	0.21287	4.7	19%	100%	100%	100%
4.8	0.18621	5.4	17%	100%	100%	100%
4.9	0.16294	6.1	15%	100%	100%	100%
5.0	0.14262	7.0	13%	100%	100%	100%
5.1	0.12484	8.0	12%	99%	100%	100%
5.2	0.10929	9.2	10%	99%	100%	100%
5.3	0.09566	10.5	9%	98%	100%	100%
5.4	0.08370	12	8%	98%	100%	100%
5.5	0.07320	14	7%	96%	100%	100%
5.6	0.06397	16	6%	95%	100%	100%
5.7	0.05586	18	5%	92%	99%	100%
5.8	0.04871	21	5%	90%	99%	100%
5.9	0.04241	24	4.1%	86%	98%	100%
6.0	0.03685	27	3.6%	83%	96%	100%
6.1	0.03194	31	3.1%	78%	95%	100%
6.2	0.02760	36	2.7%	73%	92%	100%
6.3	0.02376	42	2.3%	68%	89%	100%
6.4	0.02036	49	2.0%	63%	85%	100%
6.5	0.01735	58	1.7%	57%	81%	100%
6.6	0.01468	68	1.5%	51%	75%	100%
6.7	0.01231	81	1.2%	45%	69%	100%
6.8	0.01020	98	1.0%	39%	63%	100%
6.9	0.00833	120	0.8%	34%	56%	100%
7.0	0.00666	150	0.7%	28%	48%	100%
7.1	0.00518	193	0.5%	23%	40%	99%
7.2	0.00386	259	0.4%	17%	32%	97%
7.3	0.00268	374	0.3%	12%	23%	92%
7.4	0.00162	617	0.2%	8%	15%	79%
7.5	0.00068	1470	0.1%	3%	7%	49%

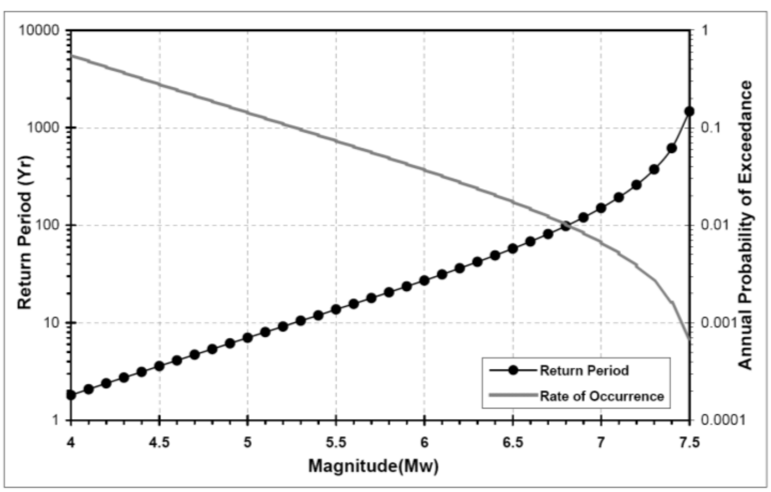

Figure 5 Return period – magnitude graph for 120 km radius area from Kiko-Graham method.

Table 2 Calculated design spectra for the Islamic Azad university site (Olum-Tahghighat) for various damping and frequencies.

Freq. (Hz)	Period (s)	Damping Ratio 0.5%	1%	2%	3%	5%	7%	8%	10%	15%	20%	Acceleration Response Spectra (g)
25.0	*0.04*	0.620	0.539	0.460	0.426	0.399	0.382	0.377	0.370	0.360	0.353	
20.0	*0.05*	0.926	0.795	0.666	0.592	0.507	0.462	0.446	0.424	0.396	0.381	
16.7	*0.06*	1.389	1.051	0.812	0.688	0.580	0.526	0.508	0.481	0.435	0.408	
14.3	*0.07*	1.360	1.093	0.867	0.768	0.655	0.589	0.565	0.526	0.462	0.425	
12.5	*0.08*	1.468	1.214	0.948	0.838	0.714	0.639	0.612	0.570	0.496	0.445	
11.1	*0.09*	1.439	1.267	1.069	0.930	0.770	0.669	0.634	0.595	0.522	0.469	
10.0	*0.1*	1.717	1.377	1.113	0.972	0.823	0.721	0.682	0.620	0.530	0.474	
6.7	*0.15*	1.952	1.622	1.301	1.127	0.912	0.791	0.745	0.670	0.545	0.474	
5.0	*0.2*	2.228	1.791	1.378	1.142	0.873	0.739	0.702	0.640	0.525	0.453	
4.0	*0.25*	1.885	1.544	1.245	1.055	0.856	0.729	0.681	0.608	0.493	0.431	
3.3	*0.3*	1.311	1.190	1.035	0.938	0.809	0.710	0.668	0.598	0.490	0.427	
2.9	*0.35*	1.242	1.135	0.995	0.898	0.763	0.669	0.633	0.574	0.466	0.396	
2.5	*0.4*	1.714	1.375	1.046	0.904	0.724	0.610	0.570	0.512	0.430	0.372	
2.2	*0.45*	1.529	1.257	1.003	0.858	0.680	0.582	0.543	0.487	0.399	0.342	
2.0	*0.5*	1.281	1.102	0.895	0.779	0.638	0.556	0.523	0.472	0.384	0.326	
1.8	*0.55*	1.046	0.919	0.780	0.703	0.601	0.528	0.500	0.453	0.367	0.313	
1.7	*0.6*	1.204	1.010	0.814	0.702	0.571	0.500	0.471	0.425	0.346	0.292	
1.5	*0.65*	1.082	0.943	0.768	0.658	0.533	0.454	0.428	0.386	0.316	0.268	
1.43	*0.7*	0.902	0.789	0.665	0.581	0.495	0.426	0.401	0.360	0.290	0.244	
1.33	*0.75*	0.853	0.732	0.602	0.544	0.456	0.391	0.365	0.326	0.263	0.224	
1.25	*0.8*	0.903	0.747	0.595	0.512	0.410	0.355	0.334	0.301	0.245	0.208	
1.18	*0.85*	0.530	0.503	0.463	0.430	0.373	0.328	0.309	0.280	0.229	0.196	
1.11	*0.9*	0.670	0.582	0.489	0.425	0.350	0.306	0.289	0.262	0.216	0.185	
1.05	*0.95*	0.621	0.558	0.466	0.405	0.328	0.282	0.264	0.240	0.200	0.172	
1.00	*1*	0.491	0.446	0.381	0.346	0.298	0.264	0.250	0.226	0.185	0.162	
0.67	*1.5*	0.309	0.281	0.245	0.219	0.183	0.160	0.151	0.137	0.114	0.099	
0.50	*2*	0.197	0.181	0.157	0.139	0.117	0.105	0.099	0.091	0.075	0.064	
0.40	*2.5*	0.118	0.110	0.098	0.090	0.079	0.073	0.071	0.066	0.056	0.049	
0.33	*3*	0.077	0.073	0.068	0.064	0.059	0.055	0.053	0.050	0.043	0.038	
0.29	*3.5*	0.073	0.066	0.058	0.053	0.047	0.043	0.041	0.038	0.033	0.030	
0.25	*4*	0.050	0.048	0.045	0.042	0.038	0.034	0.033	0.031	0.026	0.023	

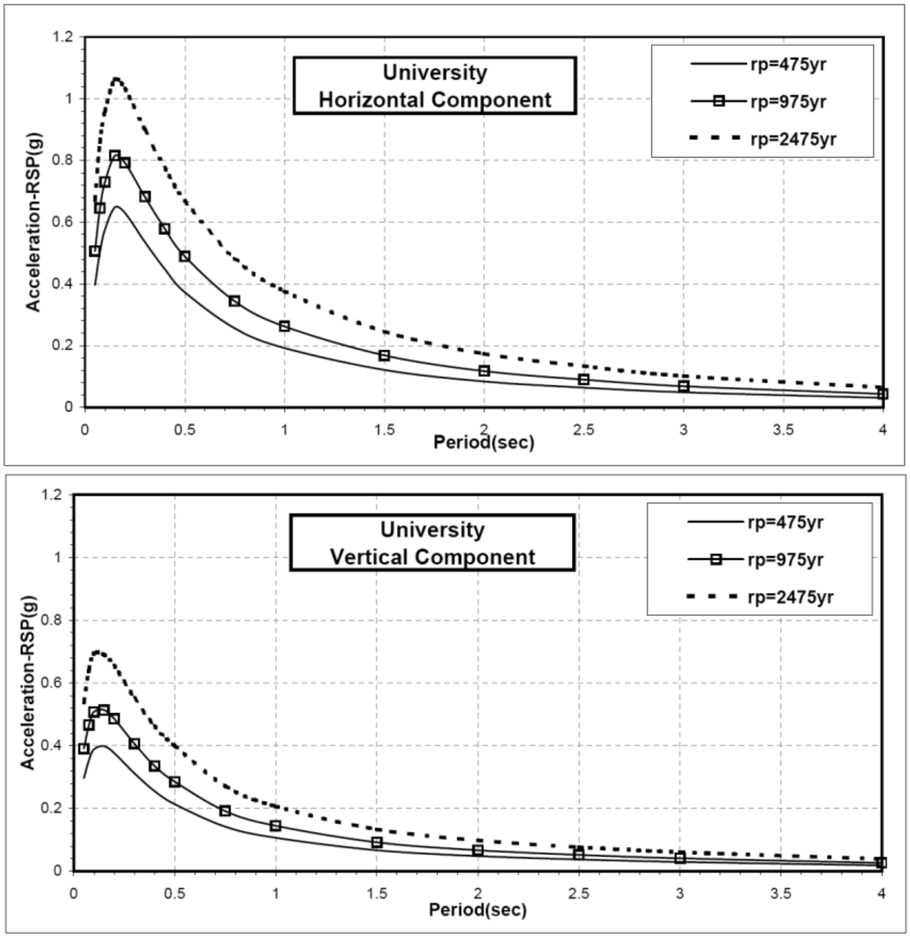

Figure 6 Horizontal and vertical response spectra for Olum-Tahghighat site for three return periods of 475, 975, and 2475 years (5% damping and mean+1σ standard deviation (84%) level).

Determining the Potential Slides in Tehran Area

Landslide hazard assessment is one of the main activities of the project. Per the "Seismic Retrofitting of Tehran Gas Pipelines Report" [2005], sliding potential exists in the northern part of Tehran, particularly in the areas close to northern fault and Abbas-Abad hills, which are considered vulnerable. Due to the relatively few steep areas in southern Tehran, no hazard was assessed. Sliding potential is basically assessed according to the information of soil condition; such as shear wave velocity, SPT values, depth of the rock beneath the soil layers, steepness of bed rock and upper alluvium layers, calculated acceleration, and amplification factor.

The research team used 34 separate sheets of Tehran regional topography map and combined various parts into one topography sheet in DWG format with ARC-GIS 9.3 computer program. Then, the gas pipelines and network maps (received from Tehran Gas Company) were corrected in a way to be compatible with the program (converted to "shp" format), and the project operation (software-related order) was implemented. Subsequently, gas pipe routes were superposed upon a Tehran topography map to show the traverse points of pipelines and potential slopes. Note that the potential slopes were extracted from visual reviewing of topography map and the landslide direction was predicted to be the steepest route of the slope. Figure 7 shows a typical identified potential landslide for the site (Islamic Azad University site in west-north of Tehran). A field survey for each predicted landslide verified the correctness of geological and geometrical considerations. For example, Figure 8 shows a potential north-south landslide and constructed structure in the Olum-Tahghighat site survey program.

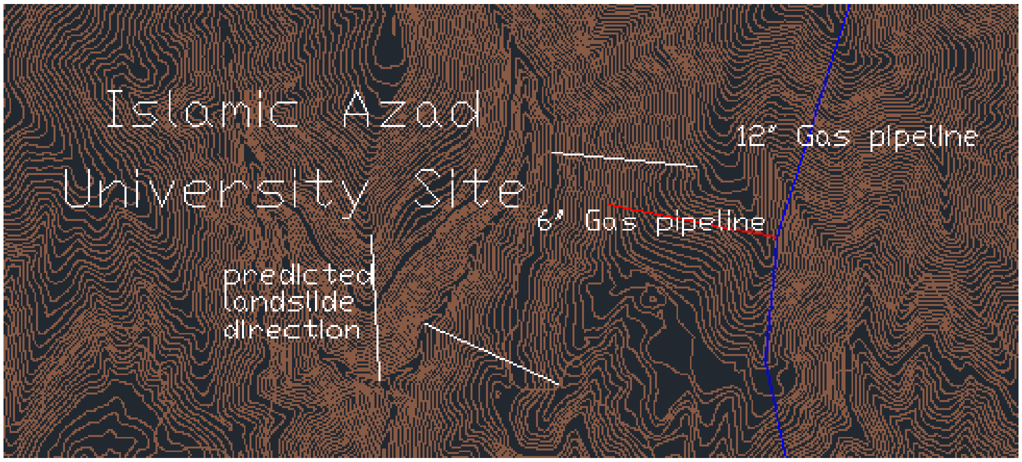

Figure 7 **Topography map of Islamic Azad University site (6 in. and 12 in. passing gas pipe and predicted landslide direction are shown).**

Figure 8 **Potential slopes in the area of Olum-Tahghighat site in western north of Tehran (eastern-north view).**

Numerical Model Characteristics

The use of finite element analysis to model the landslides under both static and dynamic failure conditions has greatly increased during last decade. The finite element program ABAQUS ver.6.10 was been used to model the slope. In order to gain the realistic results that can be a base for PGD prediction, the model specifications should be selected in a way close to natural conditions. Because in any numerical modeling, some divergences between model and prototype are inevitable, the loading condition, surrounding soil and pipe characteristics and boundary condition are selected as close as an actual continuous pipeline projecting a slope. These condition and the modeling methods for each one are described in following sections [Jafarzadeh et al. 2012].

Loading Characteristics

Pressure in main gas pipelines in Tehran is adjusted to 1000 psi, which is continuously decreased in three steps to reach the desired pressure for consumers (from 1000 psi to 250 psi and then to 60 psi and finally to fitted home consumers pressure). Therefore, the project should focus on three different pipe types that probably are composed of different materials, characteristics, and cross sections. According to the applied pressure, system equipment was divided to three main categories with high, moderate, and low earthquake vulnerability.

Although National Iranian Seismic Regulation No. 2800 proposes 0.35*g* pick acceleration for Tehran area, some seismic reports suggests the designers to consider higher levels for worse conditions. In this regard, and in parametric numerical analysis of this study, a uniform sinusoidal acceleration with 0.5*g* amplitude and 1.2 Hz frequency excitation has been applied to physical models' base for 15 sec. This loading level is compatible to moderate pressure pipelines. The dynamic step analysis was launched with implicit algorithm.

Surrounding Soil and Pipe Characteristics

Many studies have been performed to determine the Tehran cemented soil characteristics. Through studying and reviewing several related reports, including Haeri and Banasiri [2002], Fakharian. [2004],Haeri and Asghari [2004], Abdi [2008], Haeri and Rastgu [2008], and Ghanbari [2009], etc., soil slopes consisting of two layers with following parameters were assumed (see Table 3).

Table 3 Tehran soil parameters used for analysis.

Soil Layer	Layer Thickness (m)	Cohesion (kPa)	Friction angle (°)	E_{max} (MPa)
1	20	80	30	150
2	20	100	35	367

To account for stress-strain relation and to consider the strain dependent nonlinearity nature of the soil (decreasing soil strength with increasing dynamic strains), Mohr-Coulomb behavior model along with USDFLD ABAQUS subroutine written by FORTRAN compiler were used. Park et al. [2010] and Tika [2010] suggested correlations to determine G/G_o reduction curve were used to model the nonlinearity behavior [Jafarzadeh et al. 2013]. Material damping was introduced to model for two basic frequencies. The Rayleigh damping coefficients (α and β) were calculated for dynamic loading frequency (1.2 Hz) and natural frequency of the slope. This natural frequency was calculated through a frequency linear perturbation step. According to the Iranian National Gas Company, polyethylene and steel pipes can be used; however, because it is more widely used; steel pipe was selected for the analysis. The pipe grade was API-5L-X42 steel with 200 GPa elastic modulus and Poisson's ratio of 0.3.

Boundary Conditions and Model Geometry

From the studies and surveys of the potential landslides, a typical slope dimension was selected for the analyses. Figure 9 shows the slope characteristics. The steel pipe had 24 in. outer diameter and 0.312 in. wall thickness. The three-dimensional slope geometry had five boundary planes; each had its own interaction with adjacent medium. These specifications are summarized in Tables 4 and 5.

To eliminate or reduce the effect of reflecting waves from model boundaries, viscous absorbent boundary elements, with the use of dashpots as proposed by Lysmer and Kuhlemeyer [1969], were used. In addition, to overcome the redundant permanent displacement at low frequencies, normal and tangential springs developed by Kellezi [2000] were applied to unconstrained planes. Some shortcomings together with these boundary conditions at constrained planes are inevitable; therefore, in order to have a more consistent sliding style to natural condition, this technique was also applied to constrained boundary conditions. This study used penalty frictional contact (Coulomb frictional formulation) with 0.5 friction coefficient. Normal behavior was defined by hard contact and allowing separation of surfaces option.

The numerical modeling was divided to two major groups. The first one focused on relative geometry of pipe in a slope. Figure 10 describes this situation by introducing parameter "A," defining the relative burial location of pipe in the slope. For the analysis, three quantities, 0.2, 0.5 and 0.8, were selected for "A". Dynamic analysis was performed for each model, and the deformation of slope and pipe was compared in each case. The second group focused on the boundary conditions in Z=0 and Z=w planes (Figure 9 and Table 4). To account for the influence of boundary conditions, two types (Table 5) were introduced to the program, and the results of dynamic analysis were compared. Also, in the last analysis the width of the model was expanded to 60 m and the sliding pattern of the slope was studied.

Table 4 Boundary conditions for slope planes.

Plane name	U_x	U_y	U_z
X=0, X=D_r+D+D_l	Not constrained	Not constrained	Not constrained
Y=0	Not constrained	Constrained	Constrained
Z=0, Z=w	Not constrained constrained	Not constrained	Constrained

Table 5 Boundary condition types in *Z*=0, *w* planes.

Model No.	*W*	Boundary Condition
1	40	Constrained
2	40	Unconstrained
3	60	Constrained

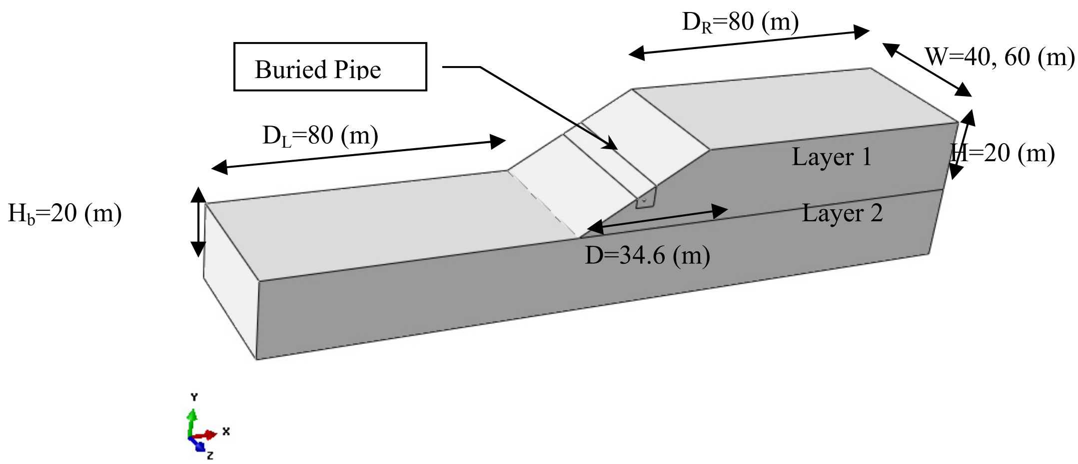

Figure 9 Typical slope dimension for the dynamic analysis.

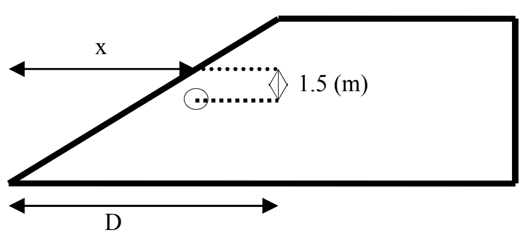

$$A = {}^{x}/_{D} \rightarrow \begin{cases} 0 < A < \frac{1}{3} \\ \frac{1}{3} < A < \frac{2}{3} \\ \frac{2}{3} < A < 1 \end{cases}$$

Figure 10 Description of parameter “A” (not to scale).

Numerical Analysis Results

To account for the relative geometry and boundary conditions, six different models were analyzed using ABAQUS. By introducing “A” parameter (Figure 10), the first type determines the influence of relative geometry of the pipe in the slope and compares the plastic strains and displacement of the pipe. Figure 11 shows the horizontal and vertical displacements for the pipe with A = 0.2, 0.5, and 0.8. These three conditions will be named A1, A2, and A3 hereafter. Maximum horizontal and vertical displacements which reflect the displacement of three parts of the slope for A1, A2, and A3 types were summarized in Table 6, respectively. The calculated resultant pipe displacements show that A1 type had the lowest deformations and, consequently, the A1 route is suggested for a pipe traversing a slope with rotational sliding pattern.

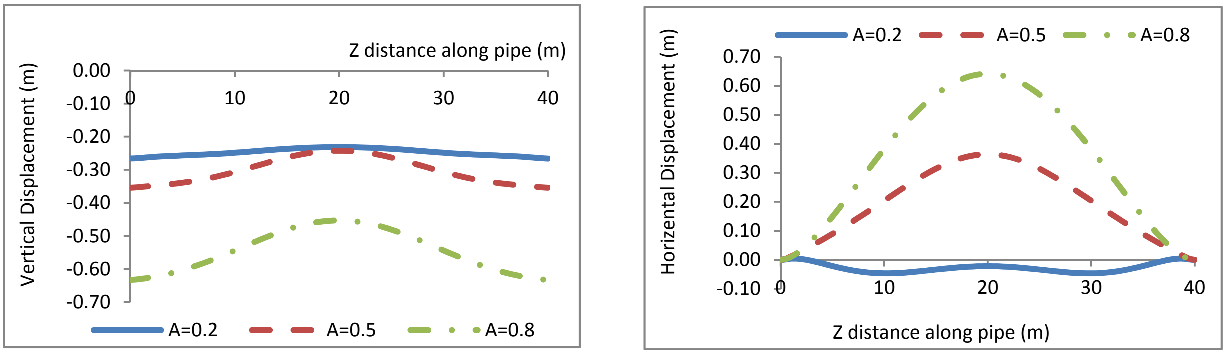

(a) (b)

Figure 11 Parameter "A": (a) vertical and (b) horizontal displacements along pipe length.

Table 6 Maximum horizontal and vertical displacements of the pipe with variation of parameter "A."

A	U_{1max} (cm)	*Z* for U_{1max}	U_{2max} (cm)
0.2	4.9	0.15<Z<0.35	26.6
0.5	36.9	0.35<Z<0. 5	35.5
0.8	64.6		63.5

Table 7 Maximum calculated horizontal displacement for mid-section of the slope.

Model No.	*Z* (m)	U_{1max} (cm)
1	40	65
2	40	21
3	60	56

In Models 1 and 2, two types of boundary conditions were considered with w = 40 m (see Table 6). In order to show the effect of boundary condition type and to be more close to natural circumstances, a w = 60 m model was also analyzed. Similar to Model 1, this model had constrained boundaries in x direction for z = 0, 60 planes. The horizontal displacement of $z= w/2$ plane for these three analysis case were compared in Table 7.

Models 3 and 4 considered two extreme boundary conditions of the planes, imposing minimum and maximum displacements in mid-section of the slope. It is logically expected that the displacement of Model 6 be between the corresponding measures of Models 1 and 2. This expectation was corroborated from the numerical analysis results presented in Figures 12 to 14. Since the displacement and strain values were symmetrically distributed in width direction, the presented values are allotted to mid-section of the models. Nevertheless, it is more accurate to extend the width of the model beyond 60 m to gain more logical values, but the model discretization and FE. calculations needed more effort and time for the analysis. So it is inferred that the Model 3 approximates the displacement closer to a natural slope.

The obvious similarities shown for displacement distribution pattern of Models 1 and 3 proved that free boundary conditions in longitudinal direction (assumed for Model 2) cannot correctly predict deformations. Furthermore, when the boundary conditions are left to be free, the whole model displacement follows a rigid mass pattern and consequently calculated deformations values are less than the other conditions.

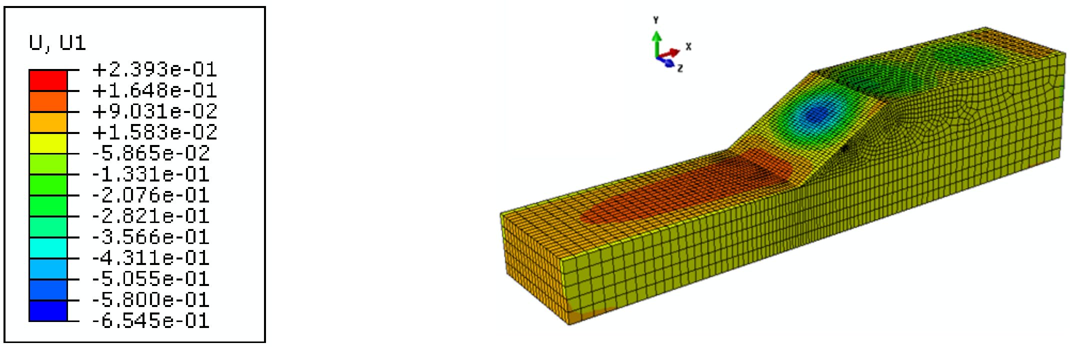

Figure 12 Horizontal displacement (m) of the slope for Model 1.

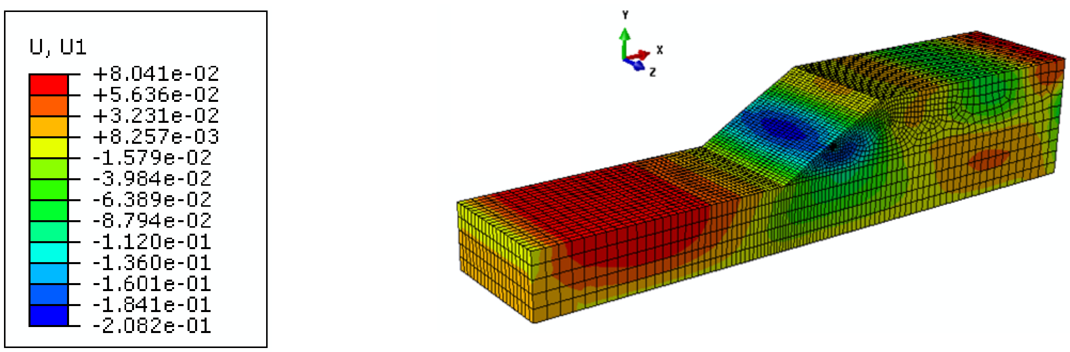

Figure 13 Horizontal displacement (m) of the slope for Model 2.

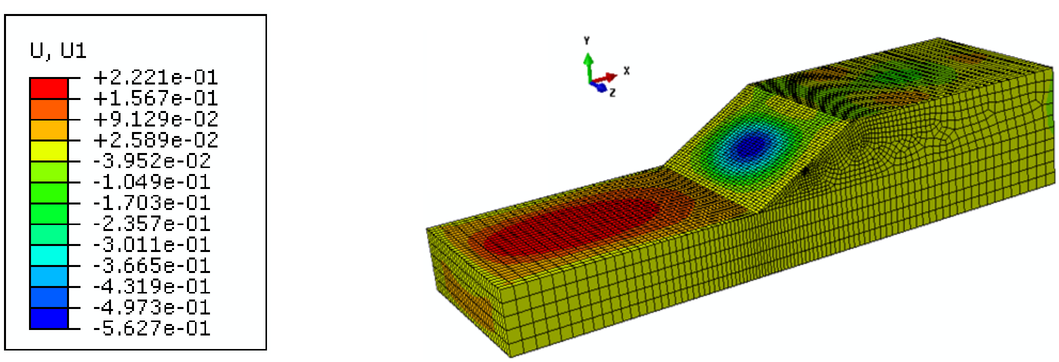

Figure 14 Horizontal displacement (m) of the slope for Model 3.

Physical Model Characteristics

The research group planned for a series of dynamic 1*g* shaking table test with the aim to model the landslides and its effect on pipe behavior. The prototype soil was Tehran cemented soil including granular materials bonded by cemented compositions. Models were constructed using Babolsar coastal sand having no cohesive materials, with a relative density of 50%. The pipe was a steel 10-in. pipe with 0.219 in. wall thickness due to API grade B materials, which was converted to an aluminum pipe having 1.67 cm diameter and 1 mm wall thickness, considering the similitude laws and conditions. Table 8 summarized the process through which the model pipe characteristics were extracted from prototype one.

The soil container was a box frame composed of steel profiles and plates. Also, a transparent Plexiglas sheet placed in front face of container, enabling monitoring of slope deformations during excitation from longitudinal side. Comparing the box dimensions [300×100×150 cm (*L.W.H.*)] with a real slope, the geometrical ratio, λ, was 10. It is assumed that the prototype and model soil have equal densities ($\lambda\rho$=1) with different shear wave velocities (V_{sp}=375 and V_{sm}=50 m/sec), resulting in $\lambda\varepsilon$=0.18. Using the mentioned assumptions, the bending strength of prototype pipe was converted to model scale by similitude laws [Iai 1989; 2005], and the model pipe dimensions were calculated.

Each test model subjected to four excitations with different amplitudes, but similar frequency and cycle numbers. In the first sub-test regarding to Iranian standard for earthquake resistant structure design specifications (regulation No. 2800), the acceleration amplitude of 0.35*g* was selected. Then by using the Seed method [Kramer 1996], a harmonic sinusoidal record having 0.23*g* amplitude, 5 Hz frequency and 25 cycles were applied to model a 7.5–8.5 magnitude earthquake. The first step acceleration amplitude was increased in following tests with regard to Table 9.

The 4 m×4 m shaking table at Sharif University of Technology was used to induce the desired excitations to the models. The table has three degree of freedoms in *x*-, *y*-direction and rotation around the *x*-*y* plane vector, with the maximum displacement of 250 and 400 mm in *x*- and *y*-directions; respectively. Also, it can sustain a model up to 20 tons in weight (the constructed slope model and the box weighted 6 tons).

Considering all given information, three physical models were constructed and tested by 1*g* shaking table device. Both models simulated a pure bending condition for the pipe and the sliding direction was perpendicular to the pipe axis. Figure 15 illustrates the model, pipe, and sensors configuration in the rigid box. Each pipe was divided to three sections in x=L/8, L/4 and L/2 length and had 3 or 4 strain gauges (with 5 *mm* length) installed. Figure 16 shows a typical pipe section and an installed strain gauge on the pipe.

The pipe supports resembled a complete hinge, allowing the aluminum pipe to be configured in any desired angle due to distributed dynamic loads around *x*- and *z*-axes. With a combination of bolts, washers, and nuts, together with a U-shaped steel profiles, the hinge support was constructed. Then the whole system was fixed to the U-shaped steel support that firmly connects the hinge to the rigid box bottom. A fastener ring fixed the aluminum pipe to the hinge support. The whole support mechanism along with an installed aluminum pipe is shown in Figure 17. The interior view of three installed aluminum pipes in the empty box and an installed one can be seen in Figure 18.

Table 8 Prototype and model pipe characteristics.

λ	$\lambda\rho$	λ_ε	λ_{EI}	EI_p	EI_m	OD_p	WT_p	I_p	I_m	WT_m	D_m
				N.m^2	N.m^2	in	in	cm^4	cm^4	mm	cm
10	1	0.18	56250	7.16E+06	127.28	10	0.219	3580	1.84E-01	1	1.67

p: prototype; ***m***: model; ***WT***: wall thickness; ***I***: moment inertia; ***D***: diameter

Table 9 Loading characteristics in each model.

Sub-Test No.	Acceleration amplitude (*g*)	Frequency (Hz)	Number of cycles
1	0.230	5	25
2	0.330		
3	0.460		
4	0.575		

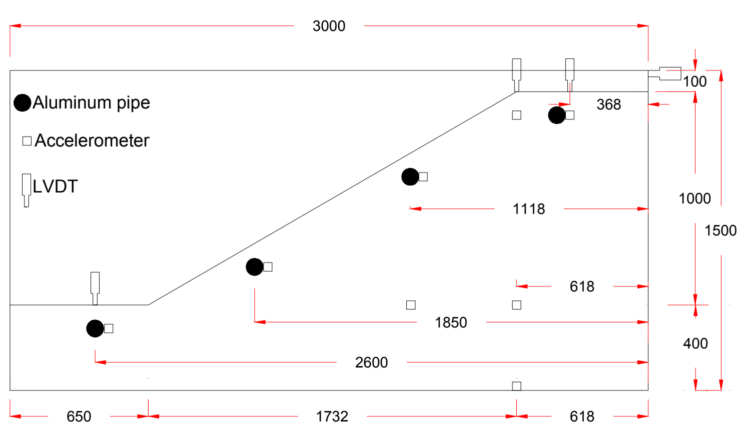

Figure 15 Soil container and pipe sensors configuration in the constructed slope.

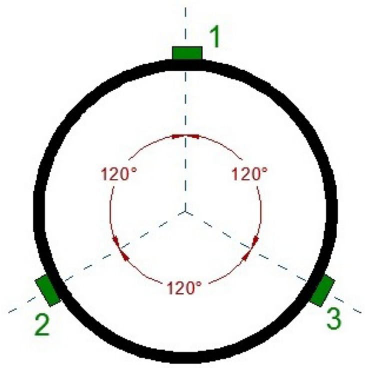

(a) (b)

Figure 16 (a) Pipe cross section showing the strain gauges confirmation; and (b) installed strain gauges on pipe wall.

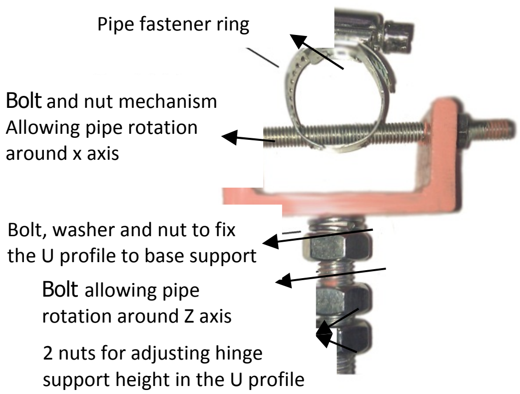

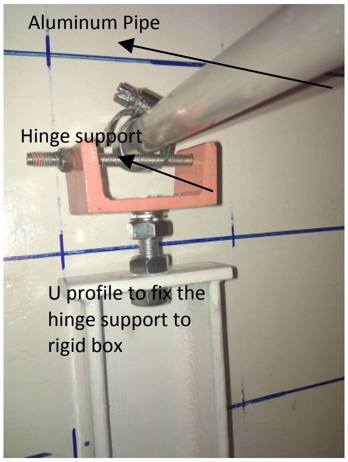

(a) (b)

Figure 17 (a) the mechanism of hinge support to allow pipe rotation around *X*-and *Z*-axis; and (b) installed hinge and base supports on the steel frame in the box.

(a) (b)

Figure 18 (a) installed aluminum pipes, hinge and base supports in the rigid box-ready for model construction; and (b) fixing the aluminum pipe in the model during slope construction.

Figure 19 Constructed slope with plaster strips showing in Model 2 before test.

In order to monitor the slope displacement during the tests, a 3-cm plaster strip was poured adjacent the Plexiglas plate at each 10-cm layer, and soil displacement pattern and failure surface formation were quantitatively determined. Figures 19 and 20 show the plaster strips before first test and after third one for Model 2. The relative densities calculated for each test are presented in Table 10. Besides the above mentioned data, Figures 21 to 24 depict the unfiltered recorded time history of accelerations in the box bottom, top, and on the pipe support. Reviewing the variation of acceleration amplitude reveals that the box behaves rigidly in height and had no effect on imposed acceleration on slope vertical surfaces.

Figure 20 **Constructed slope with deformed plaster strips showing soil displacements in Model 2 after Test 3.**

Table 10 **Relative densities before and after dynamic tests.**

Model No.	Test No.	Before test Dr (%)	After test Dr (%)
2	1	40	55
	2	55	59
	3	59	72
	4	72	90

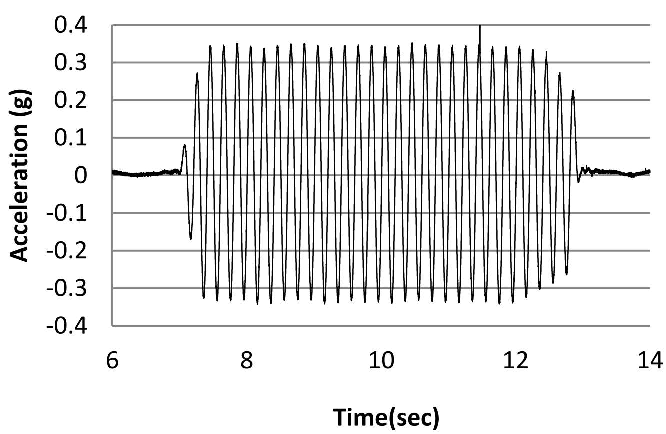

Figure 21 **Acceleration time history of accelerometer No. 0 on shaking table (Test 2).**

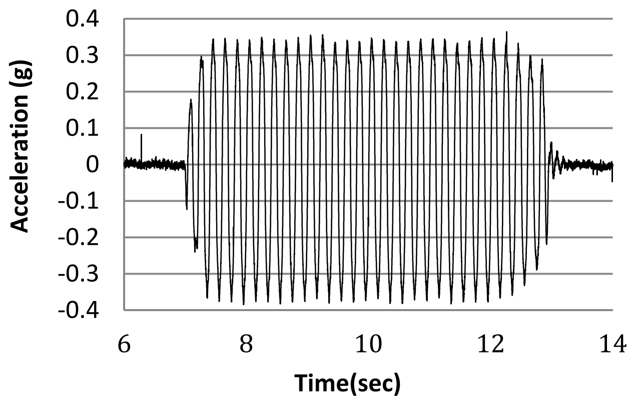

Figure 22 Acceleration time history of accelerometer No. 1 on box bottom (Test 2).

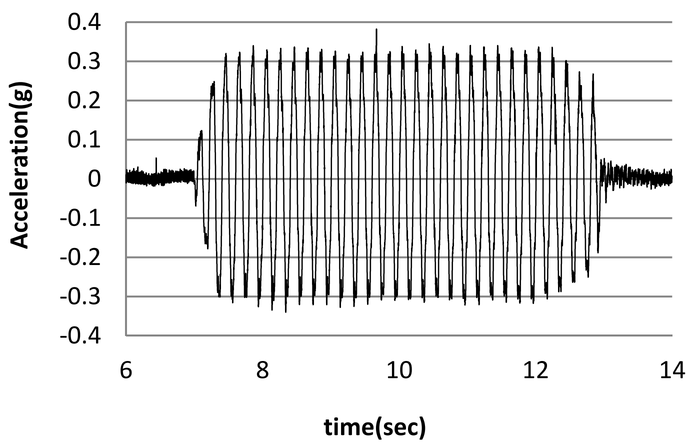

Figure 23 Acceleration time history of accelerometer No. 4 on top of the soil box (Test 2).

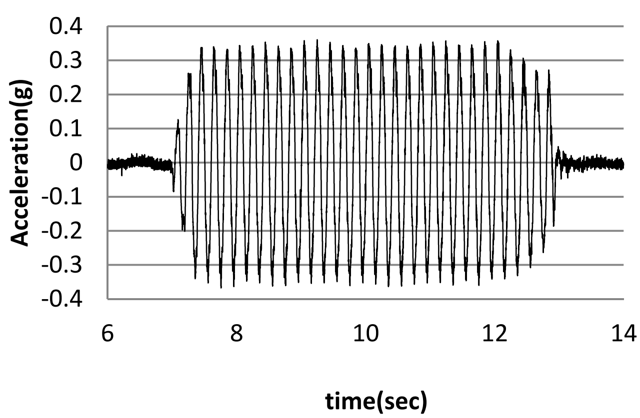

Figure 24 Acceleration time history of accelerometer No. 7 on pipe support in 30 cm height in the box (Test 2).

CONCLUSIONS

The Sharif University of Technology is engaged in a research project supported by Tehran Gas Company to investigate buried Tehran gas pipeline and network vulnerability in slopes with landslide potential during probable earthquakes. All landslide potentials in the route of gas pipes were reviewed using topographical maps and the field surveys. The studies and field observations proved the existence of potential landslides in the north and northwest of Tehran. A deterministic and probabilistic earthquake hazard analysis assisted researchers in choosing the best matching strong ground motion parameters for numerical and physical modeling.

Numerical analysis using the ABAQUS computer program together with physical modeling by means of shaking table device was performed to determine the system behavior in any earthquake-induced dynamic event. Dynamic loading, model geometry, soil and pipe characteristics, and other system configurations in both numerical and physical models were selected from available technical and scientific papers, documents received from the Tehran Gas Company, and engineering consultants.

Preliminary numerical analyses proved the importance of boundary condition features on deformations and strains. Thus, through the analysis it is inferred that fixed boundary conditions in x-direction can result in more realistic measures of displacements. In addition, it was concluded that the upper part of the slope is safer than other parts for a traversing pipe. More numerical modeling and laboratory testing are required in this regard.

In addition to numerical modeling, in 2012 a comprehensive laboratory testing program was launched at the Sharif University Earthquake Engineering Research Center; to date three dynamic physical models were constructed and tested. The record was selected to model a 975-return period earthquake and is compatible with site geological and geotechnical specifications with regard to seismicity studies. This research is an ongoing, and the analysis of dynamic models is now in progress by the research team.

REFERENCES

ABAQUS (2010). *6.10 Documentation Collection* , Dassault Systems Simulia Corp., Providence, RI.

Abdi M.R. (2008). Cementation influence on shear strength parameters of sand with direct shear test, *Proceedings, 4th National Civil Engineerimg Conference*, Sharif University of Technology, Tehran, Iran.

ALA/ASCE (2005). Guidelines for the Deisgn of Buried Steel Pipe, American Lifeline Alliance, American Society of Civil Engineers, New York, NY.

ASCE (1984). *Guidelines for the Seismic Design of Oil and Gas Pipeline Systems,* American Society of Civil Engineers, Committee and Gas and Liquid Fuel Lifelines, New York, NY.

ASCE (2010). ASCE/SEI 7 Minimum Design Loads for Buildings and Other Structures," American Society of Civil Engineers, New York, NY.

Boivin R.P., Cavanagh P.C., Clarke R.G. (1993). Directional drilling solves unstable slope along Canadian pipeline, *Oil and Gas Journal*; 91 (36).

Boore D.M. (1983). Stochastic simulation of high-frequency ground motion based on seismological models of radiated spectra, *Bull. Seismol. Soc. Am*., 73(6) 1856–1894.

Bruschi R., Spinazze M., Tomassini D., Cuscuna S. (1995). Failure modes for pipelines in landslide areas, ASME , *Proceedings, International Conference on Offshore Mechanics and Arctic Engineering,* 5: 65−78.

Brand D. (2000): MCEER-supported researchers conduct ground breaking earthquake simulation experiment at Cornell Univeristy. International earthquake-simulation experiment at Cornell is moving the earth to study forces on gas pipelines, *MCEER News*, State University of New York, Buffalo, NY.

Jafarzadeh F., Farahi Jahromi H., Yoosefi S., Sehizadeh M., Joshaghani M. (2013). Dynamic response of buried gas pipelines due to earthquake induced landslides by nonlinear numerical modeling, *Proceedings, 15th World Conference on Earthquake Engineering*, Lisbon, Portugal.

Cocchetti G., di Prisco, C., Galli A., Nova R. (2009). Soil–pipeline interaction along unstable slopes: a coupled three-dimensional approach. part 1: theoretical formulation, *Canadian Geotech. J*., 46(11): 1289-1304.

Cocchetti G., di Prisco D., Galli A.(2009). Soil–pipeline interaction along unstable slopes: a coupled three-dimensional approach. part 2: numerical analyses, *Canadian Geotech. J*., 46(11): 1305−1321.

Fakharian K. (2004). Cementation influence on the cohesion parameters of Tehran granular soils, *Proceedings, 1st National Civil Engineerimg Conference*, Sharif University of Technology, Tehran, Iran.

Ghanbari A. (2009). Study of elastic modulus of alluvium deposits in southern of Tehran, *Scientific Quarterly Journal*, Geosciences, 18(71).

Haeri S.M., Rastgou D. (2008). Study of Tehran natural cemented soil characteristics with direct shear and large scale triaxial tests, *Proceedings, 4th National Civil Engineering Conference*.

Haeri S.M., Asghari E. (2004). Cementation influence on shear strength of Tehran gravely sand with triaxial tests, *Journal of Sciences* ,University of Tehran. ISSN 1016-1104.

Haeri S.M., Banasiri J. (2002). Influence of artificial cementation on strength parameters of gravely sands with direct shear test, Proceedings, 3rd International Conference on Soil Mechanics and Geotechnical Engineering, Zurich, Switzerland.

Iai S.(1989). Similitude for shaking table tests on soil-structure-fluid model in 1g gravitational field, *Soils and Foundations*, 29(1): 105−118.

Iai S. (2005). Remediation of liquefiable soils for port structures in Japan—analysis design and performance, *J. Earthq. Eng.*, 9: 605−615.

IITK-GSDMA (1997). *Guidelines for Seismic Design of Buried Pipelines*, Indian Institute of Technology, Kanpur, Gujarat State Disaster Mangement Authority, Gujarat, India.

Japanese released standards for pipeline designs against PGDs.

Kramer S. (1996). *Geotechnical Earthquake Engineering*, Prentice Hall, Upper Saddle River, NJ.

Lysmer J., Kuhlemeyer R.L. (1969). Finite dynamic model for infinite media, ASCE, *J. Eng. Mech. Div*., 95(EM4): 859−877.

Maugeri M., Motta E., Casamichele P. (2004). Non-linear analysis of soil-pipeline interaction in unstable slopes, *Proceedings, 13th World Conference on Earthquake Engineering,* Paper No. 3161, Vancouver, B.C., Canada.

O'Rourke M.J., Liu X., Flores-Berrones R. (1995). Steel pipe wrinkling due to longitudinal permanent ground deformation, *J. Trans. Eng*., 121(5): 443−451.

O'Rourke M.J., Liu X. (1999). Response of buried pipelines subject to earthquake effects, *MCEER Monograph No. 3*, State University of New York, Buffalo, NY.

O'Rourke T. (1988). Critical aspects of soil-pipeline interaction for large ground deformation, *Proceedings, 1st Japan-U.S. Workshop on Liquefaction, Large Ground Deformation and Their Effects on Lifeline Facilities*, Assoc. for Devel. of Earthquake Prediction, Japan, pp. 118–126.

Newmark N., Hall W.J. (1975). Pipeline design to resist large fault displacements, *Proceedings, U.S. National Conference on Earthquake Engineering,* pp. 416–425, Ann Arbor, MI.

Park, K., Michael, S., Seo, W. and Stokoe, K.H., II, (2010). "Field Measurements of Linear and Nonlinear Shear Moduli of Cemented Alluvium", *Proceedings, 9th US National and 10th Canadian Conference on Earthquake Engineering*, 10 pgs, Toronto, Canada.

Qiao L., Ch. Yuan, M. Miyajima and E. Zhai (2008). Shake-table testing and flac modeling of liquefaction-induced slope failure and damage to buried pipelines, ASCE. *Proceedings, Geotechnical Earthquake Engineering and Soil Dynamics IV Congress*, GSP 181.

Suzuki N., Arata O., Suzuki I. (1988). Parametric study of deformation analysis of welded pipeline subject to liquefaction-induced permanent ground deformation, *Proceedings,, 1st Japan-U.S. Workshop on Liquefaction, Large Ground Deformation and Their Effects on Lifeline Facilities*, Assoc. for Devel. of Earthquake Prediction, Japan,, pp. 155–162.

Tehran Gas Company (2005). *Report on Seismic Retrofitting of Tehran Gas Pipelines*.

Tika T. (2010). Dynamic properties of cemented soils from Cyprus, *Bull. Eng. Geol. Environ.,* 69: 295–307.

Youd T.L. (1973). Ground movements in the Normal Lake vicinity during San Fernando, California, earthquake of February 9, 1971, U.S. Dept. Of Commerce, Vol. III, pp. 197–206.

Assessment of the Behaviour of Buried Gas Pipelines Subjected to Reverse Faulting

F. R. Rofooei[3], H, Hojat Jalali[1], Nader K. A. Attari[4], and M. Samadian[5]

ABSTRACT

Buried pipelines as one of the critical elements of infrastructure in modern cities could be endangered by different hazards such as permanent ground displacement (PGD) and/or wave propagation along their routes. Many reconnaissance reports have indicated considerable damages to gas and water supply pipelines caused by earthquakes. Over the past few decades, researchers have attempted to investigate the behaviour of buried pipelines crossing active faults. Recent studies at Cornell University and Rensselaer Polytechnic Institute focused on large-scale and centrifuge modeling techniques to study the behavior of buried high density poly-ethylene (HDPE) pipelines subjected to strike-slip faulting, respectively. In this paper, the behavior of buried steel gas pipelines with diameters equal to 4 and 6 inches subjected to reverse faulting is investigated by means of full-scale experiments and finite element analyses. The tests are performed for a dip angle of 61°. The experimental work presented herein is a part of a larger project conducted by Sharif University of Technology at Building and Housing Research Center (BHRC) for Tehran Province Gas Company. The obtained results indicate a good agreement between the measured strains from the experiments and the numerically computed strains and their distribution along the considered pipes. Based on the results of the finite element models, the maximum equivalent soil-pipe interaction forces were determined and the results were compared with those suggested by existing guidelines.

INTRODUCTION

Gas pipelines are an important part of infrastructures in today's modern cities, and therefore maintaining their operation in the case of an earthquake is of outmost importance. Since buried pipelines usually traverse large geographical distances, they cac be exposed to a variety of hazards, such as surface faulting, landslides (PGDs), and/or wave propagation. During the past century many reports have been published regarding the inflicted damages to gas and water supply pipelines caused by earthquakes such as 1906 San Francisco, [O'Rourke and McCaffrey 1984], 1978 Miyagiken-Oki [Liang and Sun 2000], 1990 Manjil [Towhata 2010], 1994 Northridge [O'Rourke and Palmer 1996], 1999 Chi-Chi [EERI 1999], and Kocaeli [JSCE 1999] earthquakes.

Faulting can occur in the forms of dip-slip (normal or reverse), strike-slip or a combination of strike-slip and reverse or normal faults, referred to as oblique faults. Figure 1 shows different types of faulting and their effects on buried pipelines. Based on the types of

[3] Department of Civil Engineering, Sharif University of Technology, Tehran, Iran.
[4] Department of Structural Engineering, Building & Housing Research center, Tehran, Iran.
[5] Director of the Research Bureau, Tehran Province Gas Company, Tehran, Iran.

faulting and the relative orientation of the pipeline with respect to the fault, the pipeline might be subjected to axial tension and bending [Figure 1(a) and 1(c) for $-\alpha$] or axial compression and bending (Figure 1(b) and 1(c) for $+\alpha$). Buried steel pipelines crossing reverse faults are subjected to a combination of axial compression and bending, which in turn can result in local buckling of the pipe. Thus, it is essential to study the effect of reverse faulting on buried steel gas pipelines to identify the potential hazards.

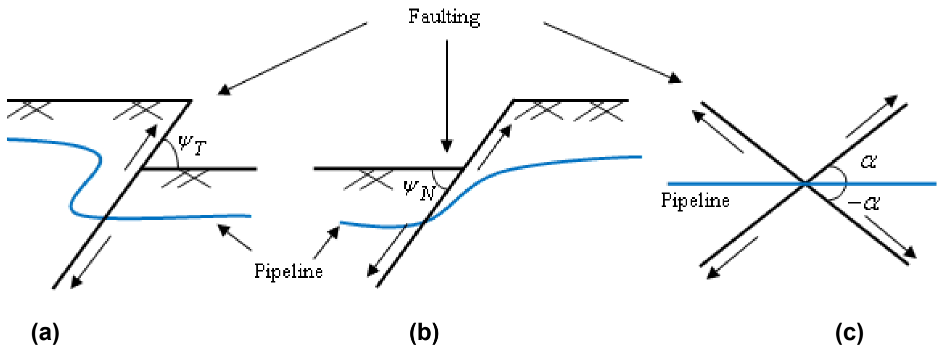

Figure 1 Different fault types and their effect on pipelines: (a) reverse fault (elevation) with angle ψ_T; (b) normal fault (elevation) with angle ψ_N; and (c) strike-slip fault (plan view) with angle α [Ha et al. 2008a].

Due to their importance, many analytical, numerical and experimental research have been conducted in recent years on buried pipelines. Analytical researches were initiated by Newmark and Hall [1975], Kennedy et al. [1977], and Wang and Yeh [1985], and extended by Karamitros et al. [2007; 2011]. O'Rourke and Liu [1999] reviewed the behavior of continuous and segmented buried pipelines subjected to peak ground deformation (PGD) and wave propagation hazards, as well as existing numerical and analytical methods to quantify their behavior.

Takada et al. [1998] performed a parametric study on shell-mode response of buried pipelines to large fault movements and considered the effect of local buckling in the analyses. Vazouras et al. [2010] performed a three-dimensional finite element study on buried steel pipelines subjected to strike-slip faulting of right angle by taking into account various parameters, such as diameter-to-thickness ratios, cohesive and non-cohesive soils, and different steel materials. Using large split-box at Cornell University, Yoshizaki et al. [2003] carried out an experimental investigation on the effects of PGD caused by strike-slip fault offset of right-angle on buried steel gas distribution pipelines with elbows during earthquakes, and calibrated the finite element models for further studies. Recent studies at Rensselaer Polytechnic Institute focused on centrifuge testing as well as finite element techniques to study the behavior of buried high density polyethylene (HDPE) pipelines subjected to strike-slip faulting [Ha et al. 2008a; 2008b; Abdoun et al. 2009; Ha et al. 2010; Xie et al. 2011].

As indicated by the existing literature, the behavior of buried pipelines subjected to reverse faulting has not been studied extensively. Therefore, a detailed joint research program was carried out by Sharif University of Technology in collaboration with Tehran Province Gas Company to study the behavior of buried gas distribution pipelines crossing reverse faults. This paper presents the results of two full-scale tests on 4- and 6-in.-diameter steel gas pipelines that were subjected to reverse faulting. Studied were the effect of different parameters such as the size of the horizontal and vertical offset of the fault, the ratio of burial depth to the pipe diameter, and pipe-diameter-to-wall thickness. Two finite element models were prepared and verified using the experimental results. In addition, the maximum soil-pipe interaction forces were calculated and compared to values suggested by ASCE's *Guidelines for the Seismic Design of Oil and Gas Pipeline Systems* [ASCE 1984].

EXPERIMENTAL SET-UP AND INSTRUMENTATION

Figure 2 shows the experimental set-up for studying the behavior of buried gas distribution pipelines subjected to reverse faulting. The dimensions of the split-box were determined such that the soil-pipeline interaction be unaffected by the boundaries of the test apparatus. The split-box was designed to test 8-m-long steel pipelines with end reaction force being around 785 kN. The approximate dimensions of the test basin are $8.5 \times 1.7 \times 2$ m (length$\times$width$\times$height) and the fault angle is considered to be 61° with respect to the horizontal plane. The fault plane is considered to be in the middle of the box, dividing the box into the fixed and moving parts. The moving part can be displaced along the faulting plane up to 90 cm; only 60 cm of uplift was exercised in the tests. The floor of the test basin is bolted to eight laterally restrained columns, each 1 m long, which are attached to their supports in the strong floor laboratory. Note that the configuration of the test basin can be reasonably modified in order to meet alternative test configurations.

Each part of the split-box when filled with sand weighs approximately 25 tons. Four rails (two at the fault interface and two on the external frames) were used to lift the moving part using three synchronized hydraulic jacks to ensure uniform displacement, with compressive load capacities of 490 kN each. High-level force-tolerating ball bearings were used inside the rails to ease the slippage of the two parts under applied loading. The external frames were considered to guarantee the stability of the moving part. The three hydraulic jacks were placed under the test basin, in the space provided by the 1-m columns and were configured as apices of a triangle aligned with the fault line.

The material properties of the sand used in this study are shown in Table 1. A well graded sand (SW) with a water content of about 4.5~5% was used and compacted to a relative density of about 75%. The steel pipelines were manufactured in accordance with API-5L Grade B, with a specified minimum yield stress and ultimate tensile strength of 241 MPa and 414 MPa, respectively, and were used with external coating to resemble field conditions.

The pipelines were instrumented with 50 strain gauges, with the ability to measure large strains up to 20% and six linear variable differential transformers (LVDTs). The 50 strain gauges were attached to crown and invert of the pipes in 20 stations in the longitudinal direction, and were more concentrated in the vicinity of the fault plane. The LVDTs were installed so that the axial displacements and the end-rotations of the pipe-ends could be measured, as shown in Figure 3. The fault offset was also measured by three independent wire displacement transducers under the moving part of the split-box.

Figure 2 Split-box test basin at structural laboratory.

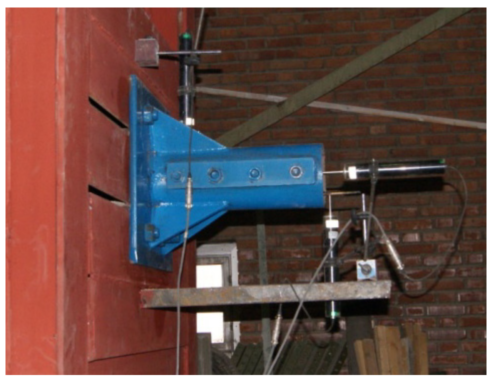

Figure 3 LVDT configuration at the pipe end connection.

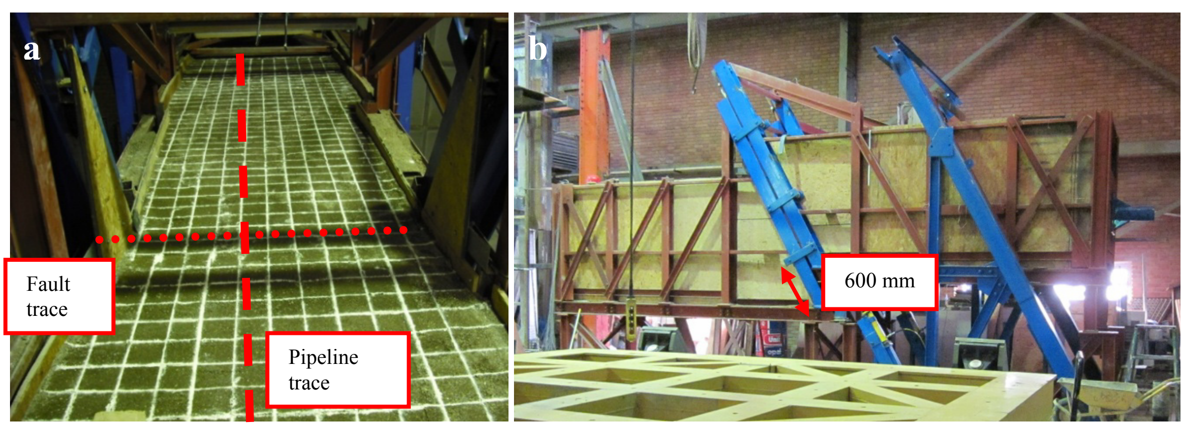

(a) (b)

Figure 4 (a) Soil surface preparation for test No. 2; and (b) split-box after 0.6 m faulting.

Table 1 Material properties for sand backfill.

Soil Property	Value
γ_d, dry unit weight (kN/m^3)	17.9
G_s, specific gravity	2.56
ϕ, friction angle (degree)	33.5
D_{50}, average particle size (mm)	1.1
C_u, coefficient of uniformity	6.69
C_c, coefficient of curvature	1.01

Table 2 Properties of the experiment.

Test No.	*D* (mm)	*t* (mm)	*D*/*t*	*H* (m)	H/D	Fault dip angle (°)	Displacement (m)
1	114.3	4.4	26	1	8.8	61	0.6
2	168.3	4.4	38	1	5.9	61	0.6

The burial depths in both tests were considered to be the same as in the field installations of these pipes, which is equal to 1 m. Approximately 20 m^3 of soil was used to perform the tests. The soil was placed in nine lifts, with 200 mm of thickness for each, and was compacted using a vibratory plate tamper. Finally, the top surface of the soil was prepared by leveling and painting gridlines at approximately 100 mm spacing; see Figure 4(a). The faulting follows a displacement-control procedure where the moving part of the test basin is lifted using the three synchronized hydraulic jacks up to a displacement of 0.6 m along the fault plane. Table 2 summarizes the two full-scale experiments. Figure 4(b) shows the split-box after applying the fault displacement. No internal pressure was considered for the pipes in these tests.

FINITE ELEMENT MODELING

A three-dimensional continuum finite element model was constructed similar to the experimental prototypes to model the soil-pipe-fault system utilizing the finite element package ABAQUS [2011]. Geometrical and material nonlinearity of both the pipe and the soil were considered. The length, width, and depth of the finite element model was considered as 8 m, 1.4 m, and 1.8m, respectively, which were established based on sensitivity analyses and are consistent with the inner dimensions of the split-box. The pipe and the surrounding soil were modeled using four-node reduced integration shell elements (S4R) and eight-node reduced-integration brick elements (C3D8R), respectively (Figure 5). A uniform mesh with about 5200 shell elements for the 4- and 6-in. pipes was used, while the soil was modeled using 5332 solid continuum elements. The fault offset was distributed over a length of 0.3 m in order to avoid discontinuity at the fault plane. This is a common assumption accepted in practice and based is on sensitivity analysis on this width and numerical investigations performed by Vazouras et al. [2010].

An elastic-plastic material behavior with von Mises plasticity model and isotropic hardening rule was assumed for the steel pipe, while the soil behavior was modeled using an elastic-perfectly plastic Mohr-Coulomb model in which the soil mass density, friction angle, dilation angle, and Poisson's ratio were determined in a way to resemble the soil used in the experiment. Note that cohesion of 5 kPa was assigned to the soil for numerical convergence. The soil-pipeline interface considered the interface friction using a Coulomb friction criterion and also allows for a separation between the soil medium and the pipe. The friction coefficient, μ, was determined based on the reduced interface friction angle between the soil and the pipe, which is suggested to be equal to two-thirds φ according to Yimsiri et al. [2003]. Thus, for this study, μ was set to 0.41. The simulation procedure included the application of a gravity loading to account for the initial stress state in the soil, followed by imposing the reverse faulting motion to the hanging wall. The surrounding and bottom faces of the footwall were restrained in all directions, simulating a fixed block. The hanging wall was displaced 0.6 m along the faulting plane at an angle of 61° with respect to the horizontal plane. The relative displacements and rotations between the soil and pipe ends measured during the tests were considered in imposing the boundary conditions of the finite element model.

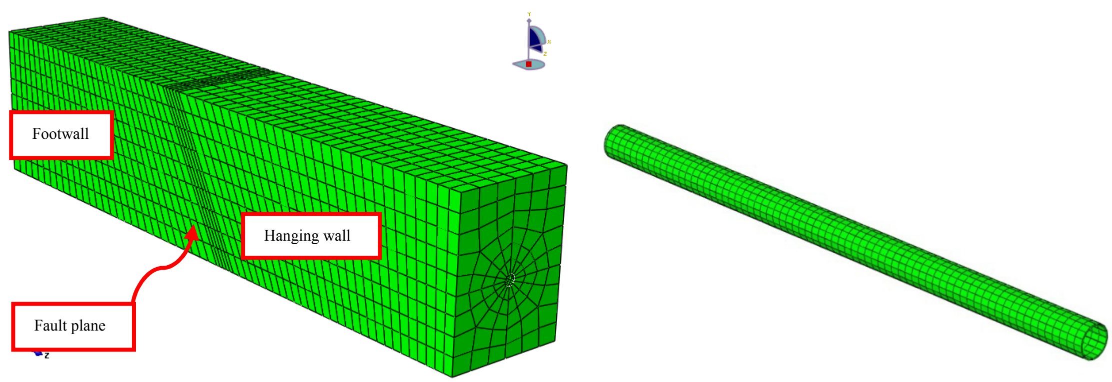

(a) (b)

Figure 5 Finite element model of the (a) soil, and (b) 4-in. steel pipe.

EXPERIMENTAL AND NUMERICAL RESULTS

The soil surface deformation for both tests showed more or less similar patterns. At the fault plane, transverse cracks were observed and propagated with increasing fault offset. As the fault offset exceeded 0.2 m, longitudinal cracks were observed above the pipeline trace in the hanging part due to the upward movement of the pipes in the moving part. With increasing fault offset, the transverse cracks were spread over a wider band at the fault trace and also transverse cracks were observed perpendicular to the longitudinal cracks. Note that no major change on the soil surface was observed at the fixed part of the split box (footwall). Figure 6 shows a closer view of the surface cracks in the region where local buckling occurred in the moving part for both tests. Both show the same trend: longitudinal cracks crossed by oblique transverse cracks moving towards the side walls and fault trace.

Figure 7 shows the deformation shape and a closer view of the buckled sections for both the 4- and 6-in. pipes, respectively. Both pipes exhibited an S-shape deformation, with the local buckling concentrated at two locations, one near the fault plane in the fixed box (footwall) and one away from the fault plane in the moving box (hanging wall); However, the location of local buckling for Test No. 1 and Test No. 2 were different. The distance between the two buckling sections for the 4- and 6-in. pipes were approximately 1.60 m and 2.20 m, respectively, and severe angular distortion of the pipe cross section was observed at these locations. There were no signs of rupture near these locations, but significance yielding and plastic deformations were observed at the buckled sections of the pipes, which could have been led to rupture if subjected to higher fault offsets or other loading types (such as settlement or cycles of frost and thaw). Note that in the vicinity of the buckling locations, the pipe coatings experienced severe cracking, and at some points the coatings had peeled off the pipes.

The soil deformation and pipe von Mises stresses after 0.6 m fault offset for the 6-in. pipe is shown in Figure 8. As it can be seen from the soil deformations, upheaval was observed at the soil surface in the hanging-wall side, which is consistent with cracks at local buckling sections in the hanging wall. The pipe deformation shape was similar to that observed in the experiments, i.e. an S-shape deformation with two buckling sections. The von Mises stress distribution for both pipes showed stress concentration at the locations of local buckling.

The experimental and finite element longitudinal crown and invert strains for the 4- and 6-in. pipes for different fault offsets are shown in Figure 9 and 10, respectively. For both pipes, strain concentration was observed in the vicinity of local buckling sections and the finite element analysis results follow the same trend as the experimental data. The maximum compressive strains for the 4- and 6-in. pipes from the experimental data are -11.7% and -9.2%, respectively. The lower maximum compressive strain for the 6-in. pipe was due to the higher relative stiffness.

(a) (b)

Figure 6 Soil deformation at pipe local buckling location in the moving part: (a) Test No. 1, and (b) Test No. 2.

(a) (b)

Figure 7 Deformed pipes after fault offset of 0.6 m: (a) Test No.1, (b) Test No. 2.

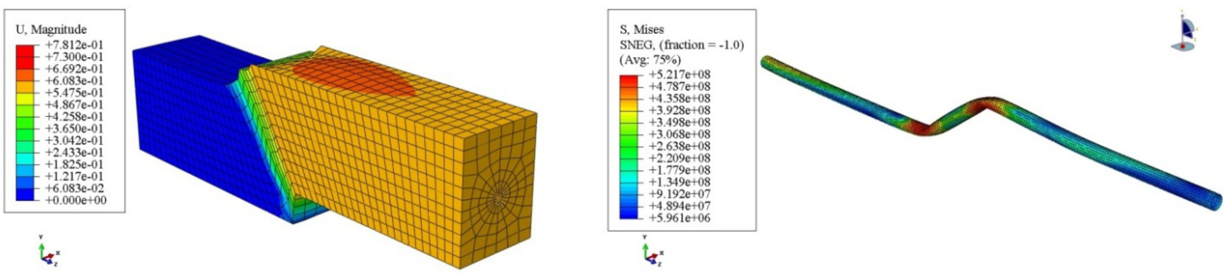

(a) (b)

Figure 8 (a) Soil deformation after 0.6 m fault offset, and (b) Von Mises stress distribution for Test No. 2.

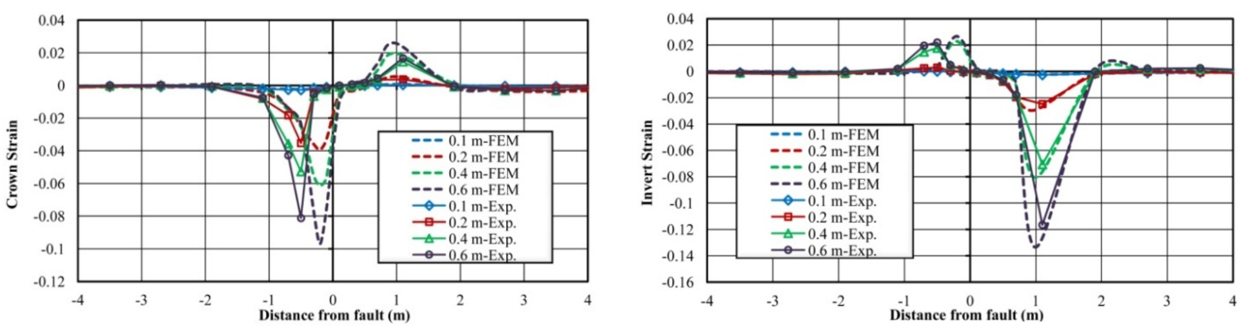

(a) (b)

Figure 9 Longitudinal strain for Test No. 1: (a) crown, and (b) invert strains.

In Figure 11 the cross-section distortion in the hanging wall obtained from finite element analyses for both pipes is compared with the experimental results. As shown, the shapes of the buckled pipes determined numerically are in good agreement with the experimental results. In general, it can be concluded that the finite element analysis results are on the safe side and are acceptable from an engineering point of view.

Next, the interaction forces were calculated based on contact pressures around the pipe in the finite element model. The pressure distribution around the pipe at a section -1.9 m away from the fault plane at a fault offset of 0.2 m is shown in Figure 12. The pressure distribution is symmetrical since the movement is only in the vertical plane. This diagram indicates that at this section the pipe is tending to move downwards with the soil reacting in the upward direction.

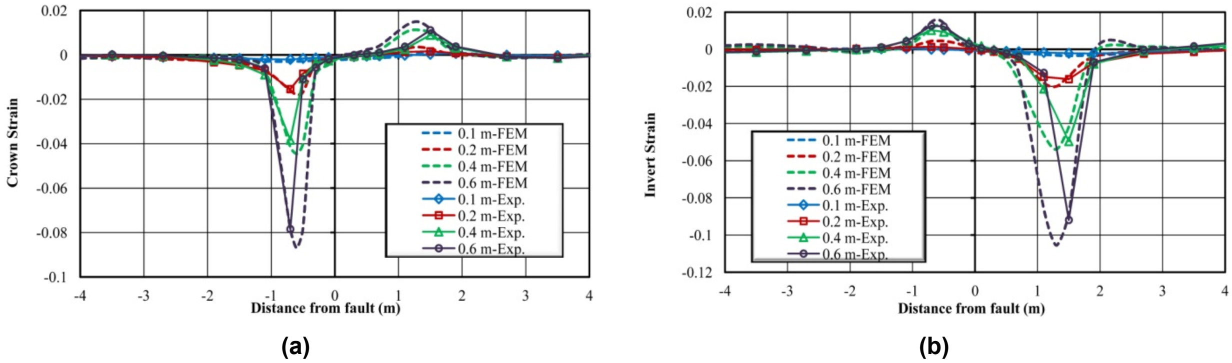

Figure 10 Longitudinal strain for Test No. 2: (a) crown, and (b) invert strains.

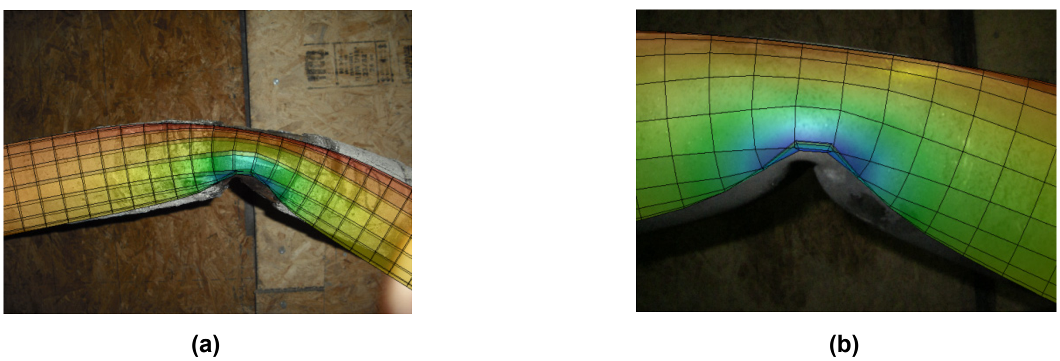

Figure 11 Finite element analysis versus experimental deformation of pipe cross-section for: (a) Test No.1, and (b) Test No.2 in the hanging part.

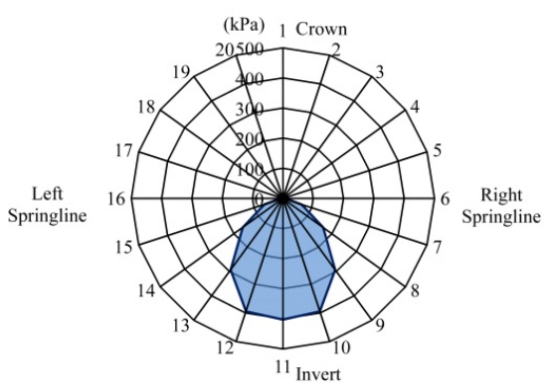

Figure 12 Pressure distribution for the 6-in. pipe at -1.5 m from the fault plane at a fault offset of 0.2 m.

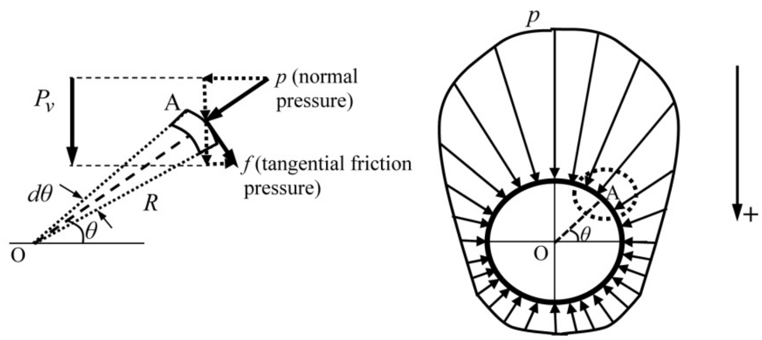

Figure 13 A schematic view of soil-pipe interaction force derived from pressure distribution around the pipe.

The soil-pipe interaction force per unit length can be calculated based on the contact pressure (see Figure 12) by integrating the pressures over the pipe perimeter, as shown in Figure 13. This method was used by Ha et al. [2010] for calculating lateral force distribution along HDPE pipes subjected to strike-slip faulting. The same methodology was used herein. In Figure 13, p , f , and P_v denote the normal, tangential friction pressure and equivalent vertical soil-pipe interaction force per unit length at the soil-pipe interface, respectively. The tangential component was calculated based on a Coulomb friction model mentioned earlier in the description of the finite element model, with a friction coefficient of 0.41. The vertical soil-pipe interaction force per unit length, P_v, was calculated by integrating the vertical components of the normal and tangential friction pressures over the pipe perimeter, as shown in Equation (1), where R, tan δ_{SI}, and θ denote the pipe outside radius, Coulomb friction coefficient, and position angle of a pipe differential segment, A, respectively. The downward direction is considered as the positive direction; therefore, a negative sign represents an upward force from the base (base reaction), and a positive sign stands for a downward force from the soil above the pipe crown.

$$P_v = \int_0^{2\pi} Rp(\theta)\sin\theta + \int_0^{2\pi} \tan\delta_{SI} Rp(\theta)\cos\theta \qquad (1)$$

Figure 14 shows the maximum upward and downward forces at different fault offsets for both pipes compared to values suggested by ASCE's *Guidelines for the Seismic Design of Oil and Gas Pipeline Systems* [1984]. The maximum downward force exceeds the corresponding values suggested by ASCE [1984], while the upward force is less than those of ASCE [1984]. After the maximum downward force was reached, it remained somewhat constant, with a slight decrease at a fault offset of 0.5 m for the 4-in. pipe. For this pipe, the maximum upward force decreased with increasing fault offset due to the upward movement of the buried pipe in the footwall (fixed) part; this resulted in a decreased in the pressure distribution to reduce, which caused the equivalent bearing force to decrease. The decrease in maximum bearing force for the 6-in. pipe occurred after a fault offset of 0.4 m. Once again this occurred because after fault offset of 0.4 m, the pipe buried in the footwall portion betan to move upward, causing the soil-pipe interaction force to decrease; before this fault offset the pipe moved downward.

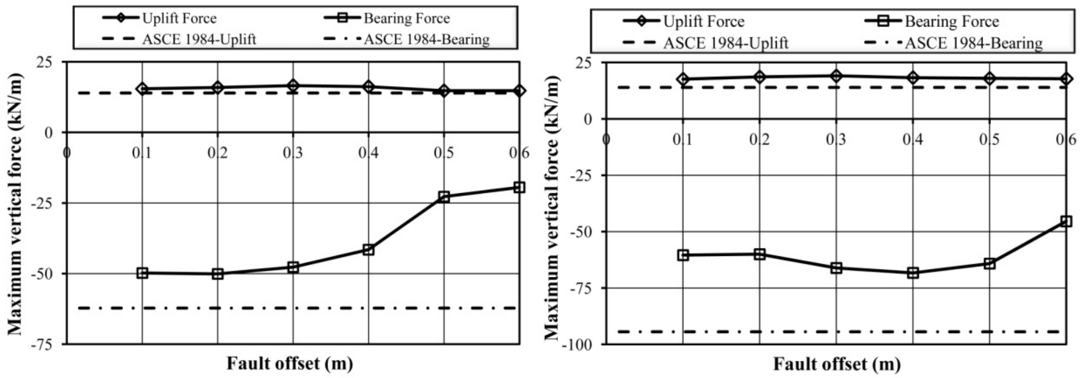

(a) (b)

Figure 14 Maximum uplift and bearing forces at different fault offsets for: (a) 4-in. pipe, and (b) 6-in. pipe.

SUMMARY AND CONCLUSIONS

The behavior of buried continuous steel pipes (API-5L Grade B) subjected to reverse faulting has been studied both experimentally and numerically for 4- and 6-in. pipes buried in sand at a depth of 1 m. Distributed crack patterns were observed at the fault plane. In the hanging wall, longitudinal and transverse cracks were observed above the buckling locations, while in the footwall no cracks were detected at the soil surface. Both pipes exhibited the same S-shape deformation, with local buckling at two locations: one near the fault plane in the footwall and one away from the fault plane in the hanging wall where severe yielding and plastic deformation were observed. The crown and invert strains were measured and compared to the finite element analysis for different fault offsets. Both the experimental and finite element analysis results showed strain concentration at local buckling locations. The peak negative strains for the 4- and 6-in. pipes were determined to be -11.7% and -9.2%, respectively. The peak compressive strains for the 6-in. pipe were lower than for the 4-in. pipe due to higher relative stiffness of the 6-in. pipe. Distortion of the pipes cross sections was compared using the experimental and finite element analysis results. In general, the results obtained from finite element analysis were in good agreement with the experimental measurements and could be used for determining soil-pipe interaction forces. The soil-pipe interaction forces were calculated using contact pressures at the soil-pipe interface by integrating the pressure around the pipe circumference. The soil-pipe interaction force in the upward direction is much higher in magnitude than the downward force. For both pipes the maximum upward force was less than the values suggested by ASCE [1984], while the maximum downward force exceeds slightly those of ASCE [1984].

ACKNOWLEDGMENTS

The experimental work presented herein is a part of a larger project conducted by Sharif University of Technology at Building and Housing Research Center (BHRC) for Tehran Province Gas Company. The authors wish to thank the Tehran Province Gas Company for their valuable support and assistance. The assistance of structural laboratory staff, especially Mr.

Alizadeh, Mr. Nooshabadi and Mr. Farrokhi is greatly acknowledged. Special thanks to Mr. Khalili for his invaluable support, advice and efforts in conducting the experimental part of the project.

REFERENCES

ABAQUS (2011). *Users' Manual, Version 6.11-1*. Providence, RI.

Abdoun T.H., Ha D., O'Rourke M.J., Symans M.D., O'Rourke T.D., Palmer M.C., Stewart H.E (2009). Factors influencing the behavior of buried pipelines subjected to earthquake faulting, *Soil. Dyn. Earthq. Eng.*, 29(3): 415–427.

ASCE (1984). *Guidelines for the Seismic Design of Oil and Gas Pipeline Systems,* American Society of Civil Engineers, Committee on Gas and Liquid Fuel Lifelines, Technical Council on Lifeline Earthquake Engineering, Reston, VA.

EERI (1999). *The Chi Chi, Taiwan earthquake of September 21, 1999, Special Earthquake Report*, Earthquake Engineering Research Institute, Oakland, CA.

Ha D., Abdoun T.H., O'Rourke M.J., Symans M.D., O'Rourke T.D., Palmer M.C., Stewart H.E. (2008a). Centrifuge modeling of earthquake effects on buried high-density Polyethylene (HDPE) pipelines crossing fault zones, *J. Geotech. Geoenviron. Eng.,* 134(10): 1501–1515.

Ha D., Abdoun T.H., O'Rourke M.J., Symans M.D., O'Rourke T.D., Palmer M.C., Stewart H.E. (2008b). Buried high-density polyethylene pipelines subjected to normal and strike-slip faulting: a centrifuge investigation, *Can. Geotech. J.*, 45(12): 1733–1742.

Ha D., Abdoun T.H., O'Rourke M.J., Symans M.D., O'Rourke T.D., Palmer M.C., Stewart H.E. (2010). Earthquake Faulting effects on buried pipelines-case history and centrifuge study, *J. Earthq. Eng.,* 14(5): 646–669.

JSCE (1999). *The 1999 Kocaeli Earthquake, Turkey, Investigation into the Damage to Civil Engineering Structures*, Japan Society of Civil Engineers, report of the Earthquake Engineering Committee, Tokyo, Japan.

Karamitros. D.K., Bouckovalas G.D., Kouretzis G.P. (2007). Stress analysis of buried pipelines at strike-slip fault crossings, *Soil. Dyn. Earthq. Eng.,* 27(3): 200–211.

Karamitros. D.K., Bouckovalas G.D., Kouretzis G.P., Gkesouli V. (2011). An analytical method for strength verification of buried steel pipelines at normal fault crossings, *Soil. Dyn. Earthq. Eng.,* 31(11): 1452–1464.

Kennedy R.P., Chow A.W., Williamson R.A. (1977). Fault movement effects on buried oil pipeline. *J. Trans. Eng.,* 103(TE5): 617–633.

Liang J., Sun S. (2000). Site effects on seismic behavior of pipelines: A review, *J. Press. Vess. Technol*., 122(4): 469–475.

Newmark N.M., Hall W.J. (1975). Pipeline design to resist large fault displacement, *Proceedings,* U.S. National Conference on Earthquake Engineering, Ann Arbor, MI, pp. 416–425.

O'Rourke M.J., Liu X. (1999). Response of buried pipelines subject to earthquake effects, *MCEER-99-MN03*. Multidisciplinary Center for Earthquake Engineering Research, Buffalo, NY.

O'Rourke T.D., McCaffrey, M.A. (1984). Buried pipeline response to permanent earthquake ground movements, *Proceedings,* 8th World Conference on Earthquake Engineering, San Francisco, California, v. VII, pp. 215–222.

O'Rourke T.D., Palmer, M.C. (1996). Earthquake performance of gas transmission pipelines, *Earthq. Spectra,* 12(3): 493–527.

Takada S., Liang J.-W., Li T. (1998). Shell-mode response of buried pipelines to large fault movements, *J. Struct. Eng.,* 44A: 1637–46.

Towhata I. (2010). *Geotechnical Earthquake Engineering*, Springer Series in Geomechanics and Geoengineering.

Vazouras, P., Karamanos, S.A., Dakoulas, P. (2010). Finite element analysis of buried steel pipelines under strike-slip fault displacements, *Soil. Dyn. Earthquake Engng.,* 30(11): 1361-1376.

Wang L.R.-L., Yeh Y.-H. (1985). A refined seismic analysis and design of buried pipeline for fault movement, *Earthq. Eng. Struct. Dyn.,* 13(1): 75–96.

Xie X., Symans M.D., O'Rourke M.J., Abdoun T.H., O'Rourke T.D., Palmer M.C., Stewart H.E. (2011). Numerical modeling of buried HDPE pipelines subjected to strike-slip faulting, *J. Earthq. Eng.*, 15(8): 1273–1296.

Yimsiri S., Soga K., Yoshiaki K., Dasari G.R., O'Rourke T.D. (2003). Lateral andupward soil-pipeline interactions in sand for deep embedment conditions, *J. Geotech. Geoenviron. Eng.,* 130(8): 830–841.

Yoshizaki K., O'Rourke T.D., Hamada M. (2003). Large scale experiments of buried steel pipelines with elbows subjected to permanent ground deformation, *J. Struct. Mech. Earthquake Eng.,* 20(1): 1s–11s.

AN OVERVIEW OF THE SEISMIC CODES PROVISIONS FOR VERTICAL IRREGULARITY CRITERIA: A PROPOSAL

H. Shakib[1] and M. Pirizadeh[2]

ABSTRACT

The vertical irregularities can influence the seismic performance of structures, depending on the limit-state or the level of seismic intensity considered. Therefore, most of seismic codes enclosed the limiting criteria for vertical irregular structures in order to prevent the discontinuity problems in the structures. In this paper, the comparative study on the different seismic codes provisions for vertical irregularities is presented. In addition, the effects of vertical irregularities on the seismic performance of steel moment frame structures are investigated from standpoint of different researchers. Based on the results, the suggestions for revision of seismic code provisions for vertical irregularities are presented.

Keywords: *seismic performance; steel buildings, vertical irregularities*

INTRODUCTION

Irregular buildings constitute a large portion of the urban elements. Experiences from the past earthquakes show that the seismic behavior of vertically irregular buildings can be significantly different in comparison to the regular counterparts. In general, vertical irregularities can be classified as non-geometric and geometric irregularities. In the geometric irregularity, the plan dimensions suddenly change over the height of building. In the non-geometric irregularity, the distribution of seismic lateral resisting properties, such as mass, lateral stiffness and strength, individually or in combination is non-uniform throughout the height of the building. The non-geometric vertical irregularities appear in the buildings due to such conditions as different uses of one floor compared to the adjacent ones or elimination of lateral resisting elements such as column, brace or shear wall in the parking or other stories due to architectural compulsions. The main types of geometric irregularities are setback buildings. Setbacks may be introduced for several reasons. The three most common ones are architectural regulations for tall buildings that entail upper floors to be set back to admit light and air to adjoining sites, program requirements that necessitate smaller floors at the upper levels, or stylistic requirements related to the building form. The lower level of a setback building with the largest floor area is usually termed the base, while the upper level with the smallest floor area is the tower. Setback buildings can be classified as one-side or two-side setbacks, based on their configurations. If the floor area of the tower is reduced from one side of the base floor plan, the structure is called a one-side setback structure, which is always asymmetric about the vertical axis of the structure. Therefore, a torsional response arises in these types of structures due to the eccentric location of the tower center mass/stiffness with respect to the base center mass/stiffness. On the other hand, if the floor area

[1] Professor, School of Civil and Environmental Engineering, Tarbiat Modares University, Tehran, Iran; email: shakib@modares.ac.ir.
2 Ph.D. Student, School of Civil and Environmental Engineering, Tarbiat Modares University, Tehran, Iran; email: pirizadeh@modares.ac.ir.

of the tower is reduced from two sides of the base floor plan, the structure is called a two-side setback structure.

The seismic performance of vertically irregular structures has been studied by many researchers. Valmundsson and Nau [1997] focused on evaluating the current seismic code requirements under which a structure can be considered vertically irregular. In addition, they compared the adequacy of simplified seismic code design procedures when applied to vertically irregular frames. Al-Ali and Krawinkler [1998] investigated criteria for limiting vertical irregularities in order to the effect of different irregularities on the seismic response of structures. They pointed out that mass irregularity has the lowest influence; whereas the influence of strength is more than stiffness on the seismic response of structure. They also concluded that the combination of strength and stiffness irregularities has the highest influence on the seismic demand. Chintanapakdee and Chopra [2004] conducted a study to compare the seismic demands for vertically irregular and regular frame buildings. They concluded that introducing a soft and/or weak story increased the drift demands on this story and some adjacent stories and decreased drift demands on other stories. Additionally, they investigated the accuracy of the modal pushover analysis for estimation of seismic demand for this type of buildings. Tremblay and Poncet [2005] determined whether or not dynamic analysis is really needed for buildings with mass irregularity as stipulated by major seismic codes.

On the basis of results obtained by two-dimensional nonlinear dynamic analysis, the authors concluded that even strong mass irregularity of structures designed with static analysis does not result in significant negative effects on their seismic response. Fragiadakis et al. [2006] evaluated the influence of vertical irregularities on a nine-story steel frame based on incremental dynamic analysis (IDA) and showed that in the inelastic limit-state ranges, some finding of previous researchers do not hold. Also, they concluded that the effects of vertical irregularities are highly dependent on the record selection and the effect of any single or multi-story vertical irregularities significantly differs depending on the limit-state or level of intensity considered. Le-Trung et al. [2010] investigated the seismic behavior of vertically irregular 20-story steel special moment frame buildings by nonlinear static and dynamic analyses. They concluded that the limitation of using ELF analysis for the design of irregular buildings may be not necessary and the limit values in the seismic codes to distinguish regular from irregular buildings should vary in accordance with the diverse positions of irregularities. They showed that the vertical irregularities placed at the bottom stories caused more serious effect than those placed at the other locations of the buildings. Also according to this study, the numbers of vertically irregular stories are significantly influential to the confidence levels of the buildings. Pirizadeh and Shakib [2013] evaluated the seismic performance of different non-geometric vertical irregular structures in comparison to a regular structure at various performance levels based on the probabilistic approach. The results showed that the non-geometric vertical irregularity influences the seismic performance of structures, especially at the limit-states close to collapse until global dynamic instability. These effects were on the seismic intensity capacity and/or on the ductility capacity of the structure, based on the type and the position of vertical irregularities. In addition, they showed that in the stiffness, strength and combined strength and stiffness vertical irregularities, when the position of irregularities is in the bottom stories of the structure, the CP and especially

GI limit-states are exceeded at the lower drift ratio capacities, compared to the regular structure. These vertical irregularities caused that damage concentration shifts towards the bottom stories and so the structure not to able to make use of its reserve ductility at the limit-states away from the collapse.

Also several researchers such as Shahrooz and Moehle [1990], Duan and Chandler [1995], and Karavasilis et al. [2008] have discussed the distribution of drifts over the height of setback frame structures and shown that the interstory drifts of the tower are larger than the corresponding level at the regular structure. Duan and Chandler [1995] focused on the torsional response of setback buildings, and they identified the need for imposing increased strength on the tower. Karavasilis et al. [2008] showed that the maximum deformation demands are concentrated in the tower for tower-like structures and in the neighborhood of the setback line for other geometrical irregularities. Pirizadeh and Shakib [2010] evaluated the seismic response of one-side setback buildings subjected to random earthquake excitations using the power spectral density (PSD) analysis. The statistical results showed that the height setback ratio, the area setback ratio and the direction of earthquake excitation significantly influence the distribution of seismic demands over the height. It is notable that the most researchers have evaluated the performance of setback buildings under unidirectional horizontal seismic excitation. However, the eccentricities in one-side setback buildings lead to coupling of the response of the structure in two directions. In addition, in another study, Shakib and Pirizadeh [2013] investigated the seismic performance of one-side setback structures under the simultaneous action of orthogonal ground motion components, based on the probabilistic approach. The results showed that the simultaneous influence of ground motion components on the seismic performance of these structures is significant over the entire range of structural responses from elasticity to global instability. They concluded that the presence of setbacks (i.e., geometric vertical irregularities) decreases the capacity of structure and the torsional effects of one-side setbacks (i.e., torsional plan irregularities) intensify this problem. Also, the confidence levels of satisfying the LS performance objective for the code-designed one-side setback structures are decreased with respect to the code-designed regular structure one, especially for critical setback ratios. Therefore, the revision of seismic codes provisions for geometric vertical irregularities seemed to be essential.

A review on the previous findings indicates that the vertical irregularities can affect the seismic performance of structures. Therefore, it is essential that the seismic codes apply the accurate analytical procedures to predict the seismic performance of this class of structures. In this paper, the provisions of five different seismic codes for vertical irregularities are studied and the approach of these seismic codes is compared.

A REVIEW ON THE SEISMIC CODES PROVISIONS FOR DEFINITION OF VERTICAL IRREGULARITY

Most of the seismic codes defined the limit values to distinguish regular from vertical irregular buildings. In general, seismic code regulations attempt to prevent the problem of discontinuity (i.e., the abrupt change of lateral load resisting properties over the height of structure). The definition of vertical irregularity in accordance with a number of seismic codes including UBC97, ASCE7-05, FEMA 450, Eurocode and Iranian seismic code is shown in Table 1. Note that most seismic codes focus on the non-geometric vertical irregularity more than the geometric irregularity. However, the Eurocode [2003] explicitly defines the ratio limits for setback structures as the main types of geometric vertical irregularities. It also defines the geometric vertical irregularity for one-side setback structures more restrictively with respect to the two-side setback structures. This can provide greater insight of designers into the unique characteristics of the one-side setback structures (i.e., the combined action of the geometric vertical irregularities with the torsional plan irregularities). It is notable that the geometric vertical irregularity did not exist in the early version of Iranian seismic code [BHRC 2010]. By considering the results of the previous research about the seismic performance of setback structures, a clear definition of setback ratio limits by the seismic codes is necessary.

All seismic codes except Eurocode [2003], have defined the same limits for mass vertical irregularities. The definition of stiffness and strength vertical irregularities is also similar in these seismic codes. However, ASCE [2006] and FEMA450 [2004] defined the extreme irregularities besides the usual stiffness and strength vertical irregularities.

Table 1 The vertical irregularity definitions in different seismic codes.

Seismic Codes	Definition of vertical Irregularity			
	Geometric	Non-geometric types		
		Mass	Stiffness	Strength
Iranian Seismic Code [16]	-	The mass of any story is more than 150% of the mass of an adjacent story.	The lateral stiffness of any story is less than 70 % of that in the story above or less than 80% of the average stiffness of the three stories above.	The lateral story strength of any story is less than 80% of that in the story above.
UBC97 [13]	The horizontal dimension of the lateral force-resisting system in any story is more than 130% of that in an adjacent story.	The effective mass of any story is more than 150% of the effective mass of an adjacent story.	The lateral stiffness of any story is less than 70 % of that in the story above or less than 80% of the average stiffness of the three stories above.	The lateral story strength of any story is less than 80% of that in the story above.
ASCE[14] FEMA450 [15]	Such as UBC 97	Such as UBC 97	Such as UBC 97 + Extreme irregularity: The lateral stiffness of any story is less than 60% of that in the story above or less than 70% of the average of the three stories above.	Such as UBC 97 + Extreme irregularity: The lateral story strength of any story is less than 65% of that in the story above.
Eurocode [17]	*One sided setback :* The setback at any story is greater than 30% of the first story plan dimension or greater than 10% of the previous story plan dimension. *Two sided single setback :* The setback at floor within the lower 15% of the total height is greater than 50% of the previous story plan dimension. The setback at floor above the lower 15% of the total height is greater than 20% of the previous story plan dimension.	*Abrupt changes exist in the mass of the individual stories from the base to the top (the amount is not declared).*	*Abrupt changes in the stiffness of the individual stories from the base to the top (the amount is not declared)*	*Abrupt changes in the strength of the adjacent stories (the amount is not declared).*

A REVIEW OF THE SEISMIC CODES LIMITATIONS FOR VERTICAL IRREGULAR STRUCTURES

The seismic codes define some limitations for vertical irregular structures. ASCE [2006] and FEMA450 [2004] do not permit to design the structures with extreme stiffness and strength vertical irregularities for very high seismic zones. This limitation can prevent from the earlier collapse and global instability in the structures located at very high seismic zones [Pirizadeh and Shakib 2013]. The codes requirements also focus on identifying the vertical irregularity conditions for which the equivalent lateral force (ELF) analysis method can be used. On the other hand, when irregularity exceeds certain nominal limit, the linear response spectrum analysis is necessitated by most seismic codes. These conditions are presented in Table 2, for different seismic codes. Some codes such as Eurocode [2003] do not permit ELF analysis method for vertical irregular buildings and most of seismic codes limit this method for mid-rise and high-rise vertical irregular structures. In addition, UBC97 [1997], ASCE [2006] and FEMA450 [2004] limit the ELF analysis method for all vertical irregular buildings located at very high seismic zones.

By considering the recently researches regarding the seismic performance of vertically irregular buildings [Fragadakis et al. 2006; Le Trung et al. 2010; Pirizadeh and Shakib 2013; Shakib and Pirizadeh 2013], the limit values to distinguish regular buildings from irregular buildings and also, the limits for ELF analysis method for this type of buildings, should preferably be defined in accordance with: (i) the expected performance objective for structure, (ii) the level of seismic intensity, (iii) the diverse positions of irregularities, (iv) the numbers of vertically irregular stories, (v) the combined action of non-geometric and geometric vertical irregularities with the torsional irregularities. Recently, the performance-based design approach to design of vertical irregular buildings can provide greater insight of designers into the unique characteristics of these structures. Therefore, for extreme cases of vertical irregularities such as extreme stiffness and strength irregularities or the setbacks more than 50% of the floor areas or the setbacks occurred within the bottom half stories of structure, we suggest that the seismic codes stipulate the explicit compulsions for implementing more accurate analysis methods such as performance-based design approach for predicting the seismic response of these types of structures. Also the assessment of code-designed setback structures by the confidence-based approaches demonstrated the poorer performance of one-side setback structures relative to the two-side setback structures because of the torsional effects of one-side setbacks. Therefore, the geometric vertical irregularity limitations for one-side setback structures may be defined more restrictively with respect to the two-side setback structures. In addition, the direct compulsion for simultaneous application of orthogonal ground motion to the one-side setback structures seems to be necessary.

Table 2 **The conditions for applying the ELF analysis method for vertical irregular structures.**

Seismic Codes	Allowable Vertical Irregular Structures for ELF Method
Iranian Seismic Code [16]	Irregular structures not more than five stories or 18 meters in height. Structures having a flexible upper portion supported on a rigid lower portion where both portions of the structure considered separately can be classified as being regular, the average story stiffness of the lower portion is at least 10 times the average story stiffness of the upper portion and the period of the entire structure is not greater than 1.1 times the period of the upper portion considered as a separate structure fixed at the base.
UBC97 [13]	All structures in Seismic Zone 1 and in Occupancy Categories 4 and 5 in Seismic Zone 2. Irregular structures not more than five stories or 65 ft(19. 8 m) in height. Structures having a flexible upper portion supported on a rigid lower portion where both portions of the structure considered separately can be classified as being regular, the average story stiffness of the lower portion is at least 10 times the average story stiffness of the upper portion and the period of the entire structure is not greater than 1.1 times the period of the upper portion considered as a separate structure fixed at the base.
ASCE[14] FEMA450 [15]	All structures in Seismic Design Category B and C. All structures with $T < 3.5T_s$ with strength irregularity or with in-plane discontinuity in vertical lateral force resisting in Seismic Design Category D, E and F.
Eurocode [17]	Not irregular structure is permitted.

CONCLUSIONS

In this paper, the geometric and non-geometric vertical irregularity provisions in the five different seismic codes are reviewed and the approaches of seismic codes for defining the limitations for vertical irregular structures are compared. In addition, based on the recently research results, the possible new approaches for revision of seismic codes provisions are presented. In brief it was found that:

- The seismic codes such as UBC97 [1997], ASCE [2006], FEMA450 [2004] and Iranian seismic code [BHRC 2010] focus on the non-geometric vertical irregularity more than geometric irregularity. However, Eurocode [2003] explicitly defines the ratio limits for setback structures as the main types of geometric vertical irregularities.
- The limitations of seismic codes such as ASCE [2006] for the design of vertical irregular structures are defined in accordance with the level of zone seismicity. They do not permit for the design of structures with extreme stiffness and strength vertical irregularities in the very high seismic zones.
- The recently researches regarding the seismic performance of vertically irregular buildings indicates that the limitations for this type of buildings should be defined preferably in accordance with: (i) the expected performance objective for structure, (ii) the level of seismic intensity, (iii) the diverse positions of irregularities over the

height, (iv) the numbers of vertically irregular stories, (v) the combined action of non-geometric and geometric vertical irregularities with the torsional irregularities.

- The geometric vertical irregularity limitations for one-side setback structures may be defined more restrictively with respect to the two-side setback structures due to the torsional responses that arise in these types of buildings. In addition, the direct compulsion for simultaneous application of orthogonal ground motion to the geometric vertical irregularities, such as one-side setback structures seems to be necessary.
- For extreme cases of vertical irregularities such as extreme stiffness and strength irregularities or the setbacks more than 50% of the floor areas or the setbacks occurred within the bottom half stories of structure, it seems to be necessary that the seismic codes stipulate the explicit compulsions for implementing more accurate analysis methods such as performance-based design approach for predicting the seismic response of these types of structures.

REFERENCES

Al-Ali A.A.K., Krawinkler H. (1998). Effects of vertical irregularities on seismic behavior of building structures. *Report No. 130*, John A. Blume Earthquake Engineering Center, Stanford University, Stanford, CA.

ASCE (2006). *Minimum Design Loads for Buildings and Other Structures, ASCE 7-05,* American Society of Civil Engineers, Reston, VA.

BHRC (2010). *Iranian Code of Practice for Seismic Resistant Design of Buildings, Standard No. 2800-05*, Building and Housing Research Center, 3rd ed., Tehran, Iran.

CEN (2003). *Design of Structures for Earthquake Resistance- Part 1: General Rules, Seismic Actions and Rules for Buildings, Eurocode 8*, Draft 6, European Committee for Standardization, Brussels..

Chintanapakdee C., Chopra A.K. (2004). Seismic response of vertically irregular frames: response history and modal pushover analysis, ASCE, *J. Struct. Eng*., 130(8): 1177–1185.

Duan X.N., Chandler A.M. (1995). Seismic torsional response and design procedures for a class of setback frame buildings, *Earthq. Eng. Struct. Dyn*., 24(5): 761–777.

FEMA (2004). *NEHRP Recommended Provisions for Seismic Regulations for New Buildings and Other Structures, FEMA450*, Building Seismic Safety Council, National Institute of Building Sciences, Washington D.C.

Fragiadakis M., Vamvatsikos D., Papadrakakis M. (2006). Evaluation of the influence of vertical irregularities on the seismic performance of a nine-storey steel frame, *Earthq. Eng. Struct. Dyn*., 35(12): 1489–1509.

ICBO (1997). *Uniform Building Code: Structural Engineering Design Provisions*, International Conference of Building Officials, Vol. 2, Whittier, CA.

Karavasilis T.L., Bazeos N., Beskos D.E. (2008). Seismic response of plane steel MRF with setbacks: Estimation of inelastic deformation demands, *J. Constr. Steel Res*., 64(6): 644–654.

Le-Trung K., Lee K., Lee J., Lee D.H. (2010). Evaluation of seismic behavior of steel special moment frame buildings with vertical irregularities, *The Structural Design of Tall & Special Buildings*.

Pirizadeh M., Shakib H. (2010). Response of setback frame buildings due to seismic random vibration analysis, *Proceedings 14th Symposium on Earthquake Engineering, Indian Institute of Technology*, Roorkee; India.

Pirizadeh M., Shakib H. (2013). Probabilistic seismic performance evaluation of non-geometric vertically irregular steel buildings, *J. Constr. Steel Res*., 82(1): 88–98.

Shahrooz B.M., Moehle J.P. (1990). Seismic response and design of setback buildings, ASCE, *J. Struct. Eng*., 116(5): 1423–1439.

Tremblay R., Poncet L. (2005). Seismic performance of concentrically braced steel frames in multistory buildings with mass irregularity, ASCE, *J. Struct. Eng*., 131(9): 1363–1375.

Valmundsson E.V., Nau J.M. (1997). Seismic response of building frames with vertical structural irregularities, ASCE, *J. Struct. Eng*., 123(1): 30–41.

Shakib H., Pirizadeh M. (2013). Probabilistic seismic performance assessment of setback buildings under bidirectional excitation, ASCE, *J. Struct. Eng*., submitted for publication.

REPORT ON RETROFIT PROCEDURE OF SCHOOL BUILDINGS IN ISLAMIC REPUBLIC OF IRAN

Alireza Mahdizadeh[1], Morteza Raissi[1], and Mohammad Yekrangnia[1]

SUMMARY

One of the most important undertakings of Iranian government in reducing the seismic vulnerability of the country against the earthquake is "Study and performing Retrofitting of the Important Buildings and Lifelines" which covers seven structural groups and was enacted since 2003 in the form of possession of stock finances. The school buildings are one of the major structural groups in the aforementioned plan. In parallel, the preliminary guideline for structural retrofit was prepared in 2003. Besides the aforesaid guideline, $4 billion U.S. was granted by the Iranian Parliament according to 4th Development Plan in order to demolish and reconstruct the seismically dangerous schools and retrofitting the vulnerable ones. "State Organization of School Renovation, Development and Mobilization of Iran” is responsible for execution of seismic risk reduction plan in the educational buildings throughout the country. This report is a brief review of the national project and achievements for retrofitting school buildings in I.R.Iran.

Keywords: *masonry school building, seismic retrofit, typical retrofitting patterns*

ENACTMENT OF THE DEMOLITION, RECONSTRUCTION, AND RETROFITTING OF SCHOOLS LAW

Iran is located in one of the most seismically active regions and catastrophic earthquakes of every decade have left a lot of casualties and financial damages. This necessitates undertaking national plan in order to reduce the earthquake prone risk to as minimum as possible. It is obvious that in this plan, the more important buildings should receive more attention and priority. The importance of each building is determined based on some parameters like functionality, serviceability of the building after earthquake, and the possible human and financial losses. School buildings, are one of the most important buildings, because, they contain accumulated population and they have crucial role in post disaster management.

Based on Code 2800 (Iranian code for seismic resistant design of buildings), school buildings are assigned to the category of the buildings with high importance which ranks second after the buildings with very high importance like nuclear facilities. Regarding this importance, $4 billion U.S. was granted by the Iranian Parliament in 2007 according to 4th Development Plan in order to demolish and reconstruct the seismically dangerous schools and retrofit the vulnerable ones. According to this law, 132000 classrooms should have been demolished and reconstructed and 126000 ones should have been retrofitted. It is noteworthy that the quality control of these projects was within International Institute of earthquake Engineering (IIEES) responsibilities.

[1] State Organization of School Renovatoin and Mobilization of Islamic Republic of Iran.

This state organization is responsible for execution of seismic risk reduction plan and the demolition and reconstruction plan (2007) in the educational buildings.

INTRODUCTION TO STATE ORGANIZATION OF SCHOOL RENOVATION, DEVELOPMENT, AND MOBILIZATION OF IRAN

The establishment of this state organization which is one of the branches of Ministry of Education dates back to 1975 and this organization formally started its work in 1976. The responsibilities of this organization are construction, development, renovation and reconstruction of the school buildings and also providing them with facilities and equipment throughout the country. Fulfilling these responsibilities leads to similar details throughout the country and also classified architectural and structural plans in school buildings.

TECHNICAL CERTIFICATE OF SCHOOL BUILDINGS

In 2004 and based on a national plan, a comprehensive database about the structural specification of all school buildings was prepared. This database consisting of 74 items includes vast spectra of information e.g., the number of students to the situation of the foundation and the building facade. The most important items in this database are: the number of students and staffs, the geometrical and technical specification of the structure, the possible hazards to the building like earthquake or landslide.

For this project, more than 380,000 classrooms in 100,000 school buildings were analyzed by the staff of the Ministry of Education. One of the most important outcomes of this database was classification of school buildings in the stability point of view in three categories: 135,000 school buildings in demolition and reconstruction category, 126,000 school buildings in vulnerable category which needed retrofitting and 139,000 school buildings in resistant category. This evaluation provided the primary tools for scheduling the first 5 years of the project from 2006 to 2010. So, the technical certificate of schools buildings had a key role in enacting of the demolish, reconstruction and retrofitting law. Based on the experiences learned during five years of execution of this project, the technical certificate of school building has been revised and completed. The new certificate is better than the previous one in different aspects. The extension in the parameters for data gathering, the method for data gathering and data storing are of examples which have been modified in the new certificate.

SELECTION OF PROJECT AND COMPATIBLE STRATEGY FOR RETROFITTING

As previously stated, this organization deals with the problematic school buildings in two ways: demolition-reconstructing and retrofitting. Considering the differences between these two ways adds to the importance of proper selection and classification of the projects. Classification and prioritizing school buildings is the first stage in projects. This classification is divided into two phases: the first phase has something to do with the general policies related to all school buildings throughout the country. The second phase concerns with the decision making processes for each school buildings. The main aim is to reach highest safety level with specific fund. The main question in this part is that "which school building should be demolished and reconstructed and which one should be retrofitted?" For answering this question, one should answer the questions below:

- How much is the price of the school building? (Combination of the structure's price, architecture preponderance and the facilities)
- How much is the cost of retrofitting? (All the structural, architectural and facilities' implementations)
- How much would be the expected life of the building after retrofit? (Architectural preponderance after retrofit)

Answering all these questions requires in-depth studies for 100000 school buildings. So at the beginning in 2004, studies were confined to rapid screening of school building. It classified all the school buildings in three structural types: satisfying, retrofit needed and demolition-reconstruction needed for general planning and budget estimation processes. In the next stage and during the retrofitting studies processes, each of the abovementioned questions was answered with an acceptable accuracy. Finally, it was decided whether a typical school building should be demolished-reconstructed or retrofitted. In 2010 and based on the experiences gained from previous projects, the technical certificate of school buildings was revised.

This time, besides the structural specifications of each building, a proper estimation about the architectural condition and the facilities of the school buildings were made in order to better answer the aforementioned questions. Accordingly, the classification of the school buildings has been modified. In the new classification, rapid screening forms have been used, and the school buildings were fallen into one of the seven types below:

- Satisfying schools: The schools which were designed based on the final version of seismic design code of Iran, and all of necessary specifications were considered. These schools were constructed after 2006.
- Buildings with low retrofitting preference: The buildings that were constructed based on previous versions of seismic design code of Iran from 2001 to 2006. Moreover, other buildings that were constructed out of this period, and were assigned to satisfying schools based on rapid screening forms were considered to this category.
- Partial rehabilitation schools: These school buildings have sufficient resistance against earthquake but have problems in slab integrity. A large number of school buildings with jack arch slab with low integrity are the main reason for considering this type of school buildings.
- Typical Retrofitting Pattern (TRP): Most Iranian single-story masonry buildings are assigned to this type. These buildings have similar deficiencies, so typical details and methods of retrofitting could increase their performance level to life safety.
- Demolition-reconstruction needed schools: The schools which retrofitting cost is more than 50% of demolition and reconstruction cost , buildings with low quality of architectural aspect, or located on developing areas that will need larger educational

area in the future are considered in this category.

- Schools without sufficient price for spending money: Most Iranian schools in rural areas and population of these areas decreases over time.
- Complete retrofitting: Frame structural buildings without any lateral load-bearing system of or serious deficiency in this mechanism are considered in this category. These school buildings should be studied in details (screening evaluation, analysis report, retrofitting preliminary plan and final retrofitting plan). As it is obvious, this process takes a long time for finalization.

In the next step, preference of retrofitting among school buildings is determined based on seismic hazard, population of schools and development program of region.

QUALITATIVE EVALUATION OF THE SCHOOL BUILDINGS TO BE RETROFITTED

The number of classrooms which should be retrofitted is more than 126,000. Most of these classrooms were constructed by a unique organization, and some similarities could be observed in these school buildings. An overview to the qualitative evaluation of these buildings could conduct the general strategy of retrofitting method or research funds.

Table1 Qualitative evaluation of school buildings.

Type of Structure	%	Number of Stories	%	Type of Roof	%
Masonry	88.53	1 story	86.09	Concrete	4.99
Steel	7.98	2 story	12.40	Wood	9.70
Concrete	2.00	3 and more	1.51	Other	5.35
Other	1.49			Jack arch	79.96

ACTIONS CYCLING IN RETROFITTING PROJECTS

Procedure of complete retrofitting is a comprehensive method of evaluation that starts from project selection and covers all steps of study and finally enters to part of construction. Project management a large amount of these projects adds to the importance of accurate control. In this circulation, selection of retrofitting and geotechnical and material consultants is the next step after the project selection stage. Totally, qualitative report, geotechnical and materials testing, analysis report, preliminary retrofitting plan, final retrofitting plan are presented. The entire process is controlled by peer reviewer.

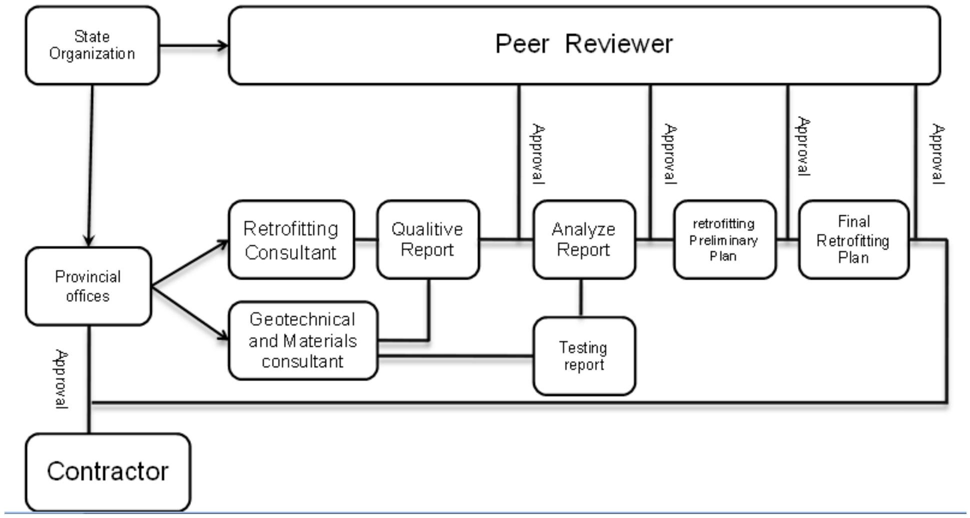

Figure1 Schematic representation of the study process of retrofitting projects.

DEVELOPMENT OF NEW METHODS FOR RETROFITTING OF SCHOOL BUILDINGS IN IRAN – TYPICAL RETROFITTING PATTERN

The results of studies reveal that the retrofitting process in Iran is a very time-consuming and costly one. Covering all the stages in this process for structures with close details and specifications has been rarely experienced before in any countries. It was because this organization has been considered new methods and criteria for its retrofitting projects. In more than two years the different methods were studied and discussed. Various reports in this realm have been published and the results finally came in the form of new instructions about the new method for retrofitting of school buildings – Typical Retrofitting Pattern (TRP). The utilization of these new instructions was started in 2009 on limited number of school buildings and led to satisfactory results.

Typical retrofitting patterns increase performance level of buildings to assumed target level with specific methods; however, minor deficiencies exist after retrofitting by this strategy. Required time for seismic evaluation based on this strategy considerably decreases because the long-time preparing and verification are eliminated. This organization follows three following goals in development of these methods:

- **Reducing the studying time of retrofitting projects:** since a lot of school buildings should have been retrofitted according to unique methods and because of the close structural details, passing all the steps in retrofitting procedure for each of them is not logical. Moreover, this will require much longer period of time to achieve our goals in retrofitting of all school buildings in 5 years.
- **Increasing the speed and quality of execution of projects:** since implementation of these instructions leads to a unique retrofitting specifications and details, this will result in fast adaptation of the contractors with the executive methods and providing them with the equipment for a repetitive process.

- **Reducing the cost of retrofitting process:** the total cost of the project greatly depends on the required time of the project, the speed of execution and the amount of necessary equipment of the contractors. So repetition of the projects details and equipment will result in considerable cost saving in the retrofitting projects.

There are four retrofitting methods developed by the organization: two of them were completed and utilized in 2010. From the two remaining, one of them is in the studying and research phase and the other which was not technically and economically justified was abandoned. The methods of this organization are as follows.

Typical Retrofitting by Shear Wall Method

In this method there are some design tables containing the capacity of the shear walls and the piles with known details of the reinforcements, concrete and soil. A typical engineer can simply calculate the base shear of the building and in doing so, can evaluate the required number and length of shear wall(s) for reaching the calculated base shear capacity. In the calculation of the number and length of shear wall(s), the load-bearing capacity of the masonry walls is neglected.

The roof of buildings, which should be retrofitted, is usually jack-arch which should be converted to composite concrete. Also specifications have been proposed for the connection of roof and walls which leads to improvement of the in-plane and out-of-plane wall performance. In this method, one meter of the upper height of walls is reinforced. This method was successfully implemented in some of school buildings in summer 2010.

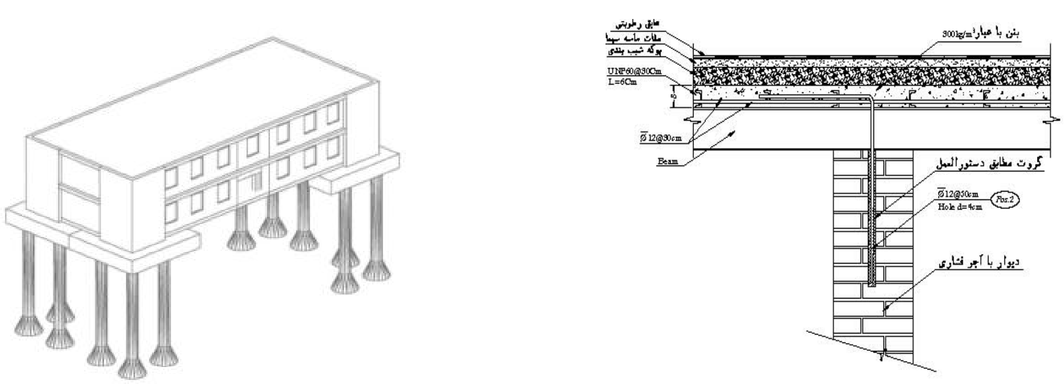

Figure 2 **Schematic overview and detail of retrofitting by shear wall pattern.**

Figure 3 Samples of retrofitted school buildings with shear walls.

Typical Retrofitting by Peripheral Shotcrete Method

This method has been chosen based on the successful experiences from other countries and numerous experiments on masonry walls. In this method, the surrounding area of the single-story URM building is shotcreted. The size of rebar and the thickness of concrete are chosen in such a way that can fulfill the seismic demand of each building. In calculation of the base shear of buildings, the total weight of the structure plus the brick walls are considered and load-bearing capacity of the walls is neglected. The roof of the buildings in this class is usually jack-arch which should be converted to composite concrete. This method was also successfully implemented in some of school buildings in 2010. Figure 5 shows some samples of this project which have been executed in summer 2010.

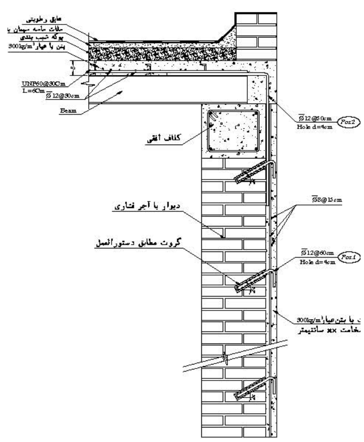

Figure 4 Samples of retrofitted school buildings with shear walls.

Figure 5 Samples of retrofitted school buildings with peripheral shotcrete.

Typical Retrofitting by Safe Room Patterm

In this method, a steel frame is constructed for each classroom regardless of the capacity of the building, the variety of construction, structural and non-structural specifications. The aim of this method is to prevent falling of the debris on the students in the classrooms. The different parts of the steel frame is designed and manufactured in order to be assembled easily and fast (in the telescoping manner). In this way it can be guaranteed that the steel frame is tight inside the classroom. Of the advantages of this method is fast recycling of the retrofitting material in the case of demolish-reconstruction plan. However this method does not have enough chances to compete with other methods technically and economically and was not implemented vastly.

Figure 6 Schematic overview on retrofitting by safe room pattern.

Typical Retrofitting by Center Core Pattern

The State Organization of School Renovation, Development and Mobilization of Iran has developed retrofitting techniques in the scope of increasing the accuracy and speed of study and execution of the projects. Also it has worked on the modern methods especially for the brick buildings with historical background. This issue seems important considering that ministry of education of Iran possesses a lot of school buildings older than 70 years of age. Moreover, there are numerous historic brick buildings in Iran and retrofitting them by the conventional retrofitting techniques can endanger and intrude their historical value.

The center core method is one of the specialized retrofitting techniques for masonry buildings against earthquakes and was first implemented in U.S. in 1987 for retrofitting of some masonry buildings. The first step of this method is excavating vertical holes with specific diameter in the whole height of the wall and in determined distances. In the next step, the holes are filled with rebar and grout and this will result in improvement in seismic performance of masonry walls. Since in this method no apparent damage is posed to the architecture of the building and all the rehabilitation actions are outside the building, this method can be the best and the only solution for the buildings with historical importance and the buildings for which it is desired to maintain their service and functionality. In Iran, numerous historic masonry buildings which require stabilization against earthquake can provide good opportunities for this method to be vastly implemented.

Figure 7 Alborz high school in Tehran, which is more than 120 years old.

GENERAL STRATEGY FOR RETROFITTING

General performance of masonry buildings in previous earthquakes shows that although strength of walls was much higher than earthquake force, several cracks appeared on them. These cracks divide the masonry walls to major parts that oscillate independent from the masonry building. Most of damages in masonry buildings are rooted in lack of stability of these elements in masonry buildings. So, retrofitting process of masonry building can be divided into two main categories: The first step is to provide sufficient total strength of masonry building against earthquake shaking, and in the next step, stability of each element should be provided. The general methods for retrofitting of masonry buildings are combination of these two methods, which have been implemented by this organization in recent years. The goals in the first step can be achieved by one of the aforementioned methods. Also the second step, i.e., providing stability of structural elements is based on two concepts: First, providing general integrity of the building and second, predicting damage location, and providing the stability of the cracked walls. Consideration of these two concepts is important to propose retrofitting patterns. In some cases providing of sufficient strength of elements leads to meeting with these two concepts' requirements. In contrast, in other cases it may not happen. As a result, besides operations to provide strength in building, additional operations should be done to provide stability of elements. Figures 8 to 10 depict some examples of the implemented methods.

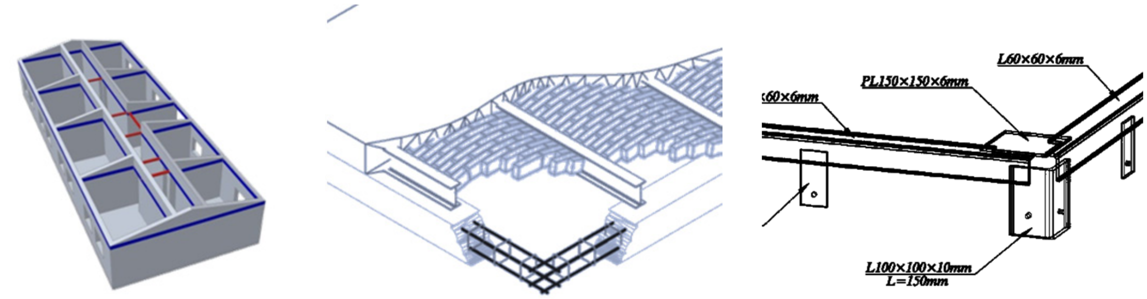

Figure 8 Providing integrity by using of steel members.

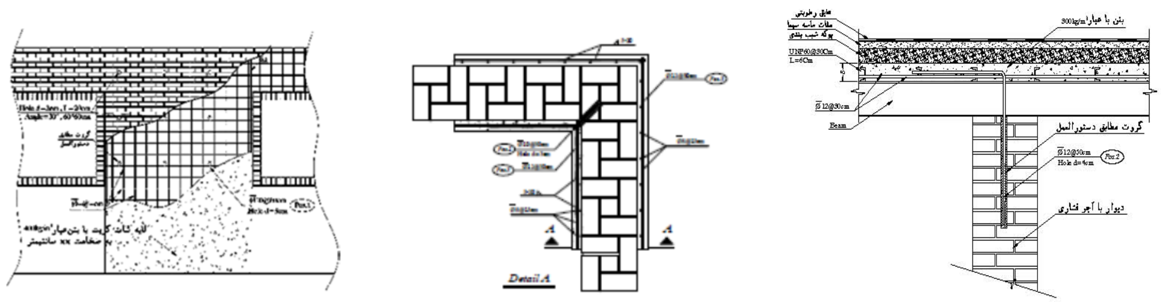

Figure 9 Current details for providing stability in masonry building.

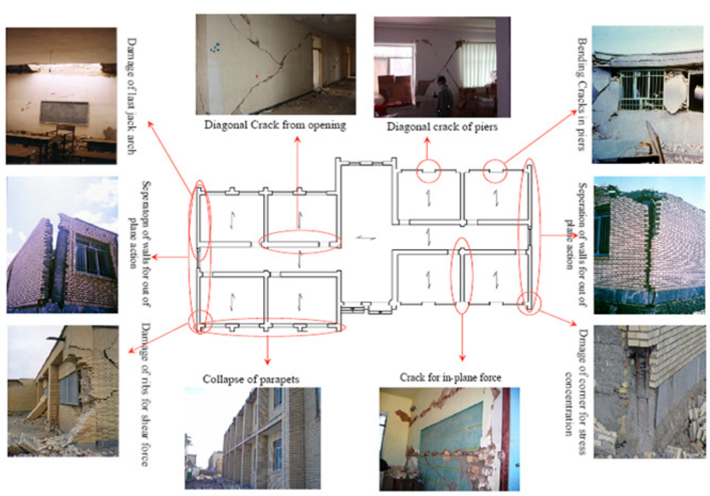

Figure 10 Damages and cracks in masonry buildings (photo courtesy of M. Yekrangnia, A. Mahdizadeh).

EFFECT OF RECENT STRATEGIES ON COST OF RETROFITTING PROJECTS

There are three approaches have been implemented in school retrofitting projects: Typical Retrofitting patterns (2010 up to now), modifying retrofitting patterns based on cost distribution and performance level of structural elements, correction of details. Figure11 shows the variation of school retrofitting cost according to time in recent years. These data is presented based on analyses of 90 schools in different provinces of Iran. As can be seen, the average retrofitting cost was about 175US$ (per m^2) in 2008 and following from the new strategies resulted in reduction of 100US$ (per m^2). Furthermore, the variation of total costs in different projects has decreased by pursuing of these strategies. Accurate estimation of time and cost is the direct result of this reduction. Also the cost of each major part of retrofit and renovation projects in complete retrofitting-renovation projects and TRP's are compared in Figure12 which shows considerable reduction in each part and also more allocation to structural part.

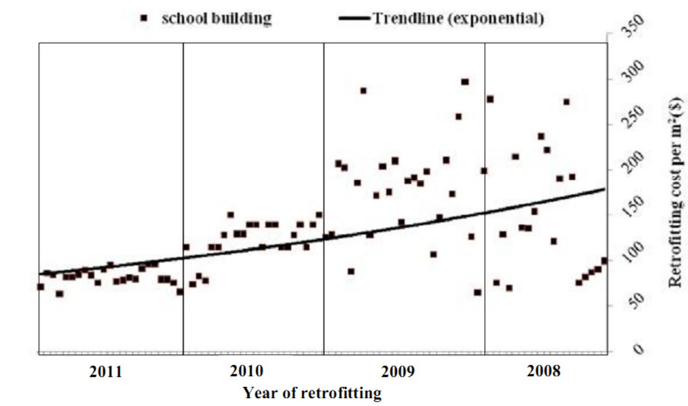

Figure 11 Variation of retrofitting cost of schools in recent years.

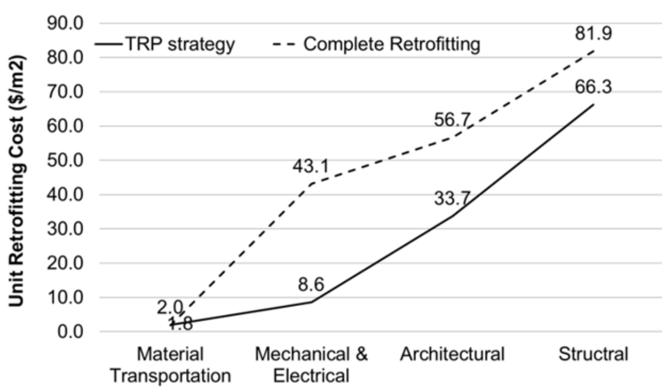

Figure12 Cost of each major part of retrofit and renovation projects.

ACHIEVEMENTS OF THE DEMOLITION, RECONSTRUCTION, AND RETROFITTING OF SCHOOLS LAW

An overview on achievement of last eight years is presented in this section. In Figures 13 and 14, numbers of retrofitted and reconstructed classrooms and fund distribution from 2006 to 2010 are shown. According to the statistics, The Islamic Republic of Iran has upgraded seismic safety of more than 28000 classrooms (equal to 1 million m^2) in the form of retrofitting and more than 55000 classrooms (equal to 6.5 million m^2) in the form demolition and reconstructing from 2005 to 2012. It is noteworthy than although the number of reconstructed classrooms is considerably higher than the retrofitted ones, the rate of retrofitting projects is increasing compared to the decreasing rate of the reconstruction projects.

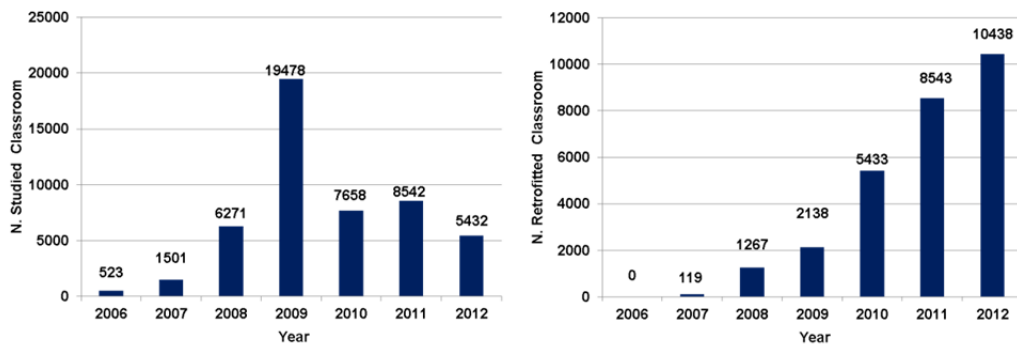

Figure 13 Number of studied and retrofitted classrooms from 2006 to 2012.

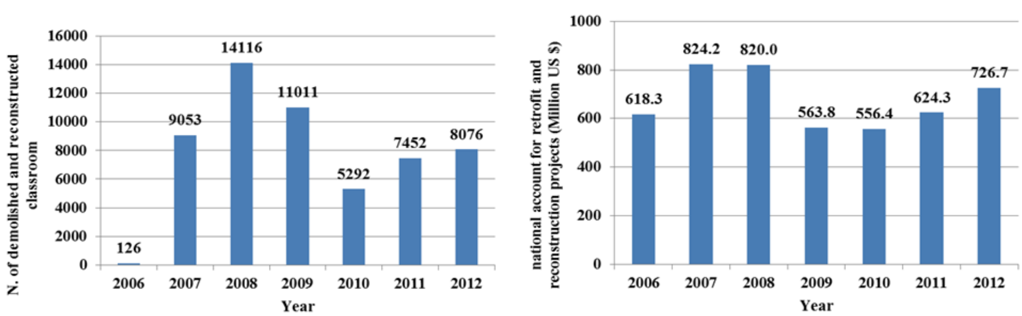

Figure 14 Number of demolished and reconstructed classrooms, the distribution of expenses from national accounts for demolition, reconstruction and retrofitting of school buildings from 2006 to 2012.

ACKNOWLEDGEMENTS

This project was supported by the State Organization of Schools Renovation and Mobilization, Deputy of Ministry of Education of Islamic Republic of Iran.

REFERENCES

BHRC (2010). Iranian Code of Practice for Seismic Resistant Design of Buildings, Standard No. 2800-05, Building and Housing Research Center, 3rd ed., Tehran, Iran.

Borzouie J., Mahdizadeh A. (2012). Peripheral shotcrete for seismic retrofitting of one-story masonry buildings, Proceedings, 6th International Conference on Seismology and Earthquake Engineering (SEE6), Tehran, Iran.

Mahdizadeh A. (2010). Report on Retrofit of School Buildings in Islamic Republic of Iran, Technical Report, State Organization of Schools Renovation and Mobilization.

Mahdizadeh A., Borzouie J. (2012). Perforating masonry walls for rehabilitation of masonry buildings using center-core method, Proceedings, 6th International Conference on Seismology and Earthquake Engineering (SEE6), Tehran, Iran.

Yekrangnia M., Mahdizadeh A. (2009). Earthquake and Masonry Buildings, Technical Report, Technical Report, State Organization of Schools Renovation and Mobilization.

PERFORMANCE OF GROOVING METHOD USED FOR FRP STRENGTHENING OF CONCRETE STRUCTURES

Davood Mostofinejad[1] and Seyed Masoud Shameli[2]

ABSTRACT

In the last two decades, Fiber Reinforced Polymer (FRP) composites have gained great application in construction industry especially for strengthening and retrofitting of existing concrete structures due to the numerous advantages such as high tensile strength, ease of application, light weight and corrosion resistance. One of the main applications of FRP materials is for flexural strengthening of concrete beams. The most well-known beam strengthening methods with FRP materials are the Externally Bonded Reinforcement (EBR) and Near Surface Mounted (NSM) techniques. However, the main obstacle that has greatly affected the performance of these methods is delamination and debonding of FRP composites from the surface of the strengthened member. Surface preparation of concrete before attaching FRP sheets has been found as a suitable procedure to postpone debonding in EBR technique, but with limited effects. Recently, a new method for strengthening of concrete beams with FRP sheets, named as grooving method (GM) has been introduced as an alternative to EBR method. According to GM, longitudinal grooves are first cut on the tension side of the concrete beam. The grooves are then cleaned with compressed air and filled with appropriate epoxy resin and carbon fiber sheets are adhered to the surface. Grooving method has shown a great promise in resolving the debonding problem and introduced as an effective method for flexural strengthening of concrete beams. To date, GM has developed rapidly from its initial stage. This paper presents a review on progresses and findings of recent studies that have been carried out in this field.

Keywords: *debonding; FRP; flexural strengthening; grooving method (GM); surface preparation*

INTRODUCTION

The probable failure of structures, especially due to earthquakes, is one of the main worries in construction industry; as a result, structural rehabilitation and strengthening have become a dynamic area of research in civil engineering. In the last two decades, fiber reinforced polymer (FRP) composites have found wide applications for strengthening of reinforced concrete (RC) structures due to their exceptional properties [Toutanji and Ortiz 2001]. Externally bonded reinforcement (EBR) is the most common method for flexural strengthening of concrete beams with FRP materials. However, the main problem associated with EBR method is the premature failure of the beam which is due to a sudden and unpredictable debonding of the FRP sheet from the concrete surface Teng et al. 2002]. The most important cause of debonding is lack of an

[1] Professor, Department of Civil Engineering, Isfahan University of Technology (IUT), Isfahan, IRAN; email: dmostofi@cc.iut.ac.ir.
[2] MSc, Department of Civil Engineering, Isfahan University of Technology (IUT), Isfahan, IRAN; email: masoud.shameli@gmail.com.

appropriate bonding interface between the FRP sheet and the concrete surface to resist stress transfer [Karbhari and Zhao 1997]. Accordingly, it is essential to provide an appropriate surface that allows for perfect bonding of the FRP sheet to the beam. Concrete surface preparation is a common procedure which is widely used for this purpose and experiments have shown that it enhances continuity and bond at the interface and delays the FRP sheet failure [Mostofinejad and Mahmoudabadi 2009]. Surface preparation procedure is accomplished by removing the weak and deteriorated concrete layer by exposing the coarse aggregates and creating an even surface. However, it has been found that surface preparation of concrete only partially delays debonding phenomenon.

Many studies have been performed to improve the performance of beams strengthened with FRP composites and postpone the debonding failure [Toutanki and Ortiz 2001; Galecki et al. 2001]. Although these studies have enhanced the efficiency of EBR method, strengthened beams are still highly prone to debonding and this limitation has affected the capability and safety of this method.

Recently, promising studies have been conducted at Isfahan University of Technology (IUT) in an attempt to develop substitutes for conventional surface preparation in EBR method which in turn led to introduction of a novel method, named as grooving method (GM) for flexural strengthening of concrete beams with FRP composites. In this paper results of some related studies on the subject of grooving method have been reported and discussed.

EXPERIMENTAL PROGRAM TO INTRODUCE ALTERNATIVES FOR SURFACE PREPARATION

In 2010, Mostofinejad and Mahmoudabadi [2010] reported an experimental investigation on concrete beam specimens with dimensions of 100×100×500 mm. The specimens were flexurally strengthened with FRP strips with the width of 70 mm and length of 360 mm. The purpose of their investigation was to evaluate the effect of surface preparation on the ultimate load carrying capacity of the beams as well as to propose new alternatives for surface preparation to enhance the ultimate limits of the strengthened beams. The specimens were divided into seven groups, categorized as groups A to G. Group A consisted of control specimens without any flexural strengthening. In group B, the specimens were strengthened by FRP sheets with EBR method but without any surface preparation; the specimens in group C, however, were strengthened after surface preparation. In group C, first a thin layer of concrete was removed; the surface was then cleaned and its porosities were filled with a suitable epoxy resin (Sikadur C31). After 72 hours another epoxy resin (Sikadur C300) was applied on the surface and the FRP sheet was attached to the beam.

The specimens of groups D to G were strengthened after subjection to alternative methods of surface preparation. These methods included creation of transverse, diagonal, or longitudinal grooves on the concrete surface (Figure 1). The strengthening procedure was as follows:

- Transverse, diagonal or longitudinal grooves were first cut in the concrete cover of the tension face of the beam.
- The grooves were cleaned with air pressure and filled with epoxy resin Sikadur C300.
- Extra resin was applied on the surface and FRP sheets were then installed to the beam.
- The epoxy in excess was removed.

Specimens' details including grooves dimensions are provided in Table 1. After strengthening, all the specimens were subjected to four-point flexural loading up to failure in order to obtain their ultimate load capacity.

(a) (b) (c)

Figure 1 Creation of grooves on the beams' surface as an alternative procedure for surface preparation [6]: (a) transverse grooves; (b) diagonal grooves; and (c) longitudinal grooves.

Table 1 Specifications of the specimens tested by Mostofinejad and Mahmoudabadi [6].

Group	f'_c (MPa)	Strengthening Technique	Dimensions of Grooves				Ultimate load (kN)
			Length	Width	Depth	Interval	
A	33.86	—	—	—	—	—	14.3
B	33.86	no surface preparation	—	—	—	—	17.2
C	33.86	surface preparation	—	—	—	—	18.6
D	32.95	transverse grooves	80	3	2	40	19.9
E	31.52	diagonal grooves	80	3	2	50	21.3
F	33.06	longitudinal grooves	370	3	2	15	23.5
G	33.06	longitudinal grooves	370	3	10	15	33.6

Experimental Results

Results showed that all the specimens except for specimens of group G failed due to FRP debonding. In Group G, debonding did not occur and the beams failed due to rupture of FRP sheet. The specimens' ultimate loads are provided in Table 1. For comparison of the effect of different strengthening procedures on the specimens' ultimate loads, average ultimate strength values of the beams in all the experimental groups are also illustrated in Figure 2.

The value for average ultimate strength in the specimens of group A (without any flexural strengthening) was 14.3 kN. In groups B and C, this value was 17.2 and 18.6 kN, respectively. This indicates that a 20% increase by FRP flexural strengthening and a 10% additional increase as a result of surface preparation have been gained in groups B and C. In groups D to G, where substitute methods of grooving have been used, higher rupture strengths were obtained compared to specimens in groups B and C. Transverse and diagonal grooves improved the failure load of the specimens to 19.9 and 21.3 kN in groups D and E respectively, indicating increase rates of 10 and 15% compared to specimens with conventional surface preparation (group C). In groups F and G with longitudinal grooving at 2 and 10 mm depths respectively, average ultimate loads were 23.5 and 33.6 kN, which represent 27 and 80% of increase compared to those of specimens with surface preparation. It can be clearly seen that in the specimens with longitudinal grooves, the highest loading capacities have been achieved. This is due to their parallel contact area to interfacial bond stress between the FRP sheet and concrete surface. It can be also concluded that in specimens with longitudinal grooves, increasing grooves depth form 2−10 mm, increases the contact area between the epoxy resin, bonding the FRP sheet and concrete, with the underlying concrete layers and delays deboning to yield higher ultimate failure loads.

The method of creation of longitudinal grooves on the concrete surface was first named as grooving method (GM); however, the specific technique of bonding FRP sheets on the surface, contained longitudinal grooves filled with epoxy resin, was later named as Externally Bonded Reinforcement on Grooves (EBROG). Figure 3(a) illustrates a schematic view of the cross section of a beam strengthened with EBROG technique.

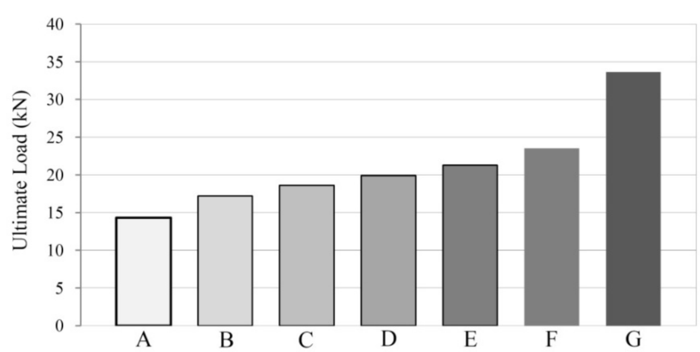

Figure 2 **Average ultimate failure loads of different groups of specimens; (A) reference beams; (B) beams strengthened without surface preparation; (C) beams strengthened after surface preparation; (D) beams with transverse grooves (2 mm deep); (E) beams with diagonal grooves (2 mm deep); (F) beams with longitudinal grooves (2 mm deep); and (G) beams with longitudinal grooves (10 mm deep) [6].**

EXPERIMENTAL PROGRAM TO IMPROVE THE PERFORMANCE OF GROOVING METHOD

In 2013 Mostofinejad and Shameli [2013] reported an experimental program to propose an improved technique to enhance the performance of grooving method. The strengthening technique introduced in their research, which is in fact Externally Bonded Reinforcement In Grooves, is named as EBRIG. According to their research, the EBRIG flexural strengthening technique are executed through the following steps:

- Longitudinal grooves are cut on the beams' tension face.

  Grooves surfaces are covered with a very thin layer of Sikadur C300.

- Carbon sheets are directly bonded to the internal surfaces of the grooves as well as the surfaces outside the grooves on the tension face of the beam.
- Epoxy resin Sikadur C300 is again applied on the surface to completely cover the carbon sheets in the grooves and on the beam surface.
- The extra resin is removed.

Figure 3(b) shows a scheme of the cross section of a beam strengthened with EBRIG technique,

The experimental specimens were 32 concrete beams with length of L=1000 mm, width of b=120 mm and height of h=140 mm. The specimens were strengthened with four distinct strengthening methods, i.e., EBR, Near Surface Mounted (NSM), EBROG and EBRIG. A group of specimens were also considered in which FRP sheets were applied to the beams using EBR technique but without any surface preparation (WSP). In addition, all of the strengthening methods were experimented for one, two and three layers of FRP sheets. Details of the specimens are available in Table 2.

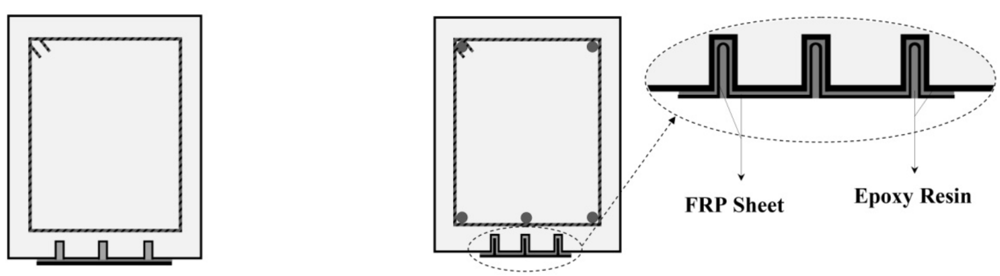

(a) (b)

Figure 3 Techniques of grooving method; (a) EBROG; smf (b) EBRIG (Mostofinejad and Shameli [2013]).

Experimental Results

The specimens subjected to four-point flexural loading to obtain their failure loads. In the following, experimental results have been reported; in addition, the effects of FRP strengthening technique as well as the effects of number of FRP strengthening layers on the beams' ultimate load have been discussed.

Effect of Strengthening Technique

In Table 2, the failure loads of the strengthened beams in different groups have been compared with failure loads of the corresponding beams strengthened without surface preparation (WSP). It can be seen that for the specimens strengthened with one FRP layer, the maximum load capacity of the EBR-1L, NSM-1L, EBROG-1L, and EBRIG-1L has respectively increased 10%, 123%, 139%, and 142% compared to that of WSP-1L. For two layers of FRP sheets, the increase in ultimate load compared to WSP-2L is 1%, 92%, 148%, and 186% for EBR-2L, NSM-2L, EBROG-2L and EBRIG-2L, respectively. For the test beams strengthened with 3 layers of FRP sheets, the increase in ultimate loads compared to WSP-3L is 10%, 67%, 99%, and 155% for EBR-3L, NSM-3L, EBROG-3L and EBRIG-3L, respectively. Figure 4 is provided for simple comparison between the ultimate loads of all the specimens. It can be understand that, due to better stress transfer in NSM, EBROG and EBRIG techniques, beams strengthened with these methods could experience much higher loads than the beams strengthened with EBR method; and among these, EBRIG technique has had the best performance.

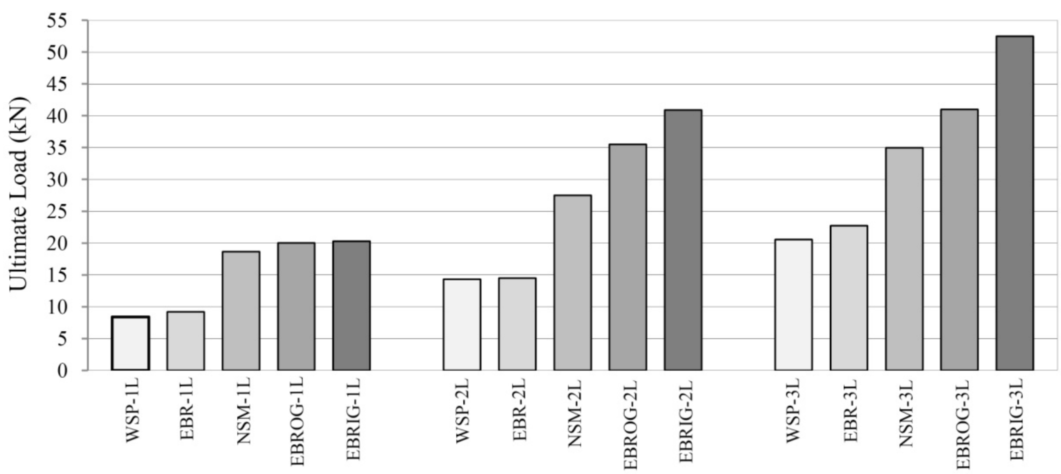

Figure 4 Comparison between the average ultimate loads of specimens with different methods of strengthening (Mostofinejad and Shameli [2013].

Table 2 **Test Results of the study executed by Mostofinejad and Shameli [2013].**

Beams	Number of FRP layers	f'_c (MPa)	Average Ultimate Load (kN)	Increase in ultimate load (%) compared to	
				WSP specimens	Reference beam
RB	0	34.8	6.8	—	—
WSP-1L	1	37.6	8.4	—	23
WSP-2L	2	38.4	14.3	—	110
WSP-3L	3	36.8	20.6	—	202
EBR-1L	1	36.7	9.2	10	35
EBR-2L	2	37.1	14.5	1	113
EBR-3L	3	35.9	22.7	10	234
NSM-1L	1	35.3	18.6	123	174
NSM-2L	2	33.9	27.5	92	304
NSM-3L	3	34.2	35	67	414
EBROG-1L	1	37.2	20	139	194
EBROG-2L	2	37.8	35.5	148	422
EBROG-3L	3	36.8	41	99	502
EBRIG-1L	1	37	20.3	142	198
EBRIG-2L	2	37.8	40.9	186	501
EBRIG-3L	3	36.3	52.5	155	672

Effect of Number of FRP Layers

Results showed that strengthening beams with two and three FRP layers considerably increase the stiffness and ultimate load of the beams compared to those strengthened with one FRP layer. From Table 2, it can be seen that for WSP-1L, EBR-1L, NSM-1L, EBROG-1L, and EBRIG-1L specimens, the increases in ultimate loads compare to reference beam were 23%, 35%, 174%, 194%, and 198%, respectively. These increases were respectively 10%, 113%, 304%, 422%, and 501% For WSP-2L, EBR-2L, NSM-2L, EBROG-2L, EBRIG-2L and 202%, 234%, 414%, 502%, and 672% for WSP-3L, EBR-3L, NSM-3L, EBROG-3L and EBRIG-3L.

CONCLUSIONS

This paper presents a review on findings of some experimental studies carried out in the field of grooving method for flexural strengthening of beams with FRP composites. The aim of the experiments was to evaluate the performance of grooving method and compare the results with other methods under the same conditions. Based on the experimental results, the following conclusions are drawn [Mostofinejad and Mahmoudabadi 2010; Mostofinejad and Shameli 2013].

- Concrete surface preparation prior to attaching FRP sheets to the beams, increases their ultimate load carrying capacity. This increase was about 10% in both studies.
- Cutting longitudinal grooves with suitable depth and width and filling them with an appropriate epoxy in EBROG technique increases the contact area between the FRP sheet and the strong underlying concrete layers along the beam; therefore, it causes considerable improvement in strengthened beams' ultimate strength.
- In EBRIG technique, in which the FRP sheet is directly adheres to the grooves surfaces, the contact area between FRP and strong concrete layer is increased even more; therefore, considerably higher failure loads can be achieved compared to other strengthening techniques.
- EBROG and EBRIG techniques noticeably postpone the debonding of FRP sheets; so these methods can be utilized to strength concrete structures against seismic loads. In the experiments presented in the current study, all the beams strengthened with EBR method failed due to debonding; however, FRP rupture just observed in the beams strengthened with EBROG or EBRIG techniques.

REFERENCES

Galecki G., Maerz N., Nanni A. (2001). Myers J. Limitations to the use of waterjets in concrete substrate preparation, *Proceedings, American Water Jet Conference*, Minneapolis, MN.

Karbhari V.M., Zhao L. (1997). Issues related to composite plating and environmental exposure effects on composite-concrete interface in external strengthening, *Composite Structures*, 40(3): 293–304.

Mostofinejad D., Mahmoudabadi E. (2009). Effect of elimination of concrete surface preparation on the debonding of FRP laminates, *Proceedings, Concrete Solutions Conference*, pp. 357–361, Italy.

Mostofinejad D., Mahmoudabadi E. (2010). Grooving as alternative method of surface preparation to postpone debonding of FRP laminates in concrete beams, ASCE, *J. Composites Construct.,* 14(6):804–11.

Mostofinejad D., Shameli S.M. (2013). Externally bonded reinforcement in grooves (EBRIG) technique to postpone debonding of FRP sheets in strengthened concrete beams, *Construct. Bldg. Mat. J.*; 38: 751–758.

Teng J.G., Chen J.F., Smith S.T., Lam L. (2002). *FRP-Strengthened RC Structures*,. John Wiley and Sons: Chichester, UK.

Toutanji H. Ortiz G. (2001). The effect of surface preparation on the bond interface between FRP sheets and concrete members, *Composite Structures*, 53: 457–462.

RECENT ADVANCES IN SEISMIC PERFORMANCE ASSESSMENT OF STRUCTURES BY ENDURANCE TIME METHOD

H.E. Estekanchi[6], A. Vafai[7], A. Mirzaee[8], M.Mashayekhi[9], and A. Nozari[10]

ABSTRACT

The concepts of ET method and recent advances in its applications in seismic assessment of structures are reviewed. Endurance Time (ET) method is a response-history based procedure in which structures are subjected to predesigned gradually intensifying dynamic excitations and their performance is assessed based on their response at different excitation levels that are correlated to particular ground motion intensities. New developments in ET methodology for performance based design are presented. A continuous Damage versus IM presentation is explained. Presentation of ET analysis results with respect to hazard return period and concepts for application of ET in life cycle cost estimation (LCC analysis) are also presented.

Keywords: *endurance time method, intensifying dynamic excitation, life-cycle cost, performance-based design, response history analysis*

INTRODUCTION

Assessment of safety and performance of structures is one of the major challenges in earthquake engineering. Reliability and accuracy of seismic analysis procedure is a key concern in almost all seismic assessment procedures for both new and existing structures. Various limitations of equivalent static and simplified dynamic analyses and design procedures, along with remarkable advances in the field of seismic resistant design have increased the tendency towards application of more realistic and reliable dynamic analysis procedures. Nonlinear pushover and response-history analyses are becoming more prevalent in design offices. It can be expected that response-history based analysis procedures will become more popular in near future due to their relatively higher reliability, applicability and accuracy. This is due to the fact that response-history analysis is the only procedure that provides the possibility of directly incorporation of nearly all sources of nonlinear and time dependent effects in the analysis. However, the relatively huge computational demand and complexity involved in this type of analysis are major obstacles in their application. The endurance time method (ET) is a new dynamic analysis procedure that tends to provide a framework where the computational demand and complexity of response-history based structural analysis can be significantly reduced, thus paving the way towards more popular application of response-history based analyses in practice. This paper provides a brief review of the history and recent advances in ET methodology and applications.

6 Professor, Department of Civil Engineering, Sharif University of Technology; email: stkanchi@sharif.edu.
7 Professor, Department of Civil Engineering, Sharif University of Technology; email: vafai@shasharif.edu.
8 PhD candidate, Department of Civil Engineering, Sharif University of Technology; email: mirzaee61@gmail.com.
9 PhD candidate, Department of Civil Engineering, Sharif University of Technology; email: mmashayekhi67@gmail.com.
10 PhD candidate, Department of Civil Engineering, Sharif University of Technology; email: bsamin2000@yahoo.com.

THE CONCEPT OF ENDURANCE TIME METHOD

The Endurance Time method is a response-history based procedure in which structures are subjected to predesigned gradually intensifying dynamic excitations and their performance is assessed based on their response at different excitation levels that are correlated to particular ground motion intensities [Estekanchi et al. 2004; Estekanchi et al. 2007; Estekanchi et al. 2011a]. The concept of the ET method is analogous to the exercise test used in medicine for assessing the fitness of athletes or patients by examining their biological measures when running on a treadmill with increasing slope and speed in a stage-wise manner [Estekanchi et al. 2009]. Endurance Time Excitation Functions (ETEFs) that have been used in recent studies are ground motion response spectrum compatible, i.e., each window of these ETAFs from start of the record to the specified time *t*, produces a response spectrum that is proportional to a template spectrum that can be either a design spectrum from code or average response spectrum from a set of ground motions. In this way, time can be correlated to the intensity level through the concept of response spectrum, thus the maximum response, e.g., interstory drift, that the structure will experience when subjected to ground motions compatible with particular response spectra can be estimated from its response up to the time where excitation intensity in ET analysis matches desired spectral intensity [Estekanchi et al. 2011b]. The point is that each ET excitation function can be made to include the entire range of equivalent intensities of interest [Valamanesh et al. 2010; Nozari and Estekanchi 2011].

By correlating the response spectrum of ETAFs with those of ground motions, two important characteristics of ground motions, i.e., the intensity and frequency content are covered in a relatively direct manner [Bazmooneh 2009]. A reasonable duration should be considered when scaling for the range of the target response spectra to be covered in the analysis. Preliminary studies suggested that a target time of 10 sec can be considered roughly a good option, not being either too short or too long compared with typical ground motions on stiff soil conditions. If the target time is too short, the structure will not undergo reasonable number of cyclic loadings before it is excited to the desired spectral intensity level, so the induced cyclic damage can be underestimated. On the other hand, if the target time is too long, the structure will experience excessive cyclic damage and if it is sensitive to cyclic degradation, the damage will be overestimated [Mashayekhi and Estekanchi 2012]. When multilevel response is to be estimated, consideration of the duration effect becomes more complicated. While it is known that higher magnitude earthquakes have longer durations on average, most concurrent analysis procedures use a scaling of the same set of considered ground motions, ignoring this aspect of duration issue. By the way, preliminary studies show that current ETAFs produce results with reasonable accuracy even in models with cyclic degradation [Riahi and Estekanchi 2010].

NEW DEVELOPMENTS IN GENERATING ET EXCITATION FUNCTIONS

The first generation of ETEFs were generated for preliminary studies of the Endurance Time method and its conceptual development [Estekanchi et al. 2004]. The second generation of ETEFs were produced in the linear range of structural analysis using a least square optimization procedure [Nozari and Estekanchi 2011]. This procedure produced ETEFs that produced acceptable results in the nonlinear range by including long-period points in objective function of the optimization procedure. The third generation of ETEFs (3G ETEFs) have been directly optimized in the nonlinear range and produced more consistent results in nonlinear studies. However, the improvements were relatively minor at about 20% as compared to second generation [Nozari and Estekanchi 2011]. For example, the E and EN set of ETEFs, which are second and third generations of ETEFs, respectively, have been produced considering average response spectra of seven earthquake records as the target spectrum. These ground motions were selected from 20 earthquakes recorded on stiff soil (type C) and proposed by FEMA 440, and their characteristics are presented in Table 1.

Figure 1 shows acceleration time-history of a typical 3G ETEF (ETA20en01), and Figure 2 indicates its acceleration response spectra at different time levels compared with objective response spectra, which have been obtained from average of response spectra of seven earthquake records as the target spectrum.

Table 1 Specifications of seven earthquake records used to develop the second and third generations of ETEFs.

Date	Earthquake Name	Magnitude (Ms)	Station Number	Scale Factor	Scaled PGA (g)	Scaled PGV (cm/sec)	Scaled PGD (cm)
6/28/1992	Landers	7.5	12149	1.10	0.56	57.0	16.8
10/17/1989	Loma Prieta	7.1	58065	3.65	0.62	73.2	47.3
10/17/1989	Loma Prieta	7.1	47006	2.63	0.64	53.2	20.2
10/17/1989	Loma Prieta	7.1	58135	2.22	0.79	63.5	14.1
10/17/1989	Loma Prieta	7.1	1652	1.45	0.74	59.7	23.6
4/24/1984	Morgan Hill	6.1	57383	2.30	1.04	42.9	8.8
1/17/1994	Northridge	6.8	24278	1.85	0.54	67.9	11.3

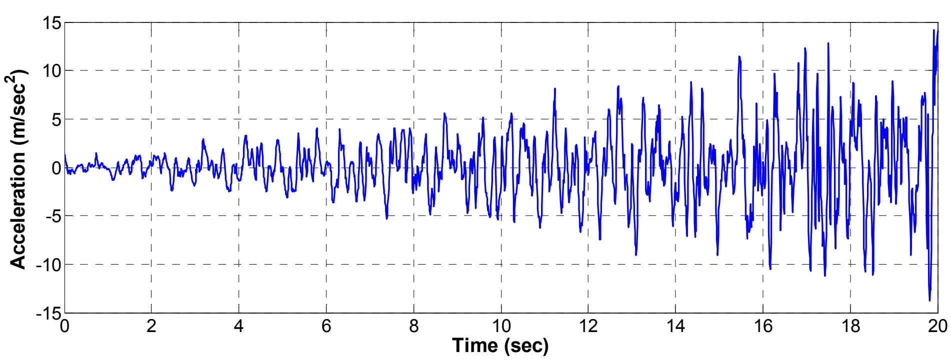

Figure 1 Acceleration time-history of a 3G ETEF (ETA20en01).

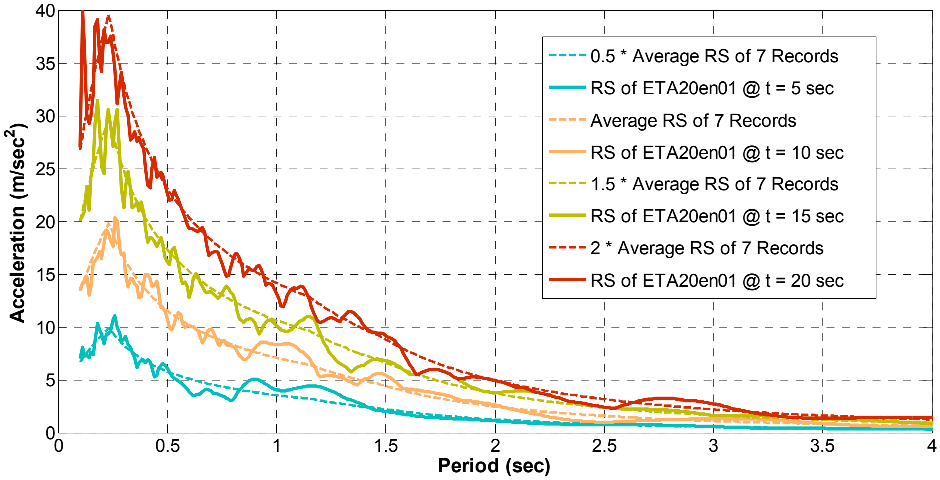

Figure 2 Acceleration response spectra of a 3G ETEF (ETA20en01) at 5th, 10th, 15th and 20th sec.

In order to develop a new generation of ETEFs which correlates with the ground motion duration it is essential to select an appropriate definition of strong-motion duration. Fundamental energy parameters of strong motions can be used for preliminary studies on correlation between the energy demand of ETEFs and real earthquake records. An important seismic parameters, i.e., cumulative Absolute Velocity (CAV) is defined as:

$$CAV = \int_0^{T_d} \left| a_g(t) \right| dt \tag{1}$$

where T_d is the total duration of ground motion, and $a_g(t)$ is the acceleration of ground motion, respectively. This energy parameter can be calculated in each time interval (from 0 to t) and plotted against time for ETEFs. However, to obtain the ideal target energy demands compatible with ground motions through time, the average value of energy parameter of seven earthquake records should be multiplied by a time variant scale function:

$$CAV_L(t) = CAV_{Ave} \times LIS(t) \tag{2}$$

where in linear intensification scheme:

$$LIS(t) = \frac{t}{t_{Target}} \tag{3}$$

Here, $LIS(t)$ is the linear increasing scale function used to indicate the objective response from the template response spectrum as a function of time. Figure 3 shows the correlation between energy parameter of the EN set of ETEFs (as 3G ETEFs) and average of seven earthquake records. As can be seen, the amounts and increasing trends of cumulative absolute velocity of 3G ETEFs are apparently distinct from those of strong motions.

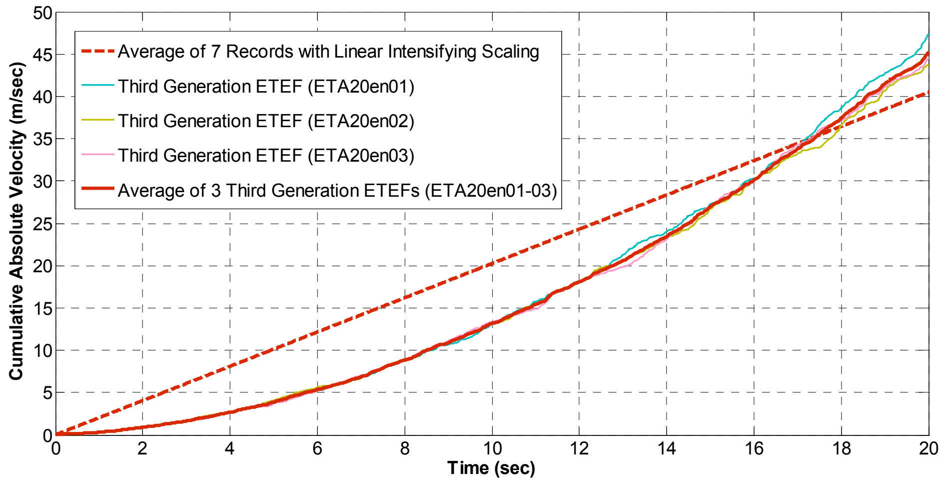

Figure 3 Time-history of cumulative absolute velocity (CAV) of 3G ETEFs versus average of linearly intensified seven earthquake records.

Cumulative absolute velocity, which is the integral of the absolute acceleration time-history, parabolically increases through time for the ETEFs; however, it linearly increases for ground motions, since they are simply multiplied by linear increasing scale factors. This can be evidently identified from Figure 3. Consequently, a new increasing scale function is required to produce a new generation of ETEFs to improve the matching. For this purpose, an exponential function is a reasonable alternative, since the integral of an exponential function preserve the exponential structure of the primary function and thus increases proportionally with it. Therefore, energy parameters of the ETEFs with exponential increasing profile would be close to those of ground motions, which are exponentially scaled. The following exponential increasing scale function is used to develop a typical fourth-generation (4G) ETEF:

$$EIS(t) = tanh(t) \times e^{\left(ln(2) \times \left[\frac{t - t_{Target}}{5} \right] \right)} \tag{4}$$

in which, the target time (t_{Target}) is defined as the 15th sec, and the total duration of ETEF is 20 sec that means t varies from 0 sec to 20 sec. It is worth nothing here the term $tanh(t)$ is to decay the exponential term at the first 3 sec of the ETEF that are not significant in the ET analysis. Figure 4 illustrates the exponential increasing scale function versus the previous linear scale function.

Considering the new exponential intensifying profile, a preliminary 4G ETEF, called "ExpAcc", is produced by the same optimization procedure utilized to produce 3G ETEFs. Figure 5 shows acceleration time-history of ExpAcc, and its acceleration response spectra at different times are depicted and compared with the objective spectra in Figure 6. The exponential increasing trend of the response spectra can be simply recognized as they increase to twice values in each 5-sec interval. Thus, since t = 15 sec is the target time of ExpAcc, its response spectra at t = 5 sec, and t = 10 sec are equal to a quarter and half of target spectrum, respectively, and reaches to twice target spectrum at t = 20 sec.

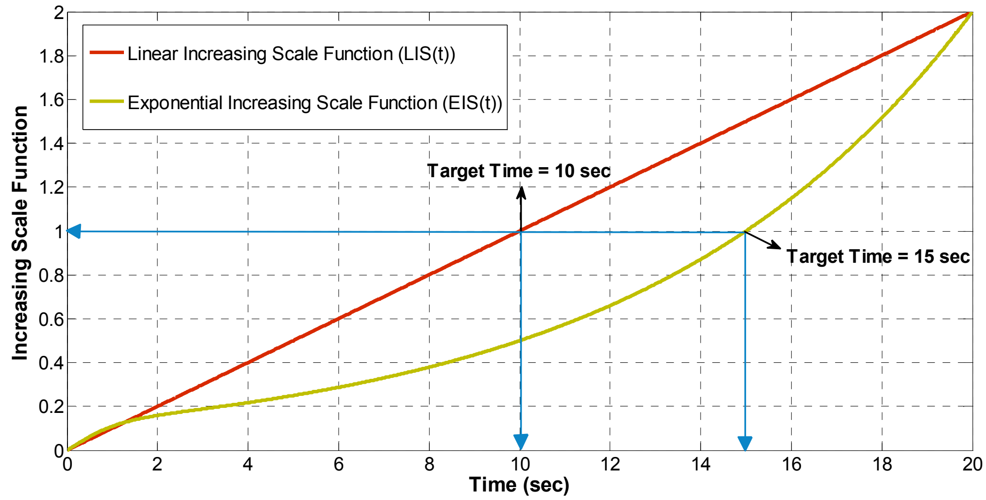

Figure 4 Exponential increasing profile used to produce a typical 4G ETEF versus linear increasing profile used to produce earlier generations of ETEFs.

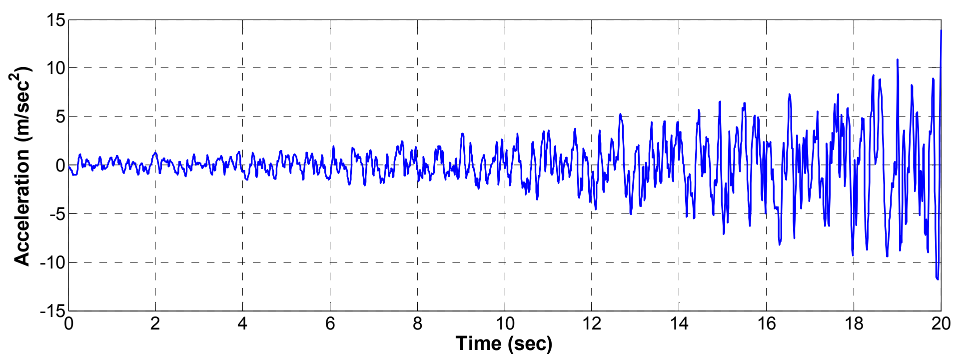

Figure 5 Acceleration time-history of a typical 4G ETEF (ExpAcc).

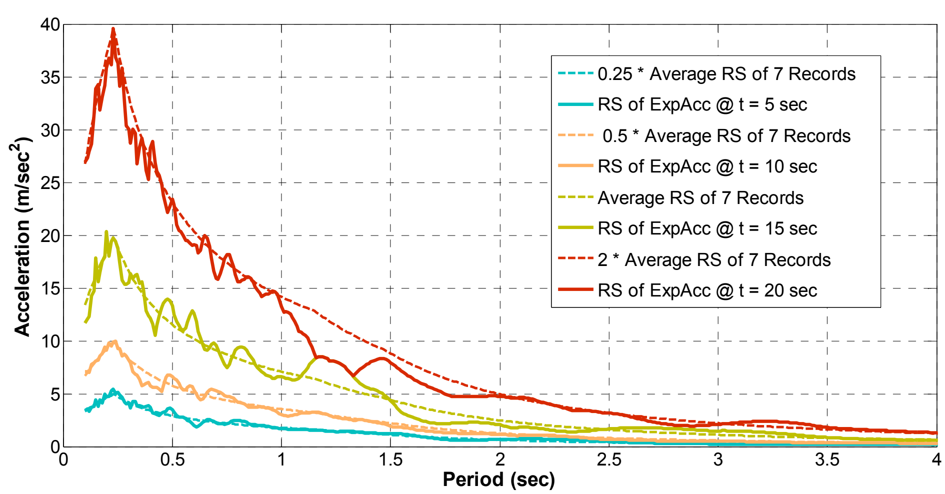

Figure 6 Acceleration response spectra of a typical 4G ETEF (ExpAcc) at 5th, 10th, 15th and 20th sec.

Figure 7 shows increasing trend of the energy parameters of ExpAcc, in comparison with the average energy demands of seven earthquake records through the time. To compare the results, the plots of CAV parameter of 3G ETEFs and seven earthquake records, with linear increasing scaling, have been re-shown in Figure 7. It can be seen that the increasing trend, but not the numerical values, of CAV of the ExpAcc, are similar to the increasing trend of energy parameters of ground motions with exponential scaling.

As a result, the change of the intensifying profile of ETEFs is an important step in producing 4G ETEFs, and the next step can be selection of the most significant energy parameter and evolving it in the objective function of optimization, when the ETEFs are initially generated. Thus, in addition to its time-variant trend, the amount of energy demand of ETEFs would be close to the average energy demand of ground motions.

Motion's number of cycles is another predictor of duration in response of structures in dynamic analysis. There are several methods for counting the cycles of a motion [Hancock and Bommer 2005; Hancock and Bommer 2007; Bommer and Martinez-Pereira 1999]. Rain flow counting and cycle counting are used in this context; either of them is used in two case namely, zero crossing and non-zero crossing. Comparison of number of cycles of an ET excitation function is depicted in Figure 8 [Riahi and Estekanchi 2010]. This figure suggests that the studied ETEFs show a higher level of cycle consistency with ground motions at higher target times. The difference is more obvious at longer periods of free vibration. These results can provide some guidelines in designing and generating the fourth-generation ETEFs.

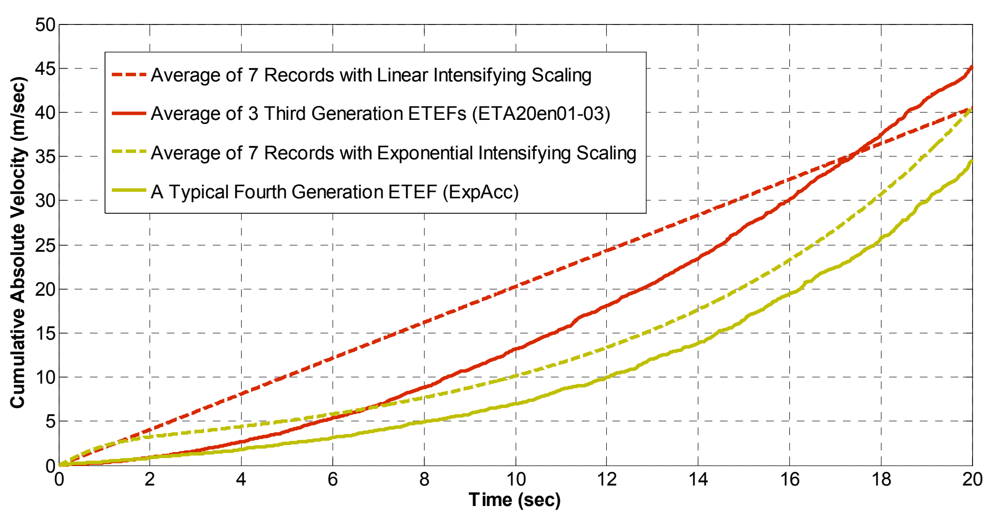

Figure 7 Time-history of CAV of a typical 4G ETEF (ExpAcc) versus average of three 3G ETEFs and average of linearly and exponentially intensified seven earthquake records.

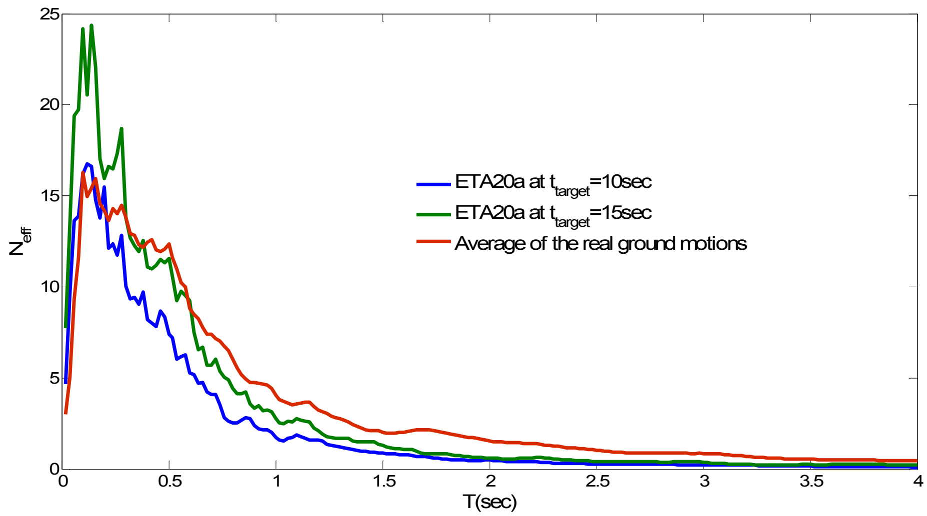

Figure 8 Comparison between the number of cycles spectrum (rain-flow counting) at proposed target time.

ADVANCES IN PERFORMANCE-BASED EARTHQUAKE ENGINEERING APPLICATION

Performance-based earthquake engineering (PBEE) is a method of design in which a preliminary model is seismically evaluated and redesigned until it fulfills some predefined performance objectives [Krawinkler and Miranda 2004]. ET method-based seismic assessment procedure has a good potential to be applied in the evaluation stage of performance-based design. The major advantage of ET analysis becomes evident when considering the huge amount of numerical effort needed for evaluating the seismic behaviour of a reasonably realistic model at multiple levels of seismic intensities. In ET analysis, elapsed time represents seismic intensity. Thus, in a single response history analysis, ET produces an estimate of performance over the entire intensity range of interest.

From Time to Hazard Return Period

Presentation of the ET analysis results can be further improved if the time variable in horizontal axis is replaced by the corresponding hazard return period. This can be based on considering a suitable intensity measure, such as acceleration response spectrum value. The time at which the response spectrum of ET excitation function matches that of the particular hazard return period can be readily calculated. In case that the spectral intensity of ET excitation do not match the intended design spectrum, consideration of the intensities at and around the fundamental structural mode of vibration is usually sufficient [Bazmooneh 2009; Mirzaee et al. 2012].

Figure 9 shows sample ET response curves in which the time has been replaced by the return period. These curves are related to different engineering demand parameters of a steel moment frame which responses are assessed over various seismic intensities. The concept of the damage level (DL) has also been applied in order to compare relative severity of different demands such as drifts, axial loads and plastic rotation [Mirzaee et al. 2010]. This figure clearly shows that in this case, the interstory drift has the higher DL in comparison to other parameters at return periods near 300 years and above, although it is below the maximum allowable level.

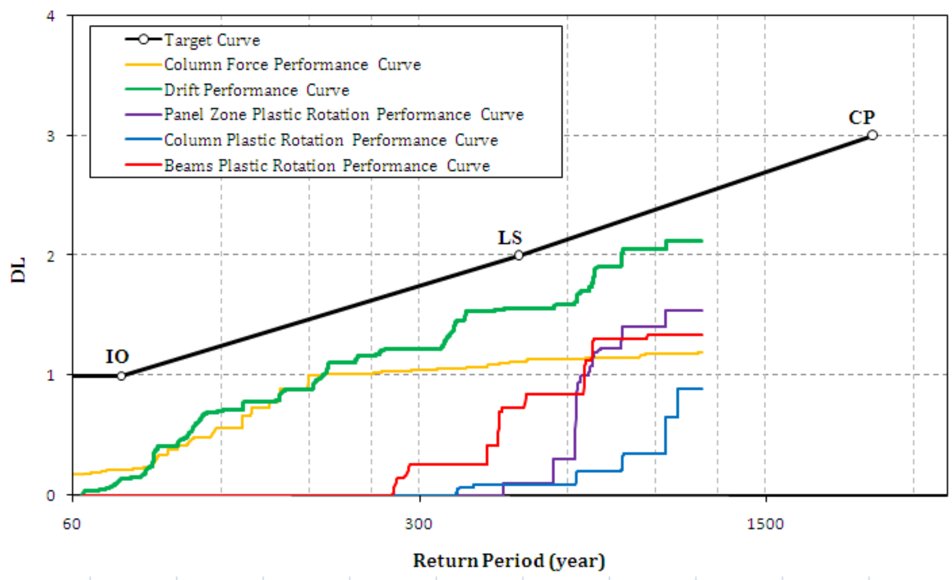

Figure 9 **New ET response curves for different engineering demand parameters in a steel moment frame.**

Life-Cycle Cost Estimation

Different types of costs may be included in the economic studies as the life-cycle costs of a structure. However, the initial construction cost and expected seismic damage cost throughout the life-time of the structure are two common types of cost which usually are considered in the life-cycle cost analyses for seismic-resistant structures. A practical approach to express the concept of seismic damage cost is considering the average annual repair cost. To calculate this parameter, the annual probability of exceedance of damage cost should be determined. Wen and Kang [2001] supposed a relation between corresponding costs of various damage states and interstory drifts. This relation has been presented in Table 2 for different damage states. Thus, having the annual probability of exceedance of interstory drift, the average annual repair cost can be obtained. The ET drift response curves can be readily used to acquire the annual probability of exceedance of interstory drift as shown in Figure 10. By reversing the return period on the x-axis to obtain the mean annual rate of exceedance and using it on the y-axis, the annual rate of exceedance of the interstory drift can be obtained.

If the interstory drift is correlated to damage cost by applying the relationship discussed previously, and considering the initial cost, the annual rate of exceedance for damage cost, i.e., the "Loss Curve" can be obtained. The area under the loss curve represents the mean annual total damage cost caused by all earthquakes in one year. Extension of ET application for Life Cycle Cost (LCC) analysis is currently under development by authors.

Table 2 Damage states, drift ratio limits, and corresponding costs [Wen and Kang 2001].

Performance level	Damage states	Drift ratio limit (%)	Cost (% of initial cost)
I	None	Δ < 0.2	0
II	Slight	0.2 < Δ < 0.5	0.5
III	Light	0.5 < Δ < 0.7	5
IV	Moderate	0.7 < Δ < 1.5	20
V	Heavy	1.5 < Δ < 2.5	45
VI	Major	2.5 < Δ < 5.0	80
VII	Destroyed	5.0 < Δ	100

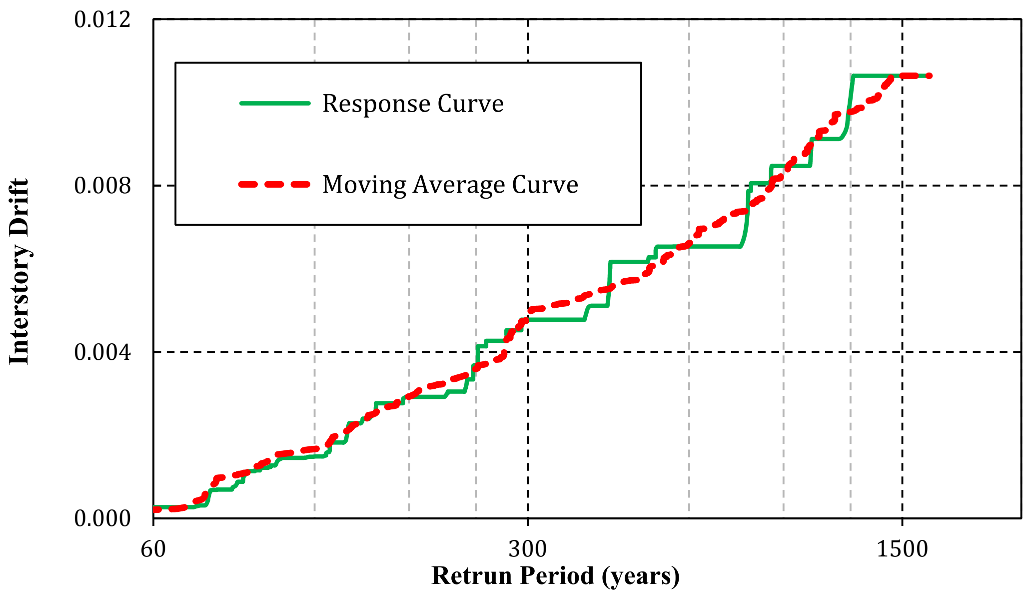

Figure 10 The ET response and ET moving average curve for drift ratio of a steel moment frame [Mirzaee and Estekanchi 2013].

REFERENCES

Bazmooneh A. (2009). *Application of Endurance Time Method in Seismic Evaluation of Existing Steel Buildings,* Thesis presented to the Department of Civil Engineering as a partial requirement for MS degree, Sharif University of Technology, Tehran, Iran.

Bommer J.J., Martinez-Pereira A. (1999). The effective duration of earthquake strong motion, *J. Earthq. Eng*., 3(2): 127–172.

Estekanchi H.E., Vafai A., Sadeghazar, M. (2004). Endurance time method for seismic analysis and design of structures, *Scientia Iranica,* 11(4): 361–370.

Estekanchi H.E., Valamanesh V., Vafai A. (2007). Application of endurance time method in linear seismic analysis, *Eng. Structures*, 29(10): 2551–2562.

Estekanchi H.E.; Riahi H.T., Vafai A. (2009). Endurance Time Method: Exercise test as applied to structures, *Asian J. Civil Eng*., 10(5): 559–577.

Estekanchi H.E., Riahi H.T., Vafai, A. (2011a). Application of Endurance Time Method in seismic assessment of steel frames, *Eng. Structures*, 33(9): 2535–2546.

Estekanchi H.E; Vafai A.; Valamanesh V.; Mirzae, A.; Nozari A., Bazmuneh A. (2011b). Recent advances in seismic assessment of structures by endurance time method, *PEER Report 2011/07*, Pacific Earthquake Engineering Research Center, University of California, Berkeley, CA.

Hancock J., Bommer J.J. (2005). The effective number of cycles of earthquake ground motion, *Earthq. Eng. Struct. Dyn*., 34(6): 637–664.

Hancock J., Bommer J.J. (2007). Using spectral matched records to explore the influence of strong-motion duration on inelastic structural response, *Soil Dyn. Earthq. Eng*., 27(4): 291–299.

Krawinkler H., Miranda, E. (2004). Performance-based earthquake engineering, in: *Earthquake Engineering: from Engineering Seismology to Performance-Based Engineering*, Y. Bozorgnia and V.V. Bertero (eds.), CRC Press, Boca Raton, FL.

Mashayekhi M., Estekanchi H.E. (2012). Significance of effective number of cycles in Endurance Time analysis, *Asian J. Civil Eng*., 13(5): 647–657.

Mirzaee A., Estekanchi H.E., Vafai, A. (2010). Application of Endurance Time Method in performance-based design of steel moment frames, *Scientia Iranica*,17: 361–370.

Mirzaee A., Estekanchi H.E., Vafai A. (2012). Improved methodology for endurance time analysis: From time to seismic hazard return period, *Scientia Iranica*, doi: 10.1016/j.scient.2012.06.023.

Nozari A., Estekanchi H.E. (2011). Optimization of Endurance Time acceleration functions for seismic assessment of structures, *Inter. J. Optimization Civil Eng*., 1(2): 257–277.

Riahi H.T., Estekanchi H.E (2010). Seismic assessment of steel frames with Endurance Time Method, *J. Constructional Steel Res*., 66(6): 780–792.

Valamanesh V., Estekanchi H.E., Vafai A. (2010). 'Characteristics of second generation endurance time accelerograms, *Scientia Iranica*, 17(1): 53–61.

Wen Y.K., Kang Y.J. (2001). Minimum building life-cycle cost design criteria, ASCE, *J. Struct. Eng*.,127: 338–346.

EFFECT OF FIRE FOLLOWING EARTHQUAKE ON COVERED AND UNCOVERED STEEL FRAME

Mahmood Yahyai[1] and Elnaz Peyghaleh[2]

ABSTRACT

Fire Following Earthquake (FFE), as an indirect seismic hazard, threats populated centers and mega-cities at earthquake prone area. There are examples of catastrophic fires following earthquakes such as the 1906 San Francisco, 1994 Northridge, and the 1995 Kobe earthquakes, that shows the importance of further studies and investigations on this phenomenon. According to current seismic codes, ductile structures are designed to suffer damages to some extent during strong earthquakes in order to avoid total collapse and therefore, safeguard human lives. However, such structures exposed to fire following earthquakes show higher vulnerability to fire than those with no structural damages. Structural elements in ductile structures, once exposed to sever ground motions may loss part of fire protection coating and therefore further penetration of heat flow in damaged elements. This in turn may result in significant reduction of structural fire resistance. In this paper, finite element models are used to study the performance of single-bay steel frames in eight cases; a steel frame with and without fire proofing cover under common fire and post-earthquake fire. It is concluded that fire following earthquake has more destructive effect on structure than ordinary fire and the structure survival time is reduced. For the case of covered frame under ordinary fire, no collapse is observed in the time period considered for the analysis of the models. However, in case of covered frame under fire following earthquake the effect of fire proofing cover is decreased and collapse can be observed. Fire proofed frames have better performance even under fire following earthquake in comparison with uncovered frames.

Keywords: *Fire Following Earthquake, fire-proofing steel structure*

INTRODUTION

Experiences from past earthquakes showed that steel structures are vulnerable to most seismic hazards such as fault rupturing, liquefaction, landslide and above all strong ground motions. Excessive damages to structures and certain utilities may cause secondary hazards such as flooding, fire, environmental pollution, etc. Fire Following Earthquake (FFE) is the major threat for cities having structures that are not resistant to fire. The cities with high pressured natural gas distribution network or air-drawn electrical transfer and distribution network are also vulnerable to fire following earthquake. During an earthquake such systems can cause ignitions and structural fire irresistibility and high density of urban areas can generate wide spread fire following big earthquakes. Fire Following Earthquake consists of many simultaneous and catastrophic fires which could result in widespread economic damages and loss of life [1,2]. Example of such historical cases is the 1906 San Francisco Earthquake with destructive

1Associate Professor, Civil Engineering Department, K. N. Toosi University of Technology, Tehran, IRAN; email: yahyai@kntu.ac.ir.
2 PhD. Student, Civil Eng. Dept., K. N. Toosi University of Technology, Tehran, IRAN; email: peyghaleh@udel.edu.

consequences [ASCE 2005; Chen and Scawthorn 2003]. More recent examples are the 1994 Northridge and the 1995 Kobe Earthquakes [NFPA 1995].

Like other fire pattern, the FFE process consists of three main phases; ignition, spread and suppression. Most of researches in recent years have focused on modeling fire spread and macro modeling of FFE and less attention is paid to study the effect of fire following earthquake on buildings from structural point of view. With regards to FFE risk modeling of ignitions, statistical correlations made between strong ground motion and ignition frequencies are mostly used as a mean to simulate this phase of an FFE model. Mizuno et al. [1978] developed the first IFE models based on statistical analyses of FFE damage data from earthquakes in Japan. Scawthorn followed this approach and expanded this concept to develop probabilistic post-earthquake fire ignition and spreading model [1986]. Using statistical data, Tokyo Fire Department [1997] developed some curves which show the ignition mean rates as functions of PGA. Zolfaghari et al.[2008] made an attempt to analytically model intrastructure ignitions following earthquakes using a probabilistic approach. Zolfaghari et al. attempted to present similar approach for estimating ignition potential from urban utility network [2009]. Besides, comprehensive researches have been carried out about fire following earthquake spread. Most of these researches are conducted for being used in FFE risk modeling. One of the most important methods in this subject is the method proposed by Hamada [1951]. In this method, the structural behaviour of buildings in fire is not considered. The Tokyo Fire Department developed the so-called TOSHO model that like Hamada model uses an oval form spread [1997]. In contrast with Hamada model, this model considers the speed of fire as a function of building material and structural collapse [Tokyo Fire Department 1997]. The most advanced model is proposed by Cousins et al. [2002] that is based on cellular automate method and like Tosho model, considers the building material type.

Since these models are developed for risk and insurance purposes, the structural behaviour in fire and especially in earthquake is not considered. The effect of seismic structure behavior is more important when the structure enters the plastic range due to a devastating earthquake and its load carrying capacity is severely decreased. When such a structure is exposed to fire, the probability of reaching to instability is increased and the survival time of structure is decreased. This matter is especially important in steel structures, since the mechanical characteristics of steel is rapidly deteriorate with increase of temperature and the steel members that have been entered to the plastic range during earthquake, loose their load carrying capacity more quickly.

Little research has been carried out considering the effect of earthquake and fire following earthquake simultaneously, such as the study conducted by Della Corte et al. [2003]. They tried to obtain some quantitative information about post-earthquake fire resistance of steel frames. A simplified modeling of earthquake induced structural damage is proposed and some numerical analysis is performed with reference to a single-bay single-story frame structure allowing the main parameters affecting the problem to be identified. Another study that has been conducted is by Yassin et al. [2008] about the performance of steel frames building structures under post-earthquake fire condition. An analytical study of two-dimensional steel frame under the effects of seismic lateral loads and subsequent fire has been presented. They concluded that

FFE performance of steel frames is affected by the lateral deformation caused by the seismic ground motion. Alderighi and Salvatore [2008] conducted a numerical investigation for the assessment of the structural fire performance of earthquake resistant composite steel-concrete frames. They tried to identify some key structural parameters that make it possible to correlate the predictable performance under seismic and fire loadings when these two are considered as independent actions.

An important point that should be noted herein is the use of fire-resisting coatings that are frequently used in steel structures during the past years. Some of experimental and analytical researches present the effect of fire proofing cover on structural performance of steel structures in fire. Kirby [1998] conducted some experimental test to study the behaviour of protected and unprotected steel members under natural fire. Extensive experimental tests carried out in Cardington [Bravery 1993; Martin et al. 1998] to investigate the protected and unprotected steel structure performance. Wald et al. [2004] studied the temperature of steel columns under natural fire. The results of the study were drawn as time-temperature curve for different points of protected columns is provided.

Although the steel profiles covered with this fire resistant have desirable behavior in common fires (not FFE) and postpone the structure collapse, the cover cannot protect the steel profiles after an earthquake. In case of FFEs, the steel members falls in plastic range due to the earthquake and plastic hinges are formed in beams and columns and many cracks are developed in fire resisting coating in the location of plastic hinges. Thus, the steel members with cracked fire resisting coating are vulnerable to fire and the mechanical properties drop quickly.

In this paper, finite element models are used to study the performance of steel frames in four cases; a steel frame with and without fire proofing cover under common fire and post-earthquake fire. The frames that are under seismic and then fire loading called EFS and the frames that are just under fire loading called FS. The steel frames are designed based on Eurocode 8 [CEN 1998] and are modeled by finite element software. In EFS models, seismic loading is applied by a lateral displacement. Fire loading in the frames without cover is simulated by increasing temperature in the bottom flange of the beam. In the case of covered steel frames, because of the large strain in plastic zones, the fire load is modeled by increasing temperature in the location of plastic hinges that is in beam for some cases and in beam and column in other ones.

SEISMIC LOADING

Performance of structures under fire following earthquake depends on several factors and large uncertainties is included in prediction of structural behavior and the intensity of external actions. One main problem is the evaluation of structural physical state after the earthquake. This structural state represents the initial condition for later fire loading. The behavior of a specific structure under earthquake loading can be predicted using complicated numerical models. Since large uncertainties are involved in both structural properties and earthquake ground motion, obtaining detailed information about the earthquake induced structural damage is difficult. Two type of damage can be occurred in structures which are mechanical and geometrical damages.

Mechanical damages are due to degradation of mechanical properties of those structural components engaged in the plastic range of deformation during the earthquake. Geometrical damages are in the form of structural geometry changes due to plastic excursion during the earthquake, such as permanent displacements and rotations.

In this paper, both geometrical and mechanical damages are considered by applying earthquake loading as a specific displacement. Although it is more accurate to apply a time-history acceleration or displacement record of an earthquake on a structure, a simplified method for simulating earthquake-induced damage is to apply a specific lateral displacement that is the structure maximum displacement caused by that earthquake record. Consequently, geometrical damages are considered by the permanent deformations of the structure after unloading. Furthermore, mechanical damages are considered since the mechanical properties of material are changed in the locations where plastic zones are formed.

For calculating the maximum displacement, limiting displacements that are presented in most seismic codes are used. These limiting displacements are calculated based on the design performance level of a structure for desired hazard level. For example, in Iranian earthquake Standard [BHRC 1999] in which the life-safety performance level is considered for structure in specific hazard level, the displacement limit is 5% of structure height. This hazard level is an earthquake having a 10% probability of being exceeded in 50 years or an earthquake with return period of 475 years.

FIRE LOADING

Fire action and the fire resistance of different structural elements should be simulated. There are several methods for applying fire load to a structure. In this paper fire is modeled by applying increasing temperature. For the bare members or the members whose cover is cracked due to earthquake and are directly exposed to fire, temperature has been assumed uniform and monotonically increasing in accordance with the time-temperature curve suggested by the standard ISO-834 [1975] shown in Figure 1(a). As it is well known the ISO curve is a purely conventional fire action model, which does not represent any particular fire that could develop in real buildings.

In cases where fire proofing cover is not used, the temperature is applied according to ISO-834 time-temperature curve as a uniform increasing temperature in columns, beam bottom flange and a part of beam web that is out of concrete slab. In the cases where fire proofing cover is used, the temperature is applied according to ISO-834 time-temperature curve as a uniform increasing temperature in plastic hinges in column, bottom beam flange and the part of beam web that is out of concrete slab, where fireproofing cover has been cracked under earthquake loading. In addition, for the areas which are covered, the temperature is applied according to time-temperature curve provided by Wald et al. [17] shown in Figure 1(b). The time-temperature curve is developed for covered column whose photo and area section are shown in Figure 2. The cover material is vermiculite cement spray and its thickness is about 18 mm. The typical location of cracked fire proofing cover that is caused by earthquake loading is shown in Figure 3(a) and the temperature loading is applied in these regions. The regions where the temperature loading is applied in uncovered frames is shown in Figure 3(b) that is the bottom beam flange and the part of beam web that is out of concrete slab; see Table 1.

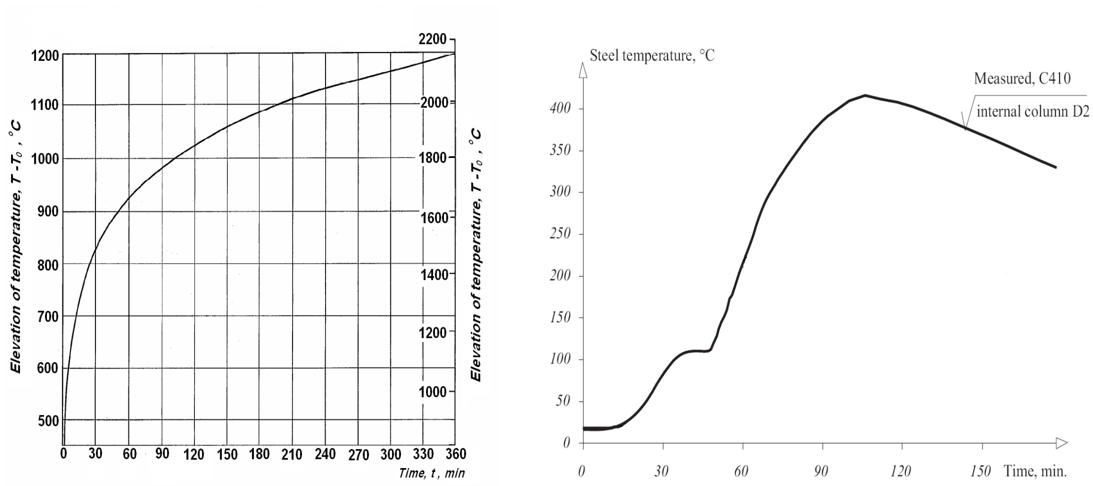

(a) (b)

Figure 1 (a) ISO standard time-temperature curve [1975; and] (b) Wald et al. column time-temperature curve [2004].

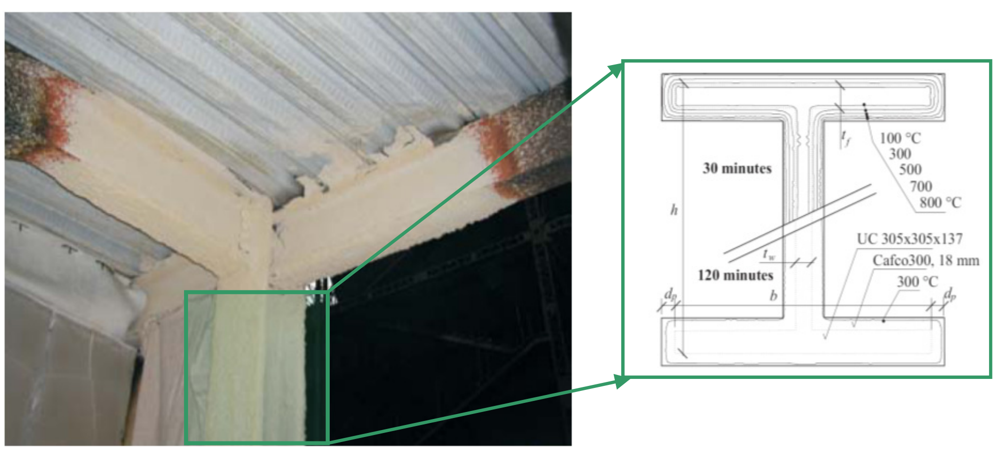

Figure 2 Photo and area section of covered steel column presented by Wald et al. [2004].

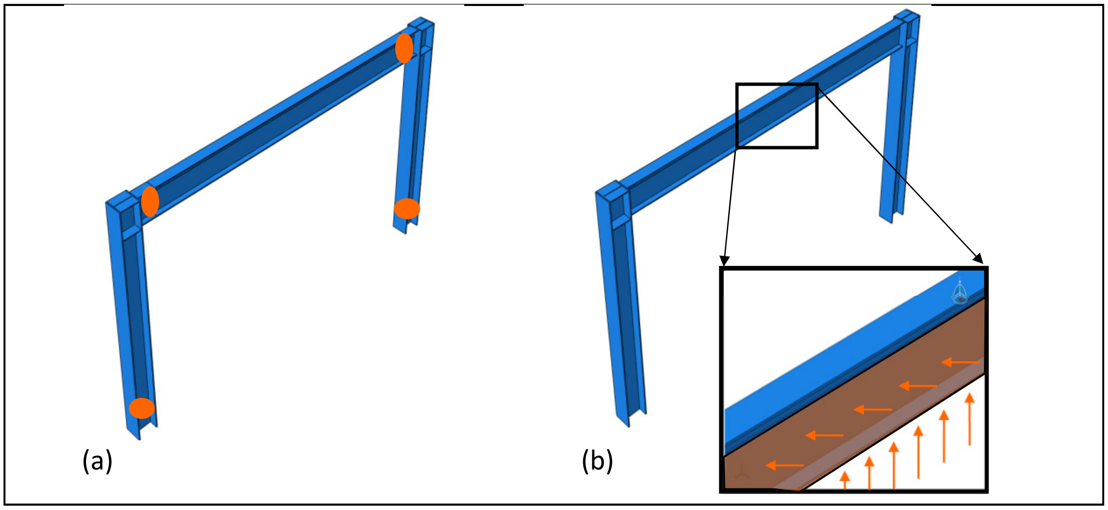

Figure 3 (a) Temperature loading in location of cracked fire proofing cover in seismically loaded frames; and (b) temperature loading in beam regions of uncovered frames.

Table 1 Characteristics of structural members.

Member	Profile	Steel	Length (cm)	M/M_p
Beam	IPEB400	ST37	600	0.1(End) 0.05 (middle span)
Column	IPB350	ST37	350	-

MODELLING APPROACH

In this paper, finite element models are used to study the performance of steel frames in eight cases. These cases are shown in Table 2. The steel frames are designed based on Eurocode 8 and are modeled by finite element software [CEN 1998]. In EFS models, earthquake load is applied by a lateral displacement equal to 5% of frame height that is a common maximum displacement that structure can sustain. Temperature has been assumed uniform in the bottom beam flange and a part of web. Temperature has been monotonically increasing in accordance with the time-temperature curve suggested by the standard ISO-834.

Table 2 The structural models.

Model Name	Seismic Load	Fire Load	Uncover	Cover-Column	Cover Beam	Time-Temperature Curve in Beam	Time-Temperature Curve in Column	Column hinge considered for temperature loading	Beam Hinge Considered for Temperatu Re-loading
FS-C	-	√	-	√	√	Wald et al. [2004]	Wald et al. [2004]	-	-
FS-NC-Beam	-	√	-	√	-	I ISO [1975]	Wald et al. [2004]	-	-
FS-NC-Frame	-	√	√	-	-	ISO [1975]	ISO [1975]	-	-
EFS-C-Beam	√	√	-	√	√	Wald et al. [2004]	Wald et al. [2004]	-	ISO [1975] in Beam plastic hinge
EFS-C-Frame1 *	√	√	-	√	√	Wald et al. [2004]	Wald et al. [2004]	ISO [1975] in Column plastic hinge	ISO [1975] in Beam plastic hinge
EFS-C-Frame2 **	√	√	-	√	√	Wald et al. [2004]	Wald et al. [2004]	ISO [1975] in Column plastic hinge	ISO [1975] in Beam plastic hinge
EFS-NC-Beam	√	√	-	√	-	Wald et al. [2004]	ISO [1975]	-	-
EFS-NC-Frame	√	√	√	-	-	ISO [1975]	ISO [1975]	-	-

*Interior columns and temperature is applied to whole part of column hinges.

** Exterior columns and temperature is applied just to column interior flange in plastic hinge area.

FINITE ELEMENT MODELLING

For FS frames the analyses consist of two steps. First, gravitational load is applied on the top flange of beam in a static form. Then, the fire loading is applied and a coupled thermal-mechanical analysis is used to simultaneously consider the effect of mechanical and temperature loading. For EFS frames, the analyses consist of three steps. First, gravitational load is applied on the top flange of beam. Then, the earthquake is simulated as a lateral displacement that is applied on the top of frame columns in a static form. Finally, the fire loading is applied and a coupled thermal-mechanical analysis is used to simultaneously consider the effect of mechanical and temperature loading.

Table 3 illustrates the variation of mechanical and thermal properties of steel material with temperature. Three-dimensional solid elements are used to model columns and beam profiles in for these frames. The beam-to-column connections are assumed to be rigid. The bases of the columns are restrained in all transitional and rotational directions. Since the concrete slab prevents the beam to have horizontal movements in direction perpendicular to the beam axis, the beam is restrained in out of plane horizontal movement [Figure 4(a)].

Table 3 Steel mechanical and thermal properties.

Temperature (°C)	Ultimate Strain	Yield strain	Yield Stress (kg/cm^2)	Thermal Expansion	Specific Heat (J/Kg°C)	Conductivity Coefficient (W/m°C)
0	0.15	0.0014	2750	0	380	54
200	0.15	0.018	2750	0.0025	500	47
400	0.15	0.02	2750	0.0055	650	41
500	0.15	0.021	2200	-	-	34
600	0.15	0.022	1300	0.0085	800	30
730	0.15	0.022	600	0.0115	850	28
800	0.15	0.022	306	0.0115	800	28
900	0.15	0.022	200	-	-	28
1000	0.15	0.022	100	0.014	700	54
1200	0.15	0.022	50	0.0175	700	47

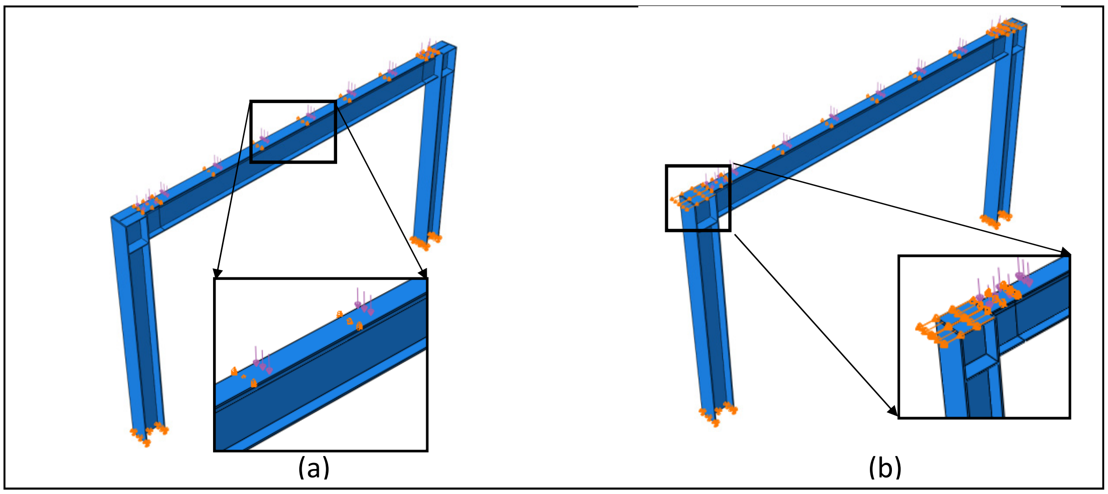

Figure 4 (a) Boundary conditions and gravitational load; and (b) boundary condition, gravitational load and earthquake load.

RESULTS AND DISCUSSION

The analysis results for each given load case are discussed in following. The typical displacement in the vertical direction under gravitational load is shown in Figure 5(a). The maximum displacement is occurred at mid span of the beam which is equal to 0.166 cm. Lateral displacement of EFS models subjected to seismic load is equal to 15.05 cm. The frame conditions after earthquake loading with plastic strain is shown in Figure 5(b). As it was anticipated, the plastic hinges are formed at the two ends of the beam and near the bases for two columns. As it can be seen in this figure, the cracks in the fireproofing covers start to develop in these locations.

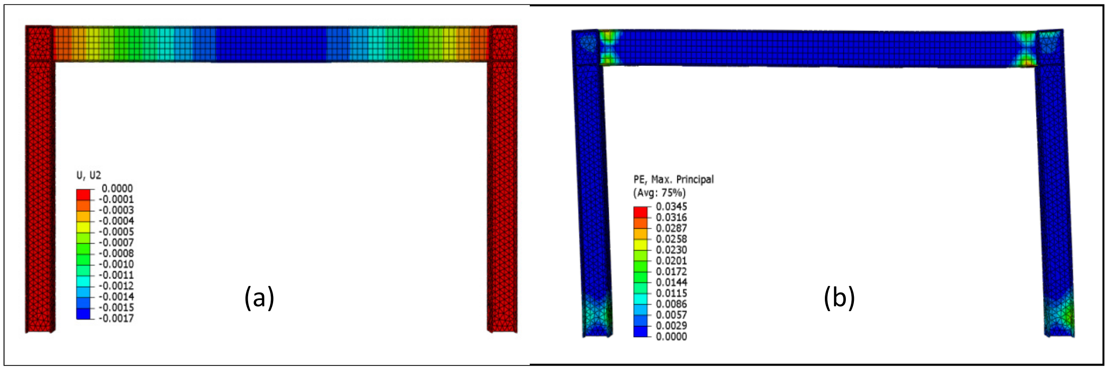

Figure 5 (a) typical displacement in vertical direction under gravitational load; and (b) plastic strain after earthquake loading.

In all cases, vertical displacements at specific time are presented in Table 4. The allowable beam deflection is estimated based on the following equation (Iranian National Building Code):

$$\beta_{allowable} = \frac{\Delta}{L_{Beam}} = \frac{1}{240}$$

where $\beta_{allowable}$, Δ, and L_{Beam} are maximum allowable beam deflection to beam length ratio, maximum beam deflection and beam length respectively. For the frames modeled in this paper, the allowable beam deflection is equal to 25 mm, which is corresponding to the $\beta_{allowable}$. Table 4 shows the ratios between vertical displacements at beam mid span to the allowable beam deflections (γ). For NC models, the ratio of beam mid span deflection to allowable deflection is very high, especially for EFS-NC models which imply beam destruction. In contrast, as it can be observed, the rise in the temperature for FS-C model has negligible effect on deflection ratio and structure remains in allowable conditions. Nevertheless, development of plastic hinges at beam and columns due to earthquake loadings reduce the effectiveness of fire resisting cover which in turn results in higher deflection ratios. In such cases, the plastic hinges are formed at the two ends of the beam and thus, the whole beam moves downward.

Variations of vertical and horizontal displacements during the time from beginning of the analysis are presented in Figures 6 and 7 respectively. In the Figure 6, sharp increase of mid span displacement in covered frames in compare with uncovered frames has been happened much later under both ordinary fire and fire following earthquake. Uncovered frame becomes unstable sooner and sustains sharp increase of displacement sooner. Also in both covered and uncovered frame under fire following earthquake, mid span displacement is increased much larger and before similar frames under ordinary fire. This is because of the earthquake effect on these frames.

The EFS frames under earthquake loading deform laterally with maximum lateral displacement of 0.15 m as it can be seen in Figure 7. The maximum horizontal displacement of the EFS-C-Beam frame after fire loading is less than the displacement applied to the frame to earthquake loading. The reason is the relaxation of elastic deformation after earthquake unloading. In EFS-C-Frames the plastic hinges are also formed in column bases and thus, the horizontal displacement of the frame is larger than that of the EFS-C-Beam case. For EFS-NC models the horizontal displacement of the frame is larger than those of fire proofed frames. In these models the sudden increase of positive displacement shows that collapse took place laterally in contrast to the FS-NC-Frame, in which both columns collapse internally and the sudden increase of negative displacement can prove this claim.

Table 4 Deflection of the models.

Model Name	Max Deflection Recording Time(Sec)	Max Deflection in Beam (cm)	γ	Time to Reach 2.5 cm Deflection in Beam Mid-Span	Time to Reach 5 cm Deflection in Beam Mid-Span
FS-C	14400	0.166	0.0664	-	-
FS-NC-Beam	7200	70	28	2966	3016
FS-NC-Frame	7200	206	82.4	2467	3092
EFS-C-Beam	14400	8.7	3.48	9023	10623
EFS-C-Frame1	14400	15.4	6.16	9124	10324
EFS-C-Frame2	14400	11.0	4.4	9032	10432
EFS-NC-Beam	7200	70	28	2861	2981
EFS-NC-Frame	7000	224	89.6	2176	2676

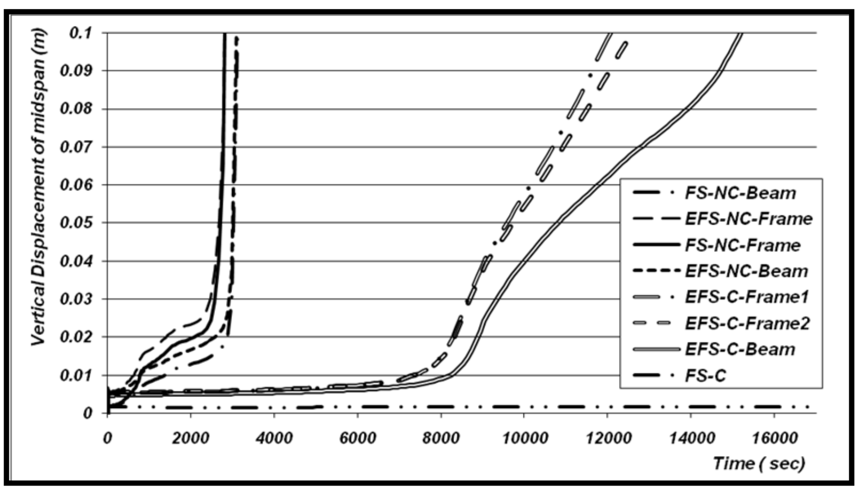

Figure 6 Vertical displacement of the mid span.

Table 3 also presents the time required to reach 25 mm and 50 mm deflection in beam mid span for each model. As it was anticipated, fire following earthquake has more destructive effect on structures than ordinary fires which results in reduction of structural survival time and sustainability, especially when the development of plastic hinges at columns are considered. As it can be seen in Figure 8(a), the frame survival time is decreased in the case of fire following earthquake. The anticipated effect of fire proofing cover on survival time of structure under fire following earthquake is also shown in Figure 8(b). However, as it can be seen, fire-proofed frames have better performance even under fire following earthquake.

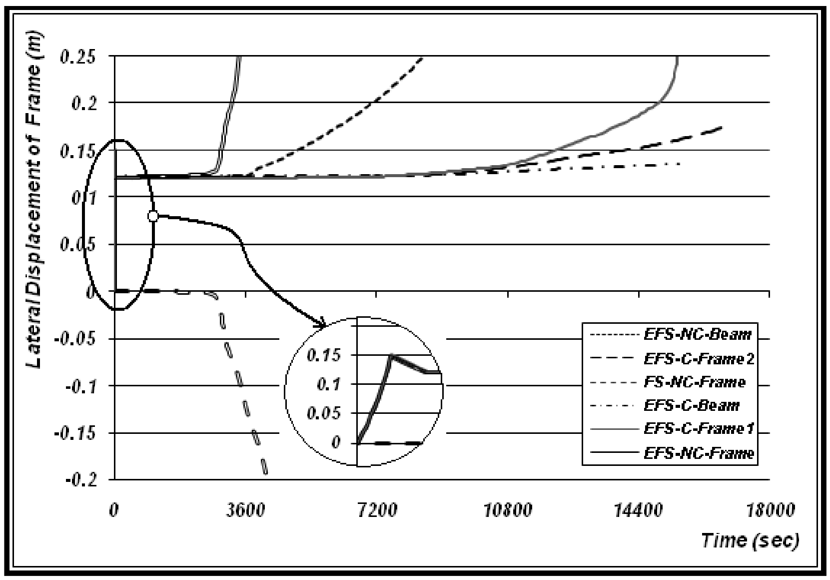

Figure 7 Vertical displacement of the mid span.

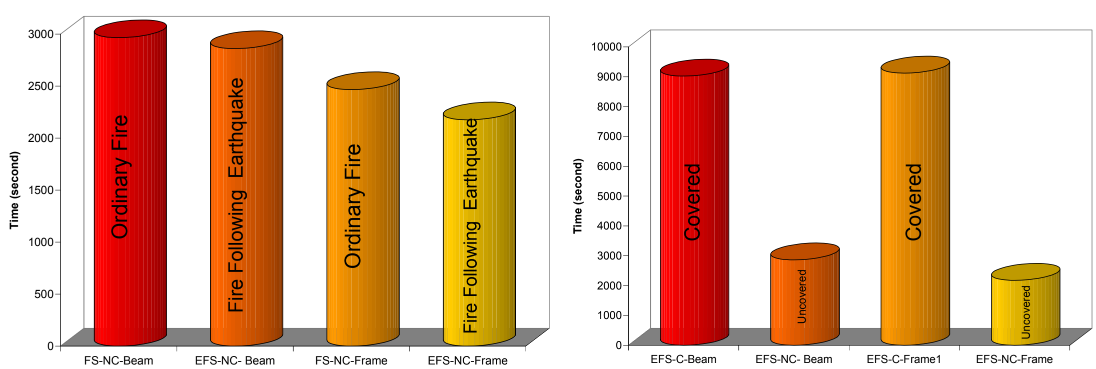

(a) (b)

Figure 8 Comparison between survival time: (a) uncovered models and (b) uncovered and covered frames under post-earthquake fire.

CONCLUSIONS

In this paper, steel frames are modeled using finite element computer software and the models are analyzed to study the differences between the performances steel structure under fire following earthquake versus ordinary fires. Furthermore, the efficiency of fire proofing cover for the case of fire following earthquake is investigated. The deflection of beam mid span is assumed as a measuring factor for structural deformation and determination of structural collapse. It is concluded that fire following earthquake has more destructive effect on structure than ordinary fires and the structure survival time is reduced, especially when the plastic hinge formation in columns is considered. For the case of covered frame under ordinary fires, no collapse is observed in the time period considered for the analyses of these models. However, in case of covered frame under fire following earthquake the effect of fire proofing cover is decreased and collapse can be observed in the time period considered for the analyses. Nevertheless, fire proofed frames have shown better performance, even under fire following earthquake in comparison with uncovered frames. As it can be seen in the case of fire following earthquake, the steel frame is collapsed laterally, whereas in the case of ordinary fire, the structure is collapsed internally. This is due to the lateral plastic deformation, formed in the structure during the earthquake. The collapse direction is important, especially for fire-fighting operations.

REFERENCES

Alderighi E., Salvatore W. (2009). Structural fire performance of earthquake-resistant composite steel-concrete frames, *Eng. Structures*, 31: 894–909.

ASCE (2005). Analysis and modeling, in: *Fire Following Earthquake 99-155*, American Society of Civil Engineers, Chapter 4, C. Scawthorn., J.M. Eidinger, and A. J. Schiff (eds.), Reston, VA.

Chen W.-F., Scawthorn C. (2003). Fire Following Earthquake, in: *Earthquake Engineering Handbook*, 1st ed., pp. (29-1)-(29-65), CRC Press, Boca Raton, FL.

Mizuno H. (1978). *On Outbreak of Fires in Earthquakes*, PhD Dissertation, Department of Architecture, Kyoto, University, Kyoto, Japan.

NFPA (1995). *Earthquake Fire, Kobe, Japan, January 17, 1995*, National Fire Protection Agency, Quincy, MA.

BHRC (1999). *Iranian Code of Practice for Seismic Resistant Design of Buildings (Standard 2800),* Chapter 2, 2nd ed., pp. 31–57, Building and Housing Research Center, Iran.

Bravery P.N.R. (1993). Cardington large building test facility, *Technical Report*, Building Research Establishment.

CEN (1988). *Structures in Seismic Region Eurocode 8*, Commission of the European Communities, Brussels.

Cousins W., Heron D., Mazzoni S. .(2002). *Estimating* risks from fire following earthquake, *Client Report 60*, Institute of Geological and Nuclear Sciences, Lower Hutt, New Zealand.

Della Corte G., Landolfo R., Mazzolani F.M. (2003). Post-earthquake fire resistance of moment resisting steel frames, *Fire Safety Journal*, 38: 593–612.

Hamada M. (1951). *On Fire Spreading Velocity in Disasters* (Tokyo: Sagami Shobo), in Japanese.

Kirby B.R. (1998). Behaviour of a multi-storey steel framed building subjected to fire attack: Experimental data, *Technical Report*, British Steel.

Martin D.M., Kirby B.R., O'Connor M.A. (1998). Behaviour of a multi-storey, steel framed building subjected to natural fire effects, *Technical Confidential Report*, British Steel.

Scawthorn C. (1986). Simulation modelling of Fire Following Earthquake, *Proceedings, U.S. National Conference on Earthquake Engineering,* Charleston, South Carolina, pp. 1675–1685.

Tokyo Fire Department (1997). *Determinations and Measures on the causes of New Fire Occurrence and Properties of Fire Spreading on an Earthquake with a Vertical Shock, Fire Prevention Deliberation*, Council Report, Page 42.

Wald F., Studecka P., Kroupa L. (2004). Temperature of steel columns under natural fire, *Acta Polytechnica*, 44:(5-6).

ISO (1975). *Fire Resistance Tests, Elements of Building Construction, ISO 834*, International Standard Organization, Geneva, Switzerland.

Yassin H., Iqbal F., Bagchi A., Kodur V.K.R. (2008). Assessment of post-earthquake fire performance of steel-frame buildings, *Proceedings, 14th World Conference on Earthquake Engineering*, Beijing, China.

Zolfaghari M.R, Peyghaleh E., Golmoradi L., Nasirzadeh G. (2008). Urban utility ıgnition model, a probabilistic approach for modelling Fire Following Earthquake, *Proceedings, 14th World Conference on Earthquake Engineering*, Beijing, China.

Zolfaghari M.R, Peyghaleh E, Nasirzadeh G. (2009). Fire Following Earthquake, Intra-structure ignition modeling, *J. Fire Sciences*, 27(1): 45−79.

PREPAREDNESS PLANNING AND THE AUGUST 23, 2011, VIRGINIA EARTHQUAKE

William A. Anderson[1]

ABSTRACT

The 5.8 magnitude Virginia earthquake that struck the East Coast of the United States on August 23, 2011 damaged buildings, including schools, near the epicenter in the state of Virginia, and a few iconic structures in nearby Washington, D.C. It also disrupted communications and transportation systems along the East Coast for some time, but fortunately caused no deaths and few injuries. Thus the event might be characterized as a "near-disaster". There was an absence of earthquake preparedness planning in the impacted jurisdictions of Maryland, Virginia and Washington, D.C. as well as in other parts of the East Coast before the earthquake. Research has shown that experience with full-fledged disasters can result in increased disaster awareness and preparedness planning. As a near-disaster, the Virginia earthquake furthered similar results at a modest but nevertheless important level. After the event, earthquake preparedness planning initiatives were undertaken involving safety guidelines, exercise drills, emergency response plans, and disaster laws.

Keywords: *earthquake; near-disaster; preparedness planning*

INTRODUCTION

On August 23, 2011, a 5.8 magnitude earthquake struck the state of Virginia in the United States damaging buildings and other structures near and beyond its epicenter in Louisa County. Damaged structures that are still under reconstruction include schools in Louisa County and the symbolically important Washington Monument and National Cathedral, both located in Washington, DC just 135 km from the epicenter (EERI 2011).

Fortunately, the earthquake resulted in no deaths and few injuries, even though it caused widespread interruptions in communications and transportation systems that disrupted life from hours to months in some cases in many East Coast communities (EERI 2011). Though considered large for the East Coast of the U.S., the Virginia earthquake was a comparatively moderate event, both in terms of its size and impact. Thus it was not a full-fledged disaster in the strictest sense but rather what might be called a "near-disaster".

Concept of Preparedness Planning

In this paper I will examine earthquake preparedness planning in the context of the Virginia earthquake. Such planning involves pre-event actions for preparing those at -risk for responding to disasters, both in terms of timeliness and appropriateness, especially during the emergency

[1] National Research Council, National Academy of Sciences (Retired), USA

phase [Kreps 1991]. When preparedness planning occurs, it is because of the recognition that mitigation actions alone will not prevent disasters which make it necessary to develop appropriate strategies to cope with them when they do occur in spite of hazard reduction efforts.

Research has well documented that disasters can lead to needed attention directed at preparedness planning by individuals, groups, and organizations [Anderson 1970; Birkland 2007; Drabek 2010; Phillips, Neal, and Webb 2012]. It has been far less clear, however, what impact a near-disaster can have on preparedness planning. The experience with the Virginia earthquake provides an opportunity to shed some light on this issue. I will focus on the states of Virginia and Maryland and Washington, DC because of their proximity to the earthquake's epicenter and because they were among the jurisdictions most affected by the near-disaster event. My analysis is based on information collected shortly after the earthquake by a team of researchers that I co-led and was assembled by the Earthquake Engineering Research Institute and included members from collaborating organizations. More recent information was obtained through telephone interviews with emergency management officials and from relevant documents, including some accessed through the Internet.

Some Principles of Preparedness Planning

I have already characterized preparedness planning as involving pre-event actions to further disaster response. Such actions need to involve the public in significant ways. In the U.S., appointed and elected officials are expected to play a leading role in furthering public disaster preparedness. Research suggests that there are several necessary public preparedness actions that decision makers can assist the public with, including [Mileti 2011]:

- Learn to be prepared
- Plan what to do
- Train and practice
- Organize supplies and equipment
- Secure building content
- Protect building structure
- Safeguard finances (insurance)

The question can be asked, then, is there evidence that decision makers in Virginia, Maryland and Washington, D.C. have attempted to help the public take such actions as a result of the Virginia earthquake experience? This did happen in some cases, as will be discussed.

It is also important to note that research has identified several important principles of disaster preparedness planning, including the following (Kreps 1991; Perry and Lindell 2007):

- Preparedness is a continuous process
- Preparedness is an educational and training activity
- Preparedness is based on knowledge

- Preparedness involves considering all hazards to which an area is exposed
- Modest planning is a reasonable outcome, especially in areas with few events

As noted below, in spite of experiencing only a near-disaster, some of the actions taken by decision makers after the Virginia earthquake matched these principles.

EARTHQUAKE PREPAREDNESS PLANNING BEFORE THE VIRGINIA EARTHQUAKE

Like citizens of other low seismic zone communities along the East Coast of the U.S., prior to the Virginia earthquake, those living in Virginia, Maryland and Washington, D.C. had little awareness of earthquakes and consequently gave little attention to preparing for them [EERI 2011]. Other hazards such as hurricanes, floods, and fires received much more consideration. For example, schools in the area held regular fire drills, but neither school children nor the general public in the region knew what protective actions to take when in a building during an earthquake. As a result, thousands of people could be seen in business districts and elsewhere inappropriately evacuating buildings, sometimes told to do so by authorities, as the shaking caused by the Virginia earthquake occurred, rather than responding by staying in place and dropping, covering under a desk or some other protective shield and holding on to it as taught in high seismic zones such as California. And many persons exposed themselves to possible collapsing walls, windows, and parapets by remaining too close to buildings they had just evacuated. Thus it was fortunate that the Virginia earthquake was a near-disaster because the public did not have the awareness or knowledge to cope with a full-fledged one. Later, however, some attempts would be made by decision makers to further pubic preparedness actions for future earthquakes.

CHANGES IN PREPAREDNESS PLANNING FOLLOWING THE EARTHQUAKE

As a near-disaster, the Virginia earthquake did convince some officials in Virginia, Maryland and Washington, D.C. that something needed to be done to advance earthquake preparedness planning in their communities. While seemingly modest in nature and low cost, as is often the case with earthquake preparedness planning, the efforts undertaken have been nevertheless important and demonstrate that a near-disaster can function as a social change agent in a similar fashion as a disaster, something very useful for risk reduction professionals to understand.

Four kinds of efforts to further earthquake preparedness planning in the region have emerged: information and guidelines on earthquake safety have been issued to the public; earthquake drills have been conducted; a state earthquake preparedness plan has been drafted; and new disaster laws have been passed by a state legislature. Collectively these actions follow key preparedness planning principles mentioned previously, including being knowledge based and educational in nature, and furthering an all-hazards approach. Time will tell if the efforts will be sustainable rather than short lived. Some of the emergency managers contacted indicated that the earthquake heightened their interest in learning from colleagues in more active seismic areas such as California so that they could better serve their citizens over the long term.

Earthquake Safety Guidelines

It didn't take long for some earthquake preparedness planning to emerge. Only one day after the earthquake, two of the emergency management agencies in the area, the District of Columbia Homeland Security and Emergency Management Agency, and the Montgomery County Office of Emergency Management and Homeland Security located just outside Washington, D.C. in suburban Maryland, posted guidelines on their Web sites on what citizens could do to further their safety before, during, and after an earthquake [EERI 2011]. These guidelines had the potential of being seen by millions of people in the area. The information offered to the public drew on current knowledge and experience regarding earthquake preparedness and safety, including such recommended actions as checking for unsecured water heaters and other potential hazards in the home before an event, acquiring disaster supplies, developing a family communication plan, staying in place during shaking, and inspecting utilities in damaged homes after an earthquake. The information reinforces guidance provided to citizens by such organizations as the Federal Emergency Management Agency and the U.S. Geological Survey, two National Earthquake Hazards Reduction Program agencies, through their Web sites and public documents and meetings.

Some universities in the region have also issued their own earthquake guidelines for students, faculty and staff. This is particularly important for students who live outside the region and are unfamiliar with its risks.

Earthquake Drills

Since the near-disaster, earthquake drills have been held for the first time in the region to promote earthquake awareness and train the public, especially students, on how to protect themselves when earthquakes occur. The state of Maryland's first large-scale earthquake drill was held on April 20, 2012, which included participation by 500 students from the state's Towson University.

Before the Virginia earthquake, the Louisa County public school system, located in the earthquake's epicenter, conducted only fire drills. But to promote awareness and earthquake safety training, the schools now hold biannual earthquake drills, including one on the anniversary of the 2011 event.

On October 18, 2012, the region made a significant breakthrough in advancing earthquake awareness and preparedness by participating in the biggest earthquake drill campaign ever to be held in the U.S. called the Great Shakeout. This was a national drill with participation by individuals, organizations, and communities from various regions of the country. The idea for such a drill originated in California in 2008 where it was very successful, then adopted in the historic New Madrid earthquake risk area in the Central U.S. a few years later, and finally also adopted in the Southeast U.S. in 2012 with participation by stakeholders in Maryland, Virginia, and Washington, D.C. and other states in the region [Jones 2009]. The Virginia earthquake paved the way for the diffusion of the drill from the other parts of the U.S. to the Southeast region and its acceptance there. Federal officials and state and local stakeholders outside the Southeast with earthquake or earthquake planning experience helped further this process and served as change agents by working with stakeholders in the Southeast region (Rogers 1995). Similar diffusion patterns related to natural disaster preparedness in the U.S. have been previously documented by researchers [Birkland 2007].

The inclusion of the Southeast region of the U.S. in the national drill for the first time was given the name the Great Southeast Shakeout. Jurisdictions within the region worked with government and various business and nonprofit groups to promote awareness of the drill and to recruit participants, including students and the public at large. Millions of people registered to participate in the drill nationwide, which focused on the drop, cover and hold on earthquake protection strategy, with educational and training activities held around the country on earthquake safety before the drill took place. Prominent local, state, and national figures lent their support to the effort. The expectation is that Maryland, Virginia, Washington, D.C. and other jurisdictions in the Southeast will participate in future Great Shakeout drills, along with states like California that are much further along in developing a culture of earthquake preparedness.

Earthquake Plan

The Virginia earthquake received significant attention in the state of Virginia because of its location as the epicenter of the event and because of the building damage it suffered, especially to schools. The state has a comprehensive preparedness plan called the Commonwealth of Virginia Emergency Operations Plan for using its resources to support local jurisdictions in their management of emergencies and disasters, including hurricanes and tropical storms. The plan takes into account federal guidelines for such planning efforts and defines the roles of leading agencies such as the Virginia Department of Emergency Management as well as those of key supporting agencies.

The basic plan describes concepts and policies and 17 emergency support functions. And annexes, including ones on hurricanes and tropical storms, address the unique challenges that specific hazards create. An annex was drafted on coping with earthquake disasters for the first time in August 2012, making the basic plan more all hazards in nature. The earthquake planning annex is integrated with the basic plan in terms of such important functions as damage assessment, search and rescue, public sheltering and mass care, and public information dissemination. In taking the lead in drafting the earthquake plan, the Virginia Department of Emergency Management collaborated with other stakeholders both within and outside government.

Disaster Laws

Virginia took a significant step in 2012 by passing two laws related to preparedness planning. One involves preparing for the emergency period of crises and the other involves preparing for financial recovery in the event of an earthquake. The first law requires that public institutions of higher education in the state develop an emergency plan. They are also mandated to conduct an annual exercise of the plan and to carry out a review every four years to keep it current. There are fifteen four-year state colleges and universities in Virginia alone, including the University of

Virginia and Virginia Tech University with their large student bodies, faculties, and staffs. Thus this law has the potential for promoting the awareness and safety of thousands of people.

The second law that was passed is aimed at making sure that homeowners have the information they need to make the best decisions about their property insurance coverage. It was only after the Virginia earthquake that many homeowners who suffered property losses learned that they did not have coverage for earthquake damage. This made it more difficult for some without coverage to recover from their losses. This caught the attention of the governor and legislators in the state. The new law requires insurance companies to inform homeowners in writing when they are renewing their policies if they do not have coverage for earthquake damage. This will enable homeowners to decide if they want to include such coverage with their insurance renewal for an additional cost since this could possibly help further their financial recovery and security after any future damaging earthquake.

CONCLUSIONS

The Virginia earthquake, a near-disaster, did indeed usher in some earthquake preparedness planning in the region. This is important to know because it demonstrates that, like major events, lesser ones may also provide opportunities for stakeholders to grasp the significance of the earthquake risk and make needed changes in preparedness planning with the public's cooperation.

As noted new preparedness planning has included the dissemination of earthquake information and safety guidelines to the public by emergency management agencies to increase awareness and encourage protective actions, the organizing of earthquake drills so that the public can practice safety responses, the crafting of a state earthquake response plan, and the passage of state laws related to emergency preparedness and earthquake insurance. Though comparatively modest and low cost, these changes are nevertheless important steps in promoting seismic safety in the Virginia, Maryland, and Washington, D.C. region. Also, by taking earthquake risks into account in even a relatively modest way, decision makers have moved the region closer to an all-hazards approach to preparedness planning.

It might be instructive to try and categorize these approaches. One suggested typology puts preparedness planning actions into three broad categories: (1) regulatory measures, which are coercive in that they attempt to control the behavior of groups, (2) incentive measures, which are non-coercive in that they attempt to encourage a desired form of behavior, rather than force it, and (3) informational measures, which enable people facing hazards to make informed decisions [Berke and Beatley 1992]. Rather than falling into a single category, the various preparedness planning measures that emerged after the Virginia earthquake seem to combine elements of the typology. For example, the earthquake safety guidelines and drill campaigns offer information on proper earthquake response as a non-coercive incentive for the public to take protective action, and the Virginia earthquake plan also largely provides information for stakeholder organizations on how to respond to future events in a coordinated fashion. The Virginia disaster laws are the only measures that fall clearly into the regulatory or coercive category. The greatest thrust of the post-earthquake measures, then, is the provision of information to stakeholders to motivate them to take appropriate actions. Perhaps this is at least partially the case because such measures are relatively low cost, not requiring the expenditure of significant resources to implement.

Such actions should continue to be promoted. Whether or not this will happen will depend greatly on the continued awareness of the earthquake risk by decision makers and the public, which might be particularly difficult if there is a long period without seismic activity in the region or other types of disaster events come into play that are more salient [Birkland 2007].

How daunting the task of keeping awareness of the earthquake risk in the purview of decision makers and the public can be seen in the fact that Hurricane Irene struck the region just a few days after the Virginia earthquake and quickly drew attention away from it. And more recently, Hurricane Sandy, which devastated parts of the East Coast in October 2012, has further imprinted the notion on the public that the region is far more hurricane than earthquake country. Despite such hurdles, decision makers have to make the case that earthquakes should be in the mix of hazards that the region prepares for, even if only at a relatively modest level.

Clearly we do not yet know how this will all evolve. Researchers will need to follow developments in the region during the years ahead to determine if the recently observed earthquake preparedness planning efforts are sustainable and perhaps even followed by other needed actions. Long-term monitoring by researchers to determine the relative benefits of the various earthquake preparedness initiatives I have discussed will also be important.

REFERENCES

Anderson W.A. (1970). Disaster and organizational change in Anchorage, in: *The Great Alaska Earthquake of 1964: Human Ecology*, National Academy of Sciences, Washington, D.C.

Berke P.R., Beatley T. (1992). *Planning for Earthquakes: Risk, Politics, and Policy*, Johns Hopkins University Press, Baltimore, MD.

Birkland T.A. (2007). *Lessons of Disaster: Policy Change after Catastrophic Events*, Georgetown University Press, Washington, D.C.

Drabek T.E. (2010). *The Human Side of Disaster,* CRC Press, Boca Raton, Florida.

Earthquake Engineering Research Institute (2011). The Mw 5.8 Virginia Earthquake of August 23, 2011; see *www.eeri.org.*

Kreps G.A. (1991). Organizing for emergency management, in: *Emergency Management: Principles and Practice for Local Government,* T.E. Drabek and G.J. Hoetmer (eds.), ICMA, Washington, D.C.

Jones L.M. (2009). Preparing a Population for an Earthquake Like Chi-Chi: The Great Southern California Shakeout, i: *Improving Earthquake Mitigation through Innovations and Applications in Seismic Science Engineering, Communication, and Response: Proceedings, U.S-Iran Seismic Workshop,* Irvine, California, Pacific Earthquake Engineering Research Center, Berkeley, CA.

Mileti D.S. (2011). Increasing Public Awareness, presentation at 44th Annual Governor's Conference on Homeland Security and Emergency Management, Middleton, WI.

Perry W.P., Lindell M.K. (2007). *Emergency Planning,* John Wiley & Sons, Hoboken, NJ.

Phillips B.D., Neal D.M., Webb G.R. (2012). *Introduction to Emergency Management*, CRC Press, Boca Raton, Florida.

Rogers E.M. (1995). *Diffusion of Innovations*, The Free Press, New York.

DESIGN AND ESTABLISHMENT OF THE "TEHRAN EARTHQUAKE DAMAGE AND LOSS ESTIMATION SYSTEM"

Maziar Hosseini[1] and Kambod Amini Hosseini[2]

ABSTRACT

Precise estimation of damages and casualties of potential earthquakes can facilitate decision-making and planning for disaster management after a seismic event. Such information can be estimated by having a network of seismometers that are in safe and continuous connection with the Emergency Operation Center (EOC) and having appropriate databases on buildings and populations and necessary software for quick damage and loss estimation. For the first time in Iran, such systems have been developed and operated in Tehran by Tehran Disaster Mitigation and Management Organization (TDMMO) with assistance of Japan International Cooperation Agency (JICA). For this purpose at the first stage 10 accelerometers have been prepared and installed in different parts of Tehran and on-line communications between these stations with EOC have been provided using ground MPLS lines (as main connection system) and satellite phones (as back up) for transmitting maximum PGA per sec continuously. In addition necessary databases on buildings and population distribution have been updated and professional software was developed for using the information in order to estimate number and distribution of damages and casualties in Tehran by using native fragility curves and casualty functions. The project has been successfully finalized in March 2010 and the system is operational now at TDMMO. The system is also applicable to estimate the existing risks in different parts of the city for planning in disaster risk mitigation and management. The details of the project will be presented in this paper.

INTRODUCTION

Iran is located in a seismic prone area in the world and experienced a lot of earthquakes during its history. One of the most important seismo-tectonic zones in Iran is Alborz Mountain Ranges. This zone is an active part of Alpine-Himalayan Orogenic belt. The city of Tehran, the Capital of Iran, is located in the central part of this zone, surrounded by several active faults. Figure 1 shows the location of the main faults and epicenter of some earthquakes occurred in the territory of Tehran during the last centuries.

Probabilistic analysis shows that the return period for Tehran Earthquake is around 173 years. Since that last seismic event has hit the city in 1830, so the seismologists expect a strong earthquake in near future that may cause considerable casualties and damages. Considering the vulnerability of urban buildings and infrastructures in Tehran, limited capacities of existing emergency management bases and insufficient preparedness among relevant authorities, the

[1] Deputy Mayor, Technical and Development Affairs, Tehran Municipality and Assistant Professor, Postgraduate School, Structural Eng. Dep., Islamic Azad University, South Tehran Branch, Tehran, Iran.
[2] Assistant Professor, International Institute of Earthquake Engineering and Seismology, Tehran, Iran.

impacts of potential earthquake may be considerable. This shows the importance of implementation necessary plans and programs for reducing the earthquake risk and improving disaster management capacities in Tehran. In this line a project carried out in Tehran Disaster Mitigation and Management Organization, TDMMO by assistance of Japan International Cooperation Agency, JICA [TDMMO and JICA, 2010].

One of the main components of this project was to develop an earthquake quick damage and loss estimation system (QD&LE) to be used for assessment the potential risk of urban fabrics and estimation casualties and damages after a potential earthquake in the city. The procedure for developing the system and its main components are introduced and discussed in this paper.

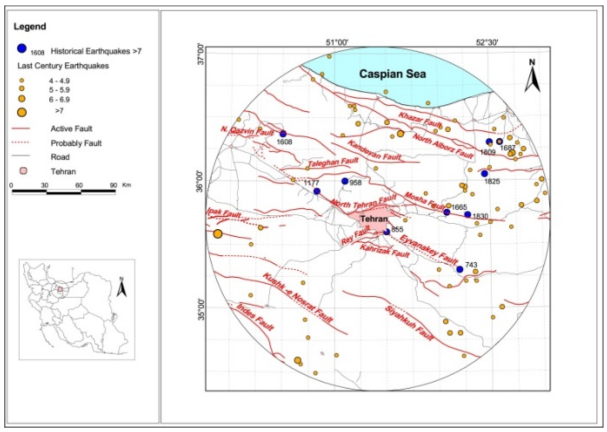

Figure 1 A schematic view on existing faults around Tehran and the historical earthquake epicenters [Jafari and Amini Hosseini 2004].

DATABASE UPDATE

One of the main issues for estimation the damages and casualties of potential earthquakes is providing the necessary databases. In the QD&LE system design procedure, the following information were used and updated to make accurate required input for the system:

- District boundary: The boundaries of urban fabrics, which is related to each district responsibilities in response activities is updated and inserted to the system;
- Population: The latest national population census was carried out in 2006 by Statistic Center of Iran. The results of this survey was used for the system;
- Building: Several building databases were available for using in the system. Since 1996, three building surveys were carried out in parallel between 2005 and 2009. However, the precision of database related to the year 1996 was more reliable, so that information was used in developing QD&LE system.
- Building Damage Function and Casualty Estimation Model: Damage and casualties functions prepared based on the experiences of Iranian recent earthquakes (especially Bam earthquake of 2003 and Manjil earthquake of 1990) were used for estimation potential damages to buildings and assessment relevant casualties.

PREPARING AND INSTALLATION OF NECESSARY MATERIALS AND EQUIPMENT IN PILOT AREAS

The QD&LE system is a complicated system consisted of several hardware and software from seismographs to alerting systems. In brief, the system must be quickly triggered after an earthquake generation by receiving reliable shaking data from an earthquake observation system. Since there was no earthquake observation system dedicated for disaster management in Iran, a new strong-motion accelerometer network system has been established in Tehran for this purpose. This was developed by installing accelerometer sensors at 10 stations, which are spread all over Tehran, selected as pilot areas. However, it was decided to increase the number of station to 50 in a five-year plan to have a dense system for better estimation of damages and casualties. Location of installed stations by the year of 2010 and the place of data acquisition center (TDMMO) is shown schematically in Figure 2.

The strong-motion accelerometer network system must reliably and in real-time (every second) send the observed earthquake data at each station to the acquisition center at TDMMO by using ground communication line or satellite phones (in case of necessity due to any problem in ground line). Output of the strong-motion accelerometer network system is used for input of the Quick Damage and Loss Estimation software. Placement and function of the strong-motion network system and the QD&LE system are shown in Figure 3.

There are five conceptual requirements for the system to properly work as follows:

- Robustness: The feature that will ensure a never-fail system even when dealing with a huge earthquake.
- Stability to measure data correctly and continuously.
- Reliability to send correct data to EOC by online communication systems.
- User-friendly to easily manipulate and generate data.
- Easy to maintain, to minimize down time and maximize use.

Features of the established strong-motion accelerometer network are shown in Figure 4. The main features of the system are summarized as follows:

- Especially designed for disaster management in emergency conditions;
- Real-time observation/recording using professional devices and relevant backup systems to assure availability of data at EOC;
- Pre-processing at station side before transmitting data to control station to reduce the time and traffic of data transmission;
- Equipping with back-up communication line (satellite phones);
- Applicable to future research purpose by recording seismic data at each station;
- Low cost operation.

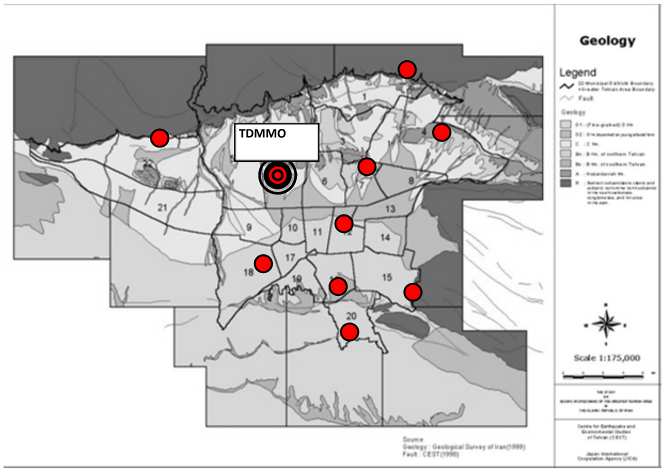

Figure 2 Location of 10 accelerometer stations and data acquisition center (TDMMO).

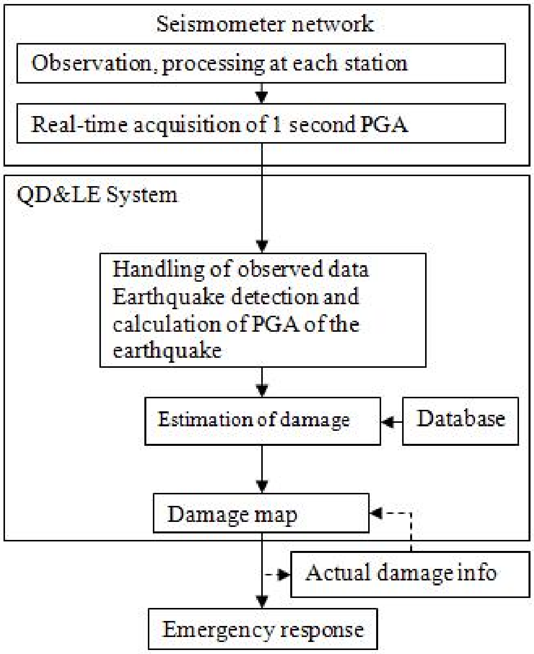

Figure 3 Placement and role of the seismometer network for the QD&LE System.

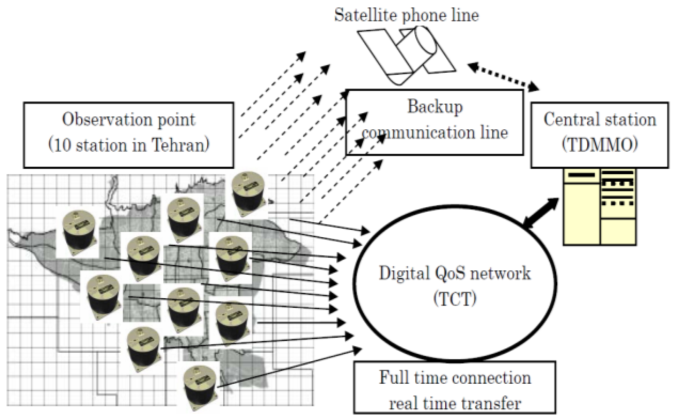

Figure 4 Features of the Strong-Motion Accelerometer Network.

SQL output function is one of the special features of the system, too. The QD&LE system can read earthquake information easily from a general SQL database written by the strong-motion network system. Originally, the available system can only record and send acceleration waveform. Waveform transmission leads to huge data traffic on the network and causes loss of the network function by collision at especially destructive earthquake. Therefore, PGA calculation function was added to the specification to keep data traffic light and avoid congestion in the network and server. In this line, it was decided to transmit only peak values of PGA data acquisition center per second.

SITE SELECTION

As mentioned earlier, at the first stage of this plan, ten pilot areas were selected as sites for installation of observation equipment after discussion with relevant experts. The criteria for site selection are as follows:

- To cover all of Tehran as homogeneous distribution;
- To have available place for sensor installation and relevant equipment;
- To avoid high vibration noise, for example, subways or highways;
- To avoid electrical noise, for example, high voltage power line;
- To keep an office environment like electric power, telephone line, and security;
- To avoid any geological/topographical anomaly in or around the site;
- To select where the bedrock is shallower to reduce ambient noises;
- To select where heavy damage is estimated to have better estimation of loss and damages;
- To select a safe and secure place.

Ten disaster management bases owned by TDMMO were selected preliminarily. Then, noise evaluation was conducted. Considering the result of the noise evaluation and actual condition of the disaster management bases, 10 station sites were finally selected as shown in Figure 2 earlier.

Preparation of Construction Site for Installation

The sensor should be fixed on the ground surface outside the observation building to prevent an artificial response caused by the building itself. Expensive equipment should be installed inside building for security. So, a duct is necessary to pass a cable connecting the sensor and other equipment. Preparation for installation was designed and completed for the station sites in 6 months. Figure 5 shows a design of a sensor pit. Preparation construction includes civil works for sensor base, trench and duct for cable laying, fixing satellite/GPS antenna, passing antenna cable, setting MPLS cable and connection, and establishment of office environment at observation room.

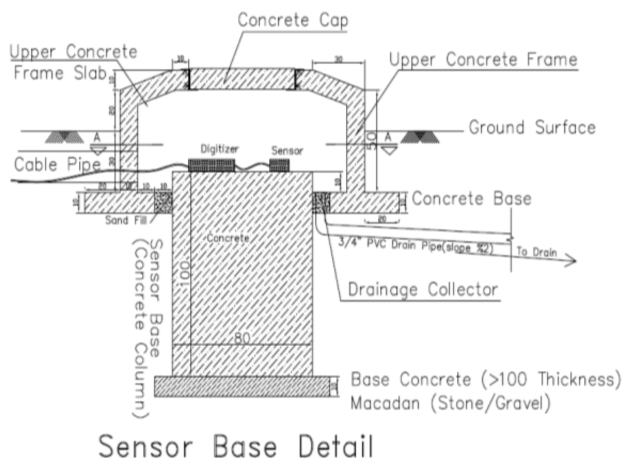

Figure 5 Design of sensor pit.

Inspection

The following inspection activities were conducted before proceeding with the installation of equipment at each station.

- Functionality: All equipment was checked to confirm their performance by simultaneous measurement test to evaluate instrumental error. To confirm instrumentation error between the equipment, three days continuous simultaneous recording using 10 sensors and digitizers were conducted while all sensors were located at the same place and aligned at the same direction (see Figure 6). Frequency response and amplitude were evaluated as that the error was in the range of +/-3% at 8 to 20Hz;
- Operation test at station: After the above-mentioned inspection, the equipment were moved to each station and installed. On-site inspection was conducted after installation.
- Total performance test after system integration: After the system integration, total performance test was conducted at TDMMO data center.

Figure 6 Simultaneous measurements tests on sensors.

DEVELOPING QD&LE SOFTWARE

In the process of QD&LE system design it was decided to outsource software development, to a system engineering team of KNT University, Tehran, which is familiar with seismic damage modeling and software development. The TDMMO experts were in close communication with the subcontractor throughout the development process, giving guidance and direction. The delivered software for damage and loss estimation that was tested in any kind of factors, has the following features.

Interface Test with Seismic Network System

The software should have the ability to receive data transmitted through seismic stations continuously. For this purpose an interface where designed to record and save the data transmitted, and software has been designed somehow to continuously read data from SQL.

Interpolation of Ground Acceleration

As the total number of stations at this stage is only ten, it was necessary to make interpolation of PGA all around Tehran by using appropriate methods. The results provided the PGA amount in each grid at bedrock and ground surface using attenuation relations and amplification factors.

Estimation of Building Damage and Casualties

In order to estimate the number of casualties and damages, relevant functions were developed and inserted into the software to assess number of death and injured as well as collapsed or damaged buildings. The software uses the maximum PGA in each grid and based on the casualty and damage functions, calculates the impacts of earthquake in less than 4 min.

Connection Test with Data Output Interfaces.

The results of all calculations should be transmitted to the relevant authorities in time. For this purpose QD&LE system uses SMS and fax and automatically prints and displays information and maps on wall screen in command center to be applicable in less than 20 minutes after the earthquake. Figure 7 depicts a screen capture photo of the prepared software.

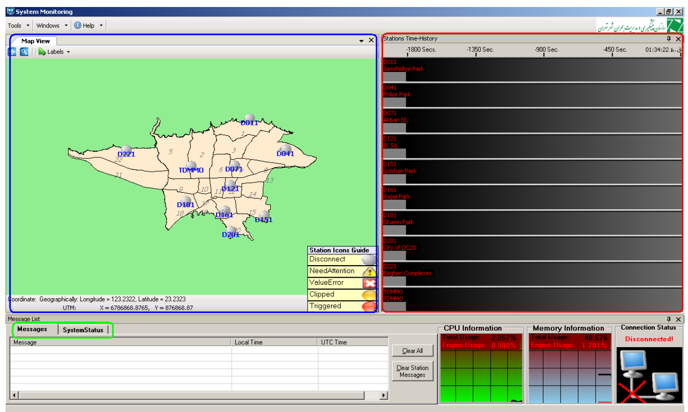

Figure 7 Screen capture of QD&LE software.

CONCLUSIONS AND RESULTS

Tehran's quick damage and loss estimation system is called "Tehran Damage Estimation System (TDES) The system has been operational in Tehran since 2010 and it is decided to make denser network in 5 years plan. Furthermore, damage and casualties functions applied in the system as well as ground models are evaluated to be updated based on local conditions of soil and construction in Tehran to provide better estimation of damages and casualties. It has the following capabilities:

- To record, transmit and read the seismic data every second. The data are transmitted via cable lines and in case of interruption the communication line through satellite phones to emergency operation center;
- To show all system components health status continuously;
- To start damage and loss estimation system when recorded PGA were exceeded 4 gal, automatically;
- To interpolate PGA distribution using ground model database ;
- To estimate building damage and human casualties using building and population database and relevant functions, and
- To transmit the output by SMS to relevant authorities and send necessary maps to printers and plotters automatically.

REFERENCES

Jafari, M.K., Amini Hosseini K. (2004). *Earthquake Risk Considerations in Preparing Tehran Master Plan*, International Institute of Earthquake Engineering and Seismology, Tehran, Iran;

Tehran Disaster Mitigation and Management Organization, TDMMO & Japan International Cooperation Agency, JICA (2010) The project on the establishment of emergency response plan for the first 72 hours after an earthquake in Iran, *Main Report, G ED.CR(10).010-019*.

ENGINEERING FOR RESILIENT COMMUNITIES

David Bonowitz[1]

INTRODUCTION

This paper discusses resilience as a potential new basis for earthquake engineering, particularly at the city or community scale. The style is informal, matching the collaborative nature of the 4th Iran-U.S. Joint Workshop, where the paper was presented on December 19, 2012. Part 1 of the paper discusses the concept of earthquake resilience, contrasting it with past and current philosophies of seismic design and mitigation. Part 2 describes an application of resilience-based planning in San Francisco. Part 3 illustrates how a resilience basis might change earthquake engineering, by reviewing reconnaissance findings from the recent Varzaghan earthquake.

EARTHQUAKE RESILIENCE

As the National Research Council has observed, "Numerous definitions of 'resilience' exist, and the term is often used loosely and inconsistently." [NRC 2011] FEMA, for example, continues to conflate ideas of community recovery with ideas of "high performance" building design, folding such disparate topics as energy conservation, "enhanced safety," and a focus on "critical facilities" into "resilience." [NIBS 2010] Others continue to focus on safety or damage reduction but *call* it resilience. Indeed, *resilience* has become something of a buzzword—more fashionable than meaningful.

But the concept of resilience goes to the heart of what it means to live with the threat of earthquakes. It is about more than structural performance, and more than simple loss prevention. Resilience is about the stability of an organization—a city, a campus, a business, a family—over time. Though not yet fully or consistently defined, earthquake resilience is commonly understood to mean an organization's capacity to recover vital pre-earthquake capabilities with manageable disruption.

From an engineer's perspective, a focus on resilience can perhaps be most easily understood as a shift in emphasis from safety to recovery. Safety, economy, and recovery are three measures of performance, though engineers might be more familiar with their opposites: the categories of measurable losses sometimes described as deaths, dollars, and downtime. Fundamentally, increasing resilience is about facilitating recovery or reducing downtime. For example, Figure 1 shows similar scenes from after the 2003 Bam earthquake and the 2008 Sichuan earthquake. The people living in these tents clearly survived, but the housing losses will obviously affect them and their neighbors, and will delay their community's full recovery, for years.

[1] Structural Engineer, San Francisco, California

Figure 1 **Tent cities following earthquakes in Bam, Iran, and Sichuan, China. (Sources: EERI, [2004] and Warwick [2008]).**

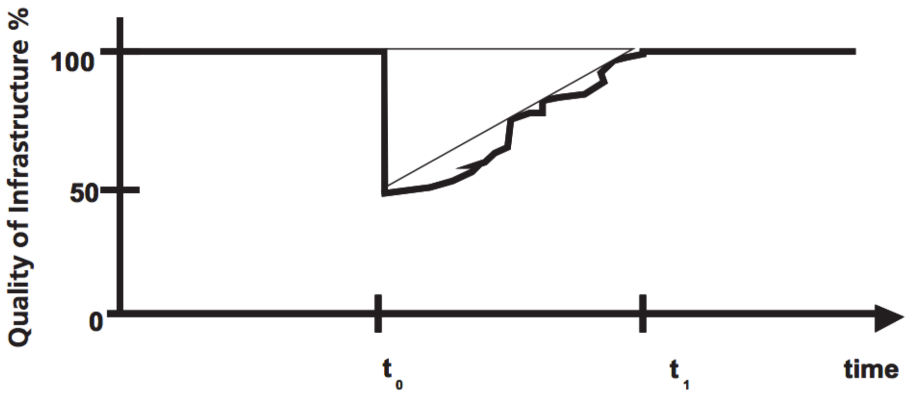

Figure 2 **The Resilience Triangle [Tierney and Bruneau 2007].**

With the focus on recovery, and taking a community-wide perspective, it becomes clear that at bottom, all the mitigation work we do as engineers—all the research, the evaluation, the insurance, the retrofit, the preparedness—is really about making recovery feasible. Like safety and economy, recovery is a function of the one thing engineers can quantify—damage—but it is also the most complex, and downtime remains the most elusive loss category, and the most difficult to predict. Still, we can see that mitigation planning and recovery planning go hand in hand: If you can't afford to mitigate an expected loss, you'd better be able to recover from it. And if you won't be able to recover from it (as in the case of life-threatening collapses), you had better mitigate. At the community level, then, an appropriate mitigation policy should be based on gaps in recovery capacity.

For this paper, a simple definition is sufficient for introducing the idea of resilience into structural engineering practice. More complete multi-dimensional descriptions have been proposed (for example, by MCEER, as described by Tierney and Bruneau [2007]), but for purposes of this paper, earthquake resilience means simply the ability of an organization to recover lost pre-event capacity in an acceptably short time. What is *acceptably short*? Basically, whatever time is necessary to prevent cascading or permanent secondary losses that harm the organization's mission. For a business, an *un*acceptable recovery time might be the time at which it loses some portion of its customer base. For a city, it might be the point at which outmigration of citizens seeking stable housing and jobs makes it more difficult to provide services for those who remain.

Two ideas are important here: First, resilience is an attribute not of buildings, but of social units: households, corporations, communities. Second, resilience is measured as a combination of functional loss and recovery time. The significance of time is illustrated by the so-called resilience triangle, as shown in Figure 2 (see also Tierney and Bruneau [2007], and NRC [2011]). The vertical axis can actually represent the level of any service. The plot shows that at the point of the earthquake, t_0, some capacity is immediately lost. Over time, the service level recovers until it reaches its pre-earthquake level at t_1. As engineers, we have traditionally focused on quantifying the initial damage: that is, the drop in service at t_0. The engineering challenge from a resilience perspective is to predict both the time to recovery and the milestones along that path.

Figure 3 shows a more nuanced version of the resilience triangle to illustrate some interesting complexities.

- Some recovery is immediate. An initial loss of service can include shut-downs to self-assess for damage or to implement emergency procedures, even in the absence of damage. At the very least, whenever people are involved, we can expect disruptions or changes in service as they adjust to what has just happened.
- Recovery typically comes in phases. For a building, the major milestones are the point at which safe re-occupancy is allowed (and when clean-up and nonstructural damage assessment can begin), a point of functional recovery at which most normal operations are restored but some cosmetic or non-critical damage remains, and full recovery at which pre-earthquake conditions are considered fully restored. Thus, the hypotenuse of the resilience triangle is rarely a straight or gradual path, but more likely a set of steps and quantum improvements.
- It is possible, even likely, that the services or functionality will eventually return to a different level than before the earthquake, either because redundancies were recognized during repairs, or because the recovery period becomes a convenient time to upgrade services as well. Indeed, even without the earthquake, service levels change over time due to a multitude of causes, some intended and some not.
- The recovery path can be altered by decisions made or implemented during response and recovery. In fact, many resilience measures involve pre-strategizing and pre-packaging the decision trees to be followed during recovery, with the express intent of altering the expected path.
- The service level can even drop during recovery to facilitate faster recovery overall. For example, a building might be vacated temporarily in order to repair it faster, or some of an organization's functions might be temporarily shut down as staff are re-assigned to post-earthquake tasks.

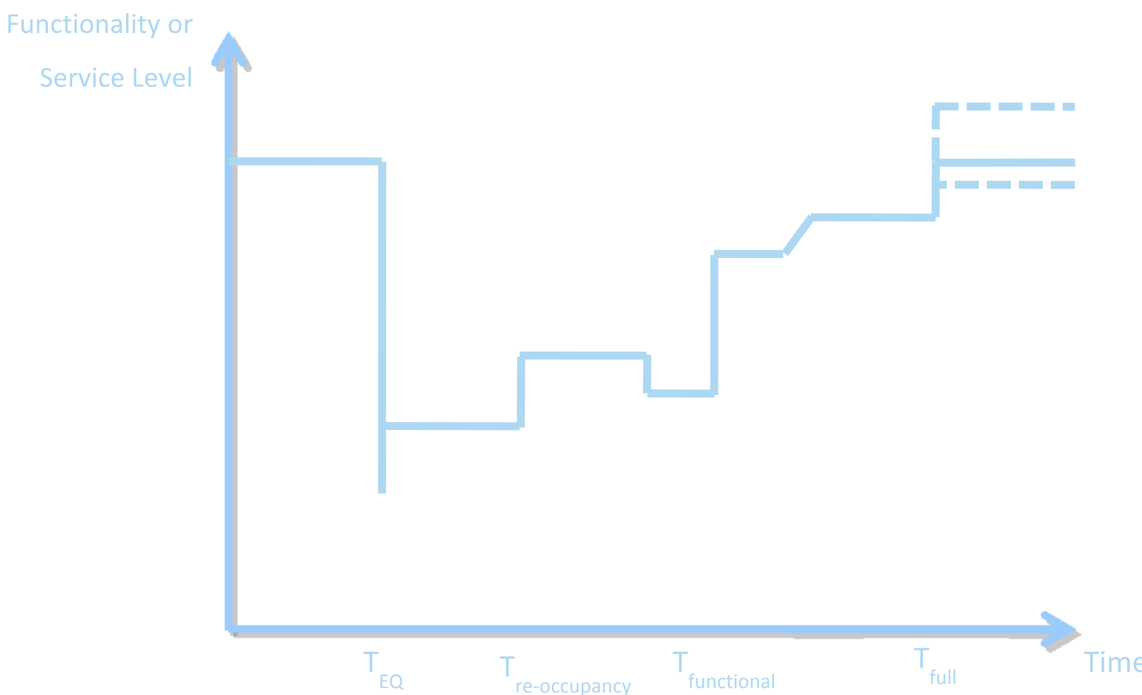

Figure 3 **A more nuanced version of the resilience triangle.**

Resilience-based engineering can be compared with our other design philosophies:

- Most engineering work is simply code-driven, or what might be called "compliance-based." That is, a building code, while technical and rational, is a policy document and a (minimum) legal standard. It embodies social and economic precedents, though not transparently, and is more useful for judging compliance—either a building complies or it doesn't—than for predicting performance.
- Our current approach, performance-based engineering, attempts to quantify the limit states of specific structural and nonstructural components, and allows the user to set a (largely technical, as opposed to socio-economic) objective by combining a desired performance level with a presumed hazard.
- Resilience-based engineering would combine some of the societal preferences of a code, many of which are occupancy-specific, with the technical approach of performance-based standards. As discussed above, it would also focus on downtime or recovery and would thus introduce time as a critical performance measure.

From this perspective, we see that resilience is not a completely new idea. However, we might consider it a new opportunity, for two reasons. First, the complexity of predicting recovery requires data and analytical tools that we have not always had. Second, the idea that we might shift our regulatory policy from mere safety to recovery is perhaps a luxury we never had before. Only now that we (in the U.S., at least) have mostly solved the problems of life-threatening collapse can we reasonably give our attention to the recovery period. In other countries, perhaps including parts of Iran, safety remains a dominant concern.

The differences between resilience-based engineering and our current approaches extends also to the larger context in which planning and mitigation is performed. This means that engineers interested in resilience might need to think about their work in new or expanded ways. For example, instead of focusing on *retrofit* of individual *buildings* for *safety*, a resilience-based approach would encourage thinking about those individual buildings and structures in the context of a *plan* for the *organization* or *community* to recover *functionality*.

As noted earlier, resilience puts the emphasis on downtime, as opposed to mere safety or repair cost. Also, because resilience is about organizations, our resilience-based codes and standards will need to give equal attention to occupancy and functionality, as opposed to just structural materials and systems. But if we want to know what programs and policies might be needed to improve a city's resilience, we should start with recovery planning—that is, by thinking about how, at a citywide scale, the post-earthquake period will or should, unfold.

As noted, resilience is an attribute of an organization, small or large, not an attribute of a building or structure. Here, I am focusing on the city as an organization, so the resilience goals will represent public policy. One thing that makes recovery prediction and resilience planning so complex, especially at this scale, is that cities and jurisdictions differ in so many more ways than buildings. Not only do the physical attributes vary—the size, topography, seismicity, and building stock—but so do the socioeconomics that determine a city's baseline functional services.

Figure 4 compares the geography of San Francisco and Tehran. While physically comparable—the size and regional population are within an order of magnitude—the financial resources, major industries, governance structure, and expectations of the citizenry, are obviously different. Thus, the resilience measures appropriate to one jurisdiction might not apply to another. Even the resilience goals of San Francisco and Los Angeles might differ significantly. Also important is the fact that mitigation policy in the U.S. is generally made at the local level, and San Francisco as a distinct city (separate jurisdictionally from Oakland, Berkeley, San Jose, etc.) is quite small compared with greater Tehran. In some ways, this is advantageous for San Francisco. In other ways, this limits San Francisco's ability to actually control its own resilience, because it is so deeply linked in functional ways—infrastructure, labor pool, etc. —to the rest of the region.

With these definitions and caveats, the question thus becomes: What does it take for a city to be resilient? What are the critical functions and services that make it a thriving city? How are they inter-related? How long can they be lost before the city, as a city, ceases to function? Even if engineers have not traditionally thought about these questions, city planners and emergency managers have. We as engineers need to learn from their work. Quite possibly, we can also contribute to it with some of our methods and ideas.

Figure 4 **San Francisco and Tehran. Although these regions are physically comparable, differences in governance, economy, and expected losses will have obvious effects on resilience goals. (Source: Google maps).**

San Francisco's Emergency Response Plan

San Francisco actually has an Emergency Response Plan that lays out how it expects, or wishes, city services to recover over time following an unspecified damaging earthquake. As illustrated in Figure 5, "critical services," including emergency utility repairs and building re-occupancy, should happen within the first week. "Ongoing social needs," including interim housing, normal utility service, and most normal city functions, should be met within a month. Everything else, including reconstruction of damaged housing, offices, and transit lines, could take years [CCSF 2008].

In a project with San Francisco Planning and Urban Research (SPUR), an NGO dedicated to city planning and governance, my colleagues and I expanded and detailed the very basic San Francisco plan in order to understand its implications, identify its shortcomings, and link it to a mitigation agenda; see Figure 5 [SPUR 2009]. The detailed matrix on the right side of the figure shows our expanded timeline, with key city services listed down the side, and a timeline across the top. Shaded cells indicate what we propose as reasonable recovery targets. An "X" indicates where what we think the current recovery time will be, given an M7.2 scenario event. Though the image is too small to read, it is clear that we do not expect most of the targets to be met.

Figure 5 City of San Francisco's Emergency Response Plan and an interpretation by SPUR.

Table 1 Recovery targets [SPUR 2009].

Service	Target
Hospitals operational	0 hours
95% housing habitable	24 hours
Emergency shelters open	24 hours
Essential City services restored	1 month
Schools reopened	1 month
Social services reopened	1 month
Community retail reopened	1 month
All businesses reopened	4 months

Table 1 shows some details from the SPUR recovery target matrix. For each service sector, we list the recovery time we feel should represent the standard for a resilient city with the size and regional significance of San Francisco. Of course, these time targets are just our judgment. One of the challenges of resilience-based engineering is that we do not yet have the social science needed to confirm that schools, for example, can only be down for a month before their loss affects the city's overall recovery.

Aside from the time targets, however, an astute engineer will immediately notice two things: First, the services are all about occupancies—hospitals, housing, etc.,—not about structure types. Second, the performance metrics are all about functionality—operational, habitable, reopened for business—not about safety or damage thresholds. This reflects another major challenge of the shift to resilience-based engineering. We will need new expertise, or at the very least we will have to translate our current expertise about structures and safety into occupancy and functionality terms. So if these are the city's resilience targets, what might the corresponding mitigation plan look like?

Consider these challenges in San Francisco:

- We already have a hospital retrofit program administered by the state of California. But if hospitals are a high priority, what about the Health Department offices, which are not part of the state's program? Are they critical too?
- What about hotels? They're not considered "essential facilities" by the building code, but they might serve as emergency housing for displaced residents or for outside emergency workers. Also, tourism is vital to San Francisco's economy.
- What about a church? Again, not traditionally a critical facility, but many small institutional buildings serve as neighborhood centers in emergencies.
- Woodframe houses generally perform well in earthquakes, but San Francisco has a disproportionate amount of "soft story" or "weak story" apartment buildings with first floors used for parking.
- And what about a neighborhood commercial street? Does it warrant new public policy, or should its recovery be left to the individual private sector owners?

In short, how might we prioritize our needs?

Figure 6 illustrates how we combined (1) what engineers know about vulnerable structure types and nonstructural components, (2) critical occupancies from the resilience target timeline, and (3) our knowledge of San Francisco's particular building stock. As engineers, we are used to thinking about vulnerability. When we think about vulnerability together with occupancy, it helps put our past and current mitigation efforts in context. For example, California already has programs to mitigate hazardous unreinforced masonry buildings (URM, the leftmost column in Figure 6) and to improve our existing hospitals (the top row). This matrix shows that those programs are working only at the extreme edges of our building stock. They are perhaps our most vulnerable and most critical buildings, but focusing only at the edges ignores the great majority of buildings, especially housing, that in the aggregate are expected to control our recovery capacity.

In Figure 6, a yellow cell indicates that the specific combination of occupancy and vulnerability *could* have some effect on citywide resilience, an orange cell indicates the combination *probably* will have some effect, and a red cell indicates a combination that we expect will *almost certainly* have a disproportionate negative impact. The pattern of shaded cells represents something of a fingerprint for San Francisco. Each city's pattern will be different. From this way of thinking, we derived a six-part mitigation agenda tied to our current recovery capacity.

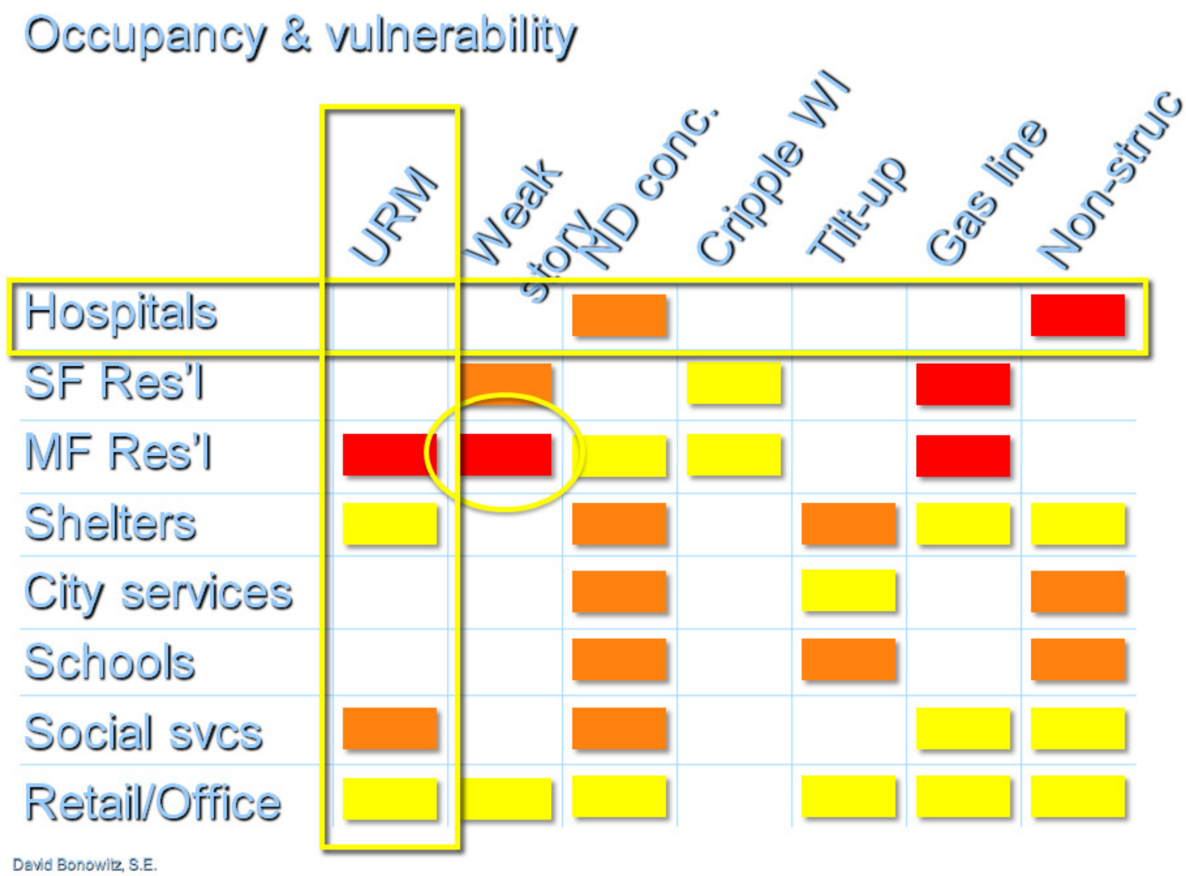

Figure 6 **Occupancy and vulnerability matrix for San Francisco.**

The six-part mitigation agenda proposed by SPUR for San Francisco, based on a conceptual resilience model:

Item 1 (shown circled in Figure 6): Weak story multi-family housing. San Francisco has several thousand such wood buildings that are prone to collapse (as shown in the 1989 Loma Prieta and 1994 Northridge earthquakes) due to inadequate first story walls; see Figure 7. After 20 years of piecemeal voluntary retrofits and mild incentives, we argued for a mandatory retrofit program. Legislation to mandate these retrofits was just introduced in February 2013 with support from the Mayor and the Board of Supervisors. If it passes, owners will have between 2 and 7 years to perform basic retrofits sufficient to keep the first story from collapsing.

Item 2: Emergency shelters. If the housing stock is so far from adequate, we know that emergency housing will be critical. Unfortunately, the buildings designated to serve as shelters, including some schools, might be inadequate themselves.

Item 3: Social services during the recovery phase. The City of San Francisco is relying on faith-based and community-based NGOs to provide services such as mass feeding, daycare, and social support services for vulnerable populations. These are services the NGOs provide every day, but if their own facilities are vulnerable, they will not be able to support the city's recovery in an emergency. If the city is relying on these private organizations, possibly the city has some responsibility to ensure that they will be adequately prepared.

Item 4: Non-ductile concrete. We know that non-ductile concrete structures can collapse, often catastrophically. But we also know that performance within this class can vary widely and is often acceptable. So for this agenda item, we are proposing to start with inventory, regardless of occupancy, so that we can develop a better sense of how our older concrete buildings, perhaps as many as 3000, will perform.

Item 5: Gas-fired utilities. Electrical components that could cause fires when damaged by an earthquake could also be in this category. Fire following earthquake could double or triple the city's losses. It is already law in California that gas-fired water tanks must be braced. Yet it is quite common to find them installed without bracing.

Item 6: Revisit our retrofitted unreinforced masonry buildings; see Figure 8. As noted above, San Francisco has had a URM retrofit program since 1992, but the criteria were minimal and safety-based, and the program did not make careful distinctions by occupancy. Though new legislation is unlikely, a resilience-based mitigation program should have a better understanding of what services are housed by these still vulnerable structures.

Figure 7 Examples of weak story wood-frame residential buildings in San Francisco. Note the relatively open first stories.

Figure 8 **Examples of unreinforced masonry buildings in San Francisco**

Figure 9 illustrates, in concept, how a multi-program mitigation agenda is intended to improve the city's resilience.

- The recovery timeline is color-coded, as shown on the right side, from immediate recovery to no recovery (meaning severe damage or collapse).
- San Francisco has about 170,000 buildings. The colored bar on the left edge of Figure 9 represents the distribution of buildings by recovery time. Some, at the top, will see very little damage, while some, at the bottom, will be near collapse.
- Consider mitigation program A: Mandatory retrofit for weak story multiunit residential buildings. (This happens to correspond to item 1 on the SPUR agenda described above, but the rest of the programs listed here do not.) The area labeled A in the left column shows the relative number of buildings targeted by this program—about 4000, currently—and indicates that their expected current recovery time is not good, typically no better than weeks, and possibly never, due to collapse.
- The similar sized area labeled A in the right column shows those same buildings, retrofitted for an improved recovery time between days and weeks. Note that the retrofitted performance need not be uniform and need not be in the range of hours. This shows that a reasonable, cost-effective retrofit objective can still contribute to the city's overall resilience.
- Similarly, other groups of buildings can be selected from the lower parts of the left column (or left to market forces alone) and reasonably retrofitted (or replaced) so that

the aggregate effect changes the recovery time distribution to the right column. Importantly, note that there will still be a range of performance, and even some collapses, but the overall effect should be enough to make the city's recovery plan feasible.

Finally, we return to the contrast between current engineering practice and resilience-based thinking. The left column of Table 2 lists topics that engineers know well. The right column suggests corresponding topics that we will need to understand and prioritize better if we are to shift to resilience-based engineering. But community resilience is not just about engineering, as suggested by the bottom row of Table 2. When mitigation programs are proposed, too often we limit ourselves by what is "doable" or cost-beneficial today. This is rational when applied to the engineering aspects of a single project. But in the aggregate, what's doable on the small scale will fail to achieve what's necessary on the large scale. For citywide resilience, especially because we still do not quite know what's necessary, we need to apply our research energies to that question. Once we have done that we will be in a better position to measure the benefit-cost ratios of various programs. But until we do that, we will never really know. Yes, our current mitigation efforts would still move forward, but slowly, almost randomly, and with blinders on.

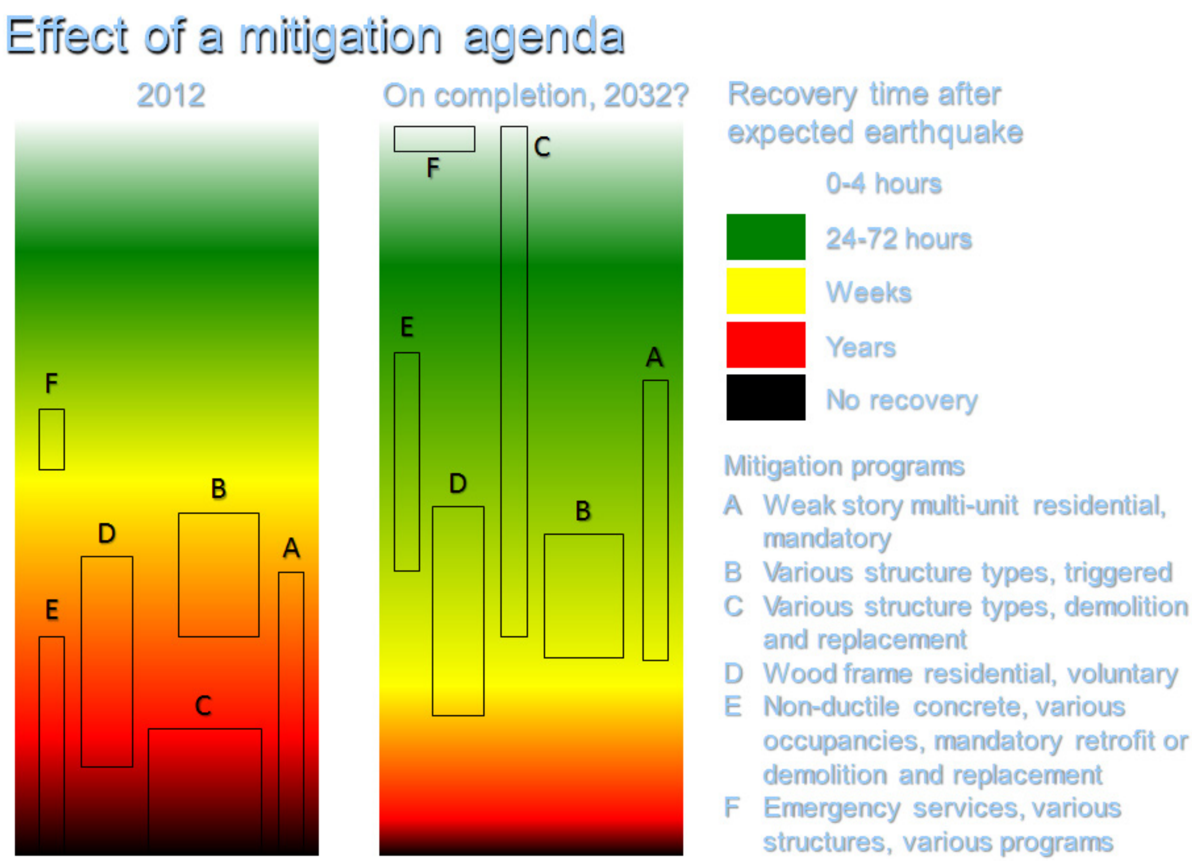

Figure 9 Multi-program mitigation agenda.

Table 2 **The subjects and priorities of current engineering practice and of resilience-based engineering.**

Codes and standards	Policy
Projects	Programs
Safety	Functionality
Structures	Occupancies
Buildings	Communities
Loss Estimation	Downtime estimation
Awareness	Action
Preparedness	Mitigation
Retrofit	Recvery planning
What's doable?	**What's necessary?**

The previous discussion described how a mitigation agenda might be derived with resilience-based thinking so that it is coordinated with a recovery plan. But resilience-based engineering has implications for other aspects of our practice as well.

- Our codes for new building design, as noted above, set a minimum compliance-based standard. In performance terms, we can be confident that they will provide safe buildings, but they promise little in terms of recovery. Why are only "essential facilities" designed with importance factors if we know that housing is likely to have a bigger impact on community resilience? The SPUR target for San Francisco housing—95% habitable within 24 hours—is probably only possible if we improve our current worst performers *and* start building new housing for better-than-code performance.
- Researchers will find many new questions opened by a resilience-based design philosophy. Some of these will be structural: What are the appropriate drift limits for habitability or continuous operation of mechanical systems, for example. But many will be in the social sciences, as we grapple with the relative importance of different occupancies and try to define critical downtime thresholds.
- Post-earthquake reconnaissance has a new resilience-based task as well. Previously we were content to study damaged buildings in isolation. Then we recognized that we needed to look at the fragility of building classes as well. Now, we will need to look not just at the performance of building classes but at the recovery timeline of key occupancy classes.

VARZAGHAN EARTHQUAKES

The final part of the paper reviews a reconnaissance report from the recent Varzaghan earthquakes [EERI 2012] from a resilience perspective. These were significant events that killed over 300 people and left approximately 30,000 homeless. The report is thorough, and the writers are obviously experts in the region with a clear understanding of the building stock and the social implications of the damage. Early recon reports are always difficult, so this review is not meant at all as a critique. Rather, the point is merely to suggest how a resilience-based frame of mind might help us to ask different questions or record different data after future events.

Considering the loss of housing, the report states simply that "residential buildings of different types were damaged in both Ahar and Varzaghan." This is not surprising, so it makes sense that a traditional recon report would not go into much detail about this sector of the building stock. From a resilience perspective, however, we might also ask:

- How many buildings were damaged, or more importantly, how many units, since units give a better sense of the number of people affected. Resilience is an attribute of an organization, like a household, not a building.
- We might also ask what portion of the housing stock saw the reported damage, since this would relate to the capacity for emergency shelters and the disruption of normal life.
- "Damaged" usefully describes the condition of the structure. But we need to know whether the building is safely habitable.
- Perhaps most important, even if the damage forced the tenants to relocate, the most important measure is how long it will be until they can re-occupy their homes.

Regarding the university, the recon report again simply lists the damage: "Several non-structural failures … infill and partition walls, damage to false ceilings, and overturning of unstable equipment …." Again, the more salient question from a resilience perspective is whether the damage prevented the buildings from being occupied, or otherwise hampered the university's mission.

As an example of resilience-based thinking for universities, U.C. Berkeley has determined that they need to supplement their ongoing safety program with mitigation measures to protect the continuity of expensive, long-term, grant-funded research. The university has set a recovery goal of one month, on the theory that a longer downtime would jeopardize a full semester, and that would interfere disproportionately with the university's mission [Comerio et al. 2006].

Regarding bridges, the Varzaghan report makes the useful observation that even while the bridges were "fully serviceable," they were inadequate to transfer the injured as needed when the main hospital was damaged. This illustrates two aspects of resilience-based planning on a citywide scale. First, it shows that different sectors of the built environment are inter-related in terms of assessing resilience. Second, it shows how certain facilities should be evaluated not only for their typical occupancy or function but also for any expected post-earthquake function.

Finally, the report looks at the local industrial facilities in Tabriz and Soufyan, noting "no observable structural damage." Again the report focuses mostly on the immediate damage. It also makes the useful observation, however, that even with no damage there was some downtime, consistent with the notes above regarding the resilience triangle. Had these facilities been damaged, the questions from a resilience perspective would have been not only about the damage but about downtime and the possible loss of jobs and income.

Industrial facilities like these can be some distance from the epicenter and still have a regional significance. This leads to two more questions that a traditional engineering approach might miss: (1) From a city's perspective, how big an area should be considered for scenario studies?; and (2) From the industry's perspective, can a distant earthquake interfere with the labor force or with market conditions? These illustrate the relative complexity of resilience-based earthquake engineering.

REFERENCES

CCSF (2008). *Emergency Response Plan: Earthquake Annex*, City and County of San Francisco, CA.

Comerio M.C., Tobriner S., Fehernkamp A. (2006). Bracing Berkeley: A guide to seismic safety on the UC Berkeley campus, *PEER Report No. 2006/01*, Pacific Earthquake Engineering Research Center, University of California, Berkeley, CA.

EERI (2004). *Social and Public Policy Issues Following the Bam, Iran, Earthquake,* Earthquake Engineering Research Institute, EERI Special Earthquake Report, Oakland, CA; available at www.eeri.org.

EERI (2012). *The MW 6.4 and MW 6.3 Iran Earthquakes of August 11, 2012*, Earthquake Engineering Research Institute, EERI Special Earthquake Report, Oakland, CA; available at www.eeri.org.

NIBS (2010). *Designing for a Resilient America: A Stakeholder Summit on High Performance Resilient Buildings and Related Infrastructure*, National Institute of Building Sciences, U.S. Department of Homeland Security, Washingon, D.C.; available at http://www.dhs.gov/xlibrary/assets/st-designing-for-resilient-america.pdf,

NRC (2011). *National Earthquake Resilience: Research, Implementation, and Outreach*, National Research Council, The National Academies Press, Washington, D.C.; available at http://www.nehrp.gov/pdf/nrc2011.pdf.

SPUR (2009). The resilient city, Part I: Before the disaster, San Francisco Planning and Urban Research Association, in: *The Urbanist*.

Tierney K., Bruneau M. (2007). *Conceptualizing and Measuring Resilience: A Key to Disaster Loss Reduction*, TR News, 250; available at http://onlinepubs.trb.org/onlinepubs/trnews/trnews250_p14-17.pdf.

Warwick M. (2008). *After the Sichuan Earthquake: Where Will People Live?,* blogs.worldbank.org, June; available at http://blogs.worldbank.org/eastasiapacific/after-the-sichuan-earthquake-where-will-people-live.

DESIGN AND DEVELOPMENT OF REAL TIME SEISMIC DAMAGE AND CASUALTY ESTIMATION TOOLS TOWARDS URBAN DISASTER MANAGEMENT

Mohammad R. Zolfaghari[1]

ABSTRACT

This paper describes the main components of an earthquake quick damage and casualty estimation system which has been designed and developed for the Tehran Disaster Management and Mitigation Organization (TDMMO). The system consists of several computer software tools plus an accelerometer network of some 10 stations, providing real-time measurement of ground accelerations across the city of Tehran. The system with its strong ground motion network, is in charge of automatic recording and zoning of peak ground acceleration for building parcels and city communes at the time of earthquake. Real-time building damage as well as statistics on human casualties are estimated in minutes after earthquake, using a computer damages estimation tools. The damage estimation system relies on a detailed database of building stocks, consisting of building database on parcel resolution for the whole city. A library of building vulnerability and casualty functions are used for this step. Upon real earthquake, the system developed under this study, generates tens of hazard, damage and casualty zoning maps and tables automatically and distributes them to disaster managers and aid agencies at the regional and municipality levels. The system also benefits from various IT communication technology such as email, SMS, fax and internet network to transfer real-time damage output to wider users. This paper summarizes some of the main characteristics of this system and also results of a few simulated earthquake scenarios which are estimated using this tool.

Keywords: *early response, earthquake hazard, seismic damage estimation*

INTRODUCTION

Tehran, the capital city of Iran is located in the southern foothills of the Alborz mountain range, surrounded by several active faults such as Mosha, North Tehran, Taleghan, Parchin, and Garmsar faults with reported large historical earthquakes (Figure 1). The city has been under rapid growth and development in the recent years with highly vulnerable built environments. The mega city of Tehran with an official population of more than seven million is Iran’s largest city. The rapid unplanned growth since 1960s has made Tehran exposed to natural catastrophes. The potential consequences of a large damaging earthquake and overall social, economic and political impacts of such event highlights the importance of effective risk management measures and a robust post-disaster strategy for this city. The city has suffered almost no earthquake damage in modern structural engineering time. This fortune is not without its disadvantages: the general public awareness for earthquake risk is comparatively low, and the national standard of

1 Associate Prof. K.N. Toosi University of Technology, Tehran, Iran; email: mzolfaghari@catrisks.com.

professional earthquake engineering is weakened by the absence of major earthquake damage experience, from which lessons may be learnt on the vulnerability of existing constructions. Though earthquakes may be of a relatively rare occurrence in cities such as Tehran, their effects could be far more devastating than originally thought. However, other cities in the near and far vicinity of Tehran have been historically and recently affected by large earthquakes with devastating consequences. Examples in the Twentieth Centuries include the Buin Zahra Earthquake in 1962 and the Manjil Earthquake in 1990.

Disaster management agencies in many developing regions have become greatly concerned about the necessary stocks of facilities and resources that are needed immediately before, during, or shortly after disasters to reduce the loss of life and economic damages. Built environment and human life in many seismically active regions in the world are exposed to various types of seismic hazards, the most important, seismic ground motions. At the time of a big earthquake in urban areas, damage and distributions caused to buildings, infrastructures and life lines result in wide spread economic damages and loss of lives. Such distributions and their interaction with other potentially hazardous urban facilities could pose secondary seismic hazard such as fire following earthquakes. Past experiences have shown that resources available to ordinary emergency response organizations at urban scales are insufficient to deal with aftermath of big natural disasters and prioritization of affected areas is required in order to make the best use of available resources. Also taking into account such limited resources, there would be need for more and immediate help on the regional, national and even international scales. Proper prioritization and organization of helps provided on such scales requires reliable as well as fast information on the extent of affected area and the volume of required help. Experiences with large recent natural disasters particularly in developing countries have shown that at the time of big events, the efficiency of normal call centers is reduced significantly due to disruptions to other infrastructure facilities. Besides, at such times, normally those who need help most are much quieter than those of no or littler need for help. Therefore, dependency of emergency response organizations entirely on such channels may result in unjustifiable distribution of help and resources. Quick estimations of geographical extent of affected area as well as volume of physical damage and number of casualties are quite crucial in emergency management and towards proper distribution of available resources. Technologies such as remote sensing and post-disaster aerial photographs have been used as such means in recent years, although not quite capable of providing detailed information, and besides with delays of hours and even sometime day after the event. The development and application of real-time damage estimation tools in recent years particularly since the 1995 Kobe earthquake have been under consideration in many seismic prone regions in the world such as Japan, United State, Turkey, and Italy. At an international scale one may name the projects such as PAGER, RISK-UE, RADIUS, and HAZUS.

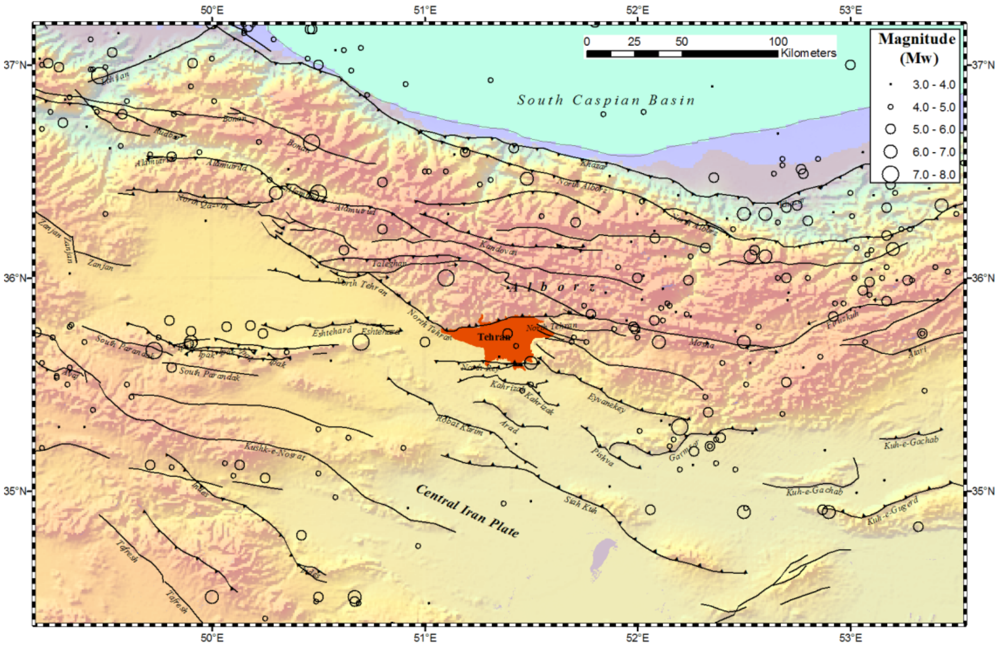

Figure 1 **Seismotectonic of northern Iran and the Alborz Mountains. Major active faults and historical and instrumental earthquakes with Mw>3.0**

TEHRAN EARTHQUAKE DAMAGE ESTIMATION SYSTEM (TEDES)

In a cooperative efforts between the Tehran Disaster Management and Mitigation Organization (TDMMO) and the Japan International Cooperation Agency (JICA), the need for design and development of Quick Damage and Loss Estimation tools was established and the author and his R&D team was commissioned for the design, development and implementation of this system. The primary objectives for this tool as a decision support system are to help disaster managers towards rapid emergency response and to minimize the secondary catastrophe damages and humanitarian crises. But the tools can also be used to provide realistic earthquake scenarios for the city which could form bases for integrated discussions between experts from different disciplines, providing clear justification for individuals, policy makers, businesses and community leaders to take necessary actions to minimize or prevent devastating losses. The system consists of several main modules responsible for earthquake detection and damage calculation, all within seconds of earthquake occurrence, using an online network of accelerograph network distributed in Tehran. Upon the triggering of accelerograph stations by any seismic event, the system makes various numerical calculations to estimate distribution of ground shaking, assess building damage, casualties and evacuees for all building blocks in Tehran. The results obtained from this system in the form of maps of different resolutions (urban block, postcode, commune, district, etc.), tables illustrating damage to the built environment, human casualty, evacuee and first aid and emergency requirement and materials. It also generates damage reports in the forms of SMS text messages, faxes, emails, and printed maps, and distributes them automatically to the authorities soon after the earthquake. Figure 2 shows the main components of this system. This system is primarily designed and developed to work as an automated tool as a disaster decision support system. However, the system also could be used and have been used as a tool for running various earthquake scenarios, using its databases of building stocks and vulnerability functions and earthquake simulation tool. The system has the ability to perform seismic damage estimation based on synthetically simulated earthquake scenarios.

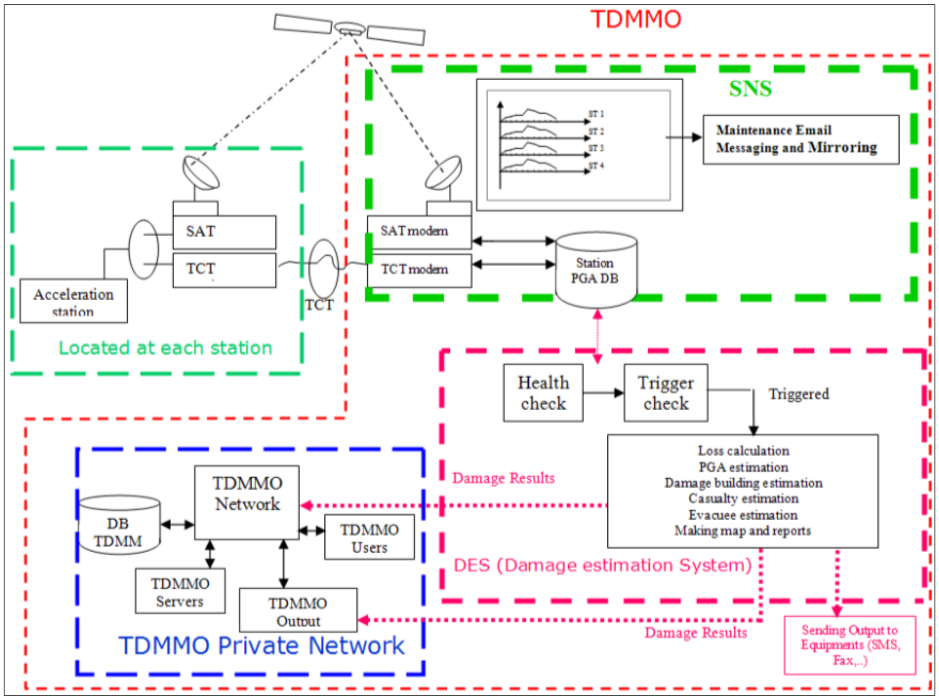

Figure 2 Main components of the TDMMO's real-time seismic damage estimation system (QD&LES).

The development of real-time damage estimation tools and supplementary hardware and software are the results of intense multidisciplinary researches on the geo-science, engineering and information technology and experiences from past earthquakes. The geographical scales for which such tools are developed and used are not always the same and such tools have been developed and used on local, regional and national/international scales; see Figure 3. The components and input data as well as output results are also dependent on the scales for which these tools are used. In a generic form, the real-time damage estimation tools consist of several main components as listed below:

- Ground motion modeling (shake map)
- Built environment inventory
    - Geographical distribution
    - Vulnerability Type
- Database of vulnerability & casualty curves
- Automatic damage estimation engine
- Digital maps

- Geotechnical zonation
- Administrative boundary maps
- Infrastructure and life-line

- Report generation tools
- Tools to distribute results to end users

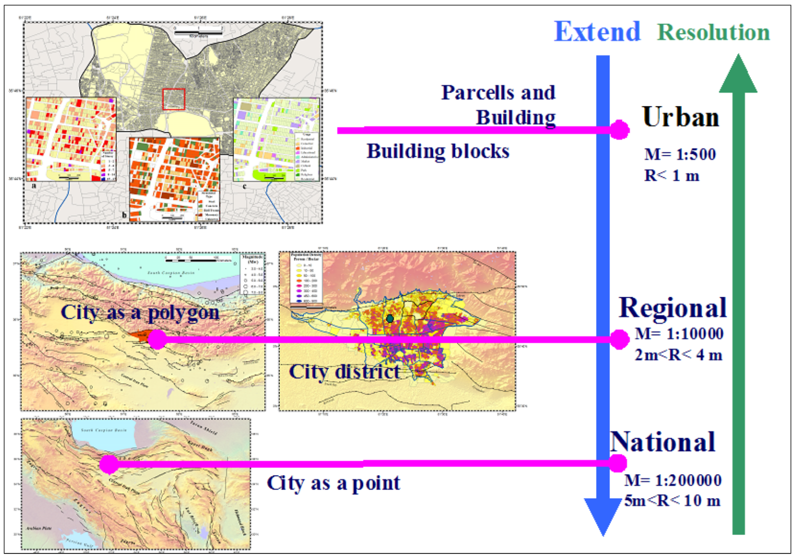

Figure 3 Geographic resolution and extend of real-time damage estimation systems.

REAL-TIME GROUND MOTION MODELING

Ground motion modeling tools are responsible for producing real-time shake maps representing the geographical distribution of shaking intensities induced by earthquake at population locations (cities, communes, postcodes, etc.). Depending on the geographical scale as well as availability of recoding instruments, one or a combination of the following two approaches can be used for this purpose:

- based on real-time data from a dense acceleration network (real ground motion data)
- based on ground motion simulation using source data and empirical attenuation models or other ground motion modeling techniques

Factors such as geographical extent of region under study, the implementation and maintenance cost and necessary communication infrastructures are against the development of on-line and real-time network of strong ground motions and therefore, majority of real-time damage estimation tools are working on the bases of strong ground motions simulation using the later approach, particularly at the national and international scales. In some cases, early estimates are provided using the second approach before more reliable estimates can be made using data from the first approach. Figure 4(a) shows the strong ground motion network for the province of

Istanbul consisting of more than 100 accelerograph stations. Figure 4(b) shows the TDMMO network currently under operation in the greater Tehran city, all connected to TDMMO control center using normal telephone network as well as wireless system.

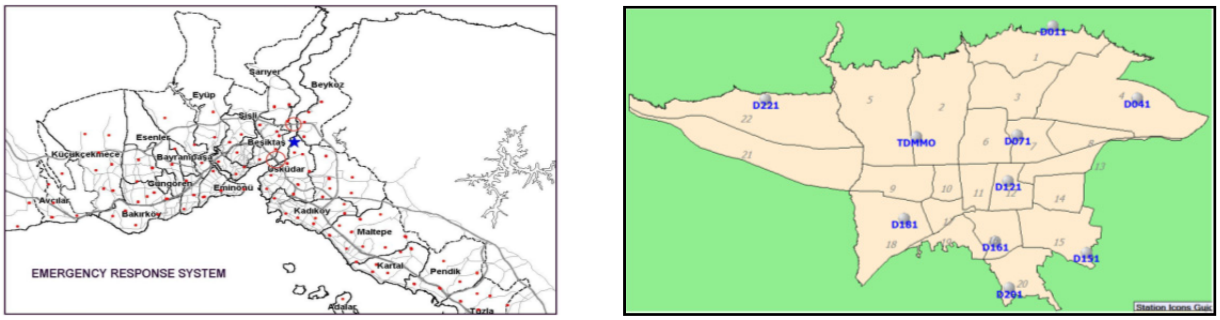

(a) (b)

Figure 4 **Dense accelerograph station network for real-time damage estimation system: (a) Province of Istanbul (Turkey); and (b) City of Tehran (Iran).**

DATABASE OF BUILDING STOCKS AND POPULATION

Another requirement for development of real-time damage estimation tools is the inventory of building data and population, provided on the usable geographical and administrative boundaries (such as parcel, block, census zones, postcode, communes, district and cities). Such data should be provided in the GIS-ready format in order to be used for damage calculation as well as report generation process. The database used for development of TEDES provides basic information with regard to the following building and population characteristics:

- administrative ID or code
- number of buildings or dwelling by vulnerability type
- number of buildings or dwelling by usage type
- population by building or administrative unit
- digital maps presenting administrative boundaries as well as geotechnical zoning
- database and maps of other urban infrastructures and emergency stocks

The extent and reliability of such data depends on the resolution for which these models are developed for. For example, if such models are developed to work on the national and international level (e.g., PAGER), a city is perhaps modeled as a point with all building stock and population aggregated on one point only. For the case of TEDES, the system relies on a detailed database of building stocks, consisting of building database on census zone level which provides building and population data on 3173 census zones (Figure 5). TEDES also provides tools for updating and change of building database as new building data being collected by the authority in this city.

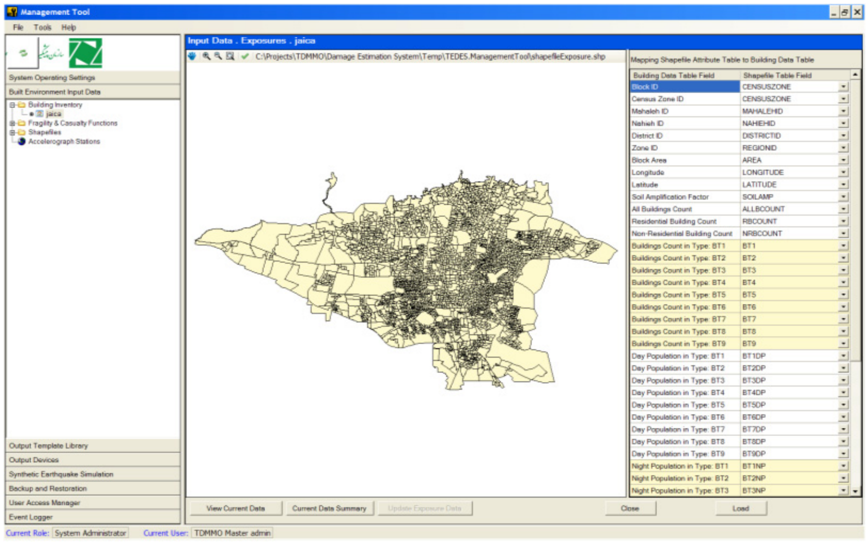

Figure 5 TEDES data management tool and Tehran Census Zone Boundary map.

DATABASE OF VULNERABILITY AND CASUALTY CURVES

In a similar manner, TEDES holds a library of building vulnerability functions and human casualty curves. These functions are PGA dependent and provide building damages in three damage states: slight, moderate and heavy damage. Figure 6 shows the fragility curves for nine typical structural types in Tehran as used by the JICA [2000] study.

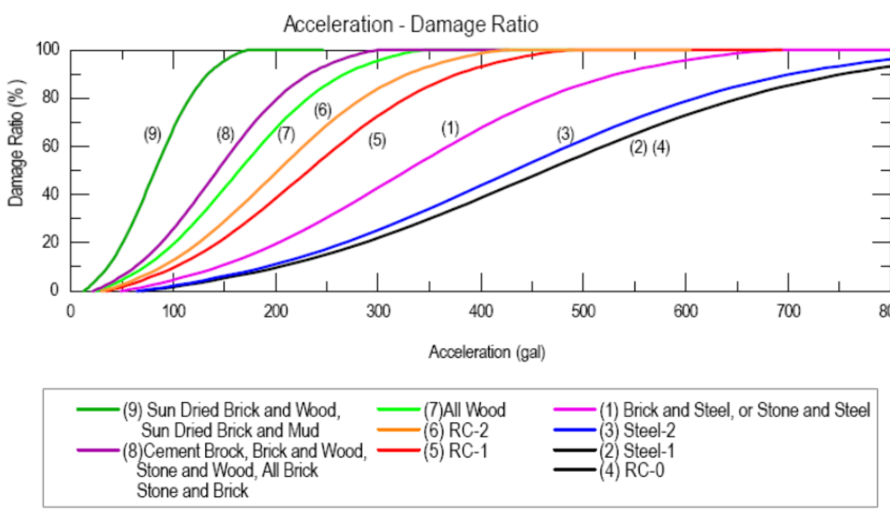

Figure 6 Building fragility curves showing damage ratios versus earthquake acceleration.

DAMAGE AND CASUALTY ESTIMATION ENGINE

Damage estimation engine is responsible for various analytical processes and forms the core of quick damage estimation system. In TEDES this engine receives ground motion data from the accelerograph network and generates shake map covering all census zones in Tehran in seconds from the earthquake. It then estimates damage to building stocks as well as human casualties using its database of building and population and also the library of fragility and casualty curves. In addition to these analytical processes, the engine is also responsible for controlling other software and hardware in charge of producing and transferring output results in form of maps, charts, reports and short messages. Upon real earthquake, the system developed under this study, generates tens of hazard, damage and casualty maps and tables automatically and distributes them to disaster managers and aid agencies at the regional and municipality levels. The system also benefits from IT communication technology such as email, SMS, fax and internet network to transfer real-time damage data to wider users. This system since its released in early 2010 has been working continuously in the disaster control room in the Tehran Municipality; see Figure 7. Necessary information for emergency response and prioritization process after a big event shall fulfill the following requirements:

- quickly accessible
- relatively reliable
- with the right format
- in the hands of right people

TEDES is therefore equipped with a configuration management tool, allowing various customizations of the system and results for use the by wider users in disaster organizations. This tool enables the administrators to configure TEDES for automatic operation and results generation, fulfilling the demands of different sectors in emergency response organization. It also enables the user to set up and prioritize the system to automatically produce and distribute the results based on the level of shaking or damage data.

Figure 7 TDMMO Emergency Management Control Hall.

APPLICATION OF TEDES TO GENERATE REALISTIC EARTHQUAKE SCENARIOS

Realist earthquake scenarios once modeled and verified can be used to improve awareness of what an earthquake can cause on the built environment and community as whole. Such scenarios could also help the authorities in disaster management organizations to plan for proper mitigation, preparation, and post disaster response measures. However, in designing such catastrophe scenarios attention is always paid to the worst case scenarios that could affect the population centers. Such extreme scenarios usually result in quite wide spread damage and casualties, although useful to highlight the vulnerability of city to the natural catastrophe, but hardly attract proper attention from authority as no one can associate a likelihood to such events. In other words there are always wide ranges of other scenarios lower than the extreme ones which is more plausible and still devastating and often not taken into account. While an earthquake scenario should show the extend of potential consequences on the built environment and population, it should also be credible and realistic enough so people and authority can associate the occurrence of such events within their life time with a reasonable likelihood. In this paper seismotectonic setting of the Alborz region plus a real-time loss and casualty estimation tool is used to model a few earthquake scenarios for the city of Tehran using the TEDES system.

In a pilot study, the TEDES system is used to run a few earthquake scenarios for the city of Tehran. Pervious examples of such scenarios were provided by the JICA [2000] study. However, in those scenarios attention was always paid to the worst case or extreme scenarios causing very wide spread damages and loss of life. In this study, the seismotectonic setting of this region as modeled by Zolfaghari [2010] is used to simulate a synthetic earthquake catalogue representing 1000 years of seismicity in this region; see Figure 8. To select a few scenarios in this study, peak ground accelerations are estimated from simulated earthquakes and based on these PGA's, a few earthquakes scenario are selected. Figure 9 shows the locations of a few selected scenarios modeled in this study. The figure also shows the geographic distribution of historical earthquakes recoded in this region in the last 12 centuries. To simulate PGA's for census zones for each earthquake scenarios, the attenuation relationship proposed by Ambraseys et al. [2005] is used here.

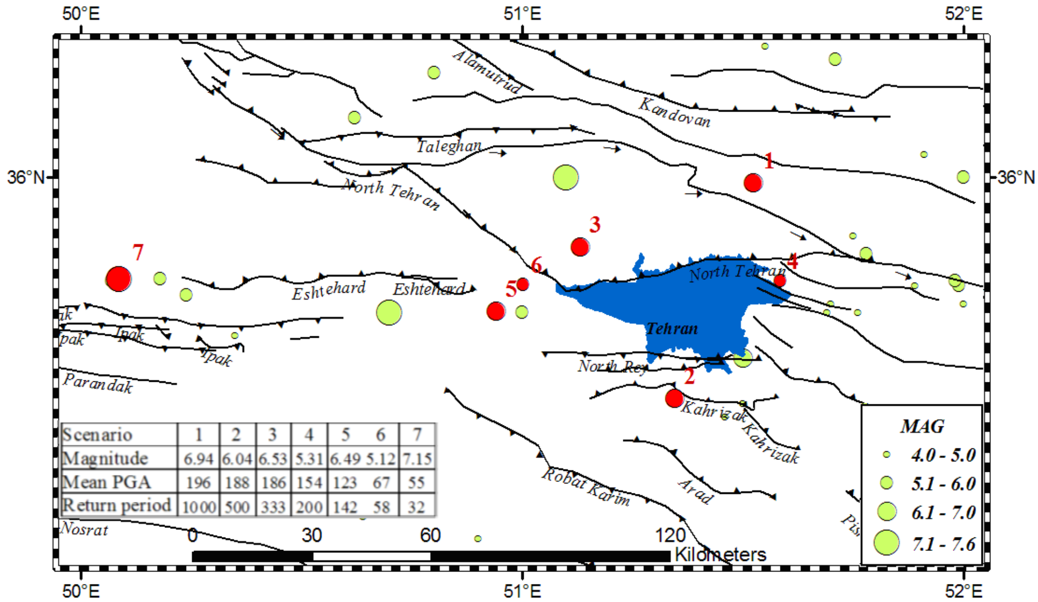

Figure 8 Historical earthquake (green circles) as well as seven selected simulated earthquake scenarios (red circles).

CONCLUSIONS

The Tehran Disaster Management and Mitigation Organization (TDMMO) has recently established a real-time damage and casualty estimation system for this city called TEDES. This paper describes the main characteristics of real-time damages estimation tools in general and the specifications for TEDES in particular. TEDES has been under continues operation since winter 2010. The system also benefits from an earthquake simulation process that enables the end user to run various type of hypothetical and realistic earthquake scenarios.

The system is equipped with a configuration management tool, allowing various customizations of the system performance and result configuration for use by wider users in disaster organizations. The primary objectives for this tool as a decision support system are to help disaster managers towards rapid response efforts and to minimize the secondary catastrophe damages and humanitarian crises. But it also has been used to provide realistic earthquake scenarios for the city which could form the bases for integrated discussions between experts from different disciplines, providing clear justification for individuals, policy makers, businesses and community leaders to take necessary actions to minimize or prevent devastating losses. This system since its release in early 2010 has been working continuously in the disaster control room in the Tehran Municipality. Additional components are being designed and developed in the next couple of years to enhance the reliability as well performance of this system.

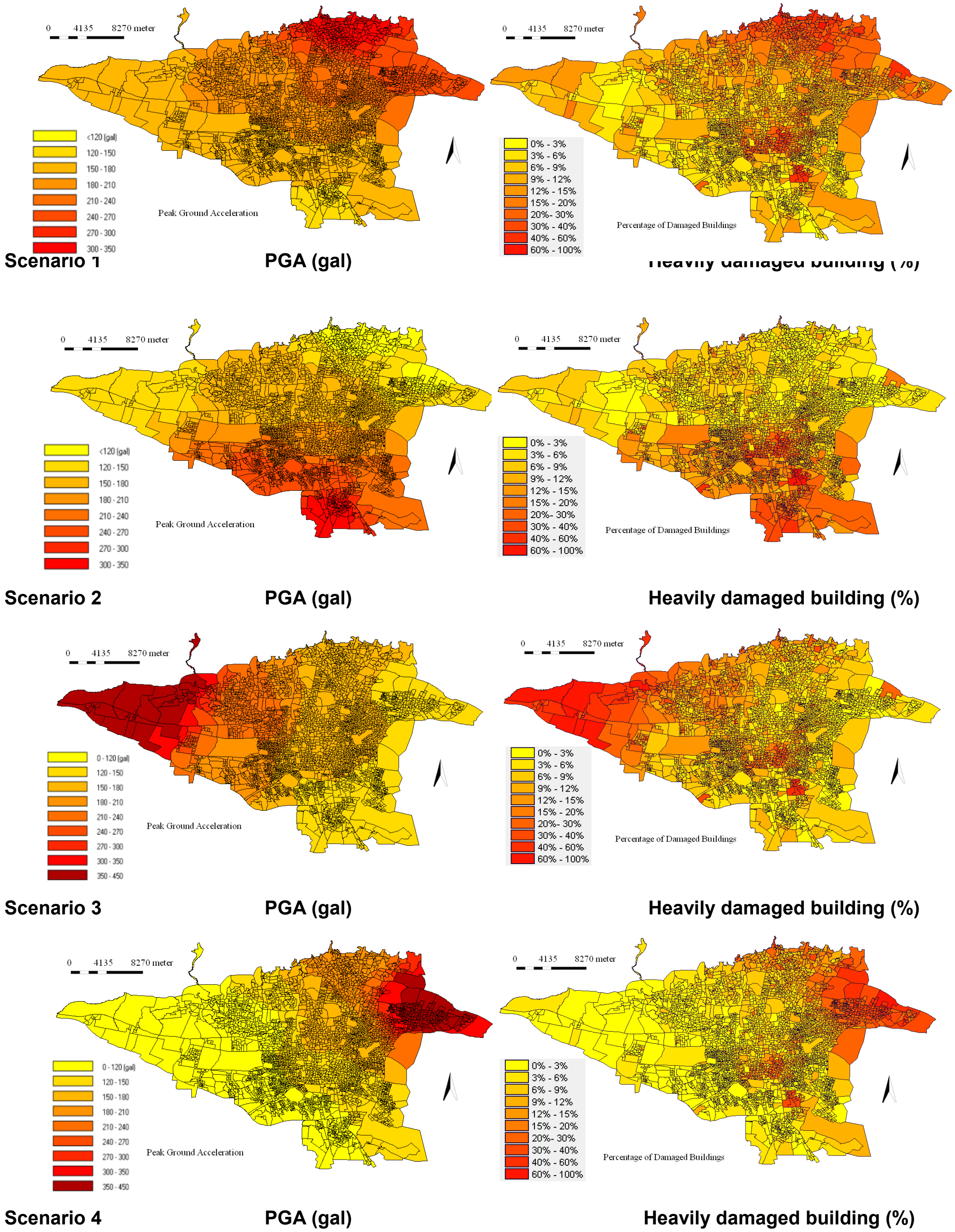

Figure 9 Damage and PGA distribution for scenarios affecting population in the greater Tehran area.

ACKNOWLEDGMENTS

TEDES tools are designed and developed by the KNTU University in cooperation with Japan International Cooperation Agency (JICA) and Tehran Disaster Management and Mitigation Organization.

REFERENCES

Ambraseys N.N., Douglas J., Sarma S.K., Smit, P.M. (2005). Equations for the estimation of strong ground motions from shallow crustal earthquakes using data from Europe and the Middle East: Horizontal peak ground acceleration and spectral acceleration, *Bull. Earthq. Eng.,* 3(1), 1–53.

Barbat A.H., Moya F.Y., Canas J.A. (1996). Damage scenarios simulation for seismic risk assessment in urban zones, *Earthq. Spectra*, 12(3): 371–394.

D'Ayala D., Spence R., Oliveira R., Pomonis A. (1997). Earthquake loss estimation for Europe's historic town centers, *Earthq. Spectra*, 3(4): 773–793.

Dolce M., Masi A., Marino M., Vona M. (2003). Earthquake damage scenarios of the building stock of Potenza (Southern Italy) including site effects, *Bull. Earthq. Eng.,* 1: 115–140.

Dolce M., Masi A., Marino M. (2002). EAEE-ESC Task Group 3 – Seismic risk and earthquake scenarios: Report of the activities. *Proceedings, 12th European Conference on Earthquake Engineering*, London, U.K.

Esteva L. (1997). An overview of seismic hazard, seismic risk, and earthquake engineering in Mexico City. *Proceedings, 1st International Earthquake and Megacities Workshop*, Seeheim, Germany.

Fah D., Kind F., Lang K., Giardini D. (2001). Earthquake scenarios for the city of Basel, *Soil Dyn. Earthq. Eng.*, 21(5): 405–413.

FEMA (1999). *HAZUS99-SR2 Technical Manual*, Federal Emergency Management Agency, Washington D.C.

JICA (2000). *The Study on Seismic Microzoning of the Greater Tehran Area in the Islamic Republic of Iran, Final Report*, Japan International Cooperation Agency, Centre for Earthquake and Environmental Studies of Tehran (CEST) Tehran Municipality.

Risk UP, http://www.risk-ue.net.

Zolfaghari M.R (2010), Definition of new seismogenic sSources to model probabilistic seismic hazard assessment for Tehran, An integrated framework for uncertaintly modelling, *Proceedings, 14th European Conference on Earthquake Engineering*, Orhid, Masedonia.

HYBRID WAVELET NEURO-PSO ALGORITHM FOR GENERATION OF PULSE-LIKE NEAR-FAULT EARTHQUAKE TIME HISTORIES COMPATIBLE WITH NGA PREDICTED SPECTRUM

G. Ghodrati Amiri[1], A. Abdolahi Rad[1], N. Khanmohamadi Hazaveh[1], and S. Aghajari[1]

ABSTRACT

In this study a new method to generate artificial pulse-like near-fault ground motion time histories compatible with NGA predicted spectrum is presented. The proposed method uses the decomposing capabilities of wavelet packet transform (WPT) on earthquake accelerograms, and the learning abilities of multilayer feed-forward (MLFF) neural network to generate spectrum-compatible near-fault artificial earthquake accelerograms. In this article, particle swarm optimization (PSO) is employed to optimize the weight values of networks. Also, to improve the training efficiency, principal component analysis (PCA) as a reduction technique is used. Implementing PCA has brought about a remarkable dimension reduction in network structures. In addition, the continuous wavelet transform (CWT) has been utilized to simulate the largest velocity pulse. In this research, to produce compatible synthetic long-period near-field ground motions with median predicted spectra, the attenuation of PGV with the close horizontal distance (R), moment magnitude ($\mathbf{M}$), and time-average shear-wave velocity from the surface to 30 m (V_{s30}) has been developed using nonlinear regression analysis. The application of the proposed approach for a number of next generation attenuation (NGA) project ground motions is presented.

INTRODUCTION

Near-field pulse type ground motions have been identified as imposing extreme demands on structures. Therefore, it is very important to comprehend the different requirements for seismic design in near-fault regions. The strong near-field earthquakes that have occurred in recent years have resulted in severe structural damage to an extent not predicted by typical measures such as response spectra (e.g., Shwe and Adeli [1993]; Alavi and Krawinkler [2001]; Mavroeidis et al. [2004]; Akkar et al. [2005]; Luco and Cornell [2007]).

Near-field effects became a focus of research after the Northridge (California, 1994), Kobe (Japan, 1995), Izmit (Turkey, 1999), and Chi-Chi (Taiwan, 1999) earthquakes. These earthquakes caused widespread damage to the urban infrastructure in the near-field region. Recent research on these earthquakes reveals that near-fault ground motions exhibit two features: (1) forward and backward directivity, which occurs when the fault rupture propagates toward the site at a velocity nearly equal to the propagation velocity of the shear waves and the direction of fault slip is aligned with the site, and (2) permanent displacement effect, which is caused by the fault slide [Somerville 2005]. The velocity time history caused by the forward directivity effect

[1] Center of Excellence for Fundamental Studies in Structural Engineering, School of Civil Engineering, Iran University of Science & Technology, P.O. Box 16765–163 Narmak, Tehran 16846, Iran.

has a strong pulse of large amplitude and long period that occurs early in the velocity time history.

For earthquake-resistant design of critical structures (such as power plants, dams, tall buildings, cable-stayed bridges, etc.) in seismically active regions, the final design is usually based on a complete time-history analysis. However, it is difficult, or maybe impossible in some cases, to choose a proper record for a design area, because the recorded and processed accelerograms of the design location are few. Many engineers select recorded motions from locations other than the project site and modify them by scaling or spectrum matching, which may result in motions with unrealistic characteristics. Moreover, the major shortcoming of response spectrum analysis lies in its inability to obtain time information for the structural responses. Such information is sometimes necessary in achieving a satisfactory design. Therefore, synthetic ground motions that incorporate key features of real earthquakes can be used as additional input.

In this study, first, the acceleration spectra of 53 pulse-like near-fault motions were studied using wavelet analysis. It was seen that the spectra of these records are larger than predicted in the region of pulse period. While the pulses were extracted from these records, the residual ground motions were well matched to predicted spectra. Therefore, to produce artificial pulse-like near fault ground motion, the generated record compatible with median predicted spectra via particle swarm optimization (PSO)-based MLFF (PSOBMLFF) network is combined with mathematical model of long-period near-field ground motion. Moreover, in this research, to produce compatible synthetic long-period near-field ground motions with median predicted spectra, the attenuation of peak ground velocity (PGV) with the close horizontal distance (R), moment magnitude (M), and the time-average shear-wave velocity from the surface to 30 m (V_{s30}) has been developed using nonlinear regression analysis. By means of a PSOBMLFF network, inverse mapping from a response spectrum to the principal components of the accelerogram's wavelet packet coefficients (WPCs) was developed. Finally, by applying PCA and inverse discrete wavelet packet transform (DWPT), an ensemble of spectrum-compatible artificial earthquake accelerograms was generated. The effectiveness of the method is demonstrated by comparing the spectral response of the simulated accelerograms with those for the real records. Comparisons have also been made between the Arias intensity curves of the simulated earthquake records with those of the original ones to show the applicability of the approach. It is shown that the produced accelerograms maintain the amplitude, energy, and frequency content of the original records.

THE PROPOSED METHOD

In this study, first, to generate the artificial pulse-like near-field accelerogram, the response spectra of near-field records are studied by a wavelet analysis. The CWT is utilized to extract the largest velocity pulse from each of the near-field records. To implement CWT, after choosing scale and translation parameters, the mother wavelet is stretched or compressed by a scaling factor to achieve a family of wavelets. In this work, the Daubechies wavelet of order 4 is used as the mother wavelet due to its similarity to the shape of many velocity pulses [Baker 2007]. The wavelet associated with this coefficient is illustrated in Figure 1(a). An extracted pulse is presented in Figure 1(b), and the residual ground motion after the pulse has been removed is shown in Figure 1(c).

Afterwards, the response spectra of each near-field records with and without the pulses are compared with the median predicted spectra (Figure 2). It is apparent that *Sa*'s are higher than predicted in the region of the pulse period, meaning that the predicted spectra do not include the near-field pulse, and a narrow-band amplification function is needed in the region of the pulse period [Baker 2008]. Therefore, in order to generate near-field artificial seismic accelerograms, first a hybrid PSOBMLFF network is employed to generate the artificial earthquake record whose response spectrum is on average in good agreement with the median predicted spectra. Subsequently, the record produced is combined with the mathematical model of long-period near-field ground motions [Mavroeidis and Papageorgiou, 2003]. In this research, a number of NGA project ground motions, which were classified as pulse-like near-field ground motions [Baker 2007], have been employed.

The suggested method is based on a modified MLFF neural network, which takes discretised ordinates of the pseudo-spectral velocity (PSV) as input, and the output of the modified MLFF neural network i produces the accelerogram's principal component of the wavelet packet coefficients c_j^i at level j of the WPT of the earthquake accelerogram:

$$c_j^i(k) = \int_{-\infty}^{\infty} a_g(t)\, \Psi_{j,k}^i(t)\, dt \tag{1}$$

where $\Psi(t)$ is the mother wavelet. Daubechies' mother wavelet offers fast execution algorithms and produces no redundancies in WPT, DB 10 wavelets are used in this study [Daubechies 1992].

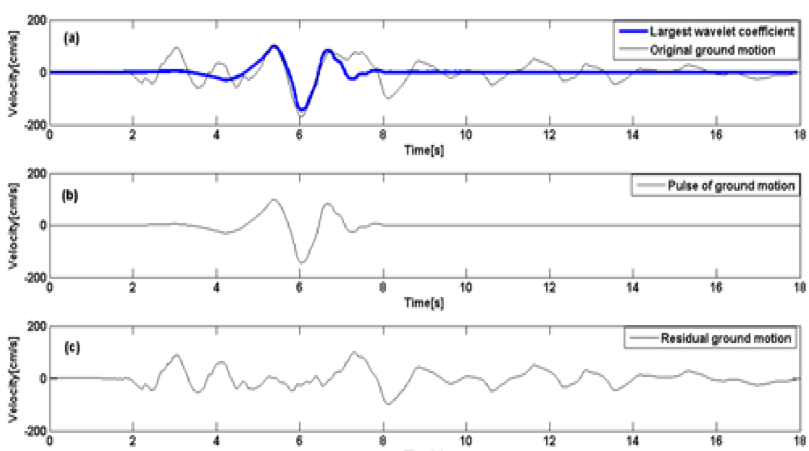

Figure 1 Illustration of the decomposition procedure used to extract the pulse portion of a ground motion (1995 Kobe, Japan, Takatori).

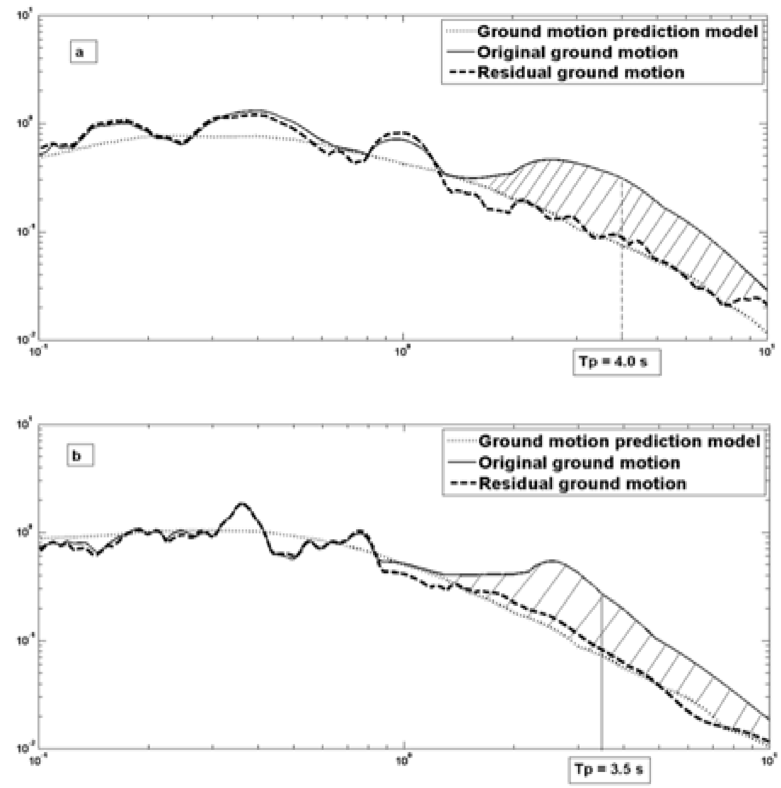

Figure 2 Response spectra of pulse-like ground motions before and after pulse extraction, and the Boore and Atkinson [2008] median prediction for each ground motion: (a) Imperial Valley, El Centro Array #5; and (b) Northridge, Jensen Filter Plant.

In this study, wavelet packet coefficients of the accelerograms were calculated at suitable DWPT decomposition levels (J). Furthermore, the accelerogram's PSV spectra have been computed numerically. Afterwards, in order to achieve better and faster convergence in training, PCA has been used for the input net layers to reduce the dimensions of the MLFF neural network structures. As mentioned previously, PCA can extract the principal components of data and arrange them according to their impressiveness. Principal component analysis is not reliably reversible, therefore it is only recommended for input processing. Outputs require reversible processing functions. The net input principal components are achieved by considering the desired effective covariance ratio for any input ($\mathrm{R}_{\mathrm{in.e}}^{\mathrm{cov-PCA}}$) data set.

$$\frac{\sum \mathrm{cov}_{\mathrm{eff-PCAcoef}}^{\mathrm{in.}}}{\sum \mathrm{cov}_{\mathrm{tot-PCAcoef}}^{\mathrm{in.}}} \leq \mathrm{R}_{\mathrm{in.e}}^{\mathrm{cov-PCA}} \tag{2}$$

where, $\mathrm{cov}_{\mathrm{eff-PCAcoef}}^{\mathrm{in.}}$ is the effective covariance (related to the effective PCA coefficients) and $\mathrm{cov}_{\mathrm{tot-PCAcoef}}^{\mathrm{in.}}$ is the total covariance (related to the total PCA coefficients), both for input data set (PSA spectra values). At the end of this stage, the input data sets have been compacted and prepared for use in the MLFF training process.

In addition, in order to train MLFF neural networks, PSO as an optimizing algorithm is implemented along with the error back-propagation training method. Application of PSO would result in the production of optimized non-unique network weight values, which will consequently lead to the generation of a suitable spectrum compatible artificial earthquake accelerogram.

The basic concept of the particle swarm optimization consists of, at each time step, changing the velocity and location of each particle towards its pbest and gbest locations according to Equations (3) and (4), respectively:

$$V_i(k+1) = wV_i(k) + c_1 r_1 (P_i - X_i(k))/\Delta t + c_2 r_2 (P_g - X_i(k))/\Delta t \tag{3}$$

$$X_i(k+1) = X_i(k) + V_i(k+1)\Delta t \tag{4}$$

where w is the inertia coefficient, which is a constant in interval [0, 1] and can be adjusted in the direction of linear decrease; c_1 and c_2 are learning rates, which are nonnegative constants; r_1 and r_2 are generated randomly in the interval [0, 1]; Δt is the time interval, commonlyset as unit; v_{id}= [-$v_{\max}$, $v_{\max}$]; and $v_{\max}$ is a designated maximum velocity. The ith particle in a D-dimensional space is represented as $X_i = (x_{i1}, \ldots, x_{id}, \ldots, x_{iD})$. The best previous position (which possesses the best fitness value) of the ith particle is recorded and represented as $P_i = (p_{i1}, \ldots, p_{id}, \ldots, p_{iD})$, which is also called pbest. The index of the best pbest among all the particles is represented by the symbol g. The location P_g is also called gbest. The velocity for the ith particle is represented as $V_i = (v_{i1}, \ldots, v_{id}, \ldots, v_{iD})$. The termination criterion for iterations is determined according to whether a maximum generation number or a designated value of the fitness is reached. For the purposes of this research, a particle represents the weight vector of neural networks, including biases.

To improve the results in this study, an iterative process has been proposed, in which the generated accelerogram using the wavelet transform is decomposed and then modified for wavelet coefficients. The wavelet coefficients cD_j are then modified for level, *j,* to coefficients cD_j mod cD_j^{Mod} such that [Mukherjee and Gupta 2002a; 2002b]:

$$cD_{\mathrm{j}}^{\mathrm{Mod}} = cD_j^* \times \frac{\int_{T_{1j}}^{T_{2j}} PSV(T)_{\mathrm{Tar}} dT}{\int_{T_{1j}}^{T_{2j}} PSV(T)_{\mathrm{Calc}} dT} \tag{5}$$

$$T_{1j} = 2^j \Delta t \quad T_{2j} = 2^{j+1}\Delta t \tag{6}$$

where T_{1j} and T_{2j} are the period range of level j of the detailed signal in wavelet transform and Δt is the time step of the digital data of $a_g(t)$. Furthermore, where $[PSV(T)]_{\mathrm{tar}}$ is the target pseudo-spectral velocity (PSV) ordinate at period *T*, and $[PSV(T)]_{\mathrm{calc}}$ is the PSV calculated from the aligned artificial accelerogram. Finally, the generated accelerogram using the inverse discrete wavelet transform is obtained.

Ultimately, the record produced, which is compatible with the median predicted spectra [Boore and Atkinson 2008], by a hybrid PSOBMLFF network is combined with the mathematical model of long-period near-field ground motions which was proposed by Mavroeidis and Papageorgiou [2003]. The equivalent pulse-type velocity can be represented by the product of a sine wave and an envelope function, that is:

$$v(t) = v_p . w(t) . \cos\left[2\pi f_p (t - t_0) + \varphi\right] \quad 0 \le t \le T \tag{7}$$

in which v_p is the peak value of the pulse-type velocity, f_p is the pulse frequency, and the pulse period is T_p=$1/f_p$,; φ denotes the phase angle of the pulse, and T denotes the duration of the velocity time history. The envelope function of the velocity history w(t) can be written as follows

$$w(t) = 0.5(1 + \cos(\alpha.\,2\pi f_p(t - t_0))) \tag{8}$$

where t_0 is the time of the peak value and α denotes the rate of peak attenuation.

The pulse period T_p, or frequency f_p, and the peak velocity v_p, in Equation (7) can be determined according to established statistical formulas. In this study, the equation which Baker [2007] obtained for a pulse period is used:

$$E\,[\ln T_p] = -5.78 + 1.02M \tag{9}$$

where T_p is the period of the pulse (as determined using wavelet analysis), E[ ] denotes an expected (mean) value, and M is the moment magnitude of the earthquake. Moreover, to produce the compatible synthetic long-period near-field ground motions with median predicted spectra [Boore and Atkinson 2008], nonlinear regression analysis has been used to produce a relationship between the PGV, close horizontal distance (R), moment magnitude (M), and the time-average shear-wave velocity from the surface to 30 m (V_{s30}). The following predictive relationship was obtained:

$$\text{Log}\,(PGV) = 1.487 + 0.069\text{M} - 0.112\text{Log}(R) + 0.0037\text{Log}\,(V_{s30}) \tag{10}$$

The standard deviation of Log (PGV) determined from this regression is 0.17. The properties of ground motions which have been used in this study are listed in Table 1.

Table1. The properties of ground motions used in this study.

No.	*Earthquake name*	*Year*	*Station name*	T_p	M_w	*R*	*PGV*	*Preferred Vs30** (m/s)*	*Fault type*
1	San Fernando	1971	Pacoima Dam (upper left abut)	1.6	6.61	1.8	116.5	2,016	RV
2	Coyote Lake	1979	Gilroy Array #6	1.2	5.74	3.1	51.5	663	SS
3	Imperial Valley-06	1979	Aeropuerto Mexicali	2.4	6.53	0.3	44.3	275	SS
4	Imperial Valley-06	1979	Agrarias	2.3	6.53	0.7	54.4	275	SS
5	Imperial Valley-06	1979	Brawley Airport	4.0	6.53	10.4	36.1	209	SS
6	Imperial Valley-06	1979	EC County Center FF	4.5	6.53	7.3	54.5	192	SS
7	Imperial Valley-06	1979	EC Meloland Overpass FF	3.3	6.53	0.1	115.0	186	SS
8	Imperial Valley-06	1979	El Centro Array #10	4.5	6.53	6.2	46.9	203	SS
9	Imperial Valley-06	1979	El Centro Array #11	7.4	6.53	12.5	41.1	196	SS
10	Imperial Valley-06	1979	El Centro Array #3	5.2	6.53	12.9	41.1	163	SS
11	Imperial Valley-06	1979	El Centro Array #4	4.6	6.53	7.1	77.9	209	SS
12	Imperial Valley-06	1979	El Centro Array #5	4.0	6.53	4.0	91.5	206	SS
13	Imperial Valley-06	1979	El Centro Array #6	3.8	6.53	1.4	111.9	203	SS
14	Imperial Valley-06	1979	El Centro Array #7	4.2	6.53	0.6	108.8	211	SS
15	Imperial Valley-06	1979	El Centro Array #8	5.4	6.53	3.9	48.6	206	SS
16	Imperial Valley-06	1979	El Centro Differential Array	5.9	6.53	5.1	59.6	202	SS
17	Imperial Valley-06	1979	Holtville Post Office	4.8	6.53	7.7	55.1	203	SS
18	Mammoth Lakes-06	1980	Long Valley Dam (Upr L Abut)	1.1	5.94	[16.23]	33.1	345	SS
19	Irpinia, Italy-01	1980	Sturno	3.1	6.90	10.8	41.5	1,000	N
20	Westmorland	1981	Parachute Test Site	3.6	5.90	16.7	35.8	349	SS
21	Coalinga-05	1983	Oil City	0.7	5.77	[8.46]	41.2	376	RV
22	Coalinga-05	1983	Transmitter Hill	0.9	5.77	[9.51]	46.1	376	RV
23	Coalinga-07	1983	Coalinga-14th & Elm (Old CHP)	0.4	5.21	[10.91]	36.1	339	RV
24	Morgan Hill	1984	Coyote Lake Dam (SW Abut)	1.0	6.19	0.5	62.3	597	SS
25	Morgan Hill	1984	Gilroy Array #6	1.2	6.19	9.9	35.4	663	SS
26	N. Palm Springs	1986	North Palm Springs	1.4	6.06	4.0	73.6	345	RV-OBL
27	San Salvador	1986	Geotech Investig Center	0.9	5.80	6.3	62.3	545	SS
28	Whittier Narrows-01	1987	Downey – Co Maint Bldg	0.8	5.99	20.8	30.4	272	RV-OBL
29	Whittier Narrows-01	1987	LB – Orange Ave	1.0	5.99	24.5	32.9	270	RV-OBL
30	Superstition Hills-02	1987	Parachute Test Site	2.3	6.54	1.0	106.8	349	SS
31	Loma Prieta	1989	Alameda Naval Air Stn Hanger	2.0	6.93	71	32.2	190	RV-OBL
32	Loma Prieta	1989	Gilroy Array #2	1.7	6.93	11.1	45.7	271	RV-OBL
33	Loma Prieta	1989	Oakland – Outer Harbor Wharf	1.8	6.93	74	49.2	249	RV-OBL
34	Loma Prieta	1989	Saratoga – Aloha Ave	4.5	6.93	8.5	55.6	371	RV-OBL
35	Erzican, Turkey	1992	Erzincan	2.7	6.69	4.4	95.4	275	SS
36	Cape Mendocino	1992	Petrolia	3.0	7.01	8.2	82.1	713	RV
37	Landers	1992	Barstow	8.9	7.28	35	30.4	371	SS
38	Landers	1992	Lucerne	5.1	7.28	2.2	140.3	685	SS
39	Landers	1992	Yermo Fire Station	7.5	7.28	23.6	53.2	354	SS
40	Northridge-01	1994	Jensen Filter Plant	3.5	6.69	5.4	67.4	526	RV
41	Northridge-01	1994	Jensen Filter Plant Generator	3.5	6.69	23.6	67.4	392	RV
42	Northridge-01	1994	LA – Wadsworth VA Hospital North	2.4	6.69	23.6	32.4	414	RV
43	Northridge-01	1994	LA Dam	1.7	6.69	5.9	77.1	629	RV
44	Northridge-01	1994	Newhall – W Pico Canyon Rd.	2.4	6.69	5.5	87.8	286	RV
45	Northridge-01	1994	Pacoima Dam (downstr)	0.5	6.69	7.0	50.4	2,016	RV
46	Northridge-01	1994	Pacoima Dam (upper left)	0.9	6.69	7.0	107.1	2,016	RV
47	Northridge-01	1994	Rinaldi Receiving Sta	1.2	6.69	6.5	167.2	282	RV
48	Northridge-01	1994	Sylmar – Converter Sta	3.5	6.69	5.4	130.3	251	RV
49	Northridge-01	1994	Sylmar – Converter Sta East	3.5	6.69	5.2	116.6	371	RV
50	Northridge-01	1994	Sylmar – Olive View Med FF	3.1	6.69	5.3	122.7	441	RV
51	Kobe, Japan	1995	Takarazuka	1.4	6.90	0.3	72.6	312	SS
52	Kobe, Japan	1995	Takatori	1.6	6.90	1.5	169.6	256	SS
53	Chi-Chi, Taiwan	1999	CHY006	2.6	7.62	9.8	64.7	438	RV-OBL

Numerical Examples

The proposed framework to generate spectrum-compatible artificial earthquake accelerogram was executed in this research for a number of the NGA project ground motions, which were classified as pulse-like near-field ground motions [Baker 2007]. Twenty one earthquake records from Table 1 were used in the training set of the modified MLFF neural network. All accelerograms are discretised at 0.01 s, i.e., $\Delta t = 0.01$ sec, and their PGAs are scaled to 1*g*. To equate the total duration of all accelerograms, in each group a time series of adequate points with zero amplitude were added at the end of shorter duration records.

The PSV spectra of all accelerograms were calculated numerically, based on the method of linear interpolation of excitation at 1000 equally spaced (in log scale) discrete periods in the range 0.01–10 sec, with a 5% damping ratio (ζ = 5%). In addition, two median predicted spectra [Boore and Atkinson 2008] with different characteristics were calculated with a 5% damping ratio (ζ = 5%) at 1000 discrete periods.

First, the CWT has been used to extract the largest velocity pulse from each near-field ground motion. Next, the largest velocity pulse is subtracted from each ground motion and the residual accelerograms using the WPT are decomposed to level 7, and at this level they have 128 sets of wavelet packet coefficients. Then, the 128 neural networks were trained with pseudo-velocity response spectra, and the wavelet packet coefficients of the earthquake accelerograms in the training group.

After training the neural networks, the trained neural networks were tested with the new accelerograms, using the accelerogram of Landers (Yermo Fire Station, 1992), Imperial Valley-06 (El Centro Array #6, 1979). Figures 3 to 6 show that the time characteristics and the response spectra obtained from the generated accelerograms are similar to those obtained from the original recorded accelerograms. In these examples, the capabilities of the proposed method in inverse mapping from response spectrum to earthquake accelerograms are presented.

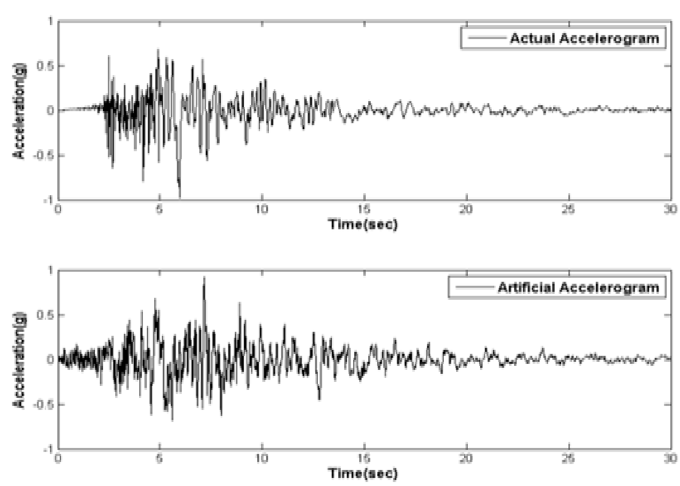

Figure 3 A test of neural networks with a new accelerogram [Imperial Valley-06 (1979)].

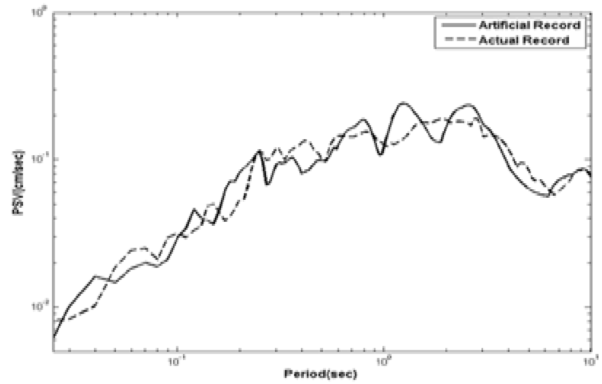

Figure 4 **A test of neural networks with a new accelerogram (Imperial Valley-06, 1979). Comparison between pseudo-velocity response spectra of actual accelerogram and artificial accelerogram.**

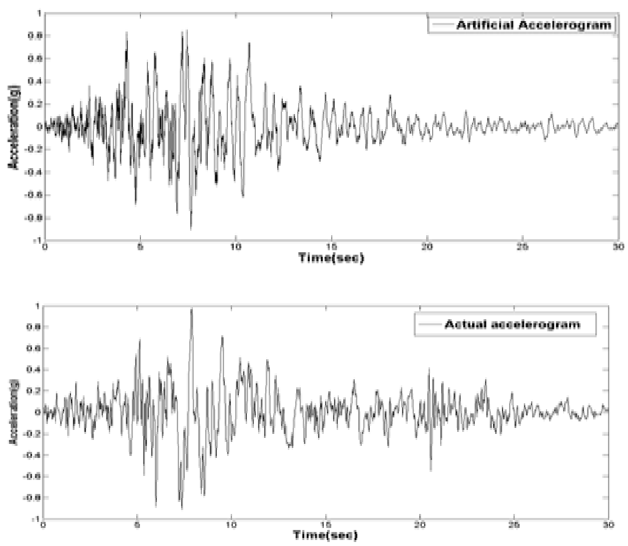

Figure 5 **Comparison between acceleration time histories of actual accelerogram and artificial accelerogram (Landers, 1992).**

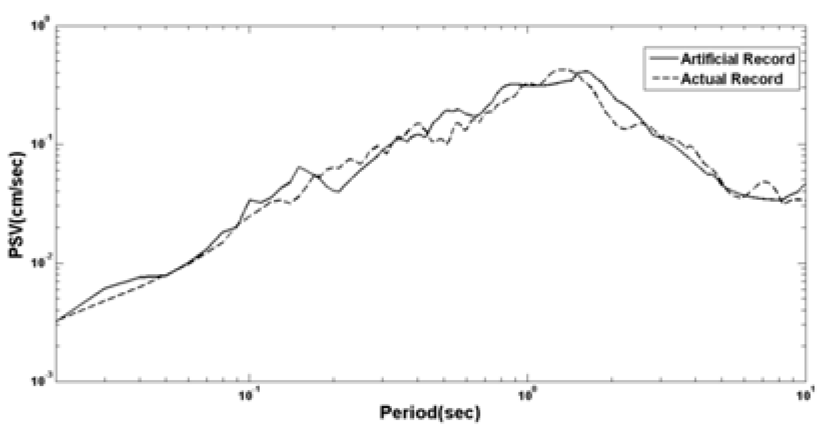

Figure 6 **Comparison between pseudo-velocity response spectra of Actual accelerogram and artificial accelerogram (Landers, 1992).**

To investigate the efficiency of the model, the Arias intensity (I_0)curves, which represent the energy parameter, obtained from the simulated accelerograms are compared with those from the actual records (Figure 7). The results reveal that there is a good agreement between the Arias intensity of simulated and actual records. Arias intensity is described by the following relationship:

$$I_0 = \frac{\pi}{2g}\int_0^\infty [a(t)]^2\, dt \tag{11}$$

To generate near-field artificial seismic accelerograms, first a hybrid PSOBMLFF network is employed to generate the artificial earthquake record whose response spectrum is on the average in good agreement with the median predicted spectra [Boore and Atkinson 2008]. Figures 8 to 9 show that the response spectra obtained from the generated accelerograms are similar to the median predicted spectra [Boore and Atkinson 2008]. Subsequently, the produced record is combined with the mathematical model of long-period near-field ground motions [Mavroeidis and Papageorgiou 2003]. The parameters of the mathematical model are obtained via the predictive relationship produced for Log (PGV) [Equation (10)]. For M_w=6.5, R = 7 km, and $V_{30} = 210$ cm/sec, PGV equals 71 cm/sec and T_p equals 2.33 sec. Figure 10 shows the shapes of the equivalent pulse model of these parameters.

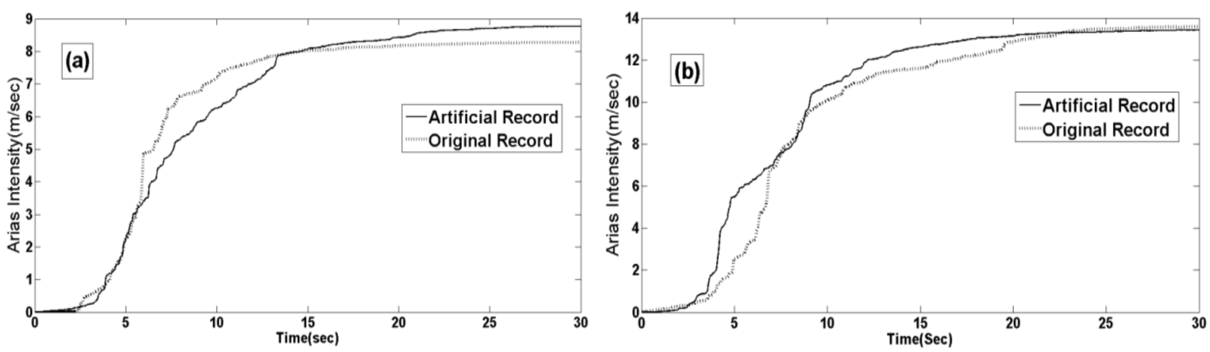

Figure 7 The arias intensity of simulated and actual records: (a) Imperial Valley-06 (1979), and (b) Landers (1992).

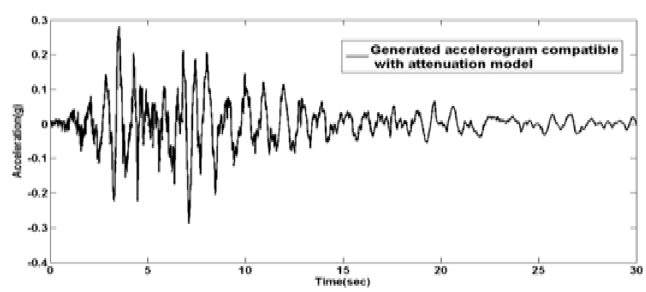

Figure 8 Generated accelerogram compatible with attenuation model [Boore and Atkinson 2008], (M_w = 6.5, R = 7 km, $V_{30} = 210$ cm/sec, fault type=SS).

Eventually, the artificial near-fault pulse-type ground motion is obtained by superimposing the equivalent pulse model and the generated artificial earthquake record from the median predicted spectra [Boore and Atkinson 2008]. Figure 11 shows the velocity time histories of the near-field accelerograms generated.

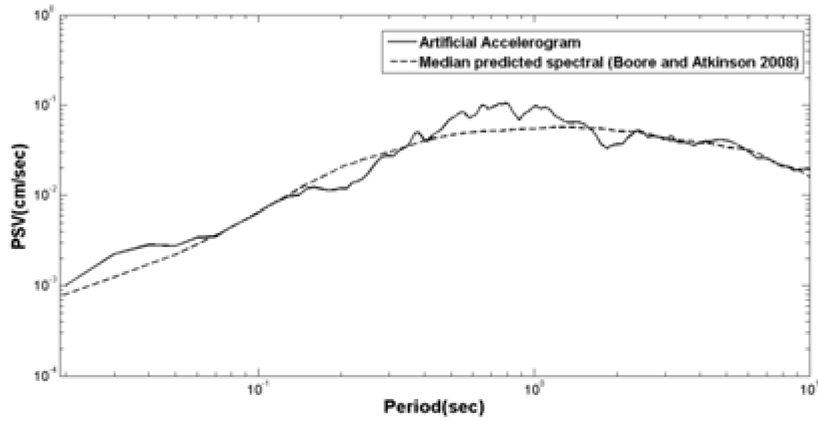

Figure 9 **The artificial earthquake record whose response spectrum is on the average in good agreement with the median predicted spectra [Boore and Atkinson 2008], (M_w=6.5, R=7 km, $V_{30} = 210$ cm/sec, fault type=SS).**

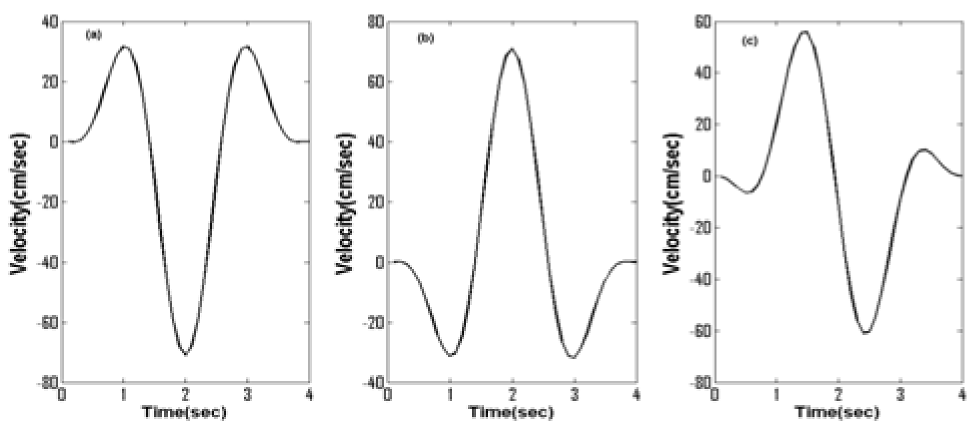

Figure 10 **Shapes of the equivalent pulse model of M_w=6.5; *R* = 7 km; $V_{30} = 210$ cm/sec; (a) φ =180;(b) $\varphi = 1$;(c) $\varphi = 100$.**

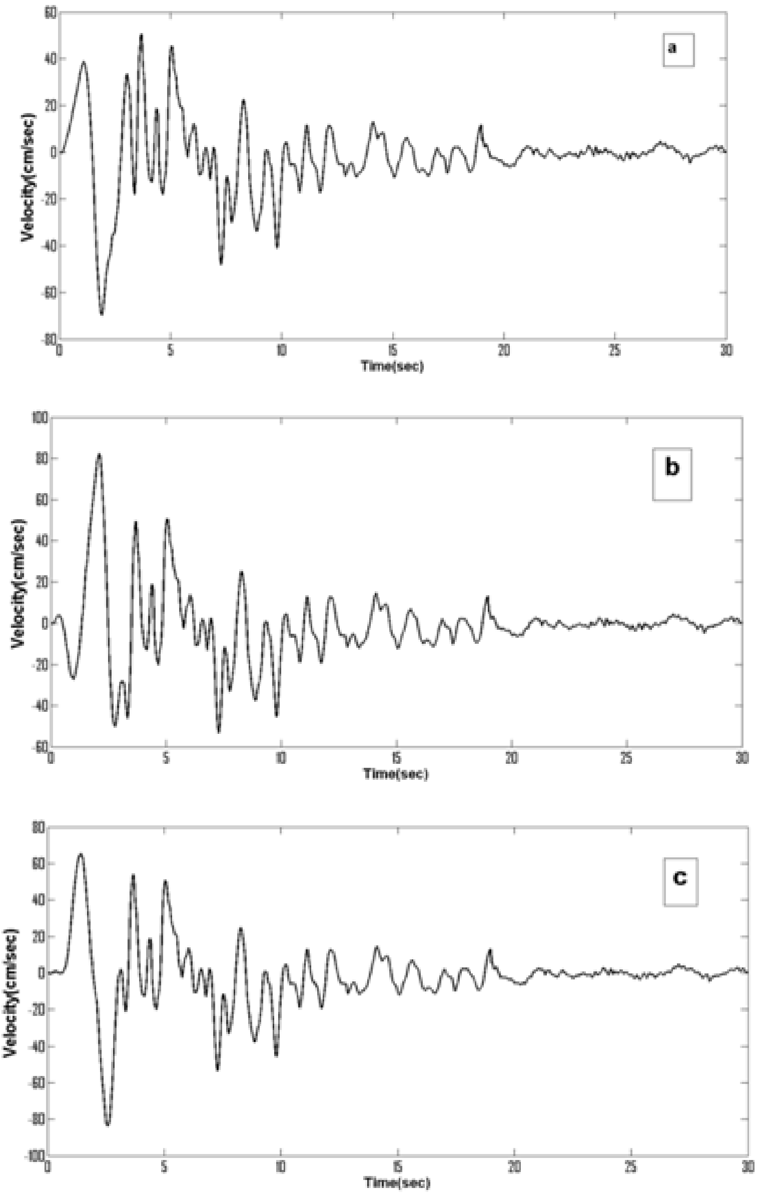

Figure 11 Velocity time histories of the generated Near-field accelerograms: Mw = 6.5; *R* = 7 km; V_{30} = 210 cm/sec; (a) φ =180; (b) $\varphi = 1$; and (c) $\varphi = 100$.

CONCLUSIONS

This article presents a PSO-based MLFF neural network framework for the generation of spectrum-compatible artificial near-field earthquake accelerograms. The proposed method uses the decomposing capabilities of WPT on earthquake accelerograms, and the learning abilities of a MLFF neural network to expand the knowledge of inverse mapping from the response spectrum to coefficients of WPT of an earthquake accelerogram. PSO is implemented as a robust search technique, with a domain independent problem-solving approach for optimizing the network's weight values, so the networks are trained through hybrid evolutionary and error-back propagation strategies. In order to improve the network's learning efficiency, PCA has been utilized as a dimension reduction strategy. Implementing principal component analysis (PCA) has notably diminished the input network's nodes.

The application of the proposed approach for a number of next generation attenuation (NGA) project ground motions is presented. The results reveal that the model proposed in this paper is able to effectively capture the significant properties of real accelerograms such as pulse period, energy, amplitude, and frequency content of near-field ground motions. The positive aspect of the current method is that it does not require exact information about the earthquake source to generate artificial ground motions. Ground motion time history and its response spectra are the only requirements for this technique. The proposed method can be used in seismic design and analysis, in conjunction with or instead of recorded ground motions.

REFERENCES

Akkar S., Yazgan U., Gulkan P. (2005). Drift estimates in frame buildings subjected to near-fault ground motions, ASCE, *J. Struct. Eng*., 131(7): 1014–1024.

Alavi B., Krawinkler H. (2001). Effects of near-fault ground motions on frame structures, *Blume Center Report 138*, Stanford University, Stanford, CA.

Baker J.W. (2008). Identification of near-fault velocity pulses and prediction of resulting response spectra, *Proceedings, Geotechnical Earthquake Engineering and Soil Dynamics IV*, Sacramento, CA.

Baker J.W. (2007). Quantitative classification of near-fault ground motions using wavelet analysis, *Bull. Seismol. Soc. Am.,* 97(5): 1486–1501.

Boore D., Atkinson G. (2008). Ground-motion prediction equations for the average horizontal component of PGA, PGV, and 5%-damped PSA at spectral periods between 0.01 s and 10.0 s, *Earthq. Spectra,* 138: 24–99.

Luco N., Cornell C.A. (2007). Structure-specific scalar intensity measures for near-source and ordinary earthquake ground motions, *Earthq. Spectra*, 23(2): 357–392.

Mavroeidis G.P., Papageorgiou A.S. (2003). A mathematical representation of near-fault ground motions, *Bull. Seismol. Soc. Am.,* 93(3): 1099–1131.

Mavroeidis G.P., Dong G., Papageorgiou A.S. (2004). Near-fault ground motions, and the response of elastic and inelastic single degree-of-freedom (SDOF) systems, *Earthq. Eng. Struct. Dyn.*, 33(9): 1023–1049.

Mukherjee S., Gupta V.K. (2002a). Wavelet-based characterization of design ground motions, *Earthq. Eng. Struct. Dyn.,* 31, 1173-90.

Mukherjee S., Gupta V.K. (2002b). Wavelet-based generation of spectrum-compatible time-histories, *Soil Dyn. Earthq. Eng*., 22: 799–804.

Shwe T.T., Adeli, H. (1993). AI and CAD for earthquake damage evaluation, *Eng. Structures*, 15(5): 315–319.

Somerville P.G. (2005). Engineering characterization of near fault ground motion, *Proceedings, New Zealand Society for Earthquake Engineering Conference*, Taupo, New Zealand.

STRUCTURAL APPLICATIONS OF HPFRCC IN EARTHQUAKE RESISTANT REINFORCED CONCRETE STRUCTURES

Ali Kheyroddin[1], Mohammad Kazem Sharbatdar[2], and Ali Hemmati[3]

ABSTRACT

High performance fiber reinforced cementitious composite (HPFRCC) materials exhibit strain hardening behavior under tensile loading. This strain hardening response occurs after the first cracking of material and concludes to multiple cracking. This unique characteristic of HPFRCC concludes to a ductile material in earthquake resistant structures. In this paper, some experimental investigations were conducted to evaluate the effect of HPFRCC on the ductility of reinforced concrete members. The test specimens which were chosen for this study were five beams with hinge supports under two-point loading and three frames with fixed supports under vertical and lateral loadings. Step by step cracking patterns, loads, displacements, mode of failure and other parameters were presented for these structures. Due to presence of fibers, multiple cracking patterns were formed in HPFRCC structures and damages not concentrated in a limited zone. Consequently HPFRCC members are appropriate for using in earthquake resistant structures. Moreover, some theoretical equations were proposed by authors for calculating the flexural characteristics of HPFRCC sections.

Keywords: *ductility, experimental, HPFRCC, reinforced concrete, ultimate load*

INTRODUCTION

High performance fiber reinforced cementitious composite (HPFRCC) is defined as a material with strain hardening response under uni-axial loading. At the first stages, Li and Wu [1992] introduced a pseudo-strain-hardening material that used only fine aggregates with reinforcing polyethylene fibers. In 1996, Naaman and Reinhardt [1996] presented a fiber reinforced cementitious material which had a matrix with no coarse aggregates, and regarded as fiber reinforced cement paste or mortar. High tensile ductility with strain hardening response are the most important characteristics of this material compared to normal concrete and fiber reinforced concrete (FRC), as shown in Figure 1 [Brandt 2008]. In recent years, a new class of HPFRCC has been emerged. Engineered Cementitious Composite (ECC) was originally developed at the University of Michigan, with a typical moderate tensile strength of 4−6 MPa and a high ductility of 3−5% [Fischer et al. 2003]. A summary of major physical properties of ECC is presented in Table 1 [Li 2007].

A great amount of researches have been performed in recent years, focused on the durability and steel corrosion of partially layered RC beams with HPFRCC material [Maalej and Li 1995; Maalej et al. 2002]. Some experimental and analytical works have been performed

[1] Professor, Civil Engineering Faculty, Semnan University, Semnan, Iran; email: kheyroddin@semnan.ac.ir.
[2] Assistant Professor, Civil Engineering Faculty, Semnan University, Semnan, Iran; email: msharbatdar@semnan.ac.ir.
[3] PhD Student, Civil Engineering Faculty, Semnan University, Semnan, Iran; email: ahemmati2000@yahoo.com.

about using HPFRCC material in RC beam-column joints in connections and plastic regions [Bayasi and Gebman 2002; Parra Montesinos et al. 2005; Chao et al. 2012]. These investigations have been concentrated on reducing the transverse reinforcements and patterns of cracking in joints. In this paper, an experimental work were carried out on five beams and three frames for assessing the step by step cracking patterns, ultimate load and deformation characteristics and ductility ratios of these structures. Moreover, some new equations were proposed for calculating the flexural characteristics of HPFRCC sections and compared with experimental works.

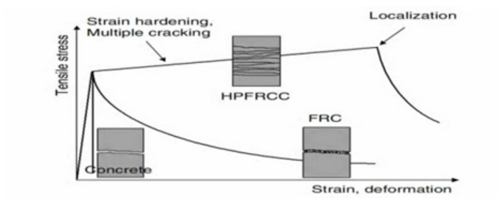

Figure 1 Tensile stress-strain curves of concrete, FRC and HPFRCC [Fischer and Li 2000].

Table 1 Major physical properties of ECC [Li 2007].

Compressive Strength (MPa)	First Cracking Strength (MPa)	Ultimate Tensile Strength (MPa)	Ultimate Tensile Strain(%)	Young's Modulus (GPa)	Flexural Strength (MPa)	Density (gr/cc)
20–95	3–7	4–12	1–8	18–34	10–30	0.95–2.3

EXPERIMENTAL PROGRAMS AND OBSERVATIONS

Beams

The test specimens chosen for this experimental study were five large scale beams with two hinged supports which have been tested by authors. The beam clear span was 2100 mm with constant cross section of 300 mm deep×200 mm wide. Two-point loading was applied on this beam, which was increased monotonically. Details of reinforcement layout and loading of these beams are shown in Figure 2.

Mix proportions of the materials are presented in Table 2. Coarse aggregate was not used in HPFRCC material, but Polypropylene (PP) fibers used for achieving the HPFRCC [Shihada 2011]. Polypropylene fibers with a length of 12 mm and diameter of 18 μm and Portland cement type II were employed for HPFRCC. Coarse aggregate gradations taking 4.75 to 12.5 mm particles and fine aggregate gradations taking particles less than 4.75 mm were used too. During the mixing, care was taken to prevent clumping of the fibers. The dry components of the mortar mix were first combined with approximately 25% of the total water required and then the fibers along with the remaining 75% of the water were intermittently added as the mixing process progressed. The fibers were added slowly, while mixing continued in order to distribute the fibers throughout the mix. Material properties are summarized in Table 3. Test set up of one reinforced concrete (RC), three reinforced composite (RCH) and one reinforced HPFRCC (RH) beams are presented in Figure 3.

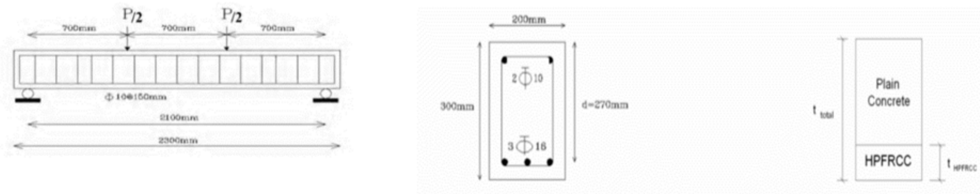

Figure 2 Details of the experimental beams.

Table 2 Mix proportion of concrete and HPFRCC.

Material	Cement	Coarse Aggregate	Fine Aggregate	Water	Fiber (volume fraction)
Concrete	1	1.72	1.72	0.45	-
HPFRCC	1	-	1	0.54	1 %

Table 3 Concrete, HPFRCC and steel properties used in the test beam.

Material properties	(RC beam)	HPFRCC beam
f'_c (MPa)	35.7	24
f_y (MPa)	400	400
E_s (MPa)	200,000	200,000

Figure 3 Test set-up for beams.

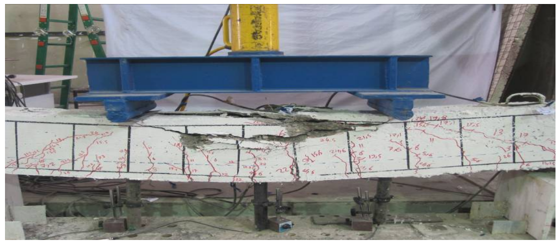

Figure 4 General view of RC beam at the end of loading.

The two-point vertical load was applied on RC beam and the first cracking observed at the load of 46 kN and mid-span deflection of 1.29 mm respectively at the mid-span of the beam. Then the yielding of steel bars occurred at the load of 161 kN and deflection of 5.97 mm. Further loading caused the cracking spread at the bottom face of the beam. Finally beam carried the load of 239.83 kN and deflection of 30.25 mm. Condition of the RC beam at the ultimate load and displacement is shown in Figure 4. As shown in this figure, the failure was in flexural mode, i.e., at first step tensile reinforcements started to yield and then compressive crushing of concrete occurred. The failure was accompanied by large tensile cracks in lower parts of the section in mid-span of the beam. The amount of damage in compressive concrete was severe and ultimate deflection was small.

At second stage, the vertical load was applied on composite beam with partially layered HPFRCC material in bottom of the normal concrete with depth of 6 mm ($\frac{t_{HPFRCC}}{t}$=0.2) and the first cracking observed at the load of 46.5 kN and mid-span deflection of 1.3 mm respectively at the mid-span of the beam. Then the yielding of steel bars occurred at the load of 169 kN and deflection of 6.5 mm. Further loading caused the cracking spread at the bottom face of the beam. Finally beam carried the load of 264.33 kN and deflection of 36.61 mm. Condition of the RCH-0.2 beam at the ultimate load and displacement is shown in Figure 5. As shown in this figure, the failure was in flexural mode and the amount of damage in compressive concrete was severed but it was less than RC beam and ultimate deflection was increased compared to RC beam. This improved behavior may be due to existence of HPFRCC material instead of normal concrete. Due to bridging of fibers, HPFRCC maintained its unity under sever loading and tensile reinforcements were closed to their plastic strain. During the loading of this specimen it was observed that the crack width in lower HPFRCC material was less than upper concrete part.

In the case of RCH-0.4, the composite beam carried the load of 275.5 kN and deflection of 41.15 mm. In the case of RCH-0.6, the composite beam carried the load of 255.17 kN and deflection of 45.86 mm. In the case of full HPFRCC beam (RH), the first cracking observed at the load of 45 kN and mid-span deflection of 1.46 mm respectively and then the yielding of steel bars occurred at the load of 160 kN and deflection of 6.22 mm. Further loading caused the cracking spread at the bottom face of the beam. Finally beam carried the load of 263.17 kN and deflection of 59.95 mm. Condition of the RH beam at the ultimate load and deflection is shown in Figure 6. Load-deflection curves of these five test specimens are presented in Figure 7. Summary of these experimental results are presented in Table 4, where, $\mu = \frac{\Delta_u}{\Delta_y}$.

Figure 5 General view of RCH-0.2 beam at the end of loading.

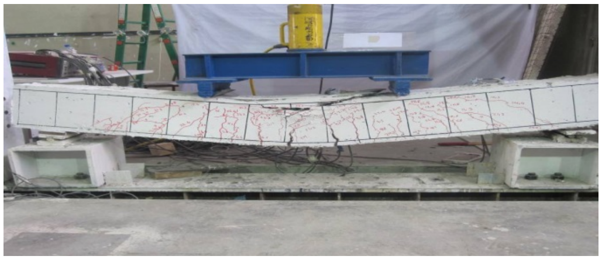

Figure 6 General view of RH beam at the end of loading.

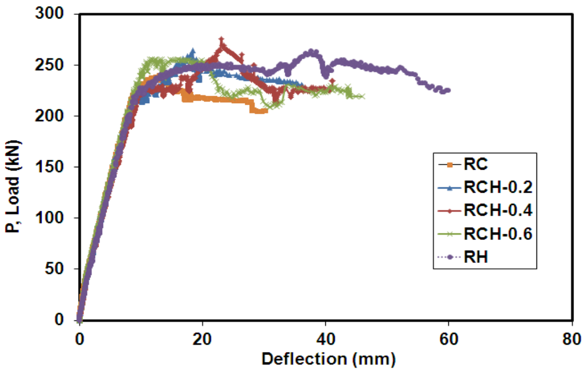

Figure 7 Load-deflection curves of experimental specimens.

Table 4 Summary of experimental results of the beams.

Specimen	P_y (kN)	P_u (kN)	Δ_y (mm)	Δ_u (mm)	μ	μ/μ_{RC}
RC	161	239.83	5.97	30.25	5.07	1
RCH-0.2	169	264.33	6.5	36.61	5.63	1.11
RCH-0.4	167	275.5	6.7	41.15	6.14	1.21
RCH-0.6	175	255.17	6.54	45.86	7.01	1.38
RH	160	263.17	6.22	59.95	9.64	1.9

Frames

The test specimens chosen for this part were three frames with fixed supports, including reinforced concrete (RC), composite (RCH) and HPFRCC (RH) frames. Clear span of the whole frames was 120 cm with total span of 160 cm. Cross section of the beams was 150 mm deep by 200 mm wide. Total height of the frames was 140 cm and cross section of the all columns was 200 mm deep×200 mm wide which is shown in Figure 8(a). Details of reinforcement layout of the frames are shown in Figure 8(b). In RC and RH frames, the whole part of frames cast with only normal concrete and HPFRCC materials, respectively. But in RCH frame, HPFRCC material used only in beam-column connection zones (30 cm in beam and 40 cm in column which are equal to the two times of the height of the beam and column, respectively) and the other parts of the frame cast by normal concrete according to Figure 8(a). Material properties are summarized in Table 5. Constant vertical and monotonic lateral loadings were applied on these frames. Vertical load was applied as a concentrated load placed on centerline of the frame and the lateral load applied on exterior side of column as shown in Figure 9.

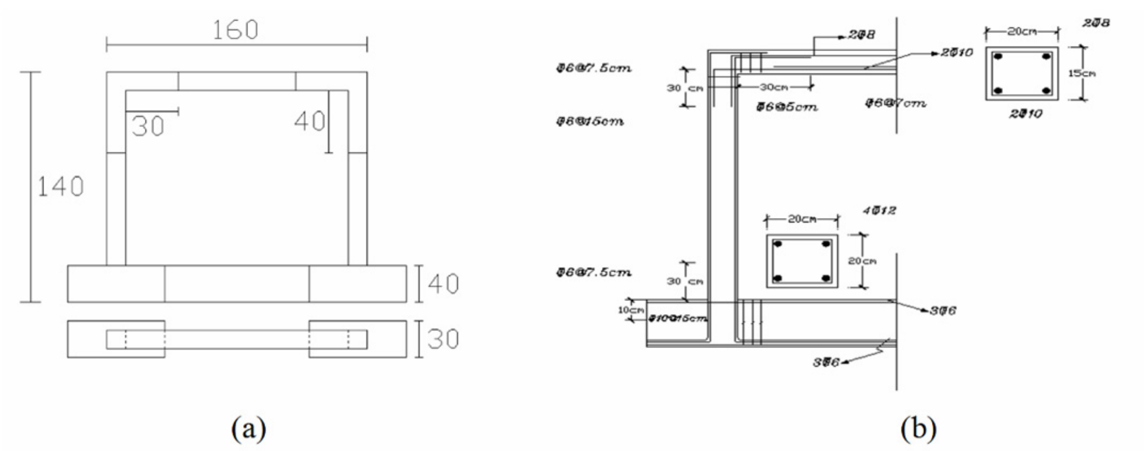

Figure 8 Dimensions and reinforcement details of the experimental specimens

Table 5 Concrete, HPFRCC, and steel properties used in frames.

Material properties	(Concrete)	(HPFRCC)
f'_c (MPa)	48	24
f_y (MPa)	400	400
E_s (MPa)	200,000	200,000

At the first step, the vertical load of 30 kN was applied on mid-span of the beam of RC frame and initial cracking in mid-span of the beam and beam to column connections formed as presented in Figure 10(a.) At the second step the lateral load applied on frame. The first cracking observed at the lateral load and displacement of 26 kN and 2.5 mm respectively at the beam top near the left beam-column junction and at the column top near the right column-foundation connection as shown in Figure 10(b). Further loading caused the cracking to spread at the beam-column junctions and column-foundation connections of RC frame. The initial yielding of the steel bars of column top near the left column-foundation connection occurred at the load of 55 kN and displacement of 11 mm and accompanied by the crushing of the concrete at the bottom face of the beam and inside the beam-column connection near the inside left corner, leading to the formation of the first plastic hinge. With further increase in load, more parts cracked. The second yielding of the steel bars of column occurred at the load of 57 kN and the displacement of 20 mm at the rear of the right column-foundation connection, leading to the formation of the second hinge, while other parts of the frame experienced more cracking and crushing. The third hinge formed at the top of beam near the left beam-column junction by the yielding of the tensile reinforcements. This phenomenon can be observed clearly from the crack patterns. At this point, the most parts of the concrete around the critical section (around the connections) cracked and crushed. Finally, the frame carried the lateral load of about 65 kN and displacement of about 66 mm. Condition of the RC frame at the ultimate load and displacement with the length of cracking in beam and columns shown in Figure 11.

Figure 9 Test set-up for frames.

(a) Vertical load of 30 kN (b) Lateral load of 40 to 52 kN

Figure 10 Initial cracks in RC frame.

Companion of RC frame, vertical load of 30 kN was initially applied on mid-span of the beam of RCH frame and initial cracking in mid-span of the beam were formed as already presented in Figure 10(a). The initial yielding of the steel bars of column in RCH frame occurred at the near the left column-foundation connection at a load of 63 kN and displacement of 9 mm and not accompanied by the crushing of the HPFRCC at the bottom face of the beam and inside the beam-column connection near the inside left corner. With increasing lateral load, more parts of frame cracked. The second yielding of the steel occurred at load of 67 kN and displacement of 12.5 mm at the beam top near the left beam column junction, leading to the formation of the second hinge, while other parts of the frame experienced more cracking. The third hinge formed at the column top near the right column-foundation connection by the yielding of the tensile reinforcements, so the most parts of the concrete around the critical section (around the connections) cracked and crushed. Therefore, the RCH frame carried the lateral load of about 75 kN and displacement of about 75 mm prior to failure shown in Figure 12.

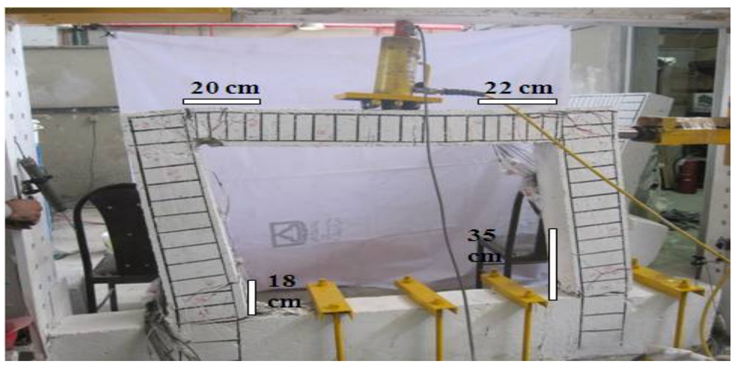

Figure 11 General view of RC frame at the end of loading.

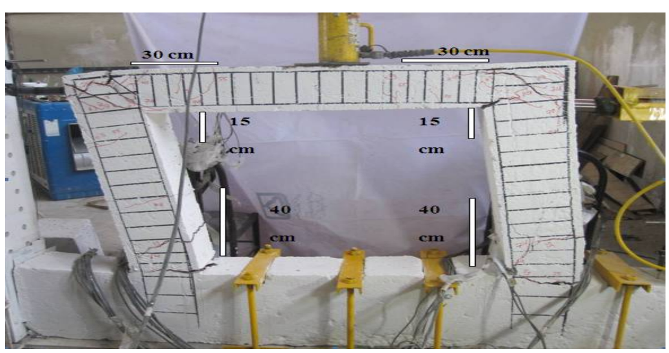

Figure 12 Condition of RCH frame at the end of loading.

Figure 12 Condition of RCH frame at the end of loading.

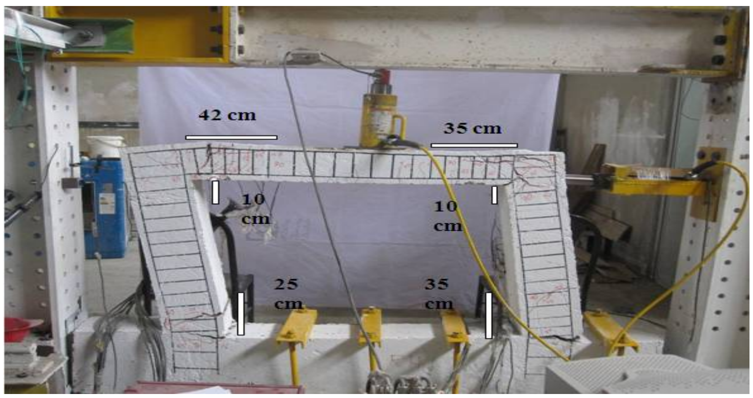

Figure 13 Condition of RH frame at the end of loading

Companion of two other frames, initial yielding of the steel bars occurred at the beam top near the left beam-column junction at a load of 55 kN and displacement of 10 mm but not accompanied by the crushing of the HPFRCC at the bottom face of the beam and inside the beam-column connection near the inside left corner. With further loading, more parts of frame cracked. The second yielding of the steel bars occurred at load of 60 kN and displacement of 20 mm at the column top near the left column-foundation connection, leading to the formation of the second hinge, while other parts of the frame experienced more cracking. The third hinge formed at the column top near the right column-foundation connection by the yielding of the tensile reinforcements. Finally, the frame carried the lateral load of about 69.5 kN and displacement of about 97 mm. Condition of the RH frame at the ultimate load and displacement with length of cracking in beam and columns shown in Figure 13.

Lateral load-displacement curves of experimental RC, RCH, and RH frames are presented in Figure 14. The area under the curve of RC, RCH and RH frames means absorbed energy are about 3.7 kN.m, 4.9 kN.m and 5.9 kN.m respectively. Therefore, the absorbed energy of RH frame is about 19.62% more than RCH frame and about 57.22% more than RC frame. It seems that due to presence of fibers in RH frame, cracking was not concentrated in columns, but spread in the beam as presented in Figure 13. Length of cracking in the beam of RH frame is about 1.4 times more than RCH and about 2.1 times of RC frame. These values in columns are about 0.625 and 0.714 too. The approximate values of l_y (length of yielding in tensile reinforcements) in the columns of RH frame is about 4% more than RCH and about 68% more than RC frame. These values in the beam are about 2.07 and 3.76 times too. The values of maximum strain in columns and beam of RH frame are about 1.13 and 1.12 times more than RCH frame and 1.87 and 1.99 times more than RC frame. In RH frame due to presence of fibers, HPFRCC material maintained its unity under the sever loading and consequently, steel reinforcement were closed to their plastic strain. The values of ductility ratio in RH frame are about 37.7% more than that in RCH frame and 60.6% more than that in RC frame. Experimental results summarized in Table 6.

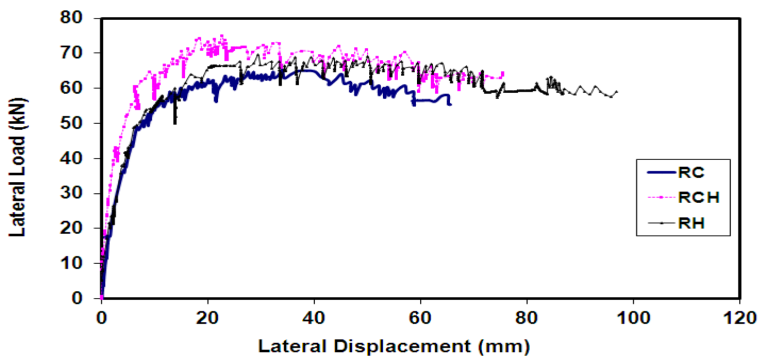

Figure 14 Experimental lateral load-displacement curve of RC, RCH and RH frames.

Table 6 Summary of experimental results of the frames.

Frame	$P_y(kN)$	$\Delta_y(mm)$	$P_u(kN)$	$\Delta_u(mm)$	$\mu=\frac{\Delta_u}{\Delta_y}$	$\mu=\frac{\mu}{\mu_{RC}}$
RC	55.31	10.9	65.31	65.61	6.02	1
RCH	64.81	9.1	75.04	75.47	8.29	1.38
RH	54.73	10.01	69.53	96.82	9.67	1.61

PROPOSED EQUATIONS

Flexural Capacity of RH beams

Strain and stress distributions in a flexural rectangular HPFRCC section are observed in Figure 15. It is assumed that the strain distribution along the height of the section is linear. As shown in Figure 15, the depth of the equivalent compressive stress block, $a=\beta_1 c$, and flexural capacity of a HPFRCC section, M_r, can be calculated as discussed below.

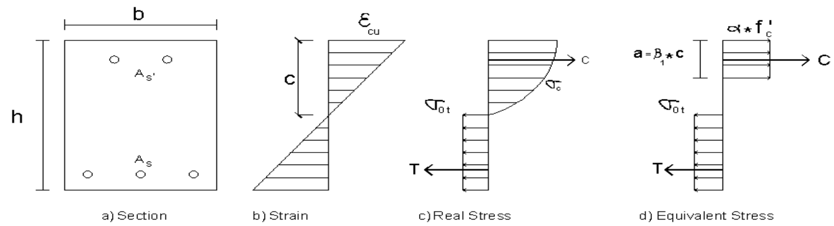

Figure 15 Strain and stress distributions in a flexural rectangular HPFRCC section.

$$\sum F_x = 0 \Rightarrow \alpha . f_c' . a . b + A_s{}' \cdot f_y - A_s . f_y - \sigma_{0t} . b . (h - c) = 0$$

$$a = \frac{(A_s - A_s{}').f_y + \sigma_{0t}.b.h}{\alpha . f_c'.b + \sigma_{0t} \cdot \dfrac{b}{\beta_1}} = \beta_1 . c$$

$$M_r = \alpha . f_c' . a . b . \left(d - \frac{a}{2} \right) + A_s{}' \cdot f_y \cdot (d - d') - \sigma_{0t} . b . (h - c) . \left[\left(\frac{h - c}{2} \right) - (h - d) \right] \tag{1}$$

where, f_c'= compressive strength of HPFRCC, b= width of the beam, f_y= yielding stress of reinforcements, A_s = area of tensile reinforcements, A_s' = area of compressive reinforcements, σ_{0t} = tensile strength of HPFRCC, h= height of the beam and d = effective height of the member. Flexural capacity of RC and RH beams which were calculated by Equation (1) ($M_r(The.)$) and experimental values ($M_r(Exp.)$) are presented in Table 7.

Table 7 Experimental and theoretical results for RC and RH beams.

Beam	σ_{0t} (MPa)	f_c' (MPa)	α	β_1	a (mm)	$M_r(The.)$ (kN.m)	$M_r(Exp.)$ (kN.m)
RC	-	35.7	0.85	0.795	29.39	60.62	83.94
HPFRCC	3.5	24	0.85	0.85	84.75	77.89	92.11

As shown in this table, because of strain hardening behavior of HPFRCC material the equivalent depth of compressive stress block (a) and flexural capacity of RH beam are more than RC beam. The difference between theoretical and experimental values in RC beam is about 38.5 %. This difference may be due to post yielding increase in tensile reinforcement forces and tensile part of concrete which has been ignored in theoretical formulation of RC beam. The flexural capacity of RH beam is about 18 % more than experimental value. This difference may be due to post yielding increase in tensile reinforcement forces which was ignored in formulations.

Flexural Capacity of RCH Beams and Maximum Reinforcement Ratio

In RCH beams with tensile HPFRCC layer (Figure 16) flexural capacity can be calculated by Equation (2).

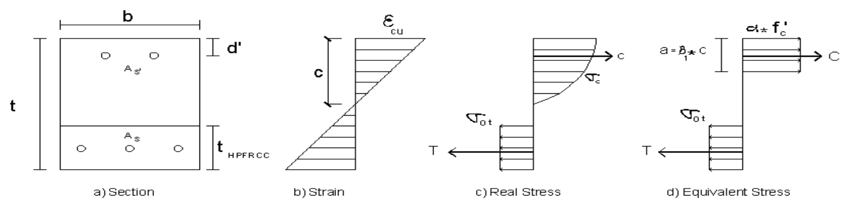

Figure 16 Strain and stress distributions in a flexural rectangular composite section.

$$M_r = \alpha . f_c' . a . b . \left(d - \frac{a}{2} \right) + A_s' . f_y \left(d - d' \right) - \sigma_{0t} . b . t_{HPFRCC} . \left[\frac{t_{HPFRCC}}{2} - (t-d) \right] \tag{2}$$

Maximum reinforcement ratio of these beams can be calculated as shown in Equation (3).

$$\alpha . f_c' . a_b . b + A_s' . f_y - A_s . f_y - \sigma_{0t} . b . t_{HPFRCC} = 0$$

$$a_b = \beta_1 c_b , \varepsilon_{cu} = 0.003, c_b = \frac{630}{630 + f_y} . d$$

$$\frac{\alpha . f_c' \cdot \beta_1 \cdot \frac{630}{630 + f_y} . d \cdot b + A_s' . f_y}{f_y \cdot b \cdot d} = \frac{A_s . f_y + \sigma_{0t} . b . t_{HPFRCC}}{f_y \cdot b \cdot d}$$

$$\rho - \rho' \le \rho_b - \frac{\sigma_{0t}}{f_y} . \frac{t_{HPFRCC}}{d} \Rightarrow \rho - \rho' \le \bar{\rho} \tag{3}$$

where, ρ = tensile reinforcement ratio, ρ' = compressive reinforcement ratio, ρ_b = maximum reinforcement ratio in RC beams and $\bar{\rho}$ = maximum reinforcement ratio in beams with tensile HPFRCC part. As could be seen in Equation (3), the amount of maximum reinforcement ratio in partially tensile HPFRCC beams is less than the corresponding value in normal reinforced concrete beams. Because tensile HPFRCC segment acts as an extra reinforcement and concludes to less maximum reinforcement ratio compared to normal concrete.

Minimum Reinforcement Ratio of RH beams

When the tension reinforcement ratio becomes extremely small in a RC member, the flexural capacity (M_r) becomes smaller than the cracking moment (M_{cr}) and steel bars may yield immediately after cracking and member shows brittle failure mode with only one crack like un-reinforced concrete. Minimum reinforcement ratio in a RH beam ($\rho_{\min}$) can be calculated as discussed below:

$$M_{cr} = M_r$$

$$M_r = \alpha . f'_c . a . b . \left(d - \frac{a}{2} \right) - \sigma_{0t} . b . (h - c) . \left[\left(\frac{h-c}{2} \right) - (h - d) \right], M_{cr} = \frac{\sigma_{0t} \cdot I_g}{y_t} = \frac{1}{6} \sigma_{0t} . b . h^2$$

$$d - \frac{a}{2} = d - \frac{\beta_1 . c}{2} = d - \frac{\beta_1 \cdot \varepsilon_{cu}}{(\varepsilon_{cu} + \varepsilon_y) \times 2} \times d = \left(1 - \frac{\beta_1 \cdot \varepsilon_{cu}}{(\varepsilon_{cu} + \varepsilon_y) \times 2} \right) \cdot d = \gamma \cdot d$$

$$h - c = h - \frac{\varepsilon_{cu}}{(\varepsilon_{cu} + \varepsilon_y)} \times d = \left(1.1 - \frac{\varepsilon_{cu}}{(\varepsilon_{cu} + \varepsilon_y)} \right) \cdot d = \phi \cdot d$$

$$\rho_{\min} = \frac{[0.2 - \phi \cdot \gamma + \frac{\phi^2}{2}] \cdot \sigma_{0t}}{f_y \cdot \gamma} \tag{4}$$

As can be seen in Equation (4), the amount of $\rho_{\min}$ is depended on values of β_1, ε_{cu}, ε_y and σ_{0t}. In the case of a RH beam with σ_{0t} = 5 MPa, the amount of $\rho_{\min}$ lies in the range of 0.25 to 0.3 times in comparison to normal concrete.

CONCLUSIONS

The following conclusions can be reached:

- The ductility ratios of RH structures are more than RCH and RC specimens due to presence of fibers and more ultimate compressive strain of HPFRCC material. In the other hand, ductile behavior for structures is attained by HPFRCC material instead of using tensile reinforcements in RC structures.
- Energy absorption of RH structures is more than RCH and RC specimens.
- Length of cracking in beam of RH frame is more than RCH and RC frame. But in columns, RH frame has the minimum length of cracking.
- HPFRCC is an appropriate material for earthquake resistant structures because of its ductile behavior.

REFERENCES

Bayasi Z., Gebman, M. (2002). Reduction of lateral reinforcement in seismic beam-column connection via application of steel fibers, *ACI Structural Journal*, 99(6): 772–780.

Brandt, A.M. (2008). Fiber reinforced cement-based (FRC) composites after 40 years of development in building and civil engineering, *Composite Structures*, 86(1-3): 3–9.

Chao C.G., Kim Y.Y., Feo L., Hui D. (2012). Cyclic response of reinforced concrete composite columns strengthened in the plastic hinge region by HPFRC mortar, *Composite Structures*, 94(7): 2246–2253.

Fischer G., Li V.C. (2000). Structural composites with ECC, *Proceedings of the ASCCS-6*, Y. Xiao and S.A. Mahin, (eds.), University of Southern California, Los Angeles, CA, pp. 1001-1008.

Fischer G., Wang S., Li V.C. (2003). Design of engineered cementitious composites for processing and workability requirements, *Proceedings, Seventh International Symposium on Brittle Matrix Composites*, pp. 29–36.

Li V.C., Wu H.C. (1992). Condition for pseudo strain-hardening in fiber reinforced brittle matrix composites, *J. App. Mech. Review*, 45(8): 390–298.

Li V.C. (2007). Engineered cementitious composites (ECC) – material, structural, and durability performance, University of Michigan, Ann Arbor, MI.

Maalej M.; Li V.C. (1995). Introduction of strain hardening engineered cementitious composites in design of reinforced concrete flexural members for improved durability, *ACI Struct. Journal*, 92(2).

Maalej M.; Ahmed S.F.U.; Paramasivam P. (2002). Corrosion durability and structural response of functionally-graded concrete beams, *Proceedings, JCI International Workshop on Ductile Fiber Reinforced Cementitious composites (DFRCC), Application and Evaluation*, Japan.

Naaman A.E., Reinhardt H.W. (1996). Characterization of high performance fiber reinforced cement composites, *HPFRCC-2*, 1–24.

Parra Montesinos G.J., Peterfreund S.W., Chao, S.H. (2005). Highly damage-tolerant beam-column joints through use of high-performance fiber-reinforced cement composites, *ACI Struct. Journal*, 102(3): 487–495.

Shihada S. (2011). Effect of polypropylene fibers on concrete fire resistance, *J. Civil Eng. and Management*, 17(2): 462–470.

A NEW REPLACEABLE BRACING SYSTEM

S.V. Kohnsari[1], G.B. England[2], M. Moradi[3], H. Farahani[4], D. Zarei[5], and M. Shahsavar-Gargari[6]

ABSTRACT

A new bracing system with new features somewhat different from those of the existing ones was devised and is presented. These features comprise some of the advantages of eccentric bracing systems including their ability to dissipate energy through bending of flexural elements while lacking some of the disadvantages of such systems including their inability of being replaced upon damage during events such as earthquakes, etc. While in traditional types of braces, including both concentric and eccentric ones, braces are under axial loading, in this new system they work in a bending capacity. As a result, the sort of flexibility which is introduced in the system in the presence of eccentric braces (definitely at the price of forcing the potential damage to occur and be concentrated at the girders/beams to which such braces are connected), is now provided by the braces and at the price of sacrificing them. Therefore, if the level of damage is such that the damaged element is no longer usable, the replacement of the braces is a more viable and economically justifiable than that of the girders. Moreover, since girders, as part of the deck/floor system, are normally engaged with other elements such as stringers/joists and/or slabs, their replacement may not be practically possible at all. Such bracing systems, called Broken Beam Bracing System (BBBS), have the potential of being used in building as well as industrial structures as originally-used elements or in a retrofit/repair capacity.

Keywords: *cyclic loading, energy dissipation, replaceable bracings, retrofitting, structural bracing systems*

INTRODUCTION

As efficient elements for controlling the deflections of structures against various lateral loads braces have a long history of service. While initially they were used to resist wind, they gradually found their way into the seismic design of structures as efficient means of controlling the lateral drift. Here they regulate the performance of the structure under dynamic cyclic earthquake induced forces.

So far, braced frames have been divided into two major categories, *viz.* Concentrically-Braced Frames (CBFs) and Eccentrically-Braced Frames (EBFs)—the former have high elastic stiffness and more rigid behaviour hence react poorly to cyclic loading. The latter have more flexible nature and good response to such loading [Bruneau et al. 1998]. EBFs which have

1 Department of Civil Engineering, Sharif University of Technology, P.O. Box 11155-9313, Tehran 14588-89694, Iran, tel: +98-21-8880 3629; email: vaheed_k@yahoo.co.uk.
2 Department of Civil & Environmental Engineering, Imperial College London, London SW7 2BU, UK, tel: +44-20-7594 5989; email: g.england@ic.ac.uk.
3 Department of Civil Engineering, Sharif University of Technology, email: mahmoudmoradi@yahoo.com.
4 Department of Civil Engineering, Sharif University of Technology, email: hosein_farahani85@yahoo.com.
5 Department of Civil Engineering, Sharif University of Technology email: da_zarei@yahoo.com.
6 Department of Civil Engineering, Sharif University of Technology email: shahmorad@yahoo.com.

become popular during the past two decades have the disadvantage of using the beam (to which the braces are connected) in a *sacrificial capacity*. Therefore, if the level of incurred damage is so high that it requires replacement, due to the engagement of the beam with the floor system (slab, joists/stringers) such replacement is basically neither technically viable nor economically justifiable.

Taking advantage of the concept of EBFs, a geometrically similar, but different in nature, system has been developed which seems to have the advantages of eccentric braces and lack their major disadvantage, *viz. irreplaceability.* Similar to eccentric braces and unlike concentric ones, they add to the weight of the structure, but what one receives is an improved performance under cyclic loading with better-shaped hysteresis loops, as demonstrated through limited number of test described in this paper.

Description of the Broken Beam Bracing System (BBBS)

Developed by the first author, the new bracing system comprises two bending-axial (beam-column) elements connected to one another through a semi-rigid joint. It resembles stair framing—in fact stair framing systems work in the same capacity. Figure 1(a) depicts a portal frame with hinge joints equipped with such system. Apparently, in such a case a minimum rigidity for the joint between the two pieces of the bracing system is required in order to maintain the stability of the frame and also limit its drift to the permissible amount required by the code. Figure 1(b) shows the detail of the semi-rigid connection between the two segments of the brace. In this Figure it has been attempted to show the fact that there is not (indeed should not be) any interaction between the beam and the horizontal segment of the brace. Moreover, the semi-rigid behaviour of the connection between the two segments of the brace is emphasized. Figure 1(c) reveals the *'two-force'* nature of the brace that emanates solely from relative overall displacements of the two ends of the brace; there being no other loading.

The following simple statics calculations show that

$$f_{AD} = \frac{f_{CD}}{\cos\alpha} = \frac{P}{\cos\alpha}$$

$$f_{DE} = f_{AD}.\sin\alpha = \frac{P}{\cos\alpha}.\sin\alpha = P.\tan\alpha = P.\frac{H}{L}$$

As it is shown in Figure 1(c), since the maximum distance between various points on the brace and the line connecting its two ends occurs at C and is equal to *h,* therefore, the maximum bending moment occurs at C,

$$M_{max} = M_C = f_{DE}.L_2 = P.\frac{H}{L}.(L - L_1) = P.\frac{H}{L}.\left(L - \frac{H}{\tan\beta}\right)$$

Here, it can be easily seen that the bending moment is a minimum when $\tan\beta$ is a minimum, i.e., when the horizontal segment of the brace diminishes and the brace turns into a straight member and works in an axial capacity, or

$$\beta \to \alpha$$

In other words, when it becomes a traditional *'Concentric Diagonal Bracing'* with no moment developing in it. And, this is very well in line with 'common sense.' On the other hand, bending moment becomes a maximum when $\tan\beta$ is a maximum, i.e., when

$$\beta \to \pi / 2$$

In other words, when the two segments of the brace are normal to one another and in fact it turns the fame into a '*Moment-Resisting Frame.'* Therefore, it is not false if we say that this bracing system, BBBS, works in such a capacity that turns the frame into something between a Concentrically-Braced Frame (CBF) and a Moment-Resisting Frame (MRF). As a result, it should be expected to see some features of the two systems being combined in this system. However, comparing with EBF systems, (despite their positive features which have made them very popular during past two decades), where damage is incurred in the main beam to which the braces are attached the new system (BBBS) should provide considerable benefits.

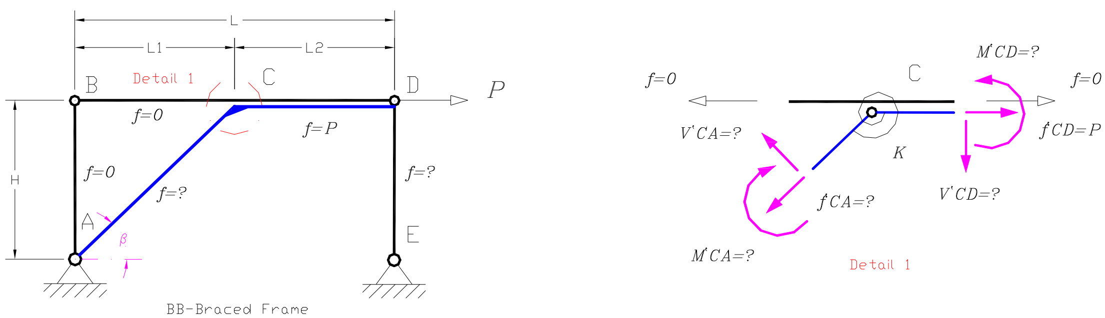

(a) **(b)**

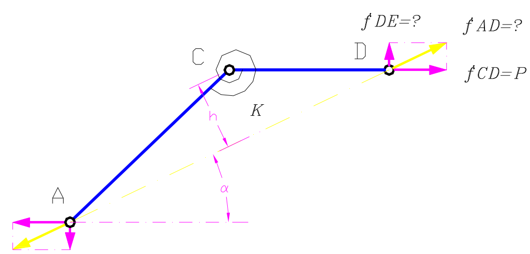

(c)

Figure 1 The Broken Beam Bracing System (BBBS) and its geometric and mechanical details: (a) The brace, shown in blue, fitted into a portal frame; (b) Detail 1 and the semi-rigid joint between the two segments of the brace and the lack of physical contact between the beam and the brace; and (c) the free-body diagram of the brace and the decomposition of its forces and the largest moment arm (*h*) which leads to the maximum bending moment occurring at the brace knee.

Experimental Program

To assess the performance of the system an experimental program was conducted. Since it is in a cyclic loading context that the performance of the new bracing system is intended to be adopted it would be meaningful to carry out the tests under cyclic loading. However, since this type of bracing has not been used in the past, there seemed to be no specifications for testing them.

Therefore, (due to the similarity which exists between the bending behaviour of this system and that of the links of EBFs), it was decided to use the instructions given by AISC for testing *Link-to-Column Connections* [2005]. Based on these instructions, the total link rotation angle, γ, is specified on a cycle by cycle basis. The corresponding loads are then monitored. Details of the recommended rotations for each cycle of testing are given in Table 1.

The test facility shown schematically in Figure 2 was used to test three braces of different section dimensions, *viz.* IPE100, HE-A100, and 2UNP100. These are standard beam, light column and channel sections, respectively, based on DIN-1025 or EURONORM-53-62 standards. In order to convert the rotation angles *γ,* given by AISC [2005], to linear displacements of the loading equipment (machine), Δ (Figure 3), the following approximate formulae were used,

$$\Delta 1 = 2L.\cos(30 - \gamma/2) - 2L.\cos 30$$

$$\Delta 2 = 2L.\cos 30 - 2L.\cos(30 + \gamma/2)$$

$$L = 580\,\text{mm}\,.$$

Approximate, in this sense means that a hinge connection is assumed to form at the joint between the two segments. Due to the differences between the geometries of the two situations, tensile and compressive, their deformations (deformation amplitudes) are different and this difference increases as the angle of rotation increases (see Table 1). All the three specimens were subjected to the above loading pattern, each up to a stage where signs of severe destruction were observed. Due to the diversity of the sections of the specimens, different types of response were observed.

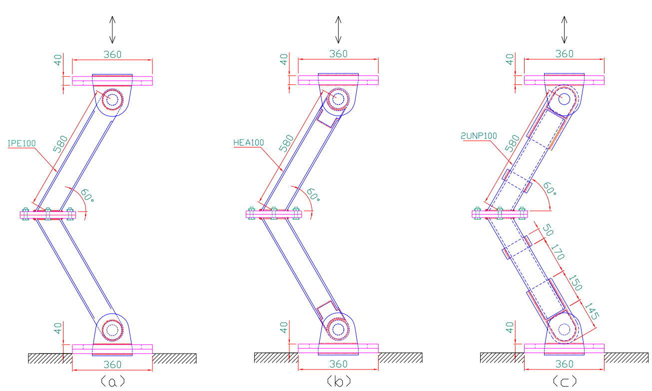

Figure 2 The test assemblies designed and fabricated to enable the authors to apply cyclic loading to the specimens of the bracing system. Brace segments were fabricated from (a) IPE100, (b) HE-A100, and (c) 2U100 sections.

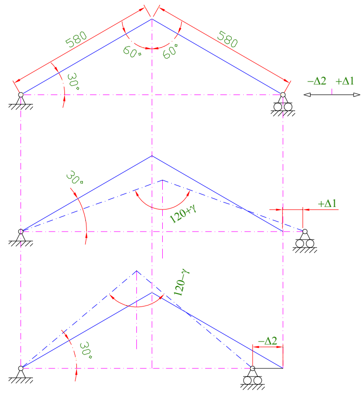

Figure 3 **The idealized model of the bracing system subjected to linear displacements in tension (Δ1) and compression (Δ2) to create the rotation angles prescribed by AISC [2005] between the two segments.**

Table 1 **The amplitudes of displacement cycles in tension and compression worked out based on the instructions given by AISC [2005] for the rotation of the links of EBFs and the simple model of Figure 3, together with the number of cycles of each stage.**

Stage	No. of Cycles	Rotation Angle	Tensile Amplitude	Compressive Amplitude
		γ (radian)	Δ1 (mm)	Δ2 (mm)
1	6	0.00375	1.0857	1.0893
2	6	0.005	1.4469	1.4531
3	6	0.0075	2.1679	2.1821
4	6	0.01	2.8874	2.9125
5	4	0.015	4.3217	4.3782
6	4	0.02	5.7497	5.8501
7	2	0.03	8.5867	8.8127
8	1	0.04	11.3983	11.8001
9	1	0.05	14.1846	14.8124
10	1	0.07	19.6806	20.9111
11	1	0.09	25.0742	27.1082
12	1	0.11	30.3649	33.4030
13	1	0.13	35.5520	39.7949
14	1	0.15	40.6351	46.2833
15	1	0.17	45.6138	52.8675
…	1	…	…	…

First Test: Using IPE100 Section

The section used for the bracing segments, IPE100, is an ordinary I section with small flange width compared to the overall section height. As a result, the ratio of the moments of inertia of the section about its two principal axes is

$$r = \frac{I_{xx}}{I_{yy}} = \frac{171}{15.9} = 10.75$$

Therefore, it was anticipated that at some point during the test signs of lateral buckling could occur. Indeed, as the test proceeded from the 11th stage the specimen started to undergo *lateral movement* with its maximum at the joint between the two segments of the brace. The effect of this phenomenon was a substantial drop in the compressive test load *(strength degradation).* Towards the end of the 14th stage the extent of lateral deformations increased to a level that was unacceptable to the test apparatus and the test was therefore halted. Figure 4 shows the first specimen before the test, while Figures 5, 6, and 7 show its side views at later stages as gradually the lateral buckling occurred during compressive half-cycles.

Figure 4 The first specimen, with IPE100 sections, before the test.

Figure 5 Side view of the first specimen showing out-of-plane displacements (lateral buckling) of the specimen.

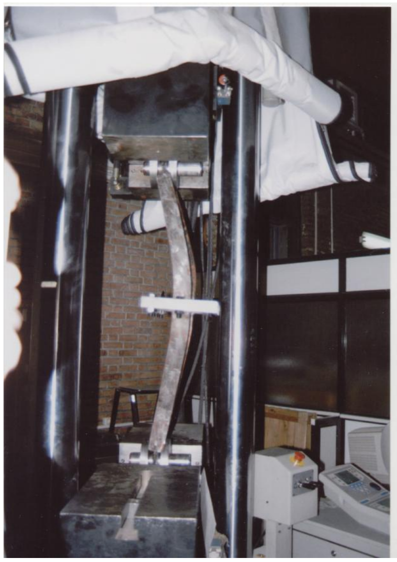

Figure 6 First specimen at a later stage where more out-of-plane displacements have emerged.

Figure 7 Side view of the first specimen at the end of the test with maximum observed out-of-plane displacements.

Although this test was terminated due to pronounced 'out-of-plane' buckling, the brace could still be used provided lateral deformations can be restricted. Figure 8 illustrates how this might be achieved, by the provision of additional bracing from adjacent frames. Some extra costs would then be involved, but overall the system could still be economically justifiable. The hysteresis loops of this test, first test, are depicted in Figure 9. The effect of buckling is clearly apparent in Figure 9 where the maximum compressive force is much less than the maximum tensile force during the latter cycles of the test.

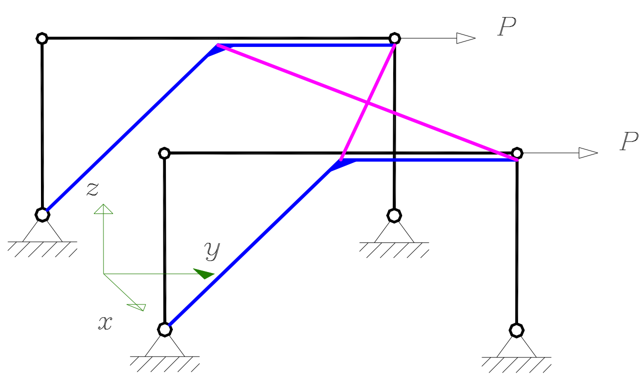

Figure 8 A suggested extra bracing system (in horizontal plane in magenta) to prevent the devised bracing system from having out-of-plane (lateral) deformations (buckling).

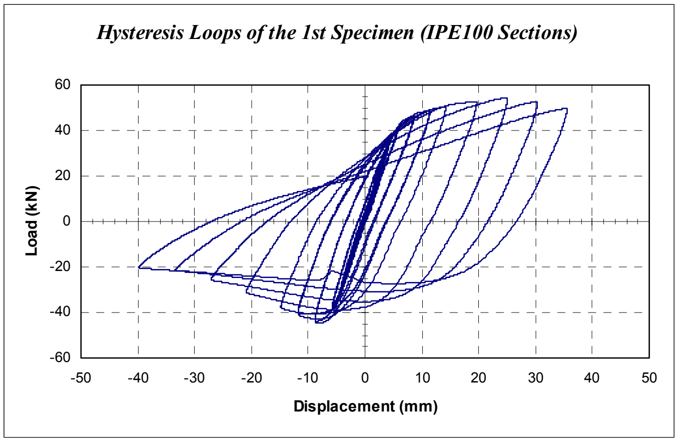

Figure 9 Hysteresis loops of the first test assembly with IPE100 sections used for the two segments of the devised Broken Beam Bracing System.

Second Test: Using HE-A100 Section

HE-A is a light wide flange section compared to HE-B and HE-M, which are medium-weight and heavy wide flange sections. The real height of HE-A100 is 96 mm while its flange width is 100 mm. The ratio of the moments of inertia about the two principal axes of this section is

$$r = \frac{Ixx}{Iyy} = \frac{349}{134} = 2.60$$

Out-of-plane buckling that was observed in the first test should not be observed in this test. Indeed no sign of lateral buckling was observed. Failure of the weld of the bracing to the endplate at the joint between the two segments halted this test. Since the overall geometry of the specimen was the same as that of the previous test, the same amplitudes for the displacements of each stage of loading were used (see Table 1). The much stronger cross section compared with that of the first test led to higher levels of resistance (load) being observed. The number of cycles to premature failure of the end plate welds was the same as for Test 1, *viz*. 40 cycles. The specimen's increased stiffness and strength were not therefore completely exploited.

Figure 10 shows the specimen before the test, whereas Figures 11 and 12 depict the weld failure and the crack that developed at the joint between the weld and the endplate. The local buckling which occurred at the lower flange of the upper segment in the vicinity of the endplate is shown in Figure 13. The hysteresis loops of this test, second test, are depicted in Figure 14.

Figure 10 The second specimen, with HE-A100 sections, before the test.

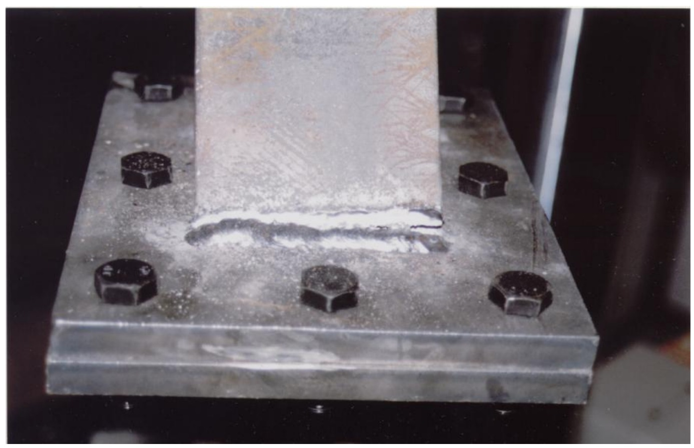

Figure 11 Developed cracks at the joint between the upper segment and its endplate caused by *'lack of fusion.'*

Figure 12 Developed cracks at the other side of the upper segment of the second test assembly with HE-A100 sections.

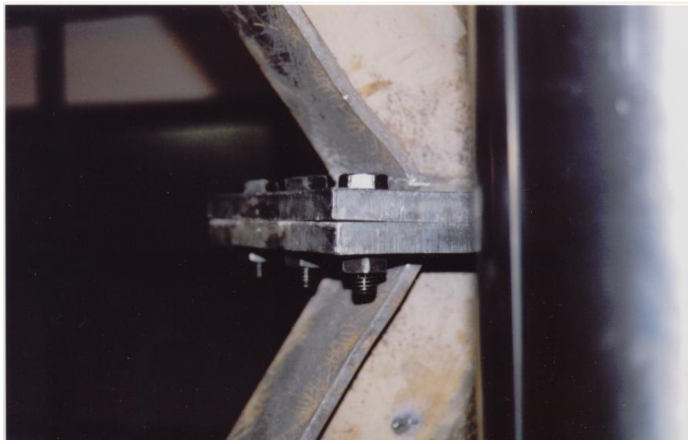

Figure 13 Local buckling of lower flange of the upper segment of the second test assembly with HE-A100 sections.

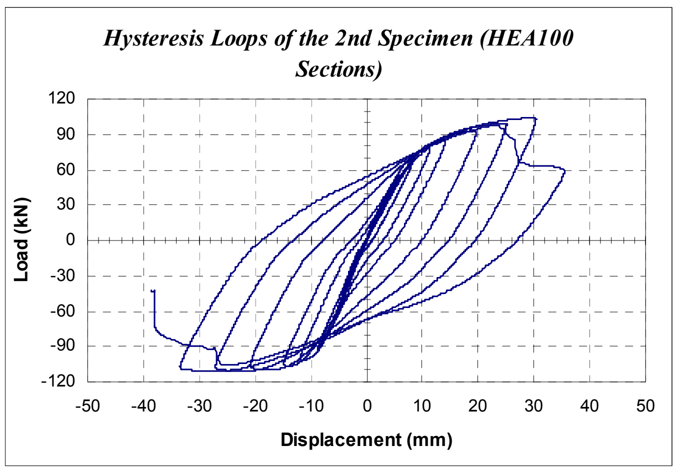

Figure 14 Hysteresis loops of the second test assembly with HE-A100 sections used for the two segments of the devised Broken Beam Bracing System.

Third Test: Using 2UNP100 Sections

As an alternative to the previous sections and in order to investigate the behaviour of a fairly commonly-used section for bracing systems, a double channel section was used. UNP100 is a Normal U Profile with 100 mm height, 50 mm flange width, 6 mm web thickness and 8.5 mm average flange thickness. For this double section (with 10 mm clear distance between their flange edges [see Figure 15]), the ratio of the moments of inertia around principal axes is

$$r = \frac{I_{xx}}{I_{yy}} = \frac{412}{480} = 0.858$$

This low ratio precluded any lateral buckling from occurring and the test was terminated when one of the welds between the element ends and the endplate fractured. As in previous tests the same displacement inputs (Table 1) were employed here.

The overall front view of the specimen is shown in Figure 16 while its side view is demonstrated in Figure 17. The developed crack in the weld of the brace-segment/brace-endplate is shown in Figure 18. The hysteresis loops of this test, third test, are depicted in Figure 19. Observation reveals considerably less ductility and less energy dissipation, cycle by cycle, compared to the previous tests. This test was halted in the 36th cycle.

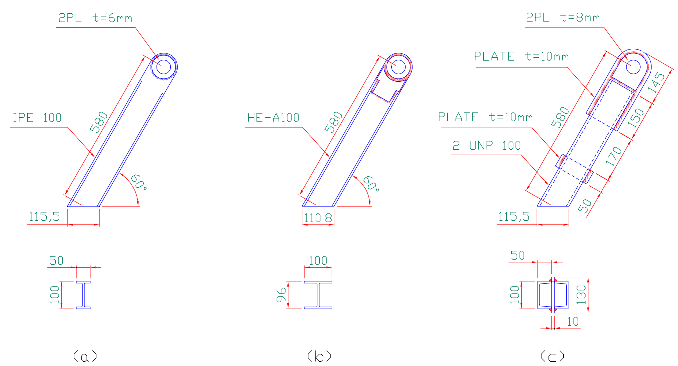

Figure 15 Details of the members of various test assemblies and their cross sections.

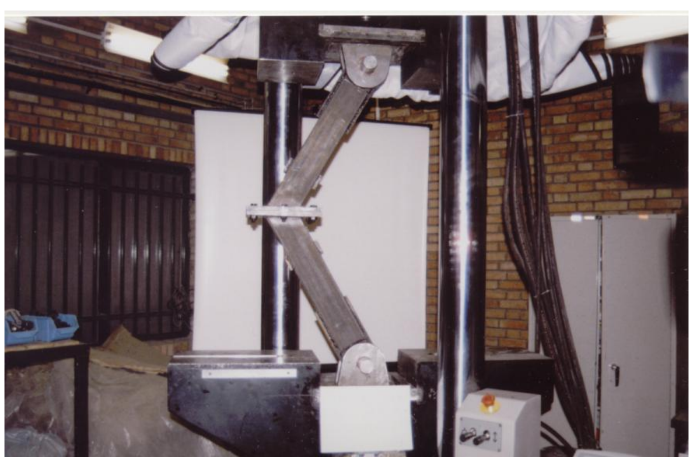

Figure 16 Overall front view of the third specimen with 2UNP100 sections attached together with 10 mm thick battens.

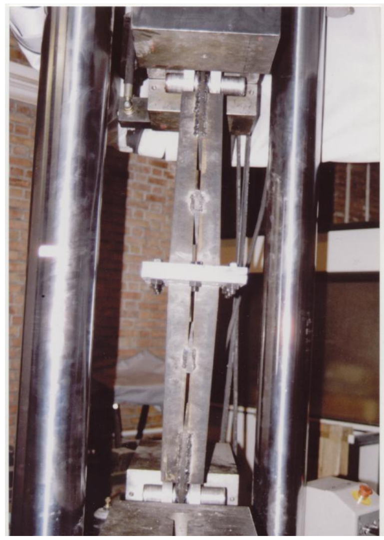

Figure 17 Side view of the third test assembly with 2UNP100 sections attached together with 10-mm batten plates—one at the middle of each segment and one being the eye-bar of the hinge connection at one end of each segment.

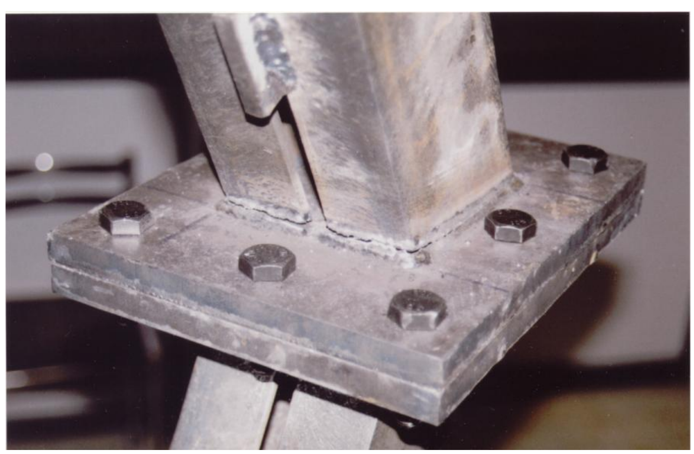

Figure 18 The developed cracks and the detachment of the upper segment and its endplate due to *'lack of fusion.'*

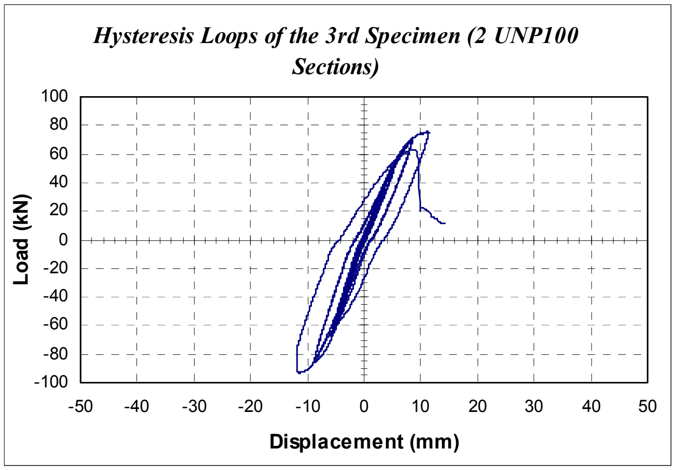

Figure 19 Hysteresis loops of the third test assembly with 2UNP100 sections used for the two segments of the devised Broken Beam Bracing System.

DISCUSSION

In order to have a proper judgment on the performance of this system, the dissipated energy for each loop (cycle) of the hysteresis curves of each test is worked out. This figure together with the total dissipated energy of each stage and also its cumulative value at the end of each stage are shown in Tables 2, 3, and 4 for the first, second, and third specimens, respectively. Moreover, for each stage of loading, the average dissipated energy per cycle is worked out and shown in these Tables. These results provide the reader with useful information to make comparisons between the different test specimens.

Although only three tests were carried out on the specimens of this type of bracing system, each was beneficial in revealing some facts about its performance. The first test was beneficial in that it showed the vulnerability of sections with low minor-axis stiffness to lateral buckling. However, despite severe out-of-plane deformations the amount of energy dissipated in each cycle of loading gradually increased as the amount of stroke increased, eventually reaching a value greater than for the other sections. This is an indication of the effectiveness of the slender elements to deform appreciably during every cycle.

The use of stiffer sections led to improvements in the cyclic behaviour of the system and dissipated more energy than the specimen of test 1, as far as the fifth loading stage and again after stage 11 when lateral buckling was observed in test 1. Due to the premature failure of the end plate welds in test 2 the final capacity of the section for the dissipation of energy was not realized.

As far as the authors are concerned, the *lack of fusion phenomenon,* about which many welding experts have already warned [Salmon and Johnson 1990], was the main cause of failure for the second and third specimens. Here, the two joining parts, the brace segment and the endplate, which in a proper welding practice should coalesce with each other and the melted electrode, had not been fused together. The molten electrode had just been stuck to the two *'un-*

melted' joining parts like an applied paste, creating a very poor bond. With a standard welding practice, this should be easily solved. Regarding the third specimen, this phenomenon existed in a much more pronounced manner, hence causing the termination of the test at an earlier stage compared with the second test. Without these premature failures these two specimens were expected to show much higher efficiency in absorbing and dissipating energy under cyclic loading and therefore be suitable for use as braces in buildings or installations built and used in environments prone to experiencing cyclic loadings such as wave or earthquake.

All of the tests suffered to some extent from premature weld failures which prevented the full plastic moment capacity of the element sections from being realized.

Table 2 The energy dissipation characteristics of the first specimen of BBBS using IPE100 profiles for the sections of the brace segments.

Stage	Cycle	Dissipated Energy per Cycle (j)	Dissipated energy per Stage (j)	Cumulative Dissipated energy (J)	Average Dissipated Energy per Cycle of each Stage (j)
1	1	1.29	5.38	5.38	0.90
	2	0.92			
	3	0.79			
	4	0.84			
	5	0.78			
	6	0.77			
2	1	1.64	7.90	13.28	1.32
	2	1.26			
	3	1.33			
	4	1.22			
	5	1.19			
	6	1.27			
3	1	4.31	18.03	31.31	3.01
	2	2.98			
	3	2.83			
	4	2.64			
	5	2.64			
	6	2.64			
4	1	8.19	34.81	66.12	5.80
	2	5.89			
	3	5.28			
	4	5.20			
	5	5.09			
	6	5.17			
5	1	32.02	96.66	162.78	24.16
	2	23.11			
	3	21.09			
	4	20.44			
6	1	82.09	306.14	468.91	76.53
	2	78.38			
	3	73.49			
	4	72.17			
7	1	332.10	692.43	1161.34	346.21
	2	360.33			
8	1	696.04	1424.32	2585.66	712.16
	2	728.28			
9	1	1051.98	1051.98	3637.64	1051.98
10	1	1732.50	1732.50	5370.14	1732.50
11	1	2245.29	2245.29	7615.43	2245.29
12	1	2542.25	2542.25	10157.68	2542.25
13	1	2779.36	2779.36	12937.04	2779.36
14*	1	269.79	269.79	13206.83	269.79

*) Incomplete Cycle

Table 3 The energy dissipation characteristics of the second specimen of BBBS using HE-A100 profiles for the sections of the brace segments.

Stage	Cycle	Dissipated Energy per Cycle (j)	Dissipated energy per Stage (j)	Cumulative Dissipated energy (J)	Average Dissipated Energy per Cycle of each Stage (j)
1	1	1.68	7.94	7.94	1.32
	2	1.47			
	3	1.21			
	4	1.17			
	5	1.18			
	6	1.24			
2	1	1.90	10.82	18.76	1.80
	2	1.84			
	3	1.91			
	4	1.74			
	5	1.75			
	6	1.68			
3	1	3.67	20.11	38.87	3.35
	2	3.44			
	3	3.31			
	4	3.31			
	5	3.20			
	6	3.17			
4	1	5.88	31.69	70.56	5.28
	2	5.31			
	3	5.26			
	4	5.01			
	5	5.11			
	6	5.12			
5	1	15.76	51.37	121.93	12.84
	2	12.18			
	3	11.80			
	4	11.62			
6	1	33.83	112.29	234.22	28.07
	2	26.73			
	3	25.94			
	4	25.79			
7	1	192.16	325.60	559.82	162.80
	2	133.44			
8	1	588.25	588.25	1148.07	588.25
9	1	1093.39	1093.39	2241.46	1093.39
10	1	2447.00	2447.00	4688.46	2447.00
11	1	4055.66	4055.66	8744.12	4055.66
12	1	5754.54	5754.54	14498.65	5754.54
13*	1	7584.39	7584.39	22083.05	7584.39

*) Incomplete Cycle

Table 4 The energy dissipation characteristics of the third specimen of BBBS using 2UNP100 profiles for the sections of the brace segments.

Stage	Cycle	Dissipated Energy per Cycle (j)	Dissipated energy per Stage (j)	Cumulative Dissipated energy (J)	Average Dissipated Energy per Cycle of each Stage (j)
1	1	1.28	6.10	6.10	1.02
	2	1.10			
	3	0.94			
	4	0.99			
	5	0.88			
	6	0.91			
2	1	1.72	9.33	15.43	1.55
	2	1.63			
	3	1.55			
	4	1.50			
	5	1.43			
	6	1.49			
3	1	4.43	21.58	37.01	3.60
	2	3.58			
	3	3.51			
	4	3.30			
	5	3.41			
	6	3.35			
4	1	8.62	42.15	79.15	7.02
	2	7.16			
	3	6.80			
	4	6.58			
	5	6.57			
	6	6.41			
5	1	33.76	99.59	178.74	24.90
	2	23.40			
	3	21.55			
	4	20.88			
6	1	84.30	274.04	452.78	68.51
	2	66.43			
	3	62.34			
	4	60.97			
7	1	341.34	651.33	1104.11	325.66
	2	309.99			
8	1	892.84	892.84	1996.95	892.84
9*	1	541.28	541.28	2538.23	541.28

*) Incomplete Cycle

CONCLUSIONS

Using the limited tests reported in this paper, the following conclusions, with some degree of caution, can be drawn.

- The hysteresis loops of the specimens have demonstrated the suitability of the bracing system for energy dissipation under cyclic loading.
- As in other types of bracing system, more traditional concentric and more modern eccentric ones, the role of the shape of the cross section is quite important. Using sections with large difference in their moments of inertia about their two principal axes makes the system susceptible to lateral buckling if the angle between the two segments of the brace is fairly large and to in-plane buckling if the angle is small.
- As in other types of bracing system, the role of connections of the braces to the frame should be considered though in this investigation such effects were not studied.
- Since the maximum bending moment in the brace occurs at the bent (breaking point), the design and fabrication of the joint between the two segments have a crucial role in the behaviour as well as service life of the system. In this regard the quality of the welds must not be compromised—full fusion welds should be used for these connections and their elements.

ACKNOWLEDGMENTS

Financial and technical support of this project by Sharif University of Technology is gratefully acknowledged.

REFERENCES

AISC (2005). *Seismic Provisions for Structural Steel Buildings*, American Institute of Steel Construction, Chicago, IL.

Bruneau M., Uang C.-M., Whittaker A.S. (1998). *Ductile Design of Steel Structures*, McGraw-Hill, Boston, MA.

Salmon C.G., Johnson J.E. (1980). *Steel Structures, Design and Behavior*, 2nd ed., Harper & Row, Publishers, N.Y.

RECENT RESEARCH ON SEISMIC BEHAVIOR OF STEEL STRUCTURES COMMONLY USED IN IRAN

Ali Akbar Aghakouchack[1]

ABSTRACT

Steel structures are widely used in construction of medium rise buildings in urban areas in Iran. This paper presents a review of the results of recent research carried out on the seismic behavior of some types of steel structures commonly used in Iran. First part of the paper is devoted to a special type of beam to column connection called Khorjeeni (saddle like). After presenting the results of cyclic tests on six samples of connection, the problem of ultra-low cycle fatigue is discussed and an algorithm is proposed to model this phenomenon in finite element models. The algorithm is validated and is used to model the crack initiation and growth in Khorjeeni connections. Based on the results of experiments and numerical analysis, some empirical formulae are developed to define characteristic values of behavior curve for this type of connection. The second part of the paper discusses the rigid connection between I beams and columns composed of double sections. Results of experiments and numerical analysis show that behavior of panel zone in this type of connection is different from that of ordinary connections of I beam to H column. Therefore a new model is developed to describe this behavior. Finally in the last part of the paper the problem of rigid connection between I beam and box column is discussed. For this type of connection, a new configuration which does not need an internal continuity plate is proposed. The behavior of this connection is compared to that of a direct widened flange connection for two types of uniaxial and biaxial loading. Using the PEEQ index for predicting initiation of ductile fracture, it is shown that the new configuration can sustain more cycles of loading and offers more superior performance in terms of plastic hinge formation.

INTRODUCTION

Steel structures are widely used in construction of medium rise buildings in urban areas in Iran. Chapter 10 of the Iranian National Building Code (INBC) [2006], which is devoted to design of steel structures, includes a section to define specific provisions for seismic design of this type of structures. Parts of the provisions are similar to those existing in international design codes; however some parts are modified to address specific needs of the country. In general braced frames and moment resisting frames are recommended for seismic design of new buildings. On the other hand during past decade, a national program for seismic rehabilitation of public buildings, especially schools, has been ongoing. This program has once again focused the attention of technical community on frames in which a specific type of connection called Khorjeeni (saddle like) connection is used. Although this type of frame in not currently recognized in the INBC, quite a number of existing buildings in Iran are composed of them.

[1] Professor of Structural Engineering, Faculty of Civil and Environmental Engineering, Tarbiat Modares University, Jalal Ale Ahmad Ave, P.O. Box 14115-143, Tehran, Iran.

This paper presents a review of the results of recent research carried out on the seismic behavior of some types of steel structures commonly used in Iran.

SADDLE-LIKE CONNECTIONS

General

Saddle-like connections are formed when the beams are not cut at their intersection with columns. The beams by-pass the columns continuously and are connected to them using top and bottom angles (Figure 1). This type of connection provides some benefits, such as ease of construction and superior behavior under gravity loads, however it has some disadvantages that can cause significant damage to the structure when subjected to seismic loads. Past studies have shown this connection is a semi-rigid connection; but its behavior does not match standard semi-rigid connections for which design guidelines are found in literature. In order to improve the behavior of saddle-like connections and provide guidelines for proper design of this type connection, a few years ago an official guideline document was published [Management and Planning Organization 2006], in which by changing the details of the connection, it is transformed to either a simple (Scissor like) connection or a fully rigid one. These guidelines may be used for design of new structures, however for existing structures in which the traditional type of details are used, in the process of seismic evaluation and rehabilitation it is necessary to have typical behavior curves and acceptance criteria for different levels of structural performance. The following sections report an attempt to address this need.

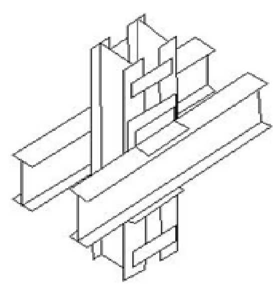

Figure 1 Traditional saddle-like connection.

Experimental Study

In order to study the behavior of traditional saddle-like connection to cyclic loads, six specimens were tested in laboratory. Table 1 shows the details of these specimens. The details were selected based on sections, which are normally found in medium rise buildings in Iran. The test set-up is shown in Figure 2. The loading protocol is shown in Figure 3.

During the tests the applied moment to the connection as well as relative rotation between the beam and box section representing the column was measured using appropriate instrumentation. As the applied moment to the connection increased, some local inelastic deformation in angles and flanges of the beam was observed. However before a general plastification of the beam section cracks started to initiate in welds connecting the angles to beam and column. These cracks then grew along the length of the weld and as a result the moment resisting capacity of the connection decreased. The cracks usually propagated at the connection of top angle with beam initially and then cracks were also observed in connection of bottom angle with beam. Cracks were also observed in the welds connecting the top and bottom angles with column usually in a later stage. Figure 4 shows a sample of cracks in top angle of a specimen. Details of experiments and the results may be found in Amiri [2012].

Table 1 Details of experimental specimens.

No.	Bottom angle	Top angle	Beam Section	Angle length (cm)
T1	100*100*10	80*80*8	IPE180	10
T2			IPE180	15
T3			IPE180	20
T4	120*120*12	100*100*10	IPE220	10
T5			IPE220	15
T6			IPE220	20

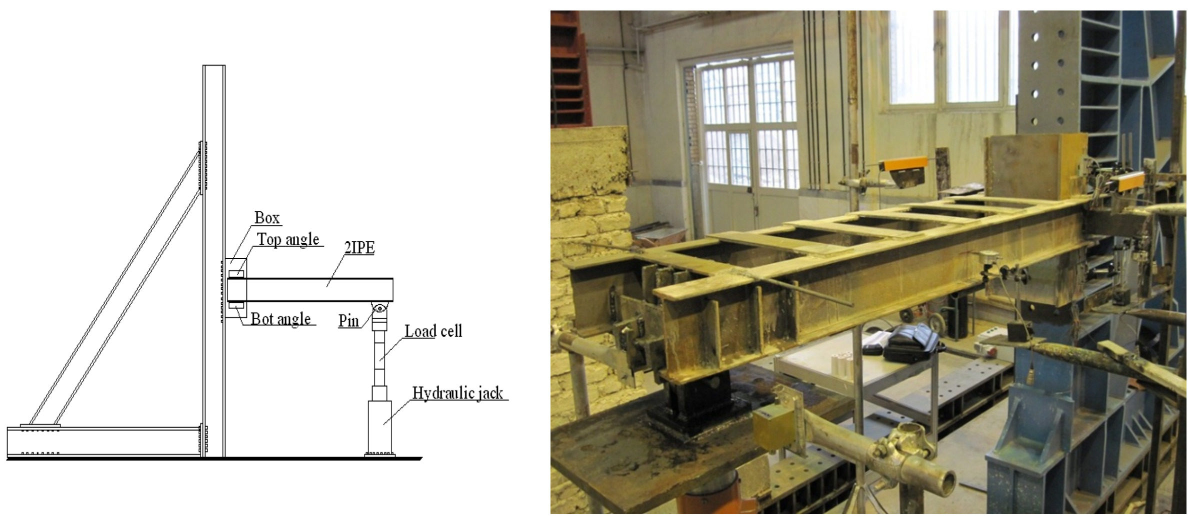

Figure 2 Test set-up.

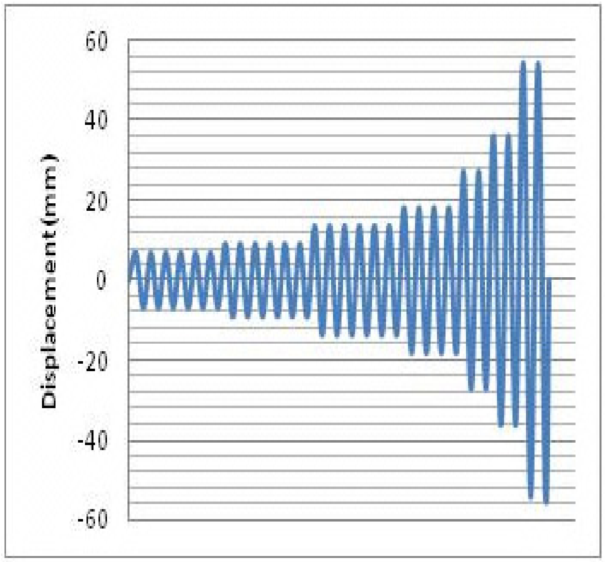

Figure 3 Loading protocol.

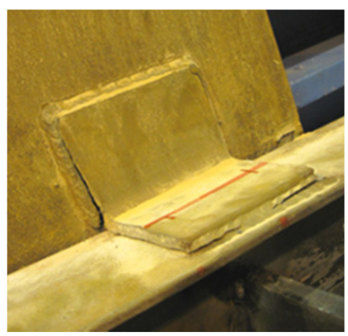

Figure 4 Cracks in welds connecting the top angle to beam and column.

Based on the results of experiments and FEMA recommendations [1997] the backbone curves, and the rotation corresponding to the different performance levels were determined. Figure 5 shows the hysteretic and backbone curves obtained for the specimens. In this figure the point in which a visible crack was found in the specimen is marked with a star. In general it was found that due to detailing of saddle-like connection initiation of crack in not the end of life for the connection and it is capable of carrying further deformation at a reduced moment. Based on these results more detailed investigation of the behavior of connection was planned using finite element simulation. Since the dominant mode of capacity reduction in these connections was found to be ductile crack initiation, propagation and fracture in the welds, a method was needed to simulate this phenomenon in the finite element model.

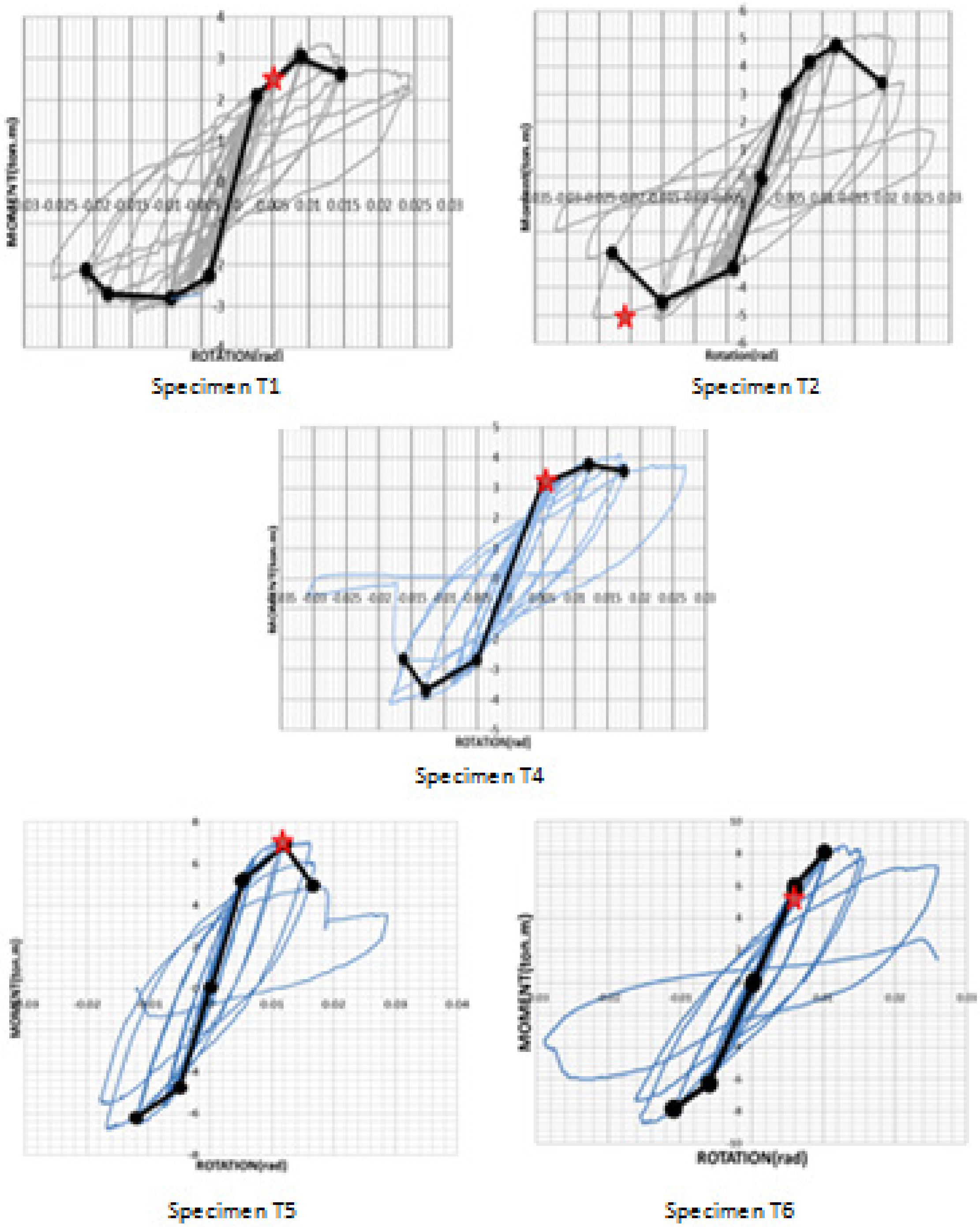

Figure 5 Hysteretic and backbone curves of tested specimens.

Ultra Low-Cycle Fatigue Modeling

Traditional high- and low-cyclic fatigue life estimation methods such as □K and □J have been mainly developed based on the assumptions of the presence of initial sharp cracks and also small scale yielding. However, when a steel structure is subjected to seismic loads, its components experience a loading history called ultra-low cycle fatigue (ULCF) whose effect is completely different in nature. In this kind of fatigue, the facture initiates due to a few (generally less than 20) cycles of large plastic strains (several times the initial yield strain). Moreover, the assumption of initial sharp cracks is subjected to considerable uncertainty in these cases. Thus the traditional fracture mechanics approaches are not so practical for treating the ULCF.

There are several methods for predicting crack initiation under ultra-low cycle fatigue, which are able to resolve these shortcomings (see, e.g., Tateishi et al. [2008; 2007]; Xue [2008]; Hommel and Meschke [2010]; Kuroda [2001]; Kanvinde and Deierlein [1995]). Among them, the micromechanically based cyclic void growth model (CVGM) introduced by Kanvinde and Deierlein [1995] is one of the newest ones proposed. They were initially developed it for the prediction of fracture initiation under monotonic loads, however it was subsequently extended to cyclic loads based on the underlying mechanism of microvoids growth and coalescence (Anderson [1005]). Afterwards, the accuracy of the method has been verified in several studies (Kanvinde [2004]; Myers [2009]).

The CVGM assumes that fracture initiates whenever a specific criterion is satisfied over a characteristic length (of order of 0.1 mm). However in many tests conducted on steel components, the crack initiation did not coincide with the final failure, i.e., the components could continue carrying loads thereafter. For example, in the tests done on column-to-base plate connections, cracks initiate quite earlier than the eventual failures (Myers [2009]; Fell et al. [2006]). Hence solely considering the crack initiation is not adequate for simulating the behavior of some components of steel structures and, for the cases in which the crack propagation phase has comparable share in the fatigue life, both phases shall be concurrently accounted for.

Numerical modeling of crack initiation and propagation in steel structures under monotonic loads has been the subject of many researches. Chen and Lambert [2003] implemented the physically based Gurson-Tevergaurd model and handled the problem within the framework of continuum damage mechanics (CDM). Xue and Wierzbicki [2008] also used damage plasticity theory for modeling ductile fracture initiation and propagation. Lequesne [2009] employed cohesive elements to model crack propagation in steel moment connections. Huang [2009] and Uriz and Mahin [2004] are among the few investigators who have studied details of crack propagation in steel structures under ultra-low cyclic loading (ULCF). They implemented a continuum damage plasticity model in the commercial LS-DYANA software to simulate the crack propagation in concentric bracings.

When steel experiences cyclic loads, cracks initiate at critical sites based on the underlying mechanism of void growth and coalescence. As new cracks are born, the stress/strain distribution is changed and new vulnerable crack initiation regions are appeared near the crack tips. Next, the voids grow and coalesce in these critically loaded volumes and thus the cracks start to grow. This is macroscopically called crack propagation. According to this explanation of the crack propagation mechanism, each macrocrack can be considered to be an assemblage of smaller cracks created in several consecutive steps. If the length of such microcracks is considered equal to l*, then the problem of simulating crack propagation reduces to a series of microcrack creation problems. A microcrack creation itself consists of the two steps of microcrack initiation and microcrack evolution. It has been already described that microcrack initiation under ULCF can be satisfactorily predicted by the CVGM. When it comes to microcrack evolution, an isotropic damage model is incorporated to simulate this phenomenon within the framework of material degradation. It needs to note that the damage model is required to correctly account for the fracture energy dissipated in the microcrack evolution phase. Hence, the damage index may simply be assumed to be a linear function of the crack opening displacement.

In order to utilize the above-mentioned concept practically, it must be implemented it in a commercial finite element code. To this end, ABAQUS as a multi-purpose finite element software is employed in this study. The numerical implementation is done using a USDFLD (user defined field) subroutine for the damage initiation in conjunction with ABAQUS built-in damage model for ductile metals [2010]. It needs to note that a USFLD subroutine allows defining field variables for the integration points. It also provides access to a number of variables such as strains and stresses, which may be used to compute the field variable.

The ABAQUS damage model for ductile metals works based on the concept of damage initiation and evolution, i.e., it checks a damage initiation criterion and, if satisfied, damage evolves by further straining. The model also provides this option that the elements whose damage indices are bigger than a predefined value are eliminated from the analysis. Figure 6 presents the flowchart of the algorithm.

To assess the accuracy of the proposed approach, the methodology is employed to simulate a series of tests on connections between columns and base plates conducted in Berkeley NEES Structures Lab. (Myers [2009]). As depicted in Figure 7, the test specimen are made of a W8X67 (W200X100) cantilever column and a 457×457×57.2 mm base plate supported on a rigid steel foundation.

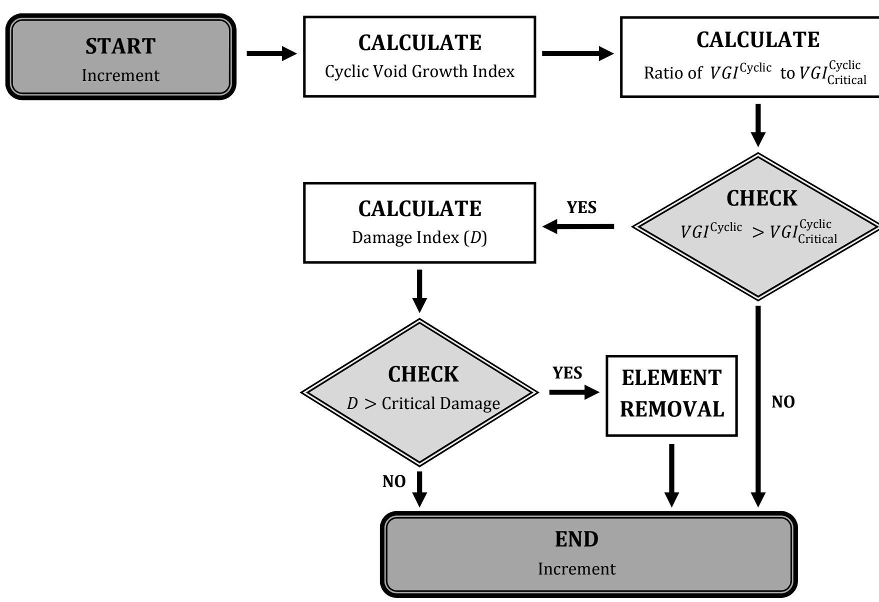

Figure 6 **Flow chart for modeling of the crack initiation and growth in finite element model based on CVGM concept.**

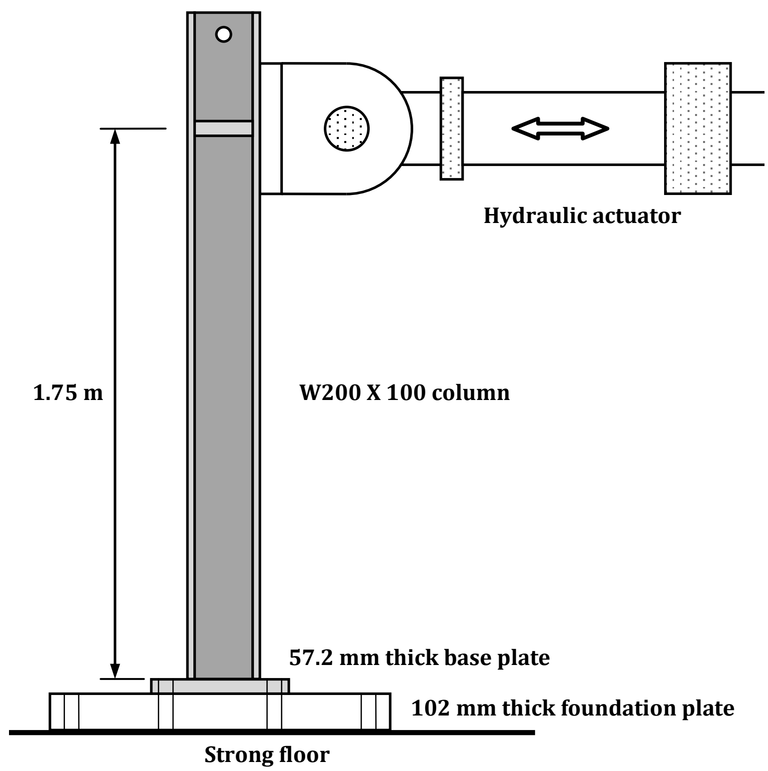

Figure 7 Experimental testing configuration [Myers 2009].

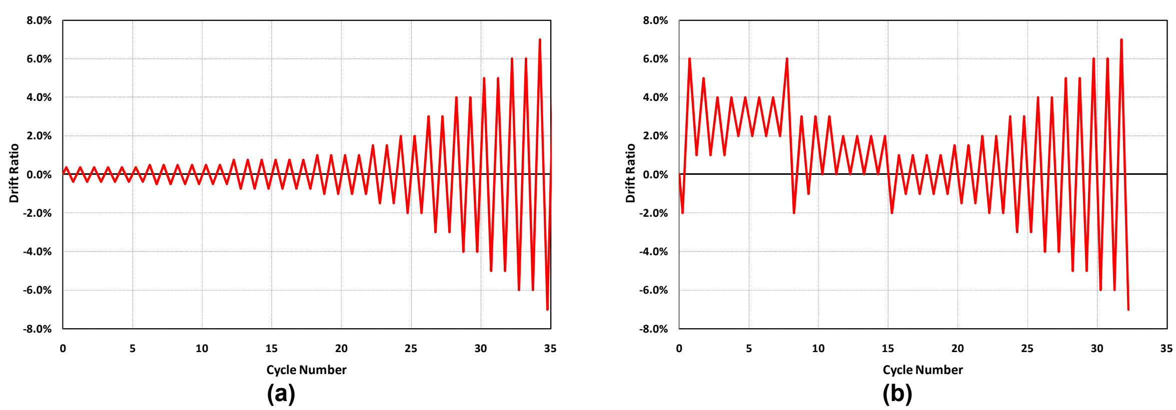

Figure 8 Loading protocols [Tsai and Popov 1988]: (a) General cyclic and (b) near fault followed by general cyclic.

The transverse loads were applied to the end of the column using a hydraulic actuator. Two alternative general cyclic [Figure 8(a)] and near-fault [Figure 8(b)] displacement histories recommended by ATC-SAC [Krawinkler et al. 2000] were adopted to realistically represent the earthquake demand.

Some four specimens previously tested in this experimental program have been selected for the validation of the method proposed in this paper. All the samples were intended to be manufactured as close as possible to the initial design, however, when the specimens were finally checked, the access hole of the third specimen was found completely different. This important issue was addressed in the numerical study of Myers [2009] and is also considered in this study.

Specimens Nos. 1, 3, and 4 were subjected to the general cyclic loading protocol while the near fault loading protocol was applied to Specimen No. 2. Taking the advantages of symmetry, only half of the column's cross section is considered in the finite element models. Eight node reduced integrated linear solid elements with hourglass control are utilized. Since, by using the standard computers, it is nearly impossible to use the global element size of about the characteristic length; this tiny mesh size (0.25 mm) is only applied to the critical regions in which the fractures are experimentally observed.

The material properties for the heat affected zone (HAZ), welds, as well as intact steel (column and base plate) have been assigned based on the experimental results of Myers [2009]. The hardening responses of these materials are approximated using a combined nonlinear isotropic-kinematic hardening model. Figure 9(a) and 9(b) compare the experimentally obtained and numerically calculated moment versus drift ratio for the first and fourth specimens, respectively. As seen, in terms of the slope, shape, and magnitude, the numerical prediction is satisfactorily consistent with the empirical results.

The crack initiations of the No. 1 and No. 4 specimens have been reported in Myers [2009] to be in the first cycle of 3% drift ratio and the first cycle of 4% drift ratio, respectively. Since no exact definition of crack initiation is in hand and considering the fact that cracks were detected visually, it is assumed in the finite element simulation that crack initiates whenever the length of damaged region is bigger than 1 mm. Based on this assumption, the FEM predicts crack initiation in the first cycle of 3% drift ratio. In terms of crack initiation site, the FEM accurately predicts it in the HAZ of the flange corner. Furthermore, as shown in Figure 10(a), the fracture path is also closely determined by the FEM. The total fractures of the finite element model and also the specimen No. 1 occurred in the second cycle of 5% drift ratio, however the specimen No. 4 fails in the second cycle of 6% drift ratio (two cycle difference).

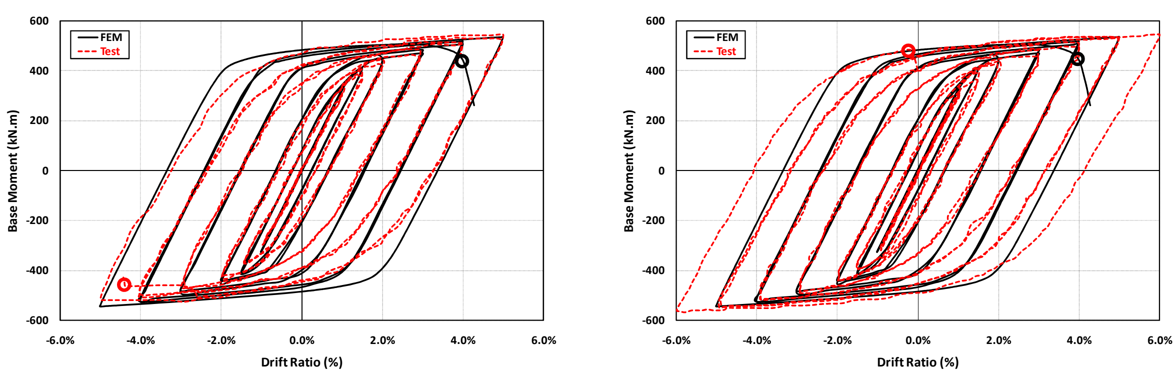

(a) (b)

Figure 9 Measured versus simulated response: (a) Specimen No. 1 and (b) Specimen No. 4.

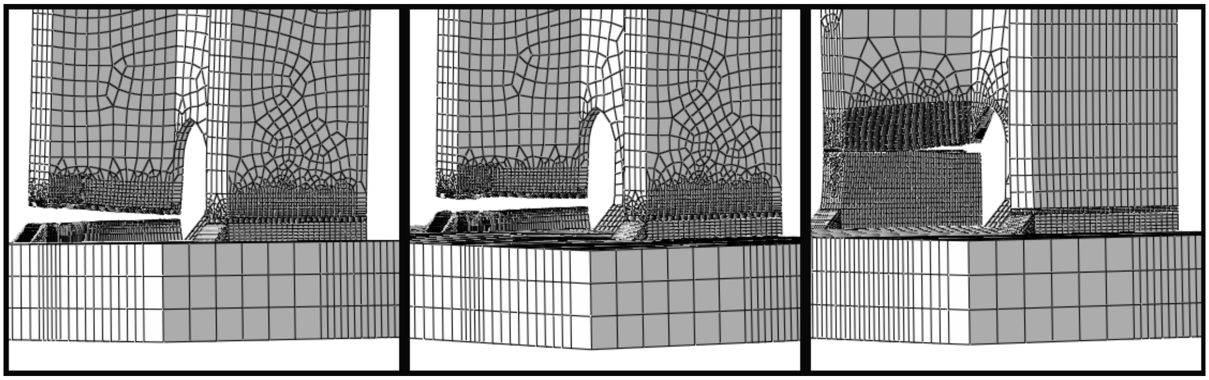

Figure 10 Fracture pattern: (a) Specimens No.1 and 4; (b) Specimen No.2; and (c) Specimen No.3.

Table 2 summarizes and compares the test results and those of the FEM. They include load cycles corresponding to crack initiation and the total flange fracture as well as drift ratios and crack locations. Here, it can be deducted that

- Crack sites of the experiments are correctly predicted by the FEM.
- In all cases examined, the crack initiation is predicted later than what experimentally observed.
- The prediction of total flange fracture is in good agreement with the experimental results.

A parameter called $\theta^{Accumulated}$ has been introduced in the original report of the experiment by Myers [2009]), which is the summation of drift angle tolerated by the specimens before total flange fracture. Table 3 compares the values of this parameter determined from tests and simulations. An average error of about 10% is observed for the simulation method which indicates fairly good overall agreement between the experimental and analytical values. This illustrates the capability of the proposed method to capture fracture processes in realistic situation in the absence of sharp crack and flaws. In all the specimens fracture predicted earlier than the test. This perhaps occurred due to using tie constraint for connecting parts to each other and coarser mesh in the opposite flange.

Table 2 Test and finite element model results.

Spec. No.	Loading Type	$\theta_{initiation}$ Test	$\theta_{initiation}$ FEM	Failure Test Cycle No.	Failure Test $\theta_{Failure}$	Failure FEM Cycle No.	Failure FEM $\theta_{Failure}$	Crack Location Test	Crack Location FEM
1	General Cyclic	3%	4%	5%	2	5%	2	Corner HAZ	Corner HAZ
2	Near Fault	6%(1)	6%(2)	5%	1	6%	1	Corner HAZ	Corner HAZ
3	General Cyclic	Not Reported	3%	6%	1	6%	2	Access Hole	Access Hole
4	General Cyclic	4%	4%	5%	2	6%	2	Corner HAZ	Corner HAZ

Table 3 Comparison between $\theta^{\text{Accumulated}}$ values of test and finite element model.

Specimen	$\theta^{\text{Accumulated}}$ TEST	$\theta^{\text{Accumulated}}$ FEM	$\frac{\theta^{\text{Accumulated}}_{\text{FEM}}}{\theta^{\text{Accumulated}}_{\text{Test}}}$
1	1.79	1.67	0.933
2	2.40	1.98	0.825
3	2.15	2.03	0.944
4	2.21	1.67	0.756

FINITE ELEMENT MODELING OF SADDLE-LIKE CONNECTION

As the method proposed in previous section proved to be successful in predicting the behavior of reference specimens under cyclic loading, it was attempted to simulate the behavior of tested saddle-like connections using the finite element model. Figure11 shows the model of Specimen No.1. As shown in this figure, a very fine mesh had to be used to model the welds and nearby regions to capture the crack initiation and growth in this region. Figure 12 shows the crack path obtained from this analysis, which agrees fairly well with experimental observations.

As the finite element modeling of tested saddle-like connections was proved to be successful in predicting the behavior of this type of connection, additional samples of the connections were modeled and analyzed and the backbone curves of them were obtained. Table 4 shows the details of these specimens. Figure 13 shows the hysteretic and backbone curves obtained for theses specimens from these analyses. The behavior curves obtained for all 14 specimens from experiments as well as finite element analysis shows that the behavior of saddle-like connections subjected to applied moment may be classified as deformation controlled.

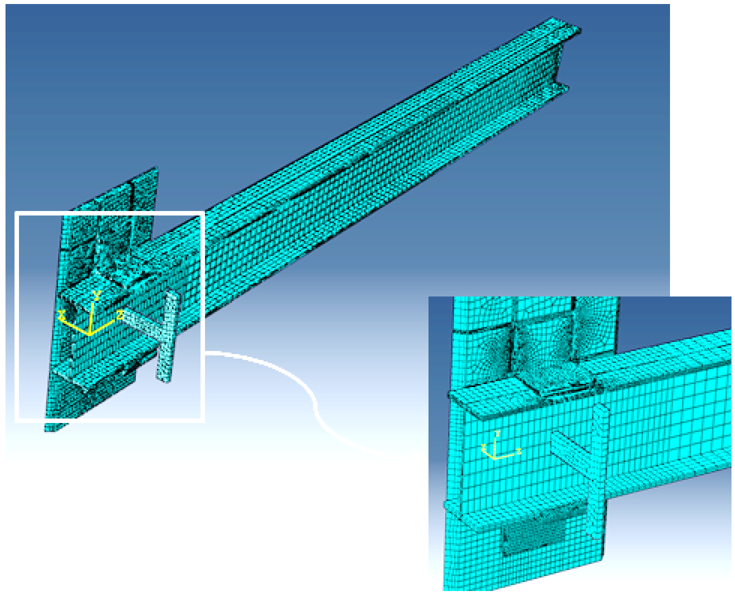

Figure 11 The finite element model of Specimen T1 of saddle-like connection.

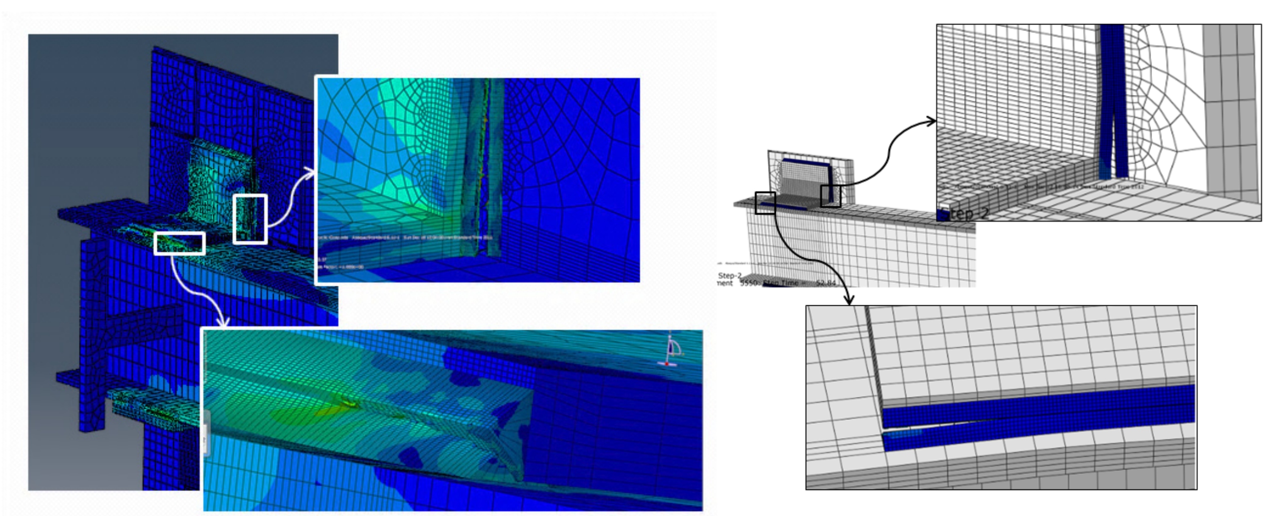

Figure 12 Crack path in the finite element model of Specimens T1 and T5 of saddle-like connection.

Table 4 Details of additional saddle-like connection specimens.

No.	Beam section	Top angle	Bot angle	Top Angle length (cm)	Bot angle length
T7	CPE160	6 ×60 × 60	10×100×100	10	15
T8	CPE160	6 ×60 × 60	10×100×100	15	15
T9	CPE160	6 ×60 × 60	10×100×100	10	20
T10	CPE160	6 ×60 × 60	10×100×100	20	20
T11	CPE180	8 ×80 × 80	10×100×100	10	15
T12	CPE180	8 ×80 × 80	10×100×100	15	15
T13	CPE180	8 ×80 × 80	10×100×100	10	20
T14	CPE180	8 ×80 × 80	10×100×100	20	20

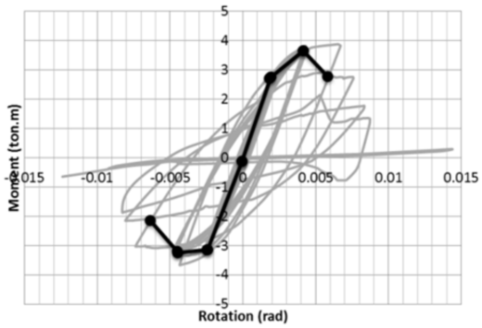

Specimen T7

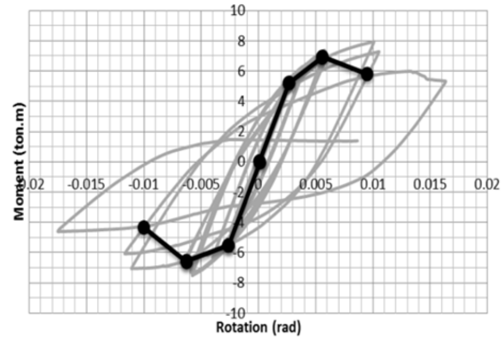

SpecimenT8

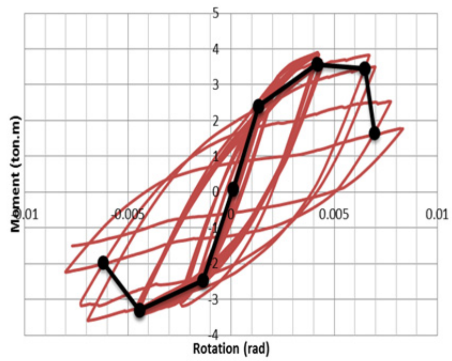

SpecimenT9

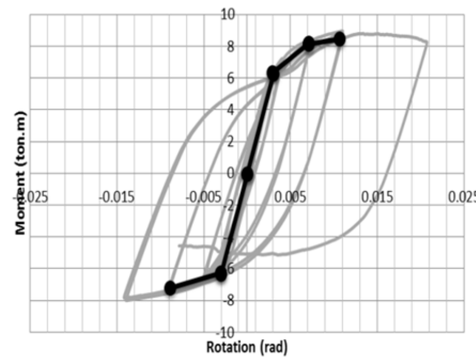

SpecimenT10

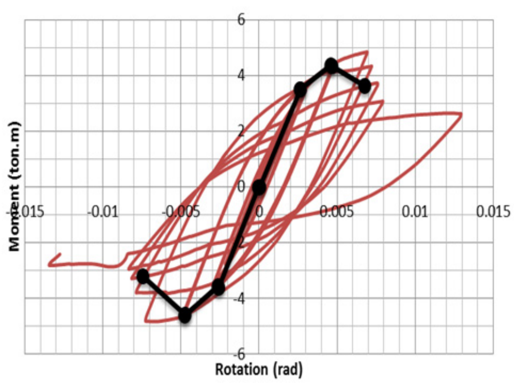

SpecimenT11

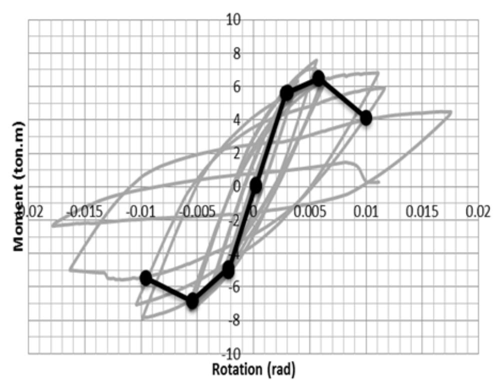

SpecimenT12

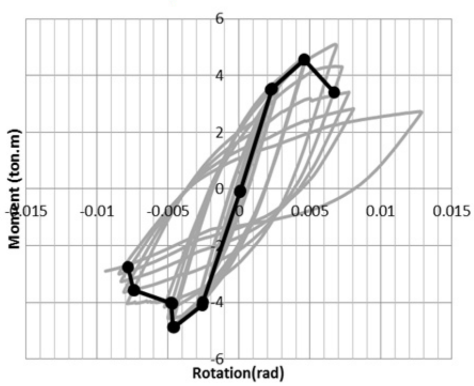

SpecimenT13

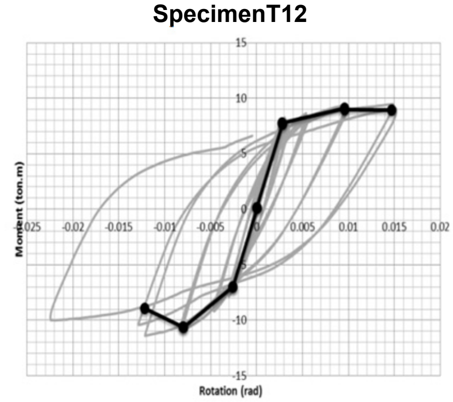

SpecimenT14

Figure13 Hysteretic and backbone curves of additional specimens.

EMPIRICAL EQUATIONS FOR CHARACTERISTIC PARAMETERS OF SADDLE-LIKE CONNECTION

Based on the results of previous sections, characteristic parameters of the behavior curve for saddle-like connections were identified as initial stiffness, yield moment, ultimate moment and ultimate rotation of the connection. Also the parameters affecting these characteristic values were found to be beam depth, H, top angle size, $D_{ta,}$ top angle length, $L_{ta,}$ and bottom angle length, $L_{ba.}$ Finally, using the regression methods, some empirical relationships were proposed for every characteristic parameter of the backbone curves as follows:

$$K=0.11*H^{2.482}*L_{ta}^{1.064}*(L_{ta}/L_{ba})^{-0.116}*D_{ta}^{-0.582}$$

$$M_y=0.011*H^{0.857}*L_{ta}^{1.16}*(L_{ta}/L_{ba})^{-0.049}*D_{ta}^{0.073}$$

$$M_u=0.067*H^{0.372}*L_{ta}^{1.141}*(L_{ta}/L_{ba})^{-0.206}*D_{ta}^{0.073}$$

$$\theta_u=0.053*H^{-0.559}*L_{ta}^{-0.238}*(L_{ta}/L_{ba})^{1.469}*D_{ta}^{0.443}$$

Concluding Remarks

Traditional saddle-like connections are semi rigid connections, whose behavior are different from semi-rigid connections found in international standard. For design of new structures, the recent guidelines, which transform this type of connection to either a simple (scissor like) or fully rigid connection, may be used. However for existing structures if a reliable lateral load resisting system such as shear wall or braced frame is provided the behavior of saddle-like connections may be modeled using the empirical equations developed in this research. In this case the behavior of this connection under applied moment may be regarded as deflection controlled and the behavior of connection may be assessed based on deformations imposed on the connection in different seismic hazard and the required performance levels.

MOMENT FRAMES COMPOSED OF BUILT-UP COLUMNS

General

Moment-resisting frame (MRF) is a structural system that is widely used in steel building construction, and thus many investigations have been carried out to determine its behavior and performance, especially in seismically active regions. Panel zone in connections of this type of frame, which is a part of the column framed by column flanges and horizontal continuity plates, has been studied extensively in the past due to its important influence on seismic behavior of. Large shear forces are induced in the panel zone when lateral load is applied to a MRF. Since well-designed joints are ductile elements, it has been proposed to design panel zones so that they yield in shear and participate in energy dissipation in severe earthquakes. Hence some design codes allow the plastic hinges to form in the panel zones of MRSFs under earthquake loading [FEMA 2000].

Deformations of the panel zone can significantly affect the frame response both in linear and nonlinear regions [Tsai and Popov 1988; Kim and Engelhardt 1995]. Therefore, some relations have been proposed to describe the elastic and inelastic behavior of this part of the structure. Several researchers as Krawinkler et al. [1971], Fielding and Huang [1971] and Wang [1988] proposed relationships between the shear force, V, and deformation, γ , in panel zone for monotonic loading. These relationships have been used as the basis of mathematical models for nonlinear rotational springs representing the panel zone. Kim and Engelhardt [2002] proposed a model with quadri-linear $M^{pa} - \gamma$ relations, in which both bending and shear deformation modes of the panel zone are included and can reasonably describe the increase of yield strength and elastic stiffness due to increase in the ratio of column flange thickness to column depth and inclusion of the bending deformation mode.

All information available in the literature regarding the panel zone behavior is about the connections in which the webs of beam and column are in the same plane. However, the use of built-up sections composed of double section profiles or box shape profiles for columns is very common in some countries such as Iran due to unavailability of large rolled sections. If an *I* beam is connected to such a column to form a rigid connection, the resulting panel zone will be different from that of an ordinary connection of an *I* beam to an *H* column. The main difference is that here, the column webs are located with a distance from each other and are not in the plane of the beam web. Examples of the two types of connections are shown in Figure 14.

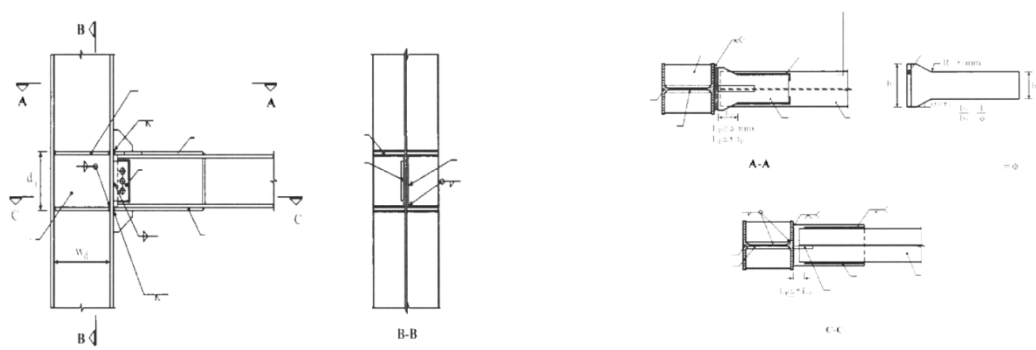

(a) ordinary connection of I beam to H column.

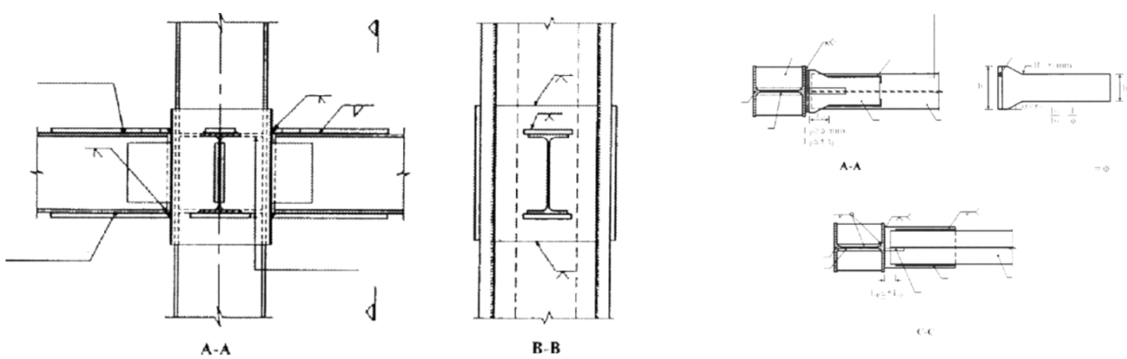

(b) connection composed of column with double section and a vertical continuity plate to *I* beam

Figure 14 Types of beam-to-column connections.

Experimental Study

To study the characteristics of connections in this type of columns and their panel zones, initially four full-scale specimens were tested under cyclic loading. The specimens were composed of a column with double sections of *IPE* profiles and a vertical continuity plate connected to a beam of *IPE* profile. Beams were connected to the column using top and bottom flange plates and web shear plates. Details of the specimens are presented in Table 5.

In the test set-up, one-half of the beams and columns length was considered at either side of the connections. The specimens were installed on the strong floor as shown in Figure 15. A pinned bearing support was provided at the column bottom, and the roller bearing supports were provided at the ends of beam sections. Hydraulic jacks were used to apply cyclic loading to the specimens at the top of column. The loading protocol introduced in the AISC Seismic Provisions was followed [ASIC41-05 2005]. The loading history of the specimens is shown in Figure 16. This loading history is based on interstory drift angle.

Table 5 Details of the specimens.

Specimen	Column Section	Beam Section	Vertical continuity plate	Column covering plate	Top flange plate of the connection						Bottom flange plate of the connection		Web shear plate	
					b_1	b_2	*L1*	*L2*	t_p	Fillet weld	Plate dimensions	Fillet weld	Plate dimensions	Fillet weld
DIP 1	2IPE 240	IPE 270	PL 75*24*1.2	PL 24*1.2	10	14	8	20	2.0	1.2	PL 28*20*1.5	1.2	PL 15*10*1.0	0.8
DIP 2	2IPE 200	IPE 240	PL 75*20*1.0	PL 22*1.0	8	12	8	15	2.0	1.0	PL 23*18*1.5	1.0	PL 15*10*1.0	0.8
DIPAL2	2IPE 200	IPE 240	PL 75*20*1.0	PL 22*1.0	8	12	8	15	2.0	1.0	PL 23*18*1.5	1.0	PL 15*10*1.0	0.8
DIP 3	2IPE 270	IPE 300	PL 80*27*1.5	PL 24*1.2	12	18	8	22	2.0	1.2	PL 30*22*2.0	1.2	PL 20*12*1.2	1.0

All dimensions are in cm.

Figure 15 Test set-up.

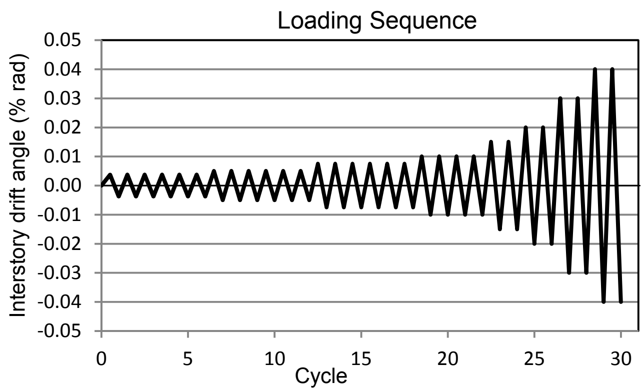

Figure16 Loading history of the specimens.

Tests Results

The value of moment applied to the connection versus angular drift of the specimens is plotted in Figure 17. The tests results in a summarized form are presented in Table 6. They include maximum tip force, tip displacement, applied moment, panel zone shear angles, and the inter-story drift. These results show that the specimens have shown ductility well above 2% drift ratio, which is needed to be qualified as intermediate ductility frame. However as fractures occurred in the welds connecting the column covering plate to the column section, the importance of the details of this plate was brought to light.

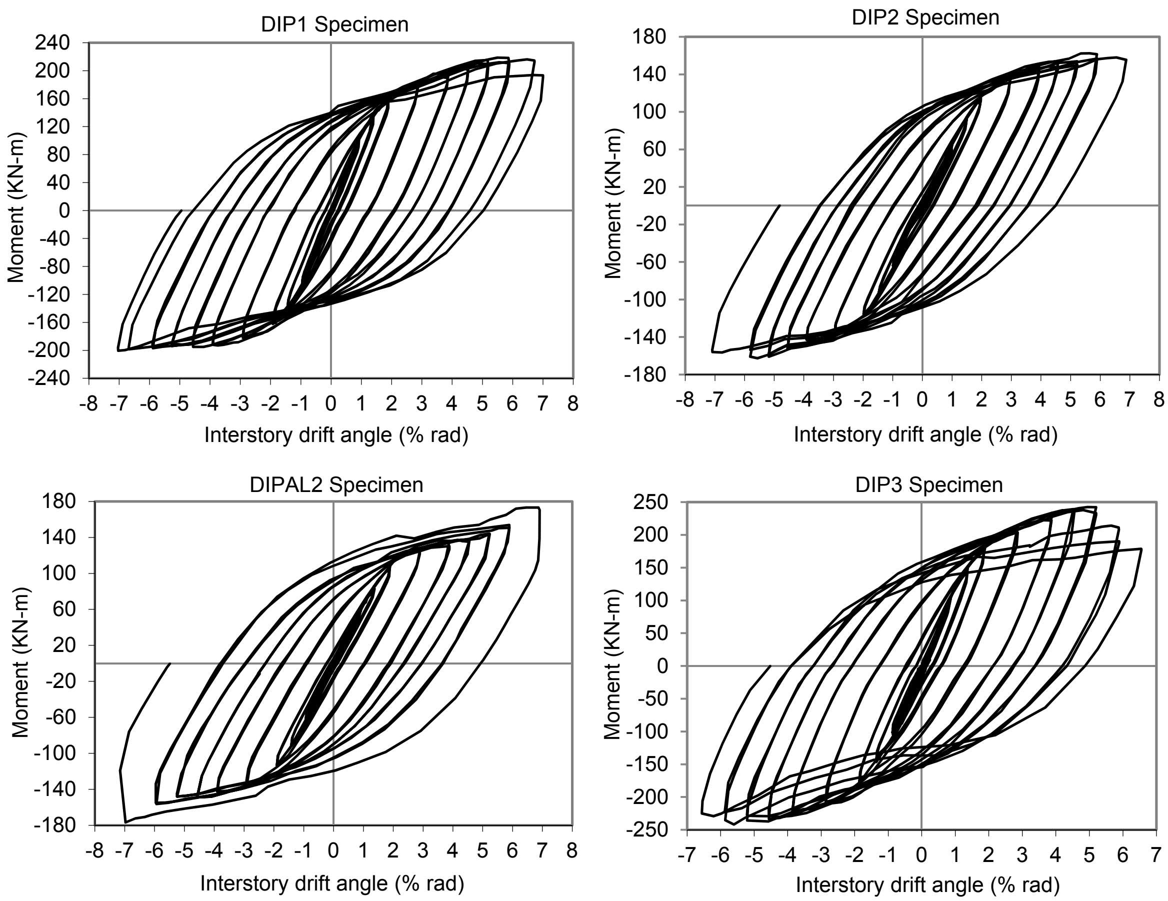

Figure 17 Moment-interstory drift angle of specimens.

Table 6 Summary of test results.

Specimen	Maximum lateral load (kN)	Maximum lateral displacement (mm)	Maximum moment (kN-m)	Maximum interstory drift ratio (%)	Maximum shear distortion of panel zone (Rad)
DIP 1	153.68	210	218.75	7	0.00799
DIP 2	113.39	210	162.68	7	0.01347
DIPAL2	123.24	210	176.82	7	0.01442
DIP 3	170.34	200	242.46	6.67	0.00602

Finite Element Modeling of the Specimens

In order to study the behavior of tested specimens in more detail and to investigate their behavior in other situations such as monotonic loading, finite element models of the specimens were also constructed (Figure 18). Solid elements were used for modeling of the components including beams, columns and plates. Contact elements were used for simulation of the contact surfaces. Geometrical nonlinearity and material nonlinearity were considered in these analyses. The Von Mises yield criteria and combined strain hardening rule were used. Material properties were specified based on the results of the coupon tensile tests. The results of finite element simulations and experiments, in the form of load- displacement curves, are shown in Figure 19. As seen in this figure, fairly good agreement has been achieved.

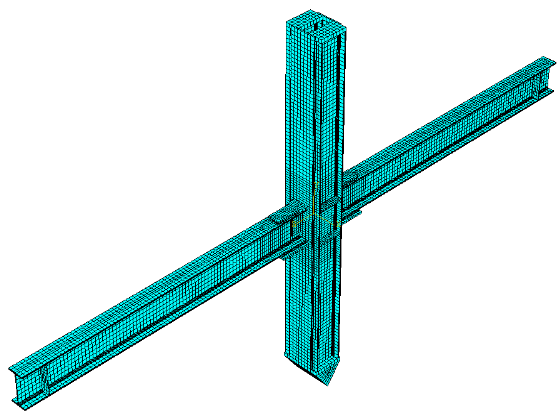

Figure 18 Finite element model of the specimens.

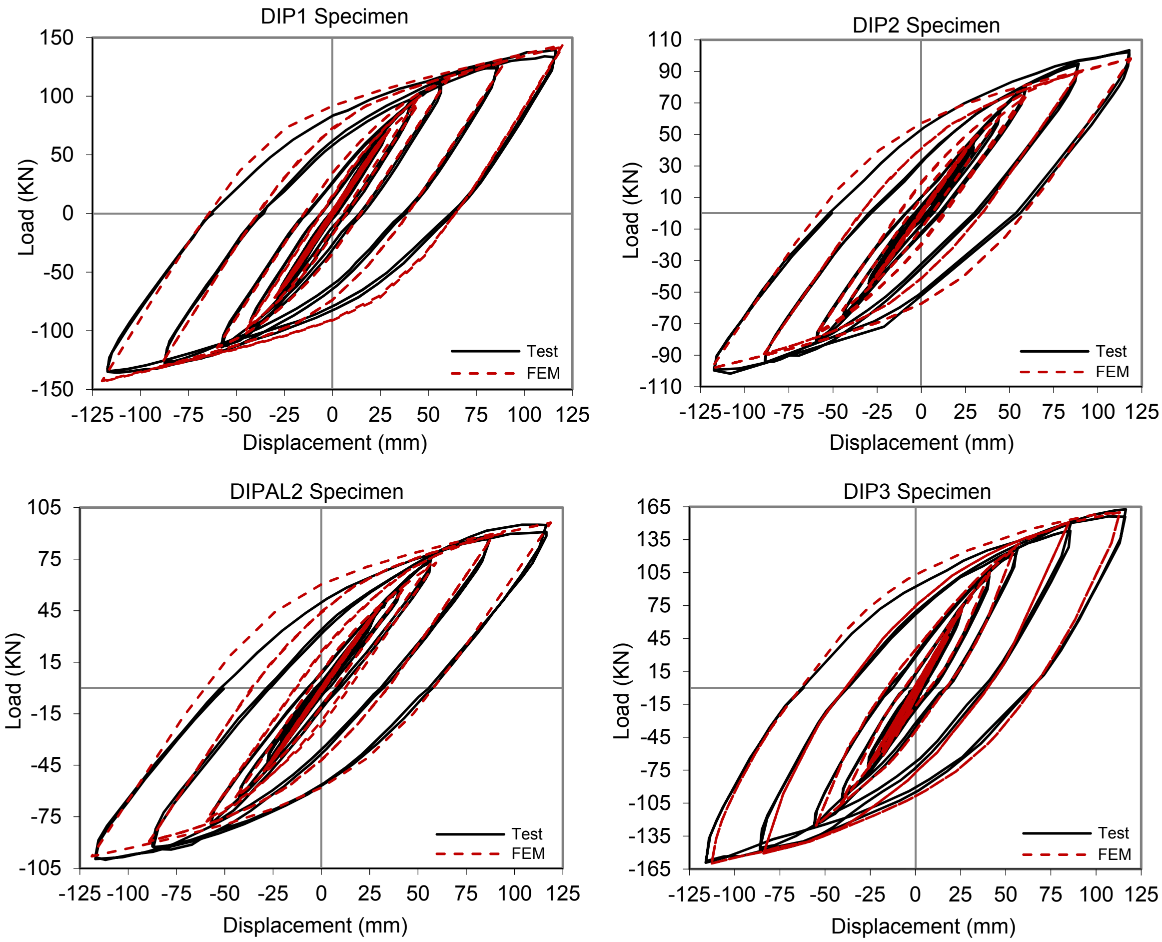

Figure 19 Comparison between the results of finite element simulations and experiments.

Panel Zone Behavior

The panel zones of connections consisting of *I*-shape beams and double section columns with a vertical continuity plate consist of three panels. First one is the middle panel, which is the vertical continuity plate, and the other two are side panels which are the webs of column sections, as shown in Figure 20. The changes in diagonal length of the side panels were measured during the tests, but for the middle panel, the access was limited and such measurements were not possible. Based on the experimental data, shear deformations of the side panels were calculated as shown in Figure 21.Since the measurement of shear deformations of the middle panel during the tests were not possible, shear deformations of the middle and side panels obtained from the finite element models were compared and it was confirmed that the middle panel undergoes larger shear deformations compared to the side panels. Considering the limitations of experiments, the finite element models of the specimens, which were calibrated by the test results, were used for more detailed study of the behavior of panel zones in other conditions such as monotonic loading.

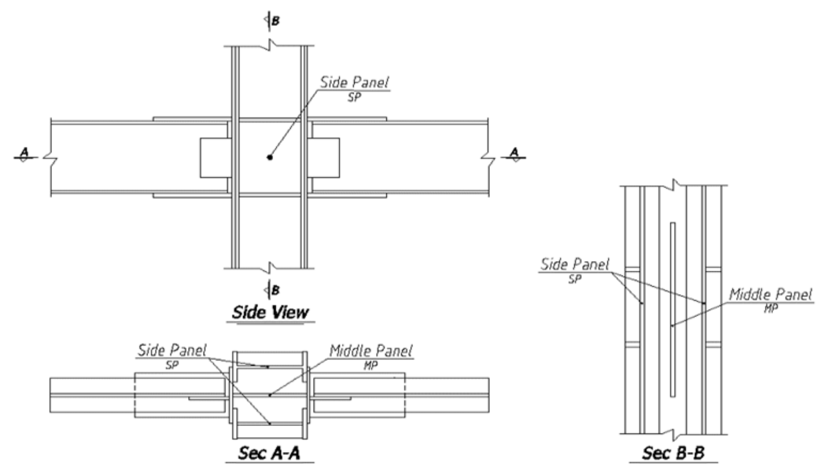

Figure 20 Connection's panel zone composed of three panels.

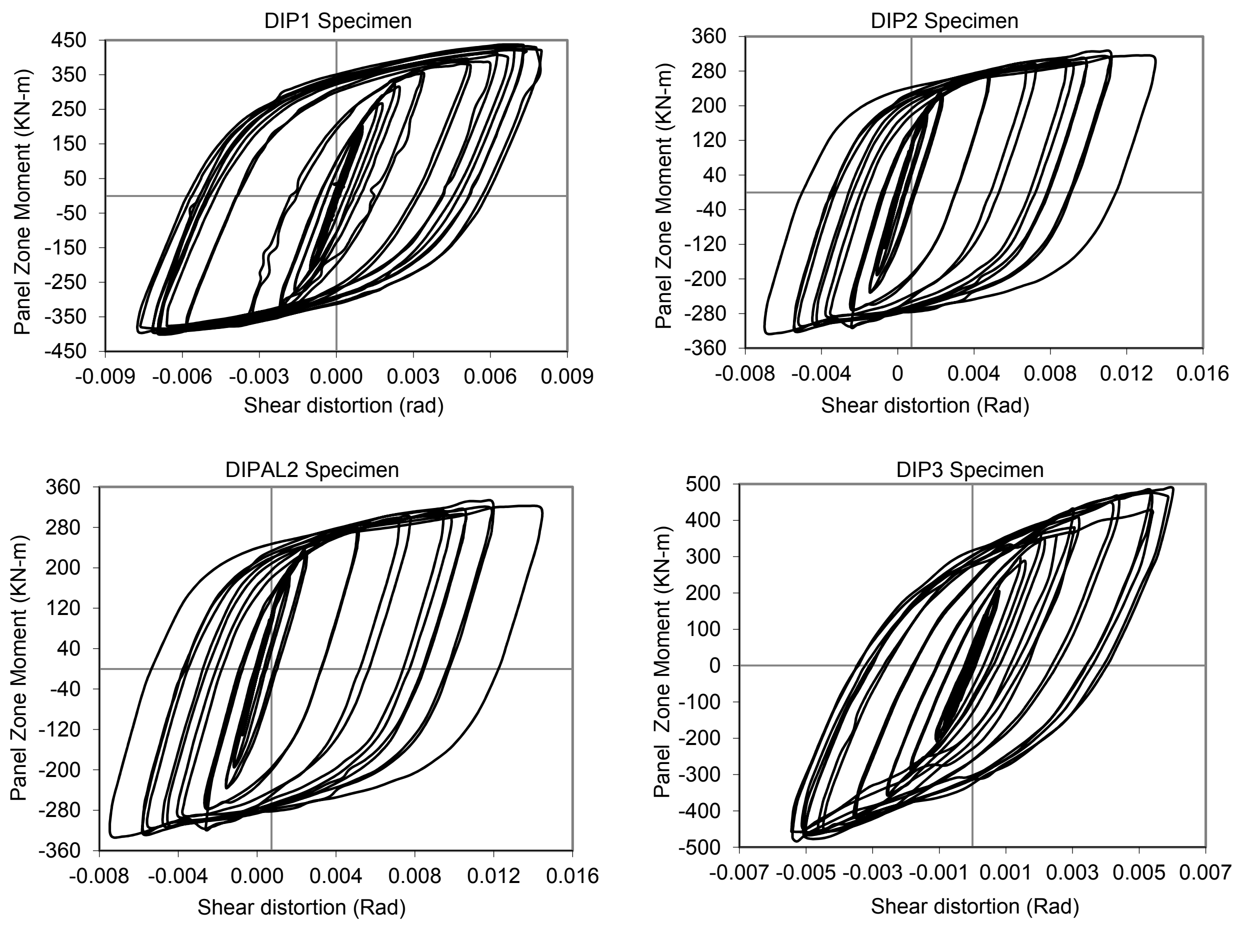

Figure 21 Shear distortion of the side panels.

Based on above mentioned observations and considering the fact that the middle panel is in the same plane as the beam web and therefore the frame behavior is primarily affected by deformations of middle panel, this panel was selected as the primary one to describe the load-deformation behavior of the whole panel zone.

Load-Deformation Characteristics of Panel Zone

Load-deformation characteristics of panel zones are usually described in terms of shear force versus shear deformation. The present mathematical models are typically based on a transformation of the boundary forces into an approximate equivalent shear force as follows:

$$V_{eq} = \frac{M_{bl}+M_{br}}{d_b-t_{bf}} - \frac{(V_{ct}+V_{cb})}{2} \quad (1)$$

where, M_{bl} , M_{br} , V_{ct} and V_{cb} are left beam moment, right beam moment, top column shear and bottom column shear, respectively; t_{bf} is the thickness of the beam flange and d_b is the beam depth. A key simplification in this analysis is that the beam moments are replaced by an equivalent couple, with the forces acting at mid-depth of the beam flanges. Equation (1) can be written as follows:

$$V_{eq} \approx \frac{M_{bl}+M_{br}}{d_b-t_{bf}}(1-\rho) = \frac{(1-\rho)}{d_b-t_{bf}} M^{pa} \quad (2)$$

where $\rho = (d_b - t_{bf})/H_c$, $M^{pa} = M_{bl} + M_{br}$ and H_c is the column height. In the following sections, the load-deformation characteristics of panel zone are discussed [Kim and Engelhardt 2002].

In early research, the elastic stiffness of the panel zone was computed by considering the pure elastic shear deformation of the effective shear area of the panel. Fielding and Huang [1971] proposed a bilinear model that includes elastic stiffness, K_e, with the following post-elastic stiffness, K_1.Krawinkler et al. [1971] and Wang [1988] each proposed different tri-linear $M^{pa} - \gamma$ relations consisting of an elastic stiffness, K_e, followed by two linear post elastic stiffness values K_1 and K_2. Kim and Engelhardt [2002] proposed a quadri-linear model, which produced more accurate results, especially where the column flanges were rather thick.

Shear deformations of the middle panel versus the total moment applied to the tested connections are shown in Figure 22and compared to the results of the model proposed by Krawinkler et al. [1971]. It is worth noting, that as discussed in previous sections, the relations proposed by previous researchers are for the case of panel zones in which the webs of beam and column are coplanar and horizontal continuity plates exist on the top and bottom of the panel zone. However, details of the connection being studied here, as seen in Figure 14(b) and Figure 20, are quite different.

In Figure 22, Krawinkler-1 represents the case where the effective shear area of panel zone, A_{eff} , has been calculated using only the thickness of vertical continuity plate and the thickness of doubler plate is neglected. In other words, it is assumed that column webs or side panels do not contribute to the stiffness and strength of the panel zone. In this figure, Krawinkler-2 represents the case where the panel zone thickness is assumed to be equal to the sum of the thicknesses of vertical continuity plate and column webs for calculating the effective shear area. In other words, in this case, it is assumed that column webs act as doubler plates for vertical continuity plate and, hence, they are completely effective in increasing the stiffness and strength of the panel zone. Considering the existence of a distance between the three panels, one can easily anticipate that Krawinkler-1 is a lower bound for the panel zone behavior and Krawinkler-2 is an upper bound for it.

It is clear from the previous discussions that existence of three panels with some distance between them, absence of continuity plate at the top and bottom of the middle panel, and details and type of beam to column connection produce different behavior of the panel zone in the connections under study compared to the models proposed by previous researchers. Therefore, in this study, a new model was proposed to describe the behavior of panel zone in such connections under monotonic loading [Sazmand and Aghakouchak 2012]. The new model is a quadri-linear model in which both shear and bending stiffness are considered for the panel zone.

The proposed monotonic model is applied to the connection described in the previous part. A comparison between the results of proposed model, the finite element model calibrated by the experimental results and Krawinkler et al.'s model [1971] is shown in Figure 23. Comparison of the proposed quadri-linear model with the results obtained from the finite element analysis of connection shows a good performance of the proposed model, especially in the elastic range.

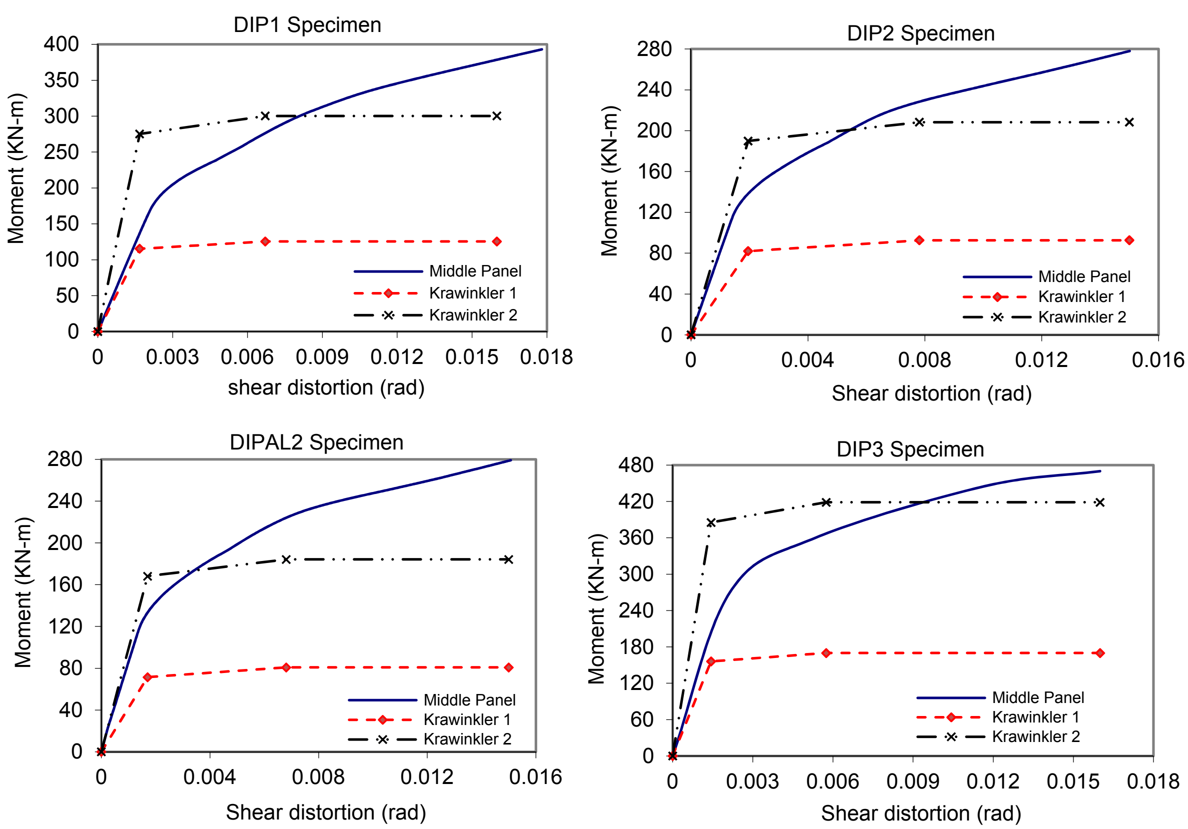

Figure 22 Comparison of the middle panel behavior with the results of the Krawinkler's model.

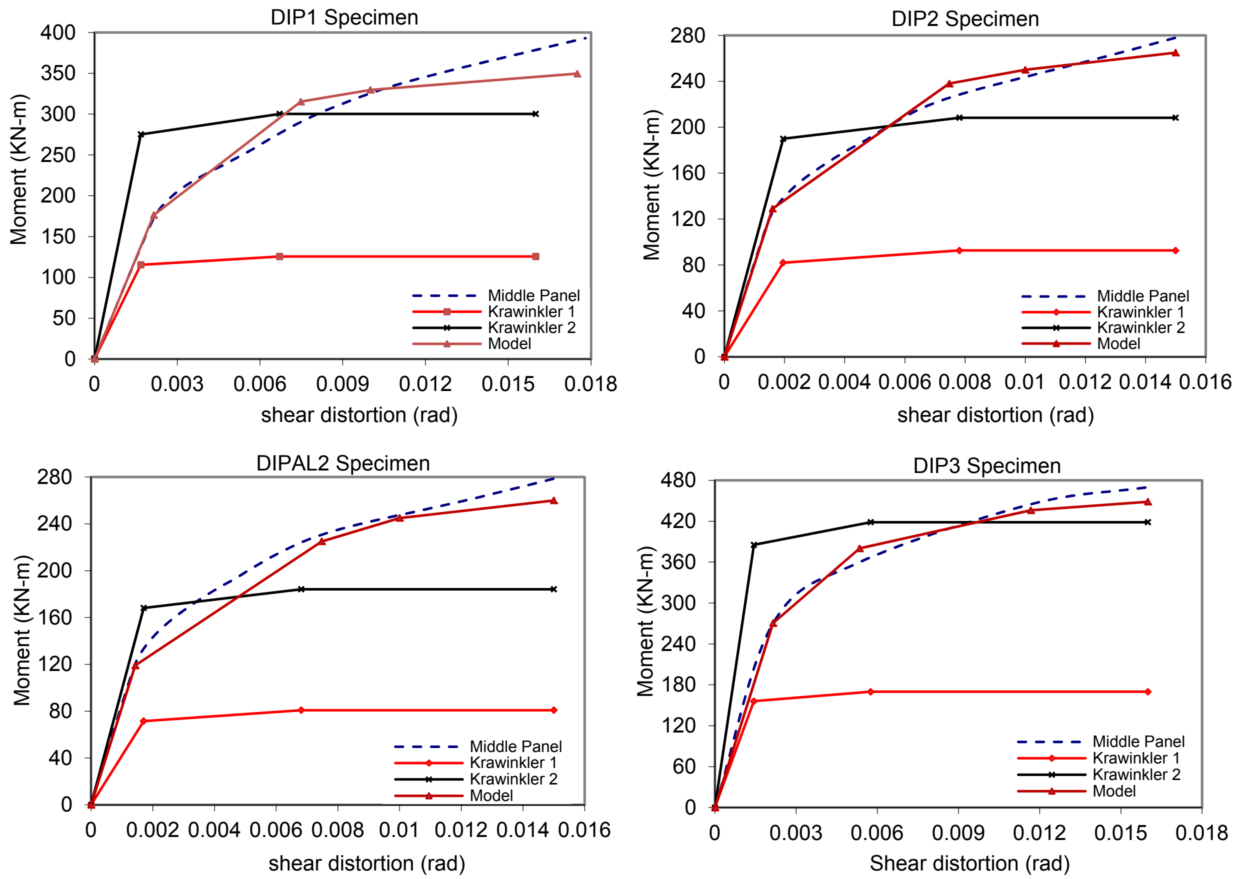

Figure 23 Comparison between the results of proposed model, the finite element model and Krawinkler's models.

Concluding Remarks

- The results of experiments and finite element simulations showed that the connection under study has sufficient stiffness, strength and ductility to be considered for intermediate ductility frame.
- The role of column cover plate is very important in avoiding premature failure in this connection and it need to be designed very carefully.
- The behavior of panel zone in this type of connection is quite different from that of ordinary IBHC connection.
- The multi linear model developed in this work may be used for assessing the panel zone and its effect on frame behavior.

MOMENT FRAMES WITH BOX SHAPE COLUMNS

General

Box shaped columns built up from four plates are successfully used in moment resisting frames (MRFs) in earthquake-prone areas. This practice is common in Japanese steel construction

[Nakashima et al. 2000] as well as some other countries. Box-columns can be used in orthogonal directions due to symmetric geometry and large bending stiffness and strength about any axis as well as high torsional stiffness and strength. In general large volume of research has been carried out on *I*-beam to *H*-column (IBHC) connections; however the studies on *I*-beam to box-column (IBBC) connections are limited [Goswami and Murty 2010]. Generalization of results and details of IBHC connections to IBBC connections is not correct due to geometric differences of box-columns compared to H-columns. Box-column flanges are weak and flexible in out-of-plane, therefore inclusion of continuity plates inside the box-columns at beam flange levels is generally recommended for IBBC connections [FEMA 2000]. However installation of continuity plates in a box-column is difficult and costly in practice.

Proposed details on IBBC connections can be divided into three categories. The first one basically uses internal continuity plates for reinforcing the joint, such as rib-reinforced welded connections [Chen et al. 2004], widened flange column-tree connection including no weld access hole detail [Chen et al. 2006], horizontal haunch connection [Tanaka 2003], connections retrofitted by T-stiffener [Ghobade et al. 2009a; Ghobadi et al. 2009b], Accordion-Web RBS connection [Mirghaderi et al. 2010a] and connections rehabilitated by welding full-depth side plates [Chou et al. 2010]. In the second category, it is tried to remove internal continuity plates by means of external features and new load paths such as connections with external T-angle or triangular plate stiffeners [Shanmugam et al. 1991; Tin et al. 1991; Shanmugam and Ting 1995], bolted moment end plate connections [Wheeler et al. 1998; Wheeler et al. 2000], inclined rib-plated collar-plated connection [Goswami and Murty 2010] and connections using a vertical plate passing through the column [Mirghaderi et al. 2010b]. In the last category, internal continuity plates are removed but the column is filled by concrete (CFT column), for example CFT column to *H*-beam welded moment connections with external T-stiffeners and penetrated elements [Shin et al. 2004; Kang et al. 2001].

In order to study seismic performance of MRF connections, researchers consider a subassemblage of moment resisting frame and study its behavior numerically or experimentally. Figure 24 shows T-shaped and cruciform subassemblages, which are commonly used. These subassemblages represent uniaxial MRF connections. In the case of dual-strong-axis MRF connections, biaxial subassemblages must be used. Only few researches have been carried out using biaxial subassemblages. Shanmugam et al. [1995] used a four-sided subassemblage to study biaxial performance of interior connections stiffened by T-sections. MNH-SMRF Systems, Inc. completed a full-scale laboratory testing of a dual-strong-axis connection at the University of California, San Diego Charles Lee Powell Structural Research Laboratories, under the direction of Uang [Uang and Latham 1995]. The dual strong axes connection was biaxially loaded by applying a static load of 30% of the beam flexural capacity to two beams in one direction while loading the beam in the other direction cyclically to failure.

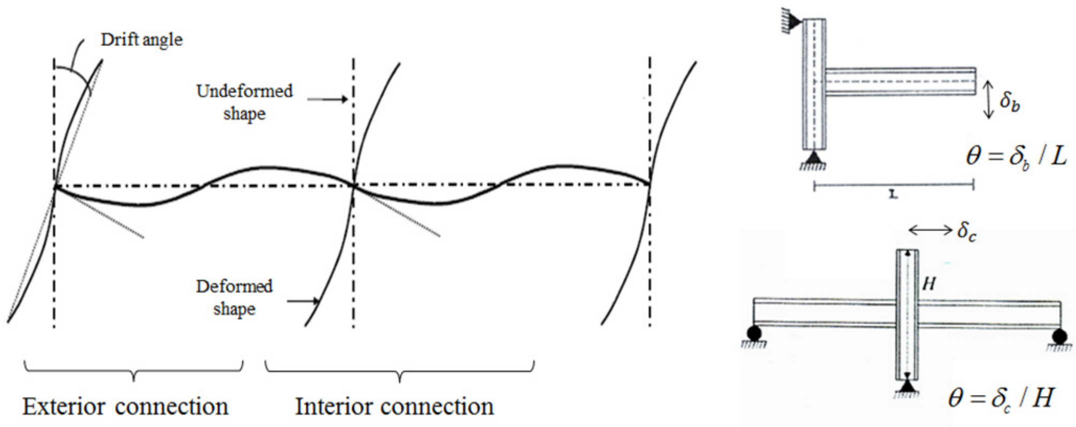

Figure 24 Uniaxial subassemblages, a T-shaped subassemblage representing an exterior connection and a cruciform subassemblage representing an interior connection.

This research introduces a new configuration for connection of *I*-beam to box-column. In this type of connection, internal continuity plates are not required. Efficiency of this new IBBC connection to resist seismic actions is proved through result of nonlinear finite element analyses of 4-sided subassemblage, which is loaded not only uniaxially but also biaxially. For this purpose the results of experiments reported in literature for another type of IBBC connection is utilized to determine a criterion for fracture initiation in critical region of the connection. The criterion is then used for evaluating the performance of the proposed connection.

Fracture in Groove Welds at the Intersection of Beam Flange and Column

Chen et al. [2004] tested a full-scale specimen of BWWF connection under cyclic loading. The subassemblage consisted of an H-shaped H588×300×12 ×20 beam, 3030 mm long and a box-column of 550×550×27×27 with 3000 mm span length. Test results revealed that the specimen failed in a brittle mode with a rapid drop in beam strength caused by the fracturing of the tensile flange of the beam during the 2.3% story drift angle cycle. The cracks originated in the nicks at the root of the CJP flange welds, and propagated rapidly through the beam flange.

In present investigation, this test is simulated numerically using finite element software to monitor inelastic behavior and fracture. For investigating fracture, the concept of plastic equivalent strain is used. PEEQ is a parameter for “plastic equivalent strain” which represents the local plastic strain demand. It is a scalar measure of all the components of plastic strain at each position in the model as follows:

$$PEEQ = \int_0^t \dot{\bar{\varepsilon}}^p \, dt \text{ A} \tag{3}$$

$$\dot{\bar{\varepsilon}}^p = \sqrt{\frac{2}{3}\dot{\varepsilon}_{ij}^p \dot{\varepsilon}_{ij}^p} \text{ A} \tag{4}$$

The PEEQ index used by researchers [Chen et al. 2004; Chen et al. 2006] is defined as the ratio of PEEQ to the yield strain.

A three-dimensional finite element model has been built on the basis of the geometric dimensions of the above referenced test specimen. Details of the material modeling in the specimen were similar to Chen's assumptions [2004]. Quadrilateral four-node shell elements having six degrees of freedom per node were employed in the modeling. Figure 25 shows Chen's finite element model and the model rebuilt in this study. Distributions of normalized longitudinal stresses at 0.5% story drift angle and PEEQ indices at 4% story drift angle, along the beam flange width at the locations of the CJP weld for both models under monotonic loading, are plotted in Figure 26(a) and (b), respectively. Usually, the story drift angle of 0.5% is selected to study the elastic behavior of the connection, while the story drift angle of 4% indicates that the connection has undergone significant inelastic deformation [Chen et al. 2004]. As shown, the results of both models are in fairly good agreement.

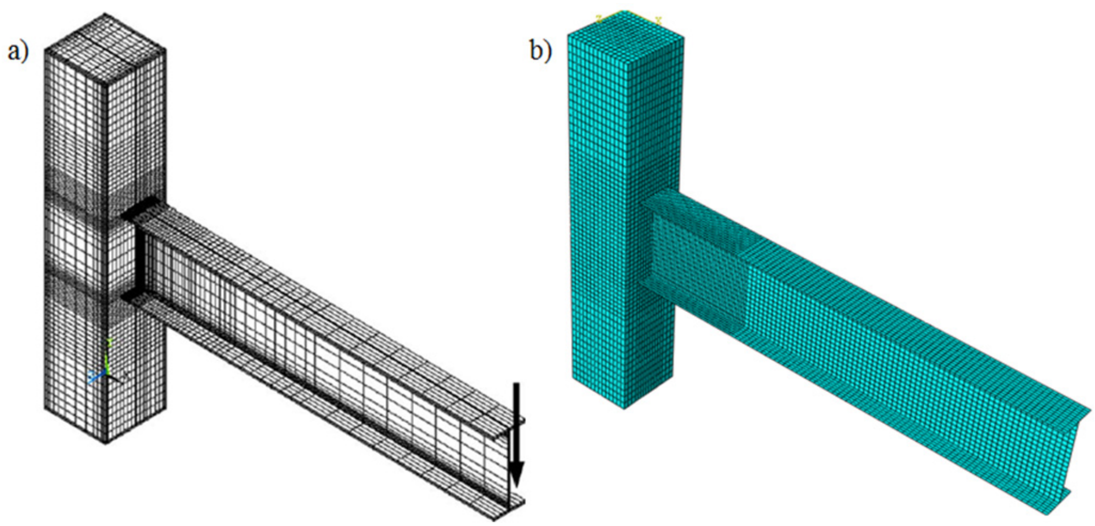

Figure 25 Finite element models: (a) Chen's model; (b) the rebuilt model in the present study.

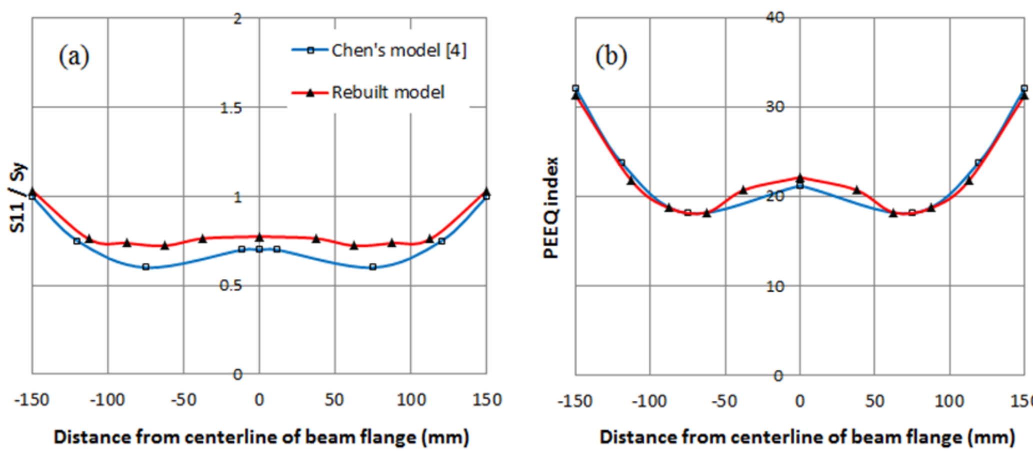

Figure 26 Comparison of two models: (a) normalized longitudinal stress at 0.5% story drift angle; and (b) PEEQ index at 4% story drift angle.

To determine critical PEEQ index, the validated rebuilt model was analyzed under cyclic loading up to the 2.3% story drift cycle (which is the story drift of crack initiation in the referred test [Chen et al. 2004]).PEEQ in the edge of the beam flange (crack region in experiment) is 0.023, Consequently PEEQ index is equal to 116 ($\varepsilon_y = 0.00198$). This value is selected as critical PEEQ index for crack initiation. It should be noted that PEEQ index is dependent on element type and mesh sizes; therefore for using the critical PEEQ index of 116, the element type and mesh sizes for other models must be similar.

Dual-Strong-Axis IBBC Connections

After a comprehensive investigation on deficiencies of traditional connections, Chen et al. [2006] proposed an IBBC connection detail. The proposed connection configuration has two distinctively improved connection details compared to previous ones, which are no weld access hole detail and a widened flange of the stub beam. The improved connection details reduce the stress concentration and plastic strain demands at the beam flange groove weld. The cyclic performance of the widened flange connection has been confirmed by the full scale tests with T-shaped subassemblage conducted by Chen et al. [2006]. In this study, a four-sided specimen of this connection detail is modeled and evaluated. Figure 27 displays this four-sided widened flange connection.

In proposed connection configuration, the box-column is subjected to bending about rotated axes. It must be noted that in the case of the dual-strong-axis connection, the box-column is normally subjected to bending about rotated axes due to moments in two directions regardless of the orientation of column section.

In this study a new connection configuration, which does not need internal continuity plates, is introduced based on column-tree construction concept. Stub beams built up from plates are connected to corner of box-column and external filler plates are installed between stub beam flanges. Stub beam webs are connected to box-column using full-depth bent plates. Figure 28 shows the proposed column-tree connection.

The bending stiffness of a member is proportional to its moment of inertia (I). In the case of members with symmetric section, such as square box, the moment of inertia about all the axes are equal. Therefore bending stiffness of them is the same about all the axes. The bending strength of a member is proportional to its plastic modulus (Z). The difference between maximum plastic modulus and minimum plastic modulus is equal to 5.72%, which can be neglected. Therefore the bending strength of a box-column about all the axes may be considered almost equal.

Note in the figures below that the behavior of square box-shaped section about rotated axes compared to principal axes is rather identical, and sometimes better, in terms of bending stiffness, bending strength and cross-section ductility. Hence rotating the column section to build the proposed connection has no detrimental effect on column behavior.

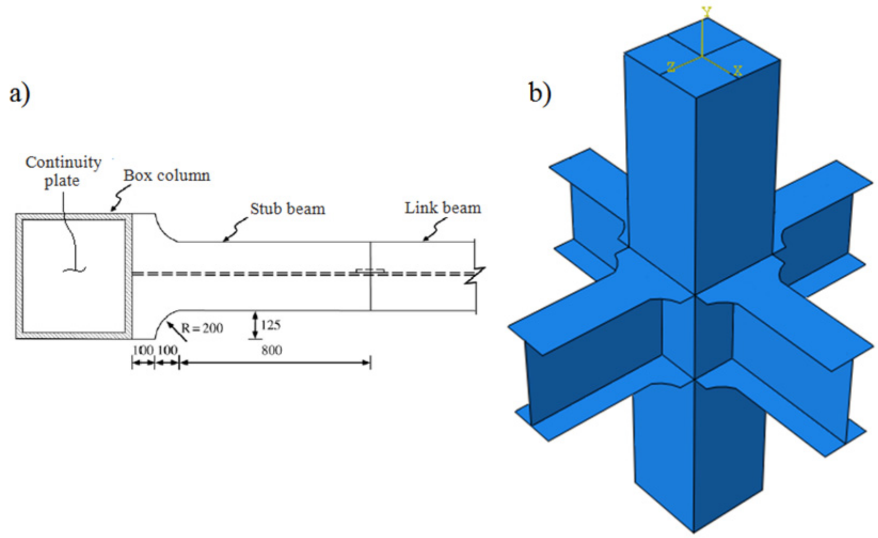

Figure 27 Widened flange column-tree connection [Chen et al. 2006]: (a) details; (b) the 4-sided specimen in the present study.

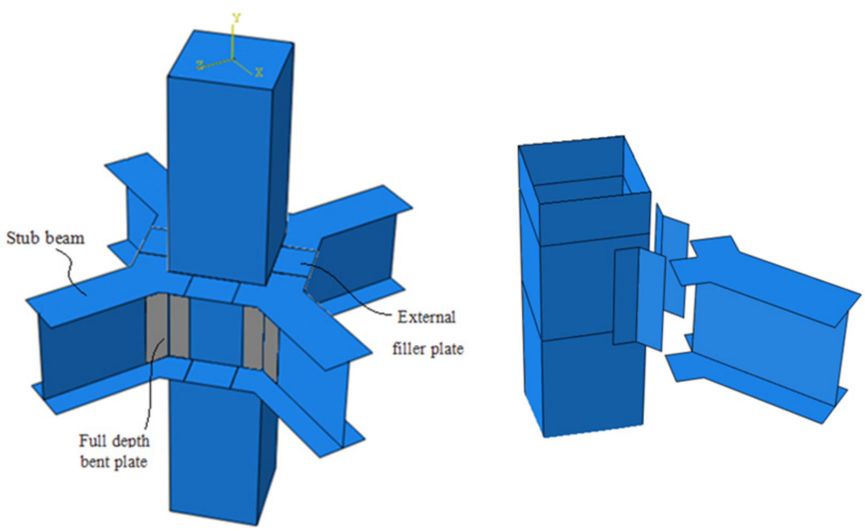

Figure 28 The proposed column-tree connection.

Finite Element Modeling

For modeling and evaluating dual-strong-axis MRF connections, symmetric fir-sided subassemblages TS1 and TS2, are used. These subassemblages, shown in Figure 29, represent an interior joint of a building structure with moment resisting frames used in orthogonal directions. In Figure 29 ‘A’ represents amplitude of applied load. The subassemblage TS1 is a cruciform subassemblage, which is subjected to a lateral displacement in one direction. In subassemblage TS2, 100% displacement in one direction and 30% displacement in another direction are applied simultaneously. Consequently, the joint is effectively subjected to moments in two axes.

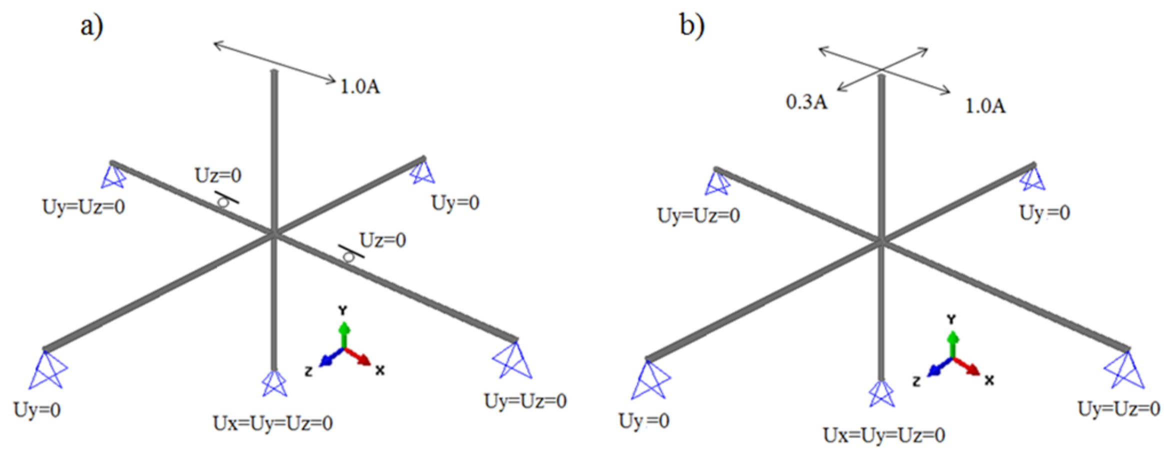

Figure 29 Studied 4-sided subassemblages: (a) subassemblage TS1; and (b) subassemblage TS2.

In this investigation, the column length is set equal to 3.0 m and distance from beam support to column centerline is 3.305 m. These sizes and also the beam and column section are similar to Chen's test [2006]. Table 7 lists the geometric sizes of the specimens. P1 and W1 represent proposed and widened flange connections, respectively. The subassemblage elements are discretized using quadrilateral four-node shell elements with six degrees of freedom at each node. Instead of modeling the welds explicitly, shell element nodes are constrained to each other to have the same displacements at the weld location. The plastic hinge area in the beam and the panel zone are modeled with a finer mesh to get more accurate results. A bilinear stress-strain relationship is considered for all components. The von Mises yield criterion is used to specify the plasticization. In analyses under monotonic and cyclic loading, the isotropic hardening rule and kinematic hardening rule are used, respectively. To mobilize the geometric nonlinearities in the model, geometric imperfections in some nodes are imposed.

Table 7 Geometric properties of the specimen.

Spec.	Column	Stub Beam						Continuity plate	External filler plate		Bent plate		
	d_c, t_c	d_b	b_{bf}	t_{bf}	t_{bw}	x	y	t_{cp}	a	b	$l1$	$l2$	t
P1	550×550×27	588	300	20	12	100	150	-	267	212	130	100	10
W1	550×550×27	588	300	20	12	-		20	-			-	

All dimensions are in mm.

Analysis Results for Uniaxial Loading (Subassemblage TS1)

Connection Rigidity

In accordance with the method proposed in AISC specifications, connection stiffness at service load is defined as $K_S = M_S / \theta_S$ where M_S and θ_S are the moment and the relative rotation between the beam end and the column, respectively. The specimens W1 and P1 were analyzed under monotonic loading up to 1% story drift which represents service loads. The moment at column face versus relative beam-column rotation is plotted in Figure 30 for both specimens. A comparison of the connections stiffness at service loads with the threshold value of 20EI/L confirms the assumption that both specimens are in the category of rigid connections. *L* and *EI* are the length and bending rigidity of the beam, respectively.

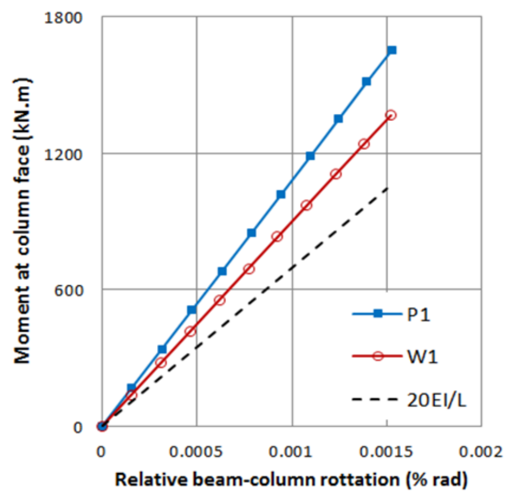

Figure 30 Rigidity of the studied connections.

Cyclic Behavior

The specimens W1 and P1 were also analyzed under cyclic loading. As shown in Figure 16, the loading history specified in the AISC seismic provisions [2005] was followed. Based on the results of cyclic analysis, the moment at column face versus total story drift is plotted in Figure 31 for both specimens. This figure shows that in both specimens W1 and P1, the moment at column face exceeds the flexural capacity of the beam section, $M_{pe} = R_y Z_b F_y$. R_y accounts for the difference between the minimum specified yield strength F_y and the expected yield strengths, based on AISC seismic provision [2005], R_y for ASTM5 72 GR50 steel plates is equal to 1.1 and Z_b represents the plastic modulus of the beam section. It proves that both connections can develop full strength of the beam.

According to Figure 31, the specimen P1 exhibits stable and reliable hysteretic behavior until end of 5% story drift cycle with 12% strength deterioration. It should be noted that the strength degradation of the specimen P1 resulted from ductile local buckling of beam flanges. Figure 32 illustrates variation of PEEQ indices at the intersection of the beam flange and the column versus loading cycles. For the specimen W1, PEEQ index exceeds the value of 116 (critical PEEQ index calculated earlier) at 27th cycle corresponding to 3% story drift. Therefore there is high probability of the brittle fracture in groove weld of the beam flange after this cycle. But in Specimen P1, the PEEQ index around the intersection is under critical for the whole loading history. To emphasize on this issue, the curves shown in Figure 31(a) have been plotted in dotted line shape when the PEEQ index is over critical.

The first cycle with 4% story drift (29th loading cycle) is selected for evaluating the distributions of the PEEQ indices along the intersection of beam flange and the column face. As shown in Figure 33 and discussed in previous section, PEEQ index in specimen P1 is smaller than critical value; therefore brittle fracture of groove welds in that location is unlikely. But PEEQ index in specimen W1 is above the critical value in middle regions of beam-column intersection and hence there is high probability of the brittle fracture in groove weld region. Generally the distribution of the PEEQ index exhibits a more desirable pattern of plasticization in Specimen P1 compared to W1.

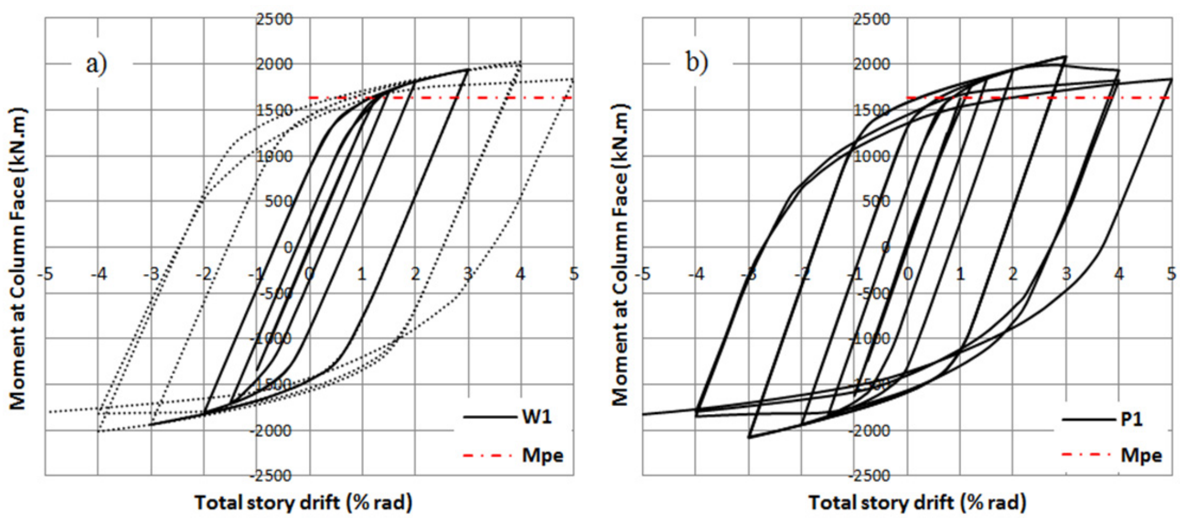

Figure 31 Hysteretic behavior (uniaxial loading): (a) W1 and (b) P1.

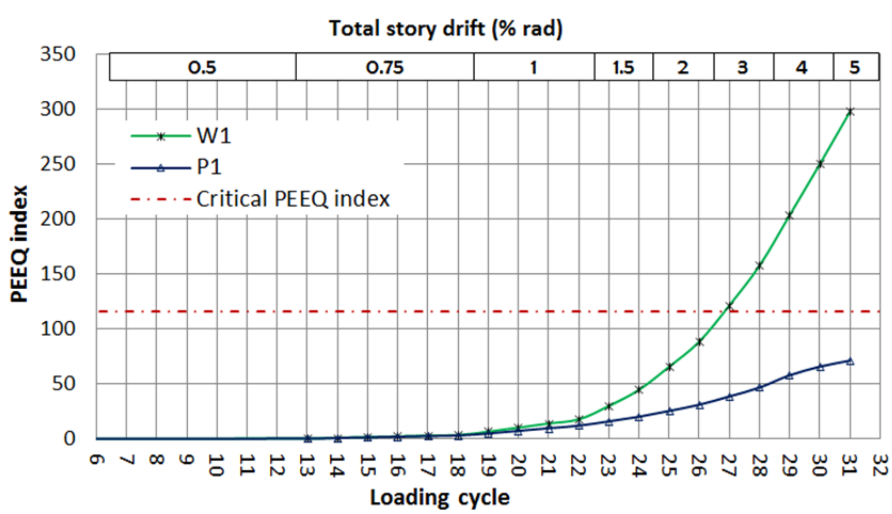

Figure 32 Maximum PEEQ index of beam-column intersection versus loading cycles.

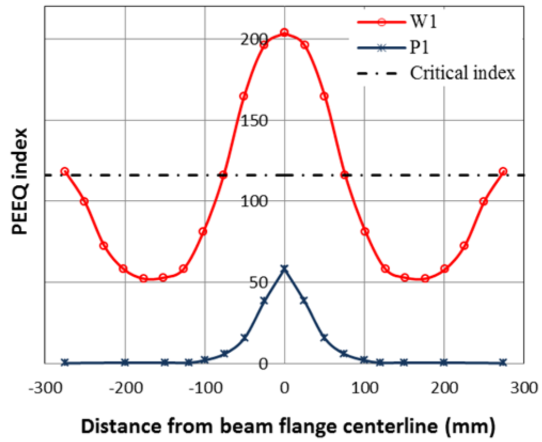

Figure 33 **Distributions of the PEEQ indices along beam-column intersection at the end of 4% story drift cycle.**

Analysis Results for Biaxial Loading (Subassemblage TS2)

Overall Behavior

For studying the overall behavior of the specimens, both specimens were analyzed under monotonic loading. For subassemblage TS2, it is assumed that total story drift may be represented by the column tip displacement in *X*-direction divided by the column height. Also the moment at column face is equal to the beam reaction force (beam in *X*-direction) times the distance. The results show that the elastic stiffness of the connections is not affected significantly.

Cyclic Behavior

Specimens P1 and W1 in TS2 configuration were also analyzed under biaxial cyclic loading. Figure 34 shows the cyclic curve of moment versus total story drift. As shown, the specimen P1 has better hysteretic performance, comparatively.

For the specimen W1, PEEQ index exceeds the value of 116 (critical PEEQ index calculated in section 2.2) at 27th cycle. But in the specimens P1, PEEQ index in weld regions is below critical value for the whole loading history. PEEQ indices indicate that plastic demand in critical regions for biaxial loading is more than uniaxial loading. The dotted line in Figure 34 correspond to parts of the results in which PEEQ index has exceeded the critical value.

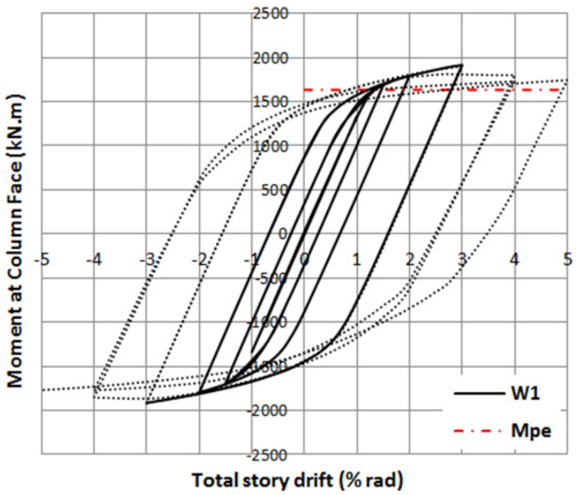

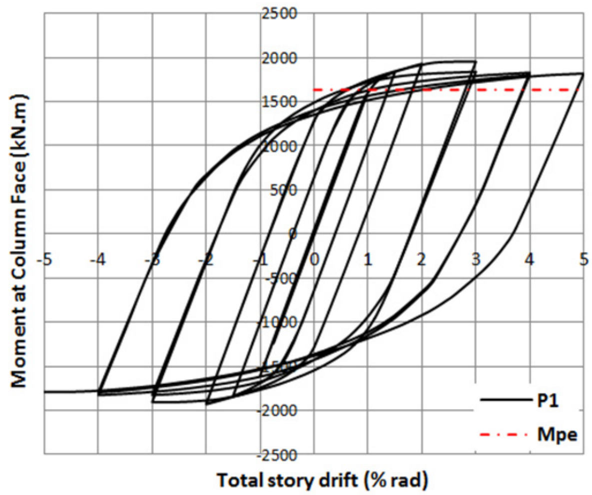

Figure 34 Hysteretic behavior (biaxial loading): (a) W1 and (b) P1.

Formation of the Plastic Hinge

Figure 35 illustrates deformed shapes and contours of PEEQ at the end of 29th cycle for both specimens. PEEQ contours show that there is some plasticization around the intersection of members in specimen W1. In other words the plastic hinge has extended to column face which is not desirable for seismic performance. However there is no significant amount of plasticization around intersection of members in specimen P1 and the plastic hinge has been formed away from column face.

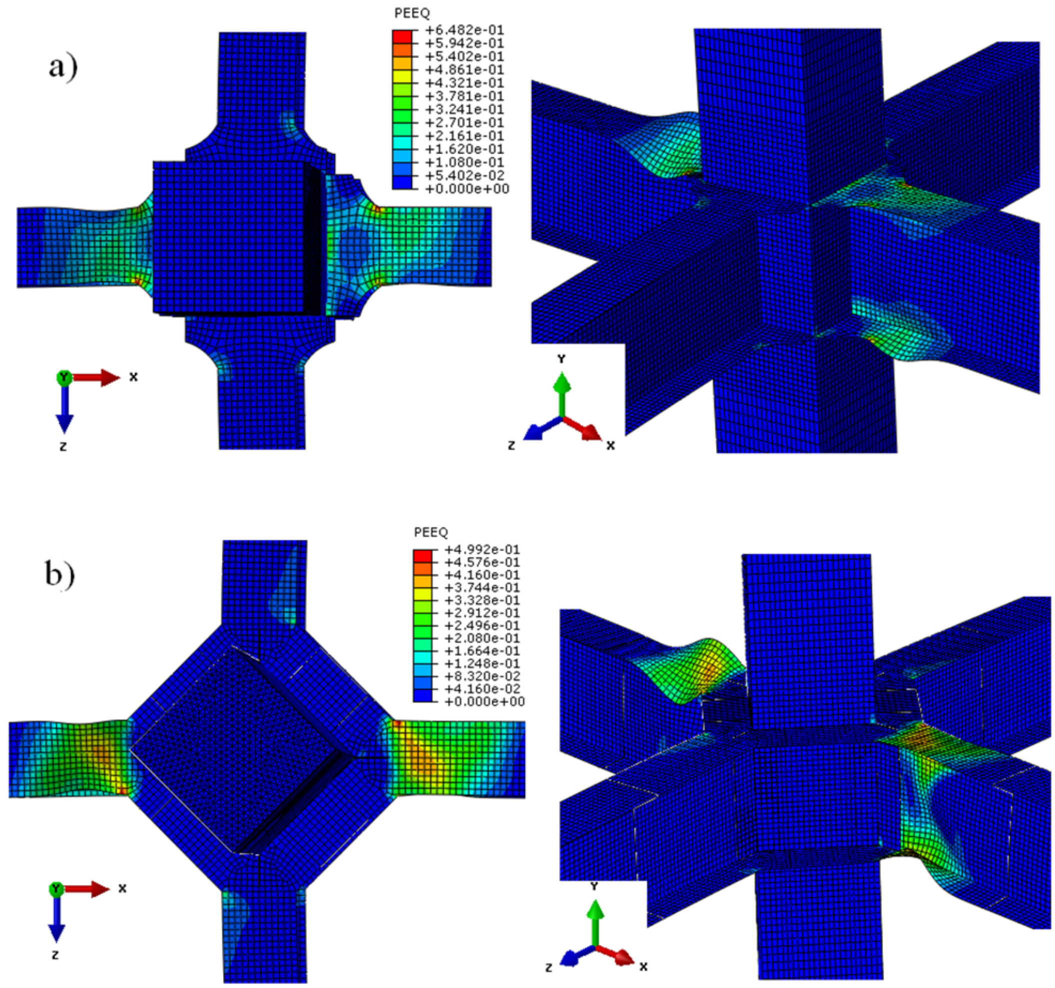

Figure 35 Deformed shapes and contours of PEEQ at the end of 29th cycle (biaxial loading): (a) specimen W1 and (b) specimen P1.

CONCLUDING REMARKS

An externally reinforced connection configuration has been presented for dual-strong-axis IBBC welded connection based on column-tree construction. The analytical results presented support the following conclusions:

- The proposed connection configuration provides a rigid moment connection between I-beams and box-columns as the connection stiffness is greater than the threshold value for a rigid connection specified in AISC standard.
- The proposed connection strength exceeds the flexural capacity of the beam in both uniaxial and biaxial loading, so this connection can develop full strength of the beam.
- The proposed connection when subjected to uniaxial cyclic loading, can tolerate at least 5% story drift and $M_{0.04}$ (the moment in column face at 4% story drift) is equal to 1.18 M_{pe}. Therefore this connection is qualified for seismic applications according to AISC

seismic provisions.

- The proposed connection when subjected to biaxial cyclic loading can tolerate at least 5% story drift and $M_{0.04}$ is equal to $1.11\,M_{pe}$
- In order to investigate the performance of dual-strong-axis moment connections, it is not sufficient to use only the uniaxial subassemblage such as T-shaped and cruciform subassemblages because such connections are subjected to moments in two directions, which may result in greater plasticization and premature buckling.

It seems that the proposed IBBC connection may be successfully used in structures where special MRFs are to be utilized in orthogonal directions. However full scale tests are required for final confirmation of their proper seismic behavior.

ACKNOWLEDGEMENTS

The author would like to thank his former graduate students Dr. Sazmand, Dr. Amiri and Mr. Sedighian who worked on different parts of the reported research during their postgraduate studies in Tarbiat Modares University. The contribution of some colleagues Dr. Shahbeyk, Dr. Mazrouei, and Professor Engelhardt who acted as co-advisor for above named students, is also gratefully appreciated.

REFERENCES

ABAQUS (2010). *User's Manual, Version 6.10*, Hibbitt, Karlsson, and Sorensen, Inc., Providence, RI

AISC (2005). *Seismic Provisions for Structural Steel Buildings, ANSI/AISC 341-05*, American Institute of Steel Construction, Inc., Chicago, IL.

Amiri H. (2012). *Analysis of the Ordinary Steel Saddle Connections Subjected To Cyclic Loading and Their Fracture Behavior*, PhD Dissertation, Tarbiat Modares University. Tehran, Iran.

Anderson T.L. (1995). *Fracture Mechanics*, 2nd ed., CRC Press, Boca Raton, FL.

Building Seismic Safety Council (1997). *NEHRP Guidelines for the Seismic Rehabilitation of Buildings, FEMA-273*, Washington, D.C.

Chen C.-C., Lin C.-C., Tsai C.-L. (2004). Evaluation of reinforced connections between steel beams and box columns, *Eng. Struct*., 26:.1889–1904.

Chen C.-C., Lin C.-C., Lin C.-H. (2006). Ductile moment connection used in steel column-tree moment-resisting frames, *J. Construct Steel Res*., 62: 793–801.

Chen Y., Lambert S. (2003). Analysis of ductile tearing of pipeline-steel in single edge notch tension specimens, *Int. J. Fracture*, 124: 179–199.

Chou C.-C., Tsai K.-C,. Wang Y.-Y., Jao C.-K. (2010). Seismic rehabilitation performance of steel side plate moment connections, *Earthq. Eng. Struct. Dyn*., 39: 23–44.

Fell B.V., Myers A.M., Deierlein G.G., Kanvinde A.M. (2006). Testing and simulation of ultra-low-cycle fracture and fatigue in steel braces, *Proceedings, 8th National Conference on Earthquake Engineering*, San Francisco, CA.

FEMA (2000). *Recommended Seismic Design Criteria for New Steel Moment-Frame Buildings, FEMA-350*, Federal Emergency Management Agency, Washington D.C.

FEMA (2000). *State of the Art Report on Connection Performance, FEMA-355D*, Federal Emergency Management Agency, Washington D.C.

Fielding D.J., Huang J.S. (1971). Shear in steel beam-to-column connections, *Welding J.*, 50(7): 313s–326 (research supplement).

Ghobadi M.S., Mazroi A., Ghassemieh M. (2009a). Cyclic response characteristics of retrofitted moment resisting connections, *J. Construct Steel Res*., 65: 586–598.

Ghobadi M.S., Ghassemieh M., Mazroi A., Abolmaali A. (2009b). Seismic performance of ductile welded connections using T-stiffener, *J. Construct Steel Res.,* 65: 766–775.

Goswami R., Murty C.V.R. (2010). Externally reinforced welded I-beam-to-box-column seismic connection, ASCE, *J. Eng. Mech.,* 136(1): 23–30.

Hommel J.H., Meschke G. (2010). A hybrid modeling concept for ultra-low cycle fatigue of metallic structures based on micropore damage and unit cell models, *Int. J. Fatigue*, 32: 1885–1894.

Huang, H (2009).0*Simulating the Inelastic Seismic Behavior of Steel Braced Frames Including the Effects of Low-Cycle Fatigue*, Ph.D. Dissertation, Department of Civil and Environmental Engineering, University of California, Berkeley ,CA.

Kang C.-H., Shin K-.J., Oh Y.-S., Moon T.-S. (2001). Hysteresis behavior of CFT column to H-beam connections with external T-stiffeners and penetrated elements, *Eng. Struct*., 23: 1194–1201.

Kanvinde A. (2004). *Micromechanical Simulation of Earthquake İnduced Fractures in Steel Structures*, PhD Dissertation, Department of Civil and Environmental Engineering, Stanford University, Stanford, CA.

Kanvinde A.M., Deierlein G.G. (2007). Cyclic void growth model to assess ductile fracture ınitiation in structural steels due to ultra low cycle fatigue, *J. Eng. Mech.,* 133(6): 701–712.

Kim K.D., Engelhardt MD. (1995). Development of analytical models for earthquake analysis of steel moment frames, *Report no. PMFSEL 95-2*, Phil M. Ferguson Structural Engineering Laboratory, The University of Texas, Austin, TX.

Kim K.D., Engelhardt M.D. (2002). Monotonic and cyclic loading models for panel zones in steel moment frames, *J. Construct Steel Res*., 58: 605–635.

Krawinkler H., Bertero V.V., Popov E.P. (1971). Inelastic behavior of steel beam-to-column subassemblages, *Report No. EERC 71/07*, Earthquake Engineering Research Center, University of California, Berkeley, CA.

Krawinkler H., Gupta A., Medina R., Luco N. (2000). Loading histories for seismic performance testing of SMRF components and assemblies, SAC Joint Venture, *Report No .SAC/BD-00/10*, Richmond. CA.

Kuroda M. (2001). Extremely low cycle fatigue life prediction based on a new cumulative fatigue damage model, *Int. J. Fatigue,* 24: 699–703.

Lequesne C. (2009). *Modeling of Fracture in Heavy Steel Welded Beam-to-Column Connection Submitted to Cyclic Loading by Finite Elements*, PhD Dissertation, University of Liege, Liege, Belgium.

Mirghaderi S.R., Torabian S., Imanpour A. (2010a). Seismic performance of the Accordion-Web RBS connection. *J. Construct Steel Res.,* 66: 277–288.

Management and Planning Organization (2006). Design criteria for Khorjeeni beam-to-column connections, *Document No. 3242006.*

Ministry of Housing and Urban Development (2006). *Iranian National Building Code*, Chapter 10, Design of steel structures.

Mirghaderi S.R., Torabian S., Keshavarzi F. (2010b). I-beam to box-column connection by a vertical plate passing through the column, *Eng. Struct*., 32(8): 2034–2048.

Myers A.T. (2009). *Testing and Probabilistic Simulation of Ductile Fracture İnitiation in Structural Steel Components and Weldments*, PhD Dissertation, Department of Civil and Environmental Engineering, Stanford University, Stanford, CA.

Nakashima M., Roeder C.W., Maruoka Y. (2000). Steel moment frames for earthquakes in United States and Japan, ASCE, *J. Struct. Eng*., 126(8): 861−868.

Sazmand E., Aghakouchak A.A. (2012). Modeling the panel zone in steel MR frames composed of built-up columns, *J. Construct Steel Res*., 77: 54–68.

Shanmugam N.E., Ting L.C. Lee S.L. (1991). Behavior of I-beam to box-column connections stiffened externally and subjected to fluctuating loads, *J. Construct Steel Res*., 20: 129−148.

Shanmugam N.E., Ting L.C. (1995). Welded interior box-column to I-beam connections, ASCE, *J. Struct. Eng*., 121(5): 824−830.

Shin K.J., Kim.Y.J., Oh Y.S., Moon T.S. (2004). Behavior of welded CFT column to H-beam connections with external stiffeners,. *Eng. Struct*., 26: 1877−1887.

Tanaka N. (2003). Evaluation of maximum strength and optimum haunch length of steel beam-end with horizontal haunch, *Eng. Struct.,* 25: 229−239.

Tateishi K, Chen T, Hanji T. (2008). Extremely low cycle fatigue assessment method for un–stiffened cantilever steel column, *J. Doboko Gakkai Ronbushuu*, 64(2): 288−296.

Tateishi K, Hanji, T, Minami K. (2007). A prediction model for extremely low cycle fatigue strength of structural steel, *Int. J. Fatigue*, 29: 887–896.

Ting L.C., Shanmugam N.E., Lee S.L. (1991). Box-column to I-beam connections with external stiffeners, J. Construct. Steel Res., 18: 209–226.

Tsai K.-C., Popov E.P. (1988). Steel beam–column joints in seismic moment resisting frames, *Report No. EERC 88/19,* Earthquake Engineering Research Center, University of California, Berkeley, CA.

Uang C.-M, Latham C. (1995). Cyclic testing of full-scale MNH-SMRF™ moment connections, *Report No. TR-95/01*, University of California, San Diego, La Jolla, CA.

Uriz P., Mahin S.A. (2004). Seismic performance assessment of concentrically braced steel frames, *Proceedings, 13th World Conference on Earthquake Engineering*, Paper No. 1639, Vancouver, Canada.

Wang S.J. (1988). *Seismic Response of Steel Building Frames with İnelastic Joint Deformation*, PhD Disseration, Department of Civil Engineering, Lehigh University, Bethlehem, PA.

Wheeler A.T., Clarke M.J., Hancock G.J., Murray T.M. (1998). Design model for bolted moment end plate connections joining rectangular hollow sections, ASCE, *J. Struct. Eng*., 124(2):164-173.

Wheeler A.T., Clarke M.J., Hancock G.J. (2000). FE modeling of four-bolt tubular moment end-plate connections, ASCE, *J. Struct. Eng*., 126(7): 816−822.

Xue L. (2008). A unified expression for low cycle fatigue and extremely low cycle fatigue and its implication for monotonic loading, *Int. J. Fatigue*, 30: 1691–1698.

Xue L. Wierzbicki T. (2008). Ductile fracture initiation and propagation modeling using damage plasticity theory, *Eng. Fracture Mech*., 75: 3276–3293.

A NEW PUSHOVER PROCEDURE FOR ESTIMATING SEISMIC DEMANDS OF TALL BUILDINGS

Faramarz Khoshnoudian[*] and Mahdi Kiani[+]

ABSTRACT

The modified consecutive modal pushover procedure as a new nonlinear static method was proposed to estimate seismic demands of one-way asymmetric-plan tall buildings with dual systems. Comparing of modified consecutive modal pushover procedure predictions with the FEMA load patterns as well as nonlinear time history analysis (NLTHA) has been carried out on one-way asymmetric–plan buildings. The estimations of the proposed procedure on seismic demands of one–way asymmetric-plan buildings with dual systems demonstrate reasonable accuracy of the procedure in comparing to an exact solution obtained from nonlinear time history analysis. In addition the new pushover procedure is more accurate than the FEMA method.

Keywords: *asymmetric-plan tall buildings, consecutive modal pushover procedure, dual system, higher-mode effects, seismic responses, torsion*

INTRODUCTION

The nonlinear static procedure (NSP) has been recognized as a common design tool to estimate maximum nonlinear responses of structures under earthquake loads. This procedure has been well established by major building codes worldwide. The procedure typically applies to simple symmetric structures with well-defined principal axes. The applicability of the NSP to asymmetric plan tall buildings has been analyzed here. Specifically the ability for NSP to account for the torsional and higher mode effects has been analyzed. In the past, several researches [Moghadam and Tso 1998; Moghadam and Tso 2000; Chopra and Goel 2004; Fajfar et al. 2008] have been dedicated to investigate the applicability of the NSP to asymmetric-plan buildings proposing well known procedures such as MPA, N2 methods. In the current study, a new NSP, a modified consecutive modal pushover (MCMP) procedure [Poursha et al. 2011], has been proposed to analyze peak nonlinear responses of one-way asymmetric-plan tall buildings with dual systems. First, the modal properties of asymmetric-plan buildings are described. Subsequently, the structural models (10, 15, and 20-story buildings with steel moment resisting frames), ground motions and underlying assumptions are briefly explained. Finally, results of the MCMP were compared to the mean of the maximum nonlinear responses obtained from the time history analyses and FEMA load distributions. The result shows that the MCMP procedure can predict seismic responses of asymmetric plan tall buildings accurately especially the plastic hinge rotations in the beams, which is difficult to estimate using the traditional NSP.

[*] Professor, Department of Civil Engineering, Amirkabir University of Technology, Tehran, Iran.
[+] M.Sc. graduated, Department of Civil Engineering, Amirkabir University of Technology, Tehran, Iran.

GOVERNING EQUATIONS OF ONE-WAY ASYMMETRIC-PLAN TALL BUILDINGS

The governing equations of *N*-story buildings under horizontal earthquake excitations can be expressed as Equation (1):

$$\begin{bmatrix} m & 0 & 0 \\ 0 & m & 0 \\ 0 & 0 & I_o \end{bmatrix} \begin{Bmatrix} \ddot{u}_x \\ \ddot{u}_y \\ \ddot{u}_\theta \end{Bmatrix} + f_s(u, sign\dot{u}) = -\begin{bmatrix} m & 0 & 0 \\ 0 & m & 0 \\ 0 & 0 & I_o \end{bmatrix} i_x \ddot{u}_{gx}(t) - \begin{bmatrix} m & 0 & 0 \\ 0 & m & 0 \\ 0 & 0 & I_o \end{bmatrix} i_y \ddot{u}_{gy}(t) \tag{1}$$

where u_x, u_y are the *x*- and *y*-lateral floor displacements vectors, and u_θ is the torsional floor displacement vector. *m* is a diagonal mass matrix with $m_{jj} = m_j$, the mass lumped at the *j*th floor diaphragm. I_o is a diagonal matrix with $I_{jj} = I_{oj}$, the polar moment of inertia corresponding to the *j*th floor diaphragm about a vertical axis through the center-of-mass (CM). In Equation (1), the influence vectors associated with the components of ground motion in the x- and y-directions ($\ddot{u}_{gx}(t)$ and $\ddot{u}_{gy}(t)$) are as follows:

$$i_x = \begin{Bmatrix} 1 \\ 0 \\ 0 \end{Bmatrix} \qquad i_y = \begin{Bmatrix} 0 \\ 1 \\ 0 \end{Bmatrix} \tag{2}$$

where each element of the $N\times1$ vector **1** is equal to unity and the $N\times1$ vector **0** is equal to zero. $f_s(u, sign\dot{u})$ is the force-deformation relation for a building that deforms into an inelastic range.

Equation (1) can be rewritten for a one-way asymmetric-plan building that is symmetric about the x-axis but asymmetric about the *y*-axis [see Figure 1] and subjected to earthquake ground motion in the *y*-direction:

$$\begin{bmatrix} m & 0 \\ 0 & I_o \end{bmatrix} \begin{Bmatrix} \ddot{u}_y \\ \ddot{u}_\theta \end{Bmatrix} + \begin{bmatrix} k_{yy} & k_{y\theta} \\ k_{\theta y} & k_{\theta\theta} \end{bmatrix} \begin{Bmatrix} u_y \\ u_\theta \end{Bmatrix} = -\begin{bmatrix} m & 0 \\ 0 & I_o \end{bmatrix} \begin{Bmatrix} 1 \\ 0 \end{Bmatrix} \ddot{u}_{gy}(t) \tag{3}$$

in which k_{yy}, $k_{y\theta}$ $k_{\theta y}$ and $k_{\theta\theta}$ are stiffness sub-matrixes. When the radius of gyration for all floor diaphragms is identical ($I_{oj} = m_j r^2$), the sub-matrix I_o, can be substituted by $I_o = r^2 m$ in the above equation.

The right side of Equation (3) can be defined as the effective earthquake forces:

$$P_{eff}(t) = -\begin{Bmatrix} m1 \\ 0 \end{Bmatrix} \ddot{u}_{gy}(t) = -s\ddot{u}_{gy}(t) \tag{4}$$

The time independent part of the spatial distribution of the effective forces in Equation (4) is the summation of modal inertia force distributions, s_n:

$$s = \begin{Bmatrix} m1 \\ 0 \end{Bmatrix} = \sum_{n=1}^{2N} s_n = \sum_{n=1}^{2N} \Gamma_n \begin{Bmatrix} m\Phi_{yn} \\ r^2 m\Phi_{\theta n} \end{Bmatrix} \tag{5}$$

Φ_{yn} and $\Phi_{\theta n}$ represent the translation in the y direction and rotation of the N floor about a vertical axis for the nth mode. The modal participating factor, Γ_n, is defined as follows:

$$\Gamma_n = \frac{L_n}{M_n} \tag{6}$$

where

$$L_n = \begin{Bmatrix} \Phi_{yn}^T & \Phi_{\theta n}^T \end{Bmatrix} \begin{Bmatrix} m1 \\ 0 \end{Bmatrix} = \Phi_{yn}^T m1 = \sum_{j=1}^{N} m_j \varphi_{jyn} \tag{7}$$

$$M_n = \begin{Bmatrix} \Phi_{yn}^T & \Phi_{\theta n}^T \end{Bmatrix} \begin{bmatrix} m & 0 \\ 0 & r^2 m \end{bmatrix} \begin{Bmatrix} \Phi_{yn} \\ \Phi_{\theta n} \end{Bmatrix} \tag{8}$$

where M_n can be expanded as follows:

$$M_n = \Phi_{yn}^T m\Phi_{yn} + r^2 \Phi_{\theta n}^T m\Phi_{\theta n} = \sum_{j=1}^{N} m_j \varphi_{jyn}^2 + r^2 \sum_{j=1}^{N} m_j \varphi_{j\theta n}^2 \tag{9}$$

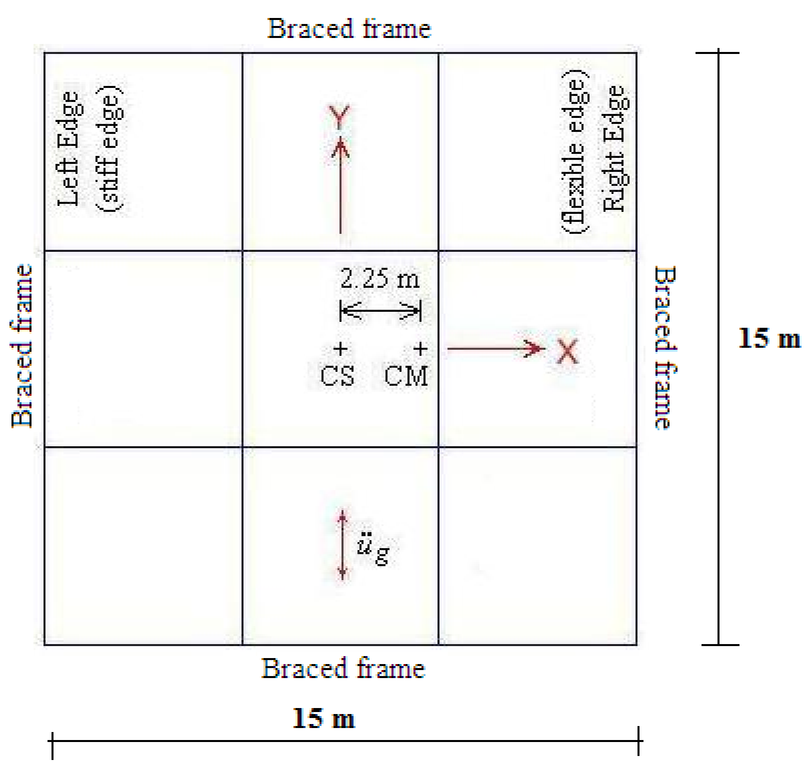

Figure 1 Plan of the analyzed one-way asymmetric-plan tall buildings.

The following results can be obtained by pre-multiplying each sub-matrix in Equation (5) by $\mathbf{1}^T$:

$$\sum_{n=1}^{2N} M_n^* = \sum_{j=1}^{N} m_j \qquad \sum_{n=1}^{2N} I_{on}^* = 0 \tag{10}$$

in which

$$M_n^* = \frac{(L_n)^2}{M_n} \qquad I_{on}^* = r^2 \Gamma_n \mathbf{1}^T m \Phi_{\theta n} \tag{11}$$

where M_n^* and I_{on}^* are the effective modal mass and modal static response for the base torque.

MODIFIED CONSECUTIVE MODAL PUSHOVER (MCMP) PROCEDURE

Unlike the traditional NSP, the modified consecutive modal pushover (MCMP) procedure involves multi-stage and single-stage pushover analyses. In each stage of the multi-stage analysis, a lateral force distribution is obtained using the elastic mode shapes. A pushover analysis is then performed using the calculated force distribution until the roof drift reaches a certain target drift. In the subsequent stage, the structure's stress and deformation were retained and the structure is further pushed to a new target drift using a new lateral force distribution.

In the MCMP procedure [Kashani 2010], the displacement increment at roof, u_{ri}, at i^{th} stage is calculated using following equation:

$$u_{ri} = \beta_i \delta_t \tag{13}$$

in which

$$\beta_i = \frac{\Gamma_i D_i}{\sum_{n=1}^{N_s} \Gamma_n D_n} \tag{14}$$

where δ_t is the target displacement at roof which can be calculated using the coefficient method or CSM [ATC 2005], β_i is a dimensionless parameter which represent the portion of the target displacement in each stage, D_i is the spectral displacement for the structure at the i^{th} mode of vibration, Γ_i is the modal participating factor of i$^{\text{th}}$ mode and N_s is number of stages to be included in the multi-stage pushover analysis.

Generally, the lateral loads ($\mathbf{s}_n^* = \mathbf{M}\Phi_n$) at each stage of the multi-stage pushover analysis involve two lateral forces and a torsional torque at each floor of asymmetric-plan buildings [Chopra and Goel 2004]. In a building with only one axis of asymmetric the lateral force excitations can be expressed as:

$$\mathbf{s}_n^* = \mathbf{M}\Phi_n = \begin{bmatrix} \mathbf{m} & 0 & 0 \\ 0 & \mathbf{m} & 0 \\ 0 & 0 & \mathbf{I_o} \end{bmatrix} \begin{Bmatrix} 0 \\ \Phi_{yn} \\ \Phi_{\theta n} \end{Bmatrix} = \begin{Bmatrix} 0 \\ \mathbf{m}\Phi_{yn} \\ \mathbf{I_o}\Phi_{\theta n} \end{Bmatrix} \tag{15}$$

m is a diagonal mass matrix with $m_{jj} = m_j$, the mass lumped at the *j*th floor diaphragm. $I_{\mathbf{o}}$ is a diagonal matrix with $I_{jj} = I_{oj}$, the inertia polar moment of the *j*th floor diaphragm about a vertical axis through the center of mass (CM).

Absolute displacement of roof (U_{ri}) at the end of each stage of multi-stage pushover analysis is defined as:

$$U_{ri} = \gamma_i \delta_t \tag{16}$$

in which

$$\gamma_i = \sum_{j=1}^{N_s} \beta_j; \qquad i \le N_S \tag{17}$$

It should be stated that the number of stages (N_S) required is based on sum of participation mass ratios when the total participating mass reaches 90% of the total seismic mass of building.

In addition to the multi stage analysis, the MCMP procedure uses a single-stage pushover analysis with an uniform load pattern. The seismic demands are obtained from enveloping the responses of multi-stage and single-stage pushover analyses. It should be noted that the responses obtained from the multi-stage pushover analysis typically dominate the response in the mid to upper stories of building. On the other hand, the responses obtained from the single-stage pushover analysis usually dominate the response in lower stories.

Prototype Model

In the current study prototype models consist of steel moment resisting frames with concentrically braced frames were included. The prototype models range from 10, 15 and 20-story buildings, which covers a wide range of structural periods. Figure 1 shows the plan view of the prototype model. The mass of the structure is purposely shifted by 15% in the *Y*-direction to create the accidental torsional effect. The same shift in mass is repeated for all floors in the structure. In addition, by modifying the ratio of the floor moment of inertia (I_{oj}) to the floor mass (m_j), two types of asymmetric-plan buildings were created [Chopra and Goel 2004]. The asymmetric-plan buildings involve torsionally stiff (TS) and torsionally flexible (TF) systems, which have different degrees of coupling between the translational and torsional motions.

In order to evaluate the MCMP procedure, nonlinear time history analyses (NLTHA) as well as pushover analysis based on FEMA load patterns have been performed. The NLTHA was carried out by using the numerical implicit $Wilson - \theta$ time integration method. A 5% mass and stiffness proportional damping was assigned to the first and third modes of vibration. Seven ground motion records were used in NLTHA. Table 1 shows the ground motion used in the analyses. The peak ground acceleration of the records were scaled to $0.9g$ and $1.15g$ for the torsionally stiff and torsionally flexible buildings, respectively. The separate scaling factor was selected to ensure enough nonlinearity behavior is observed in both systems. The second order $(P-\Delta)$ effects were included.

Table 1 List of ground motions used.

Earthquake	Date	Magnitude	Station Name	PGA (*g*)
Duzce, Turkey	1999/11/12	Ms (7.3)	Lamont	0.134
Northridge	1994/01/17	Ms (6.7)	LA - Baldwin Hills	0.239
Trinidad, California	1980/11/08	Ms (7.2)	Rio Dell Overpass, FF	0.147
Victoria, Mexico	1980/06/09	Ms (6.4)	Cerro Prieto	0.621
Hollister	1986/01/26	Ml (5.5)	SAGO South - Surface	0.09
Imperial Valley	1979/10/15	Ms (6.9)	Parachute Test Site	.204
Morgan Hill	1984/04/24	Ms (6.1)	Corralitos	0.109

Discussion of Results

The mean of the maximum displacements, inter-story drifts and plastic hinge rotations were obtained from the time history analyses and compared against the methods presented in the previous section. Figure 2 shows the floor displacement as a function of the building height for both the stiff and flexible sides of the prototype model. The result shows, the MCMP procedure can predict the displacements accurately. The results are more accurate than the NSP as outlined in the other NSP methods.

Figure 3 shows the comparison of the story drifts of the studied buildings. The result of the MCMP procedure shows the best approximation to the inter-story drift ratio as compared to the other NSP as outlined in the previous section. Especially the accuracy of proposed procedure is more remarkable in upper stories.

Figure 4 shows the maximum plastic hinge rotations at the center bay of the exterior frame. The result shows the MCMP procedure can provide an excellent match to the results obtained from the NLTHA which is difficult to obtain using the other NSP presented in FEMA. In addition where the other methods are unable to predict this response in upper stories, the proposed method due to including higher mode effects is more accurate.

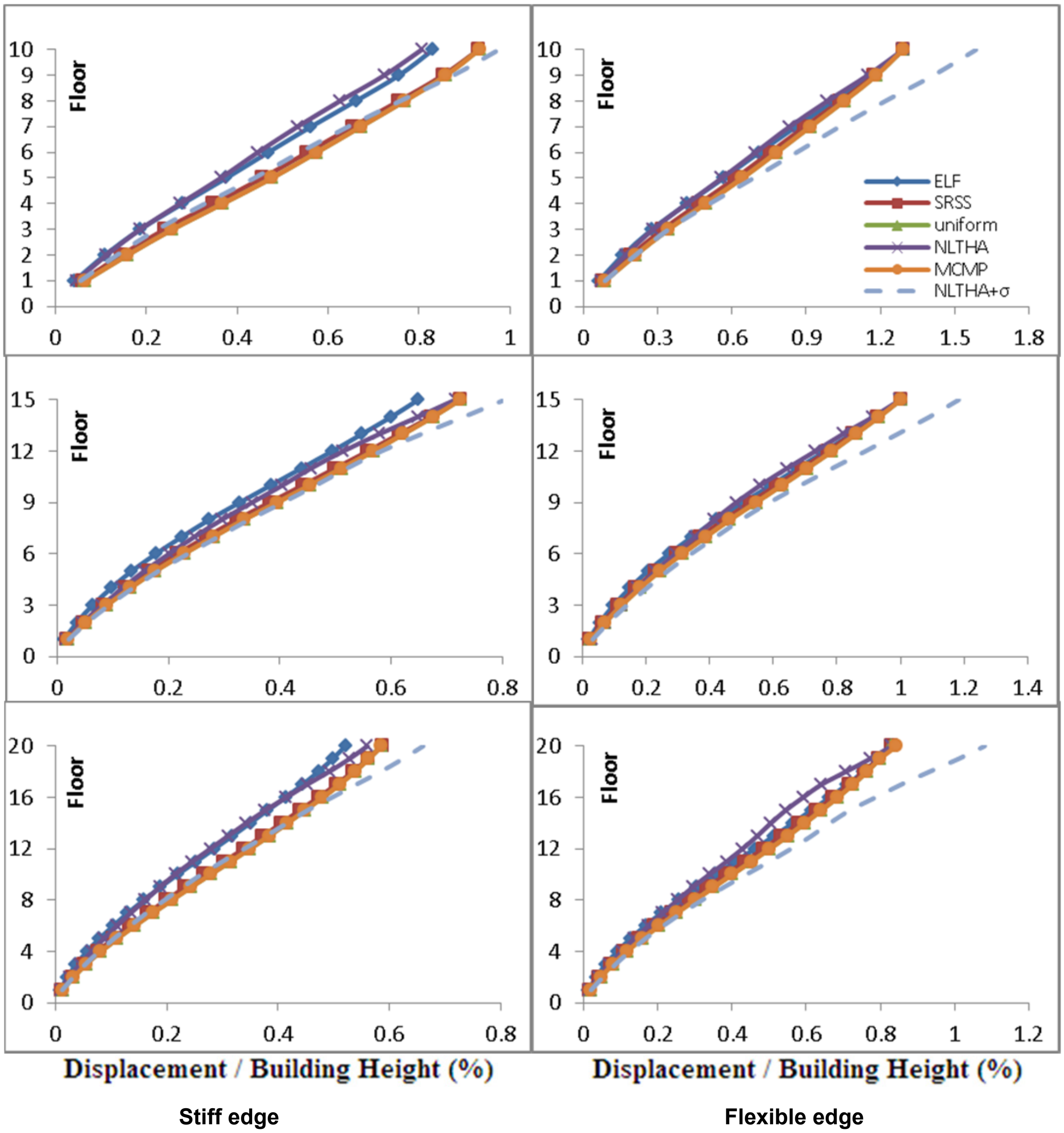

Figure 2 Height-wise variation of the displacements at the left (stiff) and right (flexible) edges of torsionally-stiff systems.

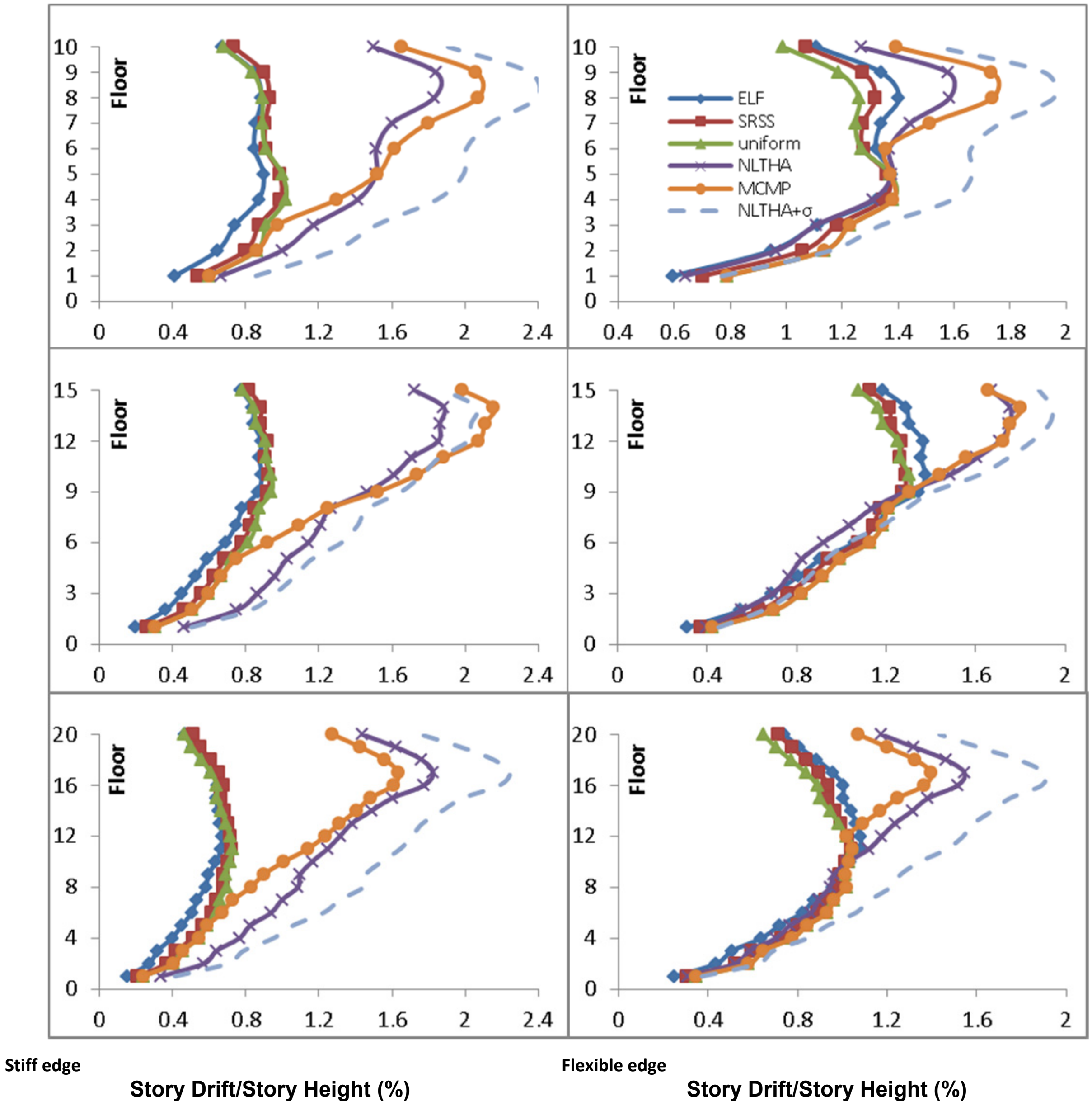

Figure 3 Height-wise variation of the story drifts at the left (stiff) and right (flexible) edges of torsionally-flexible systems.

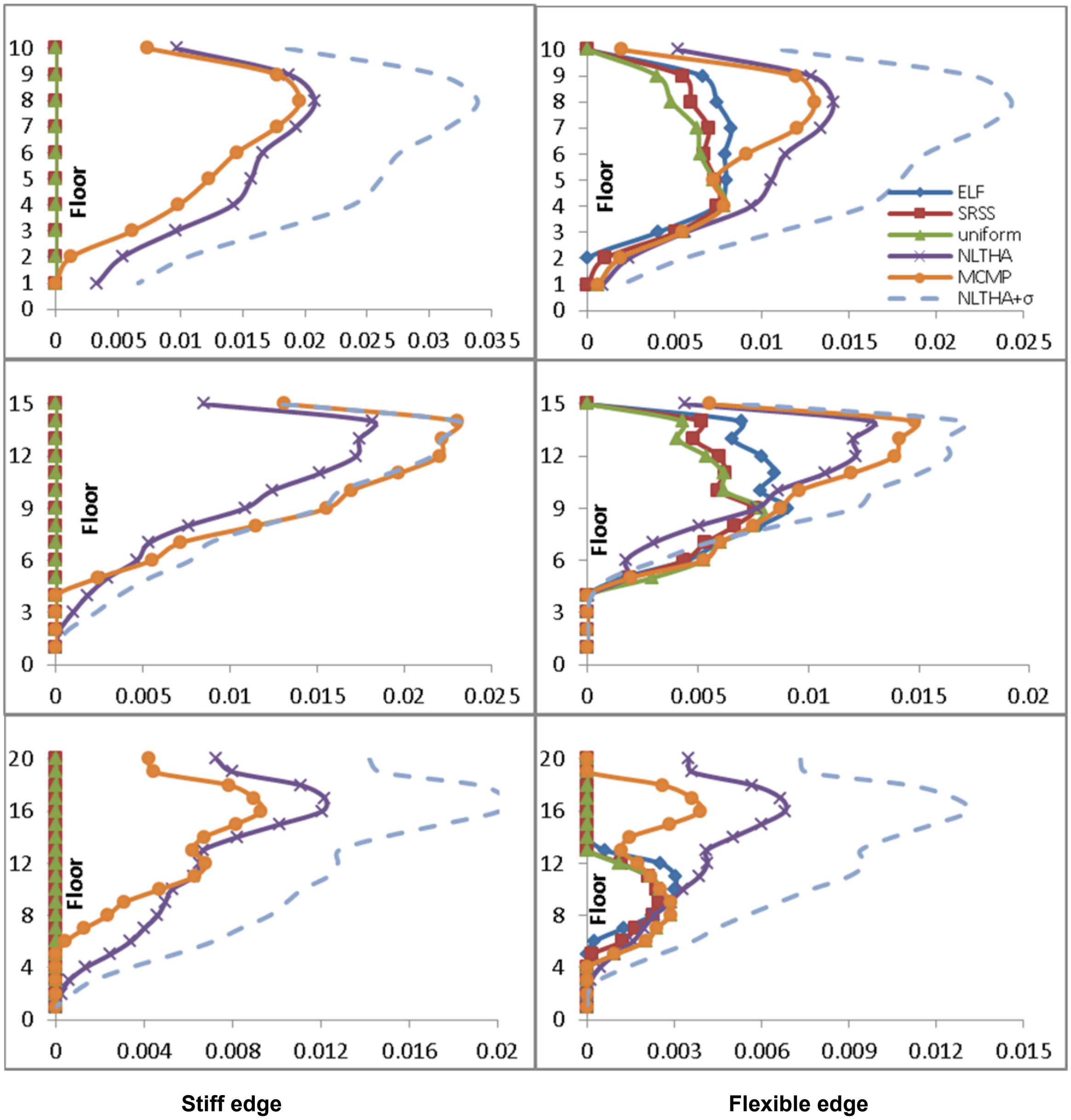

Figure 4 Height-wise variation of the plastic hinges rotation at the left (stiff) and right (flexible) edges of torsionally-flexible systems.

CONCLUSIONS

Modified consecutive modal pushover (MCMP) is developed to estimate the nonlinear response of asymmetric tall buildings. Verification of seismic demands of asymmetric tall buildings was compared using nonlinear dynamic analyses. For this purpose, several models consisting of steel moment resisting frame with concentrically braced frames, 10-, 15- and 20- story buildings were studied and seven ground motion records were used in NLTHA. The following conclusions were observed:

- The MCMP procedure was able to estimate the maximum nonlinear response of the asymmetric tall buildings more accurately compared to the ELF, SRSS and uniform NSP presented especially the story drift in the mid and upper stories.
- In addition, the MCMP was able to estimate the plastic hinge rotations of building with dual system, which is difficult to achieve using the traditional NSP approaches.
- The time-consuming of analysis is another advantage of the proposed procedure.

REFERENCES

ATC (2005). *Improvement of Nonlinear Static Seismic Analysis Procedures, FEMA-440*, Applied Technology Council, Redwood City, CA.

Chopra A.K., Goel R.K. (2004). A modal pushover analysis procedure to estimate seismic demand for asymmetric–plan buildings, *Earthq. Eng. Struct. Dyn*., 33: 903–927.

Fajfar P., Marusic D., Perus I., Kereslin M. (2008). The N2 method for asymmetric buildings, *Proceedings, Workshop of Nonlinear Static Methods for Design/Assessment of 3D Structure*s, Lisbon, Portugal.

Kashani M.M. (2010). *Evaluation of Consecutive Modal Pushover Procedure for Tall Buildings with Moment Resisting Frame and Concentrically Bracing*, M.Sc. Thesis, Department of Civil Engineering, Amirkabir University of Technology, Tehran, Iran.

Moghadam A.S., Tso W-K. (1998). Pushover analysis for asymmetrical multi-storey buildings. *Proceedings, 6th U.S. National Conference on Earthquake Engineering*, Earthquake Engineering Research Institute, Oakland, CA.

Moghadam A.S., Tso W.-K. (2000). Pushover analysis for asymmetric and set-back multi-storey buildings, *Proceedings, 12th World Conference on Earthquake Engineering*, Paper No. 1093, Auckland, New Zealand.

Poursha M., Khoshnoudian F., Moghadam A.S. (2011). Evaluation of consecutive modal pushover procedure for nonlinear static analysis of one-way asymmetric-plan tall building structures, *Eng. Struct*, 33(9): 2417–2434.

ADVANCES IN SEISMIC RESPONSE ASSESSMENT OF BRIDGES WITH SKEWED SEAT-TYPE ABUTMENTS♦

Peyman Kaviani[1], Farzin Zareian[2], and Ertugrul Taciroglu[3]

ABSTRACT

Seismic response of bridges with skew-angled abutments (a.k.a., skewed bridges) is substantially different from those with straight abutments. The inherent tendency of skewed bridges to rotate about their vertical axes under seismic excitation is a significant manifestation of this difference. This paper focuses on recent progress made in the seismic response assessment of short skewed bridges with seat-type abutments, which constitute the significant majority of recently built overcrossings in the United States. We focus on two aspects: (*i*) modeling techniques and (*ii*) performance-based seismic response assessment methods. We also introduce a probabilistic approach for multi-phase structural response assessment. This new method—*viz.,* Multi-Phase Probabilistic Assessment of Response of Structures, or M-PARS—provides a probabilistic framework for computing the complementary probability distribution function of an Engineering Demand Parameter (*EDP*), given the ground motion intensity measure, *G(EDP|IM)*. We demonstrate the implementation and utility of the M-PARS approach through a case study on a skewed bridge. We show that, by accounting for the multi-phase seismic behavior of a skewed bridge, it is possible to refine the probabilistic representation of an Engineering Demand Parameter *(EDP)* compared to the traditional method.

INTRODUCTION

Skewed bridges are the most common type of bridges in the California Highway network. They are required when the alignment of crossing roadways are not a right angle. Current state of practice for design of such bridges [Caltrans 2006; 2010] comprises using a seat-type abutment to lessen demand on foundation and allows more movement of the superstructure during seismic excitation. In transverse direction, the exterior shear keys are designed as a fuse that break off under intense impact. Similarly, under longitudinal excitation, the backwall is designed to break off and allow the generation of passive pressures on the backfill soil. The demand imposed on seat-type abutment's foundation is less than that for a diaphragm abutment, due to freedom of movement of the superstructure in different directions.

Much research has been conducted on seismic response of regular or non-skewed bridges (see, for example, Paraskeva et al. [2006], Mackie and Stojadinovic [2007], Aviram et al. [2008], Johnson et al. [2009], and Kotsoglou and Pantazopoulou [2010]. Observations from past earthquakes indicate that the unseating of the bridge deck due to in-plane rotation is the primary

---

♦ This paper was originally presented at the Seventh National Seismic Conference on Bridges & Highways.
[1] Structural Engineer, Burns & McDonnell, 1 Pointe Drive, Suite 540, Brea, CA 92821.
[2] Professor, Department of Civil and Environmental Engineering, University of California, E/4141 Engineering Gateway, Irvine, CA 92697.
[3] Professor, Department of Civil and Environmental Engineering, University of California, 5731E Boelter Hall, Los Angeles, CA 90095.

mode of failure in skewed bridges [Jennings 1971; Ghobarah and Tso 1974; Wakefield et al. 1991; Meng and Lui 2000]. This rotational response is exacerbated once the bridge is subjected to near-field motions [Shamsabadi et al. 2006]. However, there still remains significant uncertainty in models that can predict this mode of failure. Understanding the seismic behavior of skewed bridges and improving the modeling and design guidelines for this type of bridge are the main objectives of this research [Kaviani 2011].

This paper summarizes an attempt for demonstrating our research in two fronts: (1) proposing an efficient and sufficient modeling technique for representing a skewed bridge abutment; and (2) illustrating a novel analytical technique for accurate representation of seismic response of a skewed bridge given a ground motion intensity measure. Our research directly feeds into the performance-based methodology proposed by the Pacific Earthquake Engineering Research (PEER) Center, with specific extensions devised for bridges.

SKEWED BRIDGE ANALYTICAL MODEL

We have developed guidelines for proper modeling of skewed bridges along with proper criteria for defining collapse [Kaviani et al. 2012]. The proposed skewed bridge modeling technique generally follows the modeling approach described in Aviram et al. [2008]; however, we have added specifics for proper modeling of skewed bridge abutment that is both efficient and sufficient. Figure 1 shows a schematic model of a typical skewed bridge along with our proposed modeling technique. Detailed description of a skewed bridge analytical model can be found in Kaviani [2011].

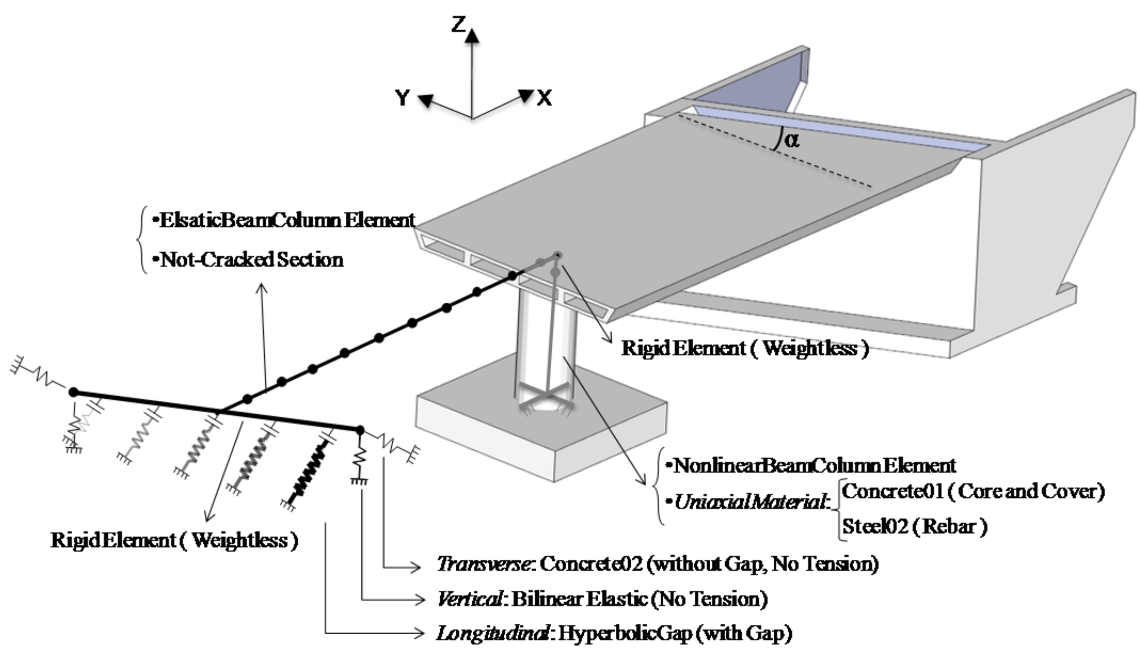

Figure 1 Schematic and generic model of a single column two span skewed bridge.

We utilize a three-dimensional spine-model of the bridge structure with line elements located at the centroid of the cross sections following the alignment of the bridge. To capture the response of the entire bridge system and individual components under specific seismic demand characteristics, three-dimensional modeling is implemented. The models developed for skewed bridges do incorporate nonlinear behavior of individual components. These components include column plastic hinges, abutment transverse and longitudinal springs, and abutment gap element. For simplicity, the superstructure, the cap beam, and the foundation springs are considered as linear elastic components.

We propose a new abutment model denoted as “Skewed Abutment Model” in this study. The Skewed Abutment Model comprises of three set of springs: (1) longitudinal springs that model response of the backfill (passive pressure) and expansion joints, (2) transverse springs that model shear key behavior, and (3) vertical springs that model bearing pads and the stemwall.

Our proposed “Skewed Abutment Model” is not verified with experimental data. Much of the research in this area is focused on lateral passive response of straight abutments [Romstad et al. 1995; Bozorgzadeh et al. 2006, Stewart et al. 2007; Shamsabadi et al. 2010]. Knowing this shortcoming, we have used our best estimate and engineering judgment to develop the proposed abutment model. We assume that the direction of the backfill passive pressure, and therefore the set of abutment springs, is perpendicular to the backwall.

Five nonlinear abutments springs model the longitudinal response in series with gap elements as shown in Figure 1. The set of nonlinear springs and the gap elements represent the passive backfill response and the expansion joint, respectively. Nonlinear properties of abutment springs are obtained from recommendations provided in the Caltrans Seismic Design Criteria (SDC) [2010] and large scale abutment testing [Romstad et al. 1995; Stewart et al. 2007]. A rigid bar represents the deck and the set of abutment springs, equally spaced, are attached to it. We postulate that the properties of the nonlinear abutment springs are different from each other. We have assumed that the difference between abutment springs is relative to the amount of backfill behind the backwall. The stiffness and strength of these springs are assumed to increase linearly, as function of abutment skew angle and distance from the obtuse angle. Finally, we have assumed that the maximum stiffness/strength variation may occur for the largest skew angle (60°), and it is equal to 30%.

The resistance provided by the exterior shear key is accounted for by the transverse springs in the Skewed Abutment Model. The capacity of the exterior shear key can be evaluated using models explained by Megally et al. [2002]. Vertical response is modeled by two springs that work in parallel; one represents the elastomeric bearing pad and the other represents the vertical stiffness of the stemwall and abutment embankment.

MULTI-PHASE PROBABILISTIC ASSESSMENT OF STRUCTURAL RESPONSE (M-PARS) TO SEISMIC EXCITATIONS

The Pacific Earthquake Engineering Research (PEER) Center Performance Based Assessment (PBA) methodology (e.g., Cornell and Krawinkler [2000]; Krawinkler and Miranda [2004]; and

Mackie and Stojadinovic [2007]) utilizes a chain of four random variables: Intensity Measure (*IM*), Engineering Demand Parameter (*EDP*), Damage Measure (*DM*), and Decision Variable (*DV*). *IM* is a scalar or vector quantity that represents the intensity of a ground motion. *EDP* is a bridge response parameter (e.g., maximum deck rotation, column drift ratio) and is estimated through nonlinear response analysis of the bridge model subjected to a ground motion. *DM* is the representation of damage (e.g., cracks in columns) and is determined based on repair strategy and many other considerations. Ultimately, *DV* is a measure of performance, with a focus on three major loss categories: direct ($) losses, downtime losses, and life losses. The PEER PBA methodology is completed by following a flow of information from *IM* to *DV* according to Equation (1) (the PEER framework equation):

$$\lambda(DV) = \iiint G(DV|DM).\,dG(DM|EDP).\,dG(EDP|IM).\,d\,\lambda(IM) \tag{1}$$

In Equation (1), $\lambda(DV)$ is the desired realization of the *DV* (e.g., mean annual frequency of exceedance) and the *G* functions represent complementary cumulative distribution functions. For instance, for downtime performance (i.e., average annual downtime for a given bridge) one can complete the PBA methodology as follows: intensity measures, *IM*s, (e.g., peak ground velocity, *PGV*), are determined from seismic hazard analysis; relevant engineering demand parameters, *EDP*s, (e.g., deck rotation, column drift ratio) are predicted from structural analysis for given values of *IM*s (and representative ground motions); component/system damage states are developed from repair strategies and *DM*s fragility curves are developed for each component/system; and finally, predictions are made on *DV*s (i.e., total amount of downtime losses of the bridge).

For the purpose of this study, our focus is on proper estimation of seismic response given the ground motion intensity. i.e., $G(EDP|IM)$. $G(EDP|IM)$ is estimated considering the information available through nonlinear response history analysis using the bridge analytical model and set of ground motion records. Traditionally, estimation of $G(EDP|IM)$ involves obtaining two types of information from nonlinear response history analysis: (1) Probability of collapse, denoted as $P(C|IM)$ using available data from ground motions that caused collapse of the bridge analytical model; and (2) distribution of *EDP* given *IM* from cases where collapse did not occur, denoted as $G(EDP|IM,NC)$. Equation (2) shows how $G(EDP|IM,NC)$ and $P(C|IM)$ can be combined to estimated $G(EDP|IM)$.

$$G(EDP|IM) = G(EDP|IM,NC).\big(1 - P(C|IM)\big) + P(C|IM) \tag{2}$$

Our investigation on seismic response of skewed bridges has shown that the behavior of a skew bridge abutment shear key can radically change the seismic response of that bridge. This sudden change in seismic response results in an bias in median and increase in dispersion of $G(EDP|IM)$ [Kaviani et. al. 2012]. We propose an approach for seismic response assessment of skewed bridges that explicitly considers changes in the nature of the bridge behavior as the ground motion intensity measure increases. This approach is denoted as the “Multi-Phase Probabilistic Assessment of Structural Response to Seismic Excitations,” or M-PARS [Kaviani 2011].

Implementation of M-PARS method for characterizing $G(EDP|IM)$ requires consideration of four possible combinations (a.k.a. phases) of skewed bridge behavior: (1) S_{11}:

shear key survives and bridge does not collapse; (2) S_{21}: shear key survives and bridge collapses; (3) S_{12}: shear key does not survive and bridge does not collapse; and (4) S_{22}: shear key does not survive and bridge collapses. Within this setting, $G(EDP|IM)$ can be estimated using Equation (2). Considering S_{21} and S_{22} phases as separate phases is redundant as they signal a bridge collapse, therefore, we simplify Equation (2) and form Equation (3).

$$
\begin{aligned}
G(EDP|IM) = G(EDP|IM, S_{11}) \times P(S_{11}|IM) + &\\
G(EDP|IM, S_{12}) \times P(S_{12}|IM) + &\\
G(EDP|IM, S_{21}) \times P(S_{21}|IM) + &\\
G(EDP|IM, S_{22}) \times P(S_{22}|IM) & \qquad (3)
\end{aligned}
$$

$$
\begin{aligned}
G(EDP|IM) = G(EDP|IM, S_{11}) \times P(S_{11}|IM) + &\\
G(EDP|IM, S_{12}) \times P(S_{12}|IM) + &\\
P(C|IM) & \qquad (4)
\end{aligned}
$$

CASE STUDY

To illustrate the implementation of our proposed skewed bridge modeling technique and seismic response assessment approach (M-PARS), we have selected a two-span single-column bridge. The Jack Tone Road On-Ramp Overcrossing is located in City of Ripon in California, and it was built after year 2000 in a region with high seismicity. This bridge is a two-span bridge with 220.4 ft (≈ 67.2 m) total length, and spans of 108.58 ft (≈ 33.105 m) and 111.82 ft (≈34.095 m). The superstructure is a continuous reinforced concrete box-girder. The column of the bent is 5.5 ft (≈ 1.68 m) in diameter supported on steel piles. The longitudinal reinforcing steel ratio of the column is approximately 2%. The bridge is non-skewed with seat-type abutments. For this paper we considered an analytical model of this bridge with equal span size. Further variation of model geometric setting can be found in Kaviani [2011].

The analytical model of the case study bridge is shown in Figure 1. The bridge structure is modeled through OpenSees [McKenna et al. 2000] finite element analysis software. The three-dimensional spine-model of the bridge structure with line elements located at the centroid of the cross sections following the alignment of the bridge is used. The deck is modeled with elastic elements because flexural yielding of deck during seismic response is not expected. Cracked section properties are used in the model to obtain realistic values for the structure's period and the seismic demands generated from the analyses. Elements that incorporate nonlinear behavior include: (1) columns, (2) shear keys, and (3) abutments. For simplicity, and as recommended by SDC [2006; 2010] guidelines, we have assumed that foundation of the bridge is rigid enough to justify a fixed–end boundary condition.

Columns are modeled using the distributed plasticity element model denoted as *NonlinearBeamColumn* element in OpenSees, *concrete01* and *concrete02* are used to model cover and core concrete in columns, respectively. The compressive strength of the unconfined concrete is equal to 5 ksi (≈ 34.5 MPa) and its concrete strain at maximum strength is equal to 0.005. For confined concrete, we assumed a compressive strength equal to 6.5 ksi (≈ 45 MPa) with concrete strain at maximum strength equal to 0.008. The ultimate strain in compression for the confined concrete is governed by the first hoop fracture, and it is set equal to 0.025. The reinforcing steel is modeled using *Steel01* material model, which has an elastic-perfectly plastic behavior. The yielding strength of the steel is equal to 60 ksi (≈ 475 MPa), and the Young's Modulus, equal to 29000 ksi (≈ 200 GPa). The maximum strain in tension depends on the type of the steel and the size of the reinforcing bars, and it is equal to 0.09. Torsional stiffness of the column is modeled assuming 20% of the gross polar moment of inertia of the column with infinite torsional strength.

Translational mass of all longitudinal elements (10 elements per span) in the three global directions of the bridge (longitudinal, transverse, and vertical) are calculated and assigned as lumped masses on each node (11 nodes per span) based on tributary lengths. The weight of normal concrete is specified by Caltrans [2006] as w = 143.96 lb/ft^3 (≈ 2286.05 kg/m^3), and therefore, a mass of ρ_c = 44.471 lb-sec^2/ft^4 (233.03 kg-sec^2/m) is used when specifying weight and material properties for concrete. We considered 5% critical damping in the first two modes of vibration.

The modeling technique and structural analysis software adopted in this study are not capable of simulating every conceivable collapse mechanism. To model non-simulated collapse, the analysis output is post-processed in order to identify collapse cases using predefined collapse criteria. Non-simulated collapse is defined as: (1) column drift ratio is greater than 8%; and (2) deck displacement relative to the abutment in the longitudinal unseating direction greater than the seat length.

The effectiveness of M-PARS method is assessing the response of the case study bridge can be seen in Figure 2. Figure 2 shows the difference between complimentary distribution functions of deck rotation given the ground motion intensity measure PGV = 55 cm/sec obtained using the M-PARS and traditional method for various skew angles. Dash lines represent $G(\theta_{rot}|$ PGV = 55 cm/sec) obtained using the traditional method and solid lines show the same distribution obtained using the M-PARS method; colors green, red, and blue show results for the case study bridge with 0, 30, and 60° abutment skewed angle, respectively. These results are obtained using the bridge analytical model as described above and a set of 40 ground motions representing seismic excitation on "soil" sites. These ground motions are not location specific and rather are standardized to accommodate comparative evaluations. These ground motions are selected from a subset of the PEER NGA Project ground motion library with ground motions from mid- to large-magnitude earthquakes at close distances. Selected ground motions have a variety of spectral shapes, durations, and directivity periods.

Figure 2 illustrates that using the traditional method for characterizing $G(\theta_{rot}|$ PGV = 55 cm/sec) can lead to an overestimation of low value seismic demands and underestimation of high value seismic demands. This discrepancy in estimation of seismic demand can lead to uneconomical and/or unsafe design of skewed bridges. The difference between estimates of $G(\theta_{rot}|$ PGV = 55 cm/sec) for all considered skew angles shows a same trend signaling that use of

M-PARS method for characterization of $G(\theta_{rot}|$ PGV = 55 cm/sec) can lead to better estimates of seismic demand distribution for skewed bridges with any skew angle.

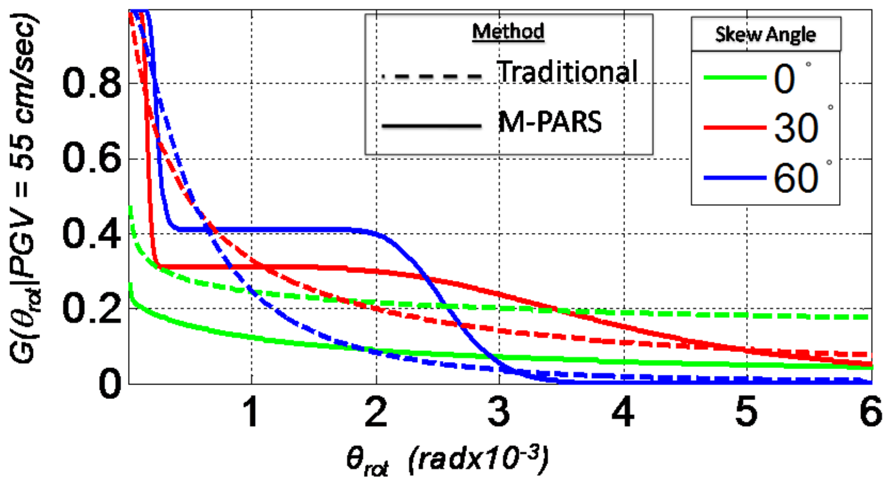

Figure 2 Complementary probability distribution function of deck rotation given ground motion intensity measure *PGV*, *G*(θ*ro*|*PGV* = 55 cm/sec), obtained using M-PARS and traditional method for skewed angles α = 0, 30, and 60°.

CONCLUSIONS

This paper summarizes our efforts for proper assessment of seismic response of skewed bridges. We introduced an enhanced technique for modeling a bridge abutment, and proposed a novel probabilistic-based method for accurate assessment of performance of a skewed bridge denoted as Multi-Phase Probabilistic Assessment of Structural Response to Seismic Excitations (M-PARS). We have briefly explained both contributions and have shown how to implement the modeling and assessment technique through a case study bridge. This case study comprises a skewed bridge with 0^o, 30^o, and 60^o abutment skew angle and we showed the accuracy of the M-PARS method in assessing the bridge performance compared to using the traditional approach. We showed that for any skew angle, a shift in the predominant phase of the seismic response of a skewed bridge from shear key survive to shear key failure can emphasize the significance of considering the multi-phase assessment concept for evaluating seismic behavior of the bridge.

ACKNOWLEDGMENTS

This study is based on work supported by the by the PEER Transportation Research Program under Grant No. UCLA-45782. This financial support is gratefully acknowledged. Any opinions, findings, and conclusions or recommendations expressed in this paper are those of the authors and do not necessarily reflect the views of sponsors. This paper was originally published in the proceedings of the Seventh National Seismic Conference on Bridges & Highways (7NSC) in

Oakland, California, May 20-22, 2013. It is republished here with the express written permission of 7NSC.

REFERENCES

Aviram A., Mackie K.R., Stojadinovic B. (2008). Guidelines for nonlinear analysis of bridge structures in California, *Technical Report 2008/3*, Pacific Earthquake Engineering Research Center, University of California, Berkeley, CA.

Bozorgzadeh A., Ashford S.A., Restrepo J.I. (2008). Effect of backfill soil type on stiffness and ultimate capacity of bridge abutments, ASCE, *Proceedings, Geotechnical Earthquake Engineering and Soil Dynamics IV*, D. Zeng; M.T. Manzari and D.R. Hiltunen (eds.), Sacramento, CA.

Caltrans (2006). *Seismic Design Criteria Version 1.4*, California Department of Transportation, Sacramento, CA.

Caltrans (2010). *Caltrans Seismic Design Criteria Version 1.6*, California Department of Transportation, Sacramento, CA.

Cornell C.A., Krawinkler H. (2000). Progress and challenges in seismic performance assessment, *PEER News 2000*, 3(2): 1–2.

Ghobarah A.A., Tso W.K. (1974). Seismic analysis of skewed highway bridges with ıntermediate supports, *Earthq. Eng. Struct. Dyn.*, 2(3): 235–248.

Jennings P.C., (ed.), Housner G.W., Hudson D.E., Trifunac M.D., Frazier G.A., Wood J.H., Scott R.F., Iwan W.D., Brady A.G. (1971). "Engineering features of the San Fernando earthquake of February 9, 1971, *Report No. EERL 71-02*, California Institute of Technology, Pasadena, CA.

Johnson N., Saiidi M.S., Sanders D. (2009). Nonlinear earthquake response modeling of a large-scale two-span concrete bridge, ASCE, *J. Bridge Eng.*, 14(6): 460–471.

Kaviani P. (2011). *Performance-Based Seismic Assessment of Skewed Bridges*, PhD Dissertation, Department of Civil and Environmental Engineering, University of California, Irvine, CA.

Kaviani P., Zareian F., Taciroglu E. (2012.) Seismic behavior of reinforced concrete bridges with skew-angled seat-type abutment, *Eng. Struct.*, 45: 137–150.

Kotsoglou A., Pantazopoulou S. (2010). "Response simulation and seismic assessment of highway overcrossings, *Earthq. Eng. Struct. Dyn.*, 39(9): 991–1013.

Krawinkler H., Miranda E. (2004). Performance-based earthquake engineering, in: *Earthquake Engineering: from Engineering Seismology to Performance-Based Engineering*, Chapter 9, pp. 9–59, Y. Bozorgnia and V.V., Bertero (eds.). CRC Press: Boca Raton, FL.

Mackie K., Stojadinovic B. (2007). Performance-based seismic bridge design for damage and loss limit states, *Earthq. Eng. Struct. Dyn.*, 36(13): 1953–1971.

McKenna F., Fenves G. L., Scott M.H. (2000). *Open System for Earthquake Engineering Simulation*, Version 2.2.2, University of California Berkeley, CA; available at: http://opensees.berkeley.edu.

Megally S., Silva P.F., Seible F. (2002). Seismic response of sacrificial shear keys in bridge abutments, *Report No. SSRP–2001/23*, University of California, San Diego, CA.

Meng J.Y., Lui E.M. (2000). Seismic analysis and assessment of a skew highway bridge, *Eng. Struct.*, 22(11): 1433–1452.

Paraskeva T.S., Kappos A.J., Sextos A.G. (2006). "Extension of modal pushover analysis to seismic assessment of bridges, *Earthq. Eng. Struct. Dyn.*, 35(10): 1269–1293.

Romstad K.M., Kutter B., Maroney B., Vanderbilt E., Griggs M., Chai, Y.-H. (1995). Experimental measurements of bridge abutment behavior, *Report No. UCD STR 95 1*, Structural Engineering Group University of California, Davis, CA.

Shamsabadi A., Kapuskar M., Martin G.M. (2006). Nonlinear seismic soil–abutment– structure ınteraction analysis of skewed bridges, *Proceedings, 5th National Seismic Conference on Bridges and Highways*, Paper No. B18, San Francisco, CA.

Shamsabadi A., Khalili-Tehrani P., Stewart J.P., Taciroglu E. (2010). Validated simulation models for lateral response of bridge abutments with typical backfills, ASCE, *J. Bridge Eng.*, 15(3): 302–311.

Stewart J.P., Wallace J.W., Taciroglu E, Ahlberg E.R., Lemnitzer A., Rha C., Tehrani P.K., Keowen S., Nigbor R.L., Salamanca A. (2007). "Full scale cyclic testing of foundation support systems for highway bridges. part ıı: abutment backwalls, *Report No. UCLA SGEL 2007/02*, Department of Civil and Environmental Engineering, University of California, Los Angeles, CA.

Wakefield R.R., Nazmy A.S., Billington D.P. (1991). Analysis of seismic failure in skewed RC bridge, ASCE, *J. Struct. Eng.*, 117(3): 972–986.

RESPONSE OF PILED RAFT FOUNDATION UNDER SEISMIC LOAD: CONNECTED AND NON-CONNECTED SYSTEMS

Alireza Saeedi Azizkandi[1] and Mohammad Hassan Baziar[2]

ABSTRACT

This paper describes a study on the behavior of piled raft foundations under dynamic loading. This research comprises four major components: the first step including the effect of granular layer on piled raft performance using centrifuge test under static load, the second step verification of numerical program with static centrifuge tests on sand pile-raft systems and then, to investigate about performing piled raft foundation with granular layer under seismic load, and the effect of granular layer on non-connected pile raft under dynamic load.

INTRODUCTION

Pile groups are conventionally designed by adopting a relatively high factor of safety to the piles and the major design criterion is the bearing capacity of the piles group. The arrangement of these piles in the group is to carry the entire load of the superstructure. Although the connection "cap" often a raft (or mat) is in close contact with the soil, its contribution to the total bearing capacity and general pile group behavior is rarely considered in the analysis and design. One of the most effective ways to decrease settlement of a mat foundation has been experienced to be the pile enhancement. The system is known as hybrid foundation or piled raft foundation (PRF). The piled-raft foundation is a recent design concept as one of the effective methods of foundation to reduce settlements of structures.

In piled-raft systems, the design procedure differs from traditional foundation design, in which the loads are assumed to be carried either by the raft or by the piles, considering the safety factor in each case. In other words the load bearing is between the piles and the raft.

Therefore, the piled raft foundation causes reduction of settlements and differential settlements in a very economical way compared to traditional foundation concepts. The raft in this system has adequate bearing capacity and therefore, the main objective of introducing these pile elements is to control or minimize the average and/or differential displacements of the piled raft system, rather than to carry the major portion of the loads

Practically, the pile head is structurally connected with, or penetrated into, the raft to form a rigid connection. In conventional piled raft design, the number of piles is normally great and the load carried by each individual pile is relatively small of total load. There is a high safety margin before the piles reach their geotechnical bearing capacity or structural failure load.

The capacity of the piles is generally governed by geotechnical considerations rather than by the compressive strength of the pile material. In addition, the resistance of piles to horizontal

[1] PhD candidate, Iran University of Science and Technology, Iran.
[2] Professor, Iran University of Science and Technology, Iran.

forces through suitably designed connections is usually adequate due to the large number of piles used. When settlement-reducing piles are designed as structural components, a low factor of safety can be applied to the geotechnical capacity of the piles and the raft alone is adequate. However, when these piles are structurally connected to the raft, as they are in traditional construction, a high axial stress may develop in the relatively small number of piles. Thus, the load-carrying capacity of these settlement-reducing piles may be governed by their structural capacity rather than by geotechnical capacity. In addition, these sparsely arranged structural piles beneath a raft may not provide adequate horizontal resistance to lateral loads. One alternative in the design of these piles is to consider them as stiffeners for the base soil so that the above-mentioned problems would be avoided

The study on the load bearing mechanism under horizontal loading or during earthquakes, however, is very limited [Mano and Nakai 2000; Horikoshi et al. 2003]. This is partially because piled raft foundations are considered as raft foundations in the current design practice. Since the behavior of a piled raft foundation during earthquakes is considered fairly complex due to dynamic interaction among a raft, piles and a soil, the design procedure should include the effect of this mechanism in an appropriate manner. In the areas where the seismic activity is considered high, such as in Iran, load that piles have to carry during an earthquake is quite large. Especially, when the inertial force of a superstructure is large, which is often the case, stresses of a pile at its head become prohibitive since the connection condition between the foundation and the piles is usually a fixed condition.

The objective of this paper is to investigate the effect of the versus non-connection condition between piles and a raft on the dynamic characteristics of a structure supported by a piled raft foundation. In this regard, a series of static centrifuge model tests and numerical modeling under seismic load have been conducted, followed by a parameter survey based on the finite element analysis.

PERFORMANCE OF PILED RAFT FOUNDATION UNDER STATIC LOAD

In order to examine the effect of the granular layer between a raft and piles (Figure 1) on the static behavior of a structure supported by a piled raft foundation, a series of centrifuge model tests have been conducted and then numerical studies are performed on the centrifuge tests.

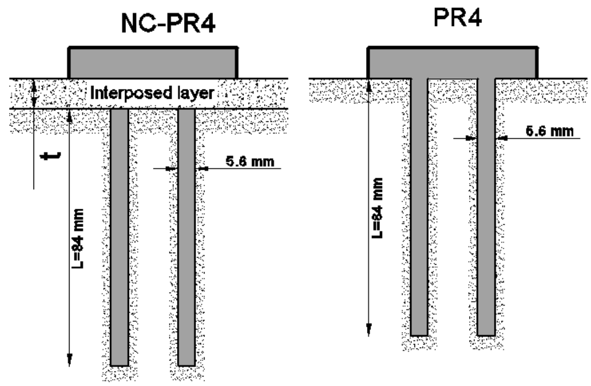

Figure 1 A schematic illustrations of the pile raft system with 4 piles and non-connected pile raft system with 4 piles and 1.5m thickness granular layer.

CENTRIFUGE MODEL TESTS

A specimen, 1/N scale of the real dimensions, in the centrifuge apparatus under the acceleration N times the gravitational acceleration is able to simulate the stress levels of the real condition for the tested specimen. Therefore the results of such model can be used for interpretation of the pile performance in the prototype condition. The observations made in the model can be correlated to the prototype behavior by the similarity equations noted in Table 1. All the models presented in this study have been tested under 100*g* acceleration and hence the scaling coefficient was N=100.

In order to measure the amount of settlement (displacements) of piles and soil, two linearly variable differential transformers (LVDT) have been used. Figure 2 shows the boundary conditions, as well as the locations of LDVT sensors and the pile raft system. Also, the broken silicate Firouzkouh sand known, as 161-Firouzkouh sand, with a uniform grading has been used for modeling of soil for piled raft system, and D11-firuzkooh sand has been used for modeling of granularly layer. In Table 2 the physical properties of the mentioned sands have been compared with Toyoura standard sands.

In the present study, all the tests have been performed in 100g acceleration, while the piles were installed under 1*g* acceleration. The acceleration has been measured at one-third of the specimen depth. Also, all the tests have been performed in sandy soil with 55% relative density. The tests specifications are summarized in Table 3.

Table 1 Similarity relationships.

Property	Prototype	Model
Acceleration	1	N
Area	N	1
Length	N^2	1
Volume	N^3	1
Velocity (projectile)	1	1
Velocity (undrained conditions)	1	N
Mass	N^3	1
Mass	N^3	1
Force	N^2	1
Stress	1	1

Table 2 Physical properties of Iran's Firouzkouh sand No. 161 compared to Toyora sand.

Sand	G_s	e_{max}	e_{min}	$D_{50(mm)}$	F.C %	ϕ	C_u	C_c	K
161-Firouzkouh sand	2.658	0.97	0.55	0.27	0.2	32	2.58	0.97	0.0125
D11-Firouzkouh sand	2.65	0.892	0.626	1.15	0.15	-	1.43	0.96	-
Toyoura 2.65 0.977 0.597	0.17	0	-	-		-		-	

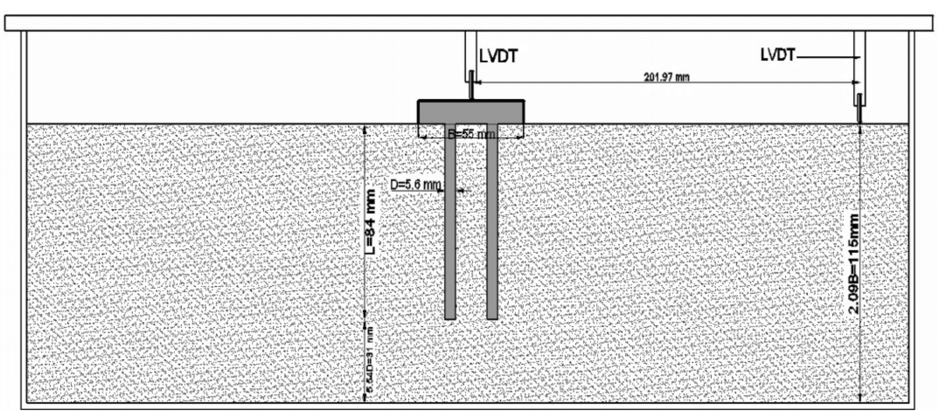

Figure 2 A schematic illustration of the boundary conditions, location of piles and LDVT sensors in the soil box.

For studying the load-settlement curve in various conditions, three tests of a single foundation, a pile group (PG4) and pile raft (PR4) system have been performed. The purposes of doing these experiments was to investigate the performance of common soil-structure load transition mechanism in sandy soil with average 55% relative density. Figure 3 shows the normalized load-settlement curves in these three tests. As can be observed, the loading capacity of a group of piles is very small compared to the raft.

In another experiment, a shallow foundation has been placed on the granular layer with 1.5 m thickness. It was observed that in low stresses, the amount of settlement does not much differ in a non-connected pile-raft system but as the stresses are increased, the amounts of settlement in two cases are considerably different (see Figure 3).

One experiment has been conducted on a connected pile raft system with 1.5m thickness granular layer. The purpose of conducting this experiment is to study the load-settlement behavior of this system and compare it with other systems. As can be observed in Figure 3, the non-connected pile raft system with granular layer has shown a better performance compared to connected pile raft systems. Also, the settlement observed in a connected pile raft system with a granular layer compared to the non-connected pile raft model did not show significant differences and they had almost similar behavior.

Table 3 Test program.

No of test	Symbol	No. of Piles	S/d	Depth of Granular Layer	D50 of Granular Layer
1	UR	0	--	--	--
2	PG	4	4.9	--	--
3	PR	4	4.9	--	--
4	NC-PR	4	4.9	1.5	1.15
5	C-PR	4	4.9	1.5	1.15

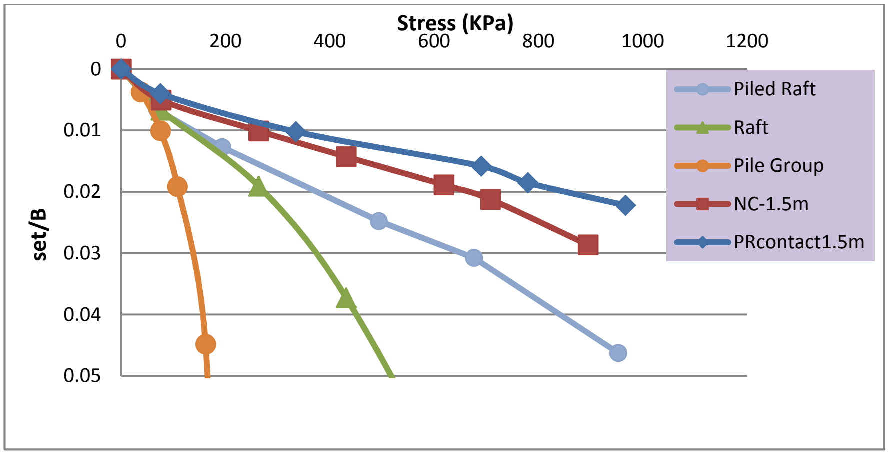

Figure 3 Normalized load settlement curve.

Numerical Modeling

The performance of piled raft under static load is investigated using ABAQUSE finite element code. To verify the code, the results of static centrifuge tests on the piled raft model are used. The studied models include four piles with ring cross section of 56cm in diameter and 8.4m in length and buried completely in sandy soil, similar to the specimens constructed in the centrifuge tests. The foundation cap dimensions are 5.5m in width and length and 0.5m in height. Figure 4 shows the geometry of the model and arrangement of piles and raft in three models. In this study the Mohr-Coulomb model applied and soil parameters like internal friction angle of soil, cohesion, young modulus, and poison ratio are selected based on centrifuge test. The load settlement curves results obtained from analysis and centrifuge test are presented in Figures. 5, 6, and 7. According to this figures, the numerical model has a good agreement with the observed behavior in the tests.

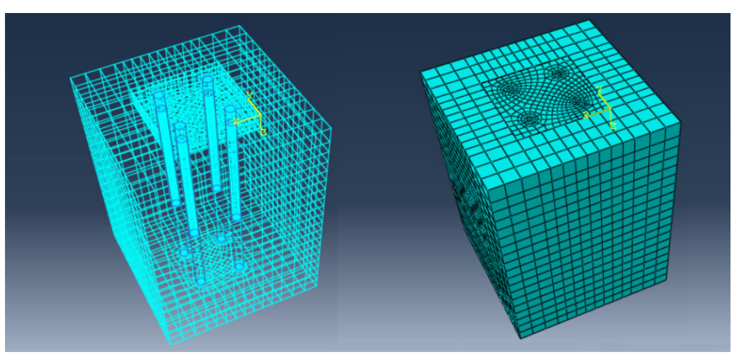

Figure 4 Three-dimensional soil- pile-raft models by finite element code ABAQUSE.

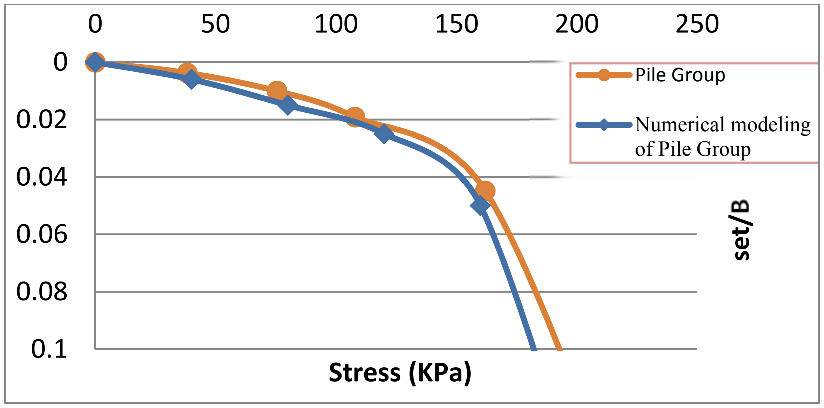

Figure 5 Comparing between pile group load-settlement curves obtained from centrifuge test and numerical modeling.

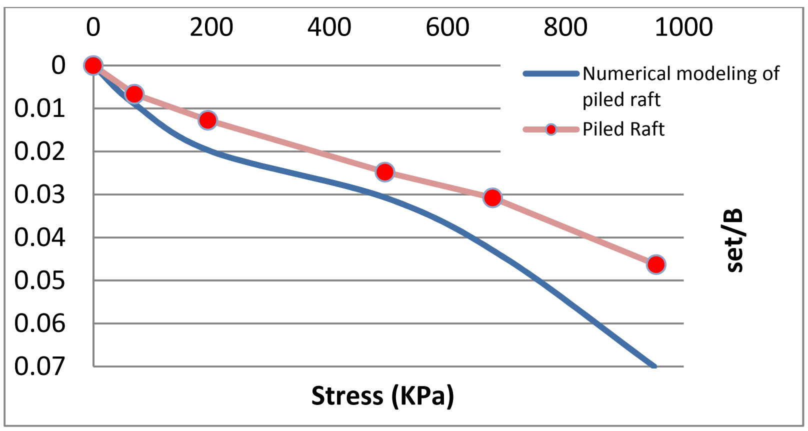

Figure 6 Comparing between piled raft load-settlement curves obtained from centrifuge test and numerical modeling.

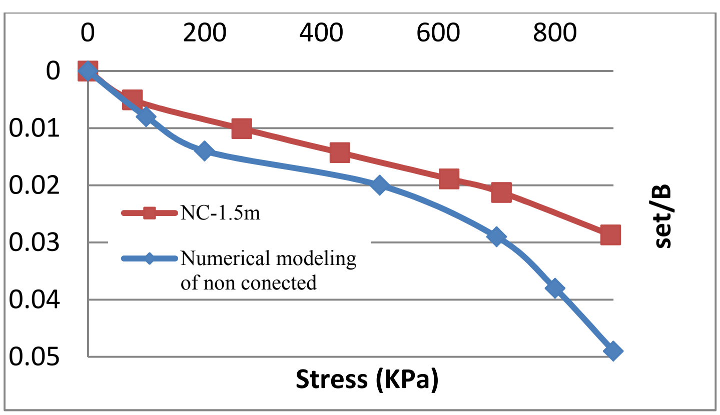

Figure 7 Comparing between non connected piled raft load-settlement curves obtained from centrifuge test and numerical modeling.

PERFORMANCE OF PILED RAFT FOUNDATION UNDER SEISMIC LOAD

The studied model include four piles similar to static conditions The center to center distance of piles is chosen so that the ratio s/d in the direction of seismic load and in the perpendicular direction are 4.9. The foundation cap dimensions are 5.5 m in width and length and 0.5 m in height. Figure 8 shows the geometry of the model and arrangement of piles and raft. In this study the Drucker Prager Hardening model is used and soil parameters like internal friction angle of soil, cohesion , young modulus, and poison ratio are selected based on centrifuge test.

The interaction between soil surface and raft is considered as rough tangential behavior. The connectivity between pile tips and corresponding surface on raft is chosen as tied. For these conditions, finite elements and infinite elements are used for studied region and boundary region and thus, there is no need for determining boundary condition in vertical boundaries. The model piles lie in the center with respect to infinite elements and often coincide with center of model or center of loading and then, the sweep technique is used for meshing and numbering infinite elements. After modeling and exerting uniform loading of 15 kN/m^2 on raft and earthquake acceleration on the base of model, the execution of the analysis has been started. The Manjil spectrum is used for studying the connections conditions of pile raft system. Acceleration histogram of this earthquake is shown in Figure 9. It is noteworthy that using infinite element significantly decreases the time of analysis. The maximum of horizontal displacement under earthquake acceleration exerted on the base for connected and non-connected piled raft foundation are shown in Table 4.

Figures 10 shows the moments along pile length under mentioned loadings. As shown in Figure 10, with change connections condition from connected piled raft to non-connected piled raft, the moment value along pile length decreases significantly. So, according to increment of horizontal displacement is small, the performance of non-connected piled raft is better than connected piled raft foundation under seismic load.

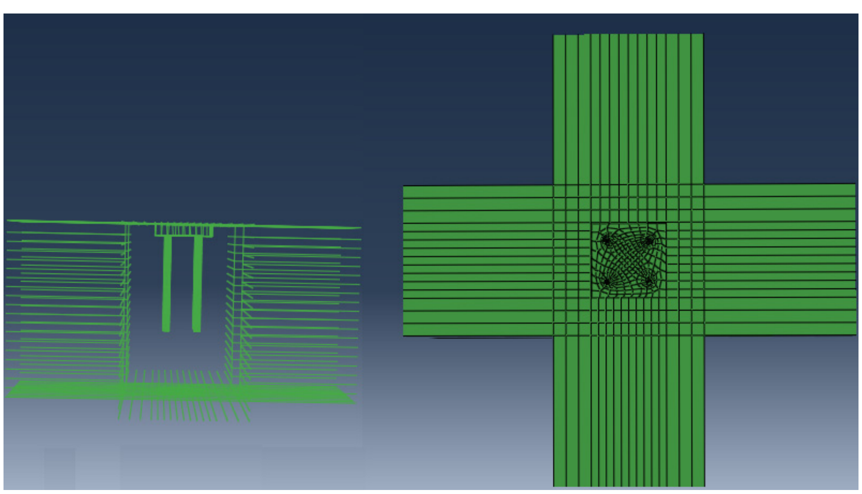

Figure 8 Three-dimensional soil- pile-raft models with infinite elements in boundaries of model by finite element code ABAQUSE.

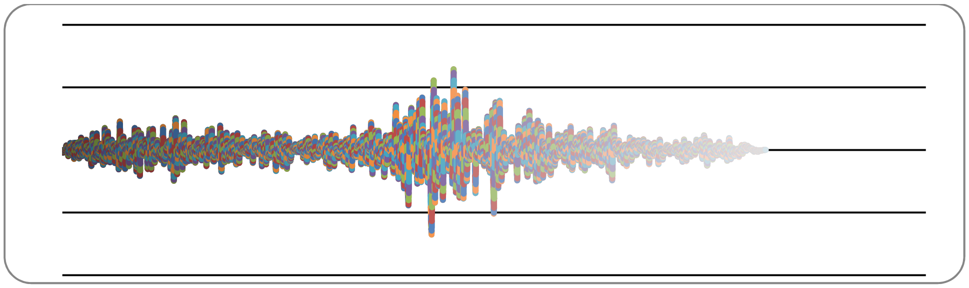

Figure 9 History of Manjil earthquake spectrum.

Table 4 **Comparison between horizontal displacement of connected and non-connected system.**

Type of piled raft foundation	Horizontal displacement (cm)
Connected piled raft foundation	**14.3**
Non-connected piled raft foundation	**18.5**

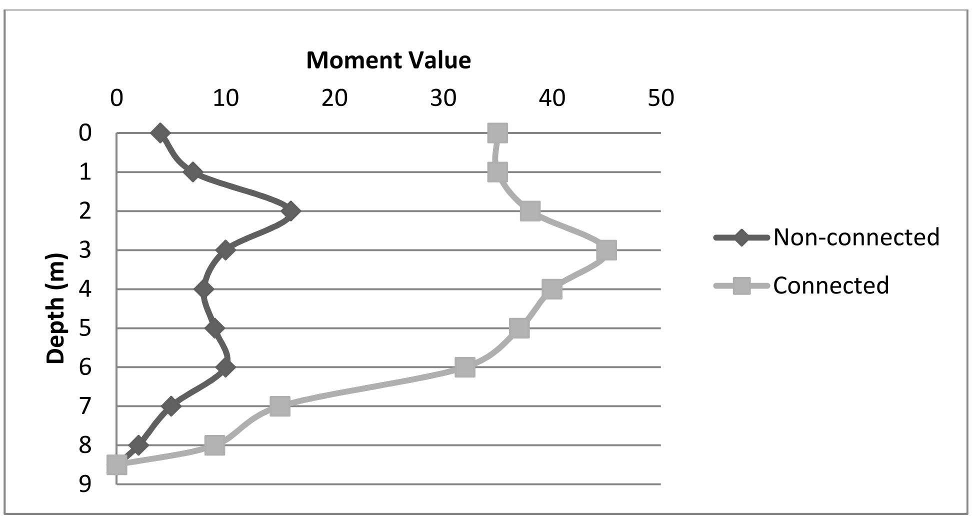

Figure 10 Bending moment graph along pile length.

CONCLUSIONS

The major conclusions of this research are as follow:

- As can be observed in results of centrifuge tests under static load, the non-connected pile raft system with granular layer has shown a better performance compared to connected pile raft systems.

- Optimum thickness of the granular layer is suggested as about 1.5m for this study.
- Regarding bearing capacity, the difference between fixed and hinged conditions piled raft foundations is very small. So, the granular layer is effective to decrease bending moment.
- The horizontal displacement is increased when using non-connected piled raft the granular layer but this different is not very large.

REFERENCES

ACS SASSI-C (1998). *An Advanced Computational Software for 3D Dynamic Analysis Including Soil-Structure Interaction*, Advanced Computational Software, Inc.

Baziar M.H., Ghorbani A., Katzenbach, R. (2009). Small-scale model test and three-dimensional analysis of pile-raft foundation on medium-dense sand, *Inter. J. Civil Eng*., 7(3).

Horikoshi K. et al. (2003). Performance of piled raft foundations subjected to dynamic loading, *Int. J. Phys. Modeling Geotech*., 2: 51–62.

Mano H., Nakai, S. (2000). An approximate analysis for stress of piles in a laterally loaded piled raft foundation, ASCE, *J. Struct. Eng*., 46B: 43–50.

Mano H., Nakai S. (2004). Stress of piles in a piled raft foundation during earthquake, *Proceedings, 11th International Conference on Soil Dynamics and Earthquake Engineering*, 1: 726–733.

Prakoso W A., Kulhawy F H. (2001). Contribution to piled raft foundation design, ASCE, *J. Geotech. Eng*. 127(1): 17–24.

Poulos H.G. (1994). An approximate numerical analysis of piled-raft interaction, *Int. J. Num. Analytical Methods Geomech*., 18 (2): 73–92.

Randolph M.F. (1994). Design methods for pile groups and piled rafts, *Proceedings, 13th International Conference on Soil Mechanics and Foundation Engineering,* 5: 61–82.

Reul O., Randolph M.F. (2004). Design strategies for piled rafts subjected to non-uniform vertical loading, ASCE, *J. Geotech. Geoenviro. Eng*., 130 (1): 1–13.

Seo Y.K., Lee H.J., Kim T.H. (2006). Numerical analysis of piled-raft foundation considering sand cushion effects, *Proceedings, 16th International Offshore and Polar Engineering Conference*, San Francisco, CA, pp. 608–613.

Sugimura Y. (2001). Pile head connection for the performance-based design, *Foundation Eng. Equip.*, 29(12): 5 (in Japanese).

Wada, A. et al. (2001). Shaking table tests for interaction of soil and structure on short-stiff-piles and long-flexible-piles, *Proceedings, 15th AIMETA Congress of Theoretical and Applied Mechanics*, Taormina, Italy.

Yamada T. et al. (1998). An example of piled raft foundation in building design, *Foundation Eng. Equip.*, 26(5): 100–103 (in Japanese).

Yamashita K. (1998). Analyses of piled raft model provided by ISSMGE TC-18 Part 2: Estimation by three-dimensional finite analysis, *Proceedings, ISSMGE TC18 JGS Meeting on Piled Rafts*.

HYBRID DEVICES TO REDUCE RESIDUAL DISPLACEMENT OF STRUCTURAL SYSTEMS SUBJECTED TO STRONG GROUND MOTION

Behrouz Asgarian[1] and Ali Jalaeefar[2]

ABSTRACT

Usage of special materials with unique properties in seismic resistant structures has increased to overcome their limited energy dissipation and ductility as a result of 1994 Northridge earthquake. Among them, shape memory alloy (SMA) is a unique metallic alloy which has the ability to undergo large deformation while reverting back to its original un-deformed shape. In This paper monotonic and cyclic static loading tests on Nitinol and steel bars are conducted to obtain their mechanical properties in tension and compression. Also a comparative low cycle fatigue test is conducted using steel and Nitinol samples. Considering the results, a simple and practical solution is developed to overcome some of the deficiencies of these two materials in seismic resisting structures. Placing the proposed device in semi-rigid bracing members of special structures will localize the energy dissipating and ductility while providing the brace with strain recovering capability and will reduce the residual drifts of the structure.

Keywords: *energy dissipating, hybrid, Nitinol, re-centering, shape memory alloy*

INTRODUCTION

One way of reducing the residual displacement of structural systems is the use of innovative materials. In particular, super-elastic shape memory alloys (SMA) have been shown to develop a flag-shape hysteresis under cyclic axial loading, which can provide a structural system with both strain recovering (re-centering) and supplemental energy dissipating and results in limiting inter-story drifts and decreasing permanent displacements of the structure.

Most of the previous studies mainly focused on SMA benefits and ignore some of its major deficiencies. Besides, SMA is much more expensive than structural steel. Thus it does not seem reasonable to substitute structural steel with shape memory alloy without taking into account all the pros and cons together. In this study the advantages and disadvantages of using Ni-Ti alloy in structural engineering is assessed. As a solution for the deficiencies of SMA, a hybrid device with parallel usage of structural steel and SMA is developed and the setup has been tested. The proposed device can be used in bracing members to reduce residual displacements due to strong ground motions.

EXPERIMENTAL INVESTIGATION OF MATERIAL PROPERTIES

In order to compare mechanical properties of shape memory alloy and steel, monotonic and cyclic tension and compression and fatigue tests are designed. The shape memory material used

[1] Associate Professor of Civil Engineering, K.N. Toosi University of Technology.
[2] PhD candidate, K.N.Toosi University of Technology; email: ali_jalaeefar@yahoo.com.

for the tests consists of commercial super-elastic Ni-Ti bars with circular cross section of 8 mm diameter provided. The alloy composition and manufacturing conditions were carefully selected so that the experimental specimens would exhibit super elastic properties at room temperature. Also 8 mm diameter bars of mild structural steel (mean yield stress=500 MPa) are provided as steel members.

Monotonic and cyclic tests are designed to obtain mechanical properties of steel and SMA namely: monotonic tension test, cyclic tension test, cyclic compression test, cyclic tension-compression test and low cycle fatigue test.

Monotonic Tensile Test

Standard specimens of Ni-Ti alloy and mild structural steel were fabricated according to ASTM E8/E8M-09 and ASTM E9/E9M-09 (Figure 1). The specimens were of 8 mm diameter at the ends from where they were clamped in the hydraulic chucks. The diameter at the gage length of the specimens was selected to be 5 mm. The specimens were tensioned up to rupture. Figures 2 and 3 show the stress-strain curves of the steel and Nitinol samples.

Figure 1 Standard tension-compression samples of steel and SMA.

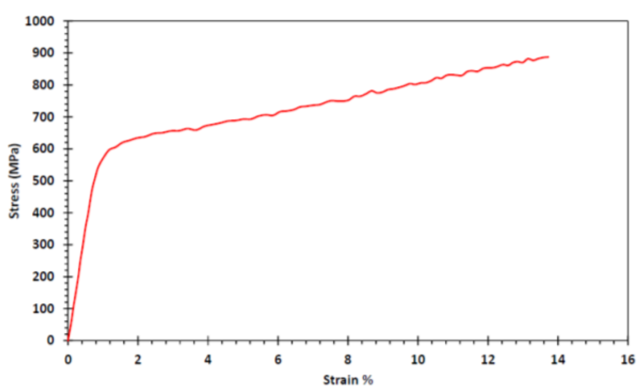

Figure 2 Stress-strain curve of structural SMA tension tests.

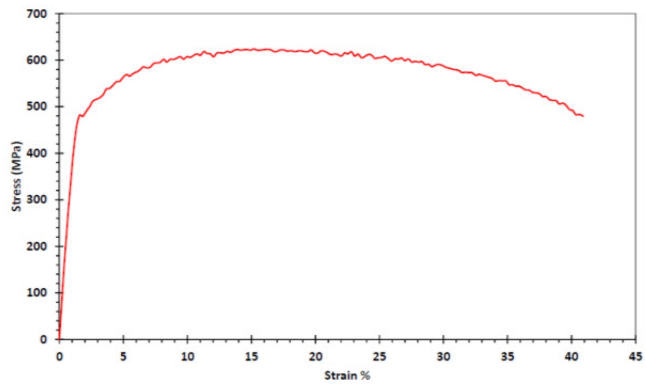

Figure 3 Stress-strain curve of structural steel tension tests.

Cyclic Tests

The same specimens which can be loaded both in tension and compression without any instability during compressive loads are used for cyclic tests (Figure 1). The loading protocols consisted of cycles of increasing strain amplitude of 1% to 6% by increments of 1%. Cyclic tension-only tests, cyclic compression-only tests and cyclic tension-compression tests are performed for Nitinol with the standard conditions of ASTM F2516-07. Figures 4 through 7 show the average of these three stress-strain curves.

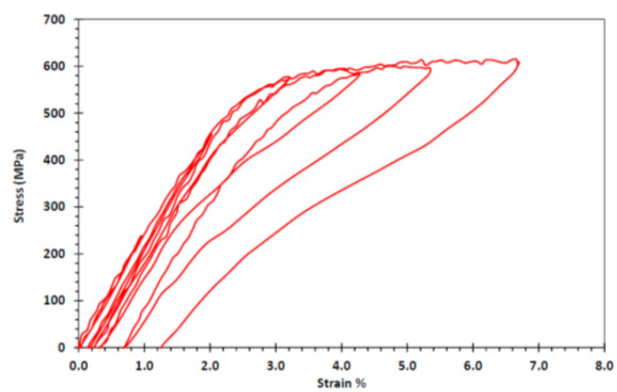

Figure 4 Stress-strain curve of Nitinol cyclic tension only tests.

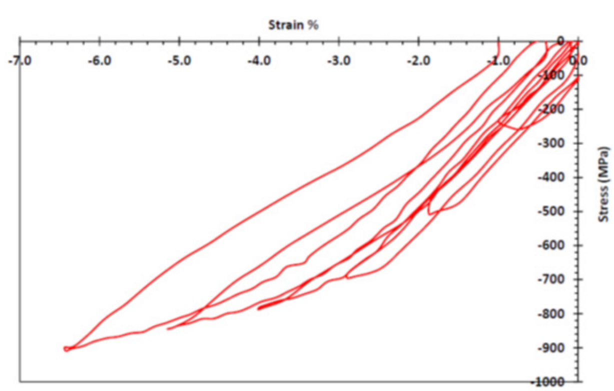

Figure 5 Stress-strain curve of Nitinol cyclic compression only tests.

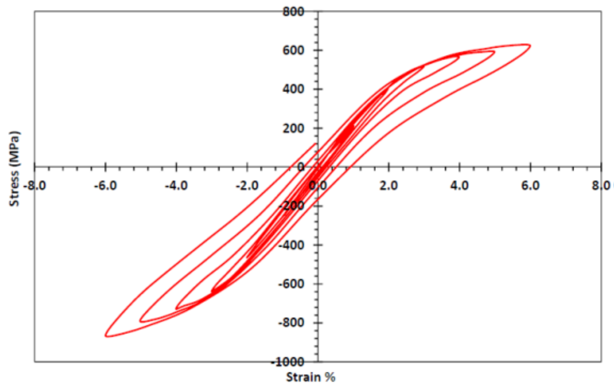

Figure 6 **Stress-strain curve of Nitinol cyclic tension-compression tests.**

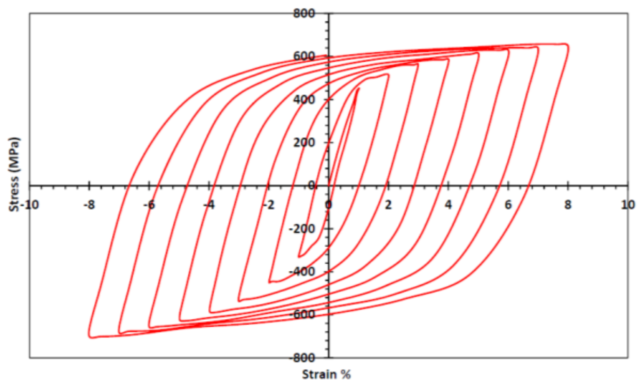

Figure 7 **Stress-strain curve of structural steel cyclic tension-compression tests**

Fatigue Test

Low-cycle fatigue test is conducted on steel and Nitinol using standard tension-compression samples similar to cyclic samples (Figure 1). For structural steel the stress varies between $0.64F_{yield}$ and $1.15F_{yield}$. For Nitinol the stress varies between $0.9F_{yield}$ and $1.45F_{yield}$. The loading frequency is assumed to be 3 Hz. Figure 8 shows the S-N curve for structural steel and Nitinol.

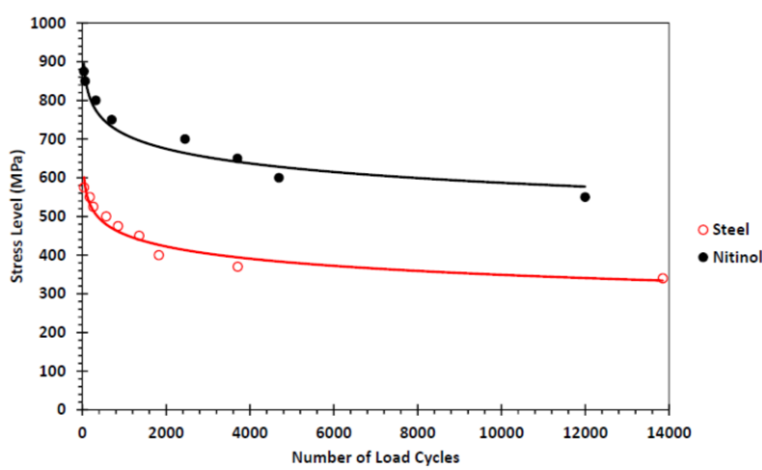

Figure 8 **Fatigue S-N curve for Nitinol and structural steel.**

Test Results

Rupture in a steel member is gradual and with definite alarming signs as necessary in structural engineering. This occurs in about 40% strain. On the other hand the rupture in Nitinol occurs in 12% strain suddenly and without any alarming signs similar to a brittle material. Figure 9 shows the different behaviors and rupture mechanisms of steel and Nitinol. As shown in this figure no necking and section reduction have occurred in the Nitinol sample and it seems that the Nitinol sample is divided into two parts with a cutting device causing a flat edge on the remaining.

Also, cyclic tests proved that the behaviors of Nitinol in tension and compression are not so much different and the alloy has considerable super-elasticity in compression as in tension. The main difference is the stress level in a same strain which is about 15–20% higher in compression. The re-centering capability is almost the same in tension and compression.

As shown in Figures 6 and 7, the cyclic dissipated energy (area surrounded by the stress-strain curve) is much more in steel than Nitinol. The stress-strain curve of steel is wide and open while Nitinol shows closed cycles with little surrounding area. On the other hand, the permanent plastic strain in steel is almost equal to the initial induced strain. But only 1% strain remains after loading Nitinol up to 6% strain and more than 80% of the induced strain is recoverable.

Taking only low cycle fatigue into account regarding to earthquake loads, structural steel will stand about 500 cycles before failure if loaded up to its yield stress while Nitinol will stand for 4700 cycles. On the other hand structural steel will fail after 40 cycles if loaded up to 1.15Fyield while Nitinol should be loaded up to 1.45 of its yield stress to fail after 40 cycles. Generally, Nitinol shows a much better behavior against fatigue than structural steel and is more reliable in seismic periodic loads.

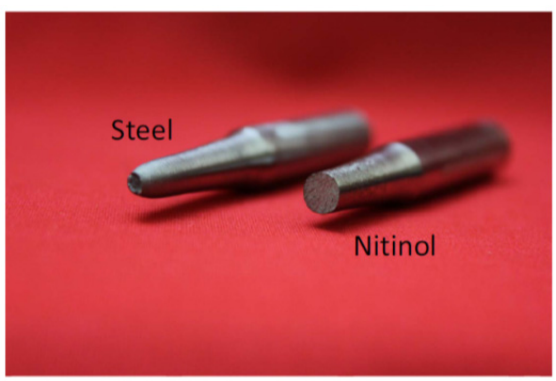

Figure 9 Ruptured remaining of steel and Nitinol tension samples.

Considering all mentioned aspects, the advantages and disadvantages of the two materials can be summarized as follows:

Structural Steel Advantages:

- Capable of bearing up to 35% strain before rupture

- Large area under stress-strain curve or high cyclic energy dissipation capacity
- Gradual and alarming fracture (showing obvious deformations)
- Softening phase in the stress-strain curve
- Similar behavior in tension and compression
- Simplicity of machining and welding
- Reasonable price

Structural Steel Disadvantages

- Large permanent plastic strain
- Weak re-centering capability
- Poor quality for making machined components such as bolts due to porosity
- Low resistance against corrosion
- Low resistance against fatigue

Shape Memory Alloy (Nitinol) Advantages

- Capable of re-centering and recovering over 80% of the induced strains
- High modules of elasticity
- Similar behavior in tension and compression
- High quality for making machined components such as bolts
- High resistance against corrosion
- High resistance against fatigue

Shape Memory Alloy (Nitinol) Disadvantages

- Small area under stress-strain curve or little cyclic energy dissipation capacity
- Semi-brittle and alarm-less fracture
- Little ultimate fracture strain (less than 15%)
- Not easily welded
- Not easily machined
- High price

SOLUTION

Using structural steel and shape memory alloy parallel with each other is a solution which leads to combining their benefits and eliminating some of the deficiencies. In this paper a simple and practical setup is proposed for parallelizing structural steel and Nitinol bars which can be utilized as an axial device in special bracing members of braced frames.

Details of the Proposed Device

Details of the proposed hybrid damping device for use in a brace member are illustrated in Figure 10. As shown, the device is made up of two thick and rigid plates at each end which are connected to each other using bars of 8 mm diameter. These bars are made up of structural steel or Nitinol and are the main load resisting elements of the device. To take advantage of these slender bars in compression in addition to tension, a high strength cement based grout fills the space around them which prevents the bars from buckling. The bars and the grout are placed in a tube providing lateral pressure for the grout. The tube is connected to only one of the end plates and is free at the other end. Also the tube and the bars are lubricated using formwork oil to minimize their friction with the grout which could affect the behavior of the device. In this way it will be possible to take advantage of the plastic potential of the steel and SMA bars without any local or global instability.

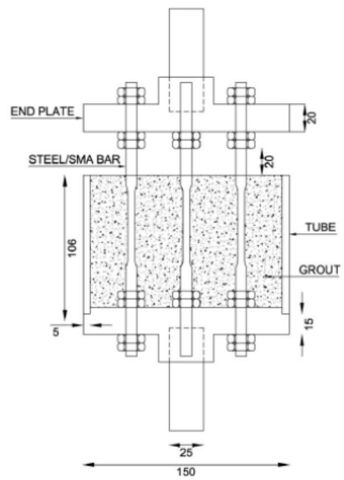

Figure 10 Details of the proposed device.

Finite Element Model

The ANSYS multi-purpose finite element modeling code was used to perform numerical modeling of the hybrid devices with both steel and SMA bars. Eight node SOLID185 elements are used for numerical modeling of the device. SOLID185 is used for three-dimensional modeling of solid structures. Displacement control static analysis is performed assuming large deformation formulation. Results of previously mentioned experimental studies on behavior of steel and Nitinol bars are used for modeling material behavior.

Three different dampers are analyzed using finite element method. The first device with steel bars exhibits an open hysteresis curve with maximum area while having a large permanent plastic strain as shown in Figure 11. But the one with SMA bars exhibits a double flag shaped hysteresis with minimum area while recovering the strains and having no permanent plastic deformations as illustrated in Figure 11. The hybrid device with both steel and Nitinol bars (hybrid device) shows both energy dissipating and re-centering together as shown in Figure

11.Thus, if the SMA/steel ratio increases, the recoverable strains increases while the cyclic dissipated energy decreases.

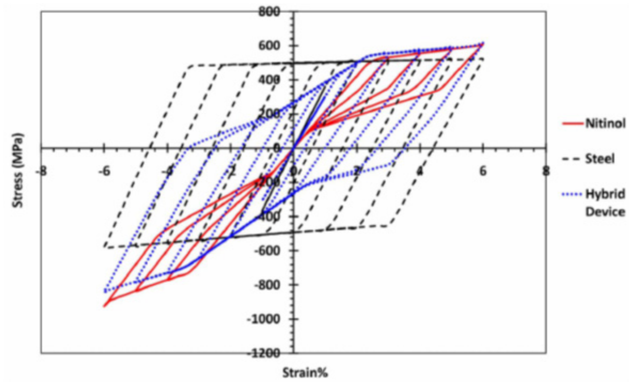

Figure 11 Analytical stress-strain curves for dampers.

Experimental Investigation of the Proposed Set-Up

The proposed device with the same details mentioned above is fabricated using five different SMA/steel proportions namely: 0, 0.67, 1, 1.5, and 2. The hybrid devices are tested to investigate the efficiency of the proposed set-up. The loading protocol consisted of cycles of increasing strain amplitude of 1% to 6% by increments of 1%. Figure 12 shows the fabricated devices and the testing setup. The results of the test are also illustrated in Figures 13 through 15. The behaviors in tension and compression are almost symmetric and no local or global instability is observed due to the bars buckling. As previously seen in finite element results, the recoverable strain increases with increase in SMA/Steel ratio, while the cyclic dissipated energy decreases.

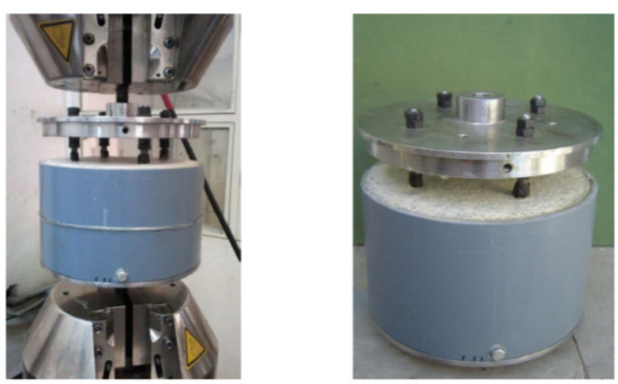

Figure 12 Fabricated hybrid device and the testing set-up.

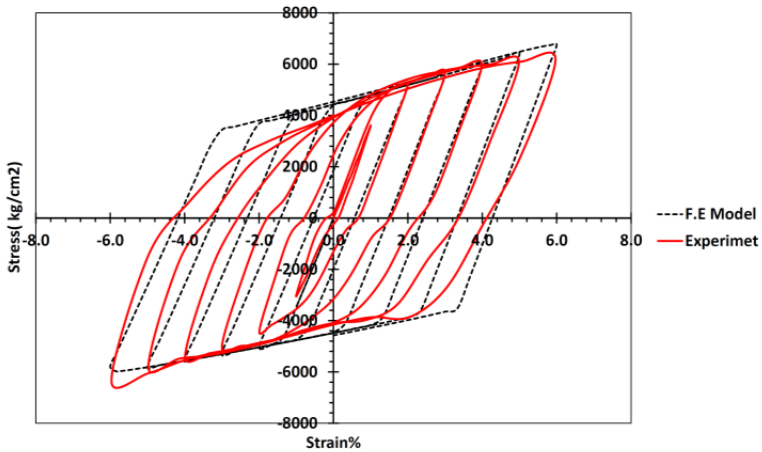

Figure 13 Result for the hybrid device with steel bars.

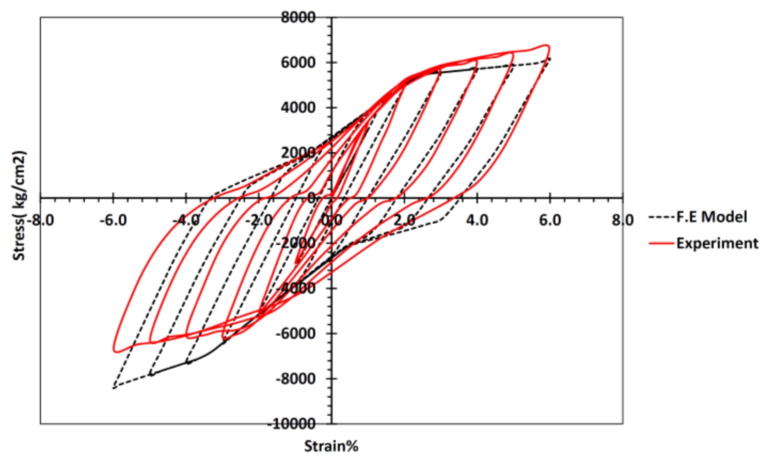

Figure 14 Result for the hybrid device with 2 steel and 2 SMA bars.

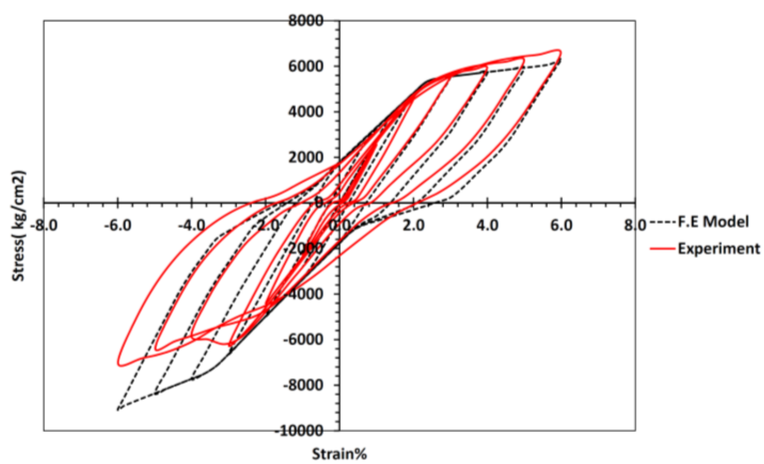

Figure 15 Result for the hybrid device with 2 steel and 4 SMA bars.

EXTENDED FINITE ELEMENT MODELS

As seen, the difference between the results of the tests and finite element models are is an acceptable and the modeling parameters are reasonably accurate. Thus the finite element modeling is extended and devices with various SMA/Steel proportions are modeled. For each device, the amount of cyclic dissipated energy and re-centering are calculated and plotted in a single graph as shown in Figure 16. Increasing the SMA/Steel proportion increases the re-centering while decreasing the cyclic dissipated energy. It is necessary to define an optimum SMA/steel ratio in which both of the two main factors would have a reasonable and acceptable amount. The intersection of the two curves is the optimum point in which both cyclic dissipated energy and re-centering capability are maximized simultaneously. This occurs in a SMA/steel ratio of about '1.33'. In this point more than 70% of total strain is recoverable while the cyclic dissipated energy ratio against structural steel is also more than 70%. Thus taking advantage of shape memory alloy parallel with structural steel leads to better performance of the device both in recovering the strains and dissipating the earthquake energy. This will not be achieved if each of the materials is used without the other.

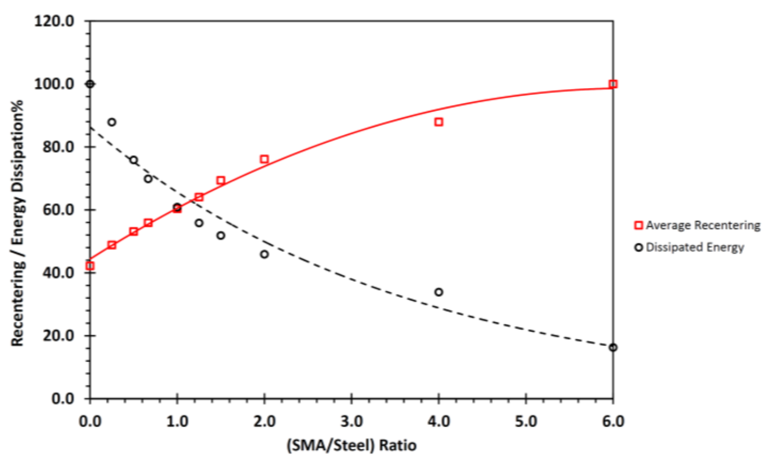

Figure 16 Optimizing the SMA/Steel ratio based on energy dissipating and re-centering

CONCLUSIONS AND SUGGESTIONS

The objective of this study is to assess the advantages and disadvantages of using Ni-Ti alloy in structural engineering and to compare its mechanical properties with structural steel according to experimental results. As a solution for some of the deficiencies of these two materials, a hybrid device with parallel usage of structural steel and SMA is developed and the setup has been tested. This idea will help to overcome the deficiencies of steel and SMA and to take advantage of them together in seismic resisting structures while reducing the costs. The following conclusions are drawn based on the results and observations presented herein:

- The behavior of shape memory alloy used in the present research is studied through monotonic and cyclic tests. Results show that behaviors of Ni-Ti alloy in tension and compression are similar. The shape of stress-strain loops are almost the same but the amounts of transformation stresses differ.

- The super-elasticity of the Ni-Ti alloy used is almost the same in compression and tension and the imposed compressive strains are recovered as well as.
- The fracture in Nitinol is sudden and with no alarming signs in about 15% strain.
- The fracture in structural is gradual and with definite alarming signs in about 35% strain.
- Nitinol shows a much better behavior against fatigue than structural steel and is more reliable in seismic periodic loads.
- A simple and practical setup is proposed for utilizing Nitinol and steel bars parallel with each other in a special bracing member. The setup can be simply used in special braced frames to improve their behavior, although more analytical and experimental studies are necessary.
- Using shape memory alloy and steel parallel with each other, the combination exhibits both strain recovering capacity and energy dissipation. Besides, this will prevent sudden and alarm less fracture of the device.

REFERENCES

ASTM. *Standard Test Method for Compression Testing of Metallic Materials at Room Temperature,* ASTM E9M, West Conshocken, PA.

ASTM. *Standard Test Methods for Tension Testing of Metallic Materials, ASTM E8/E8M-09*, West Conshocken, PA.

ASTM. *Standard Test Method for Tension Testing of Nickel-Titanium Super-elastic Materials, ASTM F2516-07*, West Conshocken, PA.

Asgarian B, Jalaeefar A (2009). Incremental Dynamic Analysis of steel braced frames designed based on the 1st, 2nd and 3rd editions of Iranian Seismic Code 2800, *Struct. Design of Tall and Special* Bldgs., 20(2): 190–207.

Auricchio F, Fugazza D, DesRoches R (2006). Earthquake performance of steel frames with Nitinol braces, J. *Earthq. Eng*., 10: 45–66.

Chuang S., Yang W., DesRoches R., Leon R. (2010). Design and analysis of braced frames with shape memory alloy and energy-absorbing hybrid devices, *Eng. Structures*, 32: 498–507.

Fugazza D. (2003). *Shape-Memory Alloy Devices for Earthquake Engineering: Mechanical Properties, Constitutive Modeling and Numerical Simulations*, Masters' Thesis, European School for Advanced Studies in Reduction of Seismic Risk, Pavia, Italy.

Fugazza D. (2005). *Use of Shape-Memory Alloy Devices in Earthquake Engineering: Mechanical Properties, Advanced Constitutive Modeling and Structural Applications*, PhD Dissertation, European School for Advanced Studies in Reduction of Seismic Risk. Pavia, Italy.

Jalaeefar A. (2012). *Experimental and Analytical Study of SMA Based Hybrid Dampers for Special Braced Frames, K.N.Toosi University of Technology*, A Thesis Submitted in Partial Fulfillment of the Requirements for the Doctor of Philosophy Degree in Structural Engineering.

Jalaeefar A., Asgarian B. (2012). A simple hybrid damping device with energy dissipating and re-centering characteristics for special structures, *Struct. Design of Tall and Special Bldgs*., DOI: 10.1002/tal.1050.

Jalaeefar A, Asgarian B (2012). Experimental investigation of mechanical properties of Nitinol, structural steel and their hybrid component, ASCE, *J. Mater. Civ. Eng*., 25(10): 1498–1505.

Lagoudas D.C. (ed.) (2008). *Shape Memory Alloys - Modeling and Engineering Applications*, Springer Science + Business Media.

Mazzoni S., McKenna F., Scott M.H., Fenves G.L. (2006). *OpenSees Command Language Manual*, Pacific Earthquake Engineering Research Center, University of California, Berkeley, CA.

McCormick J., DesRoches R., Fugazza D., Auricchio F. (2007). Seismic assessment of concentrically braced steel frames with shape memory alloy braces, ASCE, *J. Struct. Eng*., 133(6): 862–870.

McCormick J., DesRoches R., Fugazza D., Auricchio F. (2006). Seismic vibration damping using super-elastic shape memory alloys, J. *Eng. Mater. Tech*., 128: 294–301.

Motahari S.A, Ghassemieh M, Abolmaali S.A. (2007) "Implementation of shape memory alloy dampers for passive damping of structures subjected to seismic excitations, *J. Constructional Steel Res*., 63(12): 1570–1579.

Ozbulut O.E., Hurlebaus S. (2011). Optimal design of superelastic-friction base isolators for seismic protection of highway bridges against near-field earthquakes, *Earthq. Eng. Struct. Dyn*., 40: 273–291.

Ozbulut O.E., Hurlebaus S. (2011). Seismic assessment of bridge structures isolated by a shape memory alloy/rubber-based isolation system, *Smart Mater. Struct*.; doi:10.1088/0964-1726/20/1/015003.

CONCRETE FILLED STEEL TUBULAR BEAM-COLUMNS MODELING FOR NONLINEAR ANALYSIS

Ali Reza Khaloo[1], Mohammad Ali Tajally[2], and Seyyed Farshid Hosseini Khasheh Heiran[2]

ABSTRACT

This paper presents displacement-based technique (DBT) to model concrete filled steel tubular (CFST) beam-columns for nonlinear analysis and performance based design. The fiber element based formulations is used for columns in wide range of width-to-thickness ratio with both circular and rectangular sections under axial loading and uniaxial bending. In this model, new stress-strain diagram is suggested for steel and local buckling effects of steel tube are considered by offering coefficients impose in steel properties. Nonlinearity of materials is included by using total secant stiffness. Confinement effect of steel tube on concrete core and second order P-Δ effects are taken into account in this approach. The proposed DBT provides simple CFST design for columns with a wide range of steel tube strength grade and concrete strength. To ensure proper functioning of technique, several columns and a frame are modeled in OpenSees, and the results compared with corresponding experimental results. Comparison shows the capability of predicting DBT in experimental data satisfactorily.

Keywords: *CFST beam-columns; displacement based analysis; nonlinear static and dynamic analysis, steel tube local buckling*

INTRODUCTION

Combination of steel and concrete in concrete-filled steel tube in CFST provides advantages of the two materials and compensate their disadvantages. The steel tube have longitudinal and lateral reinforcement role for helping concrete core to resist against bending moment, shear and tension. Steel tube also creates confinement in concrete and increase compressive strength and prevents concrete from spalling. Concrete core increases stiffness of column and reduces capability of inward local buckling [Hu et al. 2005]. Interaction between steel and concrete provides high strength, ductility and energy absorption capacity and leads to better seismic performance of structures built with these columns [Valipour and Foster 2010].

Behaviors of CFST columns are influenced by loading, characteristics of materials and geometric of cross section such as nonlinear behavior and ultimate strength of material, shape and width-to-thickness ratio of steel tube section. Circular tubes impose more confinement effect on concrete core than rectangular cross sections. Confinement properties of concrete core are affected by width-to-thickness ratio of steel tube. Experimental studies of Schneider [1998] on short steel tubular columns demonstrate that post yield ductility of rectangular CFST columns is less than circular ones. In Schneider experiments, local buckling of rectangular CFST occurred in ductility between 2 to 8, while local buckling in circular ones appeared in ductility up 10.

[1] Professor, Sharif University of technology, Tehran, Iran.
[2] M.Sc. in Structural Engineering, Sharif University of Technology, Tehran, Iran.

Varma et al. [2002] showed that when width-to-thickness ratio or axial load level increases, monotonic curvature ductility decreases remarkably in high strength square CFST columns. However, steel yield strength did not affect the curvature ductility strongly.

Steel local buckling is the most important factor that affects behavior of CFST columns and should be considered in analysis. Ultimate strength and ductility of columns are strongly related to this factor and behavior of column under loading, changes after local buckling. In columns with large width-to-thickness ratio, steel tube may buckle locally and outward under compression forces. This phenomenon generally happens in the end regions of column and decreases ductility and ultimate strength of CFST columns remarkably [Bridge and O'Shea 1998].

Nowadays, there is a growing tendency to use CFST columns in buildings and bridges, especially in regions with high seismic activities; however, modeling of CFST columns is complicated. There are several factors that affect performance of these columns; so, it is necessary to find methods that are able to model behavior of CFST columns properly. In recent years, several investigations have been carried out to model CFST columns under axial load and uniaxial bending.

Liang [2009] proposed performance based analysis method based on fiber element formulation. He incorporated local buckling and effective width/effective strength formulas into the nonlinear analysis procedure. Munoz and Hsu [1997] suggested fiber element procedure to model short and slender CFST columns for nonlinear analysis by using incremental strain and finite different methods. Hajjar and Gourley [1996] used bounding surface plasticity models based on fiber element analysis and proposed equations for strength interaction. Lakshmi and Shanmugam [2002] used analytical model to investigate effects of local buckling on ultimate strength of CFST columns and proposed effective width formulas without considering progressive local buckling of steel tube. Chen et al. [2001] utilized Regula–Falsi numerical scheme and proposed iterative procedure to design and analyze of encased composite columns with arbitrary section shapes. Valipour and Foster [2010] used force interpolation concept to propose formulation for one dimensional elements which are used in nonlinear static and dynamic analyses of composite frames.

This paper presents appropriate nonlinear material models for confined concrete and steel tube which are used in fiber based methods. To ensure proper functioning of the proposed procedure, results attained from analytical models are compared with corresponding experimental data presented by Fujimoto et al. [2004] and Tomii and Sakino [1979].Parameters such as ultimate strength and moment curvature curves are considered in these comparisons.

An innovative aspect of this paper is considering effects of steel local buckling and shape of cross section in materials properties. This procedure makes it possible to analyze CFST columns under dynamic and static forces. Proposed displacement based technique predicts ultimate strength and ductility of concrete filled steel tubular columns for nonlinear static and dynamic analysis, and performance based designs. Also, columns in wide range of width-to-thickness ratio and with mild or high strength materials can be modeled with this method.

Finally, the proposed procedure is capable of analyzing CFST columns under axial loads, uniaxial bending, and dynamic forces such as earthquakes.

DISPLACEMENT BASED THEORY

In this paper, the presented formulation for displacement based theory is according to formulation proposed by Spacone et al. [1996]. This formulation is general in scope and can be used for any section with any material behavior [1996]. Figure 1 shows an ordinary beam–column element with two nodes and five degrees of freedom. It is assumed that axial force is constant along longitudinal of element. The generalized vectors for force and displacement are respectively denoted by Q and q.

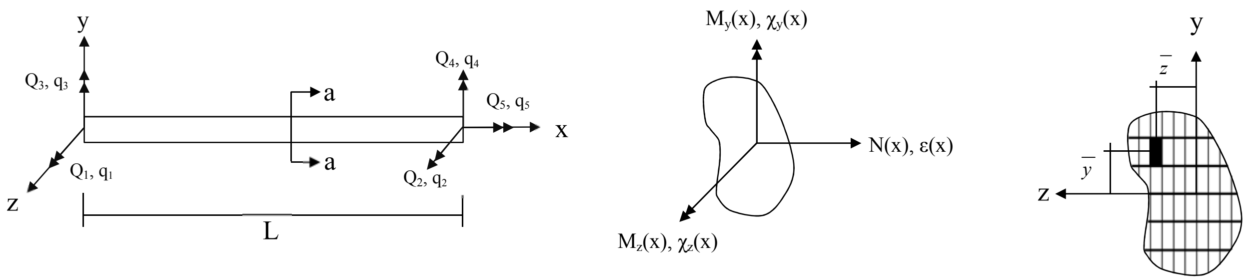

(a) **(b)**

Figure 1 (a) Nodes and degrees of freedom (b) cross section in an ordinary beam-column element.

$$Q = \{Q_1 Q_2 Q_3 Q_4 Q_5\}^T \tag{1}$$

$$q = \{q_1 q_2 q_3 q_4 q_5\}^T \tag{2}$$

The generalized force and deformation vectors for cross section are according to below where D and d denote force and deformation vectors, respectively:

$$D(x) = \{M_z(x) M_y(x) N(x)\}^T \tag{3}$$

$$d(x) = \{\chi_z(x) \chi_y(x) \bar{\varepsilon}(x)\}^T \tag{4}$$

where χ is the curvature about the respective axis, and $\bar{\varepsilon}$ is the axial strain.

Generally, in the displacement -based method, force-deformation relation of section is initially linearized about the present state, then the nonlinear force-deformation relation is satisfied by using iterative algorithm to reach an acceptable tolerance. To estimate displacement and force of any section along the element, numerical interpolation functions are used as below:

$$\Delta d(x) = a(x)\Delta q \tag{5}$$

$$\Delta D(x) = b(x)\ \Delta \mathrm{Q} \tag{6}$$

where the Δ prefix denotes to increments in corresponding quantities; $a(x)$ and $b(x)$ specify deformation and force interpolation functions, respectively.

Deformation increment in any step can be expressed as below:

$$\Delta d^{j} = f^{j-1}(x)\Delta D^{j}(x) + r^{j-1}(x) \tag{7}$$

where $f^{j-1}(x)$ and $r^{j-1}(x)$ are flexibility matrix and residual deformation vector from latest iteration and superscript j denotes to current step of iteration.

The weighted integral form of Equation (7) can be expressed as below:

$$\int_0^L \partial D^T [\Delta d^j(x) - f^{j-1}(x)\Delta D^j(x) - r^{j-1}(x)]dx = 0 \tag{8}$$

Substitution of Equations (5) and (6) in Equation (8) result in Equation (9).

$$\int_0^L \partial Q^T [T\,\Delta q^j - F^{j-1}\Delta Q^j - S^{j-1}]dx = 0 \tag{9}$$

where T is the matrix which only depends on interpolation functions. F and S are element flexibility matrix and element residual vector, respectively. The formulation of T, F, and S are expressed in below:

$$T = \int_0^L b^T(x)a(x)dx \tag{10}$$

$$F = \int_0^L b^T(x)f(x)b(x)dx \tag{11}$$

$$S = \int_0^L b^T(x)r(x)dx \tag{12}$$

Equation (9) must be independent from ∂Q^T ; thus:

$$T\,\Delta q^j - F^{j-1}\Delta Q^j - S^{j-1} = 0 \tag{13}$$

Equation (13) refers to the linearized force-deformation relation of section. By using the virtual displacement principle, equilibrium equation of element can be derived in integral form:

$$\int_0^L \partial d^T(x)[D^{j-1}(x) + \Delta D^j(x)]dx = \partial q^T Q^j \tag{14}$$

By substituting Equations (5) and (6) in Equation (14), we derive Equation (15):

$$\int_0^L \partial q^T [a^T(x)b(x)Q^{j-1} + a^T(x)b(x)\Delta Q^j]dx = \partial q^T Q^j \tag{15}$$

The above integral must be independent from ∂q^T ; thus:

$$T^T Q^{j-1} + T^T \Delta Q^j = Q^j \tag{16}$$

Combining Equation (13) with (16), and reordering leads to:

$$\begin{bmatrix} -F^{j-1} & T \\ T^T & 0 \end{bmatrix} \begin{Bmatrix} \Delta Q^j \\ \Delta q^j \end{Bmatrix} = \begin{Bmatrix} S^{j-1} \\ Q^j - T^T Q^{j-1} \end{Bmatrix} \tag{17}$$

By solving first term of Equation (17) in terms of ΔQ^j and substituting in the second term, the result can be expressed as below:

$$T^T [F^{j-1}]^{-1} (T \Delta q^j - S^{j-1}) = Q^j - T^T Q^{j-1} \tag{18}$$

By choosing proper $a(x)$ and $b(x)$ matrices, the T matrix in Equation (18) will be equal to identity matrix and can be removed from equation. If the T matrix is removed, Equation (18) becomes:

$$[F^{j-1}]^{-1} (\Delta q^j - S^{j-1}) = \Delta Q^j \tag{19}$$

Equation (19) expresses linearized matrix relation between element force increments and corresponding deformation increments ($\Delta q^j - S^{j-1}$). In this equation, $[F]^{-1}$ refers to stiffness matrix of element and implies that stiffness matrix is obtained from flexibility matrix. By using Equation (19) and imposing incremental displacements (Δq^j) to element, external reactions (Q^j) will be obtained in every step.

MATERIAL MODELING

Behavior of ordinary steel and concrete change when they are used in CFST columns. Presented material modeling procedure in this paper can be used for both nonlinear static and dynamic analysis of CFST columns in wide range of thickness to diameter ratios and for both short and medium length columns.

Concrete

In CFST columns, steel tube imposes confinement to the concrete core and increases its ultimate strength and ductility. Although, properties of confined concrete in these columns depend on geometric characteristics of section, in some cases, yield strength of steel can also affect the properties of confined concrete. Figure 2 shows the general stress-strain curve of confined concrete in CFST columns. This behavior can be modeled by using *Concrete02* material in OpenSees [McKenna et al. 2000] finite element code.

Details of this model depend on shape of cross section and thickness to diameter ratio of steel tube. Experimental studies show that steel tube increases only ductility of concrete core and has no effect on its ultimate strength in rectangular columns; however, in circular cross sections, steel tube increases both ductility and ultimate strength of concrete core. Modeling procedure for confined concrete in CFST columns is presented in next sections for circular and rectangular cross sections, separately. Both normal and high strength confined concrete can be modeled by using this procedure.

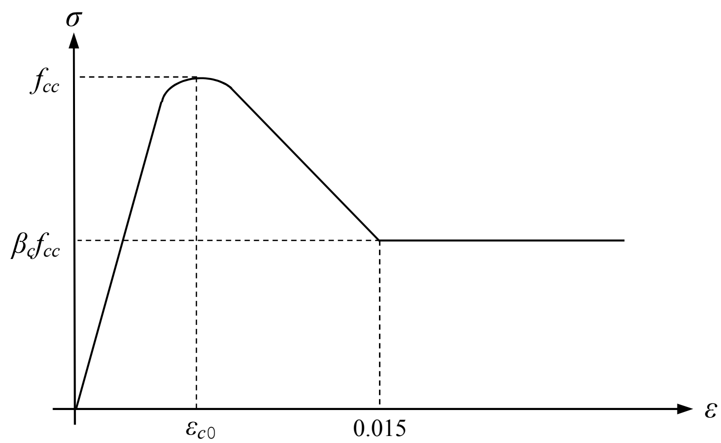

Figure 2 General stress-strain curve for confined concrete in CFST columns.

Rectangular Cross Sections

Equations that are used in this section to estimate characteristics of confined concrete are based on suggested equations by Mander et al. [1988] and Tomii and Sakino [1979] with some modifications. The corresponding equations are presented in below:

$$f_{cc} = \gamma_c f_c \tag{20}$$

$$\gamma_c = 1.85 D_i^{-0.135} \qquad (0.85 \le \gamma_c \le 1.0) \tag{21}$$

where f_{cc} is the effective compressive strength of concrete, f_c is the nominal compressive strength of concrete, and γ_c is the strength reduction factor suggested by Liang [2009]. In Equation (21), D_i refers to largest dimension of concrete core.

$$E_c = 3320\sqrt{f_c} + 6900 \tag{22}$$

$$\varepsilon_{c0} = \frac{2f_{cc}}{E_c} \tag{23}$$

where ε_{c0} is the strain at f_{cc} and E_c is the young's modulus of concrete.

To consider confinement effect of steel tube on properties of concrete core, coefficient β_c has been suggested by Tomii and Sakino [1979] according to experimental studies. This coefficient depends on width to thickness (D/t) ratio, where D is equal to largest dimension of rectangular section and t is the thickness of steel tube. The corresponding equations are presented in below:

$$\beta_c = \begin{cases} 1 & \frac{D}{t} \le 24 \\ 1.5 - \frac{1}{48}.\frac{D}{t} & 24 < \frac{D}{t} \le 48 \\ 0.5 & \frac{D}{t} > 48 \end{cases} \tag{24}$$

As relationships show, the confinement effect of steel tube decreases as width to thickness ratio of cross section increases.

Circular Cross Sections

In circular sections, steel tube not only increases ductility of concrete core but also increases ultimate strength of concrete. The amount of increase in compressive strength depends on steel tube width to thickness ratio and yield stress of steel. Additional compressive strength due to confinement effect of steel tube can be expressed as below [Fujimoto et al. 2004]:

$$f_{cc} = \gamma_c f_c + f_r \tag{25}$$

$$f_r = \frac{-1.558 F_y t}{D - 2t} \tag{26}$$

where F_y is the nominal yield stress of steel.

Steel

The innovative aspects of this paper are in the local buckling modeling of steel tube. Local buckling has the most important role in ultimate strength of CFST beam-column and its post-peak behavior. After local buckling occurrence in steel tube, compressive strength of steel decreases sharply and finally arrives to constant amount. This constant amount depends on width to thickness ratio of steel tube and yield strain of steel.

Because of concrete core existence in CFST columns, steel tube cannot buckle inward; so, local buckling delays in comparison to hollow steel tube. When concrete core is under axial compressive load, concrete tends to expand due to Poisson's effect; however this expansion is resisted by steel tube. Hence, circumferential stress is created in steel and leads to biaxial stresses which increase steel yield stress in tension and decrease in compression according to Von Mises yield criterion (Sakino et al) [17]. Figure3 shows stress-strain curve for steel material in CFST beam columns. This behavior can be modeled by bilinear material in OpenSees [14] finite element code.

The corresponding parameters in steel stress-strain curve are defined as below:

$$F_{yt} = 1.1 F_y \tag{26}$$

$$F_{yc} = \beta_s F_y \tag{27}$$

where F_{yt} is the steel yield stress in tension, F_{yt} is the steel yield stress in compression, and β_s is the reduction factor of steel yield stress in compression due to biaxial stress state and local buckling of steel tube.β_s is defined as below:

$$\beta_s = \begin{cases} 0.9 & \alpha_s \le 1.75 \\ 0.9875 - \dfrac{\alpha_s}{20} & 1.75 < \alpha_s \le 2.55 \\ \dfrac{1.0}{0.527 + 0.0976\alpha_s^2} & \alpha_s > 2.55 \end{cases} \tag{28}$$

where α_s is a parameter defined to consider effects of width to thickness ratio and steel yield strain in local buckling of steel tube, as presented in Equation (29).

$$\alpha_s = \frac{D}{t}\sqrt{\frac{F_y}{E_s}} \tag{29}$$

$$\alpha_h = \frac{F_{su} - F_y}{\varepsilon_y - \varepsilon_{su}} \tag{30}$$

$$\alpha_c = -0.2 \tag{31}$$

Equations (30) and (31) present behavior of steel after yielding and local buckling, respectively. In these equations, α_h is the strain hardening coefficient, α_c is the softening coefficient, F_{su} is the ultimate stress of steel, and ε_y and ε_{su} are yield strain and ultimate strain of steel, respectively.

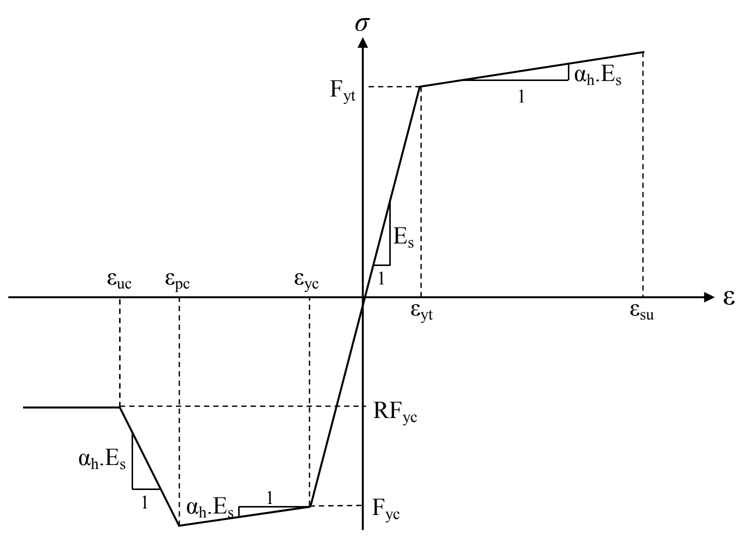

Figure 3 Stress-strain curve for steel material in CFST beam-column.

$$\varepsilon_{su} = 1.2641 - 0.173 Log(F_y) \tag{32}$$

In the suggested procedure for modeling of steel bBozoehavior, initial strain of buckling and post buckling behavior of steel are determined by Equations (33) and (34).

$$\varepsilon_{pc} = \begin{cases} \dfrac{\varepsilon_y}{0.846 - 1.2101\alpha_s + 0.2076\alpha_s^2} & \alpha_s \le 2.55 \\ \beta_s \varepsilon_y & \alpha_s > 2.55 \end{cases} \tag{33}$$

$$R = 1.2 - 0.2\alpha_s > 0 \tag{34}$$

VERIFICATION

It is not acceptable to use an analytical model without verification. Experimental results should be used to ensure proper functioning of technique. As mentioned, behavior of CFST beam-columns depends on several parameters such as concrete compressive strength, steel yield strength, section geometry, steel tube width to thickness ratio, etc. Therefore, several different sets of specimens from experimental studies of Tomii and Sakino [1979] and Fujimoto et al. [2004] are considered for verification. Also to predict performance of modeled beam-column elements in frames and under both static pushover and cyclic loads, experimental results from Han et al. [2008] were used.

Beam- Column Element Verification

In this section, the moment-curvature diagrams are comparison criteria for verification. These diagrams can show a lot of useful information such as ultimate moment capacity, initial bending stiffness, post-peak behavior and bending ductility.

Rectangular Cross Sections

For rectangular sections, comparisons were done between analytical models and corresponding experimental studies presented by Tomii and Sakino [1979]. They conducted three series of experiments with various *D*/*t* ratios from 23.5 to 45.5, concrete compressive strength from 22.4 to 45.9 MPa, and steel yield stress from 197 to 345 MPa under different levels of axial load. Material specifications and axial loads applied on each specimen are given in Table 1 [Tomii and Sakino 1979]. As diagrams show, proposed procedure can predict initial bending stiffness, ultimate resistant moment, and post peak behavior of rectangular CFST beam-columns with accuracy. Table 2 shows comparison between ultimate resistant moment obtained from experimental and analytical studies with suggested procedure. Figure 4 compares the analytical moment-curvature with experimental results some specimens.

Table 1 The material specifications and axial loads applied on rectangular specimens.

Specimen	B×D (mm)	*t* (mm)	*D*/*t*	f_y (MPa)	f_{su} (MPa)	f'_c (MPa)	P_n (kN)
I-1	100 × 100	2.29	43.67	197	352	45.9	77.7
I-2	100 × 100	2.29	43.67	197	352	45.9	160.4
I-3	100 × 100	2.29	43.67	197	352	45.9	194.3
I-6	100 × 100	2.29	43.67	197	352	45.9	335.8
II-1	100 × 100	2.27	44.05	310	397	25.9	46.8
II-2	100 × 100	2.20	45.45	345	417	25.9	93.7
II-3	100 × 100	2.20	45.45	345	417	25.9	140.5
II-4	100 × 100	2.22	45.05	294	385	25.9	187.3
III-0	100 × 100	2.98	33.56	294	408	24.7	0.0
III-1	100 × 100	2.98	33.56	294	408	24.7	51.8
III-3	100 × 100	2.99	33.44	293	411	24.7	155.4
III-4	100 × 100	2.99	33.44	293	411	24.7	207.3
IV-0	100 × 100	4.25	23.53	289	399	22.4	0.0
IV-1	100 × 100	4.25	23.53	289	399	22.4	62.8
IV-2	100 × 100	4.25	23.53	289	399	22.4	125.5
IV-3	100 × 100	4.25	23.53	290	399	22.4	188.3

Table 2 Ultimate resistant moment comparison for rectangular CFST columns.

Specimen	M_{max} Exp. (kN.m)	M_{max} Ana. (kN.m)	Difference (%)
I-1	10.85	11.01	1.47
I-2	11.38	11.07	2.70
I-3	11.45	11.08	3.24
I-6	10.26	10.53	2.63
II-1	12.35	12.49	1.13
II-2	13.22	13.25	0.23
II-3	13.00	13.21	1.62
II-4	12.15	11.70	3.70
III-0	14.87	14.88	0.07
III-1	15.90	14.95	5.97
III-3	14.60	14.86	1.78
III-4	13.55	14.81	9.30
IV-0	19.55	19.55	0.00
IV-1	20.40	19.67	3.58
IV-2	20.80	19.68	5.38
IV-3	20.10	19.70	1.99
Average=2.8			

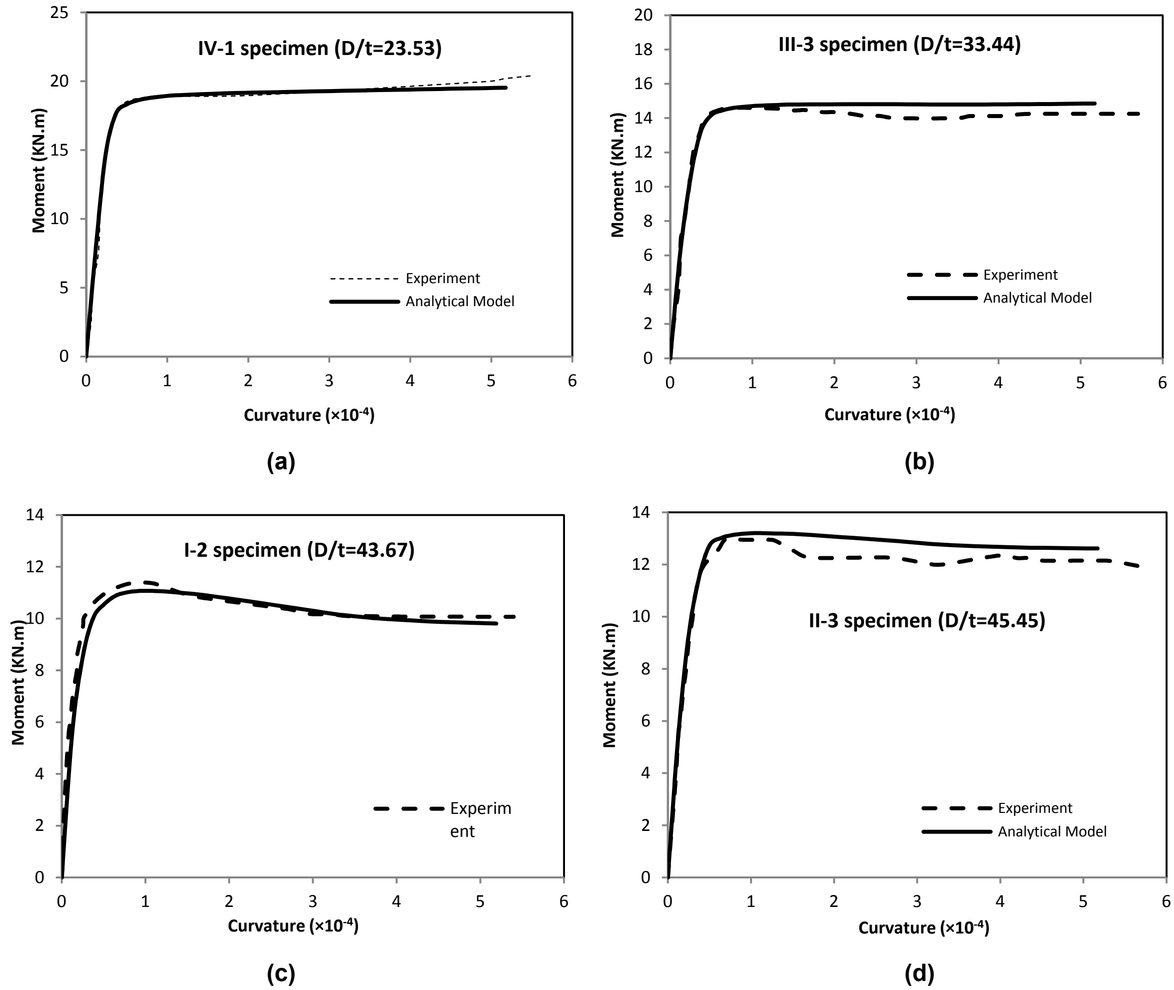

Figure 4 Moment-curvature comparison diagrams for rectangular CFST columns.

Circular Cross Sections

For circular cross sections, comparisons were made between analytical model and corresponding experimental studies presented by Fujimoto et al. [2004], who conducted several sets of experiments on circular sections with various *D*/*t* from 17 to 152, concrete compressive strength from 25.4 to 85.1 MPa and steel yield stress from 283 to 834 MPa under different axial load levels. The material specifications and axial load applied on each specimen are given in Table 3 [2004], which demonstrates that the difference between material and geometric properties of circular CFST specimens is considerable. Figure 5 compares analytical moment-curvature diagrams with experimental results.

Table 3 The material specification and axial load applied on circular specimens.

Specimen	*D* (mm)	*t* (mm)	*D*/*t*	f_y (MPa)	f_{su} (MPa)	f'_c (MPa)	P_n (kN)
EC4-A-4-035	150	2.96	50.7	283	408	39.9	359
EC4-C-8-045	300	2.96	101.4	283	408	77.6	2720
EC6-A-4-02	122	4.54	26.9	579	646	39.9	273
EC6-D-4-03	360	4.54	79.3	579	646	39.9	2050

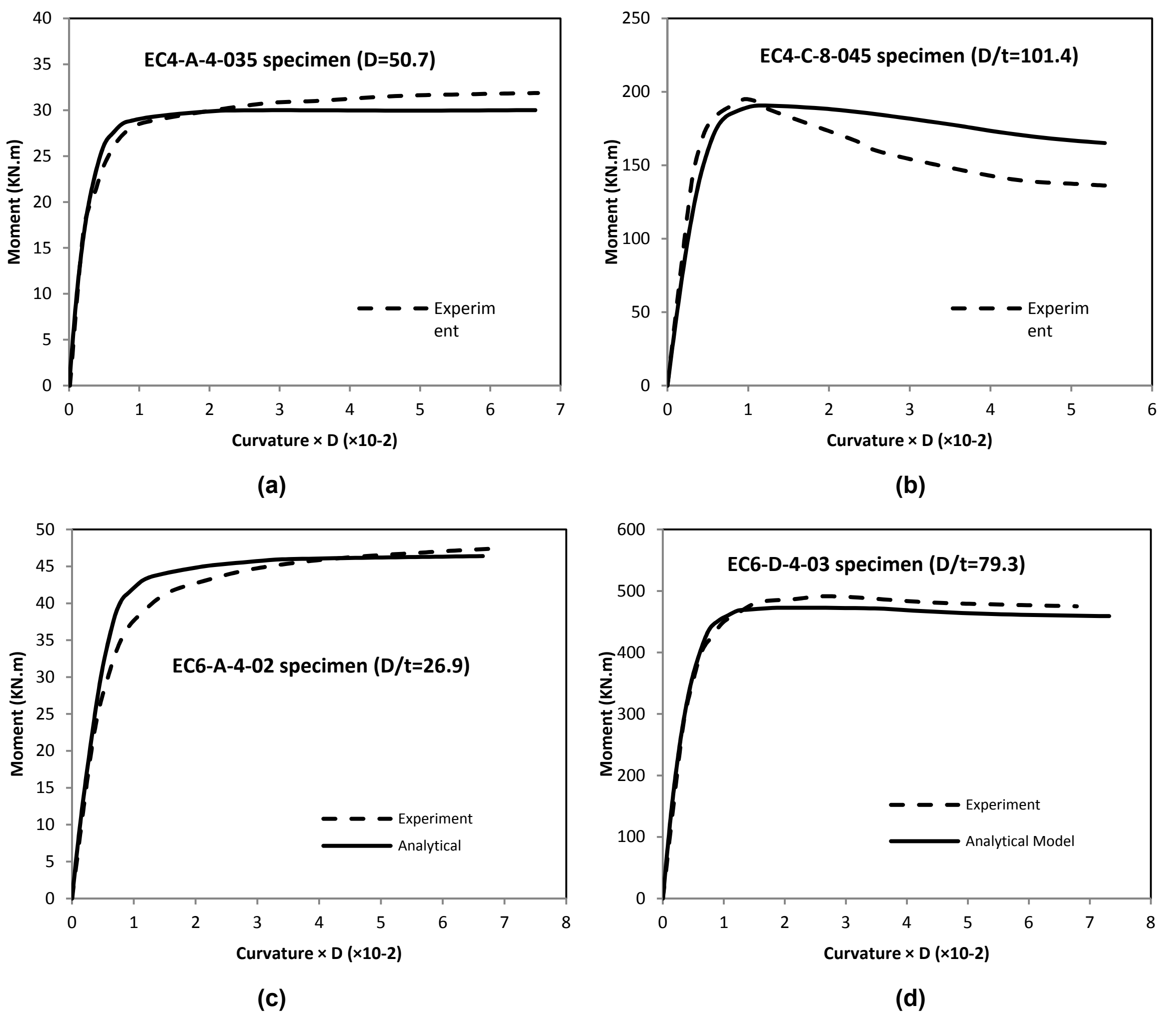

Figure 5 Moment-curvature comparison diagrams for circular CFST columns.

The diagrams show that proposed procedure predicts circular CFST columns behavior with good accuracy in initial bending stiffness and ultimate resistant moment of beam-column element; however accuracy slightly decreases in prediction of post peak behavior for specimens with high diameter to thickness ratios. Table 4 shows comparison between ultimate resistant moment obtained from experimental and analytical studies for all specimens.

Table.4 Ultimate resistant moment comparison for circular CFST columns.

Specimen	M_{max} Exp. (kNm)	M_{max} Ana. (kNm)	Difference (%)
EC4-A-4-035	31.90	30.90	3.13
EC4-C-8-045	195.06	190.71	2.23
EC6-A-4-02	47.42	46.39	2.17
EC6-D-4-03	491.42	472.80	3.79
Average=2.83			

Static Pushover and cyclic Analysis of Frame with CFST Column

To ensure proper performance of proposed modelling procedure for frames with CFST columns and also for columns under cyclic loads, experimental study of Han et al. [2008] is considered. Corresponding analytical model, modeled in OpenSEES finite element code and thelateral loadsin accordance to ATC-24 [1992] are applied. Results from both studies compared with each other. The understudy frame is a one-story frame with one span, columns are rectangular CFST and connected with ordinary I-shaped steel beam to each other. The story hight of frame and the span length are equal to 1.45 and 2.5 m, respectively. 375 KN concentrated load imposed on top of each columns where beam is load free. Table5 shows characteristics of beam and columns used in frame. Figure 6 shows comparison between analytical and experimental results for both static pushover and dynamic analysis.

As diagrams show, analytical results are very close to experimental data, which indicates the capability of proposed procedure for both CFST columns and also composite frames. In figure6 analytical displacement presented against lateral forces are in good aggrementwith experimental results and predicts lateral stiffness as good as bending stiffness. This demonstrates that proposed procedure has good accuracy under dynamic loads and can be used for seismic studies.

Table 5 Characteristics of columns and beam in studied frame for cyclic and pushover verification.

Specimen	Column				Beam				
	B (mm)	D (mm)	t (mm)	F_y (MPa)	h (mm)	b_f (mm)	t_w (mm)	t_f (mm)	F_y (MPa)
SF-22	140	140	4	361	180	80	4.34	4.34	361.6

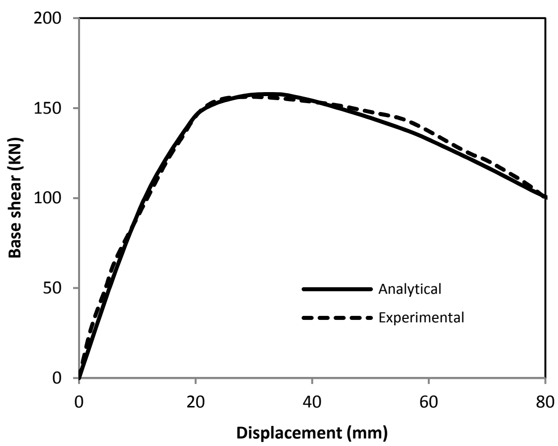

(a)

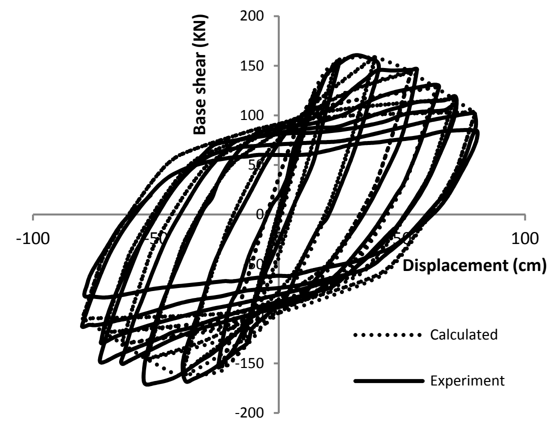

(b)

Figure 6 Comparison of analytical and experimental results for frames with CFST columns under (a) static push over; and (b) cyclic loading.

CONCLUSIONS

In this paper displacement- based analysis (DBA) technique for rectangular and circular concrete filled steel tubular (CFST) beam-columns is presented. The proposed procedure is based on fiber element formulations and can be used for both nonlinear static and dynamic studies. The innovative aspects of this paper are in the local buckling modeling of steel tube and its effects on strength and ductility performance of CFST beam-columns. In the local buckling modeling of steel tube several variables such as cross section geometry, width to thickness ratio, and strength of materials are considered. Comparisons between experimental and analytical results show that suggested formulation for steel stress-stress diagram can predict behavior of steel tube in CFST columns with good accuracy.

The proposed DBA method covers both ordinary and high strength materials and can be used for short and medium CFST beam-columns in wide range of width to thickness ratio. Due to considering local buckling in the procedure, this method can be used for CFST beam-columns with non-impact steels.

Comparisons between analytical and experimental results show that proposed DBA procedure can model ductility, strength, bending and lateral stiffness, post peak and dynamic behavior of CFST beam-columns with accuracy under several loading types such as lateral, cyclic, axial load and uniaxial bending moment.

ACKNOWLEDGMENTS

The partial supports of center of excellence in structures and earthquake engineering at Sharif University of technology is greatly appreciated.

REFERENCES

ATC (1992). *Guidelines for Cyclic Seismic Testing of Components of Steel Structures, ATC 24*, Applied Technology Council, Redwood City, CA.

Bridge R.Q., O'Shea M.D. (1998). Behavior of thin-walled steel box sections with or without internal restraint, *J. Constructional Steel Res.,* 47(1–2): 73–91.

Chen S.F., Teng J.G., Chan S.L. (2001). Design of biaxially loaded short composite columns of arbitrary section, ASCE, *J. Struct. Eng*., 127(6): 678–85.

Fujimoto T., Mukai A., Nishiyama I. (2004). Behavior of eccentrically loaded concrete-filled steel tubular columns, ASCE, *J. Struct. Eng.,* 130(2): 203–212

Hajjar J.F., Gourley B.C. (1996). Representation of concrete-filled steel tube cross-section strength, ASCE, *J. Struct. Eng*.,122(11): 1327–1336.

Han L.-H., Wang W.-D., Zhao X.-L. (2008). Behavior of steel beam to concrete-filled SHS column frames: Finite element model and verifications, *Eng. Structures*, 30(6): 1647–1658.

Hu H.T., Huang C.S., Chen Z.L. (2005). Finite element analysis of CFT columns subjected to an axial compressive force and bending moment in combination, *J. Constructional Steel Res.,* 61(12): 1692–1712.

Lakshmi B, Shanmugam N.E. (2002). Nonlinear analysis of in-filled steel–concrete composite columns ASCE, *J. Struct. Eng*., 2002;128(7): 922–933.

Liang Q.Q. (2009). Performance-based analysis of concrete-filled steel tubular beam-columns, Part I: Theory and algorithms, *J. Constructional Steel Res.,* 65(2): 363–372.

Mander J.B., Priestly M.N.J., Park R. (1988). Theoretical stress-strain model for confined concrete, ASCE, *J. Struct. Eng*., 114(8): 1804–1826.

McKenna F, Fenves G.L., Scott M.H. (2000). *Open System for Earthquake Engineering Simulation*, Pacific Earthquake Engineering Research Center, University of California, Berkeley, CA, available at: http://opensees.berkeley.edu.

Munoz P.R., Hsu C.T.T. (1997). Behavior of biaxially loaded concrete-encased composite columns, ASCE, *J. Struct. Eng*., 123(9): 1163–1171.

Sakino K., Ninakawa T., Nakahara H., Morino S. (1998). Experimental studies and design recommendations on concrete filled steel tubular columns, *Proceedings, U.S.–Japan Cooperative Earthquake Research Program. Structural Engineers World Congress*, N. K. Srivastava (ed.), Paper No. T169-3.

Schneider S.P. (1998). Axially loaded concrete-filled steel tubes, ASCE, *J. Struct. Eng.,* 124(10): 1125–1138.

Spacone E., Filippou F., Taucer F. (1996). Fibre beam–column model for non-linear analysis of R/C frames. Part 1: Formulation, *Earthq. Eng. Struct. Dyn.,* **25**(7): 711–725.

Tomii M, Sakino K. (1979). Experimental studies on the ultimate moment of concrete filled square steel tubular beam–columns, *Trans. Arch. Inst. Japan*, 275: 55–65.

Tomii M., Sakino K. (1979). Elastic-plastic behavior of concrete filled square steel tubular beam–columns, *Trans. Arch. Inst. Japan*, 280: 111–20.

Valipour H.R., Foster S.J. (2010). Nonlinear static and cyclic analysis of concrete-filled steel columns, *J. Constructional Steel Res.,* 2010; 66(6): 793–802.

Varma A.H., Ricles J.M., Sause R., Lu LW. (2002). Seismic behavior and modeling of high strength composite concrete-filled steel tube (CFT) beam–columns, *J. Constructional Steel Res.,* 58: 725–758.

ON RECENT ACHIEVEMENTS AND ACTIVITIES OF BUILDING, HOUSING, AND RESEARCH CENTER (BHRC)

Fereydoon Sinaeian[1] and Abdollah Dehhaghi[2]

ABSTRACT

This article highlights the major activities performed under the authority of Road, Housing and Urban Development Research Center, abbreviated as BHRC. The abbreviation comes from the previous title of the center- which is affiliated to the Ministry of Road and Urban Development. Firstly, the history and background declaration of BHRC is stated along with the mission statement which is then followed by the BHRC organizational structure. Secondly, various departments including their major achievements are briefly explained.

Keywords: *different departments mission statement, organizational structure*

HISTORY AND BACKGROUND DECLARATION

The idea of establishing the Building Housing and Research Center (BHRC) was formed in 1971 in the framework of United Nations Development Program “UNDP.". The duty was transferred to BHRC based on an agreement between "Ministry of Housing and Urban Development" and "UNDP." The proposed statute of BHRC was approved by the parliament in 1977 and BHRC commenced its research activities as one of the affiliated organizations to the Ministry of Housing and Urban Development, thereafter.

The BHRC as a unique Iranian research organization in the field of building and housing, it is responsible for studying and research on relevant issues associated with construction activities in the Country. Recently, as a result of the merger of the two ministries of Housing and Urban Development and Road and Transportation, some more responsibilities in the field of Roads and related industries have been added to the responsibilities of BHRC.

Organizational Structure

The BHRC is comprised of three vice-presidencies and certain departments functioning under the authorities of these vice-presidencies. See Figure 1 for the organizational chart of the BHRC.

[1] Professor, Building and Housing Research Center, Sheikh Fazlollah Noori Highway, Tehran, Islamic Republic of Iran; email: Sinaiean@bhrc.ac.ir.

[2] Professor, Building and Housing Research Center, Sheikh Fazlollah Noori Highway, Tehran, Islamic Republic of Iran; email: Dehhaghi@bhrc.ac.ir

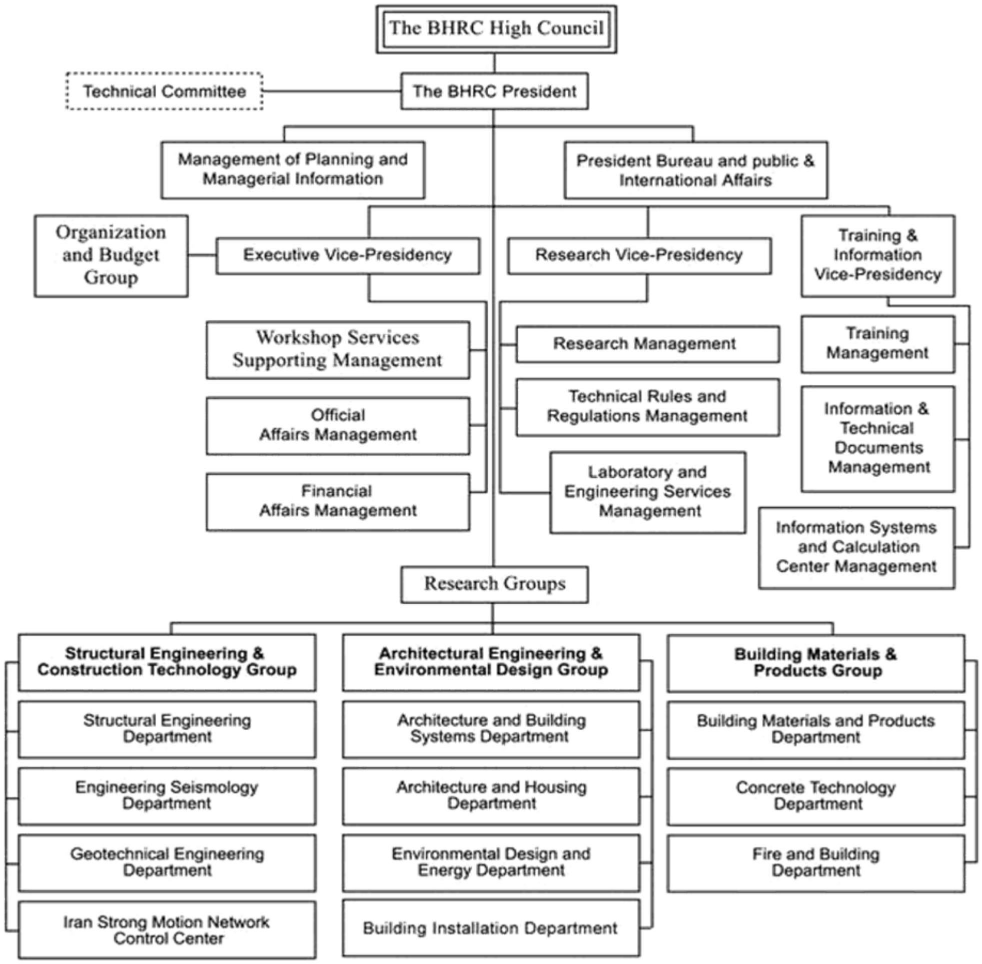

Figure 1 Organizational Chart of the BHRC.

Mission Statement

BHRC missions can be mainly classified as the following:

- Provision and publication of codes of practices and their application instructions
- Centralized provision and execution of research programs on building and housing by innovation of new methods and techniques
- Issuance of technical certificate for building products and systems
- Provision of technical guidance in construction of housing in compliance with national requirements
- Climatic and local considerations and also by consideration the need for industrialized construction within the country

BHRC High Council

In accordance with articles of the statute, BHRC performs its duties under supervision of a High Council and BHRC President who is appointed by the Minister of Road and Urban Development (after approval of the Council of Minister). This Council consists of:

- Minister of Road and Urban Development
- Minister of Industries and Mines;
- Minister of Finance and Economic Affairs
- Minister of Labor and Social Affairs
- President of Iran's Planning and Management Organization
- Minister of Agricultural Jihad
- Minister of Health Care, and Medical Training

BHRC Technical Committee

It is responsible for presenting comments on BHRC policy as well as planning and performing technical and scientific research activities. The major activity fields are as the following:

- Studying and Research on relevant problems in building such as: materials, environmental design engineering, and construction activities by using physical and laboratory equipment
- Evaluating traditional building materials from qualitative and quantitative points of view to recognize their physical and mechanical properties
- Studying and research on seismic resistant design of buildings and other destructive factors
- Development of prefabricated and industrialized building techniques
- Development of prefabricated and industrialized building techniques
- Studying construction management methods
- Evaluating local condition of Iran’s different regions
- Providing standards, criteria, and codes of practice on building and housing
- Publishing books, reports, and technical journals on building and housing
- Holding training course, seminar, and conferences in cooperation with related organization
- Implementation of technical tests and presenting research services to the building sector
- Studying and research on seismic resistance design of building s and other destructive factors
- Development of prefabricated and industrialized building techniques

- Studying construction management methods
- Evaluating local condition of Iran's different regions
- Providing standards, criteria, and codes of practice on building and housing
- Publishing books, reports, and technical journals on building and housing
- Holding training course, seminar, and conferences in cooperation with related organization
- Implementation of technical tests and presenting research services to the building sector

Educational Functions

BHRC is also actively involved in educating and retraining engineers in the field of Civil engineering:

- Holding short courses and workshops for engineers and professions
- Holding various conferences and seminars on the latest research findings
- Holding exhibitions
- Active relationship with national and international research centers, universities and other related organizations in Iran

Quality Assessment and Issuing Certificates

Control and assessment of the quality of building materials is one of the main functions of BHRC. These objectives are carried out at the relevant departments. The codes required for quality assessment of building products and systems is prepared by compiling various regulations such as codes of practice, standards and design criteria in the cooperation with the National Standard Organization of Iran. Providing related standards on building materials and tests for quality control, preparing and submitting standards to the concerned authorities for approval, and certification of technical agreements in the fields of building products and systems are the main objectives in this regard. One of the main codes in this regard have been compiled under a book titled as Iran codes of practice [Standard 2800], which is under the forth revision.

Research Departments

- Architecture
- Acoustic
- Building Installations (Mechanical and Electrical)
- Building Materials and Products
- Concrete Technology
- Engineering Seismology and Hazard Reduction
- Environmental design and Energy

- Fire Technology
- Geotechnical Engineering
- Housing and Building Systems Department
- Iran Strong Motion Network
- Socio-economical Researches
- Structural Engineering
- There are seven more departments under construction, because of the recent merger of the two Ministries

Recent Major Achievements of Department of Architecture, Housing and Building Systems

- Designing Pilot projects of a Mosque using Colbeh Nik System
- Design of Mosque based on Islamic and Iranian architecture in warm and wet climate with modular technology of Nik system
- The first modular & Ergonomic steel cottage system in Iran for rural buildings
- Application of Construction Technology for Desirable Housing
- Providing a model for green spaces application in Iran
- Application Guide of "Design Criteria for Handicapped"
- National Project of Nik System; Nik System 1 to Nik System 5

Nik System

In order to meet the need for providing housing and the accumulated need in this section, it was perceived by the BHRC in 2009 as an utmost importance to construct new buildings with a new method which is qualified to the standards of National Building Codes and has a reasonable price, namely, industrialization of building construction. Thus according to the previous studies and experiences in the center regarding the modular buildings, the center launched its first prototype. The system is totally designed by Iranian engineers. It is modular and ergonomic. It can easily be assembled and disassembled. The system can be applied for a variety of purposes such as temporary settlement, hospitals and clinics, military bases, stocks and so on. The system is prefabricated and can be manufactured industrially and can be reused several times. The parts can be stored and used after a disaster. In addition to rapid assembly, the ease of assembly, rescannable price and satisfaction of inhabitants have been taken into account. As the parts have been manufactured, material waste is considerably reduced.

Figure 2 An overview of the Nik System design process.

Recent Major Achievements of Acoustics Department

Acoustics Department and its laboratories were established in 1975 to accomplish one of the principle responsibilities of BHRC titled "Evaluation of Acoustics performance of building materials and building elements." The principle object of this department is preparing and giving information about building acoustics to reduce noise up to permissible limits and to provide reasonable listening conditions in inner spaces. Investigation on acoustical behavior of traditional non loading double leaves partitions with thermal insulation given in part 19 of national building code of Iran and also some of new partition systems in buildings.

In the most cases it is required to establish proper thermal and acoustical conditions in different parts of buildings simultaneously. Although the use of various kinds of thermal insulation in buildings creates proper thermal conditions, it may have no acoustical effectiveness.

So investigation on these walls from this mentioned point of view is very important. The information coming from this project can be used in applying the part 18 (Insulation and control of noise), 19 (Saving the energy) and 3 (Protection of buildings against fire) of national building code.

Figure 3 The Laboratory of Acoustics.

Providing Methods for Measurement of Sound Insulation and Rating of that in Buildings and of the Building Elements

In the acoustical codes, there are different regulations for the sound insulation of buildings and building elements, in order to providing acoustical comfort for the residents of dwellings. To control these regulations, it is necessary to standardize the method of acoustical measurement. So, the architects, designers and everyone who is involved in the building construction can use these values with more insurance. In addition, it is necessary to give acoustical requirements for construction of laboratories. So it will be possible to made sound insulation measurements. The result of this project is providing 17 national acoustic standards.

The Revision of Iranian National Building Code, Part 18: Insulation and Control of Noise

The role of this code is improving the sound insulation in different types of buildings and providing a comfortable acoustical environment. For preparing this code, documents and regulations from different countries and national regulations of Iran have been studied. Afterwards the previous code and its points of view were discussed in the primary committee, and then the subjects of each part were prepared, discussed and confirmed in technical committee.

This code includes two main parts and four annexes as a guideline. The first part describes the scope and acoustical definitions which are used in the second part. The second part is consisting of the acoustical regulations for different types of buildings. These include residential, educational, cultural, official and commercial buildings, hotels, hospitals and entertainment, sport and transportation centers.

Recent Major Achievements of Building Materials and Products

Conducting studies and researches in different fields of related material properties and improving their quality are among the major objectives of this department. With regard to the present approach to light weight buildings materials and systems, this Department has focused its efforts on carrying out research on lightweight building materials using modifying additives materials.

Figure 4 Building Materials and Products Laboratory.

Research Themes

- Conducting research on existing building materials by studying mechanical, physical and chemical properties
- Quantitative and qualitative studies on traditional building materials providing recommendations and guidelines
- Studying mineral, chemical, agricultural materials and industrial waste in order to produce new building materials or improving the existing ones
- Conducting research on the durability of building materials and increasing their service life
- Conducting research on light weight building materials in order to improve their quality; and

- Preparation of standards, criteria, regulations, technical instructions and codes of practice related to building materials in collaboration with Iranian Standard and Industrial Research Institute and other relevant authorities .
- Studying the mechanical characteristics of External thermal insulation composite systems (ETICS); The main objective of this project is investigation on mechanical properties of External thermal insulating composite system and submitting applicable guidelines for selection and application of them.
- Studying the Insulated Brick Cladding Systems; The main objective of this project is investigation on properties of Insulated Brick Cladding Systems and submitting applicable guidelines for their application.
- Studying various kinds of gypsum boards, preparation of related standards for quality controls and required codes of practice. The main application of gypsum plasterboards is as partition in buildings. The main advantages of these boards are high speed of construction, avoiding loss on building materials and lightweight.

Recent Major Achievements of Concrete Technology

- Propagation model and predict the service life of conventional concrete and concrete containing silica fume exposed chloride exposure in the Persian Gulf
- Concrete National Mix Design Method
- A guideline for national mix-design and its software
- Long-term durability of normal and pozzolanic concrete in condition of Persian Gulf of environmental (Phase II - Evaluation and assessment of results up to age 5 years)
- Technology of lightweight concrete semi-structural concrete
- Quality assessment the pozzolans used in five cement factory and proposing the guidelines
- The production and application of hybrid polymer fibers with glass fibers to replace asbestos fiber cement sheet manufacturing process Hatschek
- Development regulations in the construction of concrete slabs
- Characterization and application of three types of natural pozzolans mixed with polymer fibers as alternative asbestos cement boards
- Providing resources zoning in central Alborz pozzolan for cement replacement in blended cements
- Investigating the effects of different type of nano-particles on concrete properties
- Non-asbestos cement boards mix design optimization methods for production-scale plant Hchk
- Electrochemical assessment of corrosion of steel embedded in normal and silica-fume concrete

Recent Major Achievements of Engineering Seismology

- To provide comprehensive seismic risk reduction program
- Ahar-Varzeghan earthquakes report
- Information layer system of rapid response of Tehran city
- Regional Sorting for Seismic Retrofitting due to Seismic Hazard Analysis in Rural zone of Chahar Mahal va Bakhtiari
- Scenario project of Gorgan earthquake
- Providing information on seismology engineering and earthquake disaster management in Mazandaran
- Seismotectonic studies and estimation of earthquake hazard zonation in Tehran
- Seismotectonic studies and estimation of earthquake hazard zonation in Semnan
- Seismotectonic studies and Seismic Zonation in Mazandaran
- Preparing the National Catalogue of earthquakes in Iran
- Preparation of seismic zonation hazard map of Iran [Standard 2800 Annex]

Recent Major Achievements of Environmental Design and Energy

Since the beginning of its establishment, this department has performed many activities in energy efficiency solutions, in energy consumption, in building envelopes, climatic design and adjusting environmental conditions. This department attempts with selection of applied research projects suggest solutions for improving human comfort conditions in buildings and also the optimization methods in energy consumption.

- Revision and compilation of code 19 (Building regulation-Energy efficiency in buildings)
- Energy auditing of existing buildings and proposal formulation of solutions for optimal energy saving
- Guidelines for improving the architectural design of mass housing in Iran Providing rules and regulations of thermal insulation in buildings and constructing prototypes
- Iran climatic zonation-housing and residential areas
- Climatic microzonation of Iran climate from housing and residential areas standpoints
- Regulation and code revisions of urban development and architecture for physically challenged people
- Principles of green areas designing in residential areas
- Compiling national standards in insulated windows, profiles and new windows (UPVC, aluminum) the measurement methods of thermal and lighting shell of buildings
- Descriptive zonation of flood in Iran and designing the related software

- Guidelines on optimal architectural plans for mass housing in Iran
- Equipping the specialized laboratory for determining thermal performance of shells of building envelopes
- Equipping the specialized laboratory for assessment and evaluation of air-tightening and water-tightening in building envelope shells

Facilities and Equipment

- Apparatus used for measuring the amount of weather tightening and air tightening of opening windows
- Zeno test apparatus used for artificial weathering on UPVC profiles or composite sandwich panels
- Apparatus used for testing the durability and stability of sealed insulated glass units consists of frost point, high humid chamber, accelerated weather cycle chamber
- The strength measurement of UPVC profile against falling mass in low heat
- Universal traction and compression apparatus to test compress, welding test,
- Laboratory equipment and field (portable) for measuring heat, humidity, velocity and air pressure, Debbi, …
- Laboratory equipment and field (portable) for measuring electrical values and optical characteristics
- Apparatus used for testing the durability and stability of sealed insulated glass units consists of frost point, high humid chamber, accelerated weather cycle chamber

Research Activities

- Investigation of the effective parameters of textiles in flexural performance of TRC (textile reinforced concrete) composites used in exterior walls
- Investigation and identification of UPVC profile problems applied in door and windows
- Compilation of 2 standards for outdoor weathering test of plastics
- Preparation of the Guide for the Installation of PVC-U Building Windows
- Energy Performance of IGU Systems with Coated Glass in different Climates of Iran

Recent Major Achievements of Fire Technology

This department is responsible for improvement of safety of buildings in case of fire and reduction of loss of lives and properties due to fire in buildings. This is followed through applied research projects, writing of regulations, standards and guidelines and providing applied solutions to building industry.

- Investigation on fire properties of 10 building materials with Cone Calorimeter test method and simulation of fire risk with some fire models

- Development of a classification method of fire behavior of finishes with bench scale test results
- Installation and start-up of 1 m^3 fire resistance furnace
- Installation, start-up and calibration of Single Burning Item test apparatus
- Investigation and evaluation of fire behavior and fire safety requirements of some new building systems
- Technical recommendations and criteria for application of Expanded Polystyrene in buildings
- Properties and application of Polyurethane sandwich panels and thermal insulation in buildings and related fire safety recommendations
- Writing standard test methods for fire resistance of building elements
- An investigation on fires after earthquakes in the world and providing a design guide to building's fire safety, considering the probable earthquake effects.
- Bench-scale Heat release test (Cone Calorimeter)
- Ignitability test
- ISO/IMO Non-combustibility test
- ISO/IMO flame spread test
- Single Burning Item test
- Classification of reaction to fire properties of building materials
- One meter cube fire resistance test
- Test of fire protective coatings

Recent Major Achievements of Geotechnical Engineering

Geotechnical Department conducts various researches and service projects in cooperation with qualified staff and consultants who are mainly members of the Academic Board and perform the following activities:

- Evaluation studies of the static behavior of materials and foundation
- Studies on the assessment of the dynamic behavior of materials and foundation
- Preparation and compilation of codes and standards related to geotechnical engineering
- Determination of improvement methods in geotechnics engineering
- Geotechnical earthquake engineering
- Numerical studies in geotechnics engineering
- Designing and manufacturing of relevant laboratory equipment

- Geotechnical application in marine and hydrology engineering
- National Scheme for Geotechnical Database Project
- Evaluation of frequency content on properties of gravelly soils

Seismic Microzonation of Cities in Semnan Province

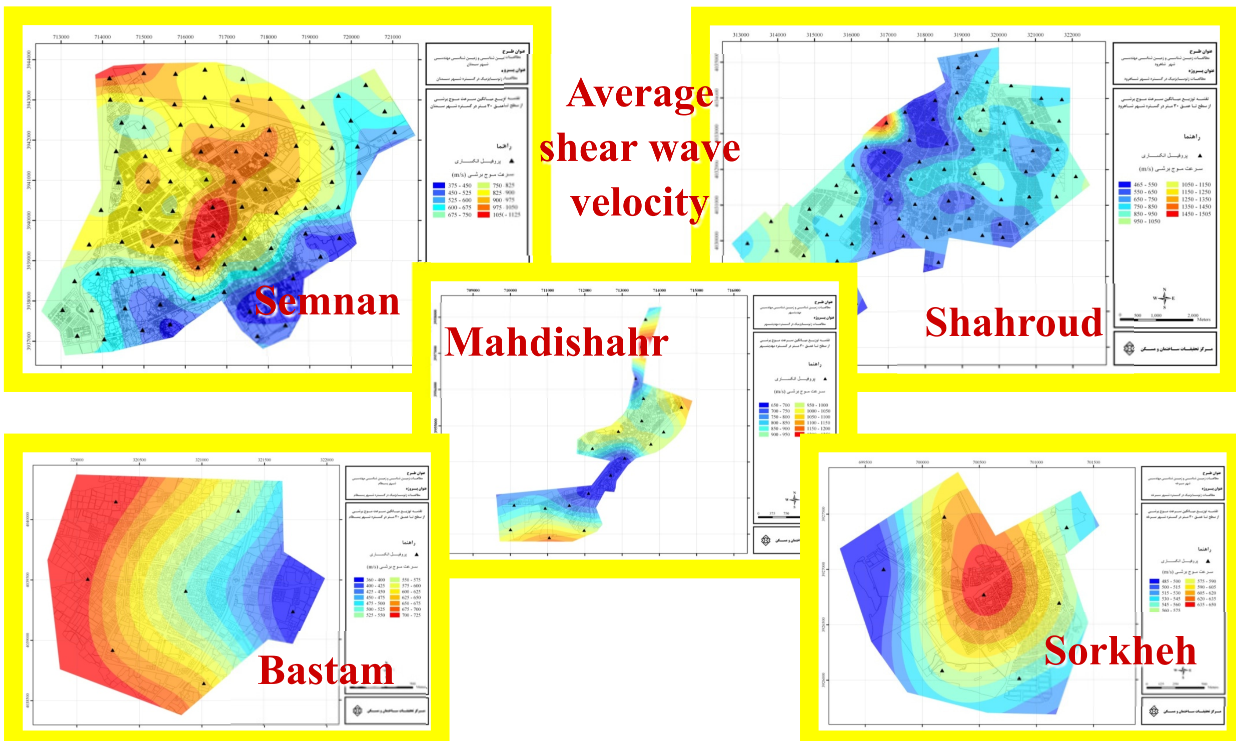

Figure 5 Seismic microzonation of cities in Semnan Province.

Iran Strong Motion Network (ISMN)

The Iran Strong-Motion Network (ISMN) was started in 1972, by installing the first accelerograph in Hamedan City, which raised to 270 in 1979. More than 1100 digital accelerographs were installed in the period of 1992–1993. This network consists of about 1160 instruments, at the time being. The majority of the instruments are located in urban complexes, taking into account the population density and the seismicity of the Iran territory. Local strong-motion arrays are also developed in some cities. More than 9000 three-component accelerograph has been recorded by this network.

The Most Important Activities and Projects of the ISMN

- Updating and maintenance of the network
- Producing a comprehensive accelerogram data bank
- Controlling and Processing of accelerograms

- Instrumentation of dams
- Geophysical Site investigation
- Earthquake and aftershock studies
- Maintenance and Calibration of Instruments
- Down hole Instrumentation (4 arrays in Tehran)
- Design and implementation a Rapid response system for Tehran city (Pilot)
- Publishing the monthly newsletter (Farsi) and Yearly Catalogue (English)
- Establishing of ISMN webpage on BHRC web site for early information of recorded data for domestic and international uses

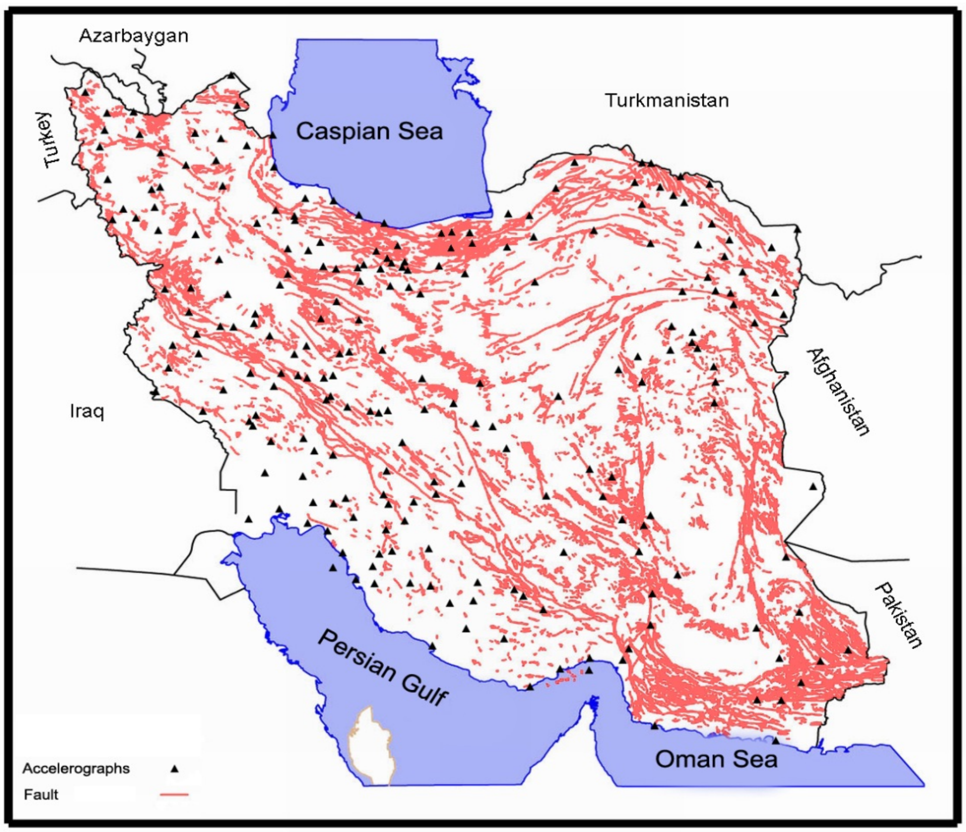

Figure 6 Iran Strong Motion Network in 1992.

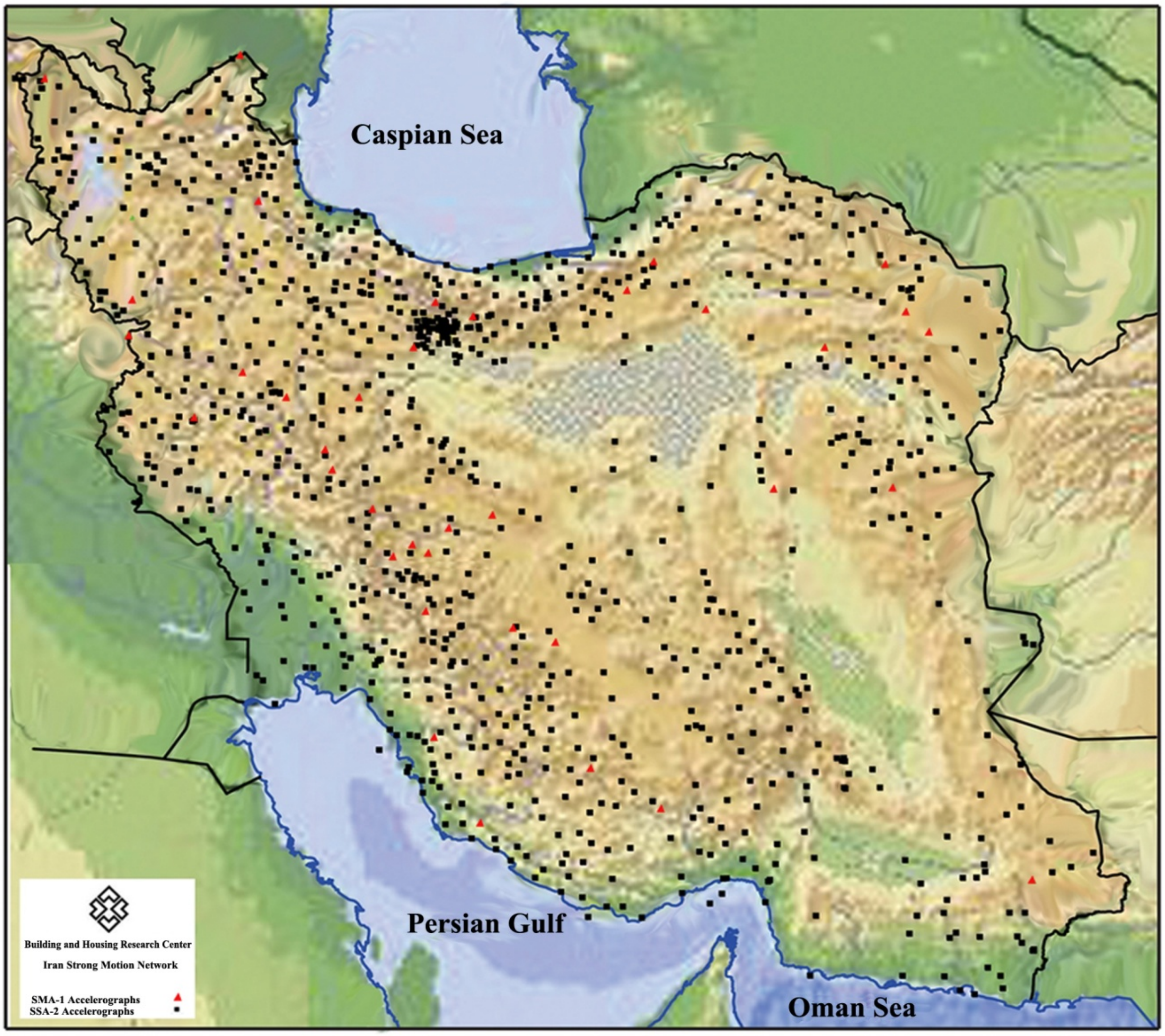

Figure 7 Iran Strong Motion Network in 2012.

Structural Engineering

As the very essence and backbone of any building, structure needs carefully applied experimental and analytical research, with regard to design, implementation and behavior standpoints. The Structural Engineering Department commenced its major activities in 1992. The main functions of the Structural Engineering Department may be defined as: Study and revision of different components of a building, impact of various forces on the structures, review and test of the structural designs, control and inspection of built structures, preparation and formulation of different codes, static and dynamic tests on various types of building structures on an appropriate scale, making new functional technologies widespread which are appropriate and compatible with conditions in the country, and cooperation with reputable university professors and scientific centers across the globe.

Laboratory Facilities and Equipment

This department is equipped with highly sophisticated laboratory instruments and advanced apparatus to carry out structural engineering research projects tests. Among the most important laboratory equipment in Structural Department are the strong floor and loading frames of different capacities

Technical Certificates

Technical Certificates Certify the performance and Quality of material, products and structural Systems meet the criteria defined in National Building Code topics and is an assured way for knowing the quality of different materials and building products. Structural Engineering Department is working on 12 technical certificate projects at the moment. In addition, 10 other projects are in their initial stages of qualification.

Current Research Activities

- Numerical and experimental study of seismic behavior of cold-formed shear walls
- Seismic performance investigation of rectangular reinforced concrete piers under combined loading including torsion and flexure
- Guide for design and construction of steel shear walls
- Investigating the seismic performance of steel shear walls in light steel frames
- Guidelines for embedded and semi- embedded reservoirs
- Review and finalizing guidelines for retrofitting urban buildings
- Comparison and evaluation of infill systems using industrial productions
- Providing guidelines for composite steel-concrete roofs
- Providing guidelines for design, fabrication, and construction of precast non-pre-stressed RC moment resisting frame systems
- Providing guidelines for design, and construction of prefab and semi prefab concrete slabs
- Investigation of the efficiency of MR dampers in promoting seismic behavior of structures
- Investigating weight reduction methods in new building systems

Some of Research Activities and Findings

- Shaking table setup and performing the first test
- A guide for design and construction of autoclaved concrete panels
- Providing a design procedure for an optimal building for industrial production
- In plane behavior of light-gauge cold-formed steel walls under cyclic loading using flat diagonal bracing fiber cement board and gypsum board sheets (experimental research)

- Studying the damage vulnerability level of the building of Housing Foundation of Islamic Revolution at Markaz , presenting rehabilitation design details and designing the top story.
- Instruction for application of FRP for strengthening and reinforcing structural elements.
- The performance evaluation of frictional damper usable in building
- Cold-formed light steel structures design and construction code
- Guidelines on design and construction of reinforced concrete building with insulating concrete forms
- Building regulations for concrete blocks in residential buildings
- Instructions for construction of reinforced concrete cast in-situ system with integrated wall form
- Instructions for construction of semi-precast reinforced concrete building structures composed of wall and ceiling panels and in-situ concrete
- Instructions for seismic evaluation and rehabilitation of conventional existing concrete buildings
- Instructions for seismic evaluation and rehabilitation of steel structure
- Instructions for seismic evaluation and rehabilitation of masonry structure
- Instructions for seismic evaluation and rehabilitation of steel structure with saddle connection
- Instructions for seismic evaluation and rehabilitation of non-structural elements
- Instructions for seismic evaluation and rehabilitation of semi frame structures

DESIGN AND CONSTRUCTION OF ELEVATED "SADR" EXPRESSWAY, TEHRAN, IRAN

Maziar Hosseini[1] and Faramarz Aminpour[2]

SYNOPSIS

Increasing traffic congestions have for some time highlighted the need for a second deck to the existing Sadr Expressway in Tehran. An elevated section is now under construction which is 6.6 km long, and is mostly of precast prestressed concrete box girder construction. This paper describes the design and construction of this elevated section.

INTRODUCTION

The existing Sadr Expressway serves the dual purpose of connecting the north-eastern suburbs of Tehran to its business center, as well as serving as an arterial road between the Capital and the north and north-east of the country. Increasing traffic congestions have highlighted the need for an expansion of the existing expressway, which could only be achieved by adding a second deck along part of its length. The new elevated structure is 6.6 km long, 5 km of which forms the main bridge; the other 1.6 km form the approach ramps. Two junctions connect to the main bridge along its length. One of the main requirements of the Client, the Municipality of Tehran, was that the bridge be completed in 18 months; a demanding task given the project size of 155 000 m^2 of deck area.

PROJECT REQUIREMENTS AND THE CHOSEN CONSTRUCTION FORM

Some project statistics are shown in Table 1; the Client's requirements are shown in Table 2. It is seen that the solutions to most of the above requirements point to a system with minimum amount of site activity and maximum use of prefabrication. It must also be noted that the main bridge constituted over 72% of the deck area, so this was where optimization of the construction process would yield the most results. An all steel alternative was rejected right at the beginning, firstly because of its very high cost, and secondly because epoxy surfacing on steel decks has not performed well in Tehran. A steel-concrete composite alternative was also considered, but rejected firstly due to its high cost, and secondly because it was felt that the construction of the concrete slab, even if precast, would involve a lot of construction activity over live traffic.

After a survey of similar bridge projects in the world, it was decided that PSC segmental box girders, precast to the full width of the bridge were the most suitable form of construction. In order to simplify handling and erection, two boxes were used in the cross section, Figure 1. For reasons explained in subsequent sections, the span-by-span method of erection using launching

[1] Deputy Mayor, Technical and Development Affairs, Tehran Municipality and Assistant Professor, Postgraduate School, Structural Eng. Dep., Islamic Azad University, South Tehran Branch, Tehran, Iran.
[2] Karane Consulting Engineers.

gantries was used for the main bridge, and the balanced-cantilever method for the ramp and junction structures.

Table 1 Project statistics.

	Length, m	Deck area, m^2	Width, m	Minimum horizontal radius, m	Maximum pier height, m
Main bridge	4 900	112 000	22.7	315	18
Ramps and junctions	4 200	43 000	7.8-13.2	40	19.2
Total	9 100	155 000			

Table 2 The client's requirements.

Requirement	Solution
Rapid construction time (18 months)	Use factory produced prefabricated units
Economy	Use local materials i.e., concrete
Minimum disturbance to existing traffic during construction	• Minimize *in situ* work; this would minimize transport and delivery activities to site. • Build superstructure from above. Starting construction of the superstructure from each end and working towards the center of the project would in effect separate the construction traffic from the road traffic below.
Minimum risk of accidents to existing traffic during construction	• Minimize *in situ* work. Minimizing the number of activities over live traffic reduces risk. • Use large prefabricated units; this would minimize site handling.
The central reserve could temporarily be widened to 7 m for construction purposes	• Use precast units not just in the superstructure, but also for pier head cross beams. Any shuttering would have to be cantilevered out from the central reserve, and would therefore be expensive.
Bridge to be aesthetically pleasing	• Use factory produced prefabricated units. This would result in a better overall finish. • Avoid wide, flat, featureless surfaces. Superstructure bottom flange widths were reduces to about 35% of the overall deck width. Grooved oval shaped piers used to minimize visual impact of the size of the columns. • Round off corners. This was done in the superstructure to soften the visual impact.

MAIN BRIDGE SUPERSTRUCTURE

General arrangement of the main bridge is shown in Figure 1 and a typical match cast segment in Figure 2. Along its 5 km alignment, the main bridge spans many roads, bridges, streams, and other obstacles. The maximum span length needed to cross these obstacles was 50 m. An optimization exercise was carried out balancing the cost of the superstructure against that of the substructure and this showed that the optimum span length was nearer 45 m. The average span length used was therefore just over 44 m. In order to limit segment weights, the maximum span of 50 m was divided into 17 segments; 15 of 3 m, and 2 of 2.425 m. The maximum segment weight was thus 85 t. In order to position the piers in an optimal way while spanning over different obstacles, it was necessary to vary the spans. By eliminating up to three segments of the 17 segments of the 50-m span, the resulting span lengths were 47, 44 and 41 m.

Generally the design of the structure was geared to simplify and thus speed up construction. Some of the design decisions taken to achieve this are shown in Table 3. The design of the superstructure was checked against three codes: British [BSI 1990; The Highways' Agency 1994], European [BSI 2004a; BSI 2005a], and American [AASHTO 2003].

The climate in Tehran can be harsh; temperatures of -17°C and 43°C have been recorded over the past 30 years. Glued segmental bridges have a 40 year history in this climate, and experience with these bridges has shown that in this king of a climate the most effective barrier against ingress of water is deck waterproofing.

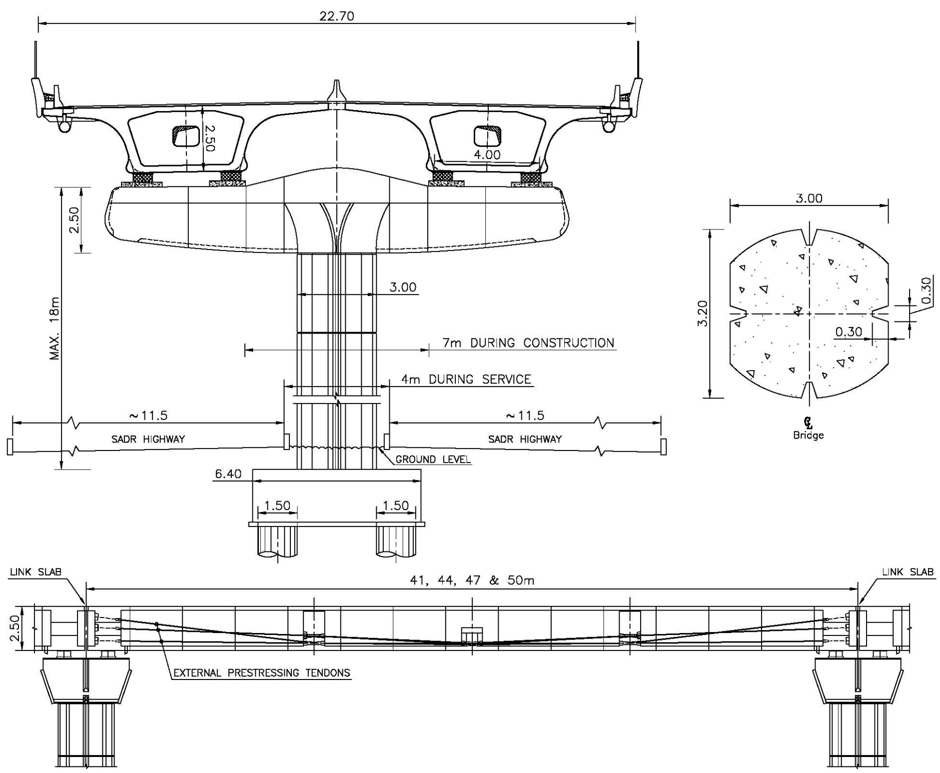

Figure 1 General arrangement of the main bridge.

Figure 2 Match cast segment.

Table 3 Design features used to simplify and speed up construction.

Design decision	Objective
Use of simply supported spans	• To eliminate the waiting time for *in situ* concrete joints to gain strength. • To minimize site activities associated with placing formwork, reinforcement, concrete etc.
Use of external tendons [Hewson 1993]	• To speed up casting of segments. Eliminating placement of prestressing ducts speeds up segment production. • To avoid potential blockage of ducts during tendon placement. Blockage of internal ducts sometimes happens when the tendon being threaded actually rips the corrugated material off the sides of the duct. This happens mostly at joints between segments. • To avoid leakage from joints during grouting operations. Grout leakage sometimes happens at joints due to incomplete gluing around the ducts. Grout leakage is always messy and gaining access to the leakage point and stopping it can be time consuming. These problems are compounded when working over traffic.
Use of dry joints [Hewson 1992]	• To eliminate gluing operations. Gluing operations can take time.
Use of a single type of saddle to cater for all cable deviations	• To eliminate mistakes in saddle placement and alignment. The alignment of the bridge follows a path of changing horizontal and vertical curves and superelevations. A single trumpet shaped saddle was designed for all ¼ span deviator locations, and a single one for the ½ span one.

Examination of several of the existing bridges has shown that where the deck waterproofing membrane was either damaged, badly detailed or badly applied, water has penetrated into the boxes, seriously damaging the concrete. The damage to the bottom slab has been more severe, because of the freeze-thaw cycles. The effect of epoxy glue at the joints seems to be insignificant. On the other hand, there are several examples where the waterproofing has performed well for nearly 30 years. For these reasons, it was considered that eliminating the glue at the joints would have negligible effect on the risk of ingress of water.

The deck waterproofing was therefore considered to be the main barrier against ingress of water into the box, and the HDPE pipes and the cement grout inside them providing the other two for the tendons. In order to minimize the number of expansion joints along the structure, the top slabs of adjacent spans were made continuous by a link-slab. This was generally done in units of 4 spans; this resulted in continuous lengths of just under 200 m. Longer lengths were not used because, as will be seen later, that would have placed too much displacement demand on the elastomeric bearings during a seismic event.

The two boxes were stitched together along their entire length by an *in situ* concrete strip. Where ramps joined or left the main bridge, the joints were treated in the same way. The chosen erection method was the span-by-span method using launching gantries. A pair of gantries, working side by side was used in order to minimize the eccentric loading on the piers. Figure 3 and 4 show the gantries assembled at each end of the bridge. It was originally planned that starting from each end of the project, the segments be fed to the gantries from behind, over the completed portions of the bridge. The pros and cons of the method are shown in Table 4. As it turned out, the contractor could not acquire enough land at the western end of the project to act as a temporary depot for the segments. At the eastern end, the ramp structures were not ready in time for launching of the gantries. The segments are now being stored during the night in the central reserve, and fed to the gantries from below.

Figure 3 Span-by-span method, east gantries starting operation.

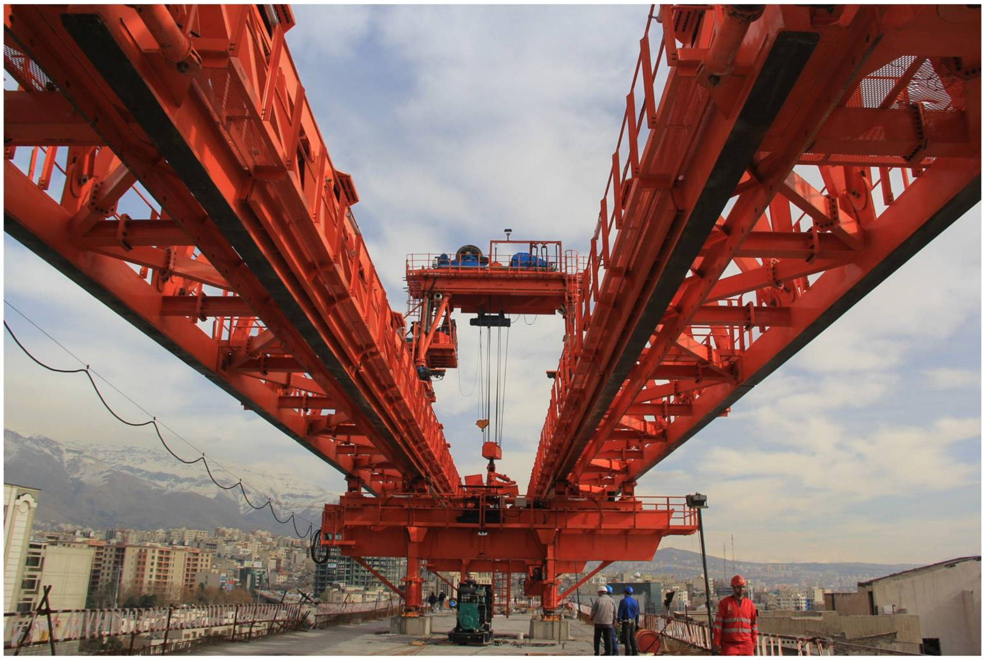

Figure 4 Span-by-span method, a west gantry being launched into position.

Table 4 Pros and cons of the span-by-span method.

Pros	Cons
• High erection rates. It was planned that in this project an average erection rate of 2.5 spans per week be achieved (main bridge formed 72% of total deck area, so speed was essential). This compared favorably with average erection rates of 3-4 spans per week reported for projects elsewhere in the world. During a site visit to the 2nd Penang Crossing in Malaysia in late 2012, potential erection rates of 12 spans per week were observed along a straight stretch of the project, well in excess of that expected in the Sadr project. • No need for access from the ground. With gantries working from each end of the project, segments could be delivered over the completed structure, and therefore the bridge could be built without causing any disruption to the road traffic below. • It was possible to feed the gantries from below, should the need arise.	• Time required for the design, fabrication, transport and erection of gantries. Construction was scheduled such that this activity could take place during the construction of the substructure and the ramp superstructures; timing however was critical. • Not suitable on tight curves. Although gantries with up to 3 hinges have been used to erect spans in curves with radii of less than 90 m, the system is mainly suited to open curves. The minimum horizontal radius along the main bridge was R_{min}=315 m. • Maximum span of approx. 60 m. This is the approximate maximum span for typical gantries. Maximum span along the alignment of the main bridge was 50 m.

RAMP AND JUNCTION SUPERSTRUCTURES

Figure 5 shows the general arrangement of the ramp and junction structures. Although the ramp and junction structures form less than 28% of the deck area, it was critical that their construction should start as soon as possible. Time wise it was not feasible to set up a casting yard for this part of the project, so the casting yard for a segmental bridge 30 km away was used. The maximum span length needed in the ramp and junction structures was 53.2 m, and it was possible to produce segments for this kind of span in that yard.

The only available means of erection was by using cranes operating from the ground, therefore the balanced-cantilever method was used which was self-supporting. Segment weights were limited to 50 t by limiting segment lengths to approximately 2 m. The only exception was the 70 t pier segment that contained a heavy diaphragm, but in that case the lifting weight was reduced to less than 50 t by casting the diaphragms on top of the piers.

The ramps crossed many roads, retaining walls, services and other obstacles, so it was decided to minimize the potential clash with these structures by using the number of piers and maximum span lengths. The standard continuous modules used were therefore 31 m – $n \times 52$ m – 31 m, where n was between 1 and 5, and generally 4. It was not possible to use longer continuous modules because of the displacement demand on the elastomeric bearings during a seismic event. Figures 6 and 7 show erection of the ramps. Sometime into construction, it was realized that modification of molds for those parts of ramps with tight curves would take longer than expected. These parts were therefore redesigned as steel-concrete composite box girders, Figure 8. They form about 5% of the total deck area. The pros and cons of the method are shown in Table 5.

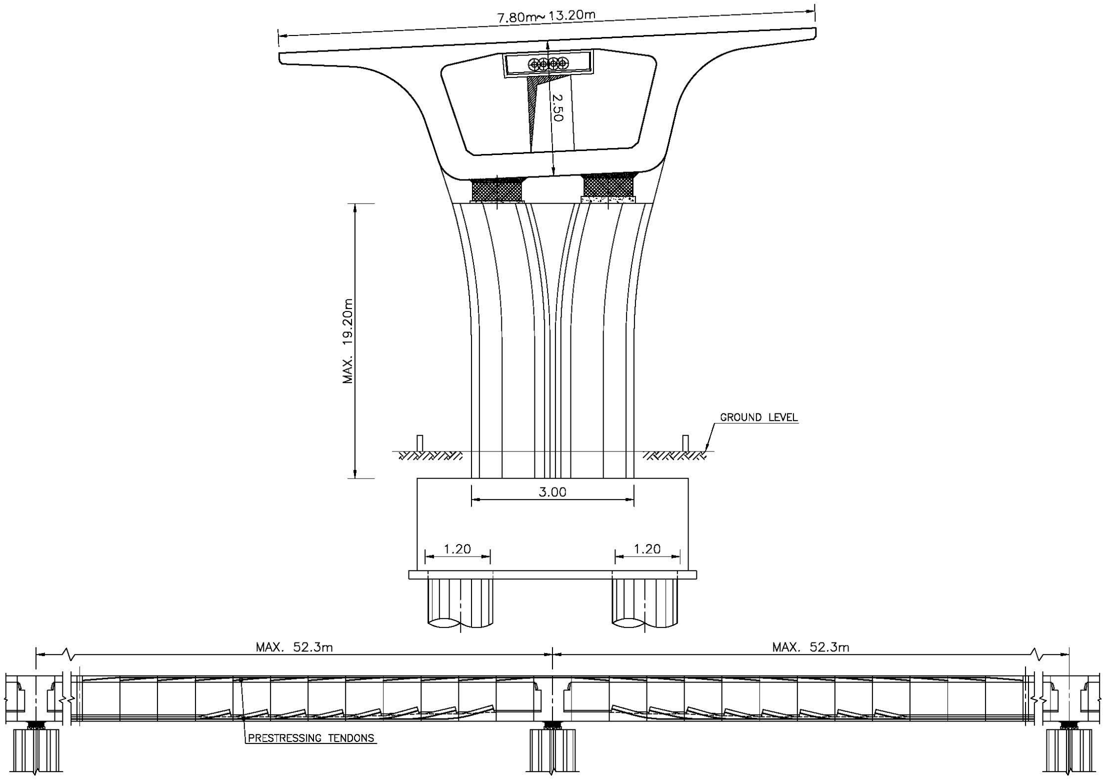

Figure 5 General arrangement of the ramp and junction structures.

Figure 6 Balanced-cantilever method, erection of a pier segment.

Figure 7 Balanced-cantilever method, erected balanced cantilevers.

Table 5 Pros and cons of the balanced-cantilever method using cranes from ground.

Pros	Cons
• No specialist machinery required; work could start immediately. The 50 t limit on segment weight meant that there were plenty of suitable cranes available. • Self-supporting; work could start immediately. Minor equipment was necessary to provide stability. • Can cope with tight curves. The existing molds could cope well with the geometry along most of the routes. Along some points in the ramps there were curves with radii as low as 40 m. This necessitated modification of the existing molds.	• Needs access from the ground. Most parts of the ramps were to the sides of the main routes, but for the other parts, lane closures combined with work at night had to be used. • Slower than span-by-span method. Normal erection rate was 1 span per week per erection team.

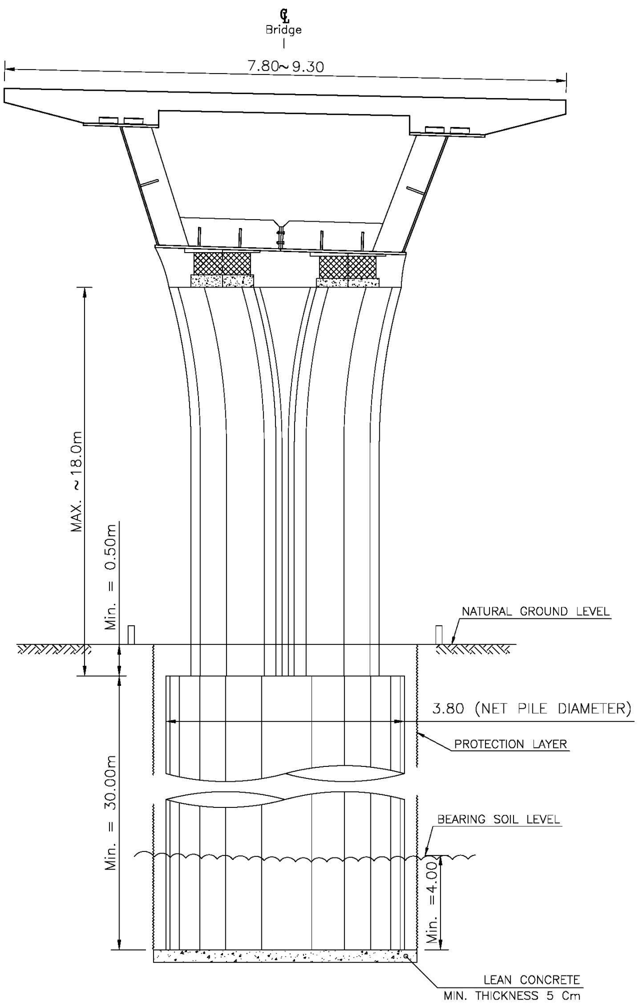

Figure 8 Steel-concrete composite box girders used in parts of ramps with tight curves.

PIERS

Tehran is situated in a seismically active zone. There are active faults believed to be capable of producing Magnitude 7 earthquakes just 5 km away from the project site. Local codes specify the design earthquake as the 475-year seismic event, with a base rock acceleration of 0.35*g*. Taking into account the soil type and the period of a particular structure, spectral horizontal accelerations can reach up to 1*g*. The effects of a 2475-year earthquake, thought to be approximately the maximum credible earthquake that these faults can generate, are roughly 1.7 times those of a 475-year earthquake. It is of course uneconomical to design for such high forces. Traditionally a structure is designed for a fraction of these forces, absorbing most of the seismic movements in plastic hinges that form at the base of the piers. These plastic hinges will of course sustain extensive damage.

A 475-year seismic event has a 19% probability of being exceeded during the lifetime of the bridge (assumed as being 100 years). With a project of this size, and given the importance of this expressway after a seismic event, it was not considered acceptable for major components of the bridge to suffer extensive damage, and therefore an alternative approach was adopted.

It was decided to absorb most of the horizontal movements of the design earthquake in flexible, easily replaceable and cheap devices. Simple low-damping elastomeric bearings proved to be sufficient for this purpose, effectively decoupling the superstructure from the substructure. In this way, although the mass of an average span was roughly 4 times the mass of an average pier, its share of bending moments at the bottom of the pier was just 11%. This also meant that the use of more elaborate systems, such as high damping elastomers, lead rubber bearings, or dampers was not necessary. The extra damping of such devices would have had negligible benefit. The seismic design of the substructure was in accordance with EN 1998 [BSI 2004b; BSI 2005].

For the 2475-year seismic event, the goal of the design was collapse prevention. During such an event, most of the displacements would again be absorbed by the elastomers and the rest by the formation of a plastic hinge at the base of the piers. The concrete in this zone was therefore confined in order to provide the necessary ductility. At an extra cost to the project of less than 5%, the resulting structure is anticipated to remain essentially elastic during a 475-year earthquake. Its main feature is that it is not particularly sensitive to the uncertainties of the seismic problem, with the added benefit that it is slender enough to comply with the 3 m width limit set for the piers.

Because of the proximity of the active faults, the vertical component of the seismic motion had to be taken into account too. The spectral response of the vertical seismic excitation was calculated for the 475-year event, taking into account the vertical flexibility of the bridge. It was found that the seismic forces were roughly equal to the traffic loading, and would therefore cause no damage to the bridge. The vertical 2475-year seismic load case proved to be less than the non-seismic ultimate limit state load case and therefore did not control the design. Figure 1 shows the general layout of the main bridge piers, and Figure 9 a row of piers after construction.

The pier cross beams were precast in order to speed up their construction, and to minimize *in situ* work. They were heavily prestressed, their design being controlled by the operation of the launching gantry. It would have been possible to substantially reduce their size by using props during gantry operation, but this was not favored by the contractor. Figures 10 through 12 show the cross-beams under construction.

Figure 9 Main bridge piers.

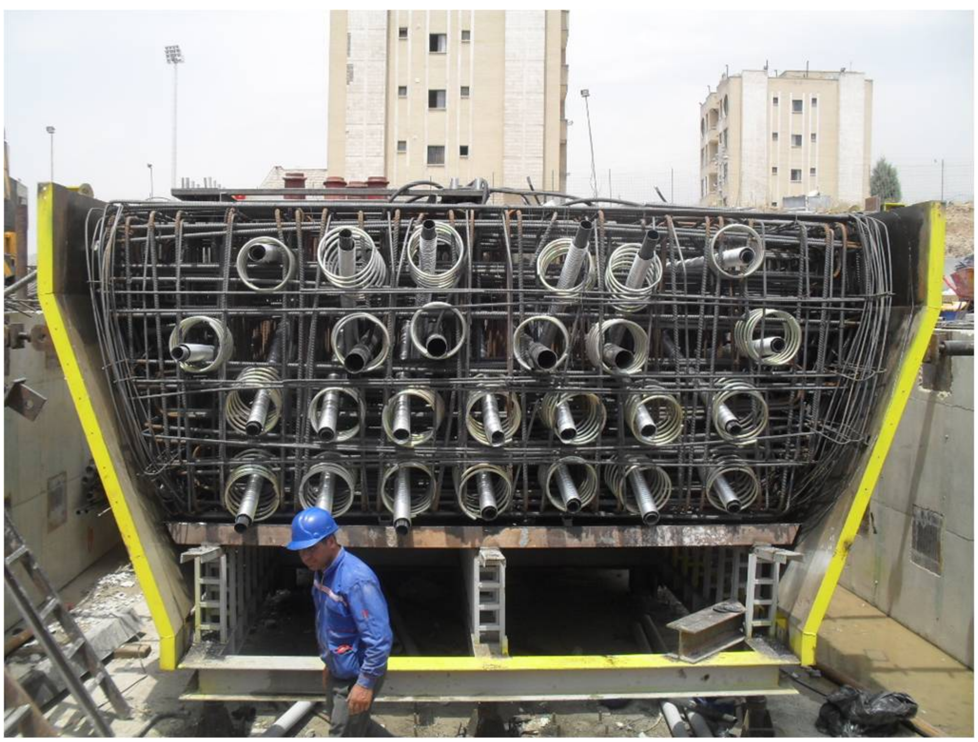

Figure 10 Pier cross-beam prestressing.

Figure 11 Cross-beam segment ready to be lifted into place.

Figure 12 Cross-beam segment ready for temporary stressing.

FOUNDATIONS

Roughly 80% of the foundations were situated either on fill material used to build the original Expressway, or on other soft soil; deep foundations were therefore used. For the other 20%, alternative spread footings were designed, but their widths were wider than the central reserve, so special construction technique had to be used. Given the availability of piling equipment, the contractor decided to use deep foundations for all foundations.

The 7 m width limit on the working area in the central reserve meant that the foundation widths had to be limited to 6.4 m, see Figure 1; therefore, up to half of the piles acted in tension during some of the seismic load cases. In some foundations the presence of various obstacles prevented the use of normal piled foundations. In these instances shafts with a diameter of approximately 4 m were used, see Figures 13 through 15. All these shafts were hand dug.

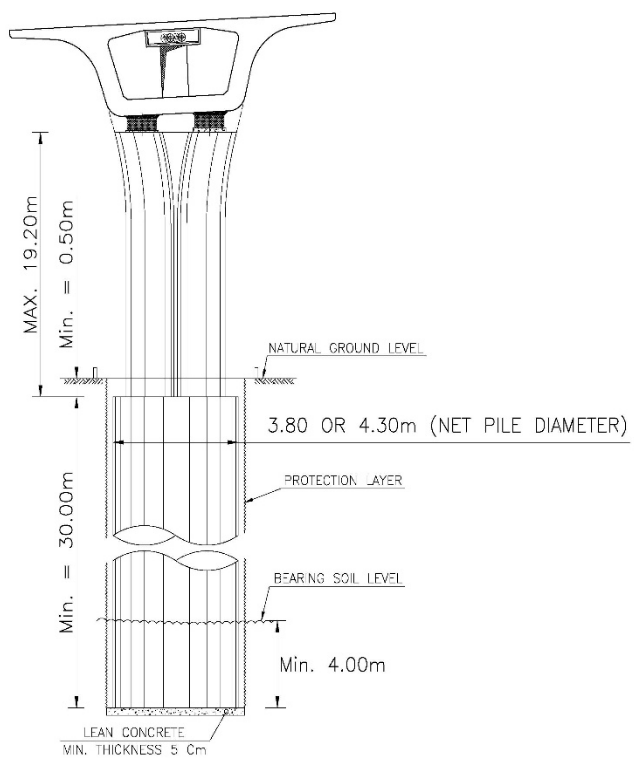

Figure 13 Shaft foundation for a ramp pier.

Figure 14 Shaft foundation with shotcrete lining.

Figure 15 Shaft foundation for a main bridge pier.

CONCLUSIONS

Match cast segmental construction has enabled the construction of Sadr Elevated Expressway to proceed rapidly, with minimum cost, while avoiding large disturbance to traffic. The balanced cantilever method, requiring the minimum of specialized equipment, was combined with the span-by-span method using launching gantries, which has speed. The result was that superstructure construction could start very early on during the project, while high erection rates could later be achieved on the main part of the project. Simple spans, external tendons, dry joints and simple detailing were used to avoid potential construction problems, with the aim of achieving a rapid rate of construction. By using simple low-damping elastomeric bearings as isolators, it is expected that the main structural members of the bridge remain essentially elastic during a 475 year seismic event. The cost burden of this favorable response was less than 5% to the project.

REFERENCES

AASHTO (2003). *2003 Interim Guide Specifications for Design and Construction of Segmental Concrete Bridges,* American Association of State Highway and Transportation Officials, 2nd ed., Washington, D.C.

BSI (1990). *Steel, Concrete and Composite Bridges—Part 4: Code of Practice for Design of Concrete Bridges, BS 5400-4,* British Standards Institution, London, U.K.

BSI (2004a). *Eurocode 2—Design of Concrete Structures, Part 1-1: General Rules and Rules for Buildings, BS EN 1992-1-1:2004,* British Standards Institution, London, U.K.

BSI (2005a). *Eurocode 2—Design of Concrete Structures, Part 2: Concrete Bridges–Design and Detailing rules, BS EN 1992-2:2005,* British Standards Institution, London, U.K.

BSI (2004b). *Eurocode 8—Design of Structures for Earthquake Resistance, Part 1: General Rules, Seismic Actions and Rules for Buildings, BS EN 1998-1:2004,* British Standards Institution, London, U.K.

BSI (2005b). *Eurocode 8—Design of Structures for Earthquake Resistance, Part 2: Bridges, BS EN 1998-2:2005,* British Standards Institution London, U.K.

Hewson N.R. (1993). The use of external tendons for the Bangkok Second Stage Expressway*, The Structural Engineer*, pp. 412–415.

Hewson N.R. (1992). The use of dry joints between precast segments for bridge decks, *Bridge Eng.*, pp. 177–184.

The Highways Agency (1994).*: The Design of Concrete Highway Bridges and Structures with External and Unbonded Prestressing, BD 58/94,* London, U.K.

ADVANCES IN EQUIVALENT LINEAR AND NONLINEAR SITE RESPONSE ANALYSIS

Youssef Hashash[1]

ABSTRACT

Studies of earthquakes that have occurred over the last 50 years and dynamic soil behavior provide ample evidence that for strains higher than 10^{-4} soil behavior during an earthquake is highly nonlinear and hysteretic. Nonlinearity has a predominant role in the behavior of soils due to dynamic loading and is a key aspect in the response of infrastructure during a seismic event.

This presentation is divided into several parts:

1. Site effects, field evidence and cyclic response of soils
2. Equivalent linear site response: history of development of an efficient approach to capture soil nonlinearity
3. History and major advances in nonlinear one-dimensional total stress site response analysis. This includes developments of simplified as well as more advanced material total and effect stress models and the challenges with capturing measured small and large strain damping in these models. The presentation will also cover issues associated with representing small and large strain damping.
4. Developments in nonlinear one-dimensional site response with porewater pressure generation using new porewater pressure generation function.
5. Discuss the main features of the software program DEEPSOIL for one-dimensional nonlinear and equivalent linear site response analysis.

Here are the two key references:

Hashash Y.M.A., Phillips C., Groholski D.R. (2010). Recent advances in non-linear site response analysis, *Proceedings, Fifth International Conference in Recent Advances in Geotechnical Earthquake Engineering and Soil Dynamics*, CD-ROM OSP 4, San Diego, CA.

Matasovic N., Hashash Y.M.A. (2012). Practices and procedures for site-specific evaluations of earthquake ground motions, a synthesis of highway practice, *NCHRP Synthesis 428*, Federal High Administration, Washington, D.C.

1 Professor, University of Illinois at Urbana-Champaign, 205 N. Mathews Ave, Urbana, IL 61801, USA, hashash@illinois.edu, tel: 217-333-6986, fax: 217-265-8041.

PEER REPORTS

PEER reports are available as a free PDF download from http://peer.berkeley.edu/publications/peer_reports_complete.html. Printed hard copies of PEER reports can be ordered directly from our printer by following the instructions at http://peer.berkeley.edu/publications/peer_reports.html. For other related questions about the PEER Report Series, contact the Pacific Earthquake Engineering Research Center, 325 Davis Hall mail code 1792, Berkeley, CA 94720. Tel.: (510) 642-3437; Fax: (510) 665-1655; Email: peer_editor@berkeley.edu

PEER 2013/26 *Urban Earthquake Engineering. Proceedings of the U.S.-Iran Seismic Workshop.* December 2013.

PEER 2013/25 *Earthquake Engineering for Resilient Communities: 2013 PEER Internship Program Research Report Collection.* Heidi Tremayne (Editor), Stephen A. Mahin (Editor), Jorge Archbold Monterossa, Matt Brosman, Shelly Dean, Katherine deLaveaga, Curtis Fong, Donovan Holder, Elizabeth Jachens, Rakeeb Khan, David Lam, Daniela Martinez Lopez, Mara Minner, Geffen Oren, Julia Pavicic, Melissa Quinonez, Lorena Rodriguez, Sean Salazar, Kelli Slaven, Vivian Steyert, Jenny Taing, and Salvador Tena. December 2013.

PEER 2013/24 *NGA-West2 Ground Motion Prediction Equations for Vertical Ground Motions.* September 2013.

PEER 2013/23 *Coordinated Planning and Preparedness for Fire Following Major Earthquakes.* Charles Scawthorn. November 2013.

PEER 2013/22 *GEM-PEER Task 3 Project: Selection of a Global Set of Ground Motion Prediction Equations.* Jonathan P. Stewart, John Douglas, Mohammad B. Javanbarg, Carola Di Alessandro, Yousef Bozorgnia, Norman A. Abrahamson, David M. Boore, Kenneth W. Campbell, Elise Delavaud, Mustafa Erdik and Peter J. Stafford. December 2013.

PEER 2013/21 *Seismic Design and Performance of Bridges with Columns on Rocking Foundations.* Grigorios Antonellis and Marios Panagiotou. September 2013.

PEER 2013/20 *Experimental and Analytical Studies on the Seismic Behavior of Conventional and Hybrid Braced Frames.* Jiun-Wei Lai and Stephen A. Mahin. September 2013.

PEER 2013/19 *Toward Resilient Communities: A Performance-Based Engineering Framework for Design and Evaluation of the Built Environment.* Michael William Mieler, Bozidar Stojadinovic, Robert J. Budnitz, Stephen A. Mahin and Mary C. Comerio. September 2013.

PEER 2013/18 *Identification of Site Parameters that Improve Predictions of Site Amplification.* Ellen M. Rathje and Sara Navidi. July 2013.

PEER 2013/17 *Response Spectrum Analysis of Concrete Gravity Dams Including Dam-Water-Foundation Interaction.* Arnkjell Løkke and Anil K. Chopra. July 2013.

PEER 2013/16 *Effect of hoop reinforcement spacing on the cyclic response of large reinforced concrete special moment frame beams.* Marios Panagiotou, Tea Visnjic, Grigorios Antonellis, Panagiotis Galanis, and Jack P. Moehle. June 2013.

PEER 2013/15 *A Probabilistic Framework to Include the Effects of Near-Fault Directivity in Seismic Hazard Assessment.* Shrey Kumar Shahi, Jack W. Baker. October 2013.

PEER 2013/14 *Hanging-Wall Scaling using Finite-Fault Simulations.* Jennifer L. Donahue and Norman A. Abrahamson. September 2013.

PEER 2013/13 *Semi-Empirical Nonlinear Site Amplification and its Application in NEHRP Site Factors.* Jonathan P. Stewart and Emel Seyhan. November 2013.

PEER 2013/12 *Nonlinear Horizontal Site Response for the NGA-West2 Project.* Ronnie Kamai, Norman A. Abramson, Walter J. Silva. May 2013.

PEER 2013/11 *Epistemic Uncertainty for NGA-West2 Models.* Linda Al Atik and Robert R. Youngs. May 2013.

PEER 2013/10 *NGA-West 2 Models for Ground-Motion Directionality.* Shrey K. Shahi and Jack W. Baker. May 2013.

PEER 2013/09 *Final Report of the NGA-West2 Directivity Working Group.* Paul Spudich, Jeffrey R. Bayless, Jack W. Baker, Brian S.J. Chiou, Badie Rowshandel, Shrey Shahi, and Paul Somerville. May 2013.

PEER 2013/08 *NGA-West2 Model for Estimating Average Horizontal Values of Pseudo-Absolute Spectral Accelerations Generated by Crustal Earthquakes.* I. M. Idriss. May 2013.

PEER 2013/07 *Update of the Chiou and Youngs NGA Ground Motion Model for Average Horizontal Component of Peak Ground Motion and Response Spectra.* Brian Chiou and Robert Youngs. May 2013.

PEER 2013/06 *NGA-West2 Campbell-Bozorgnia Ground Motion Model for the Horizontal Components of PGA, PGV, and 5%-Damped Elastic Pseudo-Acceleration Response Spectra for Periods Ranging from 0.01 to 10 sec.* Kenneth W. Campbell and Yousef Bozorgnia. May 2013.

PEER 2013/05 *NGA-West 2 Equations for Predicting Response Spectral Accelerations for Shallow Crustal Earthquakes.* David M. Boore, Jonathan P. Stewart, Emel Seyhan, Gail M. Atkinson. May 2013.

PEER 2013/04 *Update of the AS08 Ground-Motion Prediction Equations Based on the NGA-West2 Data Set.* Norman Abrahamson, Walter Silva, and Ronnie Kamai. May 2013.

PEER 2013/03 *PEER NGA-West2 Database.* Timothy D. Ancheta, Robert B. Darragh, Jonathan P. Stewart, Emel Seyhan, Walter J. Silva, Brian S.J. Chiou, Katie E. Wooddell, Robert W. Graves, Albert R. Kottke, David M. Boore, Tadahiro Kishida, and Jennifer L. Donahue. May 2013.

PEER 2013/02 *Hybrid Simulation of the Seismic Response of Squat Reinforced Concrete Shear Walls.* Catherine A. Whyte and Bozidar Stojadinovic. May 2013.

PEER 2013/01 *Housing Recovery in Chile: A Qualitative Mid-program Review.* Mary C. Comerio. February 2013.

PEER 2012/08 *Guidelines for Estimation of Shear Wave Velocity.* Bernard R. Wair, Jason T. DeJong, and Thomas Shantz. December 2012.

PEER 2012/07 *Earthquake Engineering for Resilient Communities: 2012 PEER Internship Program Research Report Collection.* Heidi Tremayne (Editor), Stephen A. Mahin (Editor), Collin Anderson, Dustin Cook, Michael Erceg, Carlos Esparza, Jose Jimenez, Dorian Krausz, Andrew Lo, Stephanie Lopez, Nicole McCurdy, Paul Shipman, Alexander Strum, Eduardo Vega. December 2012.

PEER 2012/06 *Fragilities for Precarious Rocks at Yucca Mountain.* Matthew D. Purvance, Rasool Anooshehpoor, and James N. Brune. December 2012.

PEER 2012/05 *Development of Simplified Analysis Procedure for Piles in Laterally Spreading Layered Soils.* Christopher R. McGann, Pedro Arduino, and Peter Mackenzie–Helnwein. December 2012.

PEER 2012/04 *Unbonded Pre-Tensioned Columns for Bridges in Seismic Regions.* Phillip M. Davis, Todd M. Janes, Marc O. Eberhard, and John F. Stanton. December 2012.

PEER 2012/03 *Experimental and Analytical Studies on Reinforced Concrete Buildings with Seismically Vulnerable Beam-Column Joints.* Sangjoon Park and Khalid M. Mosalam. October 2012.

PEER 2012/02 *Seismic Performance of Reinforced Concrete Bridges Allowed to Uplift during Multi-Directional Excitation.* Andres Oscar Espinoza and Stephen A. Mahin. July 2012.

PEER 2012/01 *Spectral Damping Scaling Factors for Shallow Crustal Earthquakes in Active Tectonic Regions.* Sanaz Rezaeian, Yousef Bozorgnia, I. M. Idriss, Kenneth Campbell, Norman Abrahamson, and Walter Silva. July 2012.

PEER 2011/10 *Earthquake Engineering for Resilient Communities: 2011 PEER Internship Program Research Report Collection.* Eds. Heidi Faison and Stephen A. Mahin. December 2011.

PEER 2011/09 *Calibration of Semi-Stochastic Procedure for Simulating High-Frequency Ground Motions.* Jonathan P. Stewart, Emel Seyhan, and Robert W. Graves. December 2011.

PEER 2011/08 *Water Supply in regard to Fire Following Earthquake.* Charles Scawthorn. November 2011.

PEER 2011/07 *Seismic Risk Management in Urban Areas. Proceedings of a U.S.-Iran-Turkey Seismic Workshop.* September 2011.

PEER 2011/06 *The Use of Base Isolation Systems to Achieve Complex Seismic Performance Objectives.* Troy A. Morgan and Stephen A. Mahin. July 2011.

PEER 2011/05 *Case Studies of the Seismic Performance of Tall Buildings Designed by Alternative Means.* Task 12 Report for the Tall Buildings Initiative. Jack Moehle, Yousef Bozorgnia, Nirmal Jayaram, Pierson Jones, Mohsen Rahnama, Nilesh Shome, Zeynep Tuna, John Wallace, Tony Yang, and Farzin Zareian. July 2011.

PEER 2011/04 *Recommended Design Practice for Pile Foundations in Laterally Spreading Ground.* Scott A. Ashford, Ross W. Boulanger, and Scott J. Brandenberg. June 2011.

PEER 2011/03 *New Ground Motion Selection Procedures and Selected Motions for the PEER Transportation Research Program.* Jack W. Baker, Ting Lin, Shrey K. Shahi, and Nirmal Jayaram. March 2011.

PEER 2011/02 *A Bayesian Network Methodology for Infrastructure Seismic Risk Assessment and Decision Support.* Michelle T. Bensi, Armen Der Kiureghian, and Daniel Straub. March 2011.

PEER 2011/01 *Demand Fragility Surfaces for Bridges in Liquefied and Laterally Spreading Ground.* Scott J. Brandenberg, Jian Zhang, Pirooz Kashighandi, Yili Huo, and Minxing Zhao. March 2011.

PEER 2010/05 *Guidelines for Performance-Based Seismic Design of Tall Buildings.* Developed by the Tall Buildings Initiative. November 2010.

PEER 2010/04 *Application Guide for the Design of Flexible and Rigid Bus Connections between Substation Equipment Subjected to Earthquakes.* Jean-Bernard Dastous and Armen Der Kiureghian. September 2010.

PEER 2010/03 *Shear Wave Velocity as a Statistical Function of Standard Penetration Test Resistance and Vertical Effective Stress at Caltrans Bridge Sites.* Scott J. Brandenberg, Naresh Bellana, and Thomas Shantz. June 2010.

PEER 2010/02 *Stochastic Modeling and Simulation of Ground Motions for Performance-Based Earthquake Engineering.* Sanaz Rezaeian and Armen Der Kiureghian. June 2010.

PEER 2010/01 *Structural Response and Cost Characterization of Bridge Construction Using Seismic Performance Enhancement Strategies.* Ady Aviram, Božidar Stojadinović, Gustavo J. Parra-Montesinos, and Kevin R. Mackie. March 2010.

PEER 2009/03 *The Integration of Experimental and Simulation Data in the Study of Reinforced Concrete Bridge Systems Including Soil-Foundation-Structure Interaction.* Matthew Dryden and Gregory L. Fenves. November 2009.

PEER 2009/02 *Improving Earthquake Mitigation through Innovations and Applications in Seismic Science, Engineering, Communication, and Response. Proceedings of a U.S.-Iran Seismic Workshop.* October 2009.

PEER 2009/01 *Evaluation of Ground Motion Selection and Modification Methods: Predicting Median Interstory Drift Response of Buildings.* Curt B. Haselton, Ed. June 2009.

PEER 2008/10 *Technical Manual for Strata.* Albert R. Kottke and Ellen M. Rathje. February 2009.

PEER 2008/09 *NGA Model for Average Horizontal Component of Peak Ground Motion and Response Spectra.* Brian S.-J. Chiou and Robert R. Youngs. November 2008.

PEER 2008/08 *Toward Earthquake-Resistant Design of Concentrically Braced Steel Structures.* Patxi Uriz and Stephen A. Mahin. November 2008.

PEER 2008/07 *Using OpenSees for Performance-Based Evaluation of Bridges on Liquefiable Soils.* Stephen L. Kramer, Pedro Arduino, and HyungSuk Shin. November 2008.

PEER 2008/06 *Shaking Table Tests and Numerical Investigation of Self-Centering Reinforced Concrete Bridge Columns.* Hyung IL Jeong, Junichi Sakai, and Stephen A. Mahin. September 2008.

PEER 2008/05 *Performance-Based Earthquake Engineering Design Evaluation Procedure for Bridge Foundations Undergoing Liquefaction-Induced Lateral Ground Displacement.* Christian A. Ledezma and Jonathan D. Bray. August 2008.

PEER 2008/04 *Benchmarking of Nonlinear Geotechnical Ground Response Analysis Procedures.* Jonathan P. Stewart, Annie On-Lei Kwok, Yousseff M. A. Hashash, Neven Matasovic, Robert Pyke, Zhiliang Wang, and Zhaohui Yang. August 2008.

PEER 2008/03 *Guidelines for Nonlinear Analysis of Bridge Structures in California.* Ady Aviram, Kevin R. Mackie, and Božidar Stojadinović. August 2008.

PEER 2008/02 *Treatment of Uncertainties in Seismic-Risk Analysis of Transportation Systems.* Evangelos Stergiou and Anne S. Kiremidjian. July 2008.

PEER 2008/01 *Seismic Performance Objectives for Tall Buildings.* William T. Holmes, Charles Kircher, William Petak, and Nabih Youssef. August 2008.

PEER 2007/12 *An Assessment to Benchmark the Seismic Performance of a Code-Conforming Reinforced Concrete Moment-Frame Building.* Curt Haselton, Christine A. Goulet, Judith Mitrani-Reiser, James L. Beck, Gregory G. Deierlein, Keith A. Porter, Jonathan P. Stewart, and Ertugrul Taciroglu. August 2008.

PEER 2007/11 *Bar Buckling in Reinforced Concrete Bridge Columns.* Wayne A. Brown, Dawn E. Lehman, and John F. Stanton. February 2008.

PEER 2007/10 *Computational Modeling of Progressive Collapse in Reinforced Concrete Frame Structures.* Mohamed M. Talaat and Khalid M. Mosalam. May 2008.

PEER 2007/09 *Integrated Probabilistic Performance-Based Evaluation of Benchmark Reinforced Concrete Bridges.* Kevin R. Mackie, John-Michael Wong, and Božidar Stojadinović. January 2008.

PEER 2007/08 *Assessing Seismic Collapse Safety of Modern Reinforced Concrete Moment-Frame Buildings.* Curt B. Haselton and Gregory G. Deierlein. February 2008.

PEER 2007/07 *Performance Modeling Strategies for Modern Reinforced Concrete Bridge Columns.* Michael P. Berry and Marc O. Eberhard. April 2008.

PEER 2007/06 *Development of Improved Procedures for Seismic Design of Buried and Partially Buried Structures.* Linda Al Atik and Nicholas Sitar. June 2007.

PEER 2007/05 *Uncertainty and Correlation in Seismic Risk Assessment of Transportation Systems.* Renee G. Lee and Anne S. Kiremidjian. July 2007.

PEER 2007/04 *Numerical Models for Analysis and Performance-Based Design of Shallow Foundations Subjected to Seismic Loading.* Sivapalan Gajan, Tara C. Hutchinson, Bruce L. Kutter, Prishati Raychowdhury, José A. Ugalde, and Jonathan P. Stewart. May 2008.

PEER 2007/03 *Beam-Column Element Model Calibrated for Predicting Flexural Response Leading to Global Collapse of RC Frame Buildings.* Curt B. Haselton, Abbie B. Liel, Sarah Taylor Lange, and Gregory G. Deierlein. May 2008.

PEER 2007/02 *Campbell-Bozorgnia NGA Ground Motion Relations for the Geometric Mean Horizontal Component of Peak and Spectral Ground Motion Parameters.* Kenneth W. Campbell and Yousef Bozorgnia. May 2007.

PEER 2007/01 *Boore-Atkinson NGA Ground Motion Relations for the Geometric Mean Horizontal Component of Peak and Spectral Ground Motion Parameters.* David M. Boore and Gail M. Atkinson. May. May 2007.

PEER 2006/12 *Societal Implications of Performance-Based Earthquake Engineering.* Peter J. May. May 2007.

PEER 2006/11 *Probabilistic Seismic Demand Analysis Using Advanced Ground Motion Intensity Measures, Attenuation Relationships, and Near-Fault Effects.* Polsak Tothong and C. Allin Cornell. March 2007.

PEER 2006/10 *Application of the PEER PBEE Methodology to the I-880 Viaduct.* Sashi Kunnath. February 2007.

PEER 2006/09 *Quantifying Economic Losses from Travel Forgone Following a Large Metropolitan Earthquake.* James Moore, Sungbin Cho, Yue Yue Fan, and Stuart Werner. November 2006.

PEER 2006/08 *Vector-Valued Ground Motion Intensity Measures for Probabilistic Seismic Demand Analysis.* Jack W. Baker and C. Allin Cornell. October 2006.

PEER 2006/07 *Analytical Modeling of Reinforced Concrete Walls for Predicting Flexural and Coupled–Shear-Flexural Responses.* Kutay Orakcal, Leonardo M. Massone, and John W. Wallace. October 2006.

PEER 2006/06 *Nonlinear Analysis of a Soil-Drilled Pier System under Static and Dynamic Axial Loading.* Gang Wang and Nicholas Sitar. November 2006.

PEER 2006/05 *Advanced Seismic Assessment Guidelines.* Paolo Bazzurro, C. Allin Cornell, Charles Menun, Maziar Motahari, and Nicolas Luco. September 2006.

PEER 2006/04 *Probabilistic Seismic Evaluation of Reinforced Concrete Structural Components and Systems.* Tae Hyung Lee and Khalid M. Mosalam. August 2006.

PEER 2006/03 *Performance of Lifelines Subjected to Lateral Spreading.* Scott A. Ashford and Teerawut Juirnarongrit. July 2006.

PEER 2006/02 *Pacific Earthquake Engineering Research Center Highway Demonstration Project.* Anne Kiremidjian, James Moore, Yue Yue Fan, Nesrin Basoz, Ozgur Yazali, and Meredith Williams. April 2006.

PEER 2006/01 *Bracing Berkeley. A Guide to Seismic Safety on the UC Berkeley Campus.* Mary C. Comerio, Stephen Tobriner, and Ariane Fehrenkamp. January 2006.

PEER 2005/16 *Seismic Response and Reliability of Electrical Substation Equipment and Systems.* Junho Song, Armen Der Kiureghian, and Jerome L. Sackman. April 2006.

PEER 2005/15 *CPT-Based Probabilistic Assessment of Seismic Soil Liquefaction Initiation.* R. E. S. Moss, R. B. Seed, R. E. Kayen, J. P. Stewart, and A. Der Kiureghian. April 2006.

PEER 2005/14 *Workshop on Modeling of Nonlinear Cyclic Load-Deformation Behavior of Shallow Foundations.* Bruce L. Kutter, Geoffrey Martin, Tara Hutchinson, Chad Harden, Sivapalan Gajan, and Justin Phalen. March 2006.

PEER 2005/13 *Stochastic Characterization and Decision Bases under Time-Dependent Aftershock Risk in Performance-Based Earthquake Engineering.* Gee Liek Yeo and C. Allin Cornell. July 2005.

PEER 2005/12 *PEER Testbed Study on a Laboratory Building: Exercising Seismic Performance Assessment.* Mary C. Comerio, editor. November 2005.

PEER 2005/11 *Van Nuys Hotel Building Testbed Report: Exercising Seismic Performance Assessment.* Helmut Krawinkler, editor. October 2005.

PEER 2005/10 *First NEES/E-Defense Workshop on Collapse Simulation of Reinforced Concrete Building Structures.* September 2005.

PEER 2005/09 *Test Applications of Advanced Seismic Assessment Guidelines.* Joe Maffei, Karl Telleen, Danya Mohr, William Holmes, and Yuki Nakayama. August 2006.

PEER 2005/08 *Damage Accumulation in Lightly Confined Reinforced Concrete Bridge Columns.* R. Tyler Ranf, Jared M. Nelson, Zach Price, Marc O. Eberhard, and John F. Stanton. April 2006.

PEER 2005/07 *Experimental and Analytical Studies on the Seismic Response of Freestanding and Anchored Laboratory Equipment.* Dimitrios Konstantinidis and Nicos Makris. January 2005.

PEER 2005/06 *Global Collapse of Frame Structures under Seismic Excitations.* Luis F. Ibarra and Helmut Krawinkler. September 2005.

PEER 2005//05 *Performance Characterization of Bench- and Shelf-Mounted Equipment.* Samit Ray Chaudhuri and Tara C. Hutchinson. May 2006.

PEER 2005/04 *Numerical Modeling of the Nonlinear Cyclic Response of Shallow Foundations.* Chad Harden, Tara Hutchinson, Geoffrey R. Martin, and Bruce L. Kutter. August 2005.

PEER 2005/03 *A Taxonomy of Building Components for Performance-Based Earthquake Engineering.* Keith A. Porter. September 2005.

PEER 2005/02 *Fragility Basis for California Highway Overpass Bridge Seismic Decision Making*. Kevin R. Mackie and Božidar Stojadinović. June 2005.

PEER 2005/01 *Empirical Characterization of Site Conditions on Strong Ground Motion.* Jonathan P. Stewart, Yoojoong Choi, and Robert W. Graves. June 2005.

PEER 2004/09 *Electrical Substation Equipment Interaction: Experimental Rigid Conductor Studies.* Christopher Stearns and André Filiatrault. February 2005.

PEER 2004/08 *Seismic Qualification and Fragility Testing of Line Break 550-kV Disconnect Switches.* Shakhzod M. Takhirov, Gregory L. Fenves, and Eric Fujisaki. January 2005.

PEER 2004/07 *Ground Motions for Earthquake Simulator Qualification of Electrical Substation Equipment.* Shakhzod M. Takhirov, Gregory L. Fenves, Eric Fujisaki, and Don Clyde. January 2005.

PEER 2004/06 *Performance-Based Regulation and Regulatory Regimes.* Peter J. May and Chris Koski. September 2004.

PEER 2004/05 *Performance-Based Seismic Design Concepts and Implementation: Proceedings of an International Workshop.* Peter Fajfar and Helmut Krawinkler, editors. September 2004.

PEER 2004/04 *Seismic Performance of an Instrumented Tilt-up Wall Building.* James C. Anderson and Vitelmo V. Bertero. July 2004.

PEER 2004/03 *Evaluation and Application of Concrete Tilt-up Assessment Methodologies.* Timothy Graf and James O. Malley. October 2004.

PEER 2004/02 *Analytical Investigations of New Methods for Reducing Residual Displacements of Reinforced Concrete Bridge Columns.* Junichi Sakai and Stephen A. Mahin. August 2004.

PEER 2004/01 *Seismic Performance of Masonry Buildings and Design Implications.* Kerri Anne Taeko Tokoro, James C. Anderson, and Vitelmo V. Bertero. February 2004.

PEER 2003/18 *Performance Models for Flexural Damage in Reinforced Concrete Columns.* Michael Berry and Marc Eberhard. August 2003.

PEER 2003/17 *Predicting Earthquake Damage in Older Reinforced Concrete Beam-Column Joints.* Catherine Pagni and Laura Lowes. October 2004.

PEER 2003/16 *Seismic Demands for Performance-Based Design of Bridges.* Kevin Mackie and Božidar Stojadinović. August 2003.

PEER 2003/15 *Seismic Demands for Nondeteriorating Frame Structures and Their Dependence on Ground Motions.* Ricardo Antonio Medina and Helmut Krawinkler. May 2004.

PEER 2003/14 *Finite Element Reliability and Sensitivity Methods for Performance-Based Earthquake Engineering.* Terje Haukaas and Armen Der Kiureghian. April 2004.

PEER 2003/13 *Effects of Connection Hysteretic Degradation on the Seismic Behavior of Steel Moment-Resisting Frames.* Janise E. Rodgers and Stephen A. Mahin. March 2004.

PEER 2003/12 *Implementation Manual for the Seismic Protection of Laboratory Contents: Format and Case Studies.* William T. Holmes and Mary C. Comerio. October 2003.

PEER 2003/11 *Fifth U.S.-Japan Workshop on Performance-Based Earthquake Engineering Methodology for Reinforced Concrete Building Structures.* February 2004.

PEER 2003/10 *A Beam-Column Joint Model for Simulating the Earthquake Response of Reinforced Concrete Frames.* Laura N. Lowes, Nilanjan Mitra, and Arash Altoontash. February 2004.

PEER 2003/09 *Sequencing Repairs after an Earthquake: An Economic Approach.* Marco Casari and Simon J. Wilkie. April 2004.

PEER 2003/08 *A Technical Framework for Probability-Based Demand and Capacity Factor Design (DCFD) Seismic Formats.* Fatemeh Jalayer and C. Allin Cornell. November 2003.

PEER 2003/07 *Uncertainty Specification and Propagation for Loss Estimation Using FOSM Methods.* Jack W. Baker and C. Allin Cornell. September 2003.

PEER 2003/06 *Performance of Circular Reinforced Concrete Bridge Columns under Bidirectional Earthquake Loading.* Mahmoud M. Hachem, Stephen A. Mahin, and Jack P. Moehle. February 2003.

PEER 2003/05 *Response Assessment for Building-Specific Loss Estimation.* Eduardo Miranda and Shahram Taghavi. September 2003.

PEER 2003/04 *Experimental Assessment of Columns with Short Lap Splices Subjected to Cyclic Loads.* Murat Melek, John W. Wallace, and Joel Conte. April 2003.

PEER 2003/03 *Probabilistic Response Assessment for Building-Specific Loss Estimation.* Eduardo Miranda and Hesameddin Aslani. September 2003.

PEER 2003/02 *Software Framework for Collaborative Development of Nonlinear Dynamic Analysis Program.* Jun Peng and Kincho H. Law. September 2003.

PEER 2003/01 *Shake Table Tests and Analytical Studies on the Gravity Load Collapse of Reinforced Concrete Frames.* Kenneth John Elwood and Jack P. Moehle. November 2003.

PEER 2002/24 *Performance of Beam to Column Bridge Joints Subjected to a Large Velocity Pulse.* Natalie Gibson, André Filiatrault, and Scott A. Ashford. April 2002.

PEER 2002/23 *Effects of Large Velocity Pulses on Reinforced Concrete Bridge Columns.* Greg L. Orozco and Scott A. Ashford. April 2002.

PEER 2002/22 *Characterization of Large Velocity Pulses for Laboratory Testing.* Kenneth E. Cox and Scott A. Ashford. April 2002.

PEER 2002/21 *Fourth U.S.-Japan Workshop on Performance-Based Earthquake Engineering Methodology for Reinforced Concrete Building Structures.* December 2002.

PEER 2002/20 *Barriers to Adoption and Implementation of PBEE Innovations.* Peter J. May. August 2002.

PEER 2002/19 *Economic-Engineered Integrated Models for Earthquakes: Socioeconomic Impacts.* Peter Gordon, James E. Moore II, and Harry W. Richardson. July 2002.

PEER 2002/18 *Assessment of Reinforced Concrete Building Exterior Joints with Substandard Details.* Chris P. Pantelides, Jon Hansen, Justin Nadauld, and Lawrence D. Reaveley. May 2002.

PEER 2002/17 *Structural Characterization and Seismic Response Analysis of a Highway Overcrossing Equipped with Elastomeric Bearings and Fluid Dampers: A Case Study.* Nicos Makris and Jian Zhang. November 2002.

PEER 2002/16 *Estimation of Uncertainty in Geotechnical Properties for Performance-Based Earthquake Engineering.* Allen L. Jones, Steven L. Kramer, and Pedro Arduino. December 2002.

PEER 2002/15 *Seismic Behavior of Bridge Columns Subjected to Various Loading Patterns.* Asadollah Esmaeily-Gh. and Yan Xiao. December 2002.

PEER 2002/14 *Inelastic Seismic Response of Extended Pile Shaft Supported Bridge Structures.* T.C. Hutchinson, R.W. Boulanger, Y.H. Chai, and I.M. Idriss. December 2002.

PEER 2002/13 *Probabilistic Models and Fragility Estimates for Bridge Components and Systems.* Paolo Gardoni, Armen Der Kiureghian, and Khalid M. Mosalam. June 2002.

PEER 2002/12 *Effects of Fault Dip and Slip Rake on Near-Source Ground Motions: Why Chi-Chi Was a Relatively Mild M7.6 Earthquake.* Brad T. Aagaard, John F. Hall, and Thomas H. Heaton. December 2002.

PEER 2002/11 *Analytical and Experimental Study of Fiber-Reinforced Strip Isolators*. James M. Kelly and Shakhzod M. Takhirov. September 2002.

PEER 2002/10 *Centrifuge Modeling of Settlement and Lateral Spreading with Comparisons to Numerical Analyses***.** Sivapalan Gajan and Bruce L. Kutter. January 2003.

PEER 2002/09 *Documentation and Analysis of Field Case Histories of Seismic Compression during the 1994 Northridge, California, Earthquake.* Jonathan P. Stewart, Patrick M. Smith, Daniel H. Whang, and Jonathan D. Bray. October 2002.

PEER 2002/08 *Component Testing, Stability Analysis and Characterization of Buckling-Restrained Unbonded Braces™.* Cameron Black, Nicos Makris, and Ian Aiken. September 2002.

PEER 2002/07 *Seismic Performance of Pile-Wharf Connections.* Charles W. Roeder, Robert Graff, Jennifer Soderstrom, and Jun Han Yoo. December 2001.

PEER 2002/06 *The Use of Benefit-Cost Analysis for Evaluation of Performance-Based Earthquake Engineering Decisions*. Richard O. Zerbe and Anthony Falit-Baiamonte. September 2001.

PEER 2002/05 *Guidelines, Specifications, and Seismic Performance Characterization of Nonstructural Building Components and Equipment*. André Filiatrault, Constantin Christopoulos, and Christopher Stearns. September 2001.

PEER 2002/04 *Consortium of Organizations for Strong-Motion Observation Systems and the Pacific Earthquake Engineering Research Center Lifelines Program: Invited Workshop on Archiving and Web Dissemination of Geotechnical Data, 4–5 October 2001*. September 2002.

PEER 2002/03 *Investigation of Sensitivity of Building Loss Estimates to Major Uncertain Variables for the Van Nuys Testbed.* Keith A. Porter, James L. Beck, and Rustem V. Shaikhutdinov. August 2002.

PEER 2002/02 *The Third U.S.-Japan Workshop on Performance-Based Earthquake Engineering Methodology for Reinforced Concrete Building Structures.* July 2002.

PEER 2002/01 *Nonstructural Loss Estimation: The UC Berkeley Case Study.* Mary C. Comerio and John C. Stallmeyer. December 2001.

PEER 2001/16 *Statistics of SDF-System Estimate of Roof Displacement for Pushover Analysis of Buildings.* Anil K. Chopra, Rakesh K. Goel, and Chatpan Chintanapakdee. December 2001.

PEER 2001/15 *Damage to Bridges during the 2001 Nisqually Earthquake.* R. Tyler Ranf, Marc O. Eberhard, and Michael P. Berry. November 2001.

PEER 2001/14 *Rocking Response of Equipment Anchored to a Base Foundation.* Nicos Makris and Cameron J. Black. September 2001.

PEER 2001/13 *Modeling Soil Liquefaction Hazards for Performance-Based Earthquake Engineering.* Steven L. Kramer and Ahmed-W. Elgamal. February 2001.

PEER 2001/12 *Development of Geotechnical Capabilities in OpenSees.* Boris Jeremić. September 2001.

PEER 2001/11 *Analytical and Experimental Study of Fiber-Reinforced Elastomeric Isolators*. James M. Kelly and Shakhzod M. Takhirov. September 2001.

PEER 2001/10 *Amplification Factors for Spectral Acceleration in Active Regions.* Jonathan P. Stewart, Andrew H. Liu, Yoojoong Choi, and Mehmet B. Baturay. December 2001.

PEER 2001/09 *Ground Motion Evaluation Procedures for Performance-Based Design.* Jonathan P. Stewart, Shyh-Jeng Chiou, Jonathan D. Bray, Robert W. Graves, Paul G. Somerville, and Norman A. Abrahamson. September 2001.

PEER 2001/08 *Experimental and Computational Evaluation of Reinforced Concrete Bridge Beam-Column Connections for Seismic Performance*. Clay J. Naito, Jack P. Moehle, and Khalid M. Mosalam. November 2001.

PEER 2001/07 *The Rocking Spectrum and the Shortcomings of Design Guidelines.* Nicos Makris and Dimitrios Konstantinidis. August 2001.

PEER 2001/06 *Development of an Electrical Substation Equipment Performance Database for Evaluation of Equipment Fragilities*. Thalia Agnanos. April 1999.

PEER 2001/05 *Stiffness Analysis of Fiber-Reinforced Elastomeric Isolators.* Hsiang-Chuan Tsai and James M. Kelly. May 2001.

PEER 2001/04 *Organizational and Societal Considerations for Performance-Based Earthquake Engineering.* Peter J. May. April 2001.

PEER 2001/03 *A Modal Pushover Analysis Procedure to Estimate Seismic Demands for Buildings: Theory and Preliminary Evaluation.* Anil K. Chopra and Rakesh K. Goel. January 2001.

PEER 2001/02 *Seismic Response Analysis of Highway Overcrossings Including Soil-Structure Interaction.* Jian Zhang and Nicos Makris. March 2001.

PEER 2001/01 *Experimental Study of Large Seismic Steel Beam-to-Column Connections.* Egor P. Popov and Shakhzod M. Takhirov. November 2000.

PEER 2000/10 *The Second U.S.-Japan Workshop on Performance-Based Earthquake Engineering Methodology for Reinforced Concrete Building Structures.* March 2000.

PEER 2000/09 *Structural Engineering Reconnaissance of the August 17, 1999 Earthquake: Kocaeli (Izmit), Turkey.* Halil Sezen, Kenneth J. Elwood, Andrew S. Whittaker, Khalid Mosalam, John J. Wallace, and John F. Stanton. December 2000.

PEER 2000/08 *Behavior of Reinforced Concrete Bridge Columns Having Varying Aspect Ratios and Varying Lengths of Confinement.* Anthony J. Calderone, Dawn E. Lehman, and Jack P. Moehle. January 2001.

PEER 2000/07 *Cover-Plate and Flange-Plate Reinforced Steel Moment-Resisting Connections.* Taejin Kim, Andrew S. Whittaker, Amir S. Gilani, Vitelmo V. Bertero, and Shakhzod M. Takhirov. September 2000.

PEER 2000/06 *Seismic Evaluation and Analysis of 230-kV Disconnect Switches.* Amir S. J. Gilani, Andrew S. Whittaker, Gregory L. Fenves, Chun-Hao Chen, Henry Ho, and Eric Fujisaki. July 2000.

PEER 2000/05 *Performance-Based Evaluation of Exterior Reinforced Concrete Building Joints for Seismic Excitation.* Chandra Clyde, Chris P. Pantelides, and Lawrence D. Reaveley. July 2000.

PEER 2000/04 *An Evaluation of Seismic Energy Demand: An Attenuation Approach.* Chung-Che Chou and Chia-Ming Uang. July 1999.

PEER 2000/03 *Framing Earthquake Retrofitting Decisions: The Case of Hillside Homes in Los Angeles.* Detlof von Winterfeldt, Nels Roselund, and Alicia Kitsuse. March 2000.

PEER 2000/02 *U.S.-Japan Workshop on the Effects of Near-Field Earthquake Shaking.* Andrew Whittaker, ed. July 2000.

PEER 2000/01 *Further Studies on Seismic Interaction in Interconnected Electrical Substation Equipment.* Armen Der Kiureghian, Kee-Jeung Hong, and Jerome L. Sackman. November 1999.

PEER 1999/14 *Seismic Evaluation and Retrofit of 230-kV Porcelain Transformer Bushings.* Amir S. Gilani, Andrew S. Whittaker, Gregory L. Fenves, and Eric Fujisaki. December 1999.

PEER 1999/13 *Building Vulnerability Studies: Modeling and Evaluation of Tilt-up and Steel Reinforced Concrete Buildings.* John W. Wallace, Jonathan P. Stewart, and Andrew S. Whittaker, editors. December 1999.

PEER 1999/12 *Rehabilitation of Nonductile RC Frame Building Using Encasement Plates and Energy-Dissipating Devices.* Mehrdad Sasani, Vitelmo V. Bertero, James C. Anderson. December 1999.

PEER 1999/11 *Performance Evaluation Database for Concrete Bridge Components and Systems under Simulated Seismic Loads.* Yael D. Hose and Frieder Seible. November 1999.

PEER 1999/10 *U.S.-Japan Workshop on Performance-Based Earthquake Engineering Methodology for Reinforced Concrete Building Structures.* December 1999.

PEER 1999/09 *Performance Improvement of Long Period Building Structures Subjected to Severe Pulse-Type Ground Motions*. James C. Anderson, Vitelmo V. Bertero, and Raul Bertero. October 1999.

PEER 1999/08 *Envelopes for Seismic Response Vectors.* Charles Menun and Armen Der Kiureghian. July 1999.

PEER 1999/07 *Documentation of Strengths and Weaknesses of Current Computer Analysis Methods for Seismic Performance of Reinforced Concrete Members.* William F. Cofer. November 1999.

PEER 1999/06 *Rocking Response and Overturning of Anchored Equipment under Seismic Excitations.* Nicos Makris and Jian Zhang. November 1999.

PEER 1999/05 *Seismic Evaluation of 550 kV Porcelain Transformer Bushings.* Amir S. Gilani, Andrew S. Whittaker, Gregory L. Fenves, and Eric Fujisaki. October 1999.

PEER 1999/04 *Adoption and Enforcement of Earthquake Risk-Reduction Measures.* Peter J. May, Raymond J. Burby, T. Jens Feeley, and Robert Wood.

PEER 1999/03 *Task 3 Characterization of Site Response General Site Categories*. Adrian Rodriguez-Marek, Jonathan D. Bray, and Norman Abrahamson. February 1999.

PEER 1999/02 *Capacity-Demand-Diagram Methods for Estimating Seismic Deformation of Inelastic Structures: SDF Systems*. Anil K. Chopra and Rakesh Goel. April 1999.

PEER 1999/01 *Interaction in Interconnected Electrical Substation Equipment Subjected to Earthquake Ground Motions.* Armen Der Kiureghian, Jerome L. Sackman, and Kee-Jeung Hong. February 1999.

PEER 1998/08 *Behavior and Failure Analysis of a Multiple-Frame Highway Bridge in the 1994 Northridge Earthquake.* Gregory L. Fenves and Michael Ellery. December 1998.

PEER 1998/07 *Empirical Evaluation of Inertial Soil-Structure Interaction Effects.* Jonathan P. Stewart, Raymond B. Seed, and Gregory L. Fenves. November 1998.

PEER 1998/06 *Effect of Damping Mechanisms on the Response of Seismic Isolated Structures.* Nicos Makris and Shih-Po Chang. November 1998.

PEER 1998/05 *Rocking Response and Overturning of Equipment under Horizontal Pulse-Type Motions.* Nicos Makris and Yiannis Roussos. October 1998.

PEER 1998/04 *Pacific Earthquake Engineering Research Invitational Workshop Proceedings, May 14–15, 1998: Defining the Links between Planning, Policy Analysis, Economics and Earthquake Engineering.* Mary Comerio and Peter Gordon. September 1998.

PEER 1998/03 *Repair/Upgrade Procedures for Welded Beam to Column Connections.* James C. Anderson and Xiaojing Duan. May 1998.

PEER 1998/02 *Seismic Evaluation of 196 kV Porcelain Transformer Bushings.* Amir S. Gilani, Juan W. Chavez, Gregory L. Fenves, and Andrew S. Whittaker. May 1998.

PEER 1998/01 *Seismic Performance of Well-Confined Concrete Bridge Columns.* Dawn E. Lehman and Jack P. Moehle. December 2000.

ONLINE PEER REPORTS

The following PEER reports are available by Internet only at http://peer.berkeley.edu/publications/peer_reports_complete.html.

PEER 2012/103 *Performance-Based Seismic Demand Assessment of Concentrically Braced Steel Frame Buildings.* Chui-Hsin Chen and Stephen A. Mahin. December 2012.

PEER 2012/102 *Procedure to Restart an Interrupted Hybrid Simulation: Addendum to PEER Report 2010/103.* Vesna Terzic and Bozidar Stojadinovic. October 2012.

PEER 2012/101 *Mechanics of Fiber Reinforced Bearings.* James M. Kelly and Andrea Calabrese. February 2012.

PEER 2011/107 *Nonlinear Site Response and Seismic Compression at Vertical Array Strongly Shaken by 2007 Niigata-ken Chuetsu-oki Earthquake.* Eric Yee, Jonathan P. Stewart, and Kohji Tokimatsu. December 2011.

PEER 2011/106 *Self Compacting Hybrid Fiber Reinforced Concrete Composites for Bridge Columns.* Pardeep Kumar, Gabriel Jen, William Trono, Marios Panagiotou, and Claudia Ostertag. September 2011.

PEER 2011/105 *Stochastic Dynamic Analysis of Bridges Subjected to Spacially Varying Ground Motions.* Katerina Konakli and Armen Der Kiureghian. August 2011.

PEER 2011/104 *Design and Instrumentation of the 2010 E-Defense Four-Story Reinforced Concrete and Post-Tensioned Concrete Buildings.* Takuya Nagae, Kenichi Tahara, Taizo Matsumori, Hitoshi Shiohara, Toshimi Kabeyasawa, Susumu Kono, Minehiro Nishiyama (Japanese Research Team) and John Wallace, Wassim Ghannoum, Jack Moehle, Richard Sause, Wesley Keller, Zeynep Tuna (U.S. Research Team). June 2011.

PEER 2011/103 *In-Situ Monitoring of the Force Output of Fluid Dampers: Experimental Investigation.* Dimitrios Konstantinidis, James M. Kelly, and Nicos Makris. April 2011.

PEER 2011/102 *Ground-motion prediction equations 1964 - 2010.* John Douglas. April 2011.

PEER 2011/101 *Report of the Eighth Planning Meeting of NEES/E-Defense Collaborative Research on Earthquake Engineering.* Convened by the Hyogo Earthquake Engineering Research Center (NIED), NEES Consortium, Inc. February 2011.

PEER 2010/111 *Modeling and Acceptance Criteria for Seismic Design and Analysis of Tall Buildings.* Task 7 Report for the Tall Buildings Initiative - Published jointly by the Applied Technology Council. October 2010.

PEER 2010/110 *Seismic Performance Assessment and Probabilistic Repair Cost Analysis of Precast Concrete Cladding Systems for Multistory Buildlings.* Jeffrey P. Hunt and Božidar Stojadinovic. November 2010.

PEER 2010/109 *Report of the Seventh Joint Planning Meeting of NEES/E-Defense Collaboration on Earthquake Engineering. Held at the E-Defense, Miki, and Shin-Kobe, Japan, September 18–19, 2009.* August 2010.

PEER 2010/108 *Probabilistic Tsunami Hazard in California.* Hong Kie Thio, Paul Somerville, and Jascha Polet, preparers. October 2010.

PEER 2010/107 *Performance and Reliability of Exposed Column Base Plate Connections for Steel Moment-Resisting Frames.* Ady Aviram, Božidar Stojadinovic, and Armen Der Kiureghian. August 2010.

PEER 2010/106 *Verification of Probabilistic Seismic Hazard Analysis Computer Programs.* Patricia Thomas, Ivan Wong, and Norman Abrahamson. May 2010.

PEER 2010/105 *Structural Engineering Reconnaissance of the April 6, 2009, Abruzzo, Italy, Earthquake, and Lessons Learned.* M. Selim Günay and Khalid M. Mosalam. April 2010.

PEER 2010/104 *Simulating the Inelastic Seismic Behavior of Steel Braced Frames, Including the Effects of Low-Cycle Fatigue.* Yuli Huang and Stephen A. Mahin. April 2010.

PEER 2010/103 *Post-Earthquake Traffic Capacity of Modern Bridges in California.* Vesna Terzic and Božidar Stojadinović. March 2010.

PEER 2010/102 *Analysis of Cumulative Absolute Velocity (CAV) and JMA Instrumental Seismic Intensity (I_{JMA}) Using the PEER–NGA Strong Motion Database.* Kenneth W. Campbell and Yousef Bozorgnia. February 2010.

PEER 2010/101 *Rocking Response of Bridges on Shallow Foundations.* Jose A. Ugalde, Bruce L. Kutter, and Boris Jeremic. April 2010.

PEER 2009/109 *Simulation and Performance-Based Earthquake Engineering Assessment of Self-Centering Post-Tensioned Concrete Bridge Systems.* Won K. Lee and Sarah L. Billington. December 2009.

PEER 2009/108 *PEER Lifelines Geotechnical Virtual Data Center.* J. Carl Stepp, Daniel J. Ponti, Loren L. Turner, Jennifer N. Swift, Sean Devlin, Yang Zhu, Jean Benoit, and John Bobbitt. September 2009.

PEER 2009/107 *Experimental and Computational Evaluation of Current and Innovative In-Span Hinge Details in Reinforced Concrete Box-Girder Bridges: Part 2: Post-Test Analysis and Design Recommendations.* Matias A. Hube and Khalid M. Mosalam. December 2009.

PEER 2009/106 *Shear Strength Models of Exterior Beam-Column Joints without Transverse Reinforcement.* Sangjoon Park and Khalid M. Mosalam. November 2009.

PEER 2009/105 *Reduced Uncertainty of Ground Motion Prediction Equations through Bayesian Variance Analysis.* Robb Eric S. Moss. November 2009.

PEER 2009/104 *Advanced Implementation of Hybrid Simulation.* Andreas H. Schellenberg, Stephen A. Mahin, Gregory L. Fenves. November 2009.

PEER 2009/103 *Performance Evaluation of Innovative Steel Braced Frames.* T. Y. Yang, Jack P. Moehle, and Božidar Stojadinovic. August 2009.

PEER 2009/102 *Reinvestigation of Liquefaction and Nonliquefaction Case Histories from the 1976 Tangshan Earthquake.* Robb Eric Moss, Robert E. Kayen, Liyuan Tong, Songyu Liu, Guojun Cai, and Jiaer Wu. August 2009.

PEER 2009/101 *Report of the First Joint Planning Meeting for the Second Phase of NEES/E-Defense Collaborative Research on Earthquake Engineering.* Stephen A. Mahin et al. July 2009.

PEER 2008/104 *Experimental and Analytical Study of the Seismic Performance of Retaining Structures.* Linda Al Atik and Nicholas Sitar. January 2009.

PEER 2008/103 *Experimental and Computational Evaluation of Current and Innovative In-Span Hinge Details in Reinforced Concrete Box-Girder Bridges. Part 1: Experimental Findings and Pre-Test Analysis.* Matias A. Hube and Khalid M. Mosalam. January 2009.

PEER 2008/102 *Modeling of Unreinforced Masonry Infill Walls Considering In-Plane and Out-of-Plane Interaction.* Stephen Kadysiewski and Khalid M. Mosalam. January 2009.

PEER 2008/101 *Seismic Performance Objectives for Tall Buildings.* William T. Holmes, Charles Kircher, William Petak, and Nabih Youssef. August 2008.

PEER 2007/101 *Generalized Hybrid Simulation Framework for Structural Systems Subjected to Seismic Loading.* Tarek Elkhoraibi and Khalid M. Mosalam. July 2007.

PEER 2007/100 *Seismic Evaluation of Reinforced Concrete Buildings Including Effects of Masonry Infill Walls.* Alidad Hashemi and Khalid M. Mosalam. July 2007.

The Pacific Earthquake Engineering Research Center (PEER) is a multi-institutional research and education center with headquarters at the University of California, Berkeley. Investigators from over 20 universities, several consulting companies, and researchers at various state and federal government agencies contribute to research programs focused on performance-based earthquake engineering.

These research programs aim to identify and reduce the risks from major earthquakes to life safety and to the economy by including research in a wide variety of disciplines including structural and geotechnical engineering, geology/seismology, lifelines, transportation, architecture, economics, risk management, and public policy.

PEER is supported by federal, state, local, and regional agencies, together with industry partners.

PEER Core Institutions:
University of California, Berkeley (Lead Institution)
California Institute of Technology
Oregon State University
Stanford University
University of California, Davis
University of California, Irvine
University of California, Los Angeles
University of California, San Diego
University of Southern California
University of Washington

PEER reports can be ordered at http://peer.berkeley.edu/publications/peer_reports.html or by contacting

Pacific Earthquake Engineering Research Center
University of California, Berkeley
325 Davis Hall, mail code 1792
Berkeley, CA 94720-1792
Tel: 510-642-3437
Fax: 510-642-1655
Email: peer_editor@berkeley.edu

ISSN 1547-0587X